ANALYSIS OF AUTOMOTIVE LOAD SIMULATION TECHNIQUES

by

J. M. Karwatzki

MPhil, CEng, MIMechE, MInstMC

Thesis for the degree of

Doctor of Philosophy

submitted to the

Council for National Academic Awards

August 1977

School of Mechanical, Aeronautical

and Production Engineering

Kingston Polytechnic

TEXT CUT OFF IN THE ORIGINAL

SYNOPSIS

The object of this thesis is to show how it is possible to provide simulated running conditions to a prime mover in the laboratory and to develop a test facility to provide such conditions. A generalised mathematical model is developed for prime mover/dynamometer combinations which is used as a basis for the design of a wide range of load simulation systems. The mathematical model is validated by experimental investigations of a low power simulation system for which the prime mover is a d.c. traction motor and the dynamometer is of the hydrostatic transmission system type.

A full scale engine test cell is constructed in which a 70 kW diesel engine may be loaded by two types of hydraulic dynamometer to enable comparisons to be made between each system. One of these is a hydrostatic dynamometer having the same operating principles as the low power system. The other is based upon the operation of a unique hydraulic valve, the design of which is based upon theoretical and experimental analysis of several low power prototypes. The generalised mathematical model and design method is used to predict the performance of these engine/dynamometer systems for a range of load simulation methods. The theoretical analysis is also extended to petrol engines and electric prime movers, for a range of dynamometer systems and

load simulation methods, in order that the most suitable dynamometer and simulation method may be determined for each prime mover.

To aid in the supervision of the engine test cell under running conditions, a low cost microprocessor-based monitoring system is developed to allow early warning of any large changes from the required operating conditions.

INDEX

INTRODUCTION

The need for simulating vehicle load conditions for prime movers in the laboratory has already been well established (Refs. 13, 23, 24, 25). In particular, recent American and European legislation (Refs. 1, 2) provide speed/time curves for testing engine exhaust emissions on chassis dynamometers to enable typical running conditions to be simulated. Simulation of transient performance characteristics are also of particular importance for turbocharged diesel engines which have now almost completely replaced naturally aspirated engines in heavy automotive and electric generator applications. Much work has been reported on the transient performance of turbocharged diesel engines (e.g., Refs. 15, 16, 17, 18, 22), since under sudden load application conditions the exhaust emits black smoke and under severe conditions the engine may stall.

Simulation of vehicle duty cycles is also used to improve the performance of electric vehicles to enable improved battery/motor/transmission and control systems to be chosen (Ref. 30). It has been shown that economic and environmental advantages may be obtained over internal combustion engines for certain applications (i.e., short haul deliveries, city buses, etc.).

In order to analyse the various methods by which automotive loading conditions may be simulated, it is first shown in Part 1 how a simple block diagram approach may be used to obtain a mathematical model for a range of prime mover and dynamometer systems. The model is developed using information which is generally available from the manufacturers of the prime mover or dynamometer system, i.e., torque/speed characteristics, inertia of rotating parts and time lags. Since the form of the block diagram is similar for each of the systems analysed, a generalised block diagram is proposed for typical prime mover/dynamometer configurations. Also in Part 1 it is shown how the vehicle characteristics may be simulated by using one of two basic techniques.

In the first technique the vehicle characteristics are simulated by providing torque and speed feedback control to the engine/dynamometer system so that the levels achieved are representative of typical driving conditions. For the second technique the prime mover speed is controlled through the prime mover input signal (i.e., throttle control of a petrol engine) and the vehicle characteristics are simulated by the use of a filter in either of the torque or speed feedback paths to the dynamometer input. It is shown how the root locus method provides a very suitable method of assessing the performance of typical prime mover/dynamometer systems using these means of simulating loads.

In Part 2 the analytical techniques are applied to a low power load simulation system in which a hydrostatic dynamometer is used to control an electric prime mover. The torque/speed characteristics are reasonably linear compared to other types of prime mover and dynamometer system, so that the performance predictions can be made for large changes in the operating conditions. For the typical dynamometer/prime mover configurations analysed in Parts 3, 4 and 5 a large number of the system variables are non-linear and vary with either the prime mover speed or torque (or both). For these systems a simplified analysis is performed by determining the change in root positions with speed (i.e., a root locus) at both high and low torque levels.

In Part 3 the analysis is applied to a 70 kW naturally aspirated governed diesel engine system controlled by two types of hydraulic dynamometer. The use of a governor in the system requires the analysis to include maximum fuel delivery conditions as well as the normal fuel delivery and motoring conditions. Furthermore, with the vehicle characteristics simulated by means of a filter in a feedback path of the system, it is necessary to analyse the system with the differing vehicle characteristics obtained in both high and low gear settings. Thus extensive analysis of the system is necessary since the operating conditions can vary considerably. For the purposes of comparison with the performance of the hydraulic dynamometers, further analysis is made of the system using typical coefficients for an electric dynamometer.

In Part 4 a similar theoretical analysis is applied to a 100 kW naturally aspirated petrol engine using the same range of dynamometers and load simulation methods. It is not necessary to follow the same extensive analysis as for the governed diesel engine system, since maximum fuel delivery conditions are rarely encountered by the petrol engine in practice, although the high torque low speed conditions can have a greater effect upon the stability of the petrol engine system than for the diesel engine system.

In Part 5 the analytical procedure is repeated for a 40 kW electric prime mover used in delivery vehicle applications. The analysis of load simulation techniques for this system is much simpler than for the internal combustion engine systems due to the elimination of:- (i) the prime mover actuator lag; (ii) the flexible coupling between prime mover and dynamometer; (iii) the simulation of gear changes; and (iv) the governor lag of the diesel engine system. However, the electric prime mover has a very steep torque/speed slope at low speed compared to the internal combustion engines, which is abruptly cut off as the maximum current limit of the motor is reached, so that the root positions of the system must also be investigated in this region.

In Part 6 it is shown how one of the hydraulic dynamometers has been developed in an attempt to obtain a fast response together with linear performance and high discrimination. The dynamometer is based upon the operation of a unique valve, for which previous workers have performed preliminary investigations on a low power prototype (Ref. 37). Extensive theoretical and experimental investigations on small scale valves are used to enable a full scale valve to be constructed and incorporated into the engine test cell for controlling the load on a 75 kW diesel engine. A hydrostatic dynamometer is also constructed for use in the engine test cell (based upon the principle of operation of the low power system analysed in Part 2) so that a comparison may be made between the performance of the two dynamometer systems.

Part 7 shows how the engine test cell has been developed with particular emphasis upon the safety of the start up and shut down procedures. It is also shown how a low cost microprocessor-based monitoring system has been developed to perform routine supervision of the test cell under normal running conditions, and to automatically shut down the system in the event of predefined limits being exceeded. Preliminary testing of the system is reported in Part 8, together with a general discussion on the analytical techniques developed and areas where further work may be of benefit.

PREVIOUS WORK

The great majority of previous work reported on prime mover/dynamometer control methods has been in conjunction with electrical dynamometer systems, although many papers have been presented in which hydraulic dynamometers have been used. The method of control of these systems normally falls within two categories:-

(i) Torque feedback control by dynamometer and speed feedback control by prime mover (e.g., Refs. 15, 19, 21, 25).

(ii) Speed feedback control by dynamometer and torque feedback control by prime mover (e.g., Refs. 23, 26, 27, 28).

Other control methods have also been proposed such as manifold vacuum control for truck engines, which is stipulated in certain American legislation (Refs. 1, 25). Reasons for the choice of torque or speed control by dynamometer are not discussed in any of these references, although it will be shown in this thesis that there may be significant differences between the performance of the system for the two control methods.

The control method used in a large number of cases consists of 2 or 3 term action on the torque and speed loops (Refs. 24, 26, 27). However, Oatley (Ref. 28) has used proportional control with passive lead/lag networks, whereas Clements and Richard (Ref. 25) have used just proportional control on an amplidyne type dynamometer, and Bowns (Ref. 21) has used proportional control of a hydrostatic dynamometer. Direct digital control (DDC) of prime mover/dynamometer systems has been undertaken by Winterbone et al. (Ref. 15) on a fast response water brake dynamometer for loading a 6 cylinder diesel engine. DDC has also been used by Cassidy and Rillings (Ref. 23) and Rillings et al. (Ref. 67) on an SCR controlled d.c. dynamometer for exhaust emission analysis of petrol engines, and by Pacey and Edwards (Ref. 30) on a thyristor controlled d.c. dynamometer for testing of electric prime mover systems.

Supervisory digital control over the set points of three term controllers has been used by Marzouk and Watson (Ref. 19) on an eddy current dynamometer system and by Al-Bermani and Gravestock on a d.c. thyristor controlled dynamometer system for loading of diesel engines.

Computer control languages for engine test cells are discussed by Warman (Refs. 32, 33) and certain aspects of instrumentation for computer controlled test cells are discussed by Connor (Ref. 34) and Marzouk and Watson.

For the use of dynamometers to simulate automotive loads Bates and Grimshaw first published a paper on the simulation of locomotive loads for studies on the utilisation and control of traction motors (Ref. 68). The system was, however, very complex, consisting of an amplidyne plus two generators, and an electromechanical system to solve the equation of motion for simulation of the locomotive inertia. Also, stability problems were encountered if the simulated inertia was low in comparison to the inertia of the loading generator. A method of simulating loads in this manner (using standard dynamometers) is described in detail in section 1.2.2.2 of this thesis (method 2.2).

In 1972 Clements and Richard used a dynamometer control system to simulate the driving conditions of the Californian Seven Mode Cycle by using engine speed and acceleration curves (Ref. 25). These curves were used to obtain a dynamometer torque control signal by means of an analogue computer to simulate the vehicle characteristics and the throttle signal was used to control the engine speed. This method of simulating loads is described in detail in section 1.2.1.1 of this thesis (method 1.1). In the same year Cassidy (Ref. 69) simulated the Californian cycle for petrol engines by recording the required throttle position to follow the speed/time curves on a chassis dynamometer. Using the speed curves to control an engine dynamometer and the recorded throttle curves to produce the required torque levels he showed that the engine dynamometer resulted in greater repeatability from test to test than the chassis dynamometer. This method of simulating loads (using torque control on the throttle) is described in detail in section 1.2.1.2 of this thesis (method 1.2).

Also in 1972 Odier (Ref. 70) reported on a manually controlled chassis dynamometer to simulate all aspects of the dynamic behaviour of a passenger car (braking, traction, steering, etc.). Towards the end of 1972 Huffman et al. (Ref. 24) used a 190 kW chassis dynamometer to simulate vehicle dynamic loads for testing of engine fuels and lubricants. The engine speed was used to produce a torque demand signal to the dynamometer by employing analogue modules to simulate the vehicle characteristics. The control of engine speed to follow certain duty cycles was made initially by manual control of the throttle, followed by automatic three term control. A system of this type for simulating vehicle loads is described in section 1.2.2.1 of this thesis (method 2.1).

In 1973 Soliman (Ref. 26) presented work on the hybrid simulation of vehicle loads. In the same year

Karwatzki (Ref. 13) employed a hydrostatic transmission system to simulate vehicle loads on a d.c. traction motor by using the prime mover torque to obtain a speed reference control signal for the dynamometer, with the vehicle characteristics simulated on an analogue computer (method 2.2). The paper by Winterbone et al. (1977) shows how the loading characteristics of a heavy truck were simulated on a governed turbocharged diesel engine. Under mid fuel delivery conditions the dynamometer was used to control the torque (method 1.1 - section 1.2.1.1), whereas when the governor moves the fuel control rod to maximum delivery a changeover was made to enable the dynamometer to control the engine speed (method 1.2 - section 1.2.1.2). One major disadvantage with the system is that the water brake type dynamometer used in the experimental work cannot provide the motoring condition.

Also in 1977 the paper by Pacey and Edwards showed how duty cycles for electric prime movers were simulated using the prime mover speed and acceleration signals to obtain a load torque demand for dynamometer control (method 2.2 - section 1.2.2.2). Preliminary stability investigations were made by simulating the entire system on an analogue computer. At present a large amount of work is being undertaken to develop electric vehicles in Great Britain (e.g., Refs. 71, 72, 73) and recent legislation has been introduced to increase such development in the U.S.A. (Ref. 31).

The advancement of prime mover/dynamometer control methods relies heavily upon the development of suitable mathematical models for such systems. The models presently available are either analytical in nature (using linearised transfer functions in the complex frequency or sampled data domain) or involve computer simulation (using analogue, digital or hybrid computers). Analogue simulations were used by Ledger and Walmsley in 1971 for a turbocharged diesel engine (Ref. 74), and by Al-Bermani and Gravestock in 1975 for the analysis of a complete diesel engine, dynamometer and control system. They point out that a dynamometer having a low inertia and time constant would provide an improved performance for transient response testing of the engine.

In 1973 Soliman (Ref. 27) analysed a petrol engine and eddy current dynamometer system, employing hybrid simulation techniques, in which a digital computer was used to interpolate the engine and dynamometer torques for given values of throttle setting, engine speed and dynamometer field current. Earlier, in 1971, Burrows et al. (Ref. 75) had used hybrid simulation techniques to investigate sampled data models of diesel engines. They conclude that sampled data models provide an improvement over Laplace domain transfer functions, since the pure time delay between firing cycles of an engine is sampled data in nature. This conclusion is, however, of greater significance for low speed engines, since at high speed the pure time delay becomes small.

The use of sampled data techniques for internal combustion engines was proposed first by Bowns (Ref. 21), followed by Hazell and Flower (Refs. 76, 77) in 1971.

Digital simulation techniques have also received widespread attention in the development of engine/dynamometer models. In 1968 Janota et al. (Ref. 4) used a digital simulation of the combustion process to predict the performance of multi-cylinder turbocharged diesel engines and made comparisons with an experimental 2-stroke single cylinder engine. In 1971 Streit and Borman (Ref. 17) presented a survey of the development of sub-models necessary for the detailed simulation of turbocharged diesel engines. In the same year a survey of internal combustion engine research in the U.K. was presented by the Universities Internal Combustion Engine Group (Ref. 78). Numerous refinements in the digital simulations have been proposed to date (e.g., Refs. 5, 15, 16, 18, 22).

Of great significance in the analysis of diesel engines (naturally aspirated on turbocharged) is the mathematical description of the governor, which is normally highly non-linear due to stiction and coulomb friction effects. Massey and Oldenburger presented a detailed design technique for diesel governors in 1958 (Ref. 79) and the following year Welbourn et al. applied control theory to investigate the time lags and non-linear friction effects of diesel governors (Ref. 80). Further analytical techniques, including describing functions and phase plane analysis to describe the non-linear behaviour of governors, were presented by Parnaby in 1971 (Ref. 81). In 1973 Bowns (Ref. 82) used both analogue and digital computer simulations of a naturally aspirated diesel engine to determine the effect upon engine stability of variations in governor gain, damping and undamped natural frequency.

Fairly simple analytical models have also been developed for prime mover/dynamometer systems with some success. In 1970 Monk and Comfort (Ref. 83) used electrical analogies to analyse the dynamic characteristics of a petrol engine and eddy current dynamometer system. The model gave good agreement with the experimental responses of the system for pseudo-random and frequency response tests, as well as for step input tests. The model is similar to that developed by block diagram techniques in section 4.4 of this thesis for a petrol engine and electrical dynamometer system. Monk and Comfort's model was used as a basis for the development of control parameters employing modern control theory by Munro and Hirbod in 1977 (Ref. 84). Their analysis is confined to one point of the operating range of the engine/dynamometer system and they note that any change from this point may degrade the performance of the control system.

Interest in the use of hydrostatic dynamometer systems has increased since a commercially available unit was introduced in 1967 (Ref. 85). Bowns published details of a valve controlled hydrostatic dynamometer in 1971 (Ref. 21). In 1973 Woolvet and Karwatzki (Ref. 86) reported on a hydrostatic transmission system used to control the load on a d.c. traction motor. The following year Caputo and Carnevale (Ref. 87) presented information on a fast response dynamometer using a special purpose valve to control the flow from a hydrostatic pump.

Analysis of hydrostatic transmission systems has received much attention. Thoma produced comparisons of various mathematical models for hydrostatic systems in 1969 (Ref. 88) and in the same year McCallion et al. presented experimental results of dynamic tests on a hydrostatic transmission system (Ref. 89). In 1970 Olson provided a theoretical analysis on the critical lower speed of hydrostatic transmissions (Ref. 20). The following year Green and Crossley used frequency response techniques to analyse the dynamic characteristics of the control mechanism of variable delivery hydrostatic pumps (Ref. 90). Further analysis of hydrostatic transmission systems was made by Bowns and Worton-Griffiths in 1972 (Ref. 9), and optimising techniques for hydrostatic systems were investigated by Steel in 1973 (Ref. 91).

ACKNOWLEDGEMENTS

The author gratefully wishes to acknowledge the assistance of Mr. G. A. Woolvet and the technical staff at Kingston Polytechnic and the useful discussions with Professor D. E. Bowns of Bath University throughout the course of the project. Further acknowledgements are due to the following organisations:-

Ford Motor Company Ltd.,

Lucas-CAV Ltd.,

Chloride Technical Ltd.,

Hawker Siddeley Aviation Ltd.

PART 1

THE GENERALISED APPROACH

In order to perform a generalised analysis of the methods used to simulate dynamic loads, it is helpful to first examine the actual loading situation met under automotive conditions.

1.1 Automotive Loading Conditions

The analysis of automotive loading conditions requires an examination to be made of both the prime mover and the load.

1.1.1 The Prime Mover

A generalised block diagram for prime movers is shown in Fig. 1.1. Under steady state conditions the internally developed torque will be equal to the external torque (on the prime mover shaft) and there will be no change in speed. The input to the prime mover provides changes in the internally developed torque, and hence the speed changes at a rate dependent upon the prime mover inertia. This particular form of block diagram has been developed since the coefficients for each block are easily determined for various types of prime mover. (Such information will also normally be available from the manufacturer.) It is not the intention here to develop highly detailed mathematical models for prime movers since these models would then only be appropriate to specific prime movers and would not be suitable for a generalised analysis. Also, detailed models for internal combustion engines require digital simulation of the combustion process which, in turn, requires large amounts of computer memory and processor time, Ref. (4), Ref. (5).

For a petrol engine the input consists of a throttle setting, whereas a diesel engine input is a fuel rack setting and an input to a d.c. traction motor is the voltage applied to the windings (these being the three types of prime mover most widely used for transportation purposes).

The prime mover lag will vary according to the type of prime mover used. A d.c. traction motor will have a first order lag due to the inductance of the windings. The lag for internal combustion engines is more complicated than this. For a spark ignition engine with naturally aspirated carburettor a sudden change in throttle setting will have the following effect:-

The first cylinder to fire after the change in throttle setting will produce a change in torque developed dependent upon the time taken for the combustion phase to begin. This represents a pure time delay the magnitude of which depends upon the time at which a throttle change is made in relation to the engine firing cycle (this being a random effect) as well as the engine speed. Since the change in throttle is unlikely to occur at the beginning of a suction stroke, then in general the full change in torque developed will not occur until the second or third combustion phase after the throttle change.

For compression ignition engines there is a similar pure time delay for the next combustion phase to occur, although the torque/speed characteristics for this type of prime mover remain virtually flat over the speed range. Typical torque/speed characteristics for these three prime movers are shown in graphs G1 → G3 of Appendix A. It can be seen from graph G2 that the compression ignition engine provides little in the way of torque/speed feedback path shown in the generalised block diagram of Fig. 1.1. However, for automotive purposes, an extra feedback loop is often added in the form of a governor. The operation of the governor is to adjust the fuel rack position by an amount dependent upon the difference between the required engine speed and the actual engine speed. Although the torque/speed characteristics in Fig. 1.1 are shown to be in a positive feedback loop (this being an unstable condition), this will, in fact, only occur for internal combustion engines under certain conditions. For the characteristics of the d.c. traction motor (graph G3) the torque can be seen to reduce as the speed is increased. This results in a stable system since as the speed increases, the torque developed will reduce until it equals the external torque and the prime mover will be in a steady state. If the external torque is removed the motor will run up to dangerously high speed, which is characteristic of a series wound d.c. motor under no load conditions.

For the characteristics of the internal combustion engines (graphs G1 and G2), the right-hand side of the curves indicate that the torque reduces as the speed increases, so that these prime movers are also stable over this part of the response. However, for the left-hand side of the curves the torque increases as the speed is increased, so that the prime movers are unstable over this range unless a stabilising negative feedback loop is added. For the compression ignition engine a stabilising negative feedback loop is provided by the governor (with its inherent lag).

However, for petrol engines the negative feedback loop is provided by the load, which is examined in the next section. As long as the slope of the torque/speed characteristic of the load is greater than that of the engine (when operating over the left-hand side of the curve), then the positive feedback effect is overcome and the engine is stable. Under automotive conditions the gearbox is used to change the torque/speed characteristics of the load so that the performance is stable for a wide range of loading conditions. For example, in the case of a vehicle ascending an increasing slope in high gear and full throttle, the torque will increase and the speed will reduce until the engine is operating over the left-hand side of the torque/speed characteristic. The engine will consequently stall unless a change is made to a lower gear. If this change is made then the engine speed will increase (in proportion to the change in gear ratio) so that it once again is operating over the right-hand side of the curve and is therefore stable.

For the purposes of linear analysis it is more convenient to have the generalised block diagram for the prime mover as shown in Fig. 1.2. In order to change the input to the prime mover, there must be some form of input actuator. Under actual driving conditions this is the "accelerator pedal" which is manually controlled and therefore has an inherent lag. (Under simulated driving conditions this will be a servo actuator which will also have an inherent time lag.) The result of a change in the actuator setting is to produce a torque Tb which, together with the torque Tc from the torque/speed characteristic slope, provides the internally developed torque for the prime mover.

A simple method of linearising the torque/speed curve is shown in Fig. 1.3. In range (1) the maximum torque available from the input is X, and the torque/speed characteristic slope is A (positive). In range (2) the maximum torque available is Y with slope of zero, and in range (3) there is a maximum available torque of Z, with slope C (negative). Although the slopes A and C and the magnitudes X and Z will change at lower values of prime mover input (e.g., throttle setting), average values may be taken in order to perform a linearised analysis at each range of speed.

1.1.2 The Load

For automotive conditions the load equation at the prime mover shaft will be of the following form:-

$$Te = C_c + CrN + C_w N^2 + J_4 \dot{N} + T_a \qquad \ldots\ldots (1)$$

where Te = torque on prime mover shaft,

C_c = coulomb friction coefficient for the vehicle,

Cr = rolling resistance coefficient for the vehicle,

C_w = wind resistance coefficient for the vehicle,

J_4 = inertia of vehicle referred to prime mover shaft,

N = prime mover shaft speed,

T_a = additional torque effects due to gradients, wind gusts, cornering and transmission "noise".

For small changes in conditions from a given working point the equation may be rewritten:-

$$te = J_4 \dot{n} + F_4 n + Tx \qquad \ldots\ldots (2)$$

where F_4 is a speed dependent friction coefficient (non-linear for large signals),

Tx is the non-speed dependent friction torque.

The generalised block diagram for the prime mover under automotive conditions is shown in Fig. 1.4. The disturbance torque applied at the point shown enables the speed/torque transfer function to be obtained for the prime mover under automotive loading conditions. The point chosen for the disturbance torque input is particularly convenient, since the relationship between the prime mover input and the torque at this point may be easily combined into the speed/torque transfer function to give the relationship between the vehicle speed and prime mover input (e.g., throttle). Similarly, when a prime mover is to be loaded by a dynamometer (as shown in following sections), it is possible to determine the relationship between the dynamometer input and the torque at this point. Hence the transfer function between the prime mover speed and the dynamometer input may be obtained. For this reason the speed/torque transfer functions developed henceforth will be for changes in the prime mover speed resulting from the application of a step disturbance torque at the point shown in Fig. 1.4.

It is now possible to perform a linearised dynamic analysis of the three previously mentioned prime movers under automotive conditions. The block diagram for the operation of a series wound d.c. motor under automotive conditions is shown in Fig. 1.5. By block diagram reduction the speed/torque transfer function can be obtained:-

$$\frac{n}{t_{dis}} = \frac{1 + T_2 s}{(J_4+J_1)T_2 s^2 + (J_1+J_4+T_2F_4)s + (F_4-K_1)} \qquad \ldots\ldots (3)$$

The dynamics of the d.c. motor under these conditions are governed by the roots of the characteristic equation (which in this case can be seen to be second order). Thus any means used to simulate these conditions must provide roots as close as possible to those produced from the above characteristic equation for all values of F_4 and K_1. In practice the time constant for the motor windings $(T_{\cancel{1}}^{2})$ will be a fraction of a second and will therefore be small compared to the time constant of the load (J_4/F_4) so that the response approximates to that of a first order system.

For a petrol engine under automotive conditions the block diagram is as shown in Fig. 1.6. For convenience the pure time delay transfer function $(e^{-T_1 s})$ is replaced by a first order expansion $1-T_1 s$, so that the speed/torque transfer function becomes:-

$$\frac{n}{t_{dis}} = \frac{1}{(J_1+J_4+K_1T_1)s + (-K_1+F_4)} \qquad \ldots\ldots (4)$$

This produces a first order root the time constant of which varies with speed due to the effect of F_4, T_1

and K_1 (which can be positive or negative depending on which side of the torque/speed curve is in operation). The value of the pure time delay can vary from .05 seconds for a 4 cylinder engine running at 600 rpm to .0033 seconds for a 6 cylinder engine running at 6000 rpm (assuming 4 stroke operation). Once again, in order to simulate these dynamic loading conditions it is necessary to provide a load such that a first order root is obtained which is as close as possible to that obtained for the real system over the full range of running conditions.

For a governed diesel engine under automotive conditions the block diagram is shown in Fig. 1.7. The block diagram is similar to that of the petrol engine except for the inclusion of the governor lag which is approximated by a first order transfer function.

The speed/torque transfer function reduces to:-

$$\frac{n}{t_{dis}} =$$

$$\frac{1 + T_4 s}{(J_1+J_4+T_1K_1)T_4 s^2 + (J_1+J_4+T_4F_4+T_1K_1-T_1K_8-K_1T_4)s + F_4 + K_8 - K_1} \quad \text{..... (5)}$$

This transfer function is seen to be second order, the roots of which will vary with speed over the range of F_4, T_1 and K_1 in the same manner as the petrol engine, together with an extra variable T_4 (the time constant for the first order approximation to the governor response). Frequency response curves performed by the manufacturer for a 4 cylinder GX High Speed Minimec governor and pump system are shown in graph G4 for both low and high engine speeds (engine speed = twice pump speed). Although the inertia terms for a governor result in a second order transfer function, the damping is often sufficiently high to result in a damping ratio greater than unity, e.g., Ref. (3), Ref. (11). Hence two real roots exist, one of which provides a dominant first order response as indicated by graph G4 at low speed. If the -3dB point is used to obtain the corner frequency so that a first order lag may be used as an approximation to the response, it can be seen that the time constant will vary from 0.58 seconds at low speed to 0.01 seconds at high speed (750 → 3000 rpm).

It should be noted that this change in time constant occurs under the same conditions as the pure time delay (i.e., .04 seconds at 750 rpm → .01 seconds at 3000 rpm for 4 cylinder 4 stroke engine) and therefore has a considerable effect on the dynamic performance of the engine. However, even with low values of T_1 and T_4, the second order response of the diesel engine under normal conditions will still be heavily damped such that the performance will approximate to a first order system.

The time constant of this system will be given by the dominant root of the second order response which will, in turn, depend upon F_4, T_1, K_1 and T_4 (all of which vary with engine speed, but may be assumed constant for small perturbations).

It has been shown that the three types of prime mover most widely used under automotive conditions will respond, under normal loads, in the manner of a first order system. It has been further shown that this first order approximation to the response will be affected by such highly non-linear variables as prime mover and load torque/speed characteristics and the prime mover inherent lag. Several methods by which it is possible to provide loading conditions which are as close as possible to the actual automotive conditions are suggested in the next section.

1.2 Simulated Loading Conditions

In order to provide simulated loading conditions.it is necessary to have a loading device (dynamometer) which may be controlled to provide the complete range of torque and speed of which the prime mover is capable. The dynamometer should also be able to provide power to the prime mover for simulation of the "motoring" condition, as well as being able to absorb power from the prime mover for simulation of the "loading" condition. The ideal dynamometer would have no inherent dynamic effects of its own to contribute to the simulation in order to provide loading conditions identical to the actual automotive loads. It would therefore have an infinitely fast response with no inertia and no frictional loads.

Since no such dynamometer is available, then any simulation method used will only be an approximation to the actual loading conditions.

A generalised block diagram for a prime mover connected to a dynamometer is shown in Fig. 1.8. It can be seen that the dynamometer operation is virtually identical to that of the prime mover. In spite of the differing torque/speed characteristics of the two devices, it is possible to meet the torque/speed requirements of the prime mover, for fixed prime mover input, by varying the dynamometer input. Similarly, it is possible to meet the dynamometer torque/speed requirements, for fixed dynamometer input, by varying the prime mover input. In this way the torque/speed characteristics of the two devices may be determined and this is, in fact, how the torque/speed curves for prime movers are invariably obtained. There are two basic dynamometer systems which are suitable for providing both loading and motoring conditions, these being electrical dynamometer systems and hydrostatic dynamometer systems. (Mechanical variators have been used, but these suffer from limited speed range and slow speed of response.)

The block diagram for a d.c. motor/generator type dynamometer with thyristor control is shown in Fig. 1.9. As with the prime movers, the torque/speed characteristics are linearised by assuming small perturbations and include the input torque effect to offset the base of the torque/speed slope from the origin. The time constant for the winding lag of the d.c. dynamometer will generally be in the order of 0.1 → 1 seconds, whereas the time lag for the thyristor controller can be considered to be negligible.

The block diagram for a hydrostatic dynamometer system is shown in Fig. 1.10. It will be shown in Part 2 that the hydrostatic loop time constant is proportional to the pressurised volume of oil in the loop and inversely proportional to the effective bulk modulus and leakage flow from the loop. Depending on the construction of the hydrostatic system then, the time constant could be greater than 1 second or as low as 1 millisecond. The input actuator lag for a swashplate control servo-mechanism will normally be second order, as shown, with an undamped natural frequency in the order of 3 Hz for medium power rated units (graph G 5). (In Part 5 a unique loading/motoring valve is introduced which can take the place of the actuator lag and which can be designed to have a very much faster speed of response.)

In general when a dynamometer is to be used to test an internal combustion engine, it is necessary to have some form of flexible coupling between the engine and dynamometer in order to reduce vibration on the input shaft of the dynamometer. If the stiffness and damping coefficients of the coupling are low, then a further lag is introduced to the system as shown in the block diagram of Fig. 1.11. It can be seen that a torque will only appear on the connecting shaft when there is a relative displacement from one end of the shaft to the other, in fact, it is the displacement across part of the shaft which is normally measured by a strain gauge bridge and amplifier network to provide a torque signal. The value K_2 is the stiffness coefficient, so that $K_2(N_p - N_d)/s$ provides the steady state torque on the shaft and $F_2(N_p - N_d)$ provides the transient torque (where F_2 is the viscous friction coefficient of the coupling). The block diagram may be reduced to that shown in Fig. 1.12, from which it can be seen that the coupling can be treated as introducing an extra lag to the dynamometer side of the system. For very high values of F_2 and K_2 in relation to J_2, it can be seen that the coupling lag will be fast enough to be considered negligible, resulting in the same block diagram for the system without a flexible coupling.

A simplified generalised block diagram for the prime mover and dynamometer with input actuators is shown in Fig. 1.13, and this will be used to describe the various methods by which it is possible to simulate automotive conditions. In general, for the purposes of simulation, it is necessary for the engine and dynamometer to follow a speed/time curve such that the load provided by the dynamometer is as near as possible to that obtained by running the prime mover through the same speed/time curve under actual automotive conditions. Thus there will be a required speed signal and a required torque signal to the prime mover/dynamometer system. The Federal Register Emission Standards for 1977, Ref. (1), stipulate a total of 1372 values of vehicle speed at 1 second intervals to be run on a chassis dynamometer.

To be able to run such a test on an engine dynamometer it is necessary to evaluate the torque response of the vehicle under automotive conditions as a result of such changes in speed. This evaluation may be obtained by measuring and recording the torque obtained under actual automotive conditions. Alternatively, the torque could be evaluated by computer using derived coefficients for a particular vehicle. The computation may be performed prior to the test run to obtain a torque/time curve which would be run in conjunction with the speed/time curve, or the computation could be carried out on-line (either by an analogue or digital computer).

There are two basic methods of simulating automotive loading conditions on a prime mover. In the first the required torque and speed levels are fed independently to the controllers of the prime mover/dynamometer system. These levels may be recorded from a real vehicle driven over a given route prior to the simulation run, or the torque levels may be determined from a given speed signal using the simulated characteristics of the vehicle and used either on line or recorded prior to the test run.

In the second basic method the simulated characteristics are in a feedback path of the prime mover/dynamometer system and the dynamometer is controlled so as to provide the same loading conditions as the vehicle throughout the speed range of the prime mover.

1.2.1 Basic Simulation Method (1)

1.2.1.1 Method (1.1) Speed control on prime mover Torque control on dynamometer

The block diagram for this method of simulating automotive loads is shown in Fig. 1.14. The prime mover control signal is the error between the "required speed" signal and the "actual speed" signal, whereas the dynamometer control signal is the error between the "required torque" signal and the "actual torque" signal. If the speed transducer is of the d.c. tachogenerator type, then there will normally be a response time in the order of 1 millisecond associated with the windings of the tachogenerator, together with another lag also approximately 1 millisecond for 1% rms ripple smoothing. Other methods of measuring the speed will involve frequency to d.c. conversion or pulse counting, both of which may have an appreciable time lag if reasonable accuracy is required over the low speed range (1000 rev/min).

For the measurement of torque a strain gauge bridge mounted on a torsion shaft and connected to an amplifier via slip rings will have a response time much faster than 1 millisecond (typically 20 microseconds) which may be considered negligible. Inductive type torque transducers (used to eliminate slip ring noise) will have a response time dependent upon the filtering arrangement used in the demodulator system as well as the frequency of the oscillator. Measurement of torque by means of a load cell connected to the dynamometer carcase results in a negligible time lag with low noise characteristics, but has the disadvantage of requiring calibration and there may be difficulties in mounting the dynamometer.

The speed/time curves are given in km per hour so that the "required" torque and speed signals depend upon the vehicle torque/speed characteristics, transmission ratio and driving wheel diameter. Gear changes may be simulated by reducing the output from the simulated torque/speed characteristic block and the output from the km/hour to rev/min conversion block to zero, followed by a gradual increase in the outputs from these blocks to the new torque/speed levels (i.e., for a change down in gear ratio the required speed will increase and the required torque will reduce by an amount corresponding to the change in ratio).

1.2.1.2 Method (1.2) Torque control on prime mover
Speed control on dynamometer

This method of simulating automotive loads is similar to method 1.1 as shown in the block diagram of Fig. 1.15. The difference in response to these two methods depends upon the dynamics of the prime mover in relation to the dynamometer. In particular it should be realised that the friction characteristics between internal combustion engines of the same model may vary considerably (especially at varying temperatures). However, the simulated load (representing the inertia and friction characteristics of the vehicle) will not change appreciably for vehicles of the same type. This means that simulating the motoring condition using method 1.1 (i.e., torque control by dynamometer) is likely to cause large errors in speed due to the differing friction characteristics of prime movers under the motoring condition. To avoid this possibility when repeating simulation runs for several prime movers of the same model, it is necessary to use method 1.2 (speed control by dynamometer) for the most accurate simulation of the motoring condition.

1.2.2 Basic Simulation Method (2)

1.2.2.1 Torque Reference System

With this method of load simulation the speed dependent torque characteristics are obtained not from the speed/time curves as with method (1), but from the actual speed of the prime mover shaft, as shown in the block diagram of Fig. 1.16. This method has the advantage that it is not essential to follow speed/time curves, since the system will respond to manual inputs to the prime mover in the same manner as under automotive conditions.

It can be seen that the speed is controlled by the prime mover input, whereas the dynamometer input is a torque/speed control signal. This control signal is obtained from the difference between the simulated torque signal (obtained from the "actual speed" signal via the simulated torque/speed characteristics) and the actual torque signal. Thus this control system is termed "torque reference", although the dynamometer input signal is controlled indirectly by speed feedback as well as torque feedback.

Examination of Fig. 1.16 shows that an extra block is required for basic simulation method (2), namely the dynamometer characteristic slope correction block. This block is necessary since the dynamometer torque/

speed characteristic slope is, in general, very much greater than that of the simulated friction value. Thus the block effectively reduces the steady state dynamometer torque/speed slope to zero and the required value of simulated friction is obtained from the simulated characteristics. The inertia of the dynamometer could be taken into account by including a derivative term into the dynamometer characteristic slope elimination block, but since the dynamometer inertia will normally be much less than that of the simulated inertia, this action is assumed to be unnecessary.

1.2.2.2 Speed Reference System

The difference between this system and the torque reference system is that the dynamometer input signal is the error between the actual speed signal and the simulated speed signal. The simulated speed signal is obtained from the actual torque signal via the simulated torque/speed characteristics of the vehicle, as shown in the block diagram of Fig. 1.17. The method of changing gear for simulation method (2) is the same as that suggested for method (1), although the simulated torque signal must be evaluated on line and not prior to the simulation run. It can be seen, therefore, that method (2) could be used to provide accurate simulation of automotive conditions for a manually driven vehicle on a chassis dynamometer, as well as to provide fully automatic simulation on an engine dynamometer. Method (1) however, may only be used in conjunction with speed/time curves on an engine dynamometer or with automatic speed control on a chassis dynamometer.

One basic difficulty with both method (1) and method (2) is the ability to reproduce exact automotive conditions with high repeatability. Static loading tests may be corrected for such variables as temperature, atmospheric pressure and humidity, Ref. (12). However, these variables will affect the dynamics of both the prime mover and dynamometer and consequently may have an adverse effect upon the control system performance (i.e., the dynamic error may become large).

It is possible that greater repeatability may be obtained by following prime mover input curves, rather than prime mover speed curves. Thus the error in prime mover input could be kept very small using a suitable servo system, and the dynamometer input signal could be used to obtain, as near as possible, the required torque/speed conditions using control method 2.1 or 2.2. However, since current legislation is concerned only with speed/time curves for dynamometer systems, Ref. (1), Ref. (2), this approach will not be examined further.

1.3 Controller Design Method

It has been shown that a generalised block diagram may be constructed for typical prime mover/dynamometer configurations and that two basic methods of simulation may be used. Time lags for these typical configurations have been discussed and it has been noted that there are several sources of non-linearity in the load simulation system, namely the torque/speed characteristics of the prime mover and dynamometer, as well as the simulated load torque/speed characteristics, the governor lag for governed diesel engines and the pure time delay for all internal combustion engines. Since all of these non-linearities are dependent upon the prime mover speed, it is possible to perform a linearised analysis by giving the non-linear variables constant values at various points of the speed range for small perturbations.

The problem is to design a controller to provide a good performance of load simulation under the following conditions:-

(i) Wide range of simulated inertias and friction terms (of the type given in equation (1)).

(ii) Wide range of prime movers having different inertias, torque/speed characteristics and inherent lags.

(iii) Changes in dynamometer coefficients due to heating effects (these may be significant for hydrostatic, hydrodynamic, eddy current and brake type dynamometers).

The meaning of good performance for the purposes of load simulation will depend upon the method of simulation used.

With method (1) the only criterion of good performance which can be used is to have minimum error between the "required" and "actual" torque and speed signals consistent with a stable system. Due to the inflexibility of this method of load simulation it is not possible to provide step changes in torque and compare the response to that of the "real" system under automotive conditions, as discussed in section 1.2. Since the error for the two inputs of torque and speed is to be minimised it would seem advantageous to determine the optimum control of the system using multivariable control theory.

However, optimal control can only be attempted if an exact mathematical model of the system is available. Even with the simple models previously described it has been found that the order of the system is high, contains several non-linear functions, has a fast response time and has characteristics which are highly dependent upon temperature and which therefore change with operating conditions. Also, for a comprehensive range of simulation capability a wide range of prime movers will be used, each of which will have physical differences and will therefore have a different mathematical model. Each of these effects is a major difficulty in providing optimal control using multivariable control theory.

It is therefore suggested that the most convenient way of controlling load simulation systems of the method (1) type is to use three term control, in which the integral action is as high as possible, consistent with a reasonably damped response in the prime mover/dynamometer loop. In spite of the disadvantages previously discussed for this method of load simulation, it is probably the simplest to set up from the control point of view, and in most circumstances should be quite adequate for following speed/time curves as requested by various laws concerned with emission control, Ref. (1), Ref. (2).

For method (2) the complete load simulation system has been seen to contain a large number of lags, so that the speed/torque transfer function will be of a high order. Hence the design specification is to choose a controller such that one first order root of the speed/torque transfer function is as close as possible to that of the prime mover response to actual automotive conditions, and that all other roots are made insignificant. One method of determining the relative importance of the various roots of a transfer function in response to a step input is to display the roots on the complex frequency plane. It is well known that a step input in the time domain maps into a root at the origin in the complex frequency plane. Thus the importance of the roots in response to a step input depend upon their proximity to the origin in the complex frequency plane.

It is possible that closed loop zeros (roots which make the closed loop transfer function numerator zero) may distort the relative magnitude of the closed loop pole responses. Poles are roots which make the closed loop transfer function denominator zero and therefore are the roots of the characteristic equation of the system which completely specify the closed loop dynamic performance. The magnitude of the response for each pole may be determined as the product of the phasors from the zeros to that pole divided by the product of the phasors from all remaining poles to that pole. However, it will not normally be necessary to determine the magnitude of the responses by this means since, in general, any "secondary" closed loop poles in the region of the "dominant" closed loop pole will have a detrimental effect upon the performance of the system unless their relative magnitudes of response are very small.

The three-dimensional sketch of Fig. 1.18 shows how the relative positions of the roots of a third order system affect the response of the system to a step input in the time domain. It can be seen that the first order root (on the real axis) is close to the origin and therefore has a large effect upon the response to a step input compared with the complex roots. Thus the dominant response is first order with an initial oscillatory effect due to the second order roots, as shown in Fig. 1.19.

The suggested approach to determine controller gains is as follows:-

For a given type of controller (e.g., three term action) and simulation method (e.g., method 2.1), evaluate the speed/torque transfer function for the complete system using block diagram reduction techniques. From the closed loop transfer function, obtain the characteristic equation which will give a polynomial in s of an order dependent upon the number of significant time constants in the system. Then evaluate the coefficients of the polynomial at three speed ranges (low, medium and high) and, using a root solving algorithm on a digital computer, evaluate the roots for various values of controller gains with all other variables set to average values (i.e., simulated torque/speed terms). If a reasonable response can be obtained with certain controller gain values at each speed range (i.e., if the secondary roots can be made insignificant), then use these gain values for the next step of the controller design method.

If no suitable response can be obtained, then follow the same procedure for the other simulation methods. If still no suitable response can be obtained, then determine the effect of placing filters in the torque or speed signal paths, or determine the effect of changing the physical parameters of the system, i.e., by increasing the dynamometer inertia with an inertia wheel, or reducing the dynamometer lag (possible only with hydrostatic type systems).

The next step of the design method, having determined suitable controller gains, is to examine the effect of changing other variables (e.g., simulated inertia, friction, etc.) over the required range one at a time. If the effect of the secondary roots is negligible over the range, then this step of the controller design method is complete. It is possible, however, that for certain variables the secondary roots will become significant over part of the range and that a change in controller gain will be required to reduce the effect of the secondary roots. Thus an adaptive gain controller may well prove advantageous for certain systems. It is not the intention of this work, however, to analyse such control systems. Instead, the effects of linear three term control action will be analysed for each of the methods of load simulation in the following sections.

The final stage of the controller design for method (2) is to compare the response of the complete simulation system having zero prime mover control to a step change in torque with that of the actual automotive response (equations 3 → 5) in order to determine any differences in both dynamic and steady state effects. If there are significant differences, then it may be necessary to have a calibration factor for the coefficients of the simulated torque/speed characteristics to improve the accuracy of the load simulation system. Due to the various approximations made in the development of the transfer functions for the load simulation system, it is necessary for any calibration of the simulated vehicle characteristics to be performed on the actual system (rather than use the mathematical model). However, it may be difficult to provide a step change in the actual torque of the system for the purposes of calibrating the simulated inertia, although calibration of the other simulated coefficients should provide no problem, since this can be done under steady state conditions.

1.4 The Generalised Model

By combining all the components of the prime mover/ dynamometer systems previously discussed, as well as the various methods of simulating loads, it is possible to develop a generalised block diagram of these systems as shown in Fig. 1.20. By setting the coefficients $G_1 \rightarrow G_4$ individually to zero or unity it is possible to set up in the block diagram any one of the four previously discussed load simulation methods. Further to this, by setting the coefficients of the block diagram to the required values and setting all other coefficients to zero, it is possible to set up any of the previously mentioned prime movers or dynamometer systems. (Note: the programming language used in this analysis is BASIC which accepts all coefficients as zero unless defined otherwise.) These techniques will be used in chapters 2 →5 to analyse a wide range of prime mover/dynamometer systems and load simulation methods.

The individual coefficients of the block diagram are defined as follows:-

J_1 = Prime mover inertia
J_2 = Dynamometer inertia
J_3 = Simulated inertia for method (2.2)
J_4 = Simulated inertia for method (2.1)
J_8 = J_2 for flexible coupling or 0 for no coupling
J_9 = Input actuator inertia
F_2 = Viscous damping of flexible coupling
F_3 = Simulated speed dependent friction coefficient for method (2.2)
F_4 = Simulated speed dependent friction coefficient for method (2.1)
F_9 = Input actuator viscous friction coefficient
K_1 = Torque/speed characteristic slope for prime mover
K_3 = Torque/speed characteristic slope for dynamometer
K_2 = Stiffness of flexible coupling
K_4 = Torque/voltage coefficient for dynamometer input
K_5 = Velocity transducer coefficient

K_6 = Torque transducer coefficient

K_7 = Torque/voltage coefficient for prime mover input

K_8 = Torque/speed coefficient for governor on compression ignition engine

K_9 = Input actuator gain (dynamometer)

T_1 = Pure time delay (for internal combustion engines)

T_2 = Prime mover time constant (for d.c. traction motor)

T_3 = Dynamometer time constant

T_4 = Governor time constant (for compression ignition engine)

T_5 = Velocity transducer time constant

T_6 = Input actuator time constant for prime mover

T_7 = Time constant for filter on differentiator (to reduce noise from simulated inertia effect)

a = derivative action time for dynamometer input

d = derivative action time for prime mover input

b = dynamometer input gain

e = prime mover input gain

c = integral action gain for dynamometer input

f = integral action gain for prime mover input

G_1 = 1 for velocity feedback to prime mover input, otherwise 0

G_2 = 1 for torque feedback to prime mover input, otherwise 0

G_3 = 1 for torque feedback to dynamometer, otherwise 0

G_4 = 1 for method (2), otherwise 0

$J_4 = T_7 = 0$; F_4 = 1 or 0 for velocity feedback to dynamometer input

For d.c. motor/generator type dynamometer:

$K_9 = 1 \quad T_7 = J_9 = F_9 = 0$

For d.c. traction motor as prime mover:

$K_8 = T_4 = T_1 = 0$

For spark ignition engine as prime mover:

$K_8 = T_4 = T_2 = 0$

For governed compression ignition engine as prime mover:

$T_2 = 0$

For Method (1.1):

$G_2 = J_3 = J_4 = T_7 = F_4 = 0$

$G_3 = G_1 = F_3 = 1$

For Method (1.2):

$G_1 = J_3 = J_4 = T_7 = G_3 = 0$

$F_3 = G_2 = F_4 = 1$

For Method (2.1):

$G_2 = J_3 = 0$

$G_1 = G_3 = G_4 = F_3 = 1$

For Method (2.2):

$G_2 = J_4 = T_7 = 0$

$G_1 = G_3 = G_4 = F_4 = 1$

The complete block diagram reduces to give a 14th order speed/torque transfer function $\frac{n}{t_{dis}}$, for which the characteristic equation coefficients are given in the BASIC computer program COEF of Appendix B. Once the coefficients have been entered into the generalised mathematical model it is likely that the resulting differential equation will have an order much less than 14 although normally greater than 4. The normalise procedure at the end of COEF is to remove any closed loop integrators which may have emerged in the co-efficient determination routine. This is necessary since the speed/torque transfer function does not contain single integrators under most circumstances, although they may have been created as pole-zero pairs in the block diagram reduction. The normalise procedure is also used to determine the order of the polynomial (P1).

The method of determining the roots of the characteristic equation is shown in the BASIC computer program ROOTS of Appendix B. Lin's method is initially used to determine root pairs. If convergence is not achieved upon a pair of roots within 200 iterations, the Newton-Raphson method is used to determine the lowest real root of the poly-nomial. Convergence problems are normally encountered in complex root solving algorithms when matched quadratic pairs become separated, as shown in the complex frequency plane of Fig. 1.21. This difficulty is overcome by the use of the Newton-Raphson routine to eliminate a real root whenever such a convergence problem is encountered by the Lin routine.

Due to the limits of machine accuracy (six figures on the BASIC assembler used in this analysis) it is necessary to determine the lowest valued roots first and continue through to the highest value. The self starting Lin's method performs this function automatically whereas the Newton-Raphson method has no direct control over which root it is to converge upon. To overcome this difficulty a low initial guess is made of the root value, say (-0.1). If the routine passes over the low valued root and convergences upon a root with much higher magnitude, then significant errors are likely to occur in the following roots due to the limits of accuracy of the programming language. Hence if the roots are not determined in an increasing order of magnitude, it is necessary to reduce the initial root guess (although this was rarely found to be necessary in practice).

It was mentioned (in section 1.3.1) that it is possible for a pole to emerge near the origin having a zero in close proximity which reduces the magnitude of its effect. To determine the zero positions an extension was made to the computer program COEF as shown in the program ZEROS of Appendix B. If the coefficient U9 is set to unity in the computer program VALUES then the computer will determine the numerator coefficients for the system closed loop transfer function (instead of the denominator coefficients) and continue to the root searching algorithm ROOTS.

In general, the program was found to give fast solutions with few convergence problems.

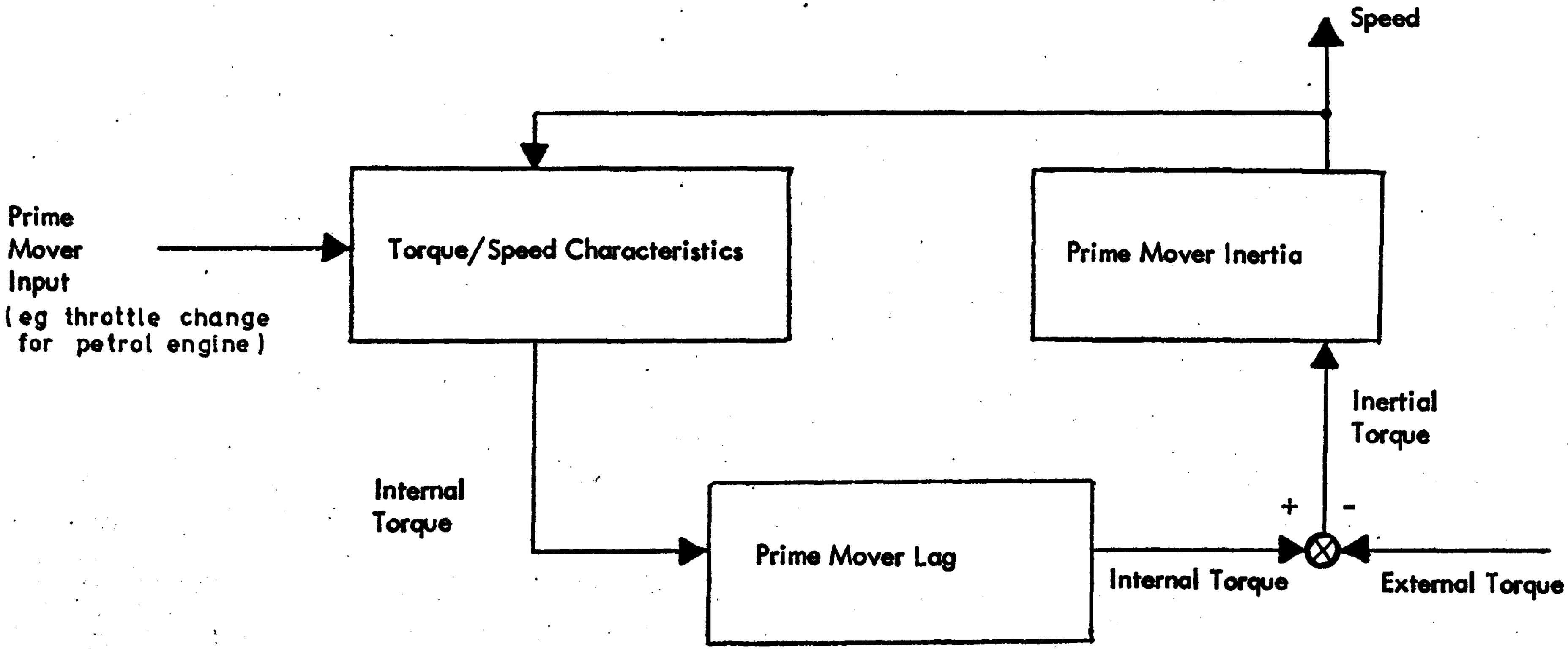

Figure 1.1 generalised block diagram for prime mover

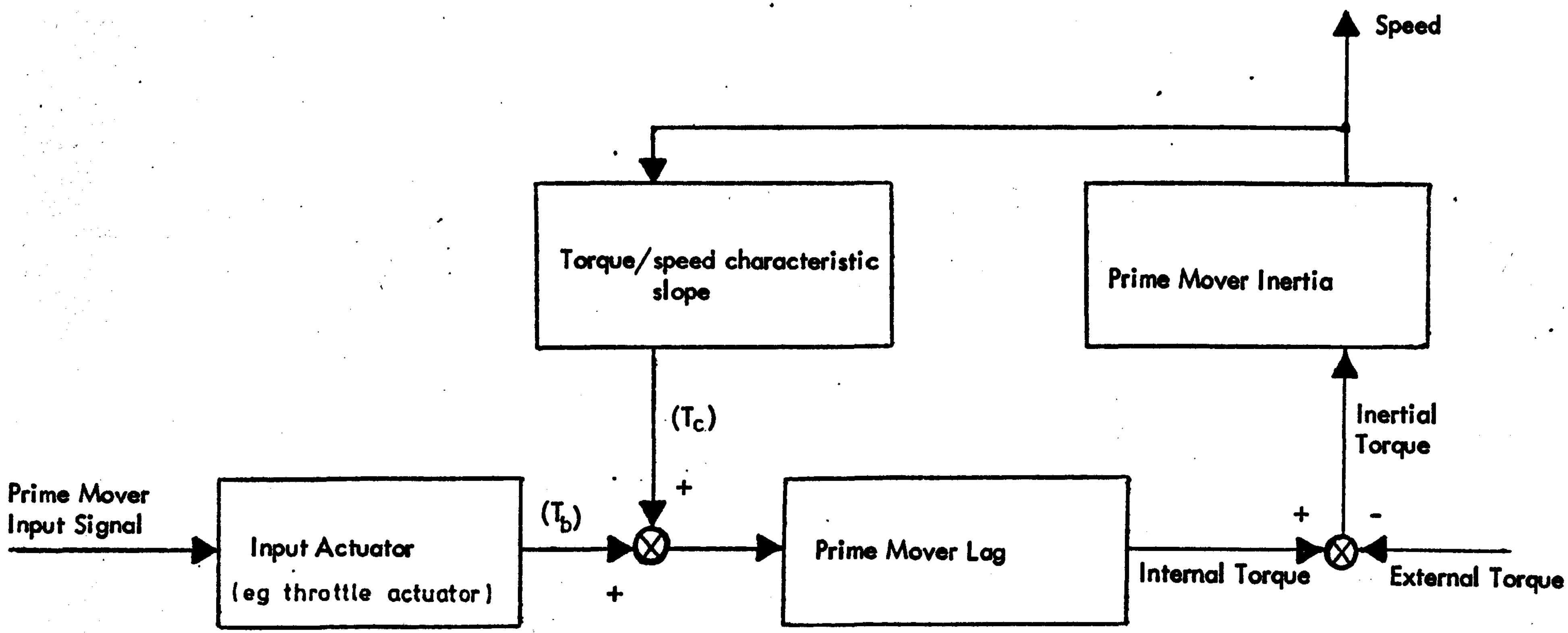

Figure 1.2 modified block diagram for prime mover

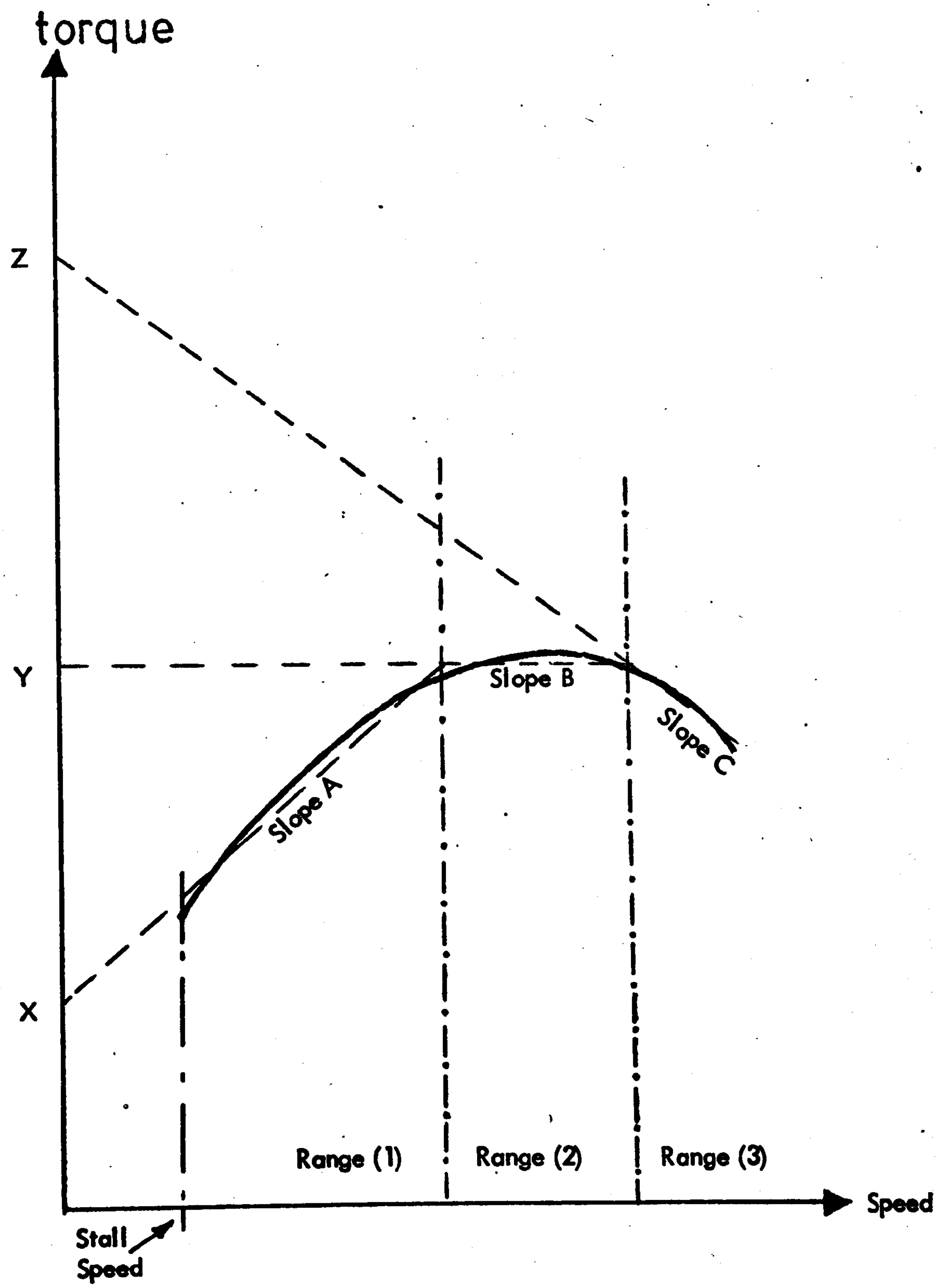

Figure 1.3

LINEARISED TORQUE/SPEED CHARACTERISTIC (FOR PETROL ENGINE WITH NATURALLY ASPIRATED CARBURETTOR)
(MAXIMUM THROTTLE SETTING)

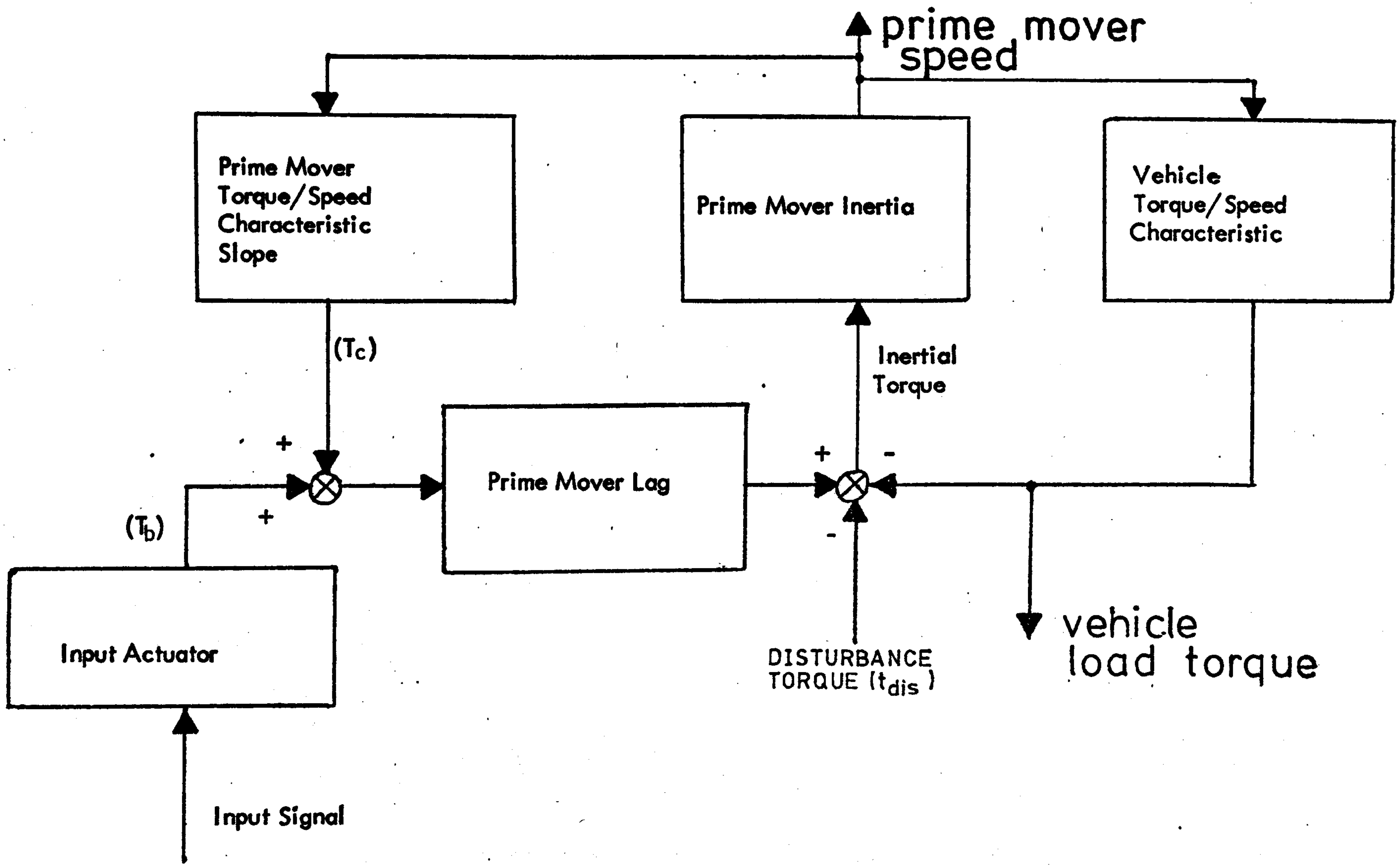

Figure 1.4 GENERALISED BLOCK DIAGRAM FOR PRIME MOVER UNDER TRANSPORTATION CONDITIONS

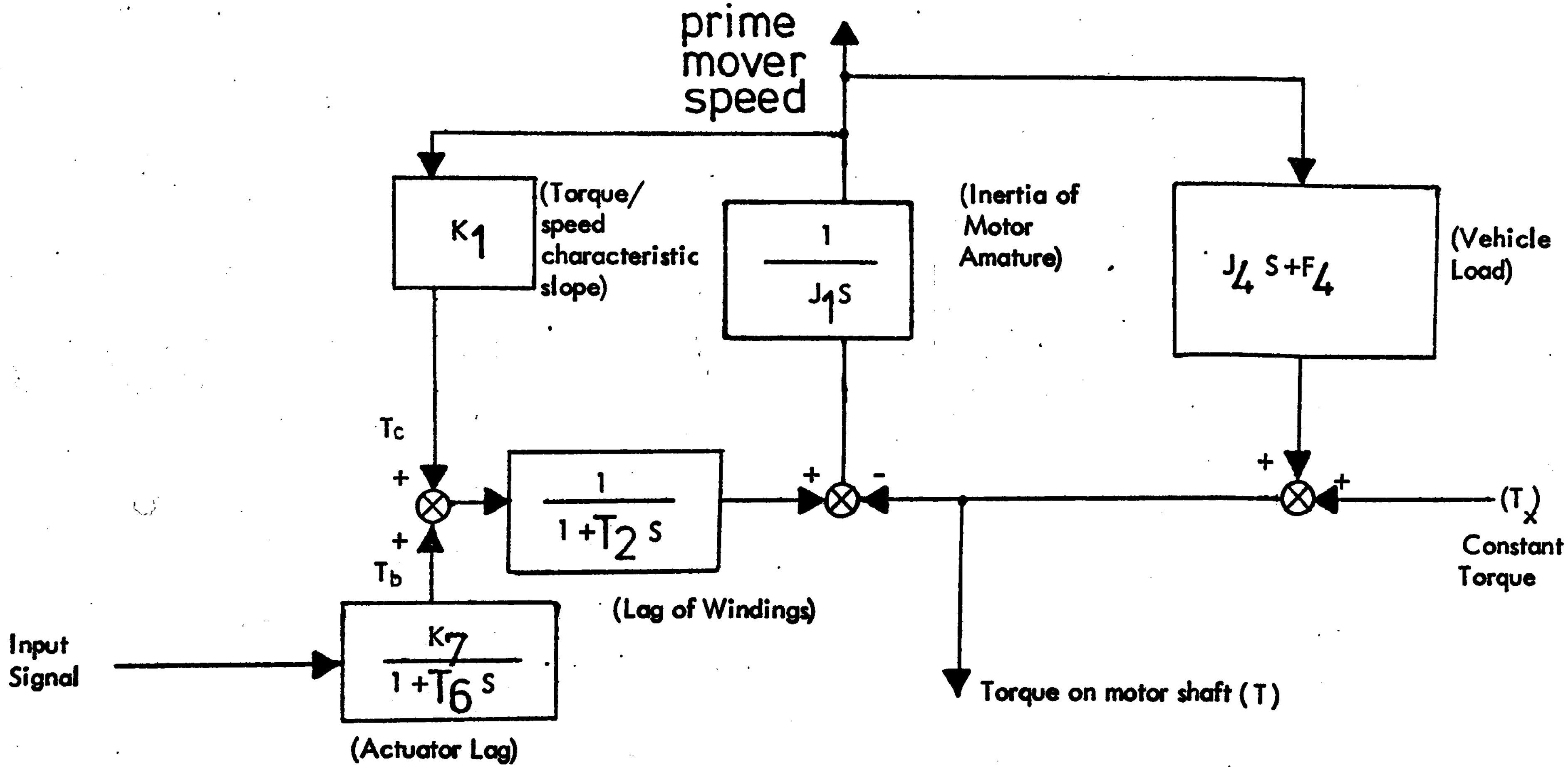

Figure 1.5 BLOCK DIAGRAM FOR SERIES WOUND D.C. MOTOR UNDER TRANSPORTATION CONDITIONS

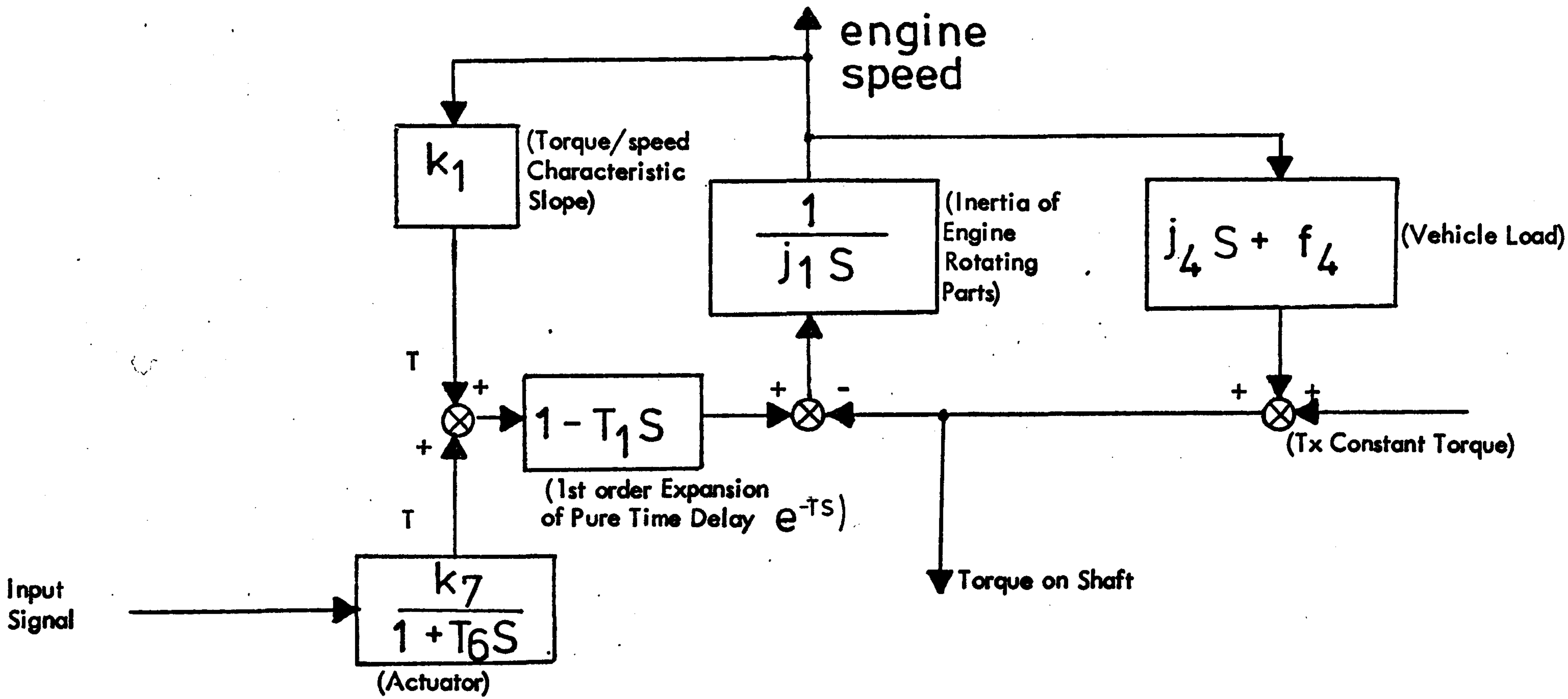

Figure 1.6 BLOCK DIAGRAM OF PETROL ENGINE UNDER TRANSPORTATION CONDITIONS

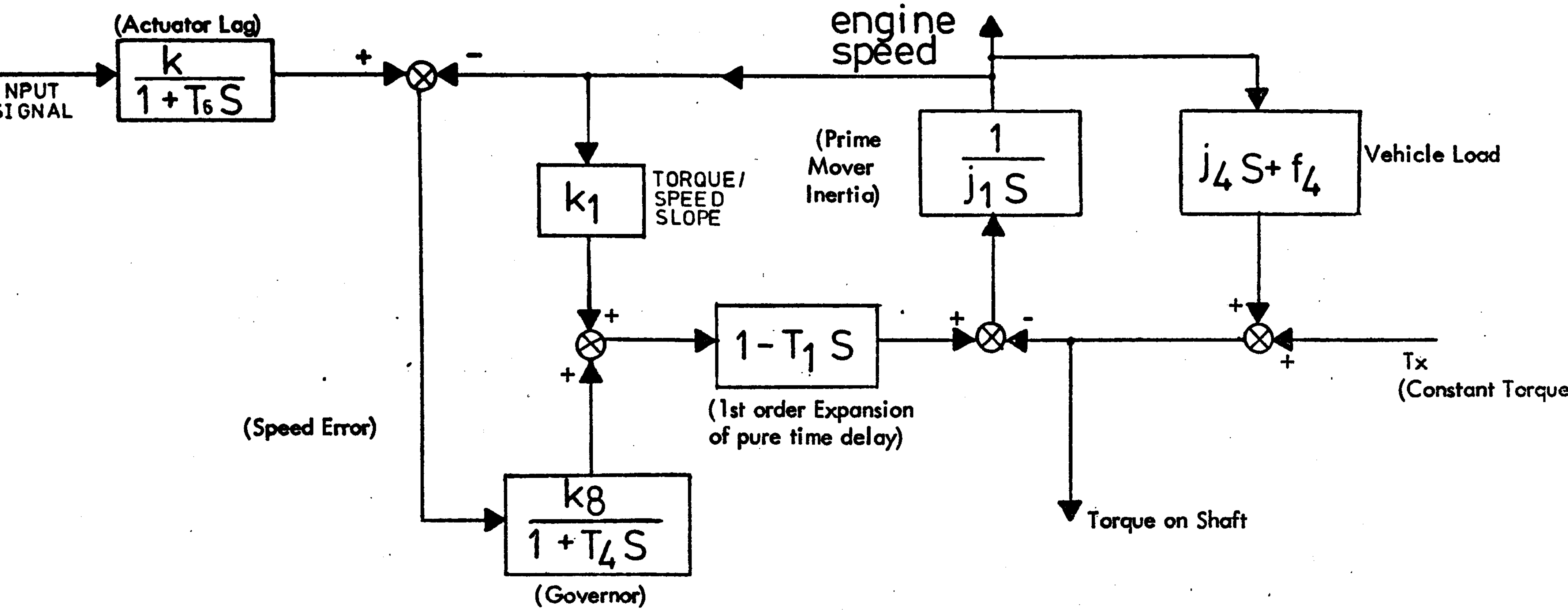

Figure 1.7 BLOCK DIAGRAM FOR GOVERNED DIESEL ENGINE UNDER TRANSPORTATION CONDITIONS

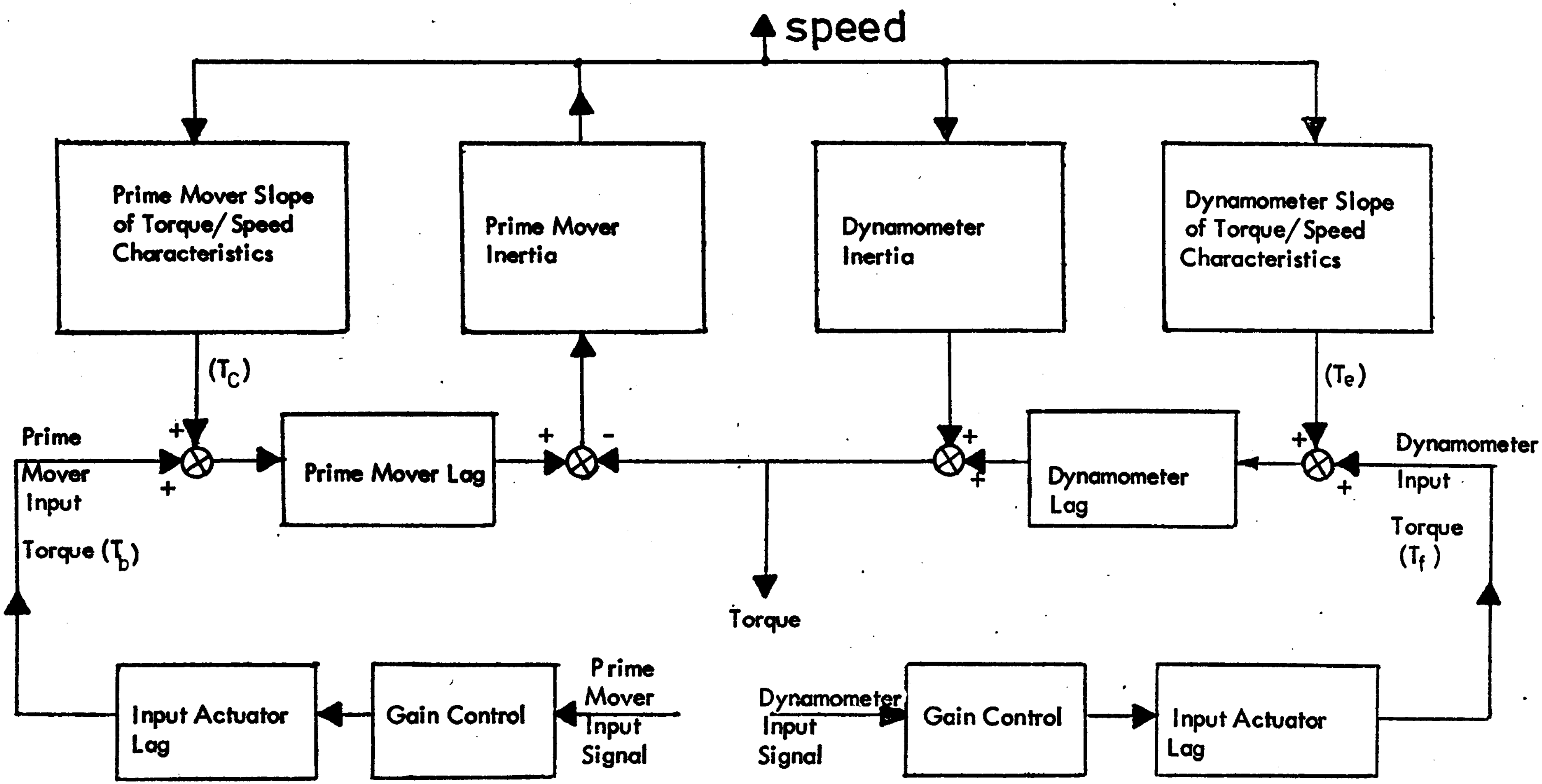

Figure 1.8 GENERALISED BLOCK DIAGRAM FOR PRIME MOVER AND DYNAMOMETER

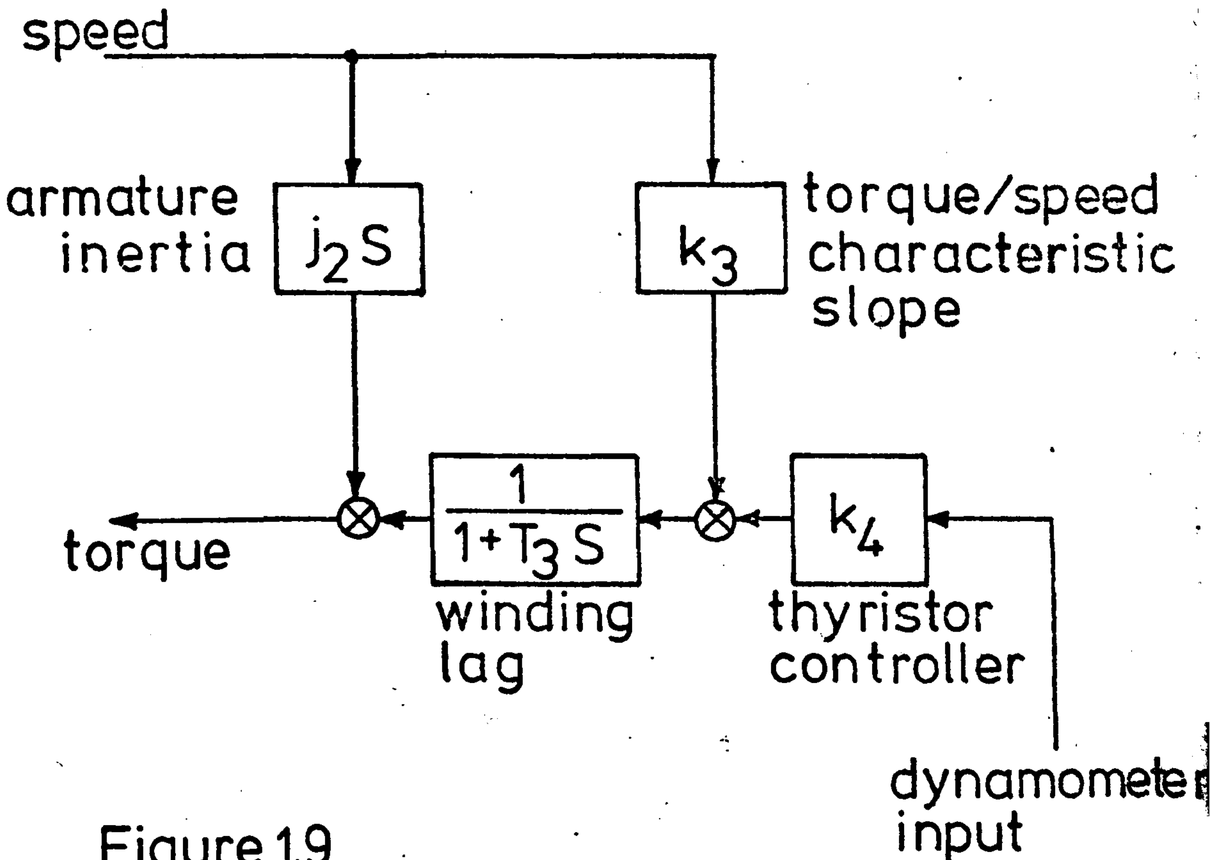

Figure 1.9

electric dynamometer with thyristor control

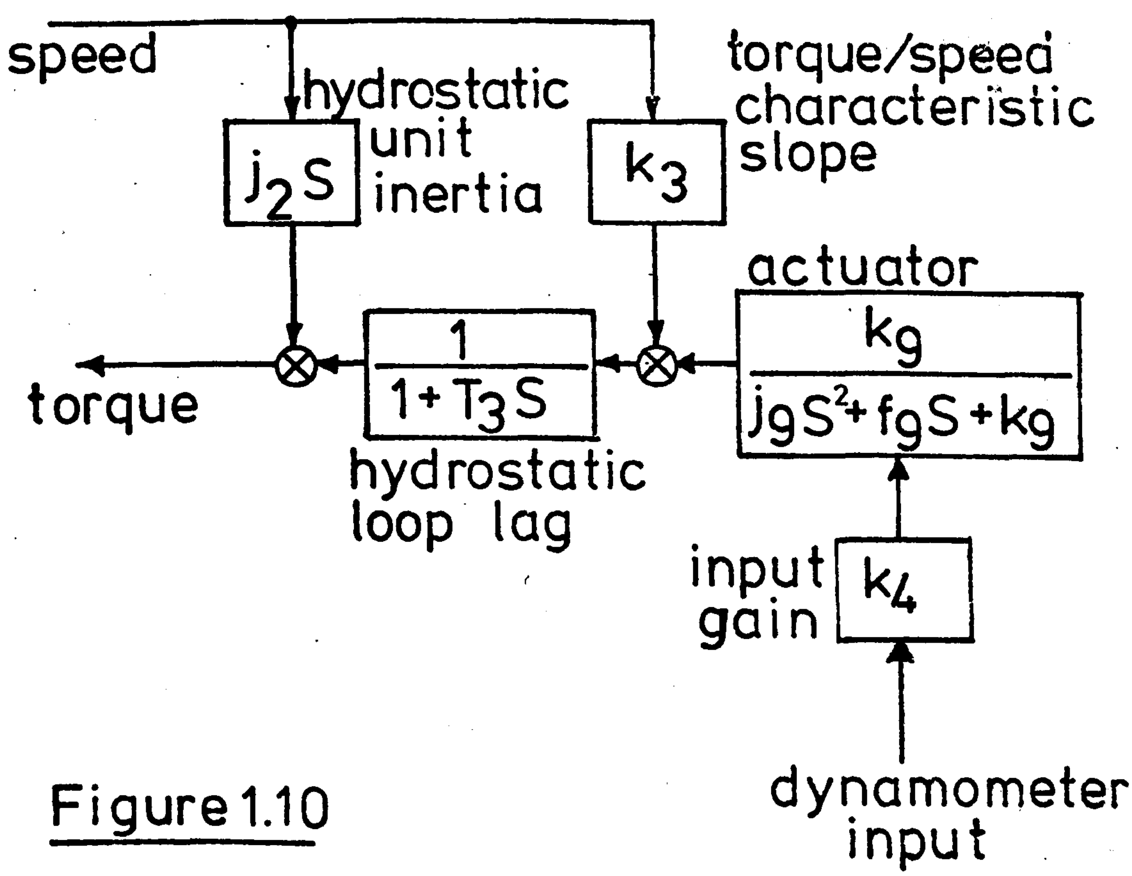

Figure 1.10

hydrostatic dynamometer

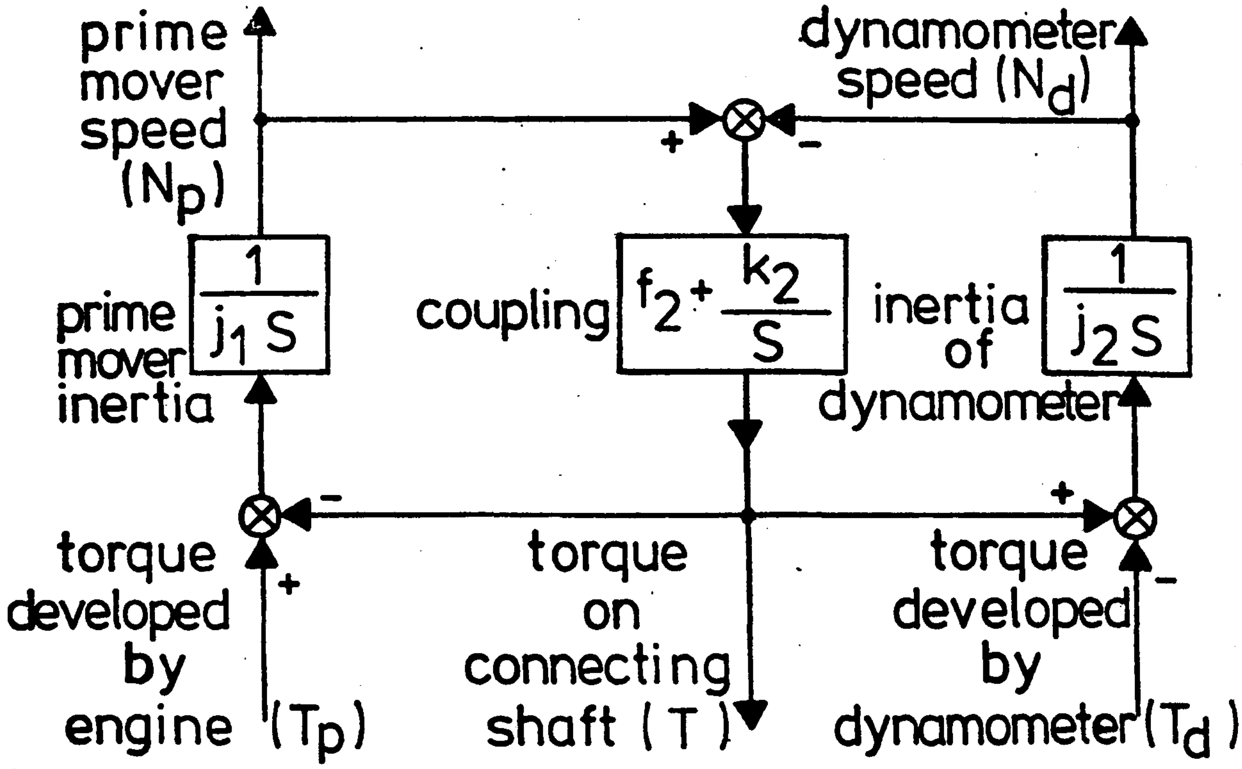

Figure1.11 block diagram for flexible coupling

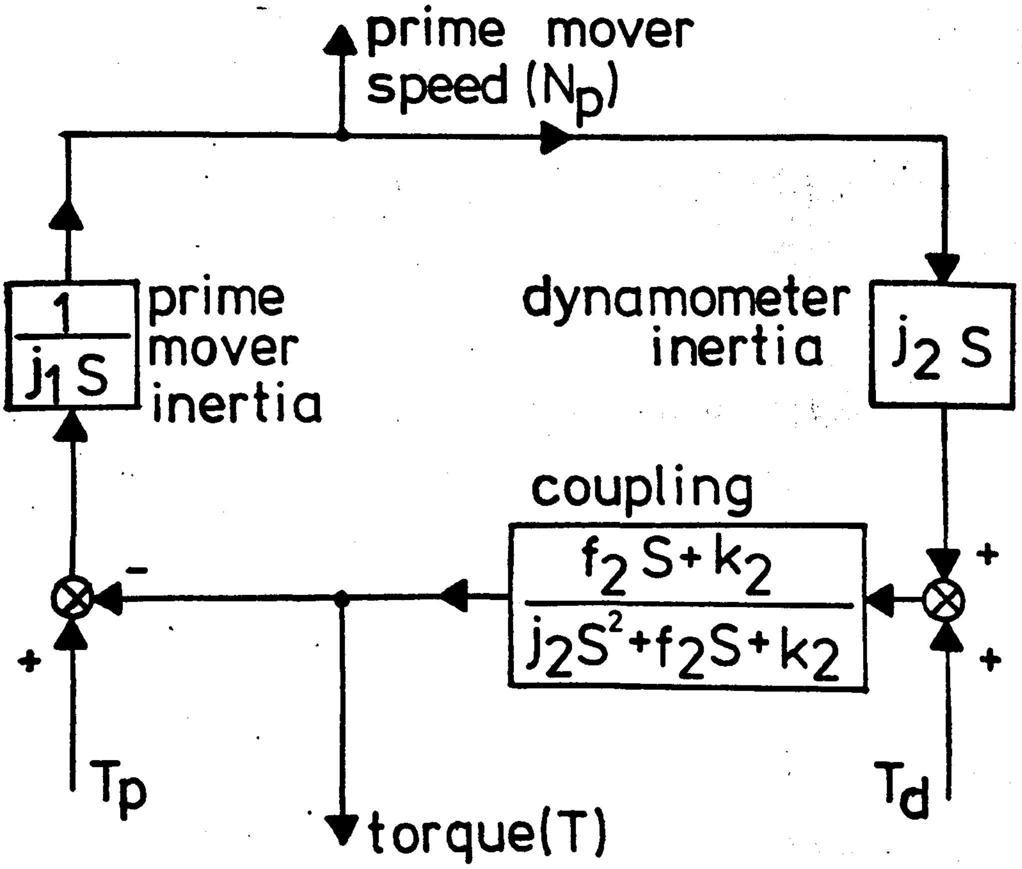

Figure1.12 simplified block diagram

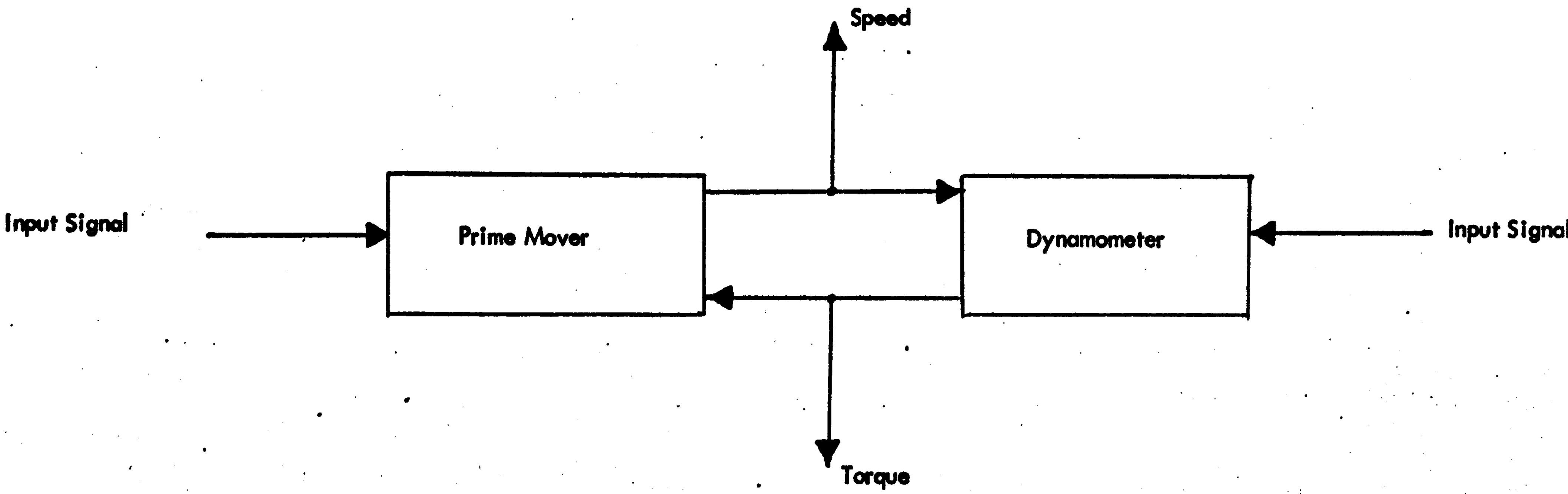

Figure 1.13 SIMPLIFIED BLOCK DIAGRAM FOR PRIME MOVER and DYNAMOMETER WITH INPUT ACTUATORS

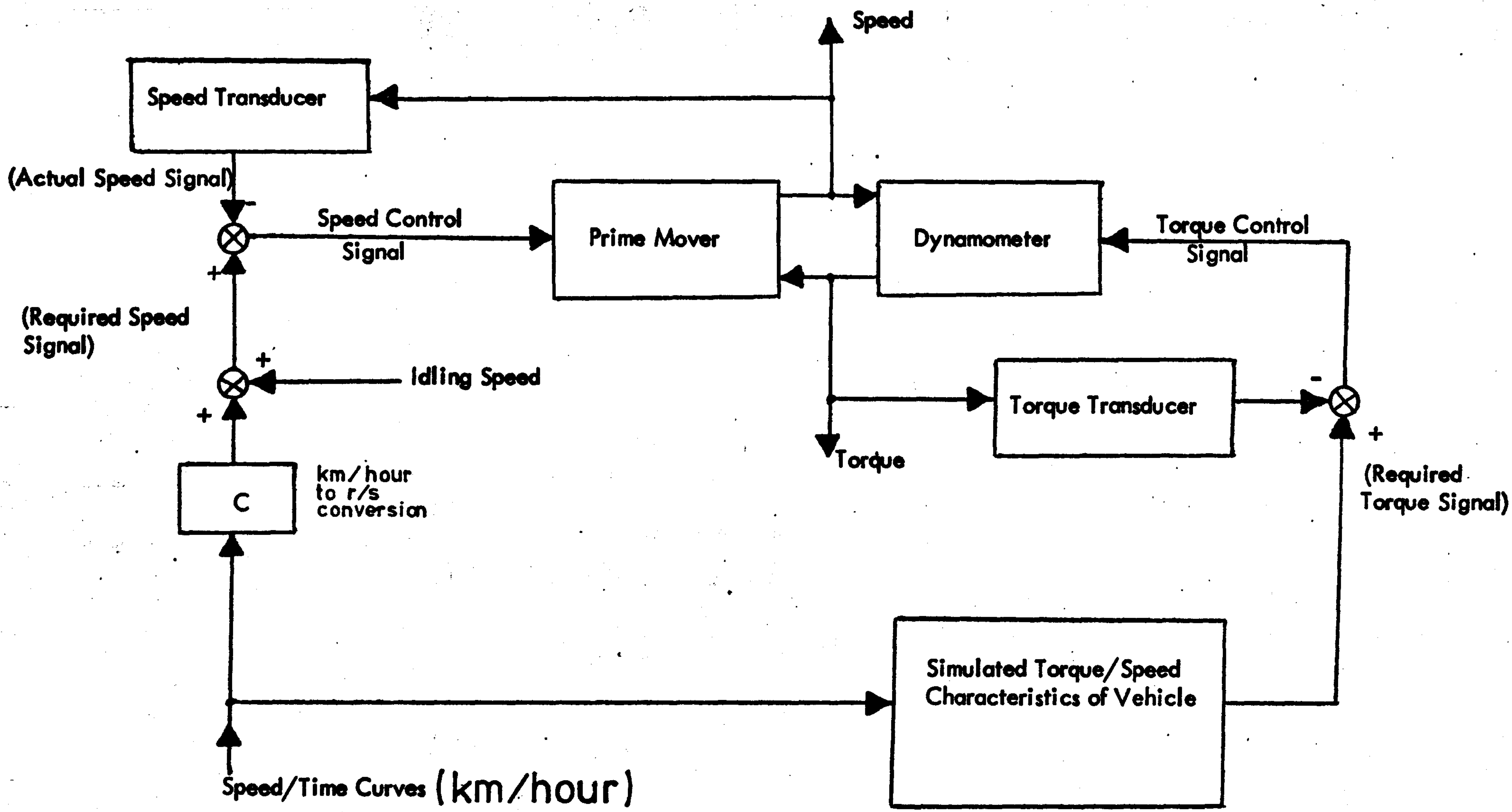

Figure1.14 simulated automotive loading conditions (method 1.1)

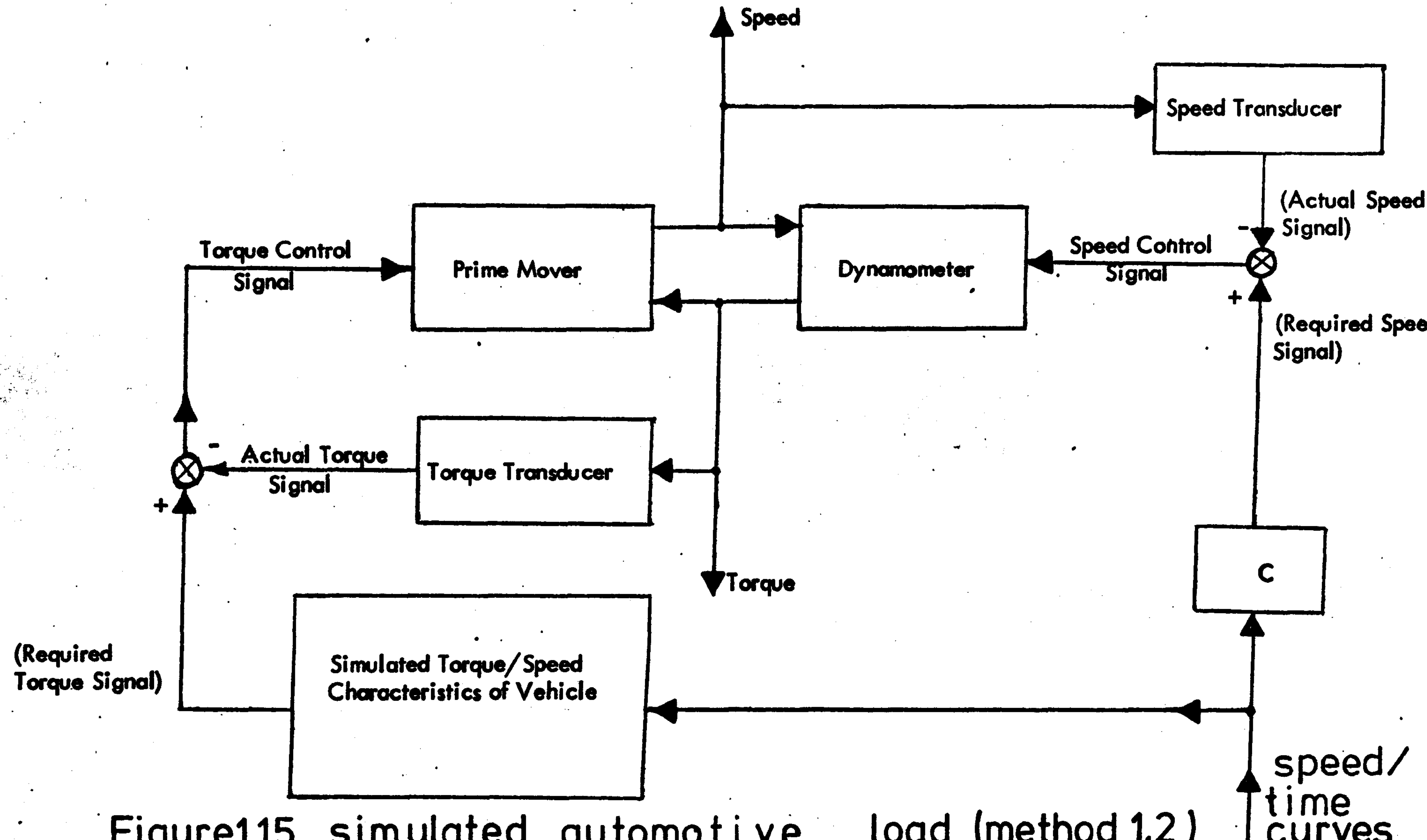

<u>Figure1.15</u> simulated automotive load (method 1.2)

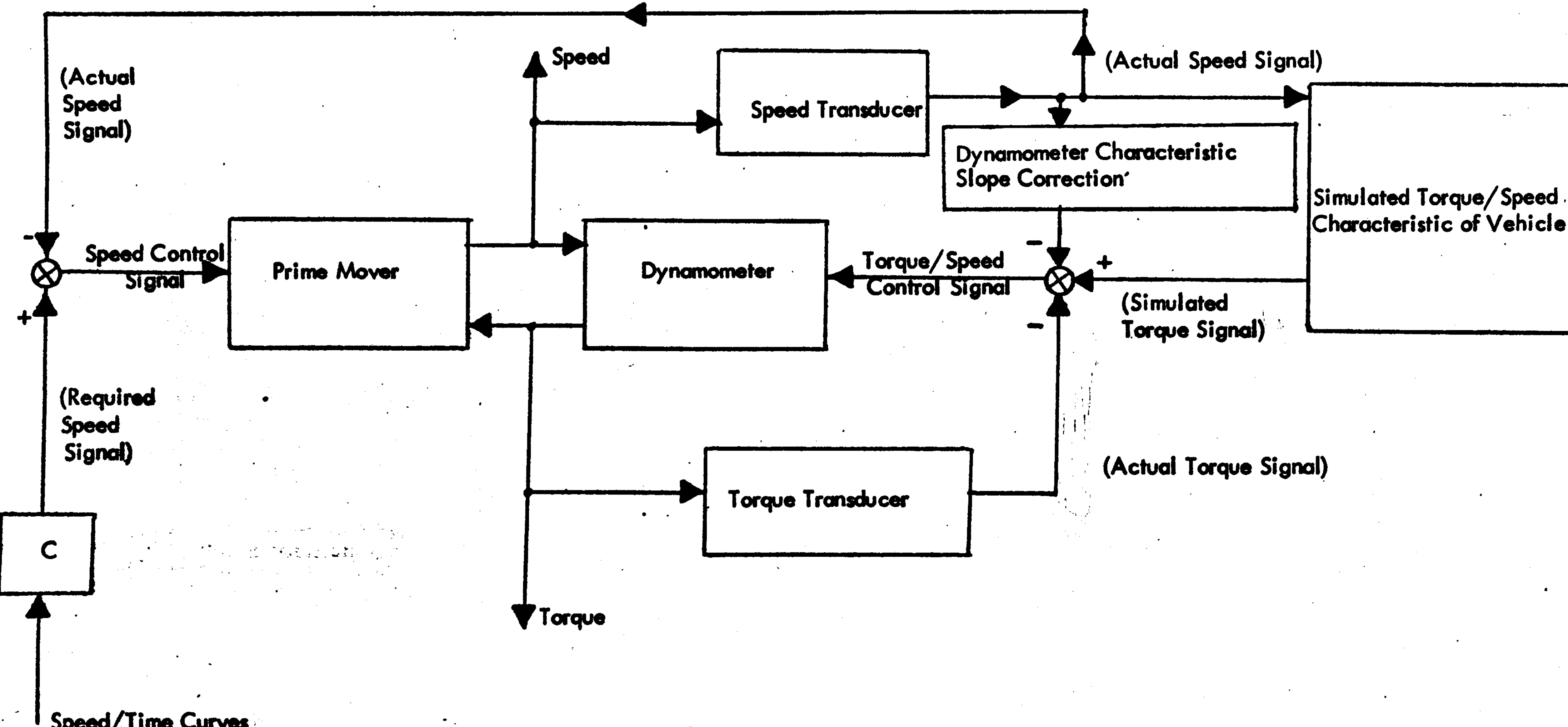

Figure 1.16 simulated automotive load (method 2.1) torque reference system

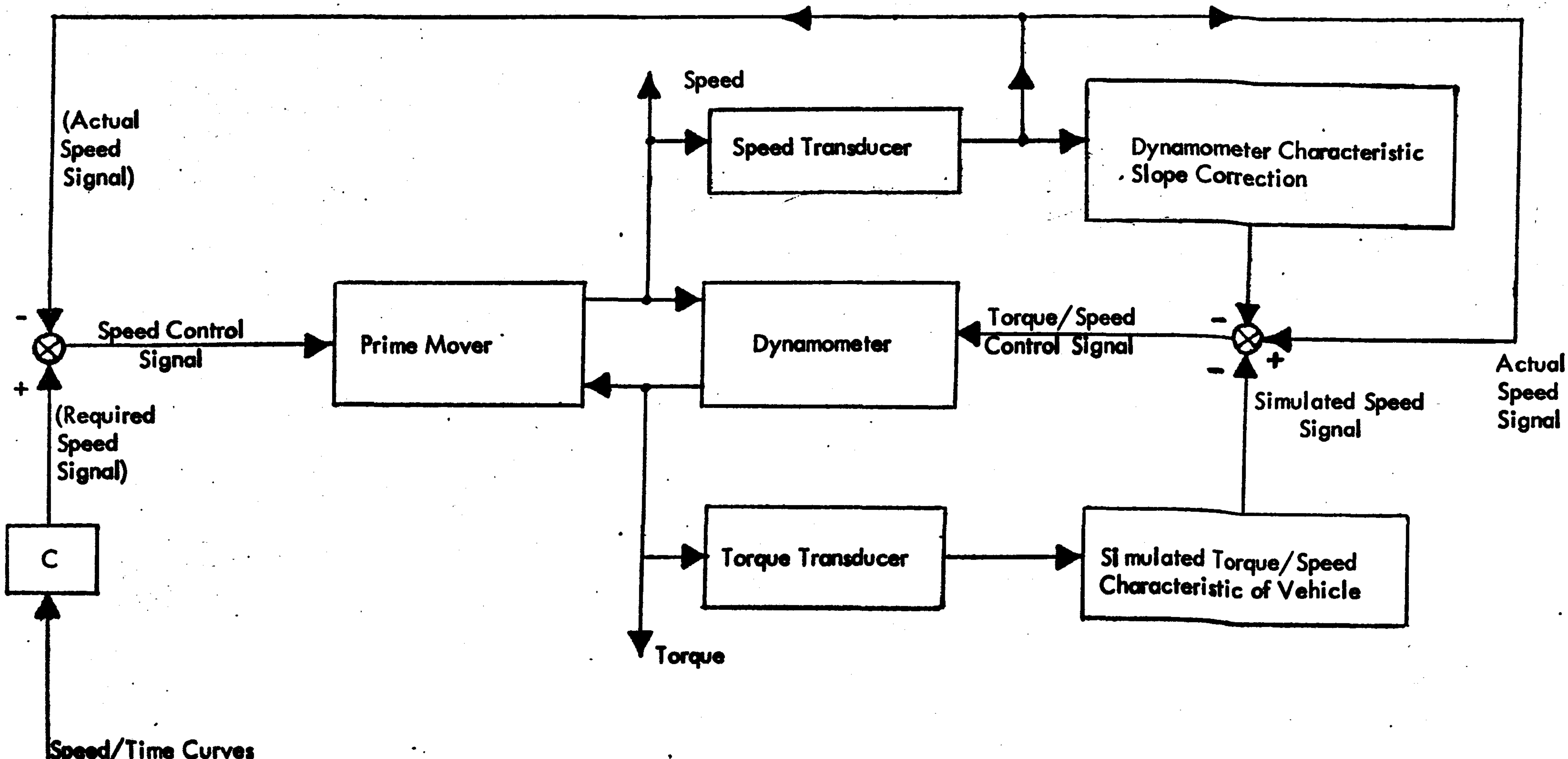

Figure 1.17 simulated automotive load (method 2.2) speed reference system

Figure 1.18 magnitude of roots on complex frequency plane in response to a step input

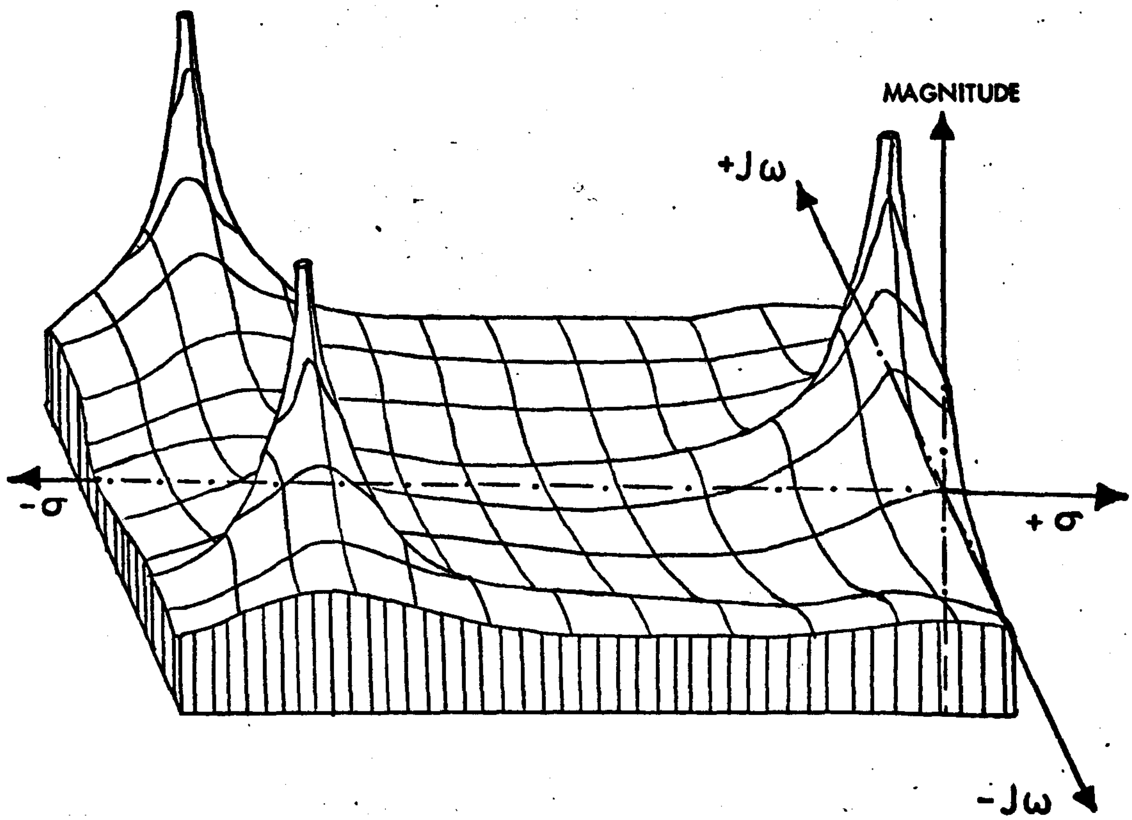

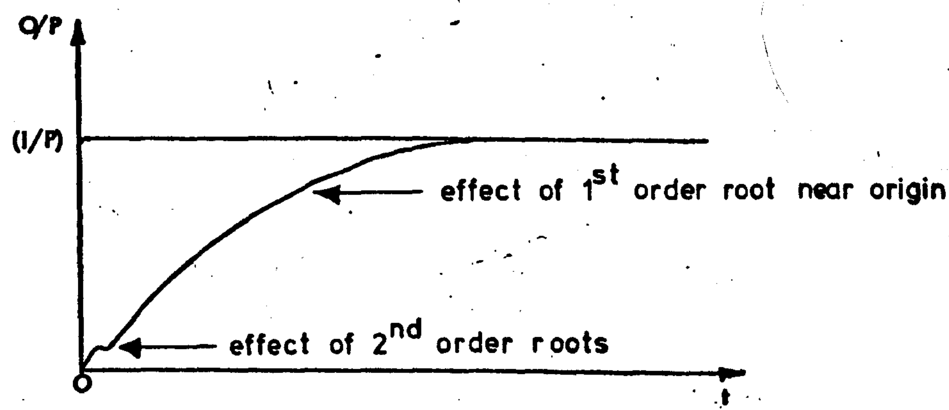

Figure. 119

time domain response to a step input for the system with roots as shown in figure 1.18

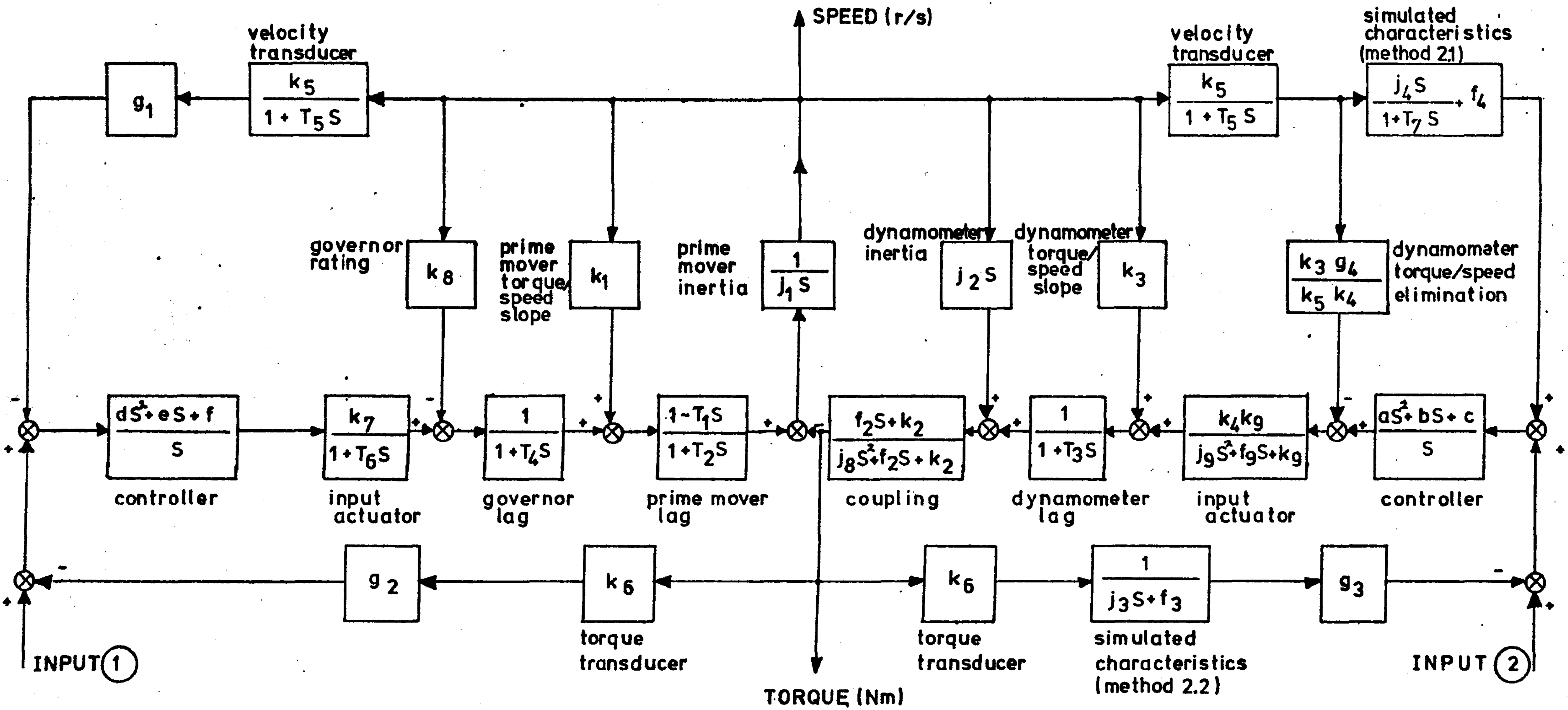

Figure 1.20 Generalised block diagram for typical prime mover/dynamometer systems and simulation methods

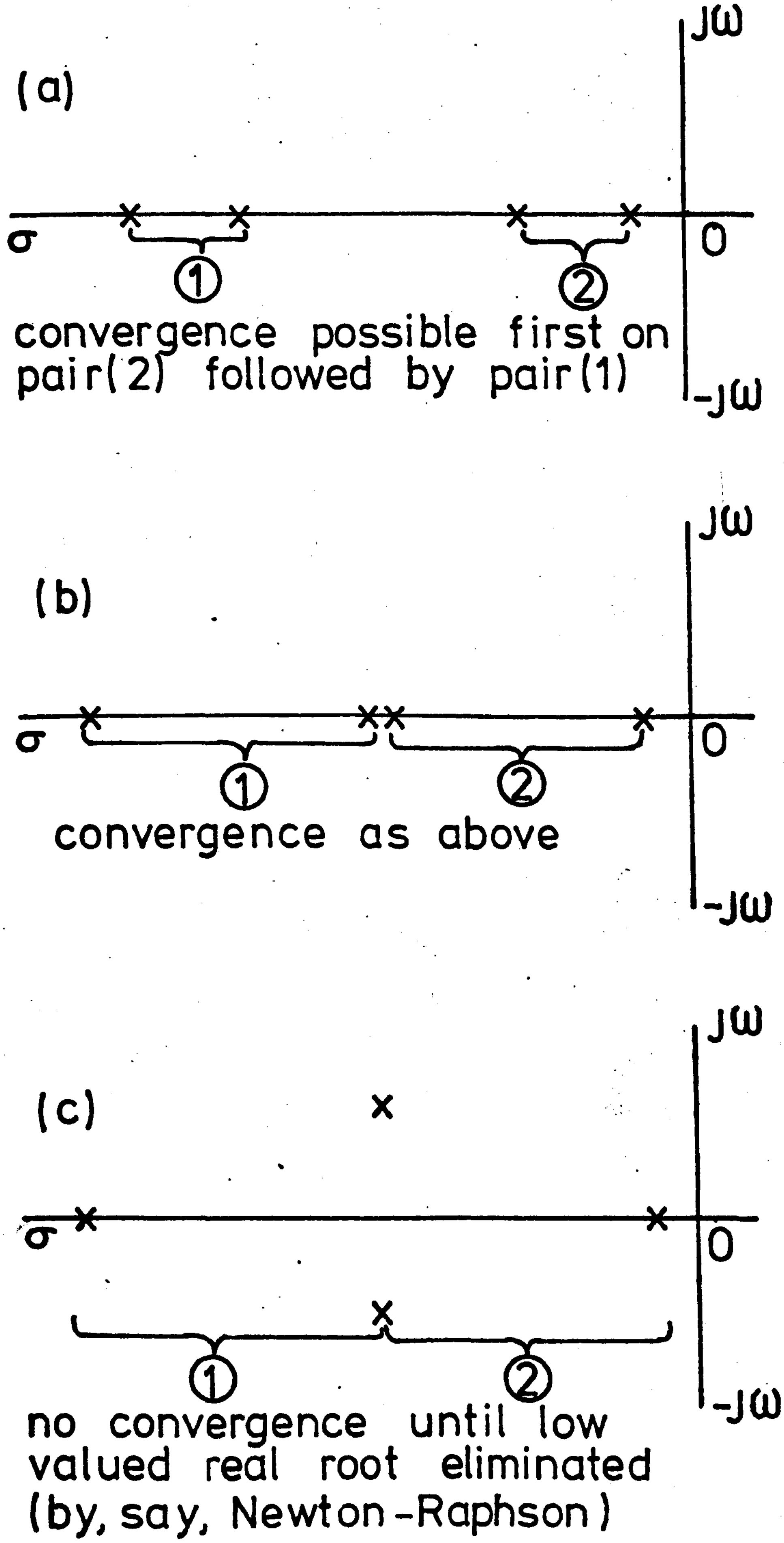

Figure 1.21 convergence difficulties with Lins method

PART 2

ANALYSIS OF A LOW POWER SIMULATOR SYSTEM

2.1 Introduction

The purpose of this section is to apply the mathematical model and analysis techniques introduced in Part 1 to a low power simulation system. The low power system was used since it was easily reconstructed from an earlier system described elsewhere, Ref. (13), and could be experimentally tested to validate the mathematical model and gain experience in the controller design method. The results will lend greater credibility to the theoretical analysis (using manufacturers' data) of a full scale load simulation system (70 kW capability) for a 3.5 litre diesel engine, the construction of which is described in Part 7. Further analysis of load simulation methods for other types of prime mover are given in Part 4 (petrol engine) and Part 5 (d.c. traction motor).

2.2 System Description

The operation of the system is based upon a hydrostatic transmission system, as shown in the schematic diagram of Fig. 2.1. The prime mover is a d.c. traction motor (9 kW) which is supplied by a manually adjustable d.c. supply (limited to 38 amps). The system performance was used to validate the generalised model developed in section 1 based on control method (2) with manually applied inputs to the prime mover.

Adjustment of the variable capacity hydrostatic unit flow rate may be used to control the oil pressure on either side of the fixed capacity unit at any speed of the prime mover. Thus pressure on one side of the hydrostatic loop will load the d.c. motor and pressure on the other side of the loop will provide the motoring condition to the d.c. motor. The variable capacity unit is of the axial piston, variable swashplate type, in which the swashplate position is controlled by an electrohydraulic servo system. The swashplate position is measured by an LVDT plus oscillator/demodulator system.

The electrohydraulic servo valve supplying the hydraulic actuator is of the two stage type with a rated flow of 0.076 litres/s and having a low current (15 mA) torque motor for flapper actuation. In order to prevent side loads to the fixed capacity hydrostatic unit (due to the torque transducer and couplings) the input shaft was retained by a ball race type bearing. The power rating of the hydrostatic units is 8 kW and that of the three phase induction motor 6 kW. The three phase induction motor was also used to power a double pump unit for supplying make up oil to the hydrostatic loop and high pressure oil to the swashplate servo system. This unit was of the gear type mounted externally to the oil reservoir and flexible hose was used on the inlet side. This had the effect of reducing audible noise under normal running conditions from 85 dBs to 70 dBs.

The circuit diagram for the electrohydraulic system is shown in Fig. 2.2 and overall views of the system are shown in Plates 2.1 and 2.2. The block diagram for the system using speed reference control is shown in Fig. 2.3. The individual coefficients are given in the following section.

2.2.1 System Identification

The time constant for the hydrostatic loop may be determined from examination of the block diagram of Fig. 2.4. The main flow of oil into the pressurised side of the hydrostatic loop will be equal to the difference in flow between the primary and secondary hydrostatic units. Assuming the three phase motor speed remains constant, then the flow from the secondary unit is proportional to the swashplate setting, whereas the flow from the primary unit is proportional to the prime mover speed. If a control signal is applied to the swashplate servo which is proportional to the prime mover speed, then the flow to either side of the hydrostatic loop at any prime mover speed will be zero. Any extra control signal applied to the swashplate servo will produce a proportional flow of oil into either side of the hydrostatic loop.

Referring once again to the block diagram of Fig. 2.4, it can be seen that oil flowing into one side of the hydrostatic loop will increase the pressure at a rate dependent upon the effective bulk modulus (βe) and volume of oil (V) in that side. The pressure will increase until the leakage flow (which is approximately proportional to the pressure) is equal to the input flow unless the maximum pressure is reached and the pressure relief valve opens (representing saturation of the system). The block diagram results in a first order transfer function of the form:-

$$\frac{P}{Q} = \frac{1/K_L}{1 + \left(\frac{V}{K_L \beta e}\right)s} \qquad \ldots\ldots (6)$$

Thus the time constant for the hydrostatic loop is proportional to the volume of oil in each side of the loop, and inversely proportional to the leakage coefficient of the two hydrostatic units. It should be noted that the time constant obtained will only be a linear approximation since the leakage coefficient is also dependent upon temperature and hydrostatic unit speed and the relationship with pressure normally follows a power law curve, Ref. (6). However, the effect this has upon the system performance may easily be seen by substituting a range of values into the root solving algorithm to determine how the root positions are altered.

Various values have been suggested for the effective bulk modulus, Ref. (7), Ref. (8), although previous workers on a similar system suggest a value of βe = 6.8×10^3 bar, Ref. (9). The leakage coefficient may be obtained from the manufacturers' data as 0.93×10^{-4} litres/min/bar giving a value of K_L for the hydrostatic loop of 1.86×10^{-4} litres/min/bar.

In order to keep the volume of oil between the primary and secondary hydrostatic units as small as possible (and therefore reduce the hydrostatic loop time constant) a manifold was constructed, as shown in Fig. 2.5. A photograph of the manifold, together with the make up check valve, high pressure relief valve, cross port shut off valve and pressure transducer, is shown in Plate 2.3. The volume of oil in the manifold, together with the dead oil volume of the two hydrostatic units, is estimated at 0.025 litres, which results in a hydrostatic loop time constant of 0.02 seconds. However, the other side of the loop (used for the motoring condition) has an oil volume of approximately 0.1 litres, which gives a time constant in the order of 0.08 seconds.

The torque/speed characteristic slope for the prime mover (K_1) was obtained by holding the prime mover input fixed at low, medium and high settings. For each setting the torque and speed were recorded for a range of swashplate positions, as shown in graph G6 of Appendix A. The average slope was found to be -0.376 Nm S, although this value is slightly higher with low prime mover input settings. The slope was found to be reasonably linear over the range of operation, unlike the typical torque/speed characteristic for this type of prime mover, due to the "pulling down" of the voltage supply as the current through the prime mover windings is increased.

By holding the secondary hydrostatic unit swashplate fixed and varying the prime mover input, the dynamometer torque/speed characteristic slope (K_3) was determined, as shown in graph G7. It can be seen that the slope varies with prime mover speed so that three ranges of the slope values need to be taken (as discussed in section 1.1.1), these being:

Low speed, $K_3 = 2$ Nm S

Medium speed, $K_3 = 1.3$ Nm S

High speed, $K_3 = 0.75$ Nm S

Also, with the hydrostatic loop pressure relief valve set at 300 bar, the torque available from the dynamometer begins to saturate at approximately 20 Nm. This effectively reduces K_3 to zero, the result of which is described in section 2.4.

The dynamometer input coefficient (K_4) was obtained by applying a range of input voltages to the swashplate servo amplifier, and for each value the prime mover input was adjusted to keep the speed constant. The results are shown in graph G8, from which it can be seen that K_4 also varies with speed so that it is necessary to use three values:

Low speed, K_4 = 64 Nm/V

Medium speed, K_4 = 55.7 Nm/V

High speed, K_4 = 41 Nm/V

Under the motoring condition the prime mover torque/speed characteristic slope becomes the mechanical friction effect of the prime mover (assuming negligible windage), which was measured at approximately -0.03 Nm S. The time constant for the prime mover windings was obtained by holding the prime mover shaft fixed and applying a medium value of current (20 amps) to the windings. The torque response was recorded as the prime mover input was suddenly switched off, and this resulted in an exponential response of time constant 0.017 seconds (T_2).

The prime mover time constant (J_1/K_1) for the speed/torque response was determined by applying a step change in prime mover input and this was found to be 0.35 seconds. Thus the prime mover inertia (J_1) is given by 0.35 x K_1, i.e., 0.129 kg m^2. It can be seen that the winding lag is small enough to justify this method of obtaining the prime mover inertia. The inertia of the hydrostatic unit rotating parts is given by the manufacturers as 4.52×10^{-4} kg m^2.

$\therefore$ Kc = 0.764 V/r/S.

The velocity transducer is a permanent magnet d.c. tachogenerator rated at 8.0 volts per 100 rev/min. To reduce the ripple effect upon the electrohydraulic servo system at high values of controller gain it was found necessary to introduce a time lag on the tacho-

O Lv generator output having a time constant of 1.0 seconds (T_5). The torque transducer is of the strain gauge bridge and amplifier type (via slip rings) and has a coefficient of 0.0656 V/Nm with negligible time constant.

K6

The transfer function for the electrohydraulic servo system was determined by a frequency response test, as shown in graph G9, using an input signal of 0.1 volts peak-to-peak amplitude. It can be seen that the transfer function approximates to that of a second order system with $\omega_n = 68\ S^{-1}$ and $\zeta = 0.6$ for small signals.

The range of inertia to be simulated on the prime mover shaft (J_3) is 0.1 → 10 kg m^2 with the value of viscous friction = 0.13 Nm S. The most suitable gains for the controller coefficients are investigated in the next section.

2.3 Comparison of Theoretical and Experimental Analysis

2.3.1 Torque Reference System

The block diagram for the torque reference system is shown in Fig. 2.6, from which it can be seen that the simulated inertia effect is obtained by the use of an angular accelerometer, rather than by differentiating the speed signal. The first order lag having a time constant T_7 is necessary to reduce extraneous high frequency signals from the accelerometer in just the same manner as the tachogenerator lag is used to reduce low speed ripple effects. Obtaining the simulated characteristics in this manner requires the following addition to be made to the BASIC computer program COEF:-

```
463  Z4 = Z4 + K4*K9*A*T5*J4*E3
473  Z3 = Z3 + K4*K9*J4*(A*E3 + B*T5*E3 - A*K5)
483  Z2 = Z2 + K4*K9*J4*(B*E3 + C*T5*E3 - B*K5)
493  Z1 = Z1 + K4*K9*C*J4*(E3 - K5)
```

where E3 is the accelerometer coefficient (0.01 $v/r/s^2$). The following change was made to the program VALUES:-

```
66  E3 = .01
67  J4 = J4*K6/E3
```

Since the secondary roots have an inherently faster response than the primary root it was decided to use the low speed coefficients for K3 and K4 in order to determine the response of the system to a step change in prime mover input. It was also decided to initially determine the effect of proportional control only (i.e., A = C = 0) and, using an accelerometer time constant of T_7 = 1 second, a root locus was constructed for a range of proportional control (B), as shown in graph G10. It can be seen that the proportional gain should be 0.1 v/v or less for a reasonably well damped response. However, a low value of proportional gain can have a very large effect upon the simulated characteristics. This is due to the value of gain chosen for the swashplate signal used to eliminate the dynamometer torque/speed characteristic slope $(\frac{K3}{K4K5})$. This value should be approximately 0.24 v/v at high speed, increasing to over 0.4 v/v at low speed, although in practice the value may be kept constant for simplicity. If a value of 0.3 v/v is chosen as an average, then at low speed the actual friction effect will be larger than the required value and at high speed it will be smaller. With low proportional gain the signal provided by the simulated friction characteristic may be much lower at high speed than the signal provided for the dynamometer torque/speed slope elimination. Such a condition may lead to positive feedback and hence an unstable system.

If a value of 0.24 v/v is chosen for the gain of the dynamometer torque/speed characteristic elimination signal, then high speed stability is ensured, although the low speed friction coefficient will be much larger than the required value, which will have a consequent detrimental effect upon both the dynamic and steady state performance of the simulator.

It is therefore important to note that the dynamometer torque/speed characteristics can have a large effect upon the performance of a load simulator system. For this system in particular, the dynamometer torque/speed characteristic slope is much greater at low speed than at high speed. For automotive loads however, the effect of wind resistance is such as to increase the equivalent friction effect at high speed, which is opposite to the effect of the dynamometer. It can be seen, therefore, that linear control of such systems will be limited in its ability to provide the best performance compared to a non-linear adaptive controller.

It is not the intention here, however, to attempt to simulate a non-linear load using non-linear adaptive gain control, but to validate the generalised model developed in section 1 by simulating simple inertia and viscous friction loads. It is expected that if reasonable performance can be obtained using linear control, then introducing non-linear adaptive control to improve the performance will not prove to be a problem.

With B = 0.1 v/v a root locus was performed for a range of simulated inertia, as shown in graph G11. An analogue computer was used to perform the load simulation and control action on the real system, for which the circuit diagram is shown in Fig. 2.7. Using a gain on the dynamometer torque/speed characteristic elimination signal (P9) of 0.24 v/v, responses were obtained for sudden changes in the prime mover input setting, as shown in graph G12. It can be seen that the responses are in close agreement with the primary root responses predicted by the root locus method. Even with the simulated inertia set to 30 kg m^2 the actual torque response indicates a highly oscillatory condition at low speed which gradually becomes less oscillatory as the speed is increased. By replacing the low speed values of K3 and K4 with the high speed values, the root locus method shows that the previously unstable roots are pulled back to the left-hand side of the complex plane resulting in a stable system.

If the real inertia and viscous friction loads were connected to the prime mover shaft, instead of simulating the values on the dynamometer, then the response to step changes in the prime mover input would be first order (since the winding lag is negligible) with time constant

on which

(J1 + J4)/(F4 - K1). The time constants obtained in this manner are compared to those obtained from the load simulator system, as well as the predicted values using the root locus method, in the following table:-

from Eq (3) page 8

$T_2 = 0$ $\qquad T_1 = 0.$

$$\frac{n}{T_{dist}} = \frac{1}{(J_1+J_4)S + F_4 - K_1} = \frac{1/(F_4-K_1)}{\frac{J_1+J_4}{F_4-K_1}S + 1} = \frac{K}{1+\tau S}$$

Inertia ($kg\ m^2$)	Real Response Time Constant (s)	Computer Predicted Simulator Response Time Constant (s)	Actual Simulator Response Time Constant (s)
0.1	0.45	4.69	3.56
1	2.23	5.34	4.7
3	6.18	6.78	6.0
10	20.0	11.8	12.76
30	59.5	26.1	28.1

Table 1

It can be seen that for this particular simulator system the effect of changing the simulated inertia is much less than actually changing real inertial loads on the prime mover at both ends of the range. Since the required range of simulated inertia is up to 10 $kg\ m^2$ (for which the real system has a time constant of 20 seconds), then this can easily be met by re-calibration of the higher values of simulated inertia. However, at the low end of the range, even with zero simulated inertia, a time constant of 3.3 seconds was obtained from the system, which is equivalent to a real inertia of 1.54 $kg\ m^2$. This effect is due to the time constant on the tachogenerator restricting the speed at which the swashplate servo system can respond as a result of changes in prime mover speed. In fact, by reducing the tachogenerator time constant (T5) to 0.1 seconds and with zero simulated inertia, a response with time constant of 1.0 seconds was obtained. Since a low proportional gain is necessary for this system, then the tachogenerator ripple will have much less effect

$T_S = 0.1$

on the electrohydraulic servo system, so that a time constant of 0.1 seconds is suitable. Using this value a root locus was constructed for the range of simulated inertia (.1 – 30 kg m^2) which indicated negligible effect upon the secondary roots (compared to a tacho time constant of 1 second), although the range of primary time constant was now extended at the lower end to give 1.2 – 23.1 seconds over the range of simulated inertia. This enables the system to have a response equivalent to a real inertia as low as 0.5 kg m^2 and as high as 10 kg m^2 with no significant secondary root effects by suitably calibrating the simulated inertia potentiometer (P6) on the analogue computer. Using suitable values for P6 responses are shown in graph G13 for the actual system with effective inertias of 0.5, 1.0, 3 and 10 kg m^2.

Although the performance of the system appears to be good so far, it was found in practice that on repeating test runs several times the effective friction of the system varied by as much as 50% per run, even though the oil temperature was kept within $\pm 3^{\circ}$ C of the average temperature (30° C). The reason for this effect is that using a constant gain for the dynamometer torque/speed characteristic slope elimination, changes in temperature will alter the magnitude of the torque error (due to the use of a constant gain), which correspondingly changes the effective viscous friction of the system. If the proportional gain (B) is low, then, referring to

Fig. 2.8, it can be seen that a 1% change in the dynamometer torque elimination signal (P9) is equivalent to a 22.4% change in the simulated friction signal (F4) (with B = 0.1 v/v, P8 = .112, P9 = 0.24). Therefore either a proportional gain (B) of at least 1 v/v should be used, or integral action should be included in the controller (or make the gain of the dynamometer torque elimination signal non-linear to match the dynamometer torque/speed characteristic exactly).

It was decided to use the root locus method to determine whether the system could be stabilised using a proportional gain (B) of 1.0 v/v. It was found that a stable response could be obtained with this value of B, for high speed K3 and K4, by increasing the accelerometer time constant (T7) in proportion to the magnitude of the simulated acceleration coefficient. By setting T7 (in seconds) equal to J4 (in kg m^2) a root locus was constructed for a range of simulated inertia (J4), as shown in graph G14. It can be seen that using the high speed values for K3 and K4 the response is just stable. Using the computer program ZEROS it was found that a zero resides in very close proximity to the highly oscillatory second order poles and therefore reduces the magnitude of their effect upon the response. In practice, this zero exists because the swashplate servomechanism cannot follow the high frequency of the second order poles (85 r/s).

Responses were obtained for the actual system as seen in graph G15 using a modified analogue computer circuit diagram, as shown in Fig. 2.8. It can be seen that the actual responses are quite stable over the range of simulated inertia, and comparisons between the primary root time constants for the real, simulated and computer predicted responses are given in the following table:-

Inertia ($kg\ m^2$)	Real Response Time Constant (s)	Computer Predicted Simulator Response Time Constant (s)	Actual Simulator Response Time Constant (s)
0.1	0.45	0.51	1.0
1.0	2.23	2.75	3.1
3	6.18	7.84	7.2
10	20.0	25.7	24.3

<u>Table 2</u>

If the time constant T7 is left constant at 1 second, then the root locus (using high speed values for K3 and K4) predicts that the system will go unstable for a simulated inertia of just over 3 kg m^2 and this was found to be the case on the actual system. One noticeable difference between the "actual" responses with T7 = 1.0 seconds and the "actual" response with T7 (s) = J4 (kg m^2) can be seen by comparing graphs G15 and G13. From graph G15 it can be seen that for large values of simulated inertia a secondary root becomes apparent with a time constant of approximately 0.5 seconds. This root is not obtained on graph G13 (with T7 = 1.0 seconds) and is not indicated by the root locus method. This effect is not due to the torque limit being reached by the dynamometer, since the response remained identical for small changes in prime mover input. In practice, however, it is not possible to provide a step change in torque by means of the prime mover input (resulting in a root at the origin), but the input is more closely approximated by an exponential change (resulting in two roots: one at the origin and the other at a position on the negative real axis determined by the time constant of the exponential change). It is this second root which becomes apparent on graph G15 since, with T7 = 1.0 s, a zero occurs at -1. This reduces the magnitude of the secondary pole effect for graph G13, but with T7 = J4 the zero moves towards the origin for large values of J4 and, consequently, the magnitude of the secondary root is not reduced.

Once again, when tests were performed on the actual system for repeatability, it was discovered that the effective simulated friction of the system reduced as the simulated inertia was increased. Examination of the accelerometer revealed a d.c. offset at zero speed of between -4 and +5 mV (depending upon its rest position). Above zero speed the offset increases from 3.8 mV at 10 r/s to 4.5 mV at 100 r/s. Although these values appear small, it can be seen from Fig. 2.8 that with a simulated inertia of 10 kg m^2 the torque error could be as high as 20 Nm at 100 r/s. This is because the setting up procedure requires the swashplate position to be zero when the hydrostatic loop is closed, so that any initial offset (including the accelerometer output) is eliminated. Thus, if the initial offset of the accelerometer is -4 mV, then at a prime mover speed of 100 r/s this is equivalent to introducing an offset of 8.5 mV which, in turn, produces a torque offset of 20 Nm. (Note that with a proportional gain (B) of 0.1 v/v the maximum possible offset becomes 0.2 Nm.)

Thus with a low proportional gain (~~N~~ B = 0.1 v/v) it has been found that the dynamometer temperature sensitivity, with linear swashplate control, causes large errors in the simulated viscous friction of the system, and for higher settings of proportional gain (B = 1 v/v) the d.c. offset of the accelerometer also creates large errors in the simulated viscous friction. It is possible to reduce the effect of the accelerometer offset by performing the initial start up procedure with the prime mover input shaft set to a position for zero accelerometer output and introducing a d.c. offset of -4.5 mV once the system is running with prime mover speeds greater than zero, but this procedure increases the complexity of start up. It should be noted that the d.c. offset is common to all seismic angular accelerometers and for this reason it is likely that a simple passive network of the type shown in Fig. 2.9 will prove more effective (and will certainly be less expensive) for the purposes of simulating inertia (unless the simulated inertia effect is calculated by digital computer).

To determine the effect of adding integral action to the system a root locus was constructed for a range of integral gain (C) with the proportional gain (B) at 0.1 v/v. The root locus, shown in graph G16, indicates that the dominant root has a very long time constant for small values of integral gain. However, examination of the system zeros showed that as the gain was reduced below 0.1 s^{-1}, a zero moved in towards the low valued pole and made its effect negligible. In fact, with C = 0, the pole and zero coincide and cancellation occurs so that the order of the system is reduced by one. As far as the secondary roots are concerned, an integral gain of 10 s^{-1} is indicated as giving the best performance, since lower values create low frequency roots near the origin and higher values create oscillatory high frequency roots causing instability for a value of C just over 20 s^{-1}.

Using an integral action gain of 10 s^{-1}, a root locus was constructed for a range of simulated inertia (J4), as shown in graph G17, which may be compared to the actual system responses shown in graph G18. From G18(b) it can be seen that one effect of integral action is to amplify low frequency torque oscillations from the system. Also, from graph G18(d), a secondary root occurs (although not indicated by the root locus) for the same reason as that shown in graph G15(d). In practice, integral action increased the complexity of starting up the system by causing "hunting" at zero speed due to dead band around the central position of the secondary unit swashplate. This can be seen at zero speed in the torque response of graph G18(b). The effect of the accelerometer d.c. offset was also found not to diminish with integral action, the reason for this being that the offset occurs in a feedback path of the system and not a forward path, so that the steady state torque error cannot be integrated out. Thus, due to the accelerometer d.c. offset, the use of proportional plus integral action was not found to improve the system performance. However, for systems which simulate the inertia characteristic by differentiating the speed signal (and which, therefore, do not suffer from the d.c. offset), the use of proportional plus integral action is necessary to counteract the effect of the torque elimination signal error when the proportional gain (B) is low. method II

Using the root locus method it was possible to determine the effect of three term control on the system. In general, for low values of proportional gain, it was found that a wide range of derivative action time had little effect on the system performance (although poles with low damping were produced their effect was made small by zeros in the same neighbourhood). However, it was found possible to increase the proportional gain (B) to 10 v/v with a derivative action time (A) of 10 seconds and integral action gain (C) of from 0 → 10 s^{-1} without adversely affecting the performance (although once again poles with low damping were produced with zeros in close proximity). However, due to noise effects, it is not usual practice to use high derivative action times with electrohydraulic servo systems and this was not attempted on the actual system. *

Having determined the effect of various control actions with the system in the loading condition, it was decided to determine the performance under the motoring condition. For the root locus method of analysis it was necessary to replace the prime mover torque/speed characteristic slope (K1) by the prime mover viscous friction effect (-.03 Nms), as well as to set the hydrostatic loop time constant (T3) to 0.08 s (for the motoring side of the loop) and to eliminate the prime mover lag time constant (T2). Using a proportional gain (B) of 1.0 v/v together with high speed values for K3 and K4, the root locus is shown in graph G19 for a range of simulated inertia (J4). The responses are shown to be highly stable (compared to the near instability of the loading condition) and the dominant root time constants are in good agreement with those obtained for the actual system as shown in graph G20.

It was shown in section 2.2.1 that the leakage coefficient of the hydrostatic loop affected the time constant (T3) and gain (included in K3 and K4) of the loop. Since the leakage coefficient depends upon the oil viscosity which, in turn, varies with temperature, it can be seen that the oil temperature may have a large effect upon the dynamic performance of the system. To determine the magnitude of this effect a root locus was constructed for a range of temperature by simultaneously varying T3, K3 and K4 in relation to the change in viscosity. The viscosity changes were obtained from a temperature-viscosity chart supplied by Shell for the oil used in the hydrostatic system (Tellus 27). It can be seen from graph G21 that with a proportional gain (B) of 1 v/v the root locus indicates that the system will go unstable at an oil temperature below 23° C. Over the range 23° → 40° C it can be seen that the effect upon the primary root time constant is small.

However, on the actual system it was found that the response was stable even at 17° C. A frequency response analysis on the electrohydraulic servo system showed that both ζ and ω_n for the servo system had increased at this lower temperature, resulting in values of F9 = 0.114 Nsm^{-1} and K9 = 6.673 Nm^{-1}. Using these values together with U7 = 1.76 (for 17° C), the root locus method indicated a stable response, with little effect upon the primary root time constant. The effect of other variables upon the system performance was investigated by the root locus method as follows:-

(a) Simulated friction (F4) was found to have little effect upon the secondary roots and the primary root time constant was reduced for values of simulated friction larger than the prime mover torque/speed characteristic slope (as would be expected under real running conditions).

(b) Dynamometer inertia (J2) increases the stability of the secondary roots as the inertia is increased, although the primary root time constant increases for dynamometer inertias greater than 1 kg m^2.

(c) Dynamometer lag (T3) was found to increase the stability of the secondary roots as the time constant was increased, with little effect upon the primary root for a time constant as high as 1 second. Thus for this particular method of simulating Loads it may be concluded that a fast response dynamometer with low inherent inertia actually gives a poorer performance than a slow response dynamometer with large inherent inertia such as a d.c. motor/ generator type dynamometer.

(d) Tachogenerator lag (T5) has little effect upon the secondary roots, although for time constants greater than 0.1 seconds the range of simulated inertia is reduced at the low end.

(e) Accelerometer lag (T7) was found to cause the secondary roots to go unstable as the time constant was reduced. Large values of time constant had little effect upon either the secondary roots or the primary root time constant.

(f) Dynamometer input actuator lag $K9/(J9s^2 + F9s + K9)$. By setting J9 and F9 to zero to eliminate the actuator lag the secondary roots in the region $-50 \pm J50$ were eliminated, which has, in fact, negligible effect upon the system performance. Increasing J9 by a factor of 100 and F9 by 10 reduces the response time of the input actuator by a factor of 10 without affecting the damping. This was also found to have little effect upon either the primary or secondary responses of the system.

Having investigated the effect of a large number of parameters upon the performance of the torque reference system, the effect of these parameters upon the speed reference system is investigated in the next section.

2.3.2 Speed Reference System

The block diagram for the speed reference system is shown in Fig. 2.3. Initial investigations were performed with proportional gain only (i.e., A = C = 0) and a root locus was constructed for a range of proportional gain (B) as shown in graph G22. It is shown that much higher gains are possible with this system compared to the torque reference system and, since the simulated characteristics are now in the torque path instead of the speed path, the size of the speed signal incorporated in the control signal is now much greater. This results in a time lag of 1 second being required on the tachogenerator (T5) to eliminate low speed ripple effects. Using the analogue computer to perform the simulated characteristics and control action, as shown in the circuit diagram of Fig. 2.10, actual responses for a range of B were obtained, as shown in graph ~~G22~~ G23. It can be seen that there is good agreement between the actual and computer predicted values, and the oscillatory nature of the secondary roots can easily be seen in graph G23(c) and (d) for B = 10 v/v. Note that this oscillatory response is well within the range of the swashplate servomechanism frequency response, so that the effect of the oscillatory poles is not reduced by zeros to the same extent as for the torque reference system.

Using a proportional gain (B) of 2 v/v a root locus was constructed for a range of simulated inertia (J4). It was discovered that the system became unstable for low values of simulated inertia (whereas the torque reference system had the opposite effect). Thus, using a gain (B) of 1 v/v, a further root locus was constructed as shown in graph G24. Highly oscillatory roots are obtained for low values of simulated inertia

J3
($J4 < 0.1$ kg m^2) and this is in agreement with the actual responses shown in graphs G25(a) and (b). For high values of simulated inertia the root locus indicates low frequency secondary roots which can be seen in the actual responses of graphs G25(d) and (e), although the actual secondary roots have lower damping than those predicted by the root locus. Time constants for the system with a "real" load are compared to the computer predicted values and the actual simulator values, for a range of inertia, in the following table:-

Inertia ($kg\ m^2$)	Real Response Time Constant (s)	Computer Predicted Simulator Response Time Constant (s)	Actual Simulator Response Time Constant (s)
0.1	0.45	0.92	0.75
1	2.23	3.3	3.1
3	6.18	8.6	9.1
10	20.0	27.1	29.4

Where do we get these values?

Table 3

One effect of the higher gain of the speed signal is that the dynamometer torque/speed characteristic elimination signal has a much smaller effect upon the system response. In fact, a 1% change in this signal (due to, say, temperature effects) is equivalent to a change of only 0.24% in the simulated friction characteristic, as can be seen from the analogue computer circuit diagram of Fig. 2.10. This effect is small in comparison to the torque reference system, for which a change of 1% in the dynamometer torque/speed characteristic elimination signal was shown to produce a 22.4% change in the simulated friction characteristic with B = .1 v/v. Also, the simulated inertia is obtained by a simple first order lag (A5 and P6 of Fig. 2.10), rather than by the use of an accelerometer, so that the starting up procedure is straightforward, without the need to take account of a d.c. offset at zero speed. In fact, after several test runs there was found to be no measurable difference in the simulated characteristics, so that calibration of potentiometer P6 for simulated inertia and P7 for simulated friction (Fig. 2.10) may be made with high repeatability.

To determine the effect of running under the motoring condition a root locus was constructed, as shown in graph G26, which may be compared to the actual responses shown in graph G27. The primary response time constants compare well with the predicted values and the oscillatory secondary roots for J3 = 0.1 kg m^2 can clearly be seen in the torque response of graph G27(b). Time constants for real responses, computer predicted and simulator responses under the motoring condition are shown in the following table:-

Inertia ($kg\ m^2$)	Real Response Time Constant (s)	Computer Predicted Simulator Response Time Constant (s)	Actual Simulator Response Time Constant (s)
0.1	1.43	ω_n=1.02 r/s; ζ =0.93	1.3
1	7.1	7.1	7
3	19.6	19.7	19
10	63.3	63.5	64

Table 4

Under the motoring condition, the simulated characteristics produce a response which is almost identical to using real values of inertia and friction on the prime mover. Since, under the loading condition, the simulator responses have a larger time constant than the "real" responses, it can be seen that a compromise must be reached in calibrating the simulated characteristics (or use a non-linear control system which can automatically change calibration factors between the loading and motoring conditions).

To determine the effect of adding integral action gain to the system a root locus was constructed as shown in graph G28. It can be seen that low values of integral gain have the same effect as for the torque reference system, i.e., a pole moves towards the origin but is closely followed by a zero which makes its effect negligible and results in cancellation when C = 0. Higher values of integral gain, however, have a greater effect upon the system performance than for the torque reference system. The secondary roots have low damping for integral gain greater than 3 s^{-1}, resulting in instability at just over 20 s^{-1}. Using an integral gain of 3 s^{-1} a root locus was performed for a range of simulated inertia as shown in graph G29, which may be compared to the actual response of the system shown in graph G30. It can be seen that low values of simulated inertia produce high frequency secondary roots whereas high values of simulated inertia produce low frequency oscillatory roots in just the same manner as the system without integral action. Thus the introduction of integral action with gain less than 3 s^{-1} has little effect upon the dynamic performance of the system. This is, in fact, similar to the effect of integral action upon the torque reference system.

To determine the effect of three term control upon the system the root locus method was used to determine the pole positions for a wide range of gain settings (A, B and C) of the three term controller. It was found that for high values of proportional gain ($B > 5$ v/v) the stability of the system was increased by the introduction of a low derivative action gain ($A < 2$ s) for a wide range of integral action ($C = 0 \rightarrow 10$ s^{-1}). Higher values of derivative action ($A > 3$ s) caused the system to go unstable for high and low settings of both integral action (C) and proportional gain (B).

The effects of other variables upon the system performance were determined by the root locus method as follows:-

(a) Temperature was found to have less effect on this system than on the torque reference system. The root locus indicated a stable response at a temperature as low as 10° C even without the extra damping effect of the electrohydraulic servo system. The effect upon the primary root response was shown to be small over the range 10 → 40° C.

(b) Simulated friction (F3) had the same effect as on the torque reference system, i.e., negligible effect upon the secondary roots and a large effect upon the primary root for values greater than the prime mover torque/speed characteristic slope (K1).

(c) Dynamometer inertia (J2) had the opposite effect to the torque reference system in that increasing the dynamometer inertia reduced the stability of the secondary roots. For an inertia above 1 kg m^2, however, the secondary roots became more stable, although the primary root response became slightly faster.

(d) Dynamometer lag (T3) was found to have negligible effect upon the primary root time constant over the range 0 → 1 s, although the secondary roots became highly oscillatory for $T3 > 0.05$ s. Thus for this method of simulating loads (speed reference) it may be concluded that a fast response dynamometer with low inherent inertia provides a better performance than a slow response dynamometer with high inherent inertia (this being the opposite result to that obtained for the torque reference system).

(e) Tachogenerator lag (T5) caused the secondary roots to become highly oscillatory for $T5 < 0.5$ s and reduced the time constant of the primary root response. Values of $T5 > 1.0$ s caused the primary root time constant to increase and thereby reduced the range of simulated inertia at the low end.

(f) Elimination of the dynamometer input actuator lag was found to have negligible effect upon system performance (as with the torque reference system). However, increasing the lag by a factor of ten introduced highly oscillatory secondary roots of low frequency to the system, although the effect upon the primary root response was negligible.

2.4 Discussion

It has been shown that the generalised model, developed in section 1 and applied to the low power simulator system, has given considerable insight into the effect of various parameters upon the system performance. In spite of the linear approximations used to describe the non-linear system, the root locus method has been found to be very effective in predicting responses under a wide range of conditions. Under certain conditions, however, it was discovered some effects indicated by the root locus method were not obtained on the actual system responses, and that other effects were obtained on the system responses which were not indicated by the root locus method. In all cases this was found to be the effect of cancellation of the system poles by zeros. In particular, it was found that where the root locus method indicated high frequency poles with very low damping ($\zeta < .1$), then if the frequency is large compared to the dynamometer cut off frequency the effect on system performance is negligible, and zeros are obtained in close proximity to the high frequency poles. However, if the frequency of the poles is lower than the dynamometer cut off frequency, then high frequency torque oscillations of large magnitude may be obtained (although this has little effect upon the speed response - see graphs G25(a) and (b)).

One difficulty encountered with high frequency poles having low damping is that of accurately determining the relative stability of the system. It is known that as the poles cross the imaginary axis the system will go unstable, but just how oscillatory the response will be as the poles approach the imaginary axis is not easy to determine. For example, graph G14 indicates a complex conjugate pole pair having a damping ratio (ζ) of 0.05 and an undamped natural frequency (ω_n) of 84 r/s. The torque and speed responses were found to have no oscillatory tendencies over the range of simulated inertia and this is due to the cancellation effect of the zeros in close proximity to the poles. However, a very small movement of the poles to the right causes the system to go unstable.

Another effect of zero cancellation was found with low values of integral gain. As the gain is reduced the dominant pole, indicated by the root locus, moves towards the origin. However, the response of the actual system was found to remain constant as the gain is reduced. It was shown that as the low valued pole moved towards the origin a zero followed closely behind (causing exact cancellation when the gain = 0) and another pole moved in to the position occupied by the previous pole. The effect of these pole movements was that the response actually remains constant (see the increased scale of graph G28).

Yet another effect of zero cancellation was found in the response of the prime mover input actuator. Since the actuator is not part of a feedback loop (for this particular method of simulation), then the lag of the actuator introduces an extra (secondary effect) pole to the root locus diagram. In practice the actuation was performed manually so that it was only possible to determine an approximate position for this pole (-0.5 ± J0). In general, it was found that a zero existed in this region, which caused a reduction in the magnitude of the effect of the pole on the system response. Under certain conditions however, the zeros moved from this region, causing the magnitude of the input pole to have a larger secondary effect, as shown in the actual responses of G15(c) and (d) and G18(c) and (d).

Since the zeros can have a large secondary effect on the system response it is important to check their relative positions when determining root loci for a range of system parameters.

It has also been shown that the non-linear torque/speed characteristic of the dynamometer can have a large effect upon the system performance, especially when a low value of proportional gain on the controller is required for stability purposes. It was found that the best estimates of the system performance resulted from using values of the dynamometer torque/speed characteristic at the higher end of the speed range. It is, however, necessary to check the effect of both low and high speed values for the dynamometer and prime mover characteristics (linear in this case) to determine the possible range of performance indicated by the root locus method.

From Fig. 2.11 it can be seen that for the same controller gain (B = 1 v/v) the effective steady state gain of the torque reference system is much lower than that of the speed reference system (using a value of simulated friction F3 = F4 = 0.13 Nm s). The result of this is that errors in the signal used to eliminate the torque/speed characteristic of the dynamometer have a much larger effect on the torque reference system than on the speed reference system. In fact, with a proportional gain (B) of 0.1 v/v on the torque reference system (to keep secondary poles well away from imaginary axis) errors in the simulated friction effect were as high as 50% from one test run to another. With the speed reference system using a proportional gain (B) of 1 v/v there was no measurable change in the simulated friction characteristic between test runs.

It may therefore be concluded that if stability considerations of the system require that the proportional gain of the controller must be low and, if this causes the torque/speed characteristics of the dynamometer to have a large effect upon the simulated friction, then it is necessary to add integral action to the controller.

Of particular importance to electrohydraulic systems, it has been seen that filters must be employed to reduce high frequency oscillations of the swashplate servomechanism. Such filters are not necessary with electrical dynamometer systems, since high frequency signals will effectively be filtered by the winding lag, and will therefore not reach the mechanical system. It has been shown that the time constant of the filter can have a large effect upon the dynamic performance of the system, especially for the lag associated with the speed transducer. For this particular system the speed transducer is a high speed tachogenerator (10,000 rev/min) which has particularly large ripple effects at low speed ($<$300 rev/min). It was therefore found necessary to have a time lag as high as 1 s to reduce these ripple effects, and this was found to be the value indicated by the root locus method as giving the best performance for the speed reference system. Over the speed range required for testing of internal combustion engines (600 - 6000 rev/min) tachogenerators are available which require a lag of only 1 ms to produce 1% rms smoothing of the ripple effect. It will be shown in Part 3 whether or not this speed of response is necessary.

For both methods of load simulation it has been shown that variation of the simulated friction characteristic over a wide range has the desired effect upon the primary root response of the system without affecting the secondary roots. This suggests that the introduction of non-linear friction effects (such as wind resistance) will also have the desired effect upon the primary response without causing stability problems of the secondary roots. It is possible to take account of the non-linear torque/speed characteristic of the dynamometer within the wind resistance effect (to avoid incorporating two non-linear loops into the system), but this method reduces the flexibility of adjusting the magnitude of the wind resistance (for simulating a range of bodyshells, for example).

Although it was stated in section 1.2 that the ideal dynamometer for the purposes of load simulation would be one with an infinitely fast response and zero inherent inertia, it was found for the torque reference method that a slow response dynamometer with large inherent inertia actually gives a better performance than a fast response dynamometer. It can be seen, therefore, that it is difficult to form general conclusions about load simulation techniques and that observations for one type of prime mover/dynamometer/ simulation method will not necessarily apply to other types.

It was shown that temperature changes can have a large effect upon the dynamometer performance by changing the torque/speed characteristics as well as the response time of the dynamometer and the input actuator. However, due to these large changes in the dynamometer characteristics occurring simultaneously it was found that over a wide temperature range the effect upon the overall simulator performance was negligible (whereas changes in these characteristics occurring one at a time were each found to have a large effect upon the secondary root responses of the system). If, however, there is an error in the dynamometer torque/speed characteristic elimination signal and if the controller gain is low (as with the torque reference system), then temperature effects may cause very large errors in the simulated friction characteristic.

The use of three term control action was found to enable much higher values of proportional and integral gain to be used, without affecting the system stability, than was possible without the use of derivative action. The result of this is to increase the repeatability of the system performance, especially for systems which otherwise require a low value of proportional gain (i.e., the torque reference system). The use of integral action was found to cause difficulties in the start up procedure of the hydrostatic system. This is due to the fact that the initial start up of the system must be performed with the hydrostatic loop open, since high pressure transients may cause sudden changes in the swashplate position with the loop closed. However, with the loop open the integral action will operate upon any drift or d.c. offset in the system, causing the swashplate to move hard over before the loop can be closed.

To avoid this effect it is necessary to introduce the integral action after the hydrostatic loop has been closed and this action may be easily programmed if digital control of the system is to be used. One other effect of integral action was to cause "hunting" in the closed loop system at zero prime mover speed (see graphs G18(b) and G30(b)). This is due to the fact that for zero prime mover speed the secondary swashplate is required to be in its mid-position (for zero flow) where there will be a certain amount of deadband. Due to the dead band the integrator action will cause the system to hunt backwards and forwards in the dead region, since the torque will continuously be pushed positive and negative around the zero position.

If the dynamometer is incapable of providing the maximum torque level required by the simulation system (due to current limit of an electrical dynamometer, or the relief valve opening at maximum pressure on a hydrostatic dynamometer), then this saturation effect will result in the type of response shown in graph G31. These responses were obtained by providing very large changes in the prime mover input (i.e., applied voltage level). It can be seen that the initial increase in speed is far higher than the required value, and the resulting large error causes the secondary swashplate to move to maximum displacement so that both hydrostatic units are pumping into the same side of the loop (with the relief valve opening at maximum pressure). When the required torque signal reduces below the maximum dynamometer torque it can be seen that the speed response gradually recovers to follow the required first order dominant response (at which point the relief valve is completely closed).

Another factor which is of importance for electro-hydraulic systems is that of deadband and stiction in the electrohydraulic servo valve. The effect this has upon the frequency response characteristics of the system is shown in graph G32(a) and the effect upon the load simulator performance is shown in graph G32(b). It can be seen that after a period of remaining stationary the system will suddenly jump to a new position of the speed and torque response. A dither signal of frequency 100 Hz and peak-to-peak amplitude 0.1 volts was used to eliminate this effect.

100W?

With all method (2) simulation systems it may be necessary to calibrate the simulated torque/speed characteristics on the actual system. Calibration of all characteristics except inertia may be easily calibrated in the steady state, but calibration of the inertia effect is not so straightforward. The best approach is probably to compute the speed response to a step disturbance torque for a range of inertia with the simulated characteristics constant. Then for each computed inertia value adjust the simulated inertia to obtain the best fit to the computed response. This approach will be particularly necessary when both the prime mover and dynamometer torque/speed characteristics are highly non-linear.

It has been found that the generalised model developed in section 1 has been highly successful in predicting the performance of method (2) type simulation systems. Since method (1) type systems do not contain the simulated torque/speed characteristics (as do method (2) systems), then the model is less complex and, it is assumed, will be just as successful in predicting system performance. The model is used to determine the effect of various simulation methods on typical prime mover/dynamometer systems in Parts 3 → 5.

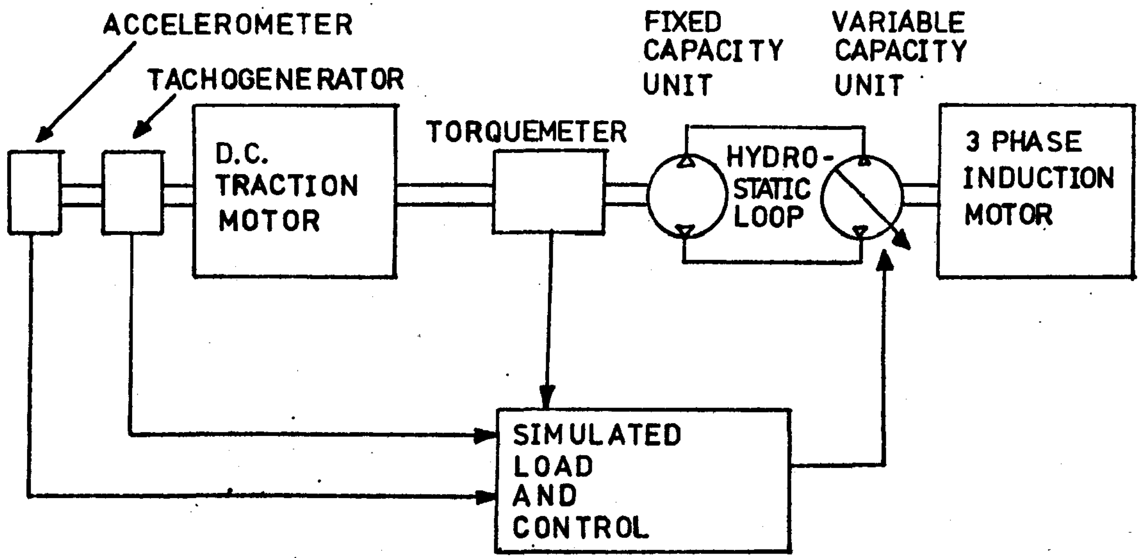

Figure 2.1 low power system schematic diagram

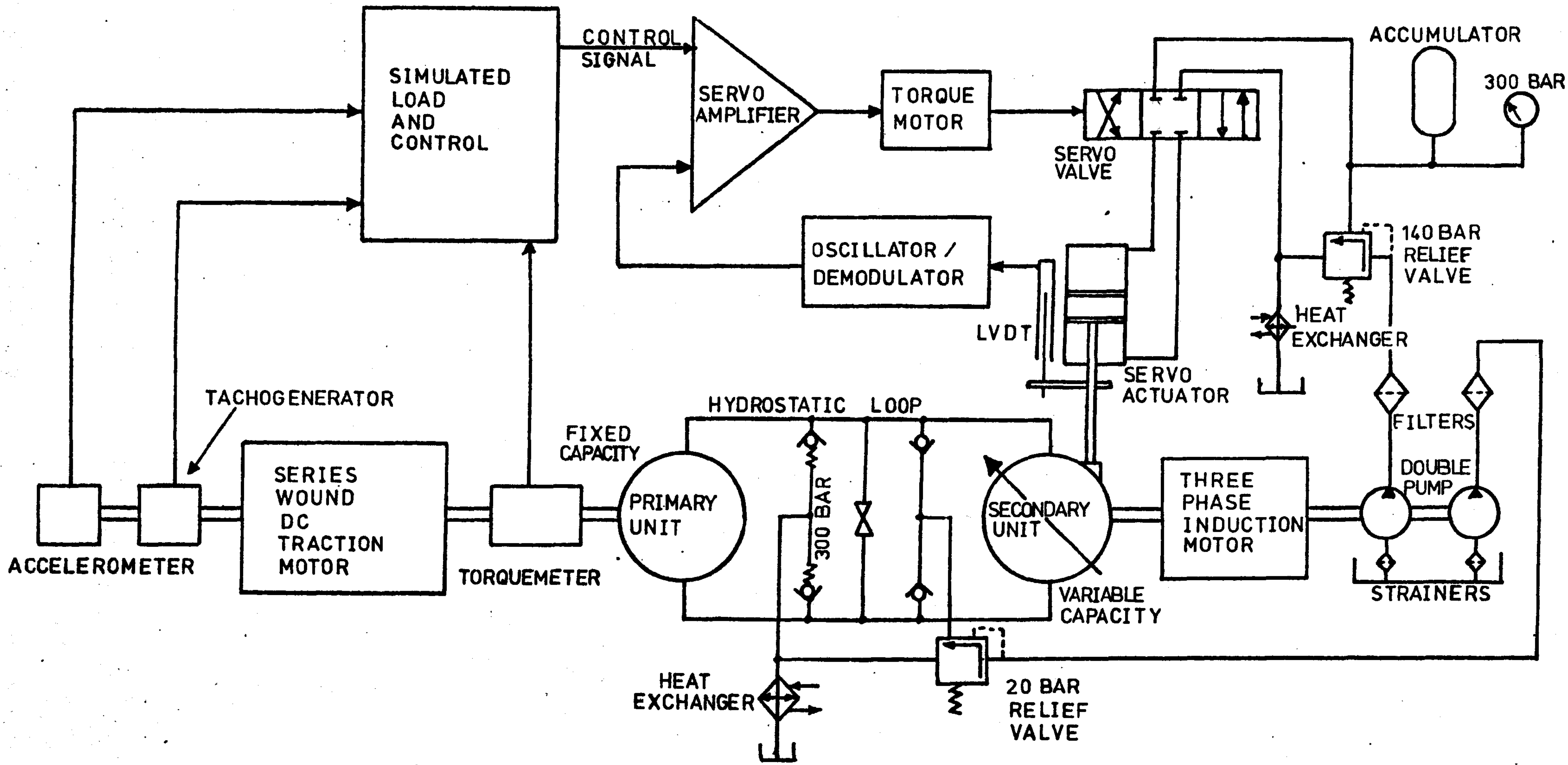

Figure 2.2 electrohydraulic system circuit diagram

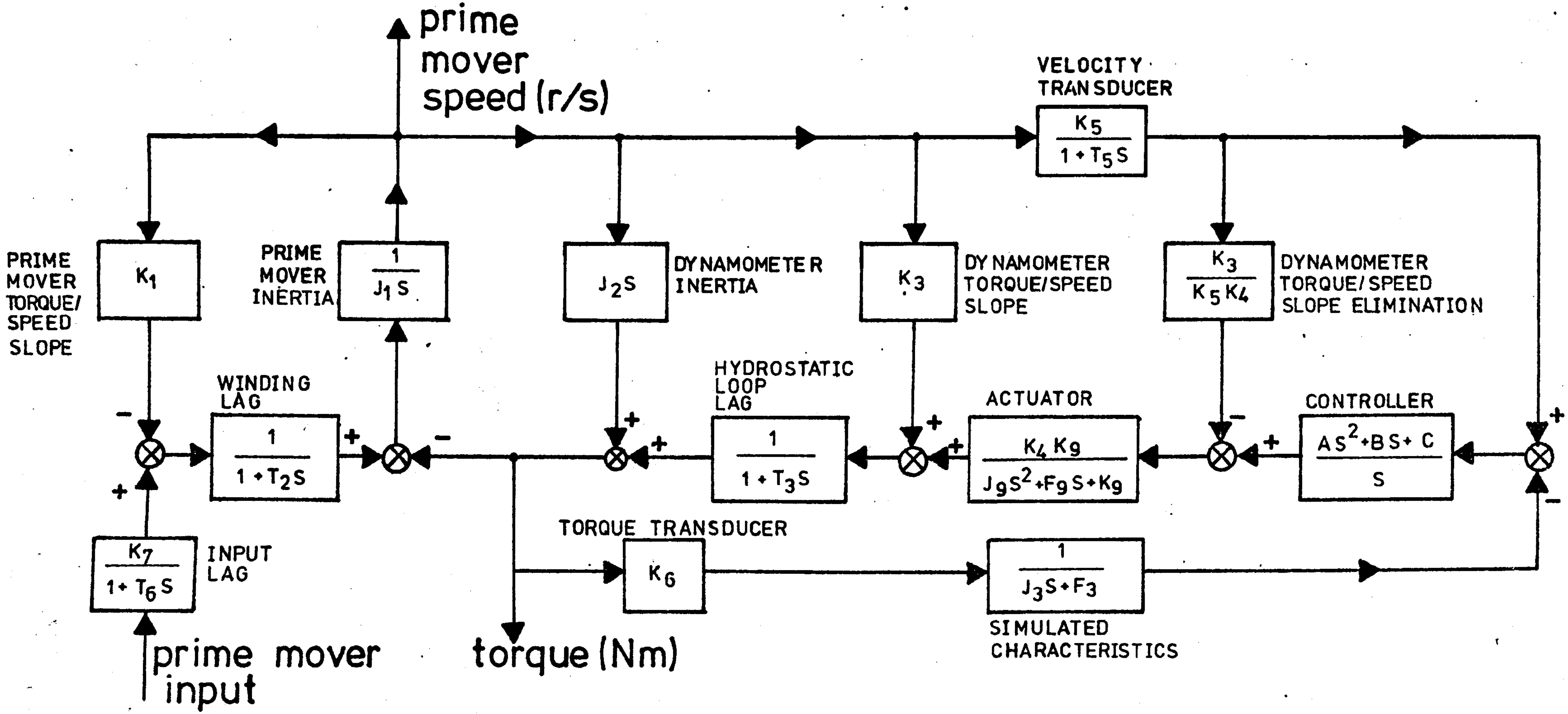

Figure 2.3 low power system block diagram (speed reference control)

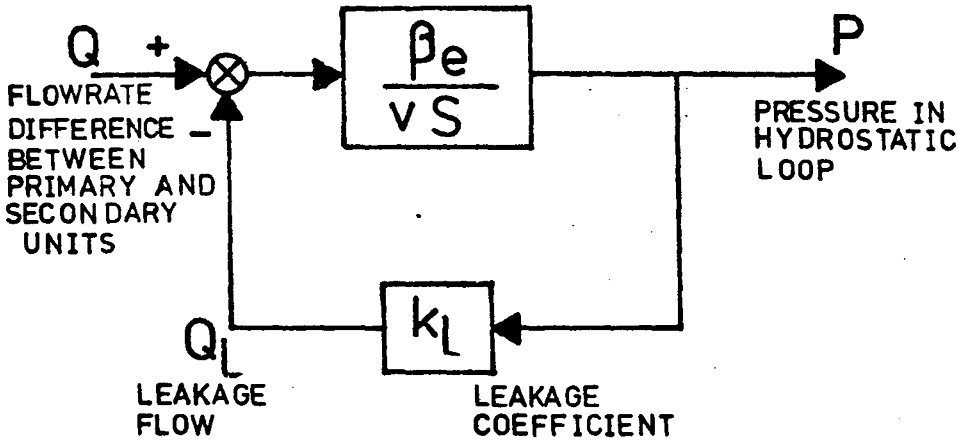

Figure 2.4 hydrostatic loop block diagram

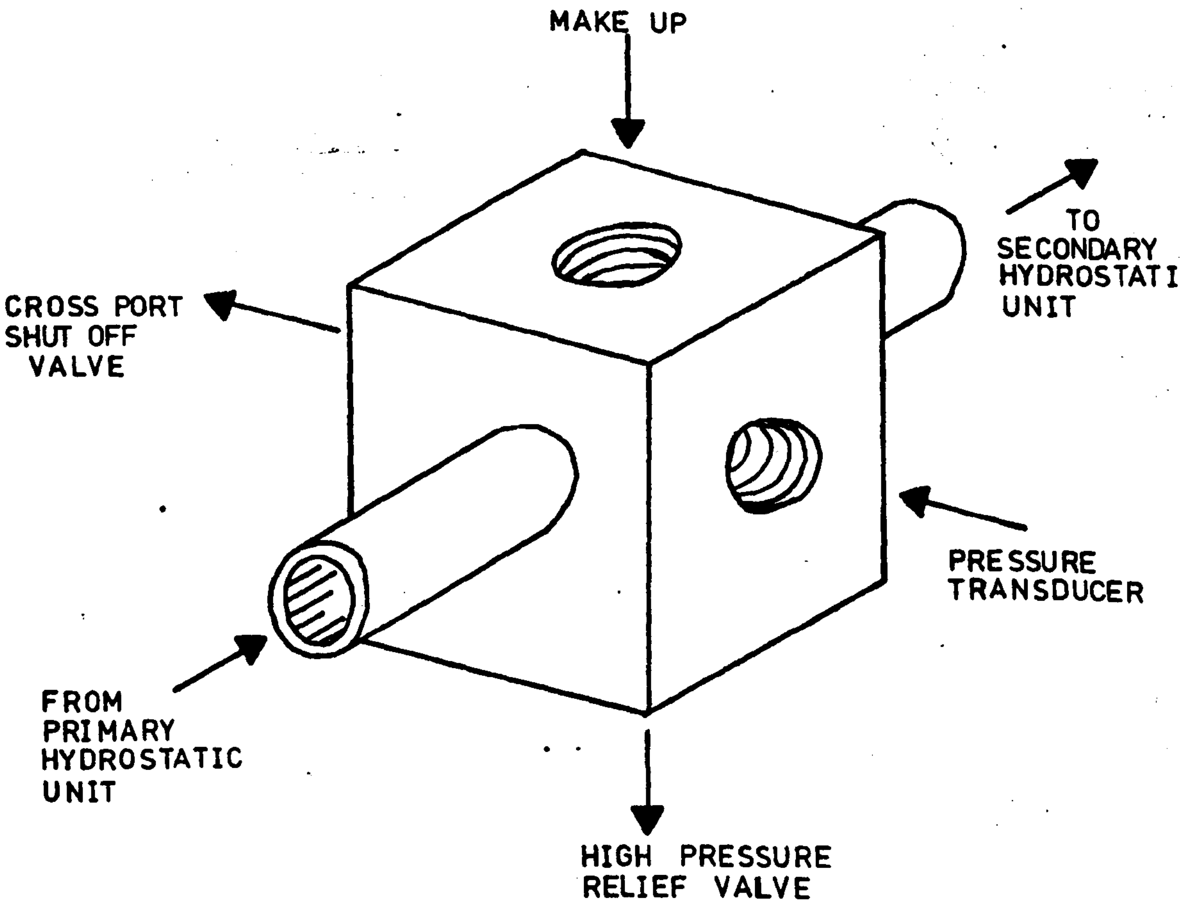

Figure 2.5 pressure loop manifold

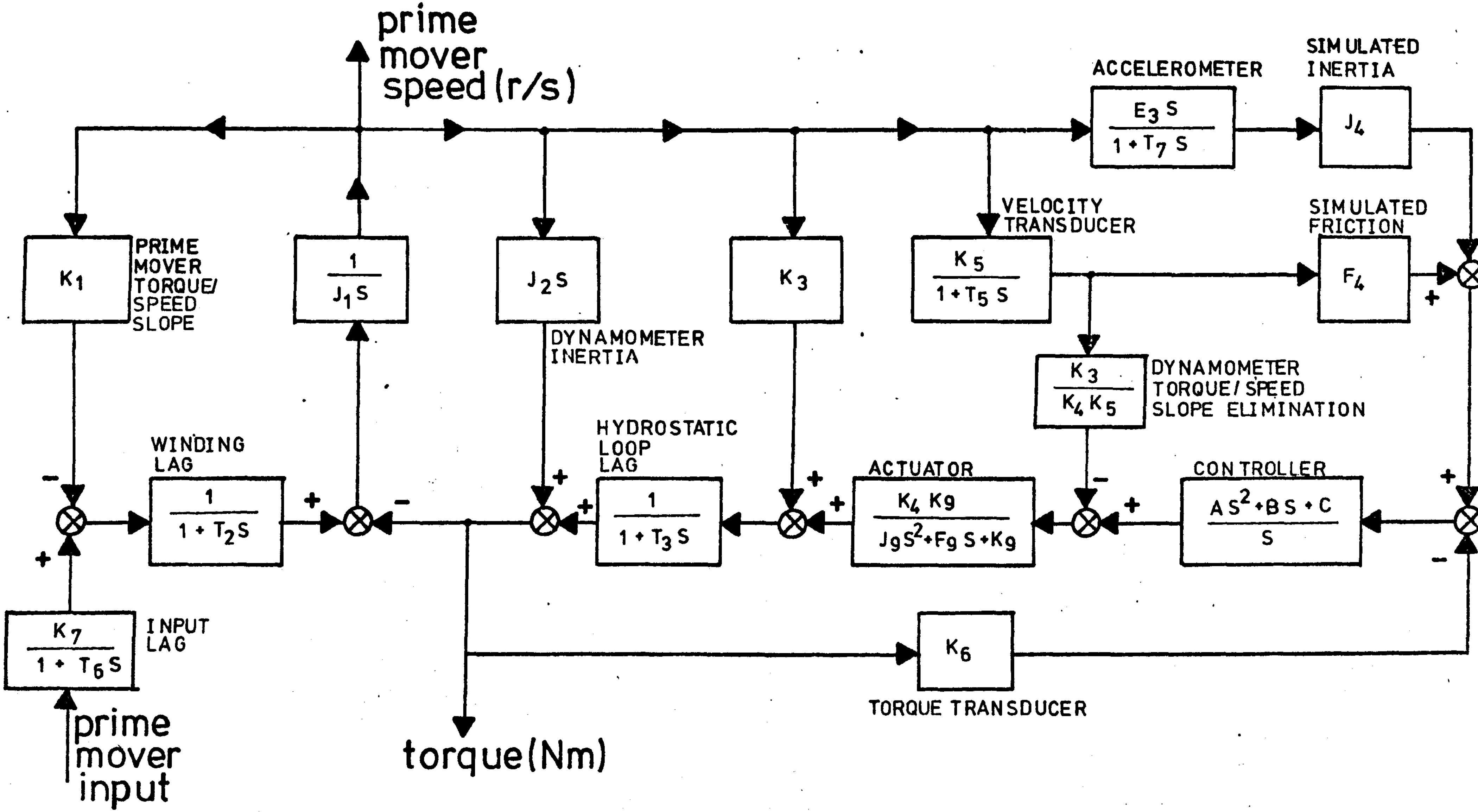

Figure 2.6 low power sytem block diagram (torque reference control)

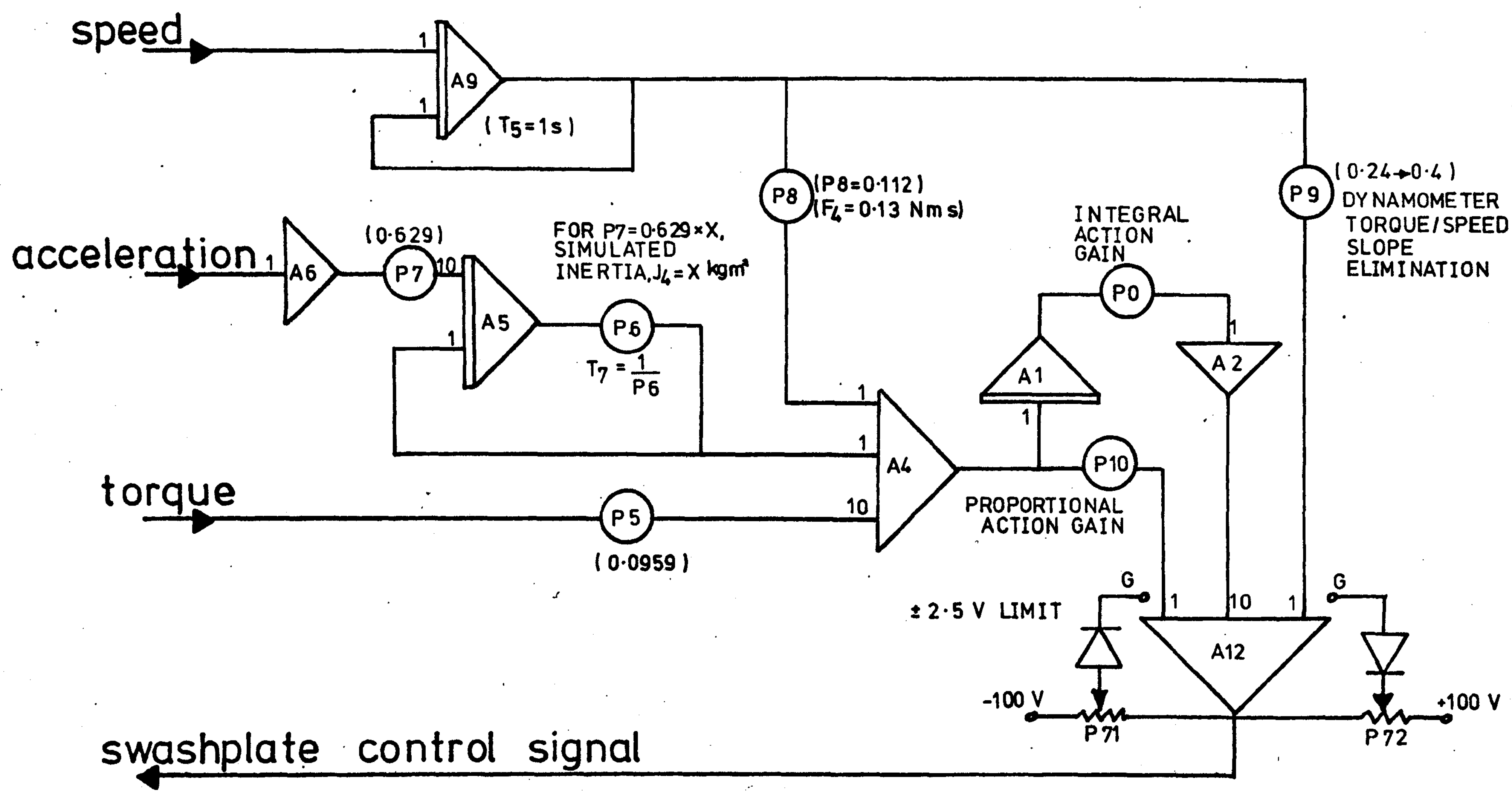

Figure 2.7 analogue computer circuit diagram (torque reference control)

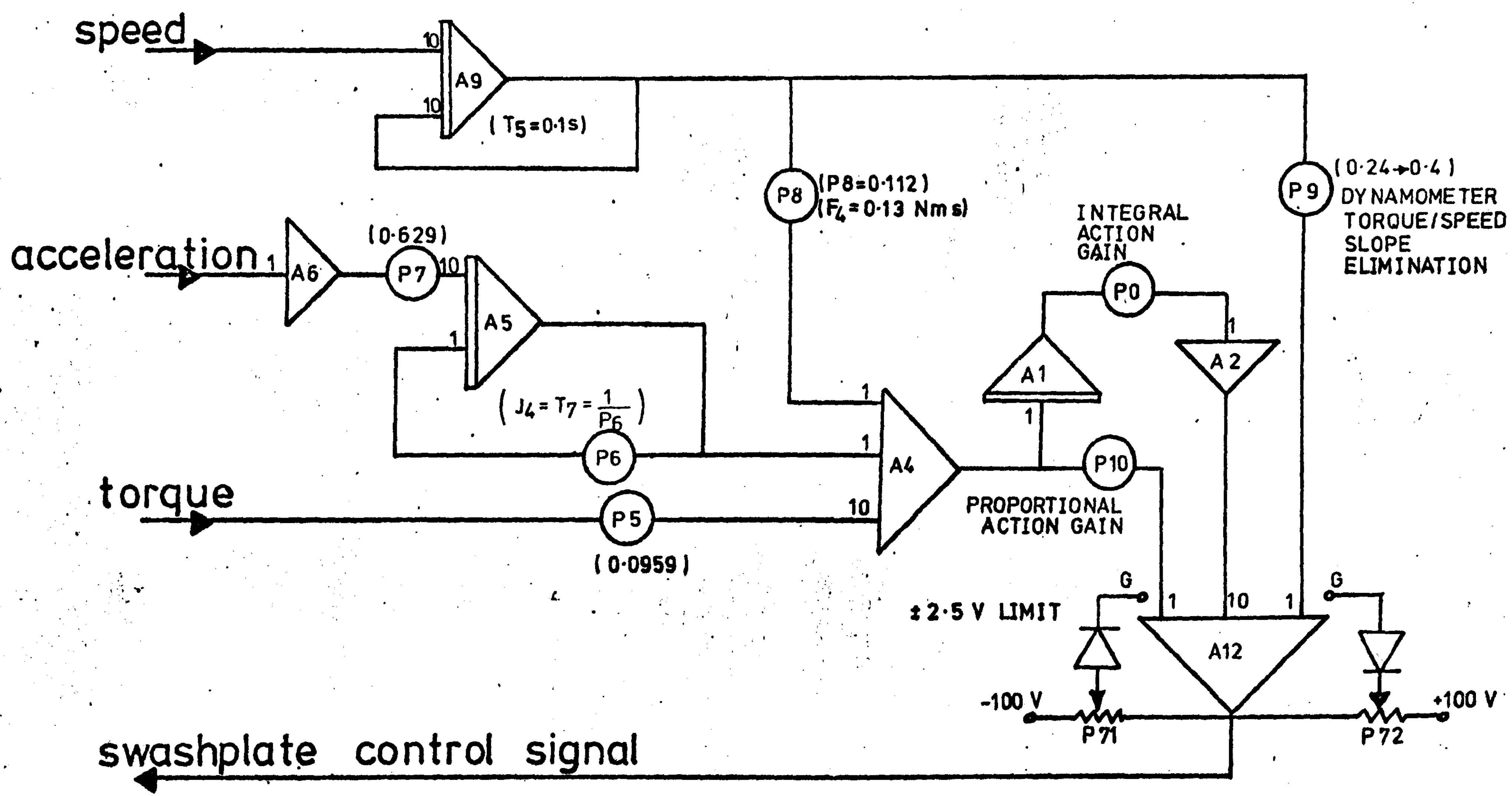

Figure 2.8 analogue computer circuit diagram – modified T_5 and J_4 (torque reference control)

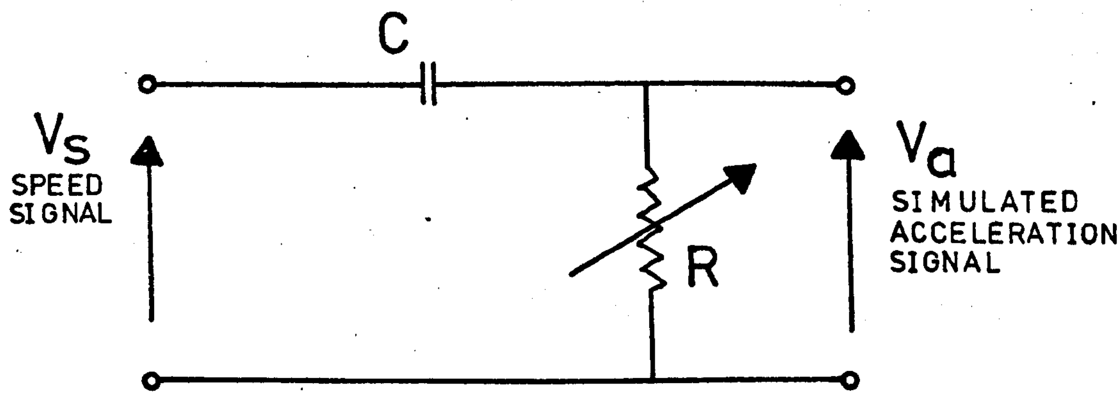

(a) schematic diagram

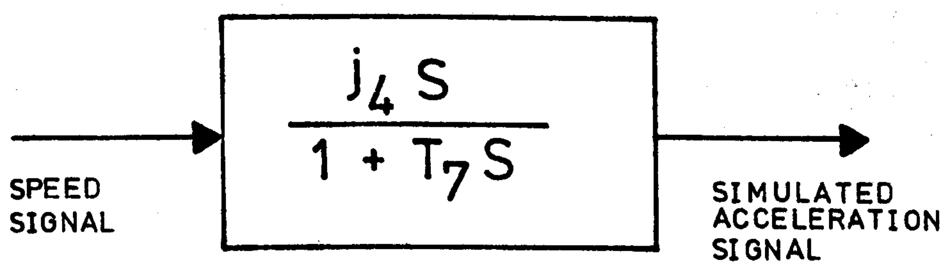

$(j_4 = T_7 = RC)$

(b) block diagram

Figure 2.9 simulated inertia using passive components

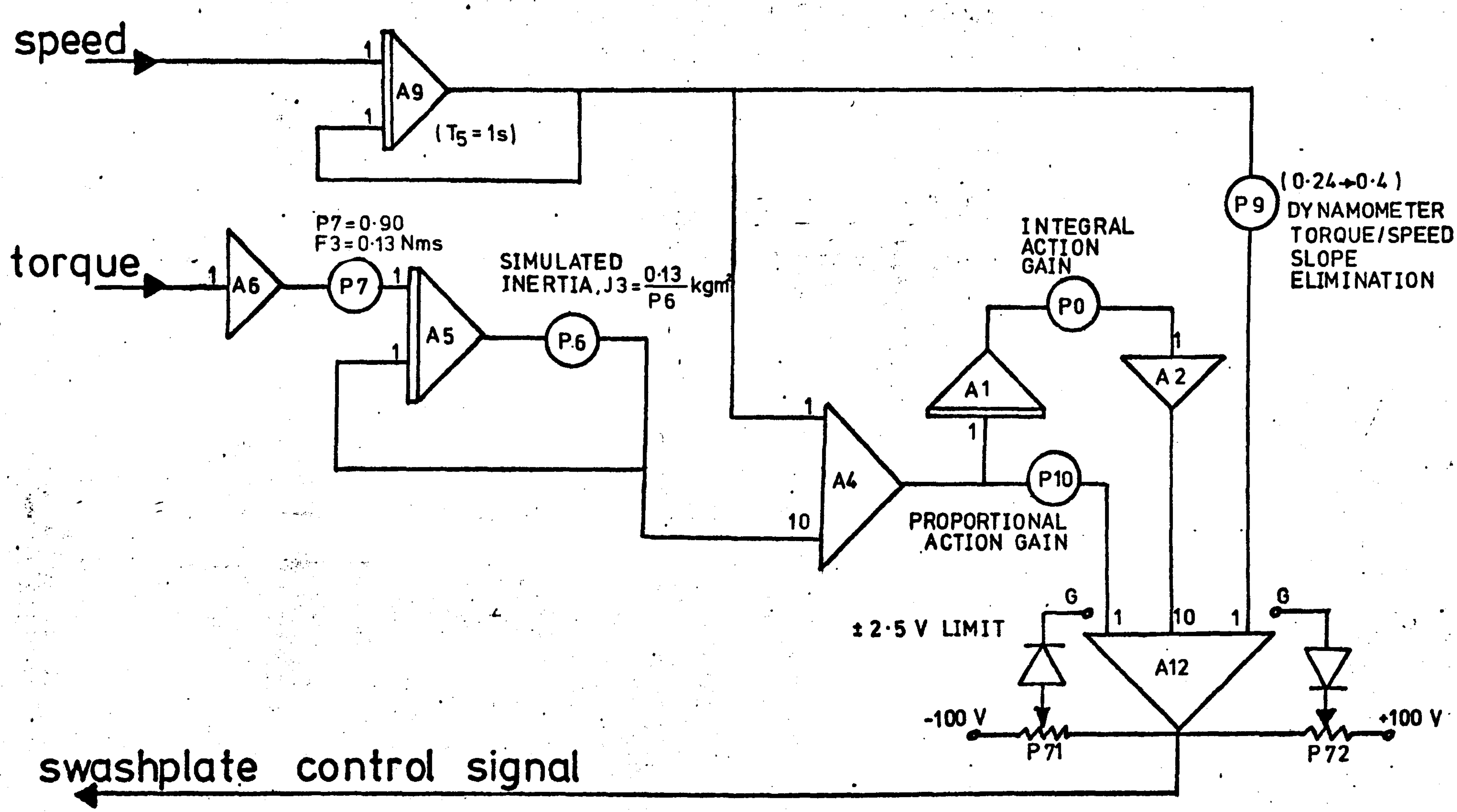

Figure 2.10 analogue computer circuit diagram (speed reference control)

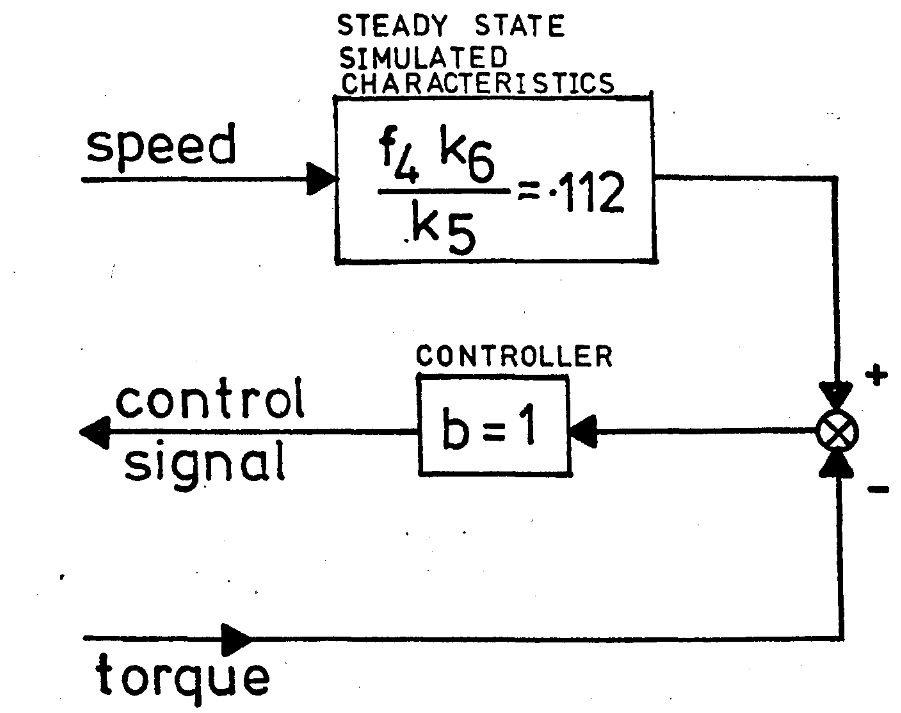

(a) steady state gain
(torque reference system)

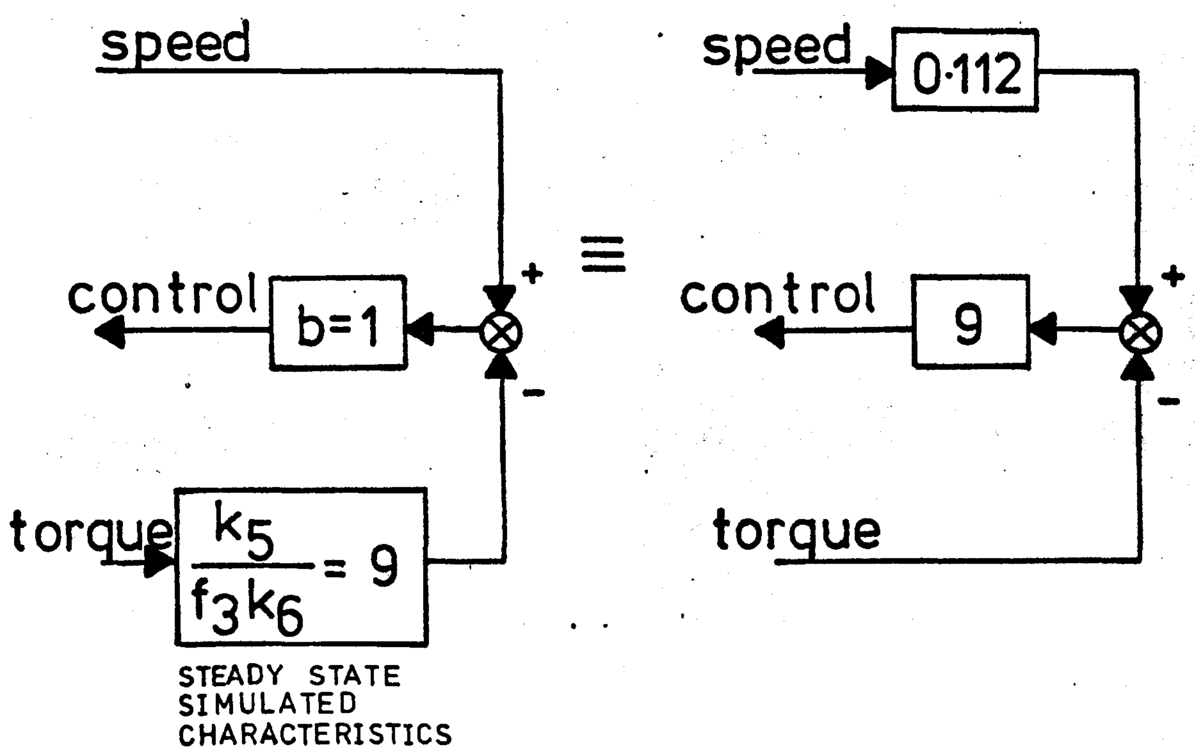

(b) steady state gain
(speed reference system)

Figure 2.11

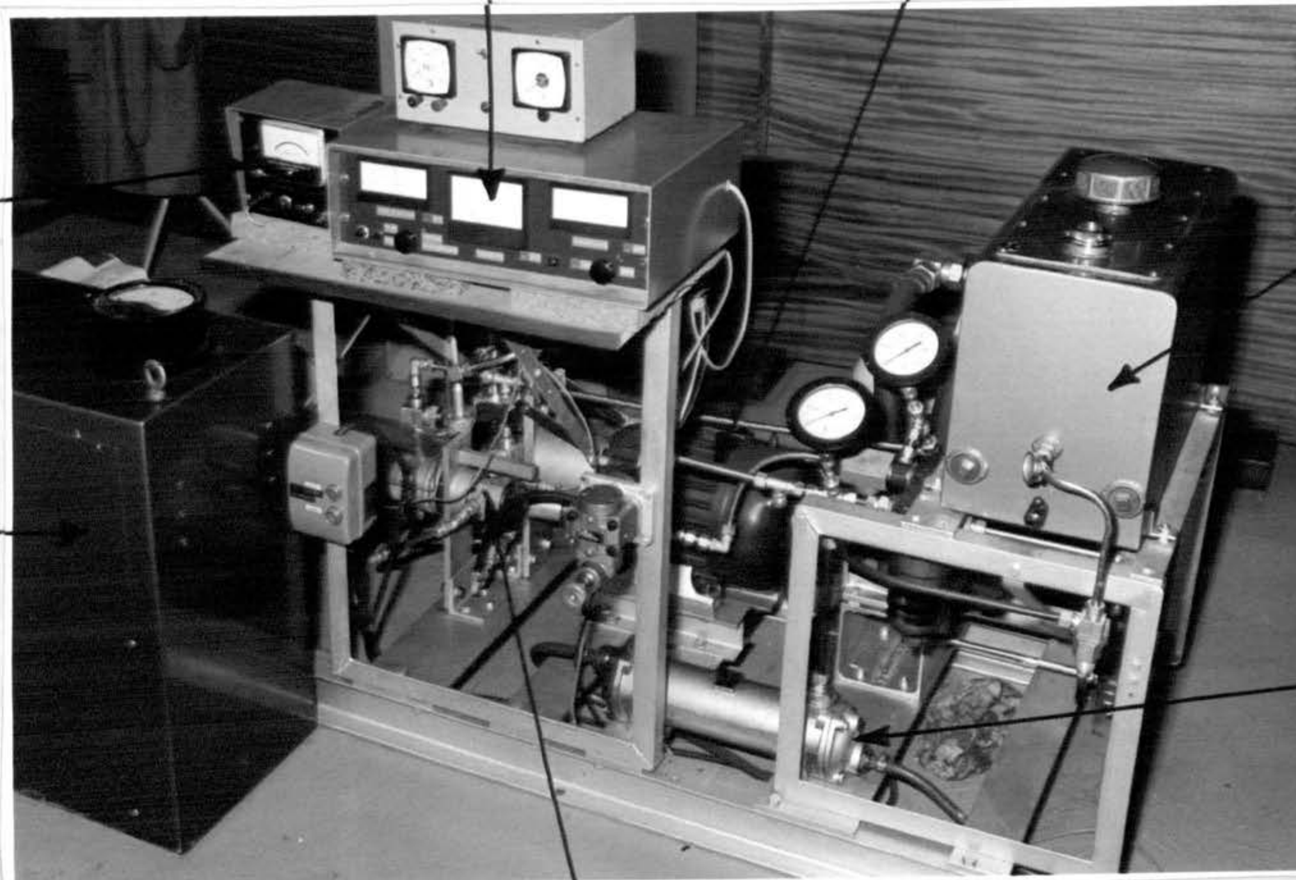

PLATE 2.1 Low power system (front view)

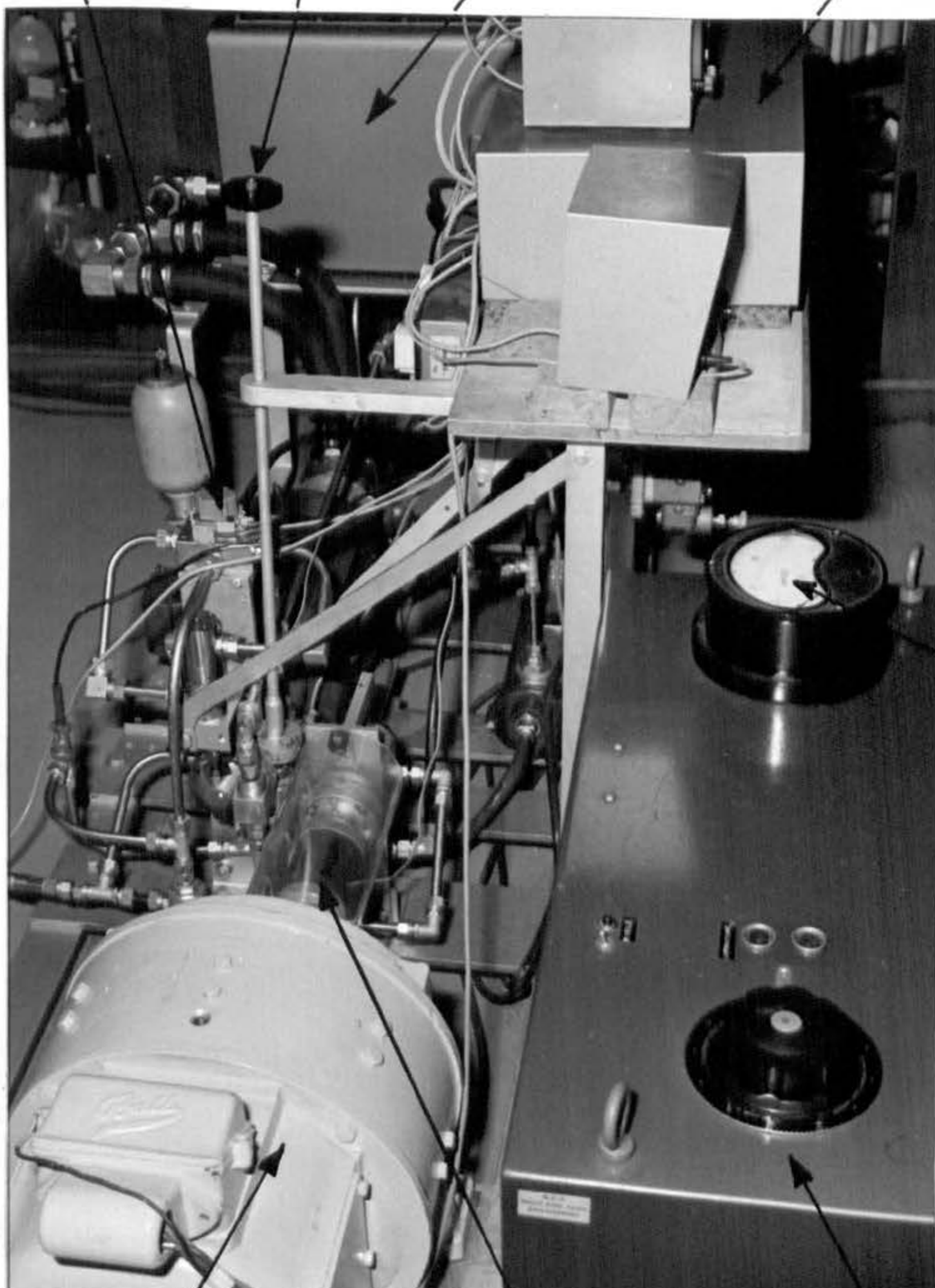

PLATE 2.2 Low power system (side view)

PLATE 2.3 Low power system manifold

PART 3

DIESEL ENGINE SYSTEMS

3.1 Introduction

The purpose of this section is to apply the method of analysis introduced in Part 1 to a 71.6 kW Ford diesel engine (Model 2402E) using ~~three~~ two types of dynamometer system for each of the methods of load simulation discussed in section 1.2. The results of the analysis will be used as a basis for the control system of an engine test cell (which is introduced in Part 7) using the Ford diesel engine and two versions of hydraulic dynamometer (for comparison). One version of the hydraulic dynamometers is based on a hydrostatic transmission system of the type used in Part 2. The other version is based on a unique electrohydraulic valve which is of simple construction and has a much faster speed of response than the hydrostatic system. The analyses and development of the valve is undertaken in Part 6.

It should be noted that for basic method (1) the root locus will be used to determine the effect of various system parameters upon the stability only, and not to determine the dominant mode of response to step inputs, as required for basic method (2).

3.2 Hydrostatic Dynamometer

3.2.1 Transfer Characteristics of Engine and Dynamometer

The block diagram for the diesel engine and hydrostatic dynamometer combination is shown in Fig. 3.1. This is obtained from a combination of Fig. 1.7 (diesel engine), Fig. 1.10 (hydrostatic dynamometer) and Fig. 1.12 (flexible coupling). For the purposes of analysis, manufacturers' data will be used where available, otherwise estimates will be made in the determination of the system coefficients.

Diesel Engine Data (supplied by the Ford Motor Company Ltd.):-

Inertia of rotating and reciprocating parts

$J_1 = 0.38$ kg m^2

Prime mover torque/speed characteristic slope (from graph G2)

K_1 (low speed) = +0.122 Nms

K_1 (medium speed) = 0

K_1 (high speed) = -0.154 Nms

Under the motoring condition K_1 is estimated by assuming a friction coefficient of half maximum torque at maximum speed, to give

K_1 (motoring) = -0.265 Nms

Pure time delay

T_1 (low speed) = .0333 s (600 rev/min)

T_1 (medium speed) = .0133 s (1500 rev/min)

T_1 (high speed) = .00667 s (3000 rev/min)

Governor Data (High Speed Minimec Governor):-

Loading:-

K_8 (low speed) = 13.2 Nms

K_8 (medium speed) = 7.4 Nms

K_8 (high speed) = 10.3 Nms

Motoring:-

$K_8 = 0$

Governor time constant (manufacturers' data available for 4 cylinder pump unit only, see graph G4)

T_4 (low speed) = 0.5 s)
)
T_4 (medium speed) = 0.07 s) Estimated values
)
T_4 (high speed) = 0.01 s)

Input Actuator:-

From Fig. 1.7 the input actuator gain (K) may be taken to give maximum prime mover speed (3600 rev/min) for maximum input signal (assumed 10 v), i.e., K = 37.7 r/s/v. Transferring this value to the generalised block diagram shown in Fig. 3.1, the prime mover input gain becomes K_7 (= K x K_8).

Hence K_7 (loading condition) becomes

K_7 (low speed) = 498 Nm/v

K_7 (medium speed) = 279 Nm/v

K_7 (high speed) = 388 Nm/v

K_7 (motoring condition) = 0

Hydrostatic Units (data supplied by Lucas Ltd.):-

Inertia of rotating parts of primary hydrostatic unit = 0.02 kg m^2

Also inertia of flexible coupling = .089 kg m^2

$\therefore J_2 = 0.109$ kg m^2

Input actuator frequency response characteristics (see graph G5)÷

Using 90^o phase shift point for second order approximation

$\omega_n \simeq 3.2$ Hz (20 r/s)

$\zeta \simeq 0.7$ (i.e., let $J_9 = .001$; $F_9 = .028$; $K_9 = 0.4$)

Leakage coefficient (obtained from manufacturers' performance characteristics for pump and motor at 50^o C)

K_L (low speed) = 0.057 litres/min/bar

K_L (medium speed) = 0.066 litres/min/bar

K_L (high speed) = 0.091 litres/min/bar

Oil volume on loading side of loop

= 0.15 litres (estimated)

∴ time constant under loading condition

(from equation (6))

T_3 (low speed) = 0.023 s

T_3 (medium speed) = 0.02 s

T_3 (high speed) = 0.015 s

Whereas oil volume on motoring side

= 0.6 litres (estimated)

∴ time constant under motoring condition

T_3 (low speed) = 0.092 s

T_3 (medium speed) = 0.08 s

T_3 (high speed) = 0.06 s

Flow capacity of primary hydrostatic unit

= 0.649 litres/min/r/s

Pressure/torque relationship of primary hydrostatic unit under loading condition (from pump characteristics)

= 1.15 Nm/bar

Pressure/torque relationship of primary hydrostatic unit under motoring condition (from motor characteristics)

= .97 Nm/bar

Hence, the dynamometer torque/speed characteristic slope (K_3) under the loading condition is obtained

from $\frac{1}{K_L} \times 1.15 \times 0.649$

$\therefore$ K_3 (low speed) = 13.09 Nm s

K_3 (medium speed) = 11.31 Nm s

K_3 (high speed) = 8.20 Nm s

and under the motoring condition

$$K_3 = \frac{1}{K_L} \times 0.97 \times 0.649$$

$\therefore$ K_3 (low speed) = 11.04 Nm s

K_3 (medium speed) = 9.54 Nm s

K_3 (high speed) = 6.92 Nm s

Assuming maximum displacement of the secondary unit swashplate will be obtained with a 10 volt signal and that the secondary unit speed remains constant at 2800 rev/min under all conditions, then the dynamometer input coefficient (K_4) becomes

$$\frac{68 \times 2.8 \times 1.15}{10 \times K_L}$$ Nm/volt under the loading condition

Hence

K_4 (low speed) = 384 Nm/volt (loading)

K_4 (medium speed) = 332 Nm/volt (loading)

K_4 (high speed) = 241 Nm/volt (loading)

And under the motoring condition

$$K_4 = \frac{68 \times 2.8 \times 0.97}{10 \times K_L}$$

Hence

K_4 (low speed) = 324 Nm/volt (motoring)

K_4 (medium speed) = 280 Nm/volt (motoring)

K_4 (high speed) = 203 Nm/volt (motoring)

Flexible Coupling Data (supplied by J. H. Fenner Ltd.)

Inertia = .089 kg m^2

K_2 = 3438 Nm/radian

Typical dynamic magnification at resonance = 7

$\therefore \zeta = \frac{1}{2 \times 7} = 0.071$ (second order approximation)

With $J_8 = J_2$ already determined at 0.109 kg m^2

then $F_2 = 2 \times \zeta \times \sqrt{Jd \times K}$

$= 2.749$ Nm s

Torque transducer + amplifier

K_6 = .00667 V/Nm (negligible time constant)

Speed transducer + amplifier

K_5 = .00637 V/r/s

$T_5 \approx 1$ second

Using these values it was decided to initially determine the root positions of the mechanical and hydraulic system with no external feedback loops, as shown in the block diagram of Fig. 3.1. The reason for this course of action was to discover the dynamic characteristics of the basic hydro-mechanical system in order to determine the effect of the flexible coupling and other parameters upon the basic system response. The root locus for this system is shown in graph G33, from which it can be seen that under the loading condition the system is basically third order, all other roots being made negligible by zero cancellation. This includes the roots due to the flexible coupling (approximately $14 \pm J200$), for which the natural frequency (32 Hz) is well above the dynamometer cut off frequency ($1/T3 = 1.7$ Hz at low speed).

However, it can be seen that for the low to medium speed range under the motoring condition there exist low frequency second order poles with low damping ($\zeta \simeq 0.33$, $\omega_n \triangleq 15$ r/s). By eliminating each of the feedback values in turn, it was discovered that these low frequency poles were due to the steep dynamometer torque/speed characteristic, as shown in Fig. 3.2. From equation (8) of Fig. 3.2 the damping of the second order roots could be improved by either reducing the time constant of the hydrostatic loop by a factor of, say, 10, or reducing the dynamometer torque/speed characteristic slope by the same factor.

In fact, if the leakage rate of the hydrostatic system is increased by a factor of 3, it can be seen that this should increase the damping ratio by the same factor without affecting the undamped natural frequency (since $T3 \propto 1/K_L$ and $K3 \propto 1/K_L$ from equation (6)). It is of interest to note that for the low power hydrostatic system analysed in Part 2 the leakage rate is high since the hydrostatic units are operated at the low efficiency end of their speed range. With the present system, however, the prime mover speed range

(600-3600 rev/min) coincides with the maximum efficiency range of the hydrostatic units, so that the leakage rate is low. Hence, to avoid the oscillatory low frequency poles imposing their effect upon the load simulator response, it is necessary to increase the leakage rate from the motoring side of the hydrostatic system.

The characteristics of the hydrostatic units were given for an oil temperature of 50° C (viscosity = 21 c.s.). Consequently, at an oil temperature of 20° C the viscosity will be approximately a factor of 4 greater from Shell viscosity charts, and it is assumed this will reduce the leakage coefficient by the same factor. Under the loading condition, using the root locus method, this was found to give highly oscillatory second order roots ($\zeta = 0.15$, $\omega_n = 34.9$ r/s) and under the motoring condition the roots became even more oscillatory ($\zeta = 0.12$, $\omega_n = 15.8$ r/s). To increase the damping by a factor of 6 at this temperature it is necessary to increase the leakage on both sides of the hydrostatic loop by 0.07 litres/min/bar (at 20° C). This is easily achieved in practice by connecting each side of the hydrostatic loop to exhaust with given lengths of small bore pipe, as will be shown in Part 7.

The introduction of this extra leakage path greatly reduces the effect of speed upon the dynamometer characteristics, enabling average values for T3, K3 and K4 to be chosen. Using these new values a root locus was constructed for the basic system with no external feedback, as shown in graph G34(a) and (b). Although the motoring condition is greatly improved, it can be seen that very low frequency secondary roots with low damping occur for the low to medium speed range under the loading condition. This is due to the influence of the governor upon the system, the effect of which becomes greater for the lower torque/speed characteristic of the dynamometer.

To determine the most suitable increase in leakage from the system under the loading condition the roots of the system were examined for a wide range of leakage values at the three ranges of speed. A value of 0.03 litres/min/bar above the normal leakage rate of the hydrostatic system gave the best response over the speed range, as shown in graph G34(c). The greatest improvement in the performance of the basic system would be obtained if the leakage rate could be made to vary with speed, since such a system could be tuned to eliminate oscillatory second order roots. Although this adds to the complexity of the hydrostatic system (and will not be examined further), the principle of operation of the fast response dynamometer, introduced in section 3.3, is based upon the control of the leakage rate of a hydraulic system.

The new leakage coefficients at 50° C become:-

Loading: K_L (low speed) = 0.087 litres/min/bar
K_L (medium speed) = 0.096 litres/min/bar
K_L (high speed) = 0.121 litres/min/bar

Motoring: K_L (low speed) = 0.34 litres/min/bar
K_L (medium speed) = 0.35 litres/min/bar
K_L (high speed) = 0.37 litres/min/bar

These coefficients result in new values for T3, K3 and K4 as shown:-

Loading:

Low speed T3 = .0150 s; K3 = 8.57 Nm s; K4 = 252 Nm/V
Medium speed T3 = .0138 s; K3 = 7.77 Nm s; K4 = 228 Nm/V
High speed T3 = .0109 s; K3 = 6.17 Nm s; K4 = 181 Nm/V

Motoring:

(Average values throughout speed range used due to small change in leakage coefficient)

T3 = 0.015 s; K3 = 1.78 Nm s; K4 = 52.7 Nm/V

3.2.2 Simulation Method 1.1 Torque control by dynamometer Speed control by prime mover

The effect of closing the speed and torque loops to provide simulation method 1.1, as shown in Fig. 1.14, was initially determined using proportional gain control for these loops (i.e., A = C = D = F = 0). For a gain of 1 v/v on the speed control signal (E) a root locus was constructed for a range of torque control signal gain (B), as shown in graph G35. This indicates that a suitable response may be obtained with a value of B = 0.3 v/v over both the low and high speed range of the system. In general, the roots obtained for the medium speed range were found to be close to those for the low speed range and are therefore not shown. Using the value B = 0.3 v/v a further root locus was constructed for a range of speed control signal gain (E), as shown in graph G36. It can be seen that very much higher gains are possible for this control signal than for the torque control signal (probably due to the fast torque response of the system compared to the slower speed response). However, high values of control signal gain also amplify noise effects from the speed transducer (as discussed in section 2.3.1), so that it was decided to use a value of E = 10 v/v.

Using these values of proportional gain for the torque and speed control loops the possible magnitude of steady state errors in speed and torque were examined. The steady state block diagram for the speed control loop is shown in Fig. 3.3, from which it may be seen that the effect of torque changes upon the speed error is small (70 rev/min at 200 Nm). However, a very large value of proportional gain is required to keep the speed error small and a gain of E = 10 v/v results in a speed error of 29% throughout the speed range. Since the gain cannot be increased (due to the effect upon the dynamic response as shown in graph G36), it is necessary to introduce integral action to eliminate steady state errors (or increase the gain of the required speed signal by 29% if steady state accuracy is not of prime importance).

The steady state torque control loop is shown in the block diagram of Fig. 3.4. In this case the effect of speed upon the torque error is very much greater than the effect of the torque control signal. For example, with a required torque signal of 2 volts (maximum) the torque T_a becomes 100 Nm, whereas this value may be achieved by T_b with a speed of only 168 rev/min. This means that at the engine idling speed (600 rev/min) a required torque signal of 7.14 volts (equivalent to a required torque of over 1000 Nm) will just be sufficient to zero the speed dependent torque T_b. To overcome this effect it is once again necessary to introduce integral action or use a dynamometer torque/speed characteristic elimination signal, as discussed in section 2.3. However, since the dynamometer torque/speed characteristic is non-linear (under the loading condition) it is necessary for the elimination signal to be non-linear, so that the introduction of integral action provides a simpler solution for this method of load simulation.

Root loci were constructed for a range of integral action gain for both the torque and speed control signals, as shown in graphs G37 and G38 respectively. It can be seen that the maximum integral action gain consistent with an adequately damped response is 1 s^{-1} for the torque control signal and 10 s^{-1} for the speed control signal. On examination of the motoring characteristic using these controller values the roots were found to be adequately damped, but there existed a pole close to the origin. It was discovered that this pole had negligible effect due to the presence of a zero in close proximity and that as the integral action (C) was reduced zero cancellation occurred (in the same manner as shown in section 2.3). As the integral action was increased, the zero moved towards a higher valued real pole, leaving the pole due to the integral action with a time constant of approximately 2 s, but also creating low frequency roots with low damping. A value of C = 10 s^{-1} was found to give a well damped response, so that to keep the torque error small it is possible to increase the integral action gain to this value when changing from the loading to the motoring condition.

To determine whether three term control could improve the damping to allow higher values of proportional plus integral gain, the root positions were investigated for a wide range of controller coefficients for both the torque and speed control signals. For each range of values investigated the introduction of derivative control action was found to actually reduce the damping of the system, resulting in instability for large values of derivative action on both the speed and torque control signals.

Using the suggested values of controller coefficients, other system parameters were investigated as follows:-

(a) Governor Lag (T4). Since the values used in the analysis were only estimates (based on manufacturers' data for a similar unit), it is necessary to assume a large margin of error for these values. It was discovered (using the root locus method) that at low speed for a governor lag greater than 1.0 s the system had low frequency oscillatory roots which became unstable for a lag greater than 2.0 s (whereas a faster response than the nominal value (0.5 s) improved the damping). At high speed it was discovered that variations of a factor of 10 either side of the nominal value (T4 = 0.01 s) had negligible effect upon the root positions.

(b) Governor Rating (K8). The data supplied by the manufacturer was for the same model of governor and fuel injection system as used on the Ford engine and the values provided should therefore be reasonably accurate. It was found that at low speed a reduction in K8 below 10 Nm s resulted in oscillatory low frequency roots which became unstable for K8 lower than 1 Nm s. Higher values of K8 (above 20 Nm s) were also found to create oscillatory low frequency roots. At high speed a factor of two change either side of the nominal value had little effect upon the low frequency roots, although reducing K8 increased the damping of the high frequency roots (which would have little effect upon the system performance).

(c) Hydrostatic Loop Lag (T3). At low speed an increase in the hydrostatic loop lag created oscillatory low frequency roots, whereas reducing T3 to 1 ms had little effect upon the low frequency roots. At high speed a range of T3 from 1 → 100 ms had little effect upon the root positions and this was also found to be the case for the motoring condition. Thus a large margin of error is permissible in the estimation of the hydrostatic loop lag under most running conditions, except that a large under-estimate may cause oscillatory secondary roots at low speed under the loading condition.

(d) Speed Transducer Lag (T5). At low speed increasing T5 above 5 s created very low frequency oscillatory roots and reducing T5 below 0.5 s created low frequency roots with low damping (although the system remained stable for T5 as low as zero). At high speed increasing T5 above 5.0 s also created very low frequency oscillatory roots, although there were no unstable roots for T5 as high as 100 s. Reducing T5 created high frequency oscillatory roots with very low damping for T5 < 0.1 s. Thus, for this method of load simulation, the speed transducer lag must be kept within the range 0.5 → 5.0 s to avoid creating oscillatory roots.

(e) Prime Mover Pure Time Delay (T1). Due to the difficulty of obtaining a good mathematical model to describe the time delay for the combustion phases to achieve a change in torque level, it was decided to use a first order approximation (1 - T1s) where T1 is the time between firing cycles. To determine possible effects of inaccuracies in this approximation T1 was varied from 30% to 300% of the nominal value at low and high speeds. It was found that higher values of T1 created low frequency roots with low damping at the low speed range, whereas lower values of T1 had negligible effect throughout the speed range.

(f) Prime Mover Inertia (J1). The effect of changes in the prime mover inertia by a factor of 0.2 to 5 times the nominal value was found to have negligible effect at high speed, although higher values of inertia created oscillatory low frequency roots at low speed. Under the motoring condition it was found that increasing the prime mover inertia had the effect of increasing the magnitude and time lag of the speed/torque response, whereas low values of inertia increased the frequency of the flexible coupling roots.

(g) Dynamometer Inertia (J2). At low speed values of dynamometer inertia above 0.5 kg m^2 created low frequency oscillatory roots, whereas reducing the inertia had negligible effect (except to move the flexible coupling roots to higher frequencies). At high speed the effect of this range of inertia was negligible (except, once again, low values moved the flexible coupling roots to high frequencies). Under the motoring condition both large and small values of dynamometer inertia had little effect upon the root positions.

(h) Dynamometer Actuator Lag $\left(\frac{K9}{J9s^2 + F9s + K9}\right)$. By simultaneously varying K9 and J9 it is possible to vary the response time of the dynamometer actuator lag without affecting the damping. A range of response times from 30% to 500% of the nominal value was found to cause no oscillatory roots over the speed range for both the loading and motoring conditions. Below 30%, however, low frequency oscillatory roots were created at low speed under the loading condition and under the motoring condition.

(i) Prime Mover Actuator Lag (T6). Faster response times for the prime mover actuator were found to have negligible effect on the root positions over the speed range. Increasing the lag above 0.1 s, however, created low frequency roots with low damping which became highly oscillatory for T6 > 1.0 s at both low and high speeds.

It can be seen, therefore, that a wide margin of error is permissible in the estimation of each of the system parameters as long as each error does not have a cumulative effect on the root positions of the system. It has been shown that to ensure stability a relatively low gain is required on the torque control loop compared to the speed control, which may create a large dynamic torque error. In particular, it has been shown that under the motoring condition, with a high value of integral action gain on the torque control signal, the system has a speed/torque dynamic lag of approximately 2 seconds. To determine whether any improvement may be obtained in these dynamic effects, simulation method 1.2 is examined in the following section.

3.2.3 Simulation Method 1.2 Speed control by dynamometer Torque control by prime mover

As with simulation method 1.1, it was decided to initially determine the root positions using proportional action on the torque and speed control loops. The root loci for a range of prime mover input gain (E) and dynamometer input gain (B) are shown for the loading condition in graph G39. For this method of load simulation the prime mover input gain (torque control) is much smaller and the dynamometer input gain (speed control) much larger for stability, compared to simulation method 1.1. Thus, regardless of whether the torque control is on the prime mover or on the dynamometer, the gain must be low in comparison to the speed control gain for load simulation method (1) (with this particular prime mover and dynamometer system). From graph G39 the most suitable values of proportional control are B = 5 v/v and E = 0.3 v/v, so that integral action is necessary for the same reasons discussed in section 3.2.2 (i.e., to eliminate steady state errors, and to avoid the use of a non-linear signal to eliminate the dynamometer torque/speed characteristic). Values of dynamometer integral action C = 10 s^{-1} and prime mover integral action F = 0.3 s^{-1} were found to give adequately damped roots over the speed range, as shown in graph G40. Under the motoring condition, however, values of dynamometer proportional action B = 10 v/v and integral action C = 10 s^{-1} were found to give a faster response with increased damping (also shown in graph G40). It should be noted that the prime mover controller settings have no effect when running under the motoring condition, since the prime mover input is assumed to be zero. If the prime mover input is not zero and negative torque is applied (i.e., the prime mover is partially motored), then the analysis under the loading condition is more appropriate.

By comparing graph G38 to graph G40 it can be seen that for this particular prime mover and dynamometer system method 1.1 results in a faster dominant response than method 1.2 with the fuel control rod between its minimum and maximum setting under the loading condition.

Due to the high gain of the governor system, however, it is clear that a small change in the required engine speed signal ($>$200 rev/min) will cause the control rod of the fuel injection system to be moved to its maximum extent. The system will remain in this condition until the actual engine speed is of the same order ($\pm$ 200 rev/min approximately) as the required speed signal. This means that under normal transient conditions the control rod will be in either its maximum or minimum condition. Thus, under these conditions, the system can be analysed as being in a saturated state by setting the prime mover controller coefficients to zero as well as the governor rating K8.

A root locus was performed under these conditions for both methods 1.1 and 1.2, as shown in graph G41. The effect of saturation of the control rod movement for method 1.1 at low speed is to cause the system to have a single unstable pole. This is in agreement with the discussion on prime movers in section 1.1.1, which shows that torque control of a prime mover operating over the left-hand side of its torque/speed characteristic results in unstable operation if there is no speed feedback signal in the system. For this system the dynamometer provides feedback through its torque/speed characteristic, but this feedback is overcome by the use of integral action on the torque control signal (in fact, elimination of the integral action was found to eliminate the non-linear root).

This instability is not a serious problem, however, since it occurs only as the prime mover speed is increasing from a low value under load. As soon as the required speed is reached the control rod is no longer in a saturated position and the system is stable. Graph G41 also shows that this unstable region does not occur using load simulation method 1.2, which is to be expected, since the system is basically operating as a speed controller of a friction and inertial load under these conditions. The unstable root for method 1.1, however, shows that it is not possible to simulate steady state maximum torque conditions with this method over the low to medium speed range. Also, under the motoring condition, the dominant response for method 1.2 was found to be much faster than method 1.1 (indicating lower dynamic errors). Hence, for the diesel engine and hydrostatic dynamometer system, the use of method 1.2 (torque control on engine, speed control on dynamometer) provides superior performance compared to method 1.1 (speed control on engine, torque control on dynamometer).

To determine whether any improvement in performance could be achieved with method 1.2 using three term control, the roots were examined for a wide range of controller coefficients for both the prime mover and dynamometer inputs. For this range of coefficients it was found that the use of derivative action created no general improvement in the root positions and normally caused a reduction in the damping of at least one pair of second order roots for both the loading and motoring conditions. The effect of variations in system parameters upon the root positions was found to be the same as for method 1.1, except for the following coefficients:-

(a) Governor Lag (T4). The second order roots were found to have greater damping at low speed for higher values of T4 using simulation method 1.2. The roots became oscillatory for $T4 > 5$ s and unstable for $T4 > 10$ s.

(b) Governor Rating (K8). The roots, once again, were found to have much greater damping at low speed for a range of K8 from $0 \rightarrow 50$ Nm s, with oscillatory second order roots being created above this value.

Hence method 1.2 is less affected by variations in the governor system than method 1.1. This result is of importance, since the governor system has already been shown to be highly non-linear with low repeatability between test runs.

(c) Speed Transducer Lag (T5). At low speed T5 could be as high as 10 s before creating oscillatory roots, whereas the roots became oscillatory for T5 > 2 at high speed. Under the motoring condition low frequency oscillatory roots were created for T5 < .5 s, and for T5 > 5 s oscillatory roots of very low frequency (< .1 Hz) resulted.

(d) Prime Mover Inertia (J1). Under the motoring condition there was no increase in the speed/torque response time lag for large values of J1 (as there was with method 1.1), although oscillatory roots occurred for J1 > 1 kg m^2.

(e) Dynamometer Inertia (J2). Increasing J2 was found to reduce the damping of the flexible coupling roots throughout the speed range for both the loading and motoring conditions. These roots were found to go unstable with J2 increased to only 0.3 kg m^2 at high speed under the loading condition.

(f) Dynamometer Actuator Lag $\left(\dfrac{K9}{J9s^2 + F9s + K9}\right)$.

Reducing the undamped natural frequency of this lag to less than 30% of the nominal value was found to introduce oscillatory low frequency roots (0.4 Hz) throughout the speed range for both the loading and motoring conditions.

It has been shown that good performance is possible with the diesel engine and hydrostatic dynamometer system using proportional plus integral action for both control loops, together with simulation method 1.2. The analysis for simulation methods 2.1 and 2.2 with this system is given in the following two sections.

3.2.4 Simulation Method 2.1 (Torque Reference System)

For this method of load simulation it is necessary to investigate not only the stability of the system (as in methods 1.1 and 1.2), but also the dominant response time constant and the effect of secondary roots (as in the low power system analysed in section 2.3). The approach will be to determine the controller coefficients for the dynamometer control loop which produce the best fit to the required load conditions on the prime mover. The best fit will be measured in terms of a comparison between the dominant speed response time constants of the prime mover under real and simulated loading conditions resulting from a step change in torque. The dominant time constant under real loading conditions will be obtained from equation (5) page 9 and for simulated loading conditions the dominant time constant will be obtained from an examination of the root positions (of the load simulation system) on the complex frequency plane.

The dynamometer controller coefficients are chosen to give the best fit over the speed range of the engine (under both loading and motoring conditions) with the prime mover controller coefficients set to zero. This is necessary since the speed control system on the prime mover input is not present under real loading conditions. Under simulated loading conditions, however, the speed control system is necessary to enable speed/time curves to be followed, and this extra loop will change the dynamics of the load simulation system. (In just the same way as the dynamic response of a vehicle would change if the extra speed control was added to it.)

Consequently the best fit to actual loading conditions must be obtained with the prime mover controller coefficients set to zero to eliminate the speed control loop. When suitable coefficients for the dynamometer input controller have been found, then the prime mover input controller coefficients may be introduced with the integral action gain set to the highest value consistent with a well damped response. In order to determine the time constants for the prime mover under real loading conditions it is necessary to determine coefficients for the load represented by the vehicle.

3.2.4.1 Vehicle Characteristics

Typical friction characteristics for a Ford A series truck were estimated from the following information:-

Air resistance = $KAV^2 \times 9.81$ (N)

where K = 0.00298

V = vehicle speed (km/hour)

A = effective frontal area = 6.6 m^2

(Including allowance for cooling fan which will not be used in test cell)

Coulomb resistance ≏ 9.81 x W x 1.1% (N)

W = vehicle mass = 5000 kg

Rolling resistance = 9.81 x W x (1.45 - 1.1)% at maximum speed

Maximum vehicle speed = 100 km/hour

Axle ratio = 5.13 : 1

Wheel coefficient = 429 revolutions/km

Transmission efficiency ≏ (100 - gear ratio x axle ratio)%

Gear ratios:-	1st	5 : 1
	2nd	2.44 : 1
	3rd	1.33 : 1
	4th	1 : 1

Hence in top gear 1 m/s vehicle speed = 13.83 r/s engine speed

Thus the inertia referred to the prime mover shaft becomes:-

$$
\begin{aligned}
\text{in 4th gear} &= 5000/(13.83)^2 &= 26.14 \ \text{kg m}^2 \\
\text{3rd gear} &= 26.14/(1.33)^2 &= 14.78 \ \text{kg m}^2 \\
\text{2nd gear} &= 26.14/(2.44)^2 &= 4.39 \ \text{kg m}^2 \\
\text{1st gear} &= 26.14/(5)^2 &= 1.046 \ \text{kg m}^2
\end{aligned}
$$

Using the values for wind resistance, rolling resistance and coulomb friction, together with the transmission efficiency estimation, a graph was plotted of the vehicle friction characteristics for each gear setting, as shown in graph G42. For each gear setting and range of speed (low, medium and high) the friction characteristics may be approximated by a viscous friction term as shown:-

Engine Speed (rev/min)		600	1500	3000
Gear Setting	Friction Characteristic F4 (Nm s)			
1		0.025	0.025	0.05
2		0.06	0.06	0.1
3		0.09	0.21	0.395
4		0.178	0.395	0.66

The speed response of the vehicle to a step change in torque can be obtained from equation (5) Page 9 with the injection pump control rod in one of three states. With the control rod at the minimum fuel delivery position (for the motoring condition) the speed/torque response becomes first order, the time constant for which may be obtained from equation (5) (by setting T1 = K8 = T4 = 0 and K1 = -0.256, i.e., the engine friction characteristic):-

Engine Speed (rev/min)		600	1500	3000
	1st	5.04	5.04	4.63
Time	2nd	15.1	15.1	13.38
Constant (s)	3rd	43.8	32.5	23.3
	4th	61.1	40.7	28.9

With the control rod in the central region the speed/torque response becomes second order (although the dominant response is first order over the higher speed range):-

Engine Speed (rev/min)		600	1500	3000
Time Constant of Dominant Response where appropriate (s)	1st	ω_n 4.3 r/s; ζ 0.164	ω_n 8.6 r/s; ζ .78	.121
	2nd	ω_n 2.3 r/s; ζ .39	.547	.438
	3rd	ω_n 1.3 r/s; ζ .74	1.91	1.38
	4th	ω_n 1 r/s; ζ .99	3.32	2.37

The speed response is shown to be highly oscillatory at low speed and in low gear. However, it should be realised that the governor rating is high, so that in first gear the maximum amplitude of oscillations would be less than ± 0.8 km/hour. The time constants of the speed response are also shown to be very fast (for a 5000 kg vehicle), but these values are only obtained when the fuel pump control rod is between the maximum and minimum settings. If an increase in engine speed of more than 200 rev/min is required, then the control rod moves to the maximum fuel delivery position, so that the response becomes first order (obtained by setting K8 = T4 = 0 in equation (5)) with time constants as shown:-

Engine Speed (rev/min)		600	1500	3000
	1st	-14.7	57	6.99
Time	2nd	-77	79.5	18.8
Constant (s)	3rd	-473.9	72.2	27.6
	4th	+473.6	67.1	32.6

At low speed and in low gear the speed response is unstable for the same reasons discussed in section 1.1.1 and 3.2.3 (i.e., that the negative feedback of the load is not large enough to overcome the positive feedback created by the prime mover operating over the left-hand side of its torque/speed characteristic). Also, at low speed, the time constants for the speed response are seen to be very large (indicating a very slow response). However, from equation (5) the steady state magnitude becomes 1/(K4 - K1), which therefore increases with the time constant. Hence, under this unstable condition, the prime mover accelerates at its maximum rate until either the required speed value is reached (when the control rod moves back from maximum position and therefore stabilises the response) or the right-hand side of the prime mover torque/speed characteristic is reached (which, once again, results in stable operation).

3.2.4.2 Analysis

Initial investigations were made to determine the most suitable values for the dynamometer controller with the system running at high speed, fuel delivery at maximum, and loading conditions for 4th gear being simulated. These conditions were chosen since a vehicle of the type being simulated will normally be in 4th gear for a greater length of time than any other gear. Also, the maximum fuel delivery condition was used (i.e., control rod saturated), since the initial analysis indicated that this caused the load simulation to be less stable (due to very low frequency oscillatory roots) than under normal fuel delivery conditions. A root locus was constructed for a range of proportional and integral gain, as shown in graph G43. The effect of derivative action was also investigated for a wide range of controller coefficients, but was not found to give any improvement in root positions. (In general, derivative action was found to create low frequency oscillatory roots and also caused the flexible coupling roots to go unstable at higher values.)

From graph G43 suitably stable values of controller gains may be obtained, B = 1 v/v and C = 0.3 s^{-1}. Using these values root loci were constructed for the speed range with both maximum and normal fuel delivery, as shown in graphs G44 (4th gear) and G45 (1st gear). Examination of the increased scales of these graphs shows that for each condition there are three roots with time constants greater than one second (although two of the roots become complex conjugate under maximum fuel delivery conditions). It is therefore necessary to check the positions of the system zeros in order to determine which pole has the dominant response. For the control rod in the maximum fuel delivery position examination of the system poles and zeros showed that the pole closest to the origin had a much greater magnitude of response than the other poles throughout the speed range (i.e., secondary root effects are negligible). This enabled the dominant response time constants to be evaluated for the load simulation system as shown:-

Control Rod Maximum Delivery

Speed (rev/min)		600	1500	3000
Time Constant (s)	1st	-18.8	ω_n=.036; ζ=.99	ω_n=.091; ζ = .6
	2nd	-64.3	78.1	21.3
	3rd	-401	84.4	42.1
	4th	444	91.3	58.5

Comparison with the time constants for the actual vehicle response (running with the control rod at maximum) shows that the values are of the same order with the closest agreement at low speed. At high speed in fourth gear the time constant for the simulation system is almost a factor of two higher than that of the real vehicle's response. This may be corrected by changing the calibration of the inertia coefficient on the load simulation system when these conditions are entered.

When the control rod is in a mid fuel delivery position, an examination of the system poles and zeros requires a careful evaluation to be made of the magnitude of the change in this region. For example, if the change in conditions is sufficient to cause the control rod to move to its maximum fuel delivery position, then it is possible that the response of the secondary roots may have a larger effect than the dominant root. The pole zero map for the system at high speed in fourth gear with the control rod between maximum and minimum is shown in Fig. 3.5(a) (the scales are distorted to show all root positions). Possible candidates for the dominant response to a step input are the poles marked A, B, C, D1 and D2.

The residue for each pole is equal to the zero vectors divided by all the other pole vectors on the pole zero map (including the pole due to the step input at the origin). For a real valued pole such as A the magnitude of response to the step input,

$$M_a = \left|\frac{R_a}{s + A}\right| = \frac{R_a}{A}$$

where R_a is the residue for A $\left(= \frac{\text{Zero Vectors to A}}{\text{Pole Vectors to A}}\right)$.

For a complex conjugate pole, such as D1, the magnitude becomes,

$$M_{d_1} = \left|\frac{R_{d_1}}{s^2 + 2\zeta\omega_n s + \omega_n^2}\right| = \frac{R_{d_1}}{\omega_n^2}$$

where R_{d_1} is the residue for D1

and ω_n is the distance from D1 to the origin.

The following magnitudes were obtained for each of the roots in response to a step input:-

$M_a = 1.27 \times 10^{-3}$; $M_b = 3.75 \times 10^{-4}$; $M_c = 1.4 \times 10^{-5}$;

$M_{d_1} = M_{d_2} = 1.2 \times 10^{-7}$

The responses due to D1 and D2 are seen to be negligible compared to A, B and C, so that the speed response to a step change in torque may be constructed as in Fig. 3.5(b). It is shown that in the linear region the response due to pole B has greater effect than that due to pole A and is therefore more dominant. A only becomes more dominant for very small changes in conditions. For large changes in conditions, however, the response due to pole C becomes much larger in relation to the linear region and may therefore have a more dominant response than that due to either A or B. Hence the speed response time constant of the system with the control rod between minimum and maximum will be very slow for very small changes in conditions (approximately 20 s time constant for a speed change less than 200 rev/min) and fast for large changes in conditions (less than 1 second for a change in required speed of 2000 rev/min). Using pole C as being most indicative of the type of response to expect under transient conditions, the following values were obtained:-

Control Rod between Minimum and Maximum

Speed (rev/min)		600	1500	3000
Time Constant (s)	1st	ω_n 7.38 r/s; ζ .41	.929	.93
	2nd	ω_n 7.38 r/s; ζ .41	1.47	1.28
	3rd	ω_n 7.38 r/s; ζ .41	1.5	1.28
	4th	ω_n 7.38 r/s; ζ .41	1.48	1.27

Comparison with the predicted time constants for the real vehicle response under these conditions shows that the values are of the same order, although the agreement is not as good as for the system with the control rod at maximum displacement. Since the load simulation system has been found to have a large number of poles in the region of importance on the complex frequency plane, then it may be possible to make changes in certain coefficients to move the secondary poles from the region and place a dominant pole (or complex conjugate pole pair) in the required position.

Changes in the controller coefficients were not found to improve the root positions and an examination was made of other system coefficients which may easily be varied. It was found that reducing the time constants for both the speed and acceleration signals (T5 = .1 s and T7 = .1 s) removed the low value secondary roots, leaving a dominant root close to the required position throughout the speed range for each gear setting. However, this action caused high frequency roots to go unstable and no values of controller coefficients were found to stabilise the system. It will be shown in the next section whether or not load simulation method 2.2 can improve upon the performance under these conditions.

Under the motoring condition the following dominant response time constants were obtained for the load simulation system using the same value of controller coefficients (i.e., B = 1 v/v; C = 0.3 s^{-1}):-

<u>Motoring Condition</u>

		600	1500	3000
Speed (rev/min)		600	1500	3000
Time Constant (s)	1st	ω_n .099 r/s; ζ .88	ω_n .099 r/s; ζ .88	ω_n .103 r/s; ζ .86
	2nd	23.7	23.7	21.2
	3rd	62.6	50.0	39.8
	4th	90	70	53

The values are approximately 50% higher than the time constants for the real vehicle response over the range of speed and gear settings (as well as causing a second order response in first gear instead of a first order response). No suitable values of the controller coefficients were found to cause a significant improvement in the agreement between the simulator response and the real vehicle response, so that it is necessary, once again, for the load simulation system to be calibrated under these conditions. The root locus for the motoring condition is shown in graph G46, from which it may be seen that the secondary root effect becomes greater for low gear settings. However, this will not have a significant effect upon the performance of the load simulator system since it is not usual practice to "motor" a vehicle in low gear (a vehicle is normally brought to a halt in third gear - the clutch being disengaged when the engine begins to labour).

Having shown that proportional plus integral control action on the dynamometer results in adequate load simulation (although calibration of the simulated coefficients of the load simulator is required), it is necessary to determine the coefficients for the prime mover controller in order that speed/time curves may be followed by the system (for example, to enable laboratory measurements of exhaust emission levels to be performed for a given vehicle on a given route). Since the prime mover controller coefficients only affect the performance of the system when the control rod is between minimum and maximum, then a root locus was constructed for this condition with a range of proportional plus integral action gains, as shown in graph G47. (Derivative action was found, once again, to give no improvement in the root positions for a wide range of controller coefficients.) Graph G47 shows that for the conditions chosen (low speed, 4th gear) suitable values of controller gains are $E = 1$ v/v, $F = 3\ s^{-1}$. Examination of the root positions for the other gear settings at each speed range showed an improvement in the damping of the low frequency roots as the speed is increased.

It has been shown, therefore, that method 2.1 is quite suitable for simulating real loading conditions (for this particular system), although it is necessary to calibrate the simulated load coefficients on the actual system. The effect of changes in various parameters upon the performance of the system was determined as follows:-

(a) Governor Lag (T4). At low speed increasing T4 above 2 s created very low frequency oscillatory roots, whereas reducing T4 below .05 s created high frequency oscillatory roots. At high speed increasing the lag by a factor of 10 created high frequency oscillatory roots, whereas a reduction of a factor of 10 had negligible effect. (These effects being for the fuel control rod between maximum and minimum only.)

(b) Governor Rating (K8). Throughout the speed range reducing K8 below 5 Nm s created very low frequency oscillatory roots and increasing K8 above 30 Nm s created high frequency oscillatory roots (once again for the fuel control rod between maximum and minimum settings).

(c) Hydrostatic Loop Lag (T3). Throughout the speed range and for both normal and maximum fuel delivery an increase in T3 above 0.1 s created high frequency oscillatory roots. Reducing T3 below 1 ms caused the flexible coupling roots to become more oscillatory throughout the speed range. This range of T3 had negligible effect upon the motoring condition.

(d) Speed Transducer Lag (T5). For mid fuel delivery, increasing the speed transducer time constant to above 3 s caused oscillatory roots of very low frequency ($<$.1 Hz) throughout the range of speed and gear settings. Under maximum fuel delivery conditions this increase created very low frequency oscillatory poles at high speed and reduced the magnitude of the single unstable pole at low speed in low gear. Reducing T5 below 0.1 s had negligible effect at high speed, although at low speed low frequency oscillatory poles ($\simeq$ 1 Hz) were formed under normal fuel delivery conditions, and for maximum fuel delivery the magnitude of the unstable pole increased. This range of T5 also had negligible effect upon the motoring condition (except to cause the dominant response to become first order in 1st gear for T5<.1 s).

(e) Prime Mover Pure Time Delay (T1). At low speed under mid fuel delivery conditions increasing T1 by a factor of 3 created low frequency oscillatory roots ($\simeq$ 1 Hz). Reducing T1 by a factor of 3 had negligible effect under all conditions.

(f) Prime Mover Inertia (J1). At low speed reducing J1 below 0.1 kg m^2 created low frequency oscillatory roots for mid fuel delivery, whereas increasing J1 above 2 kg m^2 created high frequency oscillatory roots (>5 Hz) for both mid and maximum fuel delivery conditions. This range of inertia had negligible effect at high speed and under the motoring condition for all gear settings.

(g) Dynamometer Inertia (J2). Increasing J2 above 2 kg m^2 caused the flexible coupling roots to become virtually unstable under all conditions except for mid fuel delivery at high speed. Reducing the dynamometer inertia below 0.01 kg m^2 only had the effect of increasing the frequency of the flexible coupling roots ($>$100 Hz) under all conditions.

(h) Dynamometer Actuator Lag $\left(\frac{K9}{J9s^2 + F9s + K9}\right)$.

Increasing the undamped natural frequency of the dynamometer actuator by a factor of 5 caused two roots to move out to high frequency (in the same manner as the flexible coupling roots, although with increased damping). At low speed, reducing the undamped natural frequency by a factor of 5 created low frequency oscillatory roots under normal fuel delivery conditions and had negligible effect under all other conditions.

(i) Prime Mover Actuator Lag (T6). Variations in the time constant for the prime mover input actuator ranging from 0.1 s to 1 ms had negligible effect throughout the speed range for all gear settings under both the loading and motoring conditions.

(j) Simulated Inertia (J4). Variations in the simulated inertia by a factor of 5 either side of the nominal for each gear setting were found to change only the dominant response time constants without affecting the secondary roots (except low values of inertia in fourth gear under normal fuel delivery conditions caused the dominant response to become second order). However, under mid fuel delivery conditions in first gear, reducing the simulated inertia was found not to reduce the dominant response time constant. This effect is due to the lag on the speed transducer as discovered on the low power system in section 2.3.1. For reasons already discussed in this section it will be necessary to calibrate the simulated inertia on the load simulation system by determining the effective inertia obtained for each setting.

(k) Simulated Friction (F4). Under normal fuel delivery conditions large variations in F4 had negligible effect upon the dynamic response (as indicated by the root locus method), although these variations will naturally affect the steady state values of torque and speed. The dynamic response is insensitive to changes in simulated friction due to the feedback effect of the governor system being much greater than that of the simulated friction effect. As soon as the governor has moved the fuel control rod to maximum or minimum displacement, however, then an increase in F4 above the value of the prime mover torque/speed characteristic (K1) will have a large effect upon the dominant response. In general, the secondary roots were not affected by variations in F4 except that in fourth gear, with maximum fuel delivery, low values of F4 created oscillatory secondary roots of very low frequency.

(l) Acceleration Lag (T7). As with the low power system described in Part 2, the most suitable value for the time constant on the simulated inertia signal was found to be proportional to the magnitude of the simulated inertia effect. Too low a value of T7 caused instability for large values of simulated inertia (i.e., in high gear), and too high a value of T7 caused the dominant response time constant to become too large to enable low values of inertia to be simulated.

(m) Prime Mover Torque/Speed Slope (K1). Under mid fuel delivery conditions large variations in K1 had negligible effect. Once again, this is due to the feedback effect of the governor which is large compared to K1. If the governor moves the fuel control rod to maximum or minimum settings, then variations in K1 have a large effect upon the dominant response with negligible effect upon the secondary roots (although oscillatory secondary roots of very low frequency occur in fourth gear under the motoring condition, as well as for maximum fuel delivery at low speed under the loading condition). In general, larger values of K1 reduced the dominant response time constant and smaller values of K1 had little effect at high speed. At low speed larger values of K1 increased the time constant of the unstable root (under maximum fuel delivery conditions) and lower values of K1 reduced the time constant.

Having shown that simulation method 2.1 gives adequate performance with few stability problems for large changes in conditions, the effect of using simulation method 2.2 will be examined in the following section.

3.2.5 Simulation Method 2.2 (Speed Reference System)

As with method 2.1, the dynamometer controller coefficients were determined for maximum fuel delivery at high speed in fourth gear, as shown in the root locus of graph G48 (prime mover inputs set to zero). Values of proportional gain, B = 20 v/v, and integral gain, C = 30 s^{-1}, were found to give a dominant root in good agreement with that obtained for the real vehicle response (in the previous section), together with very small secondary root effects. (Derivative action was, once again, not found to cause any improvement.) Using these values for all other conditions it was found that there was good agreement between real and simulated responses with negligible secondary root effects except in first gear. In first gear highly oscillatory secondary roots were created, so that it was necessary to determine new controller coefficients to improve the situation, as shown in graph G49 (low speed in first gear with maximum fuel delivery). Controller values of B = 3 v/v and C = 1 s^{-1} were found to give the best performance under all conditions in first gear, although low frequency secondary roots were created ($<$ 0.1 Hz) which will have a significant effect upon the dominant response.

To overcome this difficulty it was decided to use a proportional gain of B = 10 v/v only, and to zero the integral action. Although this created high frequency oscillatory roots ($\omega_n \simeq 3$ Hz; $\zeta \simeq 0.35$), the effect this has upon the dominant response is far smaller than that due to the low frequency roots with integral action in the system. The dominant time constants for each range of control rod setting are given as follows:-

<u>Control Rod Minimum (Motoring Condition)</u>

Speed (rev/min)		600	1500	3000
Time Constant (s)	1st	5.39	5.39	4.93
	2nd	15.4	15.4	13.7
	3rd	43.4	32.4	23.3
	4th	60.4	40.6	28.9

Control Rod Central (Mid Fuel Delivery)

Speed (rev/min)		600	1500	3000
Time Constant (s) (where applicable)	1st	1.02 (ω_n 5.24; ζ .111)	1.07 (ω_n 9.8; ζ .47)	1.05
	2nd	1.2 (ω_n 4.53; ζ .36)	1.6	1.43
	3rd	1.75 (ω_n 1.95; ζ .75)	2.86	2.27
	4th	2.45 (ω_n 1.6; ζ .77)	4.2	3.19

The second order roots shown in brackets are the secondary roots for the system which are close to the values obtained for the real vehicle response. If all the dominant root time constants shown above could be made faster by 1 second, then the responses would be much closer to the required values. The reason for the load simulation system having a minimum time constant of 1 second is due to the lag on the speed transducer (T5 = 1 s). If this lag is reduced the response of the load simulation system under normal fuel delivery conditions becomes much closer to the required response, although the secondary roots become more oscillatory. On the actual load simulation system (described in Part 7) it is initially intended to use a commercially manufactured speed transducer which is an integral part of the torque transducer unit. This speed transducer operates on a pulse counting principle (2 pulses per revolution) for which the filtering arrangement gives a rise time of 1 second. It is intended to develop a pulse counting network on the system (giving 720 pulses per revolution) which may be used to provide a speed signal with a very much faster speed of response. The use of this fast response speed transducer will be analysed in conjunction with the fast response dynamometer in the next section.

Control Rod Maximum (Maximum Fuel Delivery)

Speed (rev/min)		600	1500	3000
Time Constant (s)	1st	-14.3	56.9	7.25
	2nd	-75.1	79.4	19.3
	3rd	-470	72.2	27.9
	4th	471.4	67.1	32.7

These time constants are very close to those obtained for the real vehicle response (maximum error of 3%). Thus under all conditions it has been found that, for this particular prime mover/dynamometer system, load simulation method 2.2 provides a far superior performance compared to load simulation method 2.1. The predicted responses of the system using method 2.2 are so close to the required values that calibration of the simulated characteristics on the actual load simulator system will probably not be necessary.

The effects of the more significant secondary roots are shown in graphs G50 (1st gear) and G51 (4th gear), which indicate that high frequency torque oscillations will be present under the loading condition in first gear. Under all other conditions the secondary root effects will be negligible. Having determined the dynamometer controller coefficients it is necessary to determine values for the prime mover controller to enable speed/time curves to be followed (as with method 2.1). Graph G52 shows the effect of a range of integral and proportional gain of the prime mover for normal fuel delivery at high speed in fourth gear. Values of proportional gain, E = 10 v/v, and integral gain, F = 5 s^{-1}, were found to give adequate damping under all conditions except in first gear, for which highly oscillatory roots were obtained (becoming unstable at low speed). Hence it is necessary to change both the prime mover and dynamometer controller coefficients when the system is being used to simulate first gear loading conditions. Suitable values of the prime mover controller coefficients in first gear were found to be proportional gain, E = 1 v/v, and integral gain, F = 3 s^{-1}, which produce the root locus for a range of speed as shown in graph G53. At low speed it can be seen that low frequency roots are produced with very low damping which is also the case for the actual vehicle response at low speed in first gear with the fuel control rod between minimum and maximum (see section 3.2.4).

The major differences in the effect of variations in system parameters between load simulation methods 2.1 and 2.2 are given as follows:-

(a) Hydrostatic Loop Lag (T3). The effect of variations in T3 was the same as that obtained for method 2.1, except for under the motoring condition a reduction in T3 caused a reduction in the damping of the oscillatory secondary roots.

(b) Speed Transducer Lag (T5). Under maximum fuel delivery conditions increasing T5 to 3 seconds had little effect in first gear, although low frequency oscillatory roots were created in higher gears as well as under the motoring condition. Reducing T5 to 0.1 seconds created high frequency oscillatory roots under all conditions with the roots becoming unstable at low speed in high gear as well as for maximum fuel delivery at high speed in high gear. Also, for mid fuel delivery at high speed the dominant response became first order (as T5 was reduced) under all gear settings.

(c) Prime Mover Inertia (J1). In first gear, increasing J1 to 2 kg m^2 created high frequency oscillatory roots throughout the speed range, as well as causing the dominant response time constant to become larger under maximum fuel delivery conditions. For higher gear settings increasing J1 caused low frequency oscillatory roots for both loading and motoring conditions. Reducing J1 to 0.1 kg m^2 had little effect under all conditions throughout the speed range.

(d) Dynamometer Inertia (J2). Variations in J2 had the same effect as for method 2.1, except that increasing J2 also created low frequency oscillatory roots (as well as causing the flexible coupling roots to become virtually unstable).

(e) Dynamometer Actuator Lag $\left(\frac{K9}{J9s^2 + F9s + K9}\right)$.

Variations in the undamped natural frequency had the same effect as for method 2.1, except that reducing the undamped natural frequency by a factor of 5 also created low frequency oscillatory roots under maximum fuel delivery conditions (becoming unstable under the motoring condition).

(f) Simulated Inertia (J3). Increasing J3 increased the dominant response time of the system without affecting the secondary roots. Reducing J3 to 0.1 kg m^2, however, also created highly oscillatory secondary roots (becoming unstable in first gear). Unlike method 2.1, it is probable that calibration of this effect will not be necessary on the load simulator system due to the close correlation between the predicted and required responses.

(g) Simulated Friction (F3). A similar effect was obtained compared to method 2.1, except that no oscillatory roots were obtained in fourth gear.

(h) Prime Mover Torque/Speed Characteristic (K1). In first gear, for mid fuel delivery, increasing K1 to 1.0 Nm s created highly oscillatory low frequency roots. No oscillatory secondary roots were obtained under any other condition.

All other effects were found to be similar to those obtained for the torque reference system (method 2.1) analysed in the previous section. It has been shown, therefore, that the hydrostatic dynamometer is a suitable device for simulating automotive loads on a medium power diesel engine using a variety of simulation methods. In particular, it has been shown that for the basic load simulation method (1), the best performance is obtained using speed control on the prime mover with torque control on the dynamometer (method 1.1) for the loading condition, and changing to torque control on the prime mover with speed control on the dynamometer (method 1.2) when the motoring condition is entered. For basic load simulation method (2), it has been shown that, for this particular prime mover and dynamometer, the speed reference system (method 2.2) provides a superior performance compared to the torque reference system (method 2.1) under all conditions.

Having analysed the performance of the hydrostatic dynamometer, a unique fast response dynamometer is to be analysed (for the same conditions) in the following section to determine whether any improvement in performance can be obtained.

3.3 Fast Response Dynamometer

3.3.1 Transfer Characteristics

A full description of the design and method of operation of the fast response dynamometer is given in Part 6. The operation is similar to that of the hydrostatic system, except that the variable capacity hydrostatic unit is replaced by a unique spool valve which operates on hydrodynamic principles. The valve may be used to create the loading and motoring conditions by controlling the flow of oil on either side of the hydrostatic unit connected to the prime mover (see Fig. 6.9). This is similar to the method of operation of the hydrostatic dynamometer and, in fact, the same block diagram may be used to describe both systems (Fig. 3.1) with differences only in the following coefficients:- dynamometer torque/speed characteristic slope (K3), input actuator gain (K4) and lag ($K9/(J9s^2 + F9s + K9)$) and the dynamometer lag (T3).

Whereas, for the hydrostatic system, the value of K3 varies little with variations of the dynamometer input signal, for the fast response dynamometer the magnitude of K3 is directly proportional to the magnitude of the dynamometer input signal (and is therefore highly non-linear). In order to enable a linearised analysis to be performed, the maximum value of K3 will be used for each range of speed. This is justified by the fact that only high values of K3 create stability problems for the load simulation system.

By taking into account the leakage characteristics of the hydrostatic part of the system, it is shown, in Part 6, how the torque/speed characteristics may be determined for the fast response dynamometer. Graph G54 indicates the torque curves to be expected for each range of speed, which enable the following approximate values to be determined for maximum K3 and K4:-

	Low Speed	Medium Speed	High Speed
K3, loading, (Nm s)	3.2	1.27	0.637
K3, motoring, (Nm s)	3.2	1.27	0.298
K4, loading, (Nm/v)	20	250	500
K4, motoring, (Nm/v)	133	40	10

The dynamometer time constant may be obtained from

$T3 = \frac{V}{K_L \beta e}$, as shown in section 2.2.1.

In this case the leakage flow to determine K_L under the loading condition is equal to the flow through the special purpose valve plus the leakage flow from the hydrostatic system. Since the flow through the valve varies with the spool position, then K_L, and therefore T3, will also vary with the spool position. The largest value of the time constant T3 will occur when the spool position is such as to create maximum pressure drop across the hydrostatic unit. Since this provides the limiting value of T3, then these values will be used to enable a linearised stability analysis to be performed.

Under the motoring condition, the leakage flow to determine K_L consists of the make up flow minus the flow through the primary hydrostatic unit (proportional to the engine speed). Hence with estimated oil volumes of 0.3 litres (loading side) and 1.3 litres (motoring side) the following maximum values of T3 are obtained:-

	Low Speed	Medium Speed	High Speed
T3, loading, (s)	0.0129	0.0052	0.0026
T3, motoring, (s)	0.0087	0.0139	0.021 (max. speed)

Note: under the motoring condition the maximum pressure is limited by the power of the make up system. In this case the make up supply has a power rating of 37 kW which limits the pressure to 124 bar at low and medium speed. At maximum motoring speed (2400 rev/min) the required pressure is estimated at 73 bar.

For the input actuator a frequency response test indicated a 90^{o} phase shift frequency of 157 r/s (ω_n) for a well damped response corresponding to a damping ratio, $\zeta \simeq 0.7$. Hence the following values may be used:-

$J9 = .001; \quad F9 = 0.22; \quad K9 = 24.6.$

Since the dynamometer has been developed to have a fast response, then the analysis of the load simulation system will be performed with a low time constant on the velocity transducer (say T5 = .001 s).

An initial analysis was made for the basic engine - dynamometer system with no feedback control. Root loci for the speed range of the system are shown for normal and maximum fuel delivery, as well as for the motoring condition in graph G55. The curves obtained are very similar to those of the hydrostatic dynamometer basic system (graph G34), except that there are no significant secondary root effects under the motoring condition. As expected, the roots due to the flexible coupling reside in the same area as for the hydrostatic dynamometer system (approximately $15 \pm J200$).

3.3.2 Simulation Method 1.1 Torque control by dynamometer
Speed control by prime mover

Using the techniques developed in section 3.2.2 an analysis was made to determine the most suitable values of controller coefficients for simulation method 1.1. For the full speed range under both loading and motoring conditions suitable values were found to be:-

Dynamometer: proportional gain, B = 0.1 v/v;
integral gain, C = 10 s^{-1}.

Prime mover: proportional gain, E = 1 v/v;
integral gain, F = 10 s^{-1}.

The low value of proportional gain on the dynamometer was found to be necessary to maintain stability of the flexible coupling roots at high speed under the loading condition and at low speed under the motoring condition. This is due to the high value of dynamometer input gain (K4) under these conditions (see graph G54). Comparison with the root loci obtained for the hydrostatic dynamometer system using method 1.1 (graphs G38 and G41) shows that the fast response dynamometer system has far less significant secondary root effects, for the purposes of load simulation, than the hydrostatic dynamometer.

Since many of the coefficients of the mathematical model for the load simulation system have been treated as linear, although in practice they are highly non-linear, it is necessary to determine the effect of variations in system parameters upon the root positions:-

(a) Governor Lag (T4). At low speed (600 rev/min) with normal fuel delivery a governor lag greater than 2 seconds created low frequency oscillatory roots ($\omega_n \simeq .5$ Hz; $\zeta \simeq .15$), whereas at high speed (3000 rev/min) this value of lag created high frequency oscillatory roots ($\omega_n \simeq 3$ Hz; $\zeta \simeq .15$). With a governor lag of less than 0.05 seconds the roots indicate near instability at low speed ($\zeta \simeq .0017$; $\omega_n \simeq 5$ Hz), although a well damped response is obtained at high speed.

(b) Governor Rating (K8). For mid fuel delivery reducing K8 below 5 Nm s created low frequency oscillatory roots at low speed, although this change had negligible effect at high speed. Increasing K8 above 30 Nm s created high frequency oscillatory roots at low speed, whereas at high speed the speed/torque dominant time constant increased to approximately 1.5 seconds.

(c) Compressibility Lag (T3). At high speed, under the loading condition, increasing T3 by a factor of 4 (to 0.01 seconds) improved the damping of the flexible coupling roots, whereas reducing T3 to zero (obtained when torque requirement = 0) resulted in near instability of the flexible coupling roots (approximately $1 \pm J190$). At low speed, for mid fuel delivery, increasing T3 by a factor of 8 (to 0.1 seconds) created oscillatory roots of frequency $\omega_n \simeq 1.7$ Hz ($\zeta \simeq .06$). This range of T3 had negligible effect on the root positions for the motoring condition throughout the speed range.

(d) Speed Transducer Lag (T5). Variations in T5 from $0.1 \rightarrow 0$ seconds had negligible effect upon the root positions under all conditions throughout the speed range. This is because the simulated vehicle characteristics are not part of a speed feedback loop using method (1). It will be shown that this range of T5 has a much larger effect upon the system using load simulation method (2) (analysed in sections 3.3.4 and 3.3.5).

(e) Diesel Engine Pure Time Delay (T1). For normal fuel delivery, increasing T1 by a factor of 3 created highly oscillatory roots at low speed ($\omega_n \simeq 1.5$ Hz; $\zeta \simeq .03$) and slightly reduced the damping of the flexible coupling roots at high speed. Reducing T1 by a factor of 3 had negligible effect under all conditions throughout the speed range.

(f) Diesel Engine Inertia (of rotating and reciprocating parts) (J1). Increasing J1 to 2 kg m^2 caused a reduction in the dominant response time constant for maximum fuel delivery as well as under the motoring condition throughout the speed range. At high speed under the loading condition this increase in J1 caused the flexible coupling roots to become virtually unstable ($1.4 \pm J165$) and at low speed, for mid fuel delivery, oscillatory low frequency roots were created ($\omega_n \simeq 0.5$ Hz; $\zeta \simeq 0.12$). Reducing J1 to 0.1 kg m^2 caused a reduction in the dominant response time constant for maximum fuel delivery at high speed, and created oscillatory roots of high frequency (10 Hz; $\zeta \simeq 0.25$) for normal fuel delivery (again at high speed).

(g) Dynamometer Inertia (J2). Increasing the dynamometer inertia to 2 kg m^2 caused a reduction in the frequency and damping of the flexible coupling roots ($\omega_n \simeq 17$ Hz; $\zeta \simeq .03$) under all conditions throughout the speed range. For maximum fuel delivery this increase in J2 created oscillatory roots at high speed ($\zeta \simeq .23$; $\omega_n \simeq 2$ Hz) which became unstable at low speed. Reducing J2 to 0.01 kg m^2 increased the frequency and damping of the flexible coupling roots ($\omega_n \simeq$ 100 Hz; $\zeta \simeq .25$) under all conditions throughout the speed range.

(h) Dynamometer Actuator Lag $\left(\frac{K9}{J9s^2 + F9s + K9}\right)$. At high speed a reduction in the undamped natural frequency of the dynamometer input actuator by a factor of 5 created high frequency oscillatory roots $\omega_n \simeq$ 5 Hz; $\zeta \simeq 0.15$). Also at high speed an increase in the undamped natural frequency by a factor of 5 caused the flexible coupling roots to become more oscillatory at maximum fuel delivery and unstable for normal fuel delivery. This range of undamped natural frequency had negligible effect under all other conditions.

(i) Prime Mover Actuator Lag (T6). As with the hydrostatic dynamometer, variations in T6 from 0.1 → 0.001 seconds had negligible effect on the root positions under all conditions.

(j) Dynamometer Input Gain (K4). Changes in this variable are likely to be caused by variations in the oil temperature of the hydraulic system. The effect is identical to that of changes in the dynamometer controller proportional gain (B), i.e., increasing the gain reduces the stability of the system and vice versa. Increasing K4 by a factor of 2 was found to cause the flexible coupling roots to go unstable at high speed under the loading condition. At low speed increasing K4 reduced the damping of the low frequency oscillatory roots. Reducing K4 by a factor of 5 had negligible effect, except to increase the dominant response time constant under the motoring condition throughout the range of speed.

(k) Prime Mover Torque/Speed Slope (K1). Since this variable is small compared to the governor rating (K8), then its effect is only of importance for maximum fuel delivery and under the motoring condition. Under these conditions increasing K1 caused a proportional increase in the dominant response time constant, and reducing K1 caused a proportional reduction in the time constant.

(l) Dynamometer Torque/Speed Slope (K3). The values of K3 used in the analysis of the fast response dynamometer system are the maximum values (obtained when maximum torque is applied, as discussed in section 3.3.1). For zero torque the value of K3 reduces to zero and the diesel engine operates under no load conditions. At low speed for normal fuel delivery this results in an unstable system, since the engine has already been shown to be unstable under these conditions in section 3.2. (However, this is not a problem, since the fuel control rod will move either to the idling position or to maximum stroke.) Also at low speed K3 = 0 results in a reduction of the time constant of the unstable dominant root, whereas increasing K3 to 10 Nm s increases the time constant of the unstable root. This range of K3 had negligible effect at high speed under the loading condition. Under the motoring condition, an increase in K3 caused the dominant response time constant to increase and a reduction in K3 caused a reduction in the time constant.

(m) Derivative Action (A on dynamometer; D on engine). No value of derivative action was found to cause a significant improvement in the root positions. With a derivative time constant on the dynamometer of only 0.1 s the roots due to the flexible coupling were completely unstable under all conditions, except for at high speed under the motoring condition. Under normal fuel delivery conditions a derivative time constant of D = 3 s on the engine controller caused a pair of high frequency roots, as well as the flexible coupling roots, to go unstable.

In general, the root locus method indicated that the fast response dynamometer system is less sensitive to changes in system parameters than the hydrostatic system for method 1.1, except that at high speed the high gain of the special purpose valve causes a reduction in the damping of the flexible coupling roots. It has already been shown that for the hydrostatic dynamometer it is more appropriate to use speed control on the dynamometer (i.e., method 1.2) than torque control (method 1.1). This form of control is analysed for the fast response dynamometer in the following section.

3.3.3 Simulation Method 1.2 Speed control by dynamometer Torque control by prime mover

Using previously developed techniques, the root locus method was used to determine the most suitable values of controller coefficients for load simulation method 1.2. Values suitable under all conditions throughout the speed range were found to be:-

Dynamometer Controller	Proportional gain, B = 3 v/v Integral gain, C = 10 s^{-1}
Diesel Engine Controller	Proportional gain, E = 0.1 v/v Integral gain, F = 3 s^{-1}

As with the hydrostatic dynamometer system, the torque control signal proportional gain must be low in comparison to the speed control signal proportional gain, for either method 1.1 or 1.2. Using the above values, a root locus was performed for all conditions throughout the speed range, as shown in graph G57. Comparison with graph G56 (method 1.1) shows that under mid fuel delivery conditions method 1.2 has a marginally faster response than method 1.1 at high speed (although the dominant roots become second order, they are well damped). Under maximum fuel delivery conditions method 1.2 does not produce an unstable root at low speed, as does method 1.1. Hence method 1.2 can simulate steady state maximum torque conditions throughout the speed range, whereas method 1.1

can only do this at high speed.

Under the motoring condition method 1.2 has a much faster response time (approximately a factor of 10) than method 1.1 (although, once again, the roots become second order at high speed, they are well damped). Hence method 1.2 provides superior performance compared to method 1.1 for both the hydrostatic and fast response dynamometers used in conjunction with the diesel engine system.

The major differences in the effect of changes in system parameters upon the root positions between methods 1.1 and 1.2 are given as follows:-

(a) Governor Lag (T4). Same as method 1.1, except that no high frequency oscillatory roots were created at high speed.

(b) Governor Rating (K8). At high speed with mid fuel delivery, increasing K8 caused the dominant response to become second order with low damping (whereas method 1.1 under these conditions caused an increase in the time constant of the dominant response).

(c) Compressibility Lag (T3). At high speed under the loading condition reducing T3 to zero had negligible effect upon the flexible coupling roots (although for method 1.1 they became virtually unstable under these conditions).

(d) Speed Transducer Lag (T5). Increasing T5 to 0.1 seconds created oscillatory roots with low damping ($\omega_n \simeq 2$ Hz; $\zeta \simeq 0.22$) at high speed with maximum fuel delivery.

(e) Prime Mover Pure Time Delay (T1). Increasing T1 by a factor of 3 had negligible effect upon the damping of the flexible coupling roots at high speed under the loading condition (whereas the damping was reduced under these conditions using method 1.1).

(f) Prime Mover Inertia (J1). At high speed under the loading condition, increasing J1 to 2 kg m^2 also had no effect upon the damping of the flexible coupling roots, whereas the roots became unstable under these conditions using method 1.1. However, under the motoring condition, this increase in J1 at high speed caused the dominant response to become low frequency second order with low damping ($\omega_n \simeq 0$ Hz; $\zeta \simeq .35$).

(g) Dynamometer Inertia (J2). Increasing J2 to 2 kg m^2 caused the dominant response to become second order under all conditions throughout the speed range in the same manner as method 1.1, except that at high speed under the motoring condition the damping of the dominant response roots became much lower ($\omega_n \simeq 0.1$; $\zeta \simeq .3$).

(h) Dynamometer Actuator Lag $\left(\frac{K9}{J9s^2 + F9s + K9}\right)$.

Although an increase in the undamped natural frequency of the dynamometer actuator by a factor of 5 caused the flexible coupling roots to become unstable using method 1.1 (at high speed for normal fuel delivery), this increase only slightly reduced the damping of the flexible coupling roots using method 1.2.

(i) Dynamometer Input Gain (K4). Increasing K4 was found to increase the speed of response of the dominant roots under all conditions throughout the speed range. Also, increasing K1 had negligible effect upon the flexible coupling roots at high speed under the loading condition (whereas for method 1.1 under these conditions an increase in K1 of a factor of 2 caused the flexible coupling roots to become unstable). Reducing K4 was found to reduce the speed of response of the dominant roots under all conditions throughout the speed range.

(j) Prime Mover Torque/Speed Slope (K1). Varying K1 had a similar effect compared to method 1.1, except that at low speed under the motoring condition the dominant response time constant was only slightly affected by these variations.

(k) Dynamometer Torque/Speed Slope (K3). Reducing K3 to zero created a highly oscillatory dominant response at low speed for both maximum fuel delivery ($\omega_n \simeq 0.25$ Hz; $\zeta \simeq 0.15$) and mid fuel delivery ($\omega_n \simeq 0.15$ Hz; $\zeta \simeq 0.15$). However, for maximum fuel delivery maximum torque is achieved and K3 is therefore also maximum. (If a low torque value is required, then the engine will quickly accelerate to high speed away from the low stability region.) Hence, in practice, the response of the system will only be oscillatory for normal fuel delivery at low speed and not for maximum fuel delivery. (This oscillatory performance for normal fuel delivery at low torque and low speed has already been shown to be due to the unstable nature of the engine under these conditions.)

(l) Derivative Control (A on dynamometer; D on engine). As with method 1.1, no values of derivative action were found to improve the root positions, although for the dynamometer controller a value of A = 5 s could be reached before causing the flexible coupling roots to go unstable and the maximum value of D for stability was 0.1 s.

It has been seen, therefore, that the fast response dynamometer system has greatly reduced the effects of the secondary roots compared to the hydrostatic dynamometer system using method (1). The effects of using load simulation method (2) with the fast response dynamometer system are analysed in the following sections.

3.3.4 Simulation Method 2.1 (Torque Reference System)

One major difference between simulation methods (1) and (2) is that for method (2) it is necessary to have an extra control signal to eliminate the steady state torque/speed characteristic of the dynamometer (as discussed in section 2.3.1). The effect this has upon the performance of the basic system is shown in the root locus of graph G58, which may be compared to that of the basic hydrostatic dynamometer system shown in graph G34. For mid fuel delivery at low speed the root locus for the fast response dynamometer indicates two marginally stable roots, whereas a comparison with graph G34 shows that the hydrostatic dynamometer is reasonably stable under these conditions. The reason for this is that the engine is unstable under low torque and speed conditions. The use of the dynamometer torque elimination signal creates this low torque condition, although the signal has the lag of the velocity transducer and of the input actuator to dampen its effect. The lag on the hydrostatic dynamometer system is much greater than on the fast response dynamometer system and therefore the stabilising effect upon the engine is much greater.

Thus, at low speed for normal fuel delivery, the basic fast response dynamometer system is inherently much more oscillatory than the basic hydrostatic dynamometer system using method (2), and this may cause difficulties in the control of the load simulation system. By closing the feedback loops to provide load simulation method 2.1 (setting G1 = 1 and G3 = 1 on the computer program VALUES) a value of proportional gain, B = 3 v/v, was found to improve the stability at low speed with normal fuel delivery. However, this value of gain at high speed was found to cause the flexible coupling roots to go unstable (due to the increased gain of the special purpose valve). Hence the gain requirements are conflicting, i.e., at low speed a high gain is required to stabilise the unstable engine roots, and at high speed a low gain is required to maintain stability of the flexible coupling roots. It is therefore necessary to use either an adaptive gain controller or use the gain appropriate to the high speed stability requirements (since it has been shown in section 3.2.4.1 that the actual vehicle performance is highly oscillatory at low speed for normal fuel delivery). To maintain simplicity of the control system the latter method was adopted for further analysis of the load simulation system using method 2.1. Root loci are shown for the speed range under all conditions in graphs G59 (4th gear) and G60 (1st gear) using the following values of controller gains:-

Dynamometer Controller	Proportional gain, B = .05 v/v Integral gain, C = 10 s^{-1}
Diesel Engine Controller	Proportional gain, E = 1 v/v Integral gain, F = 10 s^{-1}

The graphs show that the system is more stable in low gear and that in 4th gear the secondary roots are highly oscillatory at high speed under the motoring condition and low speed under the loading condition. The dominant response time constants for each condition (which may be compared with the actual vehicle response time constants in section 3.2.4.1) are tabulated below:-

Motoring Condition

Engine Speed (rev/min)		600	1500	3000
Time Constant (s)	1st	5.33	5.84	6.06
	2nd	17.4	18.7	17.8
	3rd	52.8	45.9	37.7
	4th	79.5	65.4	54.6

Loading Condition (mid fuel delivery)

(No engine control as discussed in section 3.2.4)

Engine Speed (rev/min)		600	1500	3000
Time Constant (s)	1st	Unstable	ω_n 15.8r/s; ζ .256	ω_n 35.14r/s; ζ .676
	2nd	Unstable	ω_n 15.8r/s; ζ .253	ω_n 35.1r/s; ζ .674
	3rd	Unstable	ω_n 16.0r/s; ζ .249	ω_n 35.5r/s; ζ .66
	4th	Unstable	ω_n 16.2r/s; ζ .246	ω_n 35.8r/s; ζ .648

Loading Condition (maximum fuel delivery)

Engine Speed (rev/min)		600	1500	3000
Time Constant (s)	1st	-12.1	57	7.7
	2nd	-64.1	82.1	22.7
	3rd	-408	85.2	41.9
	4th	450	91.7	58.2

Comparison with the actual vehicle response shows that the time constants predicted for the load simulation system are of the same order with the greatest difference occurring under mid fuel delivery conditions. The measure of agreement is, in fact, approximately the same as for the hydrostatic dynamometer using the same load simulation method (2.1), except for the unstable response at low speed and normal fuel delivery. Hence for load simulation method 2.1 the predicted performance of the fast response dynamometer system shows no improvement over that of the slower hydrostatic dynamometer system. In fact, it has been shown that the faster speed of response tends to de-stabilise the system under low speed conditions.

Root positions which were significantly affected by changes in system parameters were determined under the worst case conditions (i.e., low speed - loading; high speed - motoring) as follows:-

(a) Velocity Transducer Lag (T5). It has already been suggested that the reason for the system roots to go unstable at low speed under mid fuel delivery conditions is due to the fast response of the dynamometer effectively reducing the damping under these conditions. By increasing the velocity transducer lag to 1 s the unstable roots were found to be stabilised. However, with T5 = 1 s, the low frequency roots become virtually unstable for maximum fuel delivery. Although instability can be tolerated under normal fuel delivery conditions, the system must be well damped for maximum fuel delivery and motoring so that the faster value of T5 (.001 s) must be used.

(b) Acceleration Lag (T7). The most suitable value of this lag was found to be proportional to the simulated inertia (J4), as with method 2.1 for the low power simulation system of section 2.3.1. Reducing the value of T7 was found to stabilise the system at low speed for mid fuel delivery, although at high speed under both mid and maximum fuel delivery conditions this reduction caused the flexible coupling roots to go unstable.

(c) Simulated Inertia (J4). Variations from 1 → 100 kg m^2 of the simulated inertia had a proportional effect upon the dominant root time constant under maximum fuel delivery and motoring conditions with negligible effect upon the secondary roots.

(d) Simulated Friction (F4). Reducing F4 by up to a factor of 10 was found to increase the dominant response time constant without affecting the secondary roots. Increasing F4 was found to reduce the dominant response time constant as well as to reduce the damping of the low frequency oscillatory roots.

(e) Prime Mover Inertia (J1). Increasing the diesel engine inertia of rotating and reciprocating parts up to 2 kg m^2 was found to improve the damping of the low frequency secondary roots, whereas reducing the inertia to 0.1 kg m^2 caused a reduction in the damping of these roots with near instability at low speed for maximum fuel delivery.

(f) Dynamometer Inertia (J2). Increasing the dynamometer inertia to 2 kg m^2 created very low frequency oscillatory roots under maximum fuel delivery and motoring conditions (ω_n = .1 Hz; ζ = .15), as well as reducing the damping of the flexible coupling roots. Reducing J2 to 0.01 kg m^2 merely increased the frequency of the flexible coupling roots.

(g) Dynamometer Input Gain (K4). At low speed under maximum fuel delivery conditions increasing K4 to 100 Nm/v caused the low frequency oscillatory roots to become well damped, whereas reducing K4 to 2 Nm/v caused the roots to become unstable. (This is due to the same effect of the dynamometer proportional gain controller upon stability as discussed earlier.) Under the motoring condition this range of K4 had little effect upon the damping of the low frequency roots.

(h) Diesel Engine Torque/Speed Characteristic Slope (K1). Increasing this slope at low speed under maximum fuel delivery conditions caused the low frequency secondary roots to become unstable. At high speed under the motoring condition reducing the slope created a reduction in the damping of the low frequency roots.

(i) Derivative Control. The effect of derivative action was found to be the same as for previous systems, i.e., a relatively low value of derivative action time on either the dynamometer controller or diesel engine controller caused the flexible coupling roots to go unstable.

To determine whether any improvement in performance can be obtained with the fast response dynamometer (especially under normal fuel delivery conditions at low speed), simulation method 2.2 is analysed in the following section.

3.3.5 Simulation Method 2.2 (Speed Reference System)

Values of controller coefficients found to give suitable performance for simulation method 2.2 under all speeds and gear settings were as follows:-

Dynamometer Controller	Proportional gain, B = 5 v/v Integral gain, C = 1 s^{-1}
Diesel Engine Controller	Proportional gain, E = 1 v/v Integral gain, F = 1 s^{-1}

Using these values root loci are shown for the speed range under all conditions in graphs G61 (1st gear) and G62 (4th gear). Under the motoring condition in 1st gear the dominant speed/torque response is shown to be second order at low and medium speeds. However, this second order response is well damped and has the same order of time response as that of the real vehicle analysed in section 3.2.3.1. Besides this, under normal driving conditions a vehicle will "motor" to a halt in 3rd gear, so that the motoring condition in 1st gear will not normally occur in practice. Under the loading condition with mid fuel delivery for both 1st and 4th gears the low frequency root effects (shown in the increased scales) are made negligible by having zeros in close proximity. The dominant response time constants are tabulated for each speed and gear setting under all loading and motoring conditions as follows:-

Motoring Condition

Engine Speed (rev/min)		600	1500	3000
Time Constant (s)	1st	ω_n .2 r/s; ζ .99	ω_n .197; ζ .957	ω_n .184; ζ .857
	2nd	14.3	13.5	ω_n .099; ζ .91
	3rd	42.4	31.2	20.53
	4th	59.6	39.7	27.1

Loading Condition (mid fuel delivery)

(Engine control = 0 as discussed in section 3.2.4)

Engine Speed (rev/min)		600	1500	3000
Dominant Response	1st	ω_n 7.3 r/s; ζ .084	.232	.173
	2nd	ω_n 7.3 r/s; ζ .089	1.28	.709
	3rd	ω_n 7.3 r/s; ζ .089	ω_n .231 r/s; .816	ω_n .297 r/s; ζ .965
	4th	ω_n 7.3 r/s; ζ .09	ω_n .176 r/s; .657	ω_n .226 r/s; ζ .855

Loading Condition (maximum fuel delivery)

Engine Speed (rev/min)		600	1500	3000
Time Constant (s)	1st	-14.2	57	6.94
	2nd	-75.4	79.5	18.7
	3rd	-470	72.2	27.6
	4th	+471.5	67.1	32.5

Under the motoring condition and the loading condition for maximum fuel delivery the predicted dominant response time constants are in very close agreement with those of the actual vehicle response, analysed in section 3.2.4.1. This was also found to be the case with the hydrostatic dynamometer using simulation method 2.2 as analysed in section 3.2.5. For mid fuel delivery conditions the predicted responses are very much closer to the actual vehicle response than those using method 2.1 with the fast response dynamometer, although not as good as the hydrostatic dynamometer system using method 2.2 (section 3.2.5). Significant differences in root positions as a result of changes of system parameters between methods 2.1 and 2.2 were determined as follows:-

(a) Velocity Transducer Lag (T5). Since simulation method 2.2 has already been shown to produce significantly greater damping than method 2.1 (as well as providing dominant responses closer to the actual vehicle response), then for mid fuel delivery conditions at low speed, increasing T5 produced even greater damping of the low frequency roots. Also, for maximum fuel delivery, increasing T5 to 1 second resulted in stable low frequency roots (ζ .4; ω_n .2 r/s), whereas for method 2.1 under these conditions the low frequency roots became completely unstable.

(b) Simulated Inertia (J3). Variations in J3 had negligible effect upon the secondary roots (as with method 2.1) and the dominant response time constants were very close to those for the real vehicle.

(c) Simulated Friction (F3). Reducing F3 was found to have negligible effect upon either the dominant or secondary roots at low speed due to the fact that F3 is already small in value at low speed compared to high speed (resulting from the simulation of wind resistance).

(d) Prime Mover Inertia (J1). Increasing J1 to 2 kg m^2 improved the damping of the low frequency roots for mid fuel delivery and created oscillatory low frequency roots for maximum fuel delivery at low speed. Under the motoring condition this increase in J1 caused the dominant response time constant to increase by a factor of 2. Reducing J1 to 0.1 kg m^2 had negligible effect upon the root positions for maximum fuel delivery and motoring conditions, although for normal fuel delivery the low frequency roots became unstable. (For method 2.1 variations in J1 had the opposite effect to those reported above under all conditions.)

(e) Dynamometer Inertia (J2). Increasing J2 to 2 kg m^2 caused the dominant response under the motoring condition to become first order with time constants in close agreement with those for the real vehicle response. (Whereas for method 2.1 under the motoring condition this increase in J2 created low frequency roots with very low damping.) Under mid fuel delivery conditions this increase improved the damping of the low frequency roots.

(f) Dynamometer Input Gain (K4). Increasing K4 by a factor of 5 had negligible effect upon the root positions, except that under the motoring condition this increase created high frequency secondary roots with very low damping (ω_n 15 Hz; ζ .05). Under the loading condition for both maximum and mid fuel delivery a reduction in K4 by a factor of 10 caused the low frequency roots to go unstable, and under the motoring condition this reduction in K4 caused a reduction in the damping of the dominant response roots.

(g) Diesel Engine Torque/Speed Characteristic Slope (K1). Reducing K1 under the motoring condition caused the dominant response to become first order, the time constant of which increased in proportion to the reduction in K1. Increasing K1 under the same conditions also caused the dominant response to become first order, for which the time constant reduced in proportion to the increase in K1.

(h) Derivative Control. Although derivative action on the dynamometer controller was not found to create any improvement in root positions, it was found that at low speed for normal fuel delivery a value of derivative action on the engine controller of D = 1 s caused the oscillatory low frequency roots to become well damped. However, at high speed under this condition the same value of derivative action caused the flexible coupling roots to go unstable.

It has been shown, therefore, that the fast response dynamometer system has significant advantages over the hydrostatic dynamometer system in that secondary root effects are much lower. Also, for method 2.2, very close correlation with real vehicle performance may be achieved without the need for changing controller gains in first gear (as was the case for the hydrostatic dynamometer system). However, one disadvantage with the fast response dynamometer system, when used in conjunction with a governed diesel engine, is that it cannot effectively dampen the oscillatory nature of the engine-governor combination at low speed under low load conditions. These effects do not occur with petrol engines or d.c. traction motors used for automotive purposes, and the performance of the fast response dynamometer in conjunction with these prime movers is investigated in Part 4 and Part 5.

It should be noted that one further advantage of the fast response dynamometer is that its speed of response combined with low inherent loading characteristics make the system suitable for transient and frequency response testing of prime movers (since the dynamic effects of the dynamometer will be low in comparison to those of the prime mover). Because the number of hydrostatic dynamometer systems in common usage at present is small compared to electric dynamometers, the effects of using an electric dynamometer to simulate loads on the diesel engine are investigated in the following section.

3.4 Electrical Dynamometer

The analysis presented in this section is to determine the ability of a separately excited d.c. motor/generator type dynamometer to simulate loading characteristics of the Ford A Series truck for the diesel engine analysed in the preceding sections. The analysis is purely theoretical and typical characteristics will be chosen for the d.c. motor/generator to enable a performance comparison to be made with the hydrostatic and fast response dynamometer systems.

3.4.1 Transfer Characteristics

The basic block diagram for the diesel engine and electrical dynamometer with thyristor control is shown in Fig. 3.6. The block diagram is similar to the hydrostatic and fast response dynamometer systems, except that the dynamometer input actuator lag is replaced by thyristor control (which is assumed to have a negligible time constant compared to an electrohydraulic actuator). The dynamometer to be used in the analysis has 100 kW power rating, for which the torque/speed curve at maximum power is shown in graph G63. Since the internal power losses in a d.c. motor/generator are relatively small, then the same torque/speed curve will be used for the dynamometer as both a motor and a generator. This means that under the loading condition the dynamometer torque/speed slope (K3) is negative, thereby resulting in positive feedback and possible instability.

However, for the diesel engine the negative feedback of the governor (K8) is much greater than K3 and hence stable operating conditions will result. It should be noted that for a petrol engine not having a governor the system will be unstable at low speed (when operating over the left-hand side of the engine torque/speed characteristics) unless an external feedback loop is added. This feedback may be to control engine torque (or generator current), engine speed (or terminal voltage), or both (i.e., power output).

For the theoretical system under investigation linearised values of the dynamometer torque/speed slope (K3) and gain (K4) may be obtained at each range of speed as follows:-

K3, Loading Condition:

At low speed (600 rev/min) the maximum level of torque required by the diesel engine is 170 Nm (from graph G2), whereas the dynamometer is capable of supplying 1590 Nm (from graph G63). Hence the maximum value of K3 under these conditions becomes:-

$$K3_{max} \text{ (low speed)} = -24.7 * \frac{170}{1590} = -2.64 \text{ Nm s}$$

Similarly at medium and high speed:-

$$K3_{max} \text{ (medium speed)} = -4.05 * \frac{200}{630} = -1.286 \text{ Nm s}$$

$$K3_{max} \text{ (high speed)} = -0.931 * \frac{190}{315} = -0.562 \text{ Nm s}$$

K3, Motoring Condition:

Under the motoring condition the torque available to motor the diesel engine reduces as the speed is increased, so that the dynamometer provides negative feedback and K3 is therefore positive. Also, the torque/speed slope of the diesel engine is estimated as linear with a required torque of 100 Nm to reach maximum speed (3000 rev/min). Hence at low speed (600 rev/min) the diesel engine requires a torque of (100*600/3600) Nm, whereas the dynamometer can provide 1590 Nm. Thus

$$K3_{max} \text{ (low speed)} = +24.7 * \frac{600}{3600} * \frac{100}{1590} = 0.259 \text{ Nm s}$$

Similarly for medium and high speeds:-

$$K3_{max} \text{ (medium speed)} = +4.05 * \frac{1500}{3600} * \frac{100}{1590} = 0.106 \text{ Nm s}$$

$$K3_{max} \text{ (high speed)} = +0.931 * \frac{3000}{3600} * \frac{100}{1590} = 0.0488 \text{ Nm s}$$

It should be noted that under normal operating conditions K3 will vary from zero up to these maximum values (in the same manner as for the fast response dynamometer), so that it will be necessary to determine the effect of this range upon the root positions when analysing the system performance.

K4, Loading and Motoring Conditions:

Since the same torque/speed curve has been used for the loading and motoring conditions, then the dynamometer input gain (K4) will remain the same for both conditions. For a maximum control signal of 10 volts the values of K4 may be obtained for each range of speed from graph G63 as follows:-

K4 (low speed) = 313 Nm/v;

K4 (medium speed) = 126 Nm/v;

K4 (high speed) = 61 Nm/v.

Other values used for the dynamometer were:-

Electrical time constant due to windings = 0.2 s (T3)

Armature inertia = 3 kg m^2 (J2)

Thyristor controller lag zero $\therefore$ J9 = F9 = 0;

K9 = 1

Flexible coupling to have the same stiffness and dynamic magnification as the hydrostatic system,

i.e., K2 = 3438 Nm/radian

$$\zeta = \frac{1}{2 \times 7} = 0.071$$

$$\therefore F2 = 2*0.071\sqrt{3*3438} = 14.42 \text{ Nm s}$$

To determine the characteristics of the basic engine-dynamometer system with no feedback, a root locus was constructed for the range of speed under both loading and motoring conditions, as shown in graph G64. Comparisons with the basic system root loci for the fast response dynamometer (graph G55) and the hydrostatic dynamometer (graph G34) show that the basic electrical dynamometer + diesel engine system has a much slower speed of response under all conditions. Also, for maximum fuel delivery, there is a single unstable root throughout the speed range. This is due to the fact that under the loading condition the system is stabilised by the negative feedback of the governor, which becomes saturated for maximum fuel delivery.

The only second order roots for the basic system (other than the oscillatory engine roots for low speed maximum fuel delivery) are due to the flexible coupling (approximately $-20 \pm J100$), so that the basic system is well damped in comparison to the hydrostatic and fast response dynamometer systems. The following sections will show how this affects the electrical dynamometer system performance under load simulation conditions.

3.4.2 Simulation Method 1.1 Torque control by dynamometer Speed control by prime mover

Under the loading condition suitable values of controller coefficients were found to be:-

Dynamometer Controller	Derivative action, A = 0.2 s Proportional action, B = 0.3 v/v Integral action, C = 1.0 s^{-1}
Diesel Engine Controller	Derivative action, D = 0.3 s Proportional action, E = 1 v/v Integral action, F = 3 s^{-1}

It was found that derivative action allowed higher values of proportional gain to be used on both the engine and dynamometer controllers without de-stabilising the oscillatory engine roots at low speed for normal fuel delivery. The reason that derivative action improves the performance of the electrical dynamometer system and not the previously analysed hydraulic dynamometer systems is due to the low cut off frequency of the electrical dynamometer windings. This effectively prevents fast changing control signals (amplified by the derivative action) from exciting the flexible coupling, whereas the faster hydraulic dynamometers allow these fast changing signals through.

Under the motoring condition the above values of controller coefficients were found to produce a dominant second order response with low damping. To improve the performance under this condition it was found necessary to eliminate the derivative action and increase the dynamometer proportional gain to B = 10 v/v (or, preferably, change to simulation method 1.2 for reasons discussed in section 1.2.1.2). Using these values root loci were constructed for the speed range under each condition as shown in graph G65.

For mid fuel delivery throughout the speed range the low frequency roots are well damped and approximately the same magnitude as those for the hydrostatic system under the same conditions (graph G38). For maximum fuel delivery, however, the dominant first order response is well into the unstable region at low speed, becoming second order at high speed (due to the positive feedback of the dynamometer under the loading condition). For the hydrostatic and fast response dynamometer systems under these conditions (graphs G41 and G56 respectively) the dominant first order response becomes stable above the mid speed range. This would indicate that it is not possible to simulate maximum torque conditions (i.e., fuel control rod at maximum) at high speed with the electrical dynamometer system using method 1.1, since the dominant response is unstable until the control rod is pulled back from maximum (thereby reducing the maximum torque). It is of intcrest to note that this effect may cause errors in the steady state calibration of prime mover torque/speed characteristics if torque feedback is applied to an electrical dynamometer system with three term control. Under the motoring condition (with B = 10 v/v and A = 0) the dominant response is well damped and of the same order of magnitude as the fast response dynamometer system.

The effect of variations in system parameters was determined as follows:-

(a) Governor Lag (T4). At low speed for mid fuel delivery increasing T4 to 2 seconds caused the oscillatory low frequency roots to go unstable, whereas reducing T4 to 0.05 seconds caused the flexible coupling roots to go unstable.

(b) Governor Rating (K8). At low speed for mid fuel delivery reducing K8 to 5 Nm s caused one pair of low frequency roots to go unstable, whereas increasing K8 to 30 Nm s increased the dominant response time constant and caused the other pair of low frequency roots to become highly oscillatory.

(c) Dynamometer Lag (T3). Increasing the dynamometer lag to 1 second caused the major secondary root time constant to increase at high speed for maximum fuel delivery, and reduced the damping of the low frequency roots at low speed for mid fuel delivery. Reducing the dynamometer lag to 0.01 seconds resulted in a very fast secondary root time constant (.018 seconds) at high speed for maximum fuel delivery, and an increase in the damping of the flexible coupling roots at low speed for mid fuel delivery. This range of T3 had negligible effect upon the motoring condition.

(d) Velocity Transducer Lag (T5). Increasing T5 up to 1 second had negligible effect under all conditions, except to cause the dominant response to become second order at low speed for mid fuel delivery.

(e) Diesel Engine Pure Time Delay (T1). Values of T1 from 30% to 300% of the nominal value had negligible effect under all conditions, except to reduce the damping of the low frequency roots and flexible coupling roots at low speed for mid fuel delivery.

(f) Diesel Engine Inertia (J1). At high speed under the motoring condition, increasing J1 to 2 kg m^2

caused the flexible coupling roots to become virtually unstable and the dominant response to become second order with very low natural frequency ($\omega_n \simeq .013$ Hz; $\zeta \simeq .9$). At low speed for mid fuel delivery this increase reduced the damping of the low frequency roots and also reduced the frequency of the flexible coupling roots under all conditions. Reducing J1 to 0.1 kg m^2 was found to increase the frequency of the flexible coupling roots under all conditions. At high speed the unstable dominant roots were stabilised under maximum fuel delivery conditions and under the motoring condition the dominant response time constant was reduced (due to zero cancellation of a low valued pole).

(g) Dynamometer Armature Inertia (J2). Reducing the dynamometer inertia to 0.3 kg m^2 increased the damping and natural frequency of the flexible coupling roots under all conditions. At high speed under the motoring condition this reduction increased the speed of response of the dominant first order root (once again due to zero cancellation of a low valued pole) and reduced the damping of the low frequency roots throughout the speed range under the loading condition. Increasing J2 to 10 kg m^2 caused the dominant response at high speed under the motoring condition to become second order ($\omega_n \simeq .01$ Hz; $\zeta \simeq .65$) and under maximum fuel delivery conditions the unstable roots moved closer to the left-hand side of the complex frequency plane. This increase caused the low frequency roots to become virtually unstable at low speed for mid fuel delivery.

(h) Diesel Engine Actuator Lag (T6). Variations in T6 from .001 to 0.1 seconds had negligible effect upon the root positions under all conditions throughout the speed range (as with all previously analysed systems).

(i) Dynamometer Input Gain (K4). Increasing K4 caused the low frequency roots to become more oscillatory at low speed for mid fuel delivery, whereas at high speed for maximum fuel delivery the dominant unstable roots became stabilised. Also, increasing K4 caused the damping of the flexible coupling roots to be reduced at high speed under the motoring condition and to be increased at low speed for mid fuel delivery. Reducing K4 caused an increase in the dominant response time constant under the motoring condition and a reduction in the dominant response time constant at low speed for mid fuel delivery.

(j) Diesel Engine Torque/Speed Slope (K1). Reducing K1 to -0.01 Nm s caused the dominant root under the motoring condition at high speed to become unstable. Increasing K1 to -1 Nm s resulted in a fast dominant response time constant (approximately 1 second) under the same conditions, and stabilised the dominant roots, at high speed for maximum fuel delivery.

(k) Dynamometer Torque/Speed Slope (K3). Reducing K3 tended to stabilise the unstable dominant roots at high speed for maximum fuel delivery, whereas increasing K3 caused the low frequency roots to become unstable at low speed for mid fuel delivery, and increased the dominant time constant at high speed under the motoring condition.

(l) Derivative Action. Reducing the dynamometer derivative gain to zero created unstable low frequency roots at low speed for mid fuel delivery. Increasing the dynamometer derivative action increased the damping of the flexible coupling roots, but caused the dominant low frequency roots to become highly oscillatory. Reducing the derivative action on the diesel engine also caused the dominant low frequency roots to become highly oscillatory, whereas increasing the derivative action resulted in a reduction in the damping of the flexible coupling roots and of the secondary low frequency roots.

Hence the electric dynamometer system has been shown to provide satisfactory load simulation for the diesel engine using method 1.1 (torque control by dynamometer; speed control by prime mover), except for possibly large dynamic errors when the fuel control rod is between maximum and minimum. The performance using simulation method 2.2 (speed control by dynamometer; torque control by prime mover) is investigated in the following section.

3.4.3 Simulation Method 1.2 Speed control by dynamometer Torque control by prime mover

Values of controller gains suitable throughout the speed range under all conditions were found to be:-

Dynamometer Controller	Derivative action, A = 3 s Proportional action, B = 30 v/v Integral action, C = 3 s^{-1}
Diesel Controller	Proportional action, E = 0.1 v/v Integral action, F = 1 s^{-1}

Once again derivative action on the dynamometer controller allowed higher values of proportional and integral gains without resulting in oscillatory low frequency roots. Any value of derivative action on the diesel engine controller, however, resulted in unstable flexible coupling roots. Using the above values, root loci were constructed for each condition throughout the speed range, as shown in graph G66. The dominant response time constant for each condition remained within the range of 9 → 10 seconds and the root loci show only the secondary root positions. With a dominant time constant of approximately 10 seconds the torque and speed errors for the system are likely to be large under transient conditions in comparison to the fast response and hydrostatic dynamometer systems. The root loci, however, show that the secondary root effects are well damped and insignificant compared to the primary root response for the maximum fuel delivery and motoring conditions. Also, for maximum fuel delivery there are no unstable single roots throughout the speed range, so that there is no problem simulating maximum torque conditions at high speed.

Significant differences between methods 1.1 and 1.2 in the effects of variations in system parameters were noted as follows:-

(a) Governor Lag (T4). Variations in T4 had less effect than for method 1.1 in that increasing T4 to 2 seconds reduced the damping of the low frequency roots and reducing T4 to 0.05 seconds reduced the damping of the flexible coupling roots without causing either to go unstable.

(b) Governor Rating (K8). Variations in K8 from 5 to 30 Nm s had negligible effect upon the root positions at low speed for mid fuel delivery, whereas for method 1.1 reducing K8 created unstable roots and increasing K8 caused highly oscillatory low frequency roots under the same conditions.

(c) Dynamometer Lag (T3). Increasing the dynamometer lag to 1 second resulted in low frequency oscillatory roots ($\omega_n \doteq .3$ Hz; ζ .3) at high speed under both maximum fuel delivery and motoring conditions. Reducing T3 to 0.01 seconds caused the flexible coupling roots to go unstable at low speed for mid fuel delivery, whereas method 1.1 increased the damping of the flexible coupling roots under these conditions.

(d) Velocity Transducer Lag (T5). Increasing T5 to 1 second created highly oscillatory low frequency roots under all conditions, becoming virtually unstable at low speed for mid fuel delivery.

(e) Diesel Engine Pure Time Delay (T1). Variations in T1 from 30% to 300% of the nominal value had negligible effect under all conditions.

(f) Diesel Engine Inertia of Rotating and Reciprocating Parts (J1). Increasing J1 to 2 kg m^2 reduced the damping of the flexible coupling roots under all conditions, becoming nearly unstable at low speed for mid fuel delivery. Reducing J1 to 0.1 kg m^2 had the same effect as for method 1.1 in increasing the frequency and damping of the flexible coupling roots under all conditions.

(g) Dynamometer Armature Inertia (J2). Increasing J2 to 10 kg m^2 had negligible effect under all conditions and reducing J2 to 0.3 kg m^2 merely increased the damping and frequency of the flexible coupling roots at high speed.

(h) Dynamometer Input Gain (K4). Increasing K4 had negligible effect under all conditions, except to cause a reduction in the damping of the flexible coupling roots at low speed for mid fuel delivery. Reducing K4 caused low frequency oscillatory roots under both maximum and mid fuel delivery conditions, and reduced the dominant response time constant under the motoring condition.

(i) Diesel Engine Torque/Speed Slope (K1). Variations in K1 of a factor of 10 either side of the nominal value had negligible effect under all conditions throughout the speed range.

(j) Dynamometer Torque/Speed Slope (K3). Increasing K3 by a factor of 10 reduced the dominant response time constant for mid and maximum fuel delivery with negligible effect upon the motoring condition. Reducing K3 by a factor of 10 had negligible effect under all conditions.

(k) Derivative Action. Increasing the derivative action on the dynamometer to A = 10 s resulted in a reduction in the damping of the flexible coupling roots at low speed for mid fuel delivery. Reducing the derivative action to zero resulted in oscillatory low frequency roots ($\omega_n \doteq 1.5$ Hz; ζ 0.2) under the same conditions. Derivative action on the diesel engine controller of D = 0.1 s resulted in unstable flexible coupling roots also at low speed for mid fuel delivery.

The most noticeable effect of variations in system parameters for simulation method 1.2 is that the system is well damped and insensitive to most changes in conditions. Under all conditions the system roots are better placed from the stability point of view than the roots for the system using method 1.1 Hence for load simulation on a governed diesel engine using any of the three previously analysed dynamometer systems, the root locus method indicates that better performance may be obtained using speed control on the dynamometer and torque control on the engine (i.e., method 1.2), than for torque control on the dynamometer and speed control on the engine (method 1.1) under both loading and motoring conditions.

Performance comparisons between methods 2.1 and 2.2 are made in the following sections.

3.4.4 Simulation Method 2.1 (Torque Reference Control)

As with the hydrostatic and fast response dynamometer systems it was first decided to determine the performance of the basic system with no feedback except for the dynamometer torque elimination signal (G4 = 1). Root loci for this basic system are shown under each condition for the range of speed in graph G67. The dominant roots for the system are second order at low speed under the motoring condition and for mid fuel delivery, as well as at high speed for maximum fuel delivery. Suitable values of controller coefficients to maintain stability under all conditions were found to be:-

Dynamometer Controller	Derivative gain, A = 3 s Proportional gain, B = 5 v/v Integral gain, C = 2 s^{-1}
Engine Controller	Derivative gain, D = 0.3 s Proportional gain, E = 1 v/v Integral gain, F = 10 s^{-1}

It was found that a reasonably high value of proportional gain was necessary on the dynamometer controller to maintain stability under maximum fuel delivery conditions at low speed, even though this reduced the damping of the low frequency roots under the mid fuel delivery condition. Derivative action on both controllers was used to increase the damping of these roots, although too high a value on the engine controller caused the flexible coupling roots to become unstable at high speed. Using these controller coefficients, root loci were constructed for the speed range, as shown in graph G68 (1st gear) and G69 (4th gear). In general, the secondary roots are much more significant than those of the fast response dynamometer system (graphs G59 and G60) or the hydrostatic dynamometer system (graph G47). Although the secondary roots of the electric dynamometer are well damped under all conditions, these roots are slow enough to have a large effect upon the performance of the load simulator system using method 2.1. Eliminating the derivative action on the dynamometer had the effect shown in graph G70. For maximum fuel delivery and motoring conditions the secondary roots become first order and even closer to the origin, so that they have a much larger effect upon the dominant response. For mid fuel delivery the low frequency roots become virtually unstable at low speed. Using the original controller values the dominant response time constants under each condition (which may be compared to those for the real vehicle response in section 3.2.4.1) are tabulated as follows:-

<u>Motoring Condition</u>

Engine Speed (rev/min)		600	1500	3000
Time Constant (s)	1st	4.88	ω_n .255; ζ .99	ω_n .22; ζ .85
	2nd	17.7	18.9	17.3
	3rd	53.8	46.6	37.5
	4th	80.9	66.2	54.5

Loading Condition (mid fuel delivery)

(D = E = F = O)

Engine Speed (rev/min)		600	1500	3000
Dominant Response	1st	ω_n 7.5; ζ .178	ω_n 14.6; ζ .52	.682 s
	2nd	ω_n 7.63; ζ .179	ω_n 14.6 ζ .52	.664 s
	3rd	ω_n 7.65; ζ .182	ω_n 14.7; ζ .53	.666 s
	4th	ω_n 7.68; ζ .19	ω_n 14.9; ζ .53	.669 s

Loading Condition (maximum fuel delivery)

Engine Speed (rev/min)		600	1500	3000
Time Constant (s)	1st	-13.2	55.5	ω_n .18; ζ .9
	2nd	-65.4	81.7	22.8
	3rd	-410.3	85.2	42
	4th	449.9	91.7	58.5

These predicted dominant time constants for the load simulation system using method 2.1 are larger than those for the real vehicle response, especially in high gear. The values are, however, very close to those of the hydrostatic and fast response dynamometer systems using method 2.1, as shown in sections 3.2.4.2 and 3.3.4 respectively (except for the mid fuel delivery condition, under which the hydrostatic dynamometer system has the closest correlation with the real vehicle response).

Thus as far as the dominant response is concerned, it would appear there is little difference between the three types of dynamometer system used in conjunction with the diesel engine for method 2.1.

However, due to the large lag of the electrical dynamometer compared to the hydraulic dynamometer, it was possible to reduce the acceleration lag (T7) without causing stability problems when simulating large inertias. It was found that reducing T7 resulted in the dominant response time constants of the simulation system being much closer to the real vehicle values. A value of T7 = 1 second was found to improve this correlation under all conditions in each gear (without causing stability problems) as shown:-

<u>Motoring Condition</u>

Engine Speed (rev/min)		600	1500	3000
Time Constant (s)	1st	4.84	ω_n .253; ζ .98	ω_n .217; ζ .85
	2nd	15.3	15.7	14.06
	3rd	43.5	33.1	24.1
	4th	60.8	41.3	29.8

Loading Condition (mid fuel delivery)

(D = E = F = 0)

Engine Speed (rev/min)		600	1500	3000
Time Constant (s)	1st	ω_n 7.5; ζ .18	ω_n 14.6; ζ .53	.687
	2nd	ω_n 8; ζ .61	ω_n 1; ζ 1	.79
	3rd	2.4	3.74	4.03
	4th	3.04	5.04	4.86

Loading Condition (maximum fuel delivery)

Engine Speed (rev/min)		600	1500	3000
Time Constant (s)	1st	-13.2	55.5	ω_n .176; ζ .89
	2nd	-74.1	79.7	19.6
	3rd	-468.8	72.9	28.6
	4th	472.2	67.9	23.6

When compared with the actual vehicle time constants shown in section 3.2.4.1, the correlation is very close under the motoring condition and under the loading condition for maximum fuel delivery. The effect of this reduction in T7 upon the secondary roots is negligible for low gear settings, although for higher gear settings an improvement is obtained in both the damping and speed of response of the secondary roots, as shown in graph G71 (4th gear). Hence the electrical dynamometer system can provide superior performance compared to the hydrostatic dynamometer system (in that the dominant responses are much closer to the required values), although the secondary root effects are still large compared to those for the fast response dynamometer system. The effects of variations in system parameters (in 4th gear with T7 = 1 second) were determined as follows:-

(a) Velocity Transducer Lag (T5). Increasing T5 up to 1 second improved the damping of the flexible coupling roots, but also created oscillatory low frequency roots under all conditions, becoming virtually unstable at low speed for mid fuel delivery.

(b) Acceleration Lag (T7). Reducing the acceleration lag to 0.1 second caused the flexible coupling roots to become unstable under all conditions. Increasing the lag above 10 seconds improved the damping of the flexible coupling roots but caused the dominant response time constants to become larger than those for the real vehicle response, as well as to create oscillatory low frequency roots at low speed for mid fuel delivery in all gears.

(c) Simulated Inertia (J4). In 4th gear increasing the simulated inertia by a factor of 10 (to 260 kg m^2) resulted in the flexible coupling roots becoming unstable without a similar increase in the acceleration lag T7. Hence if it is required to simulate a wide range of inertia using method 2.1, then it is necessary to have a value of T7 proportional to J4. Reducing the simulated inertia to 1 kg m^2 caused the dominant response to become second order under all conditions.

(d) Simulated Friction (F4). For mid fuel delivery conditions variations in the simulated friction coefficient had negligible effect upon the root positions. Under maximum fuel delivery and motoring conditions variations from 10% to 10 times the nominal value had a proportional effect upon the dominant response without affecting the secondary roots.

(e) Diesel Engine Inertia of Rotating and Reciprocating Parts (J1). Increasing J1 to 2 kg m^2 caused a slight reduction in the damping of the flexible coupling roots, whereas reducing J1 to 0.1 kg m^2 resulted in an improvement in the damping of the flexible coupling roots with negligible effect upon all other root positions.

(f) Dynamometer Inertia (J2). Variations in J2 had a similar effect to J1 in that increasing the dynamometer inertia up to 10 kg m^2 caused a slight reduction in the damping of the flexible coupling roots, whereas reducing the inertia to 0.3 kg m^2 resulted in an increase in the damping of these roots with negligible effect upon all other root positions.

(g) Dynamometer Input Gain (K4). Increasing the dynamometer gain by a factor of 10 resulted in an increase in the damping of the flexible coupling roots under all conditions with a slight reduction in the dominant response time constant at low speed for mid fuel delivery. Under the same condition a reduction in the dynamometer gain by a factor of 10 caused an increase in the dominant response time constant as well as a reduction in the damping of the flexible coupling roots with negligible effect under all other conditions.

(h) Engine Input Gain (K7). At low speed for mid fuel delivery increasing K7 by a factor of 10 reduced the damping of the flexible coupling roots and of the low frequency engine roots. Reducing K7 by a factor of 10 caused the dominant response to become second order with low natural frequency under the same conditions.

(i) Dynamometer Torque/Speed Slope (K3). Variations in K3 from 10% to 10 times the nominal values had negligible effect upon the root positions under all conditions.

(j) Diesel Engine Torque/Speed Slope (K1). Increasing K1 by a factor of 10 resulted in a reduction in the dominant response time constants for maximum fuel delivery and motoring conditions. Reducing K1 by a factor of 10 resulted in a slight increase in these time constants under the same conditions with negligible effect on all other root positions.

(k) Derivative Action. Increasing the derivative action on the diesel engine controller to D = 1 s caused the flexible coupling roots to become unstable at high speed for mid fuel delivery. Reducing this derivative action resulted in a reduction in the damping of the oscillatory engine roots for mid fuel delivery at low speed in low gear. Increasing the dynamometer derivative action to A = 20 s resulted in oscillatory roots of very low frequency under all conditions ($\omega_n \simeq .05$ Hz; ζ .4) with an increase in the damping of the flexible coupling roots. Reducing the dynamometer derivative action to zero resulted in oscillatory low frequency roots under all conditions, with a reduction in the damping of the flexible coupling roots at low speed for mid fuel delivery.

It has been shown that the electric dynamometer using simulation method 2.1 produces simulated loads on the diesel engine with dominant responses in very close agreement with the real vehicle response. However, it has also been shown that the secondary roots, although well damped, may have a large influence upon the dominant response. Simulation method 2.2 is investigated in the following section to determine whether any improvement can be obtained upon this performance.

3.4.5 Simulation Method 2.2 (Speed Reference Control)

The following values of controller coefficients were found to give excellent performance characteristics under all conditions:-

Dynamometer Controller	Derivative gain, A = 3 s Proportional gain, B = 30 v/v Integral gain, C = 30 s^{-1}
Engine Controller	Proportional gain, E = .3 v/v Integral gain, F = 1 s^{-1}

Derivative action on the engine controller was found to reduce the damping of the flexible coupling roots without improving the damping of the low frequency roots. Derivative action on the dynamometer controller, however, enabled high values of proportional and integral gain to be used without creating unstable roots at low speed for mid fuel delivery. These high values of proportional and integral gain on the dynamometer controller caused the secondary roots to become relatively fast (less than 1 second time constant, which therefore has little effect upon the primary response) under the maximum fuel delivery and motoring conditions, as shown in graphs G71 (1st gear) and G73 (4th gear). The roots are well damped under all conditions, except for low speed with mid fuel delivery in low gear. Under this condition, however, the oscillatory roots are of the same order of magnitude as those of the real vehicle, as shown in section 3.2.4.1. In fact, the correlation between the actual vehicle response and the dominant response of the load simulation system using method 2.2 is very close under all conditions, as shown in the following table:-

Motoring Condition

Engine Speed (rev/min)		600	1500	3000
Time Constant (s)	1st	4.89	4.92	4.55
	2nd	14.6	14.7	13.1
	3rd	42.7	31.9	23.0
	4th	59.8	40.2	28.7

Loading Condition (mid fuel delivery)

(D = E = F = 0)

Engine Speed (rev/min)	600	1500	3000
1st	$\omega_n 4.3; \zeta .078$	.143	.170
2nd	$\omega_n 2.3; \zeta .42$	$\omega_n 1.45; \zeta .94$	$\omega_n 1.51; \zeta .78$
3rd	$\omega_n 1; \zeta .73$	$\omega_n .72; \zeta .96$	$\omega_n .71; \zeta .74$
4th	$\omega_n .7; \zeta .84$	2.91	$\omega_n .53; \zeta .82$

Loading Condition (maximum fuel delivery)

Engine Speed (rev/min)		600	1500	3000
Time Constant (s)	1st	-14.7	57.0	7.0
	2nd	-77.0	79.5	18.8
	3rd	-473.8	72.2	27.6
	4th	473.6	67.1	32.6

The time constants given for the loading condition with maximum fuel delivery are an exact match with those given for the real vehicle in section 3.2.4.1. Under the motoring condition the greatest difference between the simulation system time constants and those for the real vehicle is approximately 2%. Also, for mid fuel delivery, the dominant responses of the simulation system are closer to those of the real vehicle than either the hydrostatic or fast response dynamometers using method 2.2. Hence the electrical dynamometer with its large lag and inherent inertia has been shown to provide more effective simulation of automotive loading conditions for the diesel engine than the faster acting hydraulic dynamometers with low inherent inertia. In fact, the addition of its own inherent characteristics, together with the ability to enable higher controller gains to be used compared to the hydraulic dynamometers, results in a basic load on the diesel engine which is of the same order of magnitude as the actual vehicle load. The result of this is that the load simulation system does not have to make very large changes in the dynamometer loading characteristics in order to meet the required conditions.

The effects of variations in system parameters upon the root positions are compared to the effects of such variations using method 2.1 as follows:-

(a) Velocity Transducer Lag (T5). Increasing T5 up to 1 second caused the low frequency roots to become unstable under all conditions.

(b) Simulated Inertia (J3). At high speed variations in the simulated inertia from 1 to 260 kg m^2 had negligible effect upon the damping of the flexible coupling roots, whereas for method 2.1 the flexible coupling roots became unstable for J4 = 260 kg m^2.

(c) Diesel Engine Inertia of Rotating and Reciprocating Parts (J1). Increasing J1 to 2 kg m^2 caused a large reduction in the damping of the flexible coupling roots, becoming nearly unstable at low speed for mid fuel delivery ($\omega_n \doteq 10$ Hz; ζ .05).

(d) Dynamometer Armature Inertia (J2). Increasing the inertia of the dynamometer armature to 10 kg m^2 had negligible effect at low speed for mid fuel delivery, but created oscillatory low frequency roots at high speed for maximum fuel delivery and motoring conditions.

(e) Dynamometer Input Gain (K4). Variations in K4 had the opposite effect for method 2.2 compared to method 2.1. Increasing K4 by a factor of 10 was found to reduce the damping of the flexible coupling roots under all conditions, becoming unstable at low speed for mid fuel delivery. Reducing K4 by a factor of 10 created oscillatory low frequency roots under all conditions.

(f) Engine Input Gain (K7). Increasing K7 by a factor of 10 caused the low frequency roots to have very low damping in 4th gear at low speed with mid fuel delivery (although the flexible coupling remained unaffected).

(g) Derivative Action. Increasing the derivative action on the dynamometer controller (A) had a similar effect compared to method 2.1, except that the damping of the flexible coupling roots was reduced at low speed for mid fuel delivery. The effect of derivative action on the engine controller was to cause the flexible coupling roots to become virtually unstable at low speed for mid fuel delivery.

Variations in all other parameters had a similar effect compared to method 2.1.

3.5 Discussion

The most significant findings in the analysis so far lie in an understanding of how the control loops of each type of simulation system affect the basic interaction between the diesel engine and dynamometer. For example, the diesel engine has been shown to have a highly oscillatory response when the fuel delivery is between minimum and maximum in low gear and at low speed (under actual automotive conditions for an A series truck). This inherent condition causes problems for the fast response dynamometer which cannot provide sufficient inherent damping to enable the control system to accurately simulate these low speed conditions for method (2) (in which the simulated characteristics are in a feedback loop of the control system). For the electric dynamometer, however, the inherent damping is large enough to enable high values of proportional and integral action to be used without creating stability problems for the control system under the same conditions. These high values of controller gains therefore enable the simulated conditions to be much closer to those of the actual vehicle. A further factor affecting the performance of the fast response dynamometer at low speed lies in the fact that its gain (K4) at low speed is very much lower than at high speed (see graph G54). Unless an adaptive gain controller is used, this results in the overall effective gain of the fast response dynamometer and simulation system being low at low speed, thereby increasing the error between simulated and actual loading conditions.

Also, at higher speeds for both maximum fuel delivery and under the motoring condition the low value of integral action necessary for stability of the fast response dynamometer at high speed using method 2.2 results in the time constants of the secondary roots being large (although the magnitude of these roots is kept small by zeros in close proximity). For the hydrostatic dynamometer system using method 2.2 the secondary root time constants are fast (in the order of 0.5 seconds) with close correlation being achieved between the actual and simulated dominant responses. This is due to the high values of the dynamometer gain (K4) and controller gains (B and C) of which the system is capable without causing stability problems. The correlation under mid fuel delivery conditions (section 3.2.5) is not as good as for the electrical dynamometer system due to the large lag found to be necessary on the velocity transducer (T5) to maintain adequate damping of the secondary roots under all conditions. This value of lag is not necessary for the electric dynamometer system, since the dynamometer winding lag effectively filters out fast changing signals.

For each of the three dynamometer systems analysed it was found that simulation method 2.2 provided much closer correlation with the actual vehicle response than method 2.1. This was due to the necessity of having a low pass filter (in the case of this analysis a first order lag was used) on the acceleration signal for method 2.1 to maintain stability of the control system under all conditions. For the hydrostatic and fast response dynamometer systems the value of this lag (T7) needed to be considerably larger than for the electric dynamometer system to maintain stability, hence the dominant response errors (compared to the actual vehicle response) are much larger for these systems than for the electric dynamometer system.

One further effect of systems using simulation method (2) is due to the dynamometer torque/speed elimination signal. This signal attempts to eliminate the inherent torque/speed characteristics of the dynamometer so that they may be replaced by the simulated characteristics. By using a large value of integral action on the dynamometer controller the use of this signal becomes unnecessary. This is shown by the fact that the difference in root positions for the electrical dynamometer (having high integral action) with or without the torque/speed elimination signal was found to be negligible for both method 2.1 and 2.2. For the hydrostatic dynamometer with method 2.2 (having high values of gain on the dynamometer controller) there is also negligible effect upon the root positions if the torque/speed elimination signal is removed, whereas for method 2.1 (having low values of gain on the dynamometer controller) the effect of removing the torque/speed elimination signal is to increase the dominant response by a factor of 2.

For method (1) (in which the simulated characteristics are in a forward path of the control system) the root locus analysis indicates that the slow response and large inherent inertia of the electric dynamometer system does not provide the same advantages as for the basic simulation method (2). For method 1.2 the root locus for the electrical dynamometer system (graph G66) shows that the dominant response to a step disturbance torque has a time constant of approximately 10 seconds under all conditions. This indicates that the dynamic error may be large when attempting to follow speed/time curves under transient conditions. For method 1.1 the root locus shown in graph G65 indicates that for maximum fuel delivery the electrical dynamometer system has an unstable root at all speeds. This means that it is not possible to simulate steady state maximum fuel delivery conditions (i.e., for gradients) at any speed with this system using method 1.1 (i.e., speed control on engine; torque control on dynamometer). It should be noted, however, that present legislation for exhaust emission testing, Ref. (1), Ref. (2), does not require maximum load steady state conditions to be simulated on dynamometer test systems.

For the hydrostatic dynamometer the dominant responses for method 1.2 are much faster than for the electric dynamometer (approximately 1 second for maximum fuel delivery and 0.4 second under the motoring condition) so that the dynamic error when following speed/time curves will be low. For the fast response dynamometer using method 1.2 the dominant response at maximum fuel delivery varies from 2.5 seconds at low speed to 0.25 seconds at high speed (due to the inherent gain variations of the special purpose valve). For method 1.1 both the fast response and hydrostatic dynamometer systems have an unstable root only at low speed. Hence the faster response hydraulic dynamometer systems with low inherent inertia would appear to give superior performance compared to the electric dynamometer system when the simulated characteristics are in a forward path of the control system (method (1)), whereas the electric dynamometer system with its slower response and large inherent inertia gives superior performance when the simulated characteristics are in a feedback path of the control system (method (2)).

However, an assessment of the accuracy of simulation using method (1) is not easy with the root locus method (although it provides a clear indication of stability conditions) and it may be better to use the mathematical model of the system to determine some performance index (e.g., ISE or IAE) for the torque and speed responses over a given set of speed/time curves.

The virtue of the root locus method lies in its ability to show how the performance of the load simulation system varies over the speed range, since, for a given torque level, the non-linear functions of the system depend mainly on speed. Furthermore, it is possible to identify the root positions of various components of the system, such as the roots due to the flexible coupling; the input actuators for the engine and dynamometer; the low pass filter lags (T5 and T7); and the oscillatory low frequency roots at low speed resulting from the high governor gain. It is therefore possible to determine how these roots are affected by changes in speed, as well as changes in other parameters of the system (e.g., dynamometer inertia, simulated friction coefficients, etc.). All of these capabilities with the root locus method give considerable insight and understanding into the overall nature of load simulation techniques.

The following two chapters will show briefly the effects of load simulation techniques for the two other basic types of prime mover used for automotive purposes:- (a) Petrol engine (Part 4); (b) D.C. traction motor (Part 5). These chapters are basically to be used for comparison with the work undertaken in this chapter and will therefore not contain the same degree of detailed analytical work that has been necessary so far. The discussion of Part 5 includes a comparison of the basic dynamometer systems for the three types of prime mover.

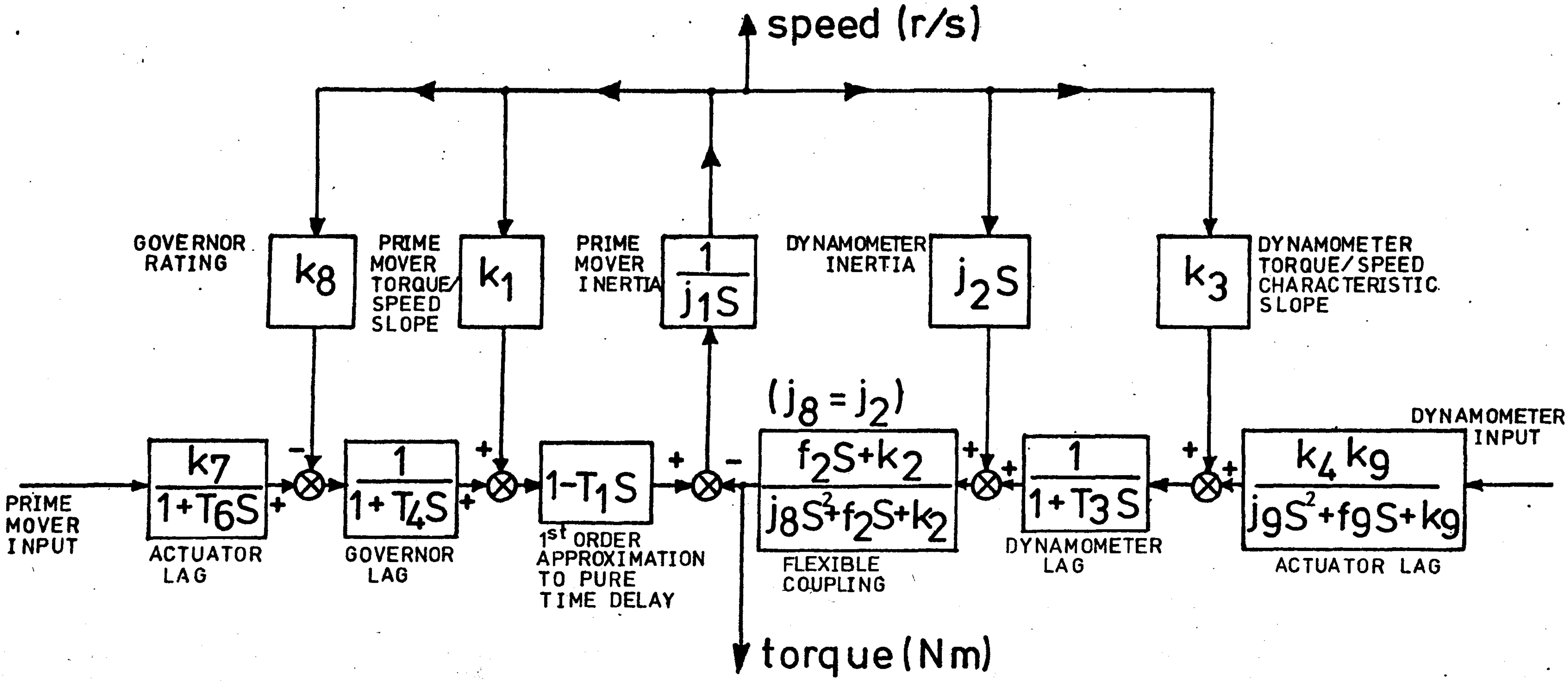

Figure 3.1 diesel engine and hydrostatic dynamometer block diagram

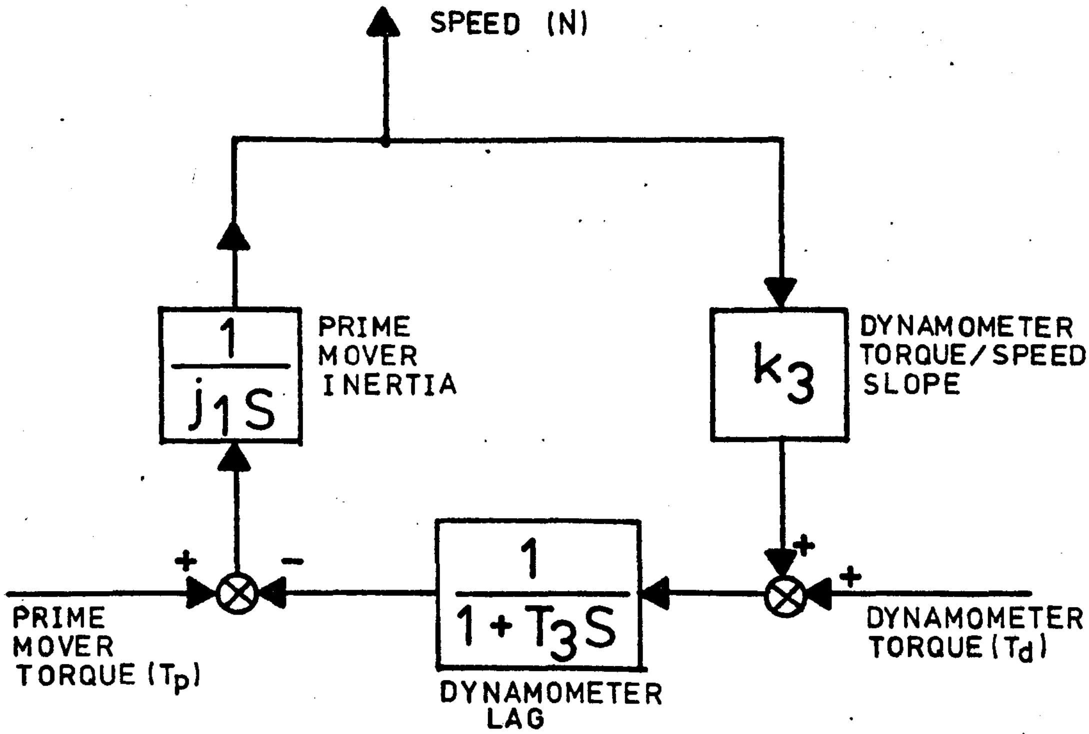

$$\frac{N}{T_p} = \frac{1 + T_3 S}{j_1 T_3 S^2 + j_1 S + k_3} \qquad (7)$$

$$\zeta = \frac{j_1}{2\sqrt{j_1 T_3 k_3}} = 0{\cdot}31 \text{ (low speed)} \qquad (8)$$

$$\omega_n = \sqrt{\frac{k_3}{j_1 T_3}} = 17{\cdot}8 \text{ r/s (low speed)} \qquad (9)$$

Figure 3.2 determination of low frequency roots (motoring condition)

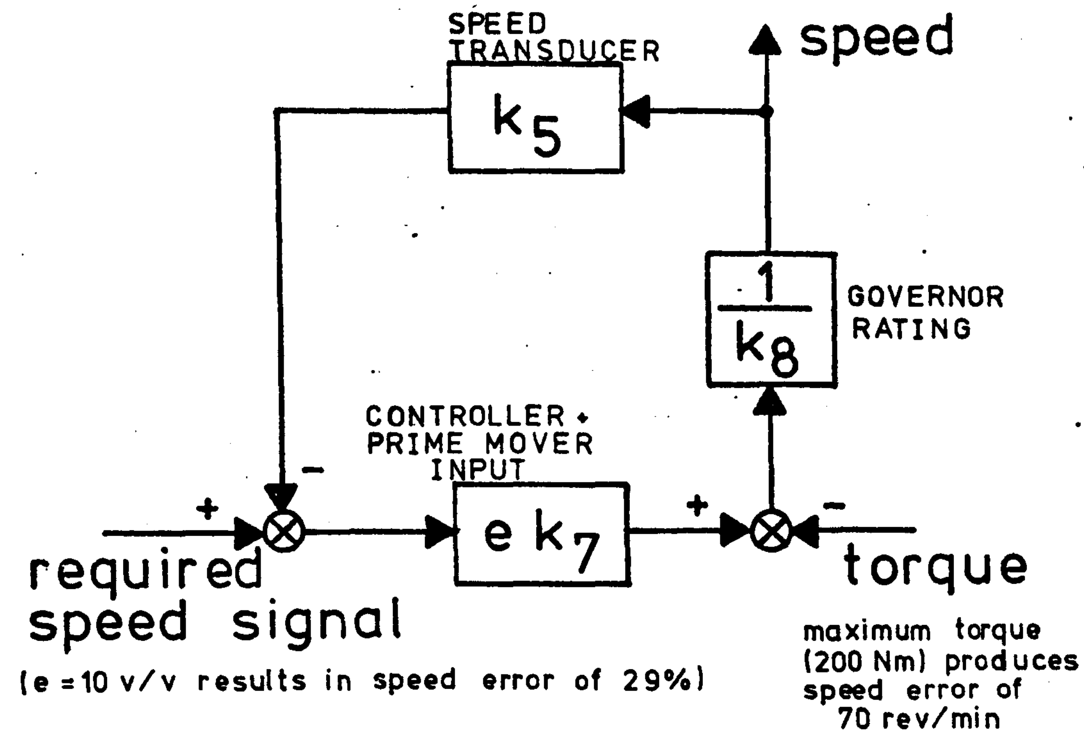

Figure 3.3 steady state block diagram for speed control loop

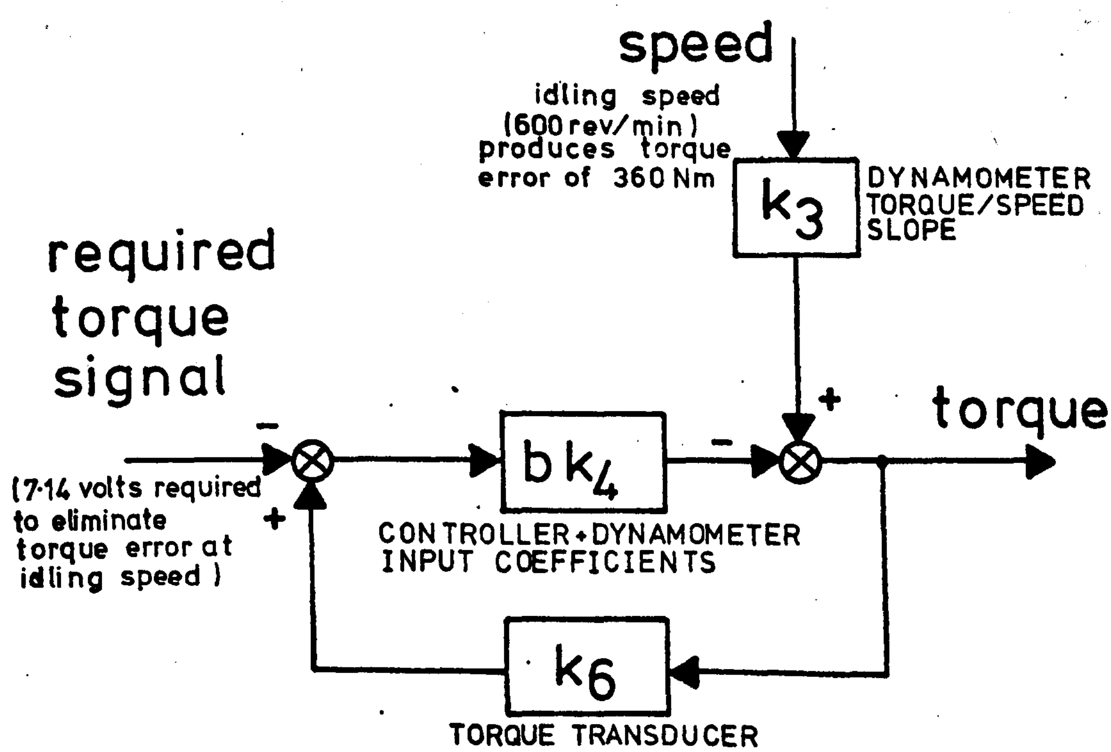

Figure 3.4 steady state block diagram for torque control loop

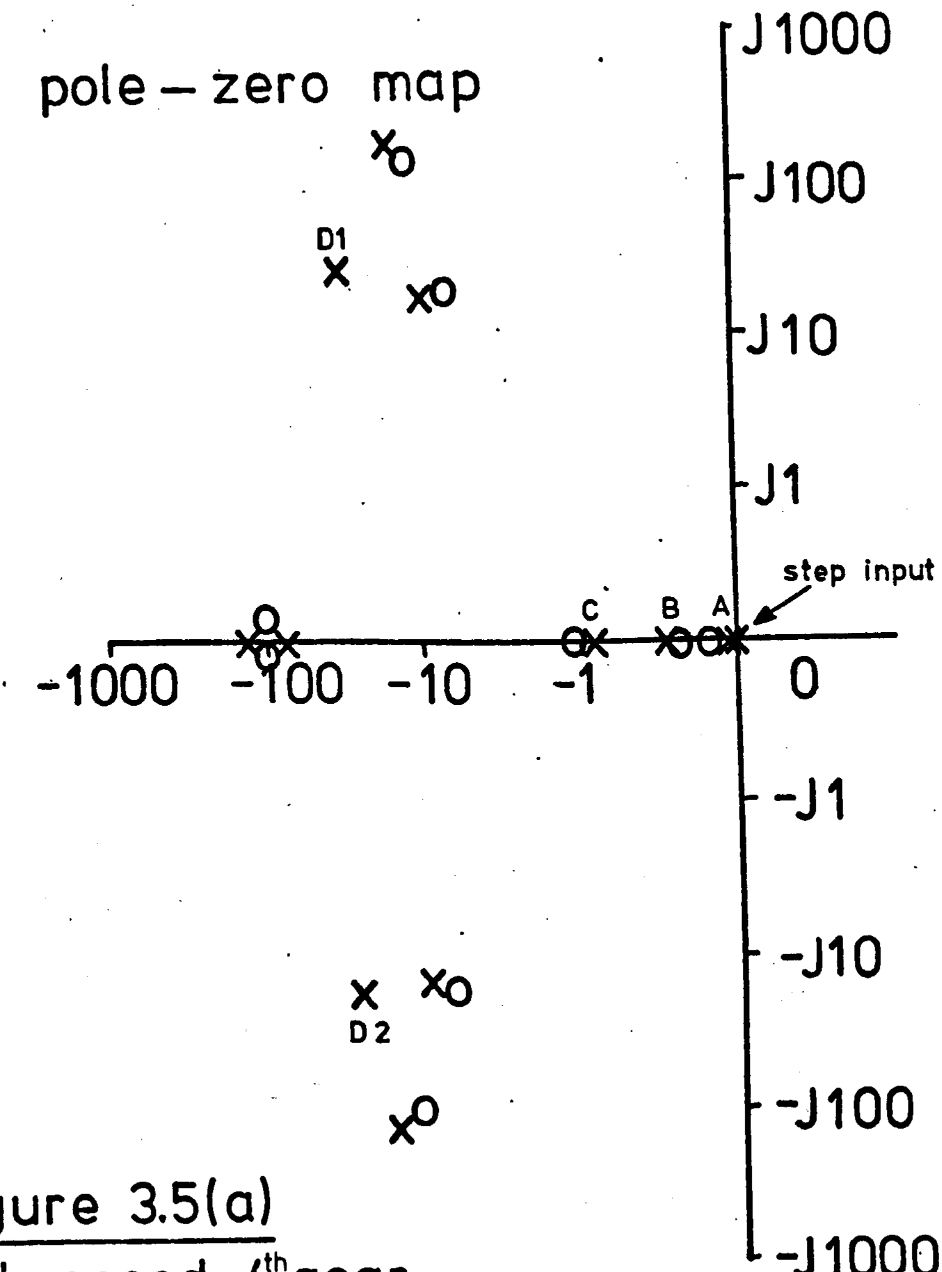

Figure 3.5(a)

high speed; 4th gear; normal fuel delivery

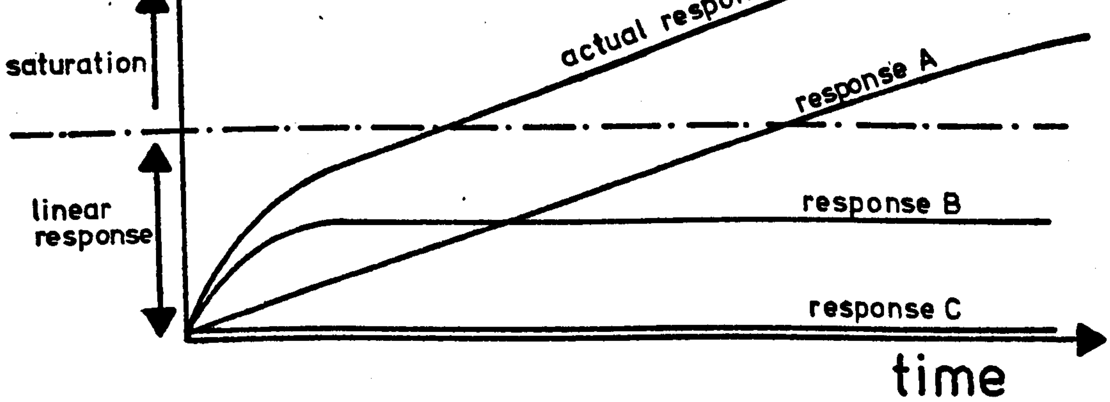

Figure 3.5(b)

speed response to step change in torque

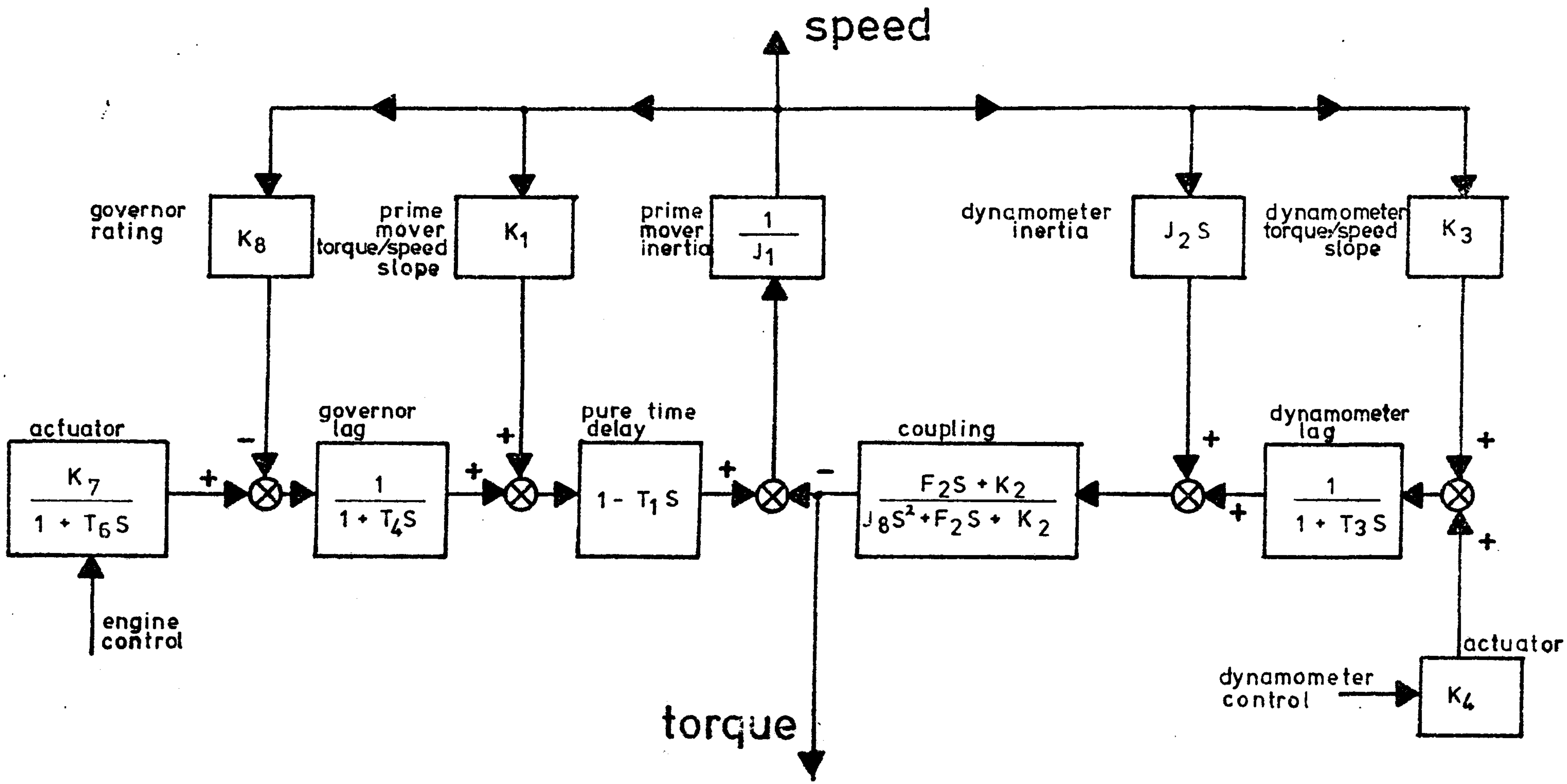

Figure 3.6 Basic block diagram for diesel engine +electric dynamometer

PART 4

PETROL ENGINE SYSTEMS

4.1 Introduction

The purpose of this section is to continue the analytical methods used in Part 3 for a 101.5 kW Ford petrol engine (model 2614E) to be tested in conjunction with the three dynamometer systems and two basic methods of load simulation analysed in Part 3. The same vehicle characteristics (Ford A series truck) are used with slight modifications due to the higher speed range of the petrol engine (600 → 6000 rev/min) compared to the diesel engine (600 → 3600 rev/min). One major difficulty with this higher speed range in connection with hydrostatic systems is that commercially available high power hydrostatic pumps (> 100 kW) are not capable of reaching such high speeds.

To overcome this difficulty it is necessary either to use a reducing gearbox in connection with the hydrostatic pump or use a combination of lower power hydrostatic pumps (having a higher speed range) connected in tandem. To enable comparisons to be made with the systems analysed in Part 3 the following speed ranges are used:-

Low speed - 1000 rev/min; Medium speed - 2500 rev/min;
High speed - 4000 rev/min.

A linear interpolation will be made for each of the dynamometer systems analysed in Part 3 to give the dynamometer transfer characteristics at these higher speed ranges for use in conjunction with the petrol engine system.

4.2 Hydrostatic Dynamometer

4.2.1 Transfer Characteristics of Engine + Dynamometer

The basic block diagram for the petrol engine and hydrostatic dynamometer system is shown in Fig. 4.1. The engine transfer characteristics were obtained from the Ford Motor Co. Ltd. as follows:-

Inertia of rotating and reciprocating parts,

$J1 = 0.1798$ kg m^2

The torque/speed characteristics (as shown in graph G1 for full throttle) provide the following information:-

K1 (low speed, 1000 rev/min) = +0.269 Nm s

K1 (medium speed, 2500 rev/min) = 0

K1 (high speed, 4000 rev/min) = -0.367 Nm s

Under the motoring condition K1 is estimated from half the maximum power rating, i.e.,

K1 = -95 Nm @ 5000 rev/min = -0.181 Nm s

Information on the engine characteristics at less than maximum throttle setting was not made available to the author, although typical characteristics are given in Ref. (10). In practice, the positive torque/speed slope at low speed is eliminated at low throttle settings and the slope becomes negative throughout the speed range (resulting in negative feedback under all conditions). An estimation to this performance was made by choosing a torque/speed slope, K1 = -.223 Nm s, and a prime mover input gain, K7 = 22 Nm/v.

Input gains (for full throttle position obtained by 10 v signal):-

K7 (low speed) = 17.2 Nm/v

K7 (medium speed) = 23.2 Nm/v

K7 (high speed) = 38 Nm/v

Pure time delay (between firing cycles):-

T1 (low speed) = 0.02 s

T1 (medium speed) = 0.008 s

T1 (high speed) = 0.005 s

Dynamometer characteristics:-

Inertia = .109 kg m^2 (as previously)

Under the loading condition the following values were interpolated from the dynamometer characteristics of section 3.2.1:-

Low speed (1000 rev/min):

$T3 = .0145$ s; $K3 = 8.3$ Nm s; $K4 = 241$ Nm/v

Medium speed (3500 rev/min):

$T3 = .0119$ s; $K3 = 6.7$ Nm s; $K4 = 197$ Nm/v

High speed (4000 rev/min):

$T3 = .0082$ s; $K3 = 5.1$ Nm s; $K4 = 149$ Nm/v

Under the motoring condition the characteristics of the hydrostatic dynamometer remain relatively constant over the speed range (due to the large leakage rate from the hydrostatic system), hence the same values may be used:-

$T3 = .015$ s; $K3 = 1.78$ Nm s; $K4 = 52.7$ Nm/v

The characteristics of the dynamometer and prime mover input actuators remain the same as given in section 3.2.1, as well as the characteristics of the flexible coupling.

Using these values a root locus was constructed for the speed range of the basic petrol engine and dynamometer system (with no external feedback loops), as shown in graph G74. The basic system is seen to be well damped with a very fast response under both the loading and motoring conditions. Maximum fuel delivery conditions resulting in zero prime mover control will not be examined with this system since the petrol engine is normally operated at maximum throttle for only a small percentage of its operating life in comparison to the governed diesel engine. At low speed under the loading condition the high frequency second order roots result not from the positive feedback effect of the left-hand side of the engine torque/speed characteristic as the throttle setting approaches maximum (as would be expected), but from the increased gain of the dynamometer torque/speed slope at low speed. In fact, the magnitude of the torque/speed slope of the petrol engine is small compared to that of the hydrostatic dynamometer under all conditions.

4.2.2 Simulation Method 1.1 Torque control by dynamometer Speed control by prime mover

By setting G1 and G3 to unity on the computer program VALUES it was possible to determine the effect of various settings of controller coefficients upon the root positions of the petrol engine and hydrostatic dynamometer system using simulation method 1.1. Suitable values of controller coefficients were found to be:-

Dynamometer	(	Proportional gain, B = 1 v/v
	(	
Controller	(	Integral gain, C = 5 s^{-1}

Engine	(	Proportional gain, E = 5 v/v
	(	
Controller	(	Integral gain, F = 0.3 s^{-1}

The low value of integral gain on the engine controller was necessary since higher gains caused low frequency roots to become unstable under the loading condition. This low value of integral gain (F) in conjunction with the high proportional gain (E) results in a very slow dominant speed response to disturbance torques, as shown in the root locus of graph G75 (using the above controller coefficients). This slow response is due to the low valued root (S + F/E) which results from the engine controller transfer function = $\frac{ES + F}{S}$. If the integral action on the engine controller is eliminated then the low valued root disappears, although this will result in large steady state speed errors (to achieve full throttle setting would require a speed error of 600 rev/min with a proportional gain, E = 5 v/v).

The use of derivative action on either the engine or dynamometer controller was not found to improve the damping of the low frequency roots under any conditions. From graph G75 under the motoring condition the above values of controller coefficients result in first order dominant and secondary roots. By increasing the gain of the dynamometer controller (engine control becomes zero under the motoring condition) it is possible to increase the speed of response under the motoring condition, although, for reasons discussed in Part 1, it is more appropriate to use method 1.2 under this condition.

For method 1.1, reducing the velocity transducer time constant (T5) to 1 ms had negligible effect upon the root positions, except to reduce the time constant of the real secondary root at low speed under the loading condition. Varying the speed of response of the engine actuator by a factor of 10 either side of the nominal value (i.e., 0.001 → 0.1 seconds) was also found to have negligible effect upon the root positions at all speeds. (This was found to be the case for the diesel engine actuator under all conditions analysed in Part 3.)

4.2.3 Simulation Method 1.2 Speed control by dynamometer Torque control by prime mover

By setting G2 and F4 to unity (with G1 = G3 = 0) in the computer program VALUES the following values of controller coefficients were found to give suitable performance for simulation method 1.2:-

Dynamometer Controller	Proportional gain, B = 10 v/v Integral gain, C = 10 s^{-1}
Engine Controller	Proportional gain, E = 0.3 v/v Integral gain, F = 30 s^{-1}

The low value of proportional gain on the engine controller (E) was found necessary to prevent the flexible coupling roots from going unstable, although it was possible to use a large value of integral action (F). This meant that together with the high gains on the dynamometer controller the primary root responses were very fast for both the loading and motoring condition, as indicated in the root locus of graph G76. The root locus also shows that the secondary roots are well damped at all speeds under both the loading and motoring conditions. Under the loading condition it was found that higher gain values on the dynamometer controller (B = 20 v/v; C = 40 s^{-1}) resulted in a faster dominant response without reducing the damping of the secondary roots, although these gain values were found to reduce the damping of the dominant response under the motoring condition. No values of derivative action were found to cause any improvement in the root positions under any conditions.

Under low torque loading conditions at low speed (which results in the engine torque/speed characteristic slope becoming negative and therefore providing negative feedback), the change in root positions compared to high torque conditions is negligible. This is due to the fact that the feedback provided by the engine torque/speed characteristic is small compared to that provided by the hydrostatic dynamometer.

For this method of load simulation the effect of the velocity transducer lag and the engine actuator lag become significant. At high speed under the loading condition reducing the velocity transducer time constant (T5) to 1 ms caused high frequency roots to become virtually unstable ($\omega_n \simeq 4$ Hz; $\zeta \simeq 0.08$). Under the same conditions, increasing the engine actuator time constant (T6) to 0.1 second created oscillatory secondary roots ($\omega_n \simeq 1$ Hz; $\zeta \simeq 0.4$).

4.2.4 Simulation Method 2.1 (Torque Reference System)

4.2.4.1 Vehicle Characteristics

The vehicle inertia values referred to the engine shaft in each gear remain the same as in section 3.2.4.1. The friction values over the higher range of speed were obtained from graph G42 as follows:-

Gear	Low Speed (1000 rev/min)	Medium Speed (2500 rev/min)	High Speed (4000 rev/min)
4th	0.2	0.54	1.0
3rd	0.17	0.33	0.87
2nd	0.06	0.12	0.28
1st	0.025	0.038	0.063

These values were substituted into equation (4) to determine the time constants of the first order response of the real vehicle under all conditions as follows:-

Loading Condition (Throttle near maximum)

Engine Speed (rev/min)		1000	2500	4000
Time Constant (s)	1st	-5.03	32.2	2.85
	2nd	-21.9	38.1	7.06
	3rd	-151.1	45.3	12.1
	4th	-381.5	48.7	19.2

Motoring Condition

Engine Speed (rev/min)		1000	2500	4000
Time Constant (s)	1st	5.93	5.59	5.02
	2nd	18.9	15.2	9.91
	3rd	42.6	29.2	14.2
	4th	69.1	36.5	22.3

At low speed under the loading condition the response is unstable in all gears with the throttle setting approaching maximum. This is due to the fact that the friction characteristics of the vehicle at low speed have a much lower negative torque/speed slope than the positive torque/speed slope of the engine characteristics for high throttle settings. In practice this unstable response shows that the vehicle will accelerate at an increasing rate for a given throttle setting. As the speed increases the response becomes stable and settles down with the time constant which occurs at high speed. Lower throttle settings are not shown since under these conditions the engine torque/speed slope becomes positive throughout the speed range so that the response is always stable. At medium speed the time constants appear excessively large, considering the throttle is near maximum. However, from equation (4) the magnitude of the response is inversely proportional to (F4 - K1), i.e., the vehicle torque/speed slope minus the engine torque/speed slope. Under these conditions (F4 - K1) becomes small so that the magnitude of the response becomes large and the actual response is faster than indicated by the time constant at high speed.

Under the motoring condition the real vehicle response appears to be slow at low speed. In practice the real vehicle reduces speed somewhat faster than indicated, due to coulomb friction effects. Coulomb friction terms, however, are constant in nature and therefore do not affect the transient performance of the vehicle. The time constants obtained for the real vehicle under both loading and motoring conditions will be used to determine the performance of load simulation methods 2.1 and 2.2 for each type of dynamometer system (in conjunction with the petrol engine) throughout the remainder of Part 4.

4.2.4.2 <u>Analysis</u>

For simulation method 2.1 the following values of controller coefficients were found to result in suitable performance with a time constant for the acceleration signal of T7 = 1 s:-

Dynamometer Controller	(	Proportional gain, B = 1 v/v
	(	Integral gain, C = 1 s^{-1}
Engine Controller	(	Proportional gain, E = 20 v/v
	(	Integral gain, F = 1 s^{-1}

It was found possible to use this constant value of T7 without creating the stability problems encountered with the diesel engine system, since the oscillatory low speed performance (due to the high gain governor on the diesel engine) does not occur with the petrol engine system. The low gain values on the dynamometer controller were necessary to prevent low frequency roots from becoming oscillatory under all conditions, although too low a value of proportional gain (B) resulted in oscillatory low frequency roots occurring under the motoring condition at high speed in high gear. Under the loading condition lower values of proportional gain on the engine controller resulted in oscillatory roots of very low frequency occurring throughout the speed range for all gear settings, whereas higher values of integral gain on the engine controller resulted in oscillatory low frequency roots occurring at low speed in high gear only.

Lower values of throttle setting at low speed under the loading condition (resulting in a negative torque/speed slope for the engine) had little effect upon the root positions except to slightly increase the damping of the dominant response in high gear. Using these values of controller coefficients root loci were constructed for the range of speed in 1st gear (graph G77) and 4th gear (graph G78) under both loading and motoring conditions. These root loci show that the system is well damped under all conditions, although the dominant response under the motoring condition becomes second order in low gear. This is not a problem, however, since it has already been discussed in Part 3 that under actual automotive conditions it is not normal practice to "motor" a vehicle in low gear. The dominant response time constants (which may be compared with those for the real vehicle shown in section 4.2.4.1) were obtained as follows:-

<u>Loading Condition</u>

(Throttle near maximum; E = F = 0)

Engine Speed (rev/min)		1000	2500	4000
Time Constant (s)	1st	-6.1	27.5	ω_n .255; ζ .69
	2nd	-20.1	37.7	7.86
	3rd	-146.1	45.9	13.3
	4th	-374.4	49.5	20.5

<u>Motoring Condition</u>

Engine Speed (rev/min)		1000	2500	4000
Time Constant (s)	1st	ω_n.173; ζ .87	ω_n.178; ζ .85	ω_n.188; ζ .82
	2nd	21.4	17.1	11.0
	3rd	45.1	31.2	15.4
	4th	71.6	38.2	23.6

The correlation between these predicted values for the load simulation system and those for the real vehicle is quite close, with the greatest differences occurring in 1st gear under both the loading and motoring conditions. For this system the effect of increasing the acceleration lag (T7) to 10 seconds was to increase the dominant response time constant under all conditions, as well as to create oscillatory low frequency roots at low speed under the motoring condition. Reducing T7 to 0.1 s resulted in low frequency roots becoming unstable in high gear under both loading and motoring conditions.

Reducing the velocity transducer time constant to 1 ms had negligible effect in low gear, although in high gear oscillatory roots ($\omega_n \simeq 3.5$ Hz; $\zeta \simeq .06$) were created under the loading condition, whereas under the motoring condition these roots became unstable. Variations in the engine actuator lag from 1 ms to 0.1 s had negligible effect upon the root positions under all conditions.

4.2.5 Simulation Method 2.2 (Speed Reference System)

For simulation method 2.2 no values of controller coefficients could be found to give good performance in all gears. The following values were found suitable for 2nd, 3rd and 4th gears:-

Dynamometer Controller	(Proportional gain, B = 10 v/v (Integral gain, C = 3 s^{-1}
Engine Controller	(Proportional gain, E = 30 v/v (Integral gain, F = 1 s^{-1}

In 1st gear suitable performance could be obtained with the same dynamometer controller coefficients but with a reduction in the engine controller coefficients as follows:-

Engine Controller (1st gear)	(Proportional gain, E = 6 v/v (Integral gain, F = 0.3 s^{-1}

In Part 3 it was discovered that the diesel engine and hydrostatic dynamometer system also required modification of the controller coefficients when 1st gear loading conditions were simulated using method 2.2. This effect is due to the limited ability of simulation method 2.2 to simulate low values of inertia as discovered with the low power simulation system in section 2.3.2.

In general, for higher gear settings it was found possible to have higher gain values for both the engine and dynamometer controller without causing stability problems. The least favourable stability conditions at high controller gains were found to occur at low speed in low gear. Under the motoring condition higher values of proportional gain on the dynamometer controller increased the lag of the secondary root response, whereas reducing this gain resulted in oscillatory low frequency roots. Also, under the motoring condition, higher values of integral gain on the dynamometer controller increased the speed of response of the secondary roots (thereby reducing their effect) and lower values reduced this speed of response. Using the above values of controller coefficients root loci are shown for the range of speed in 1st gear (graph G79) and 4th gear (graph G80).

The roots are well damped under all conditions although, from the increased scale of graph G80 it can be seen that under the motoring condition in 4th gear the time constant of the most significant secondary root is large (approximately 3 seconds). Hence, to improve dynamic accuracy under the motoring condition an increase in the integral gain of the dynamometer controller is required as this condition is entered. Slow secondary roots also occur under the loading condition and to improve overall dynamic accuracy it is necessary to use the largest value of integral action in each gear consistent with a well damped response (i.e., higher values in high gear reducing for lower gear values).

The primary response time constants (which may be compared with those for the real vehicle in section 4.2.4.1) were obtained as follows:-

Loading Condition

(Throttle near maximum; E = F = 0)

Engine Speed (rev/min)		1000	2500	4000
Time Constant (s)	1st	-4.36	32.1	4.29
	2nd	-20.7	38.0	7.71
	3rd	-148.3	45.3	12.4
	4th	-377.4	48.7	19.5

Motoring Condition

Engine Speed (rev/min)		1000	2500	4000
Time Constant (s)	1st	6.89	6.49	5.87
	2nd	19.6	17.7	10.3
	3rd	43.1	29.6	14.4
	4th	69.5	36.7	22.4

These values are significantly closer to those of the real vehicle response than for the system using simulation method 2.1, although (as with method 2.1) the greatest differences occur in 1st gear.

The effect of reducing the velocity transducer time constant to T5 = 1 ms was to create high frequency oscillatory roots ($\omega_n \triangleq 3$ Hz; $\zeta \triangleq 0.3$) under all conditions, except for under the loading condition at high speed in high gear. Variations in the engine actuator lag from 0.1 s to 1 ms had negligible effect upon the root positions under all conditions.

The hydrostatic dynamometer has been shown to provide satisfactory performance for simulating automotive loads on the petrol engine system, with few of the stability problems encountered by the governed diesel engine system analysed in section 3.2. This is basically due to the de-stabilising effect of the high gain governor of the diesel engine upon the control loops of the various load simulation systems. The effect of using the fast response dynamometer upon the performance of the various load simulation systems in conjunction with the petrol engine is analysed in the following section.

4.3 Fast Response Dynamometer

4.3.1 Simulation Method 1.1 Torque control by dynamometer
Speed control by prime mover

The basic block diagram for the fast response dynamometer used in conjunction with the petrol engine is identical to that shown in Fig. 4.1 (for the hydrostatic dynamometer system). As with the hydrostatic dynamometer the coefficients for the fast response dynamometer at the higher speed ranges of the petrol engine were interpolated from the values obtained in section 3.3.1 as shown:-

Loading Condition:

Low speed (1000 rev/min)

T3 = .0081 s; K3 = 2.07 Nm s; K4 = 123 Nm/v

Medium speed (2500 rev/min)

T3 = .0030 s; K3 = 0.75 Nm s; K4 = 423 Nm/v

High speed (4000 rev/min)

T3 = .0024 s; K3 = 0.55 Nm s; K4 = 610 Nm/v

Motoring Condition:

Low speed (1000 rev/min)

T3 = .011 s; K3 = 2.07 Nm s; K4 = 72 Nm/v

Medium speed (2500 rev/min)

T3 = .0188 s; K3 = 0.50 Nm s; K4 = 15 Nm/v

High speed (4000 rev/min)

T3 = .0245 s; K3 = 0.15 Nm s; K4 = 5.0 Nm/v

Using these values suitable magnitudes were determined for the controller coefficients using simulation method 1.1 as follows:-

Dynamometer	(	Proportional gain, B = 0.1 v/v
	(	
Controller	(	Integral gain, C = 30 s^{-1}
Engine	(	Proportional gain, E = 10 v/v
	(	
Controller	(	Integral gain, F = 12 s^{-1}

As with the diesel engine system of section 3.3.2, the low value of proportional gain on the dynamometer controller is necessary to maintain stability of the flexible coupling roots at high speed under the loading condition (due to the high gain of the special purpose valve under this condition). A high integral gain is necessary on the dynamometer controller since lower values create oscillatory low frequency roots at low speed under the loading condition as well as to increase the dominant response time constant under the motoring condition. For the engine controller, lower values of proportional control (E) result in oscillatory low frequency roots at high speed under the loading condition, which become unstable at low speed. Lower values of integral action (F), however, increase the dominant response time constant (and therefore increase the dynamic error).

Using these values of controller coefficients a root locus was constructed for the range of speed, as shown in graph G81. The dominant response is fast and well damped under both the loading and motoring conditions and the secondary roots (not shown) were found to be fast enough to have negligible effect upon the response. Under the motoring condition all secondary poles were found to have zeros in close proximity so that higher values of integral gain on the dynamometer controller could be used to increase the dynamic accuracy without creating stability problems.

It was shown in section 3.3.1 that for the fast response dynamometer the magnitude of the dynamometer torque/ speed slope (K3) is proportional to the level of torque set up on the engine shaft. Also, in section 4.2.1, it was shown that the engine torque/speed characteristics are similarly affected by the torque level on the engine shaft. By varying these coefficients to determine the effect of simulating low torque levels upon the performance of the load simulation system it was found that low torque levels created no detrimental effects and actually improved the damping of the dominant response at low speed under the loading condition.

The effect of increasing the velocity transducer lag (T5) to 1.0 s was negligible under the motoring condition, whereas under the loading condition highly oscillatory low frequency roots were created at high speed, becoming unstable at low speed. Also under the loading condition the effect of increasing the lag of the engine actuator to 0.1 s was to create oscillatory roots having high frequency at high speed ($\omega_n \doteq 2$ Hz; $\zeta \doteq 0.4$) and low frequency at low speed ($\omega_n \doteq 0.5$ Hz; $\zeta \doteq 0.6$).

4.3.2 <u>Simulation Method 1.2</u> <u>Speed control by dynamometer</u> <u>Torque control by prime mover</u>

For simulation method 1.2 it was found that under the loading condition a low value of proportional action on the dynamometer controller (B) was necessary to maintain stability of the dynamometer actuator roots (i.e., the electrohydraulic servomechanism) at high speed. However, at high speed under the motoring condition a high value of proportional gain on the dynamometer controller is necessary to maintain an adequately damped dominant response (due to the low value of dynamometer gain (K4) which occurs under these conditions). Hence the following values of controller coefficients were found to be most suitable:-

Loading Condition:

Dynamometer Controller	Proportional gain, B = 3 v/v Integral gain, C = 30 s^{-1}
Engine Controller	Proportional gain, E = 0.3 v/v Integral gain, F = 30 s^{-1}

Motoring Condition:

Dynamometer Controller	Proportional gain, B = 20 v/v Integral gain, C = 30 s^{-1}

The high values of integral action on both controllers were found to produce a fast response without creating stability problems throughout the speed range. The low value of proportional gain on the dynamometer controller was necessary to prevent the flexible coupling roots from becoming unstable at low speed under the loading condition. Using these values of controller coefficients a root locus was constructed for the range of speed under both loading and motoring conditions, as shown in graph G82. The response is very fast under both the loading and motoring conditions (indicating good dynamic accuracy) with all roots being well damped.

The effect of increasing the velocity transducer lag to 1 s was to create oscillatory low frequency roots under both the loading and motoring conditions, becoming unstable at high speed under the loading condition. Increasing the engine actuator lag (T6) to 0.1 s was found to increase the speed of response under the loading condition throughout the speed range (although the response became second order at high speed).

4.3.3 Simulation Method 2.1 (Torque Reference System)

Using a lag on the acceleration signal (T7) of 1 second it was found necessary to have a lower value of proportional gain for the dynamometer controller (B) under the loading condition than under the motoring condition. The following values of controller coefficients were found to give suitable performance under each condition:-

Loading:

Dynamometer	(	Proportional action, B = 0.1 v/v
	(	
Controller	(	Integral action, C = 3 s^{-1}
Engine	(	Proportional action, E = 30 v/v
	(	
Controller	(	Integral action, F = 2 s^{-1}

Motoring:

Dynamometer	(	Proportional action, B = 1 v/v
	(	
Controller	(	Integral action, C = 3 s^{-1}

Under the loading condition higher values of proportional gain on the dynamometer controller (B) resulted in the flexible coupling roots becoming unstable at high speed for all gear settings. Under the motoring condition, however, lower values of proportional action (B) resulted in oscillatory secondary roots with low damping in high gear.

Higher values of integral action on the dynamometer controller caused the roots due to the electrohydraulic servomechanism to become unstable at all speeds in 4th gear under the loading condition, and reduced the damping of the secondary roots under the motoring condition. For the engine controller the high value of proportional gain (E) was necessary to prevent the dominant response from becoming too oscillatory in high gear under the loading condition. Higher values of integral action (F) were found to have a similar effect upon the dominant response under the same conditions.

Using the above values of controller coefficients root loci were constructed for the range of speed, as shown in graph G83 (1st gear) and graph G84 (4th gear). Under the motoring condition the secondary roots are fast and well damped, whereas under the loading condition the secondary roots are slower and therefore have a more significant effect upon the response. This is due to the speed control system for the engine, which modifies the characteristics of the overall load simulation system as discussed in section 3.2.4. The dominant responses of the system (for comparison with the real vehicle responses of section 4.2.4.1) were obtained as follows:-

Loading Condition

(Engine control zero; throttle near maximum)

Engine Speed (rev/min)		1000	2500	4000
Time Constant (s)	1st	-3.84	33.06	3.77
	2nd	-20.4	39.0	8.06
	3rd	-149	46.3	13.1
	4th	-379	49.7	20.26

Motoring Condition

Engine Speed (rev/min)		1000	2500	4000
Time Constant (s)	1st	7.25	8.54	12.0
	2nd	20.4	17.9	14.2
	3rd	43.9	31.3	16.7
	4th	70.4	38.3	24.7

The values are reasonably close to those of the real vehicle with the greatest errors occurring at high speed under the motoring condition. This is due to the fact that the dynamometer coefficients were interpolated from the low speed values of section 3.3.1. In practice, however, the special purpose valve would need to be re-designed for use with the higher flowrate requirements of the petrol engine system (due to the higher speed range). This would result in higher values for the torque/speed characteristics (K3 and K4) than were interpolated from the low speed values, thereby increasing the dynamic accuracy at high speed.

The effect of increasing the velocity transducer lag (T5) to 1 second was to create oscillatory low frequency roots in low gear which become unstable throughout the speed range in high gear under the loading condition. The effect of increasing the engine actuator lag (T6) to 0.1 s was to create oscillatory high frequency roots throughout the speed range under the loading condition. For the acceleration lag (T7) increasing T7 in high gear was found to improve the damping of the secondary roots, as well as reducing T7 in low gear. However, increasing T7 also caused an increase in the dominant response time constant, thereby increasing the dynamic error between the real vehicle response and that for the simulation system. As with basic simulation method (1) (vehicle characteristics in forward path), the effect of simulating low torque values in the system by varying the coefficients K1, K7, T3 and K3 simultaneously was found to have negligible effect upon the root positions.

4.3.4 Simulation Method 2.2 (Speed Reference System)

As with method 2.1 it was found that for an acceleration signal lag of T7 = 1 s it became necessary to have a low value of proportional gain on the dynamometer controller (B) under the loading condition, and a high value of gain under the motoring condition. This is because higher values of gain (B) caused the roots due to the dynamometer electrohydraulic actuator to become unstable at high speed under the loading condition, whereas low values of B created low frequency oscillatory secondary roots at all speeds under the motoring condition. Suitable controller gains were found to be:-

Loading:

Dynamometer Controller	Proportional gain, B = 2 v/v Integral gain, C = 10 s^{-1}
Engine Controller	Proportional gain, E = 30 v/v Integral gain, F = 1 s^{-1}

Motoring:

Dynamometer Controller	Proportional gain, B = 10 v/v Integral gain, C = 10 s^{-1}

Using these values root loci were constructed for the range of speed, as shown in graphs G85 (1st gear) and G86 (4th gear). Under the motoring condition the secondary roots in 4th gear have a greater influence upon the response than those obtained using method 2.1, whereas in 1st gear the secondary roots are slightly less significant. The high value of integral action on the dynamometer controller was found to reduce the significance of the secondary roots under all conditions by moving these roots away from the origin on the complex frequency plane. As with method 2.1, it was found that lower values of proportional action on the engine controller (E) created a highly oscillatory dominant response in high gear under the loading condition, although for method 2.2 this effect also occurred at low speed in low gear under the loading condition.

The low value of integral action on the engine controller (F) was necessary for the same reasons as with method 2.1, in that higher values created an oscillatory dominant response in high gear under the loading condition. The dominant responses for the system using these values of controller coefficients were determined as follows:-

<u>Loading Condition</u>

(Throttle near maximum; engine control zero)

Engine Speed (rev/min)		1000	2500	4000
Time Constant (s)	1st	-5.03	32.2	2.84
	2nd	-21.9	38.1	7.05
	3rd	-151	45.5	12.1
	4th	-382	48.8	19.3

Motoring Condition

Engine Speed (rev/min)		1000	2500	4000
Time Constant (s)	1st	5.93	5.50	4.72
	2nd	18.95	15.1	9.72
	3rd	42.7	29.2	14.1
	4th	69.1	36.5	22.2

Comparison of these values with those for the real vehicle (section 4.2.4.1) shows very close correlation under all conditions with the greatest errors occurring at high speed in low gear under the motoring condition (for the same reasons discussed in the previous section). Outside of these conditions the maximum error for this method of simulation is less than 0.5%.

At low speed under the loading condition the simulation of low torque values had negligible effect upon the root positions in high gear, although in low gear the damping of the low frequency secondary roots was reduced. The effect of increasing the velocity transducer lag (T5) to 1 second was to create highly oscillatory roots at high speed under both the loading condition ($\omega_n \triangleq 1$ Hz; $\zeta \triangleq .15$) and the motoring condition ($\omega_n \triangleq 0.15$ Hz; $\zeta \triangleq 0.3$) for all gear settings. At low speed these oscillatory roots became unstable under the loading condition, although under the motoring condition the damping of the secondary roots was greatly increased. The effect of increasing the engine actuator lag (T6) was negligible at high speed, although at low speed slightly oscillatory secondary roots ($\omega_n \doteq 2$ Hz; $\zeta \doteq 0.45$) were created in all gear settings.

It was shown in the previous section that the hydrostatic dynamometer provided satisfactory load simulation performance for the petrol engine with few stability problems. In this section it has been shown that the fast response dynamometer has a superior performance for both basic simulation methods (1) and (2), since the response under method (1) is faster than for the hydrostatic dynamometer (with a consequent smaller dynamic error). For method (2) the secondary roots are also much faster than for the hydrostatic dynamometer (and therefore less significant) and the dominant responses using method 2.2 are closer to the real vehicle values (although for method 2.1 the errors between real and predicted responses are approximately the same for both the hydrostatic and fast response dynamometer systems).

4.4 Electric Dynamometer

4.4.1 Simulation Method 1.1 Torque control by dynamometer
Speed control by prime mover

The block diagram for the basic electric dynamometer and petrol engine system is shown in Fig. 4.2. As with the hydrostatic and fast response dynamometer systems, the coefficients for the electric dynamometer were interpolated from the lower speed values of section 3.4.1 as follows:-

Loading Condition

Engine Speed (rev/min)	1000	2500	4000
K3 (Nm s)	-1.9	-.74	-.39
K4 (Nm/v)	198	80	43

Motoring Condition

Engine Speed (rev/min)	1000	2500	4000
K3 (Nm s)	.154	.062	.035
K4 (Nm/v)	198	80	43

Using these values, together with the same dynamometer time constant (T3 = 0.2 s), suitable values of controller coefficients for both the loading and motoring conditions were found to be:-

Dynamometer Controller	Proportional gain, B = 30 v/v Integral gain, C = 15 s^{-1}
Engine Controller	Proportional gain, E = 10 v/v Integral gain, F = 8 s^{-1}

Unlike the diesel engine system of section 3.4 no values of derivative action on either the engine controller or dynamometer controller were found to improve the root positions of the petrol engine system. Using these controller values a root locus was constructed for the range of speed under both the loading and motoring conditions, as shown in graph G87. The system roots are well damped with the dominant response under both conditions considerably faster than for the hydrostatic dynamometer (graph G75) and nearly as fast as for the fast response dynamometer (graph G81).

This is due to the high values of controller gains which are possible with this system (resulting in low dynamic errors). Under the loading condition lower values of proportional action on either the dynamometer or engine controller caused the secondary roots to become highly oscillatory at high speed and unstable at low speed. Under the motoring condition, however, lower values of proportional action on the dynamometer controller (B) caused the dominant response to become highly oscillatory at high speed.

Under the loading condition, lower values of integral action on the dynamometer controller (C) had negligible effect on the dominant response (although a low valued pole was created it was eliminated by zero cancellation), whereas under the motoring condition lower values of integral action (C) caused the dominant response to become first order (although, once again, a low valued pole was created which was eliminated by zero cancellation). Reducing the integral action on the engine controller (under the loading condition) resulted in the dominant response becoming slower, since a low valued pole was created without any zeros in close proximity.

As with the fast response dynamometer the simulation of low torque values results in a reduction of the dynamometer torque/speed slope K3 (as well as to cause the engine torque/speed slope to become negative at low speed). By simultaneously varying K1, K7 and K3 it was found that the simulation of low torque values had little effect upon the root positions compared to the simulation of near maximum torque conditions.

The effect of increasing the velocity transducer lag (T5) to 1 second had negligible effect under the motoring condition, whereas under the loading condition oscillatory secondary roots were created at high speed, becoming unstable at low speed. Increasing the lag of the engine actuator (T6) to 0.1 second created oscillatory secondary roots throughout the speed range under the loading condition.

4.4.2 Simulation Method 1.2 Speed control by dynamometer Torque control by prime mover

For simulation method 1.2 suitable values of controller gains were found to be:-

Dynamometer Controller	Derivative action, A = 5 s Proportional gain, B = 30 v/v Integral gain, C = 30 s^{-1}

Engine	(	Proportional gain, E = 1 v/v
Controller	(	Integral gain, F = 30 s^{-1}

The use of derivative action on the dynamometer controller enabled high values of proportional gain to be used without creating highly oscillatory secondary roots under both the loading and motoring conditions (although high values of derivative action caused the dominant response to become second order with low damping under all conditions). Using the above values of controller coefficients root loci were constructed for the range of speed under the loading and motoring conditions, as shown in graph G88. As with method 1.1, the response is well damped and fast, although not as fast as for the hydrostatic dynamometer (graph G76) or the fast response dynamometer (graph G82).

The low value of proportional gain on the dynamometer controller (E) was necessary to prevent the flexible coupling roots from becoming unstable under the loading condition. The use of derivative action on the engine controller (D) was found to make these roots go unstable for even lower values of proportional gain (E). Simulating low torque values on the system (by simultaneously varying K1, K7 and K3) had little effect upon the root positions, as was the case with method 1.1. The effect of increasing the velocity transducer lag (T5) to 1 second was to create unstable roots under both the loading and motoring conditions, whereas increasing the engine actuator lag (T6) to 0.1 s had negligible effect under all conditions.

4.4.3 Simulation Method 2.1 (Torque Reference System)

For simulation method 2.1 suitable values of controller coefficients were as follows:-

Dynamometer Controller	(	Derivative action, A = 1 s
	(	Proportional gain, B = 30 v/v
	(	Integral gain, C = 30 s^{-1}
Engine Controller	(	Proportional gain, E = 30 v/v
	(	Integral gain, F = 2 s^{-1}

As with simulation method 1.2, the use of derivative action on the dynamometer controller (A) enabled high values of proportional gain (B) to be used without creating highly oscillatory secondary roots. Low values of integral action on the engine controller (F) were necessary to prevent the dominant response from becoming second order with low damping under the loading condition in high gear. Derivative action on the engine controller (D) was, once again, not found to cause any improvement in root positions under all conditions.

Lower values of integral action on the dynamometer controller (C) have little effect upon the dynamic performance, since the low valued root which emerges is eliminated by zero cancellation. However, lower values of proportional gain on the engine controller (E) caused the dominant response to become second order with low damping at low speed for all gear settings, as well as throughout the speed range in high gear under the loading condition. Using these controller coefficients root loci were constructed for the range of speed, as shown in graphs G89 (1st gear) and G90 (4th gear). Under all conditions the secondary roots are fast and well damped. In particular, under the motoring condition, the secondary root nearest the origin (time constant approximately 1 s) has negligible effect due to a zero residing in close proximity, so that all secondary root effects are very small under this condition. The primary root responses (for comparison with the real vehicle response of section 4.2.4.1) were obtained as follows:-

<u>Loading Condition</u>

(Throttle near maximum; E = F = 0)

Engine Speed (rev/min)		1000	2500	4000
Time Constant (s)	1st	-4.27	32.9	3.60
	2nd	-20.9	39.0	8.02
	3rd	-150.1	46.3	13.1
	4th	-380.4	49.7	20.3

Motoring Condition

Engine Speed (rev/min)		1000	2500	4000
Time Constant (s)	1st	6.79	6.38	5.73
	2nd	19.93	16.1	10.85
	3rd	43.6	30.27	15.22
	4th	70.1	37.5	23.3

These values are in reasonable agreement with the real vehicle responses, although the error becomes large at low speed under both the loading and motoring conditions. In most cases the difference in time constant between real and predicted values is of the order of 1 second. This is due to the lag on the acceleration signal (T7) which is necessary to prevent instability of the flexible coupling roots when simulating large inertia values (i.e., in high gear). Increasing the lag of the velocity transducer (T5) to 1 second created unstable roots under all conditions and increasing the lag of the engine actuator (T6) created oscillatory secondary roots at high speed for all gear settings under the loading condition as well as at low speed for low gear settings.

4.4.4 Simulation Method 2.2 (Speed Reference Control)

For method 2.2 the following values of controller coefficients result in good performance under all conditions:-

Dynamometer Controller:
- Derivative action, A = 10 s
- Proportional gain, B = 30 v/v
- Integral gain, C = 30 s^{-1}

Engine Controller	(	Proportional gain, E = 30 v/v
	(	Integral gain, F = 2 s^{-1}

As discovered in the previous analysis, the use of derivative action on the dynamometer controller (A) enabled high values of proportional gain (B) to be used without creating highly oscillatory roots under both the loading and motoring conditions. Also, low values of integral action on the engine controller (F) were necessary to prevent the dominant response from becoming second order with low damping under the loading condition in high gear. Although the controller gains are similar to those used for method 2.1 in the previous section, the secondary roots are faster, as shown by the root loci of graphs G91 and G92 (1st and 4th gears respectively) and the dominant response time constants are much closer to those for the real vehicle (given in section 4.2.4.1), as shown in the following table:-

<u>Loading Condition</u>

(Throttle near maximum; E = F = 0)

Engine Speed	(rev/min)	1000	2500	4000
Time Constant (s)	1st	-5.05	32.2	2.93
	2nd	-21.9	38.1	7.07
	3rd	-151.1	45.3	12.1
	4th	-381.5	48.7	19.2

Motoring Condition

Engine Speed (rev/min)		1000	2500	4000
Time Constant (s)	1st	5.96	5.62	5.06
	2nd	18.96	15.2	9.92
	3rd	42.6	29.3	14.2
	4th	69.1	36.5	22.3

Increasing the velocity transducer lag (T5) to 1 second created oscillatory low frequency roots under all conditions, becoming unstable in low gear under the loading condition. Hence the electric dynamometer has been shown to give good performance for each of the methods of load simulation with the petrol engine system.

4.5 Discussion

Examination of the root loci for each of the dynamometer/petrol engine systems (graphs G74 → G92) shows similar trends compared to the diesel engine system. For basic simulation method (2) (with the simulated vehicle characteristics in a feedback path of the system) the use of speed reference control (method 2.2) results in dominant responses much closer to those of the real vehicle than for torque reference control (method 2.1). This is due to the lag on the acceleration signal (for simulation of the inertia characteristic) which is necessary to prevent low frequency roots from becoming unstable using method 2.1.

For basic simulation method (1) (with the simulated characteristics in a forward path of the system) the dominant responses are much faster using method 1.2 (speed control on dynamometer; torque control on prime mover) than method 1.1. Although for the diesel engine system the dominant responses were marginally faster for the hydraulic dynamometer under the loading condition using method 1.1.

One major difference between the control of the diesel and petrol engine systems is that for the petrol engine system the second order roots maintain a reasonable degree of damping even with high gain values on the engine and dynamometer controllers. For the diesel engine system under mid fuel delivery conditions, however, the high gain governor was shown to create highly oscillatory secondary roots at low speed regardless of the gains of the controller coefficients.

Comparison of dynamometer performance for the petrol engine system shows that for method 2.2 the fast response and electric dynamometer systems provide dominant responses much closer to those of the actual vehicle than for the hydrostatic dynamometer system, and have faster secondary roots under all conditions. However, for method 1.2 the situation is reversed and the hydrostatic dynamometer provides a faster response that the electric dynamometer, under both the loading and motoring conditions, resulting in a lower dynamic error. The relationship between speed of response (to a step disturbance torque) and dynamic error for simulation method (1) is due to the length of time taken for the integral action of both controllers to integrate out the torque and speed errors, resulting from the step disturbance torque, as shown in Fig. 4.3. In general, slow responses (low dominant roots) were due to the necessity of having low values of integral action to prevent instability of the secondary roots.

Although it was originally considered that the positive torque/speed slope for the petrol engine under low speed, high torque conditions might result in unstable operation (especially with the positive feedback effect of the electrical dynamometer system), it was found that this slope was small in comparison to the effect of the engine torque/speed control loops (due to the high controller gains) and unstable operation was only encountered with low controller gain settings.

One possible difficulty with the testing of spark ignition engines using hydrostatic systems is due to the limited speed range of high power hydrostatic units commercially available at present (generally less than 4000 rev/min for power ratings greater than 100 kW). Although a gearbox may be used to overcome this difficulty, this increases the complexity of the basic mechanical system, as well as increasing the torque "noise" on the engine shaft (due to gearbox chatter) and possibly creating torque control problems when changing from the loading to motoring conditions (due to backlash in the gear train).

As with the diesel engine system the use of derivative action was not found to improve the root positions for the hydrostatic and fast response dynamometer systems. Also, for the fast response and electrical dynamometer systems, larger values of the velocity transducer lag reduced the stability of the secondary roots (so that modifications to the controller coefficients are necessary if slower response transducers are to be used). Under certain conditions increasing the engine actuator lag (T6) by up to a factor of 10 created low frequency oscillatory secondary roots, whereas for the diesel engine such an increase had negligible effect.

The time constants obtained for the real vehicle response (as well as for simulation method (2)) were found to give a misleading indication of the speed of response of the vehicle at low and medium speeds. By examination of Fig. 4.4 it can be seen how the variation of time constant with speed affects the overall performance. At low and medium speeds the dominant roots are close to the origin and therefore have a high gain in response to a step input. As the speed increases the dominant root moves away from the origin so that the gain and time constant both reduce, resulting in an actual response with an average time constant slightly faster than the high speed value.

Having examined the performance of various load simulation systems for the two main prime movers used for automotive purposes (namely, the diesel and petrol engines), a brief analysis will be made in the following section for an electric traction motor, the use of which, for automotive purposes, is presently being encouraged for both economic and environmental reasons, Ref. (31).

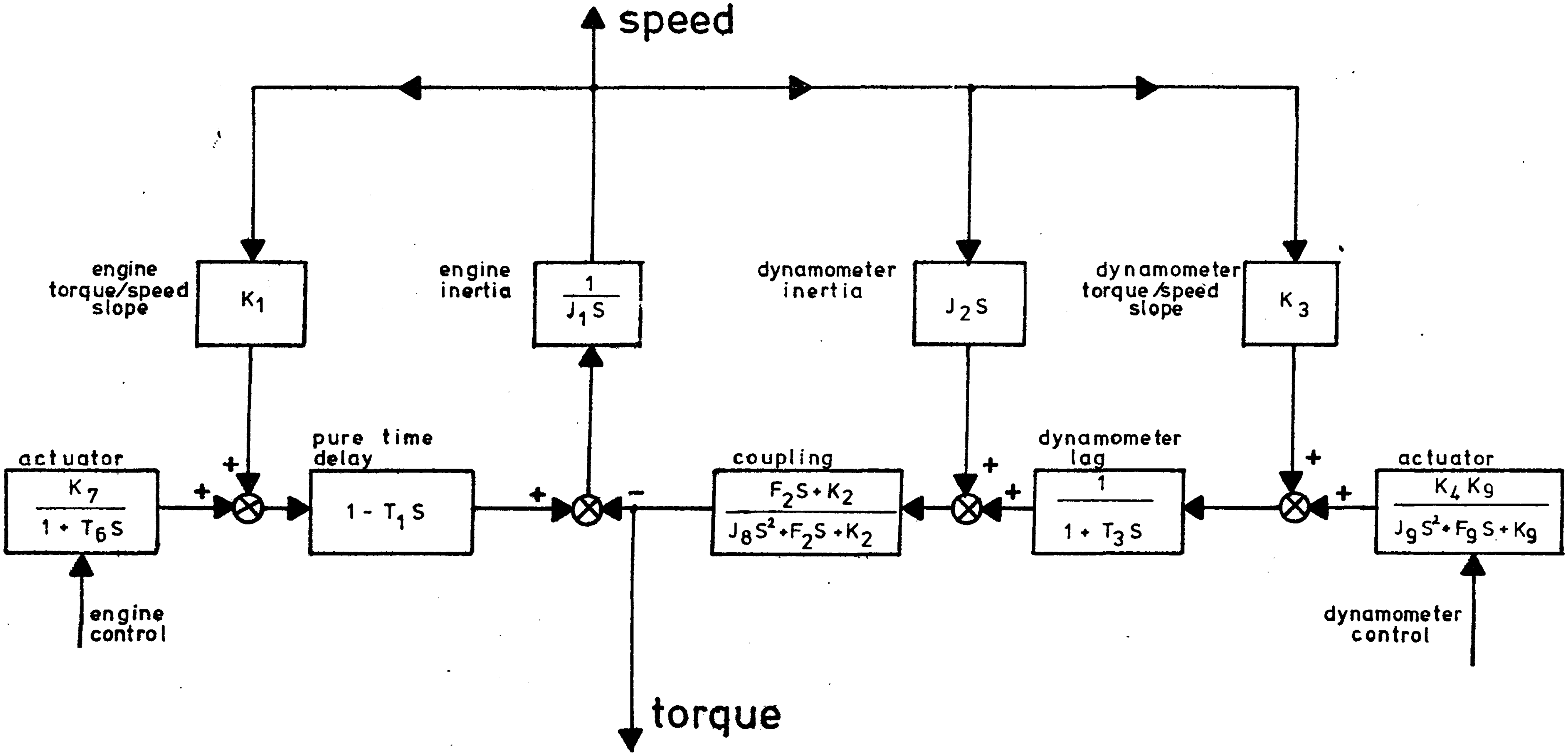

Figure 4.1 Basic block diagram for petrol engine + hydrostatic dynamometer

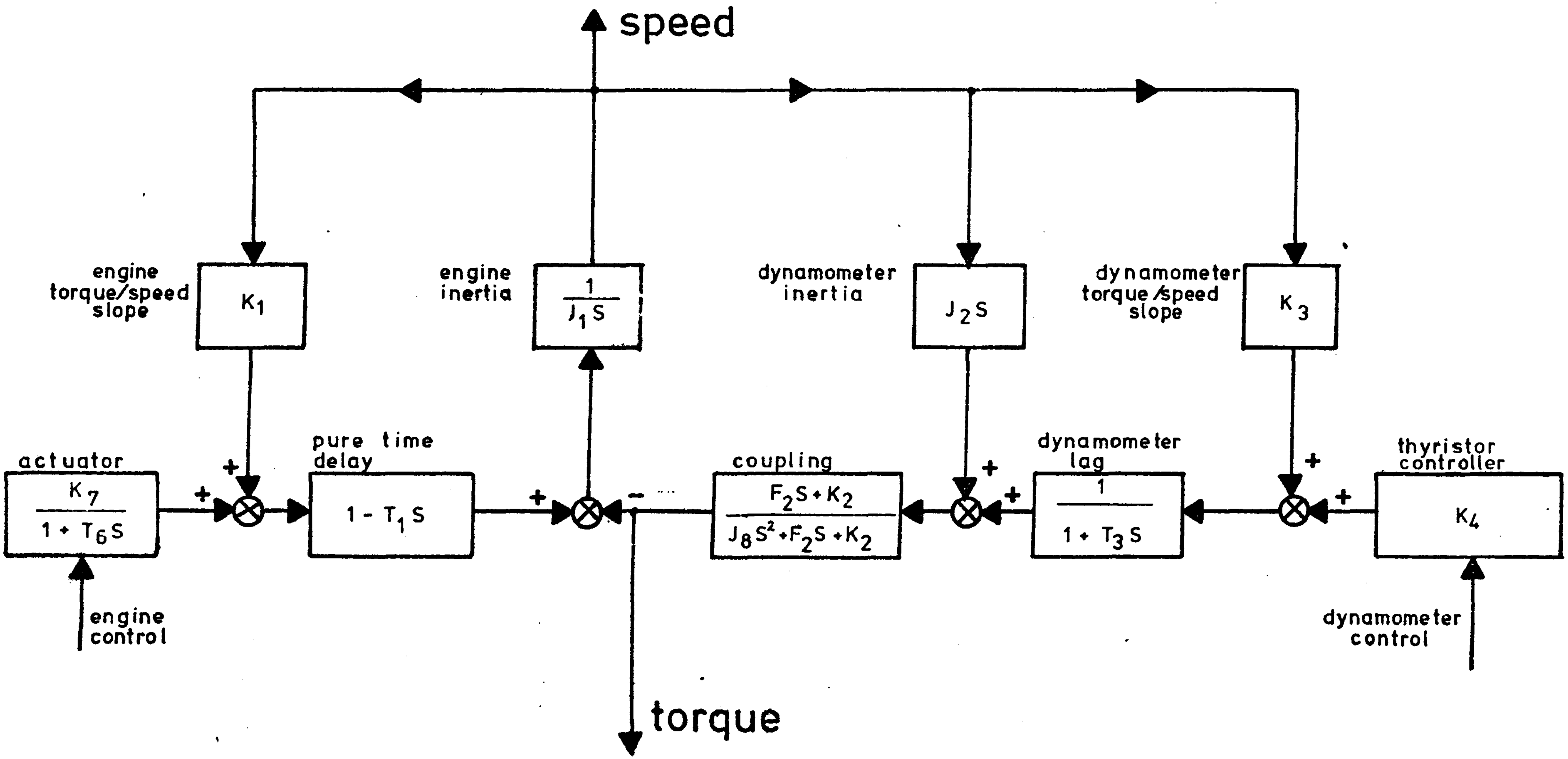

Figure 4.2 Basic block diagram for petrol engine + electric dynamometer

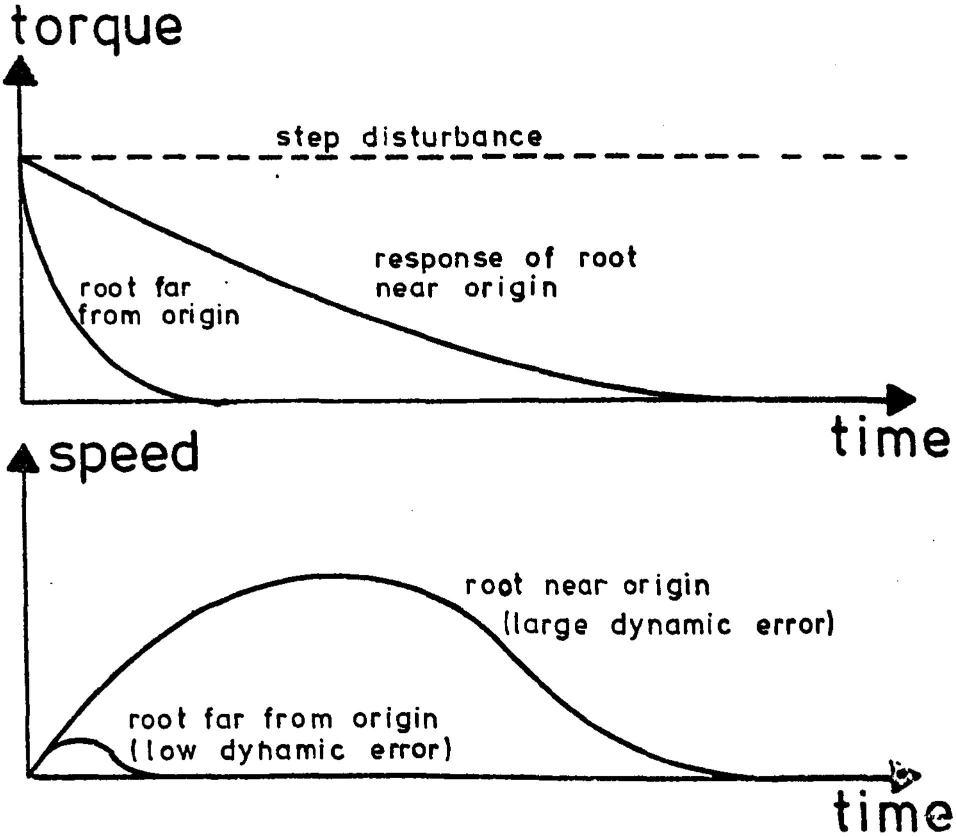

Figure 4.3 RELATIONSHIP BETWEEN DYNAMIC ERROR AND SPEED OF RESPONSE FOR BASIC SIMULATION METHOD (1)

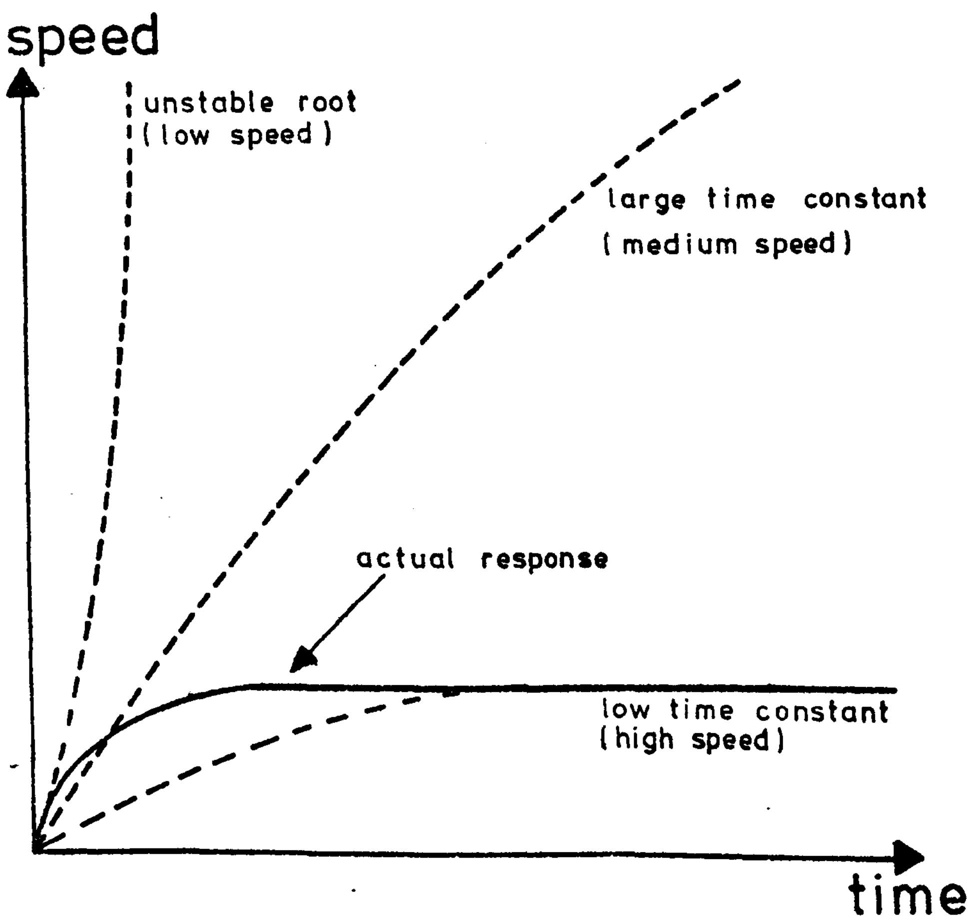

Figure 4.4 EFFECT OF TIME CONSTANT VARYING WITH SPEED FOR BASIC SIMULATION METHOD (2)

PART 5

ELECTRIC PRIME MOVER SYSTEM

5.1 Introduction

The purpose of this section is to continue the analytical methods used in Parts 3 and 4 for a prime mover which is becoming increasingly advantageous (from both economic and environmental viewpoints) for use in short haul vehicles, namely the electric traction motor. Manufacturers of electric vehicles are currently attempting to improve battery/motor/transmission/load characteristics for certain duty cycles for which the use of a vehicle load simulator in the laboratory provides obvious advantages, Ref. (30).

The analysis of this section will be to show the suitability of the previously analysed dynamometers and simulation methods for the simulation of a 7.5 tonne delivery vehicle (Silent Karrier developed by Chloride Ltd.) on a 75 kW separately excited d.c. traction motor with regenerative control. To increase the distance capability of the Silent Karrier the current supply is limited to give an effective power rating for the prime mover/controller of 48.5 kW. The speed range of the motor is 0 → 3000 rev/min so that the same speed ranges can be used as for the diesel engine systems of Part 3, i.e., low speed, 600 rev/min;

medium speed, 1500 rev/min; high speed, 3000 rev/min.

5.2 Transfer Characteristics of Motor and Vehicle

(Information supplied by Chloride Ltd.)

Vehicle weight = 7.5 tonnes

Transmission ratio = 6.81 : 1

Efficiency of transmission = 96%

Maximum vehicle speed = 64.4 km/hr

Maximum motor speed = 3000 rev/min

Hence vehicle inertia referred to motor shaft

$= 7500/(17.57)^2 = 24.3 \text{ kg m}^2$ (J3; J4)

(1 m/s vehicle speed = 17.57 r/s motor speed)

Vehicle friction characteristics referred to motor shaft obtained from graph G93:-

Low speed, F3 = F4 = 0.0425 Nm s

Medium speed, F3 = F4 = 0.11 Nm s

High speed, F3 = F4 = 0.248 Nm s

Motor armature inertia = 0.965 kg m^2

From the motor torque/speed characteristics of graph G3:-

(a) Loading condition:

Low speed (K1 = -15.6 Nm s (maximum)
(K7 = 175 Nm/v

Medium speed	(	K1	=	-1.74 Nm s (maximum)
	(	K7	=	58.3 Nm/v
High speed	(	K1	=	-0.21 Nm s (maximum)
	(	K7	=	22.0 Nm/v

The values given for the motor torque/speed slope (K1) represent the maximum values obtained under maximum power conditions. It will be necessary to check throughout the analysis whether or not lower values of K1 affect the performance of the load simulation system for values of controller coefficients determined at maximum K1.

(b) Motoring condition:

Under the motoring condition the effect of simulating the regeneration of power to the batteries may be achieved by retaining the same value of K7 and setting K1 positive with the same maximum magnitude as under the loading condition.

Also, for an electric prime mover, it is not necessary to use a flexible coupling to connect to the dynamometer system, as with prime movers of the internal combustion engine type.

Hence K2 = 1; F2 = J8 = 0

Due to thyristor control, the lag of the prime mover actuator becomes negligible, i.e., T6 = 0. For the prime mover field windings there is an inductance of 4.5 H and resistance of 6.5 Ω resulting in a prime mover time constant of T2 = 0.692 s. Substituting the motor and vehicle coefficients into equation (3) enables the dominant response time constants for the real vehicle (speed response to a step disturbance torque) to be evaluated as follows:-

(a) Loading:

Prime mover speed (rev/min)	600	1500	3000
Dominant response	ω_n .945 r/s ζ .765	τ = 12.547 s	τ = 54.85 s

(b) Motoring:

Prime mover speed (rev/min)	600	1500	3000
Dominant response	τ = -2.149 s	τ = -16.79 s	τ = +668.9 s

$\underbrace{\tau = -2.149\text{ s} \quad \tau = -16.79\text{ s}}_{\text{Unstable roots}}$

At very low speeds (less than 600 rev/min) the current limit causes the prime mover torque/speed slope to become zero (graph G3), which results in the same dominant response time constant under both the loading and motoring conditions of τ = 594.5 s. As with previous analysis these time constants do not provide a very good indication of the real time response of the vehicle (to a step disturbance torque) for the same reasons given in the discussion of Part 4 and shown in the responses of Fig. 4.4. In fact, under the motoring condition, the dominant root remains fairly close to the origin throughout the speed range. This indicates that, under the motoring condition, the dominant speed response of the vehicle to a step change in disturbance torque will be in the form of a ramp change rather than the exponential responses of the previously analysed prime mover systems.

5.3 Hydrostatic Dynamometer

Since the electric prime mover can achieve a very high torque at low speed, it is necessary for the hydrostatic units to have a much higher power rating than those analysed in Parts 3 and 4 in order to be able to simulate this high torque/low speed condition. As an approximation to this higher power rating the dynamometer coefficients K3, K4 and J2 were increased by a factor of 2.5 under all conditions, with all other dynamometer coefficients remaining as given in section 3.2.1.

5.3.1 Simulation Method 1.1 Torque control by dynamometer
Speed control by prime mover

For simulation method 1.1 suitable values of controller gains were found to be:-

Dynamometer Controller	(	Proportional gain, B = 1 v/v
	(	Integral gain, C = 3 s^{-1}
Prime mover Controller	(	Derivative gain, D = 10 s
	(	Proportional gain, E = 10 v/v
	(	Integral gain, F = 3 s^{-1} (loading); F = 0 (motoring)

It was necessary to zero the integral action on the prime mover controller (F) under the motoring condition, since the use of integral action in conjunction with the positive feedback effect of the prime mover (under the motoring condition) created two unstable roots at low and medium speed. Under the loading condition higher values of integral action (F) could not be used, since this caused the dominant response to become second order with low damping for low values of the prime mover torque/speed slope (these occur at very low speed due to the current limit on the prime mover, and at high speed).

The high value of proportional gain on the prime mover controller (E) was necessary to stabilise the single unstable root which occurs throughout the speed range under the motoring condition (due to the positive feedback effect of the prime mover torque/speed slope). The use of derivative action on the prime mover controller (D) improved the damping of the secondary roots under all conditions.

On the dynamometer controller the low value of proportional gain (B) was necessary to maintain the stability of the electrohydraulic actuator roots under all conditions. Higher values of integrator gain (C) resulted in oscillatory low frequency roots throughout the speed range under the loading condition and at very low speed under the motoring condition. The use of derivative action on the dynamometer controller (A) was not found to cause any significant improvement in root positions under all conditions.

Using these controller values root loci were constructed for the range of speed under both the loading and motoring conditions, as shown in graph G94. The roots are well damped under all conditions except at low speed under the loading condition. Also, the dominant response is slow at low and medium speeds under the loading condition (indicating possible large dynamic errors) and it is not possible to maintain steady state conditions at low speed under the motoring condition (600-800 rev/min), as indicated by the single unstable root on the right-hand side of the complex frequency plane. However, this effect is not a problem for the purposes of load simulation, since the dominant response of the real vehicle under the motoring condition has already been shown to be represented by a single unstable root at low and medium speeds (for maximum power regeneration).

The simulation of low torque values (determined by reducing the prime mover torque/speed slope, K1) was found to have little effect upon the root positions under all conditions, except to stabilise the dominant unstable root at low speed under the motoring condition. The effect of reducing the time constant of the velocity transducer (T5) was to improve the damping of the low frequency roots under all conditions at the expense of an increase in the dominant response time constant.

5.3.2 Simulation Method 1.2 Speed control by dynamometer Torque control by prime mover

For simulation method 1.2 much higher controller gains were possible than for method 1.1 as shown:-

Dynamometer Controller	Proportional action, B = 15 v/v Integral action, C = 20 s^{-1}
Prime mover Controller	Derivative action, D = 10 s Proportional action, E = 20 v/v Integral action, F = 20 s^{-1}

These high controller gains resulted in a fast response (hence low dynamic error) with well damped roots, as indicated by the root loci of graph G95. In particular the high values of proportional action on both controllers resulted in no unstable single roots under the motoring condition (as occurred with method 1.1). The use of derivative action on the prime mover controller (D) enabled high values of proportional and integral action to be used without creating oscillatory secondary roots under all conditions, although derivative action on the dynamometer controller (A) was not found to cause any significant improvements in root positions.

Due to the use of high values of proportional action on both controllers it was necessary for the integral gain of both controllers also to be high, since low values resulted in a slow dominant response under all conditions. The effect of simulating low torque values (by reducing the magnitude of the prime mover torque/ speed slope, K1) was found to be negligible throughout the speed range under both loading and motoring conditions, and the effect of reducing the velocity transducer time constant (T5) to 1 ms was to create high frequency roots ($\omega_n \triangleq 3 \rightarrow 6$ Hz) with very low damping under all conditions, becoming unstable at low speed under the motoring condition.

5.3.3 Simulation Method 2.1 (Torque Reference System)

For this method of load simulation it was found necessary to use low values of controller gains as shown:-

Dynamometer Controller (Loading and motoring)	(	Proportional gain, B = 1 v/v
	(	
	(	
	(	Integral gain, C = 1 s^{-1}

Prime mover Controller

(Loading)	Proportional gain, E = 30 v/v Integral gain, F = 2 s^{-1}
(Motoring)	Proportional gain, E = 1 v/v Integral gain, F = 0

Higher values of proportional gain on the dynamometer controller (B) caused high frequency roots to become unstable under both the loading and motoring conditions. Although a high value of proportional gain on the prime mover controller (E) was necessary to prevent oscillatory low frequency roots under the loading condition, under the motoring condition a low value of E was necessary to prevent oscillatory roots of very low frequency ($\triangleq$ 0.1 Hz) from occurring at low speed. Higher values of integral action on the dynamometer controller (C) created oscillatory low frequency roots ($\omega_n \triangleq 0.7$ Hz) under all conditions, and higher values of integral action on the prime mover controller (F) resulted in the dominant response becoming oscillatory at high speed under the loading condition (whereas any value of F under the motoring condition resulted in 2 unstable roots at low speed, which become highly oscillatory at high speed).

The use of derivative action on either controller was not found to improve the damping of the secondary roots, which would enable higher values of proportional plus integral action to be employed. The root loci obtained for these controller gains are shown in graph G96, from which it is shown that under the motoring condition the dominant response is slow and the secondary roots have low damping. It was found that the damping of these secondary roots could be improved by reducing the time constant (T7) on the acceleration signal (for the simulated inertia effect), although under the motoring condition this reduced the damping of the secondary roots.

Also under the motoring condition, the dominant root remains unstable for the major part of the speed range. This means that steady state motoring conditions cannot be simulated with this method, although in practice, the real vehicle also cannot remain in the steady state motoring condition at low and medium speeds for maximum power regeneration (as indicated by the real vehicle responses of section 5.2). By zeroing the prime mover controller coefficients the dominant responses for the load simulation system (which may be compared with the real vehicle responses) were obtained as shown:-

Prime mover speed (rev/min)		<600	600	1500	3000
Time Constant (s)	Loading	595.1	2.92	14.9	56.2
	Motoring	595.1	-0.495	-13.3	657.5

Due to the low gain values on the dynamometer controller the correlation of these values with those for the real vehicle is not very close, especially at low speed (600 rev/min).

The simulation of low torque values in the system (determined by reducing K1) had little effect upon the root positions under all conditions. Reducing the velocity transducer time constant (T5) to 1 ms resulted in oscillatory high frequency roots under the motoring condition ($\omega_n \simeq 3$ Hz; $\zeta \simeq 0.3$) which become virtually unstable under the loading condition ($\omega_n \simeq 6$ Hz; $\zeta \simeq .05$).

5.3.4 Simulation Method 2.2 (Speed Reference System)

As with previous systems using simulation method 2.2 it was found possible to use high controller values under the loading condition without creating stability problems:-

Dynamometer Controller (Loading)	Proportional gain, B = 30 v/v Integral gain, C = 30 s^{-1}
Prime mover Controller (Loading)	Proportional gain, E = 30 v/v Integral gain, F = 3 s^{-1}

The somewhat lower value of integral gain on the prime mover controller (F) is necessary to prevent the dominant response from becoming too oscillatory at high speed under the loading condition. Derivative action on either controller did not result in any significant change of the root positions. Under the motoring condition lower values of controller gains, together with the elimination of integral action on the prime mover controller, were necessary to maintain stable performance throughout the speed range:-

Dynamometer Controller (Motoring)	Proportional gain, B = 10 v/v Integral gain, C = 1 s^{-1}
Prime mover Controller (Motoring)	Proportional gain, E = 5 v/v Integral gain, F = 0

This is because any value of integral action (F) creates two unstable roots at low speed which become highly oscillatory at higher speeds. Low values of integral action on the dynamometer controller (C) were necessary to prevent the creation of oscillatory low frequency secondary roots which become unstable at low speed. This effect was also obtained with lower values of proportional gain on the dynamometer controller (B). Higher values of proportional gain on the prime mover controller (E) created oscillatory low frequency roots at low speed. As with the loading condition, no values of derivative action were found to improve the root positions under the motoring condition.

Using these controller values root loci were constructed for the range of speed, as shown in graph G97. Under the loading condition the dominant response is relatively slow throughout the speed range. From the following table the correlation between the real vehicle response and the response of the load simulation system with zero prime mover control is closer than for method 2.1 (although the error is still large at low speed, 600 rev/min).

Prime mover speed (rev/min)		<600	600	1500	3000
Time Constant (s)	Loading	594.4	2.04	13.9	55.27
	Motoring	594.4	-0.561	-14.17	661.6

Under the motoring condition from the root locus the dominant response at low speed is given by a single unstable root under maximum regeneration conditions (although for lower regenerative torque levels this root becomes stable). At higher speeds the dominant response is stable but very slow (time constant greater than 25 seconds) for all torque levels, which indicates the possibility of large dynamic speed errors. There will also be a steady state speed error for this system at high speed under the motoring condition due to the elimination of integral action on the prime mover controller (necessary to prevent an unstable second order response). For a controller gain of E = 5 v/v a speed of 3000 rev/min is necessary to obtain the maximum prime mover control signal of 10 volts.

Reducing the velocity transducer time constant (T5) had negligible effect under the motoring condition, although under the loading condition a value of T5 = 1 ms resulted in high frequency roots becoming unstable at all speeds. Also, under the loading condition, the simulation of low torque values resulted in slightly oscillatory secondary roots ($\omega_n \triangleq 1 r/s; \zeta \triangleq 0.5$) at low speed.

Hence the use of the hydrostatic dynamometer in conjunction with the electric prime mover was found to result in good performance only for simulation method 1.2 (speed control by dynamometer, torque control by prime mover). This is due to the large difference in the torque/speed characteristics of the two devices, especially at low speed, creating difficulties when speed control is applied to the prime mover.

The effects of the torque/speed characteristics for the fast response dynamometer upon the performance of the load simulation systems are examined in the following section.

5.4 Fast Response Dynamometer

As with the hydrostatic dynamometer, it is necessary for the fast response dynamometer to have a higher power rating than for those used in the internal combustion engine systems, due to the high torque capability of the electric prime mover at low speed. As an approximation to the necessary higher power rating the dynamometer coefficients J2, K3 and K4 were also increased by a factor of 2.5 under all conditions with all other dynamometer coefficients as given in section 3.3.1.

5.4.1 Simulation Method 1.1 Torque control by dynamometer Speed control by prime mover

The fast response dynamometer using simulation method 1.1 enables much higher values of integral action to be used on each controller than the hydrostatic dynamometer system, under both loading and motoring conditions:-

Dynamometer Controller	Proportional gain, B = 0.1 v/v Integral gain, C = 10 s^{-1}
Prime mover Controller	Derivative action, D = 30 s Proportional gain, E = 30 v/v Integral gain, F = 30 s^{-1}

As with previous systems it was necessary to have a low value of proportional gain on the dynamometer controller (B) to prevent the roots due to the electrohydraulic actuator from becoming unstable at high speed under the loading condition (at which point the dynamometer gain becomes very large). The use of a high value of integral action on the dynamometer controller (C) in relation to the magnitude of proportional action (B) had little effect upon the dominant response of the system under all conditions, although the secondary roots were made considerably faster. Derivative action on the dynamometer controller (A) did not create any improvement in root positions, although derivative action on the prime mover controller (D) enabled high values of proportional and integral gains (E and F) to be used with creating oscillatory low frequency roots under all conditions.

Root loci were constructed using these controller values (graph G98) which show that the system response is fast and well damped under all conditions. For this system the effect of simulating low torque values can be determined by simultaneously reducing the magnitudes of the dynamometer torque/speed slope (K3) and time constant (T3) as well as the prime mover torque/speed slope (K1). Under all conditions the simulation of low torque values was found to have negligible effect, except to slightly increase the speed of response of the dominant roots at low speed under both loading and motoring conditions. Increasing the velocity transducer time constant (T5) created highly oscillatory low frequency roots under all conditions.

5.4.2 Simulation Method 1.2 Speed control by dynamometer Torque control by prime mover

For method 1.2 even higher values of controller gains were possible than for method 1.1, although it was necessary to change the dynamometer controller gains between the loading and motoring conditions:-

Dynamometer Controller (Loading)	Proportional gain, B = 3 v/v Integral gain, C = 30 s^{-1}
Dynamometer Controller (Motoring)	Derivative action, A = 0.2 s Proportional gain, B = 20 v/v Integral gain, C = 30 s^{-1}
Prime mover Controller (Loading and motoring)	Derivative action, D = 10 s Proportional gain, E = 30 v/v Integral gain, F = 30 s^{-1}

The high value of proportional gain on the dynamometer controller (B) is necessary under the motoring condition to prevent low frequency secondary roots from becoming highly oscillatory at high speed (due to the low gain of the fast response dynamometer under these conditions). This high value of gain, however, results in high frequency oscillatory roots ($\omega_n \triangleq 11$ Hz; $\zeta \triangleq 0.15$) at low speed under the motoring condition, although the damping of these roots was greatly increased by the use of a low value of derivative action on the dynamometer controller (A). Values of A greater than 0.2 s were found to reduce the damping of these high frequency roots, becoming virtually unstable at approximately A = 1 s.

Under the loading condition it was necessary to reduce the proportional gain B to prevent the high frequency roots due to the electrohydraulic actuator from becoming unstable at high speed (although a much higher value of B is possible than for method 1.1, since the dynamometer is now in a speed control loop as opposed to torque control). Under these conditions the use of derivative action on the dynamometer controller (A) created no improvement in root positions. Due to the higher values of proportional action B it was necessary to maintain a high value of integral action on the dynamometer controller (C) to keep a fast dominant response under all conditions. The use of derivative action on the prime mover controller (D) enabled high values of proportional plus integral action (E and F respectively) to be used without creating high frequency oscillatory roots ($\omega_n \simeq 5$ Hz; $\zeta \simeq .2$) at low speed under both the loading and motoring conditions.

The root loci for these controller gains (graph G99) show the system to have a fast and well damped response under all conditions. The effect of simulating low torque values in the system (determined by reducing K1, K3 and T3) was to cause a slight improvement in the damping of the high frequency secondary roots under all conditions, together with an increase in the speed of response of the dominant roots throughout the speed range under the motoring condition. The effect of increasing the velocity transducer time constant to 1 s was to increase the speed of response of the dominant roots at low speed under the motoring condition, as well as to improve the damping of the high frequency roots, although at high speed the low frequency secondary roots became unstable under both motoring and loading conditions.

5.4.3 Simulation Method 2.1 (Torque Reference System)

Suitable controller values for method 2.1 were found to be:-

Dynamometer Controller (Loading)	Derivative action, A = .001 s Proportional gain, B = 0.3 v/v Integral gain, C = 30 s^{-1}
Dynamometer Controller (Motoring)	Derivative action, A = 0.1 s Proportional gain, B = 10 v/v Integral gain, C = 30 s^{-1}
Prime mover Controller (Loading and motoring)	Derivative action, D = 0 Proportional gain, E = 30 v/v Integral gain, F = 5 s^{-1}

The low values of derivative action on the dynamometer controller (A) prevent the creation of virtually unstable roots at high speed under the loading condition ($\zeta \triangleq .03$; $\omega_n \triangleq 40$ Hz) which become unstable at low speed under the motoring condition. However, too high a value of A results in the creation of oscillatory roots throughout the speed range under the loading condition ($\omega_n \triangleq 3$ Hz; $\zeta \triangleq 0.1$ for A = 0.1 s).

Under the loading condition the low value of proportional gain on the dynamometer controller (B) prevented the electrohydraulic actuator roots from becoming unstable throughout the speed range. Under the motoring condition, however, a high value of B is necessary to prevent the creation of oscillatory secondary roots throughout the speed range ($\omega_n \triangleq 1$ Hz; $\zeta \triangleq 0.15$ at high speed). Lower values of integral action on the dynamometer controller (C) had little effect under the motoring condition except to improve the damping of the dominant response at high speed, although under the loading condition lower values of C created oscillatory secondary roots at high speed.

No value of derivative action on the prime mover controller (D) was found to improve the root positions under either the loading or motoring conditions. The value of integral action on the prime mover controller (F) was limited to 5 s^{-1} in order to prevent the creation of oscillatory low frequency roots ($\omega_n \triangleq 0.06$ Hz; $\zeta \triangleq 0.4$) at high speed under both loading and motoring conditions. The root loci for these controller values (graph G100) show the dominant roots to be well damped under all conditions. Removal of the prime mover controller gains enables the predicted dominant responses for the simulation system to be compared to those for the real vehicle (section 5.2) as follows:-

Prime mover speed (rev/min)		600	600	1500	3000
Time Constant (s)	Loading	595.4	2.06	13.99	55.8
	Motoring	595.4	-1.44	-15.16	667.4

These values show slightly better correlation with the real vehicle response than for the hydrostatic dynamometer of the previous section, although the error is still large at low speed under the loading condition due to the low gain of the fast response dynamometer under these conditions. Increasing the lag on the simulated inertia signal (T7) resulted in a slower dominant response as well as to create oscillatory low frequency secondary roots ($\omega_n \simeq 1$ Hz; $\zeta \simeq 0.3$ for T7 = 10 s) throughout the speed range under both the loading and motoring conditions. Lower values of T7, however, caused the electro-hydraulic actuator roots to become unstable under all conditions. Simulation of low torque levels in the system was found to improve the damping of the high frequency secondary roots under all conditions. Increasing the velocity transducer lag (T5) to 1 s resulted in the low frequency secondary roots becoming highly oscillatory under all conditions (unstable at low speed under the motoring condition).

5.4.4 Simulation Method 2.2 (Speed Reference System)

For method 2.2 the following controller values gave suitable performance throughout the speed range:-

Dynamometer Controller (Loading)	Proportional gain, B = 3 v/v Integral gain, C = 30 s^{-1}
Dynamometer Controller (Motoring)	Proportional gain, B = 30 v/v Integral gain, C = 30 s^{-1}
Prime mover Controller (Loading)	Derivative action, D = 20 s Proportional gain, E = 20 v/v Integral gain, F = 2 s^{-1}
Prime mover Controller (Motoring)	Derivative action, D = 20 s Proportional action, E = 30 v/v Integral gain, F = 2 s^{-1}

Using these values root loci were constructed, as shown in graph G101, which indicate a very similar performance compared to simulation method 2.1. Although a much higher value of proportional gain on the dynamometer controller (B) could be used than for method 2.1, it was found that under the loading condition increasing B above 3 v/v caused the electrohydraulic actuator roots to become highly oscillatory at high speed. Under the motoring condition, however, too low a value of B created oscillatory secondary roots at low speed. The use of derivative action on the dynamometer controller

(A) produced no improvement in root positions under any condition, whereas derivative action on the prime mover controller (D) was used to improve the damping of oscillatory secondary roots ($\omega_n \simeq 1.5$ Hz; $\zeta \simeq 0.25$ with D = 0) at low speed under the loading condition.

Under the motoring condition, an increase in the proportional gain on the prime mover controller (E) was necessary to improve the damping of the dominant response throughout the speed range. Higher values of integral action (F) reduced the damping of the dominant roots under all conditions. The dominant response time constants (with zero prime mover control) were obtained as follows:-

Prime mover speed (rev/min)		<600	600	1500	3000
Time Constant (s)	Loading	594.4	ω_n .8 r/s; ζ .66	13.0	54.8
	Motoring	594.4	-1.97	-16.0	668.2

The correlation between these values and those for the real vehicle (section 5.2) are much closer than for any of the previously analysed systems and the secondary roots (with zero prime mover control) are fast and relatively insignificant.

Higher values of velocity transducer time constant (T5) reduced the damping of the low frequency secondary roots, which became unstable at high speed under the loading condition for T5 = 1 s. The effect of simulating low torque values in the system was negligible under all conditions, except to reduce the speed of response at low speed under the motoring condition. Hence the fast response dynamometer system provides superior performance for simulating vehicle loads on an electric prime mover compared to the hydrostatic dynamometer system. It has been noted, however, that in order to use the hydrostatic and fast response dynamometer systems in conjunction with the electric prime mover, the power rating of the hydraulic units has to be much larger than that of the prime mover in order to achieve the high torque/low speed capability of the electric prime mover.

One further possible disadvantage is that the speed range of the electric prime mover extends to zero rev/min under normal operating conditions. For positive displacement hydraulic units there exists a critical speed below which stick/slip conditions become large, Ref. (20). It is possible that these conditions may have a large effect upon the operation of high power dynamometer systems, although for the low power system analysed in Part 2 the effect was small. In the following section an analysis is made of the electric prime mover used in conjunction with the electric dynamometer system for the purposes of comparison with the hydrostatic and fast response dynamometer systems.

5.5 Electric Dynamometer

The same electric dynamometer may be used for this system as for the diesel engine system of section 3.4 (100 kW d.c. motor/generator with thyristor control). However, due to the much higher torque capability at low speed it is necessary to modify the torque/speed slope values for the dynamometer under both the loading and motoring conditions.

At low speed (600 rev/min) the maximum torque capability of the prime mover = 765 Nm, and for the dynamometer = 1590 Nm. Hence the torque/speed slope for the dynamometer at maximum power (-24.7 Nm s from graph G63) must be reduced to the maximum power level of the prime mover, i.e., K3 (low speed) $= -24.7 * \frac{765}{1590} = -11.88$ Nm s

similarly, K3 (medium speed) $= -4.05 * \frac{312}{630} = -2.006$ Nm s

K3 (high speed) $= -0.931 * \frac{160}{315} = -0.473$ Nm s

(these being the maximum possible values of K3) and K3 (very low speed) = 0 ($<$ 600 rev/min).

Under regenerative conditions the magnitudes for K3 remain the same although the sign becomes positive in the same manner as for the electrical dynamometer system of section 3.4. The values of J2, T3 and K4 remain as given in section 3.4, although an extra value for K4 is required for speeds less than 600 rev/min:-

K4 (very low speed) = 191 Nm/v (from graph G63)

The second order terms for the flexible coupling and dynamometer actuator are eliminated:-

K2 = K9 = 1; F9 = J9 = F2 = J8 = 0

The basic block diagram for the electric prime mover/ dynamometer system is shown in Fig. 5.1.

5.5.1 Simulation Method 1.1 Torque control by dynamometer
Speed control by prime mover

For the electric dynamometer using simulation method 1.1 it was possible to use very high values of controller coefficients under both the loading and motoring conditions:-

Dynamometer Controller	Proportional gain, B = 30 v/v Integral gain, C = 30 s^{-1}
Prime mover Controller	Derivative action, D = 30 s Proportional gain, E = 30 v/v Integral gain, F = 30 s^{-1}

The use of derivative action on the prime mover controller (D) was necessary to maintain the stability of the secondary roots throughout the speed range, whereas derivative action on the dynamometer controller (A) caused little change in root positions. The root loci using these controller values (shown in graph G102) indicate a fast and well damped response with similar characteristics to the fast response dynamometer system using method 1.1 (graph G98). This is due to the fact that the high controller gains overcome the effect of the large lags and inertia values inherent in the system, as well as the de-stabilising influence of the positive torque/speed slope of the dynamometer under the loading condition.

The effect of simulating low torque levels in the system is negligible at high speed, whereas at low speed the dominant response becomes faster, together with an increase in damping of the dominant roots under the motoring condition. The effect of increasing the velocity transducer time constant (T5) is to cause the dominant response to become highly oscillatory under all conditions.

5.5.2 <u>Simulation Method 1.2</u> <u>Torque control by prime mover</u>
<u>Speed control by dynamometer</u>

Very high controller gains were also possible with method 1.2 under both the loading and motoring conditions:-

Dynamometer Controller	Derivative action, A = 3 s Proportional gain, B = 30 v/v Integral gain, C = 30 s^{-1}

Prime mover	(	Derivative action, D = 10 s
	(	Proportional gain, E = 30 v/v
Controller	(	Integral gain, F = 30 s^{-1}

In this case derivative action on the dynamometer controller (A) was necessary to prevent oscillatory roots occurring at low and very low speeds ($\omega_n \triangleq 1.5$ Hz; $\zeta \triangleq .25$) under both the loading and motoring conditions, although too high a value of (A) reduced the speed of response of the dominant roots at high speed. The magnitude of derivative action on the prime mover controller (D) is lower than for method 1.1, since this lower value increased the speed of response of the dominant roots under all conditions, although too low a value of D created a further reduction in the speed of response. The effect of simulating low torque values (determined by reducing K1 and K3 simultaneously) was negligible at high speed, although at low speed the dominant response became slightly faster under the motoring condition and slower under the loading condition.

The root locus for the system using the above controller values (shown in graph G103) indicates that the system will have a fast response with well damped roots (resulting in low dynamic errors). The performance characteristics are similar to both the hydrostatic dynamometer system (graph G95) and the fast response dynamometer system (graph G99) for the electric prime mover using method 1.2. The effect of increasing the velocity transducer time constant (T5) to 1 s was to cause the low frequency secondary roots to become unstable under all conditions.

5.5.3 Simulation Method 2.1 (Torque Reference System)

Although high values of proportional plus integral action were possible on the dynamometer controller for method 2.1, it was necessary to have a lower value of integral action on the prime mover controller (F) than for simulation methods 1.1 and 1.2. This was in order to maintain adequate damping of the dominant roots at high speed under both the loading and motoring conditions. The following controller values were found suitable:-

Dynamometer Controller	Derivative action, A = 3 s Proportional gain, B = 30 v/v Integral gain, C = 30 s^{-1}
Prime mover Controller	Proportional gain, E = 30 v/v Integral gain, F = 5 s^{-1}

Derivative action on the dynamometer controller (A) was used to increase the damping of high frequency secondary roots at high speed under both the loading and motoring conditions although, in practice, these roots would have little effect upon the system response without the use of derivative action ($\omega_n \simeq 3$ Hz; $\zeta \simeq .45$) due to the large dynamometer and prime mover lags (T3 and T2 respectively). The use of derivative action on the dynamometer controller (D) had little effect upon the root positions.

Using these controller values root loci were constructed for the range of speed, as shown in graph G104. The root loci show the system to be well damped under all conditions with similar performance characteristics compared to the fast response dynamometer using method 2.1. The dominant responses with zero prime mover control (which may be compared with those for the real vehicle in section 5.2) were determined as follows:-

Prime mover speed (rev/min)		<600	600	1500	3000
Time Constant (s)	Loading	595.3	2.07	14.02	55.8
	Motoring	595.3	-1.45	-15.26	669.05

These time constants are very similar to those obtained for the fast response dynamometer system (section 5.4.3), and show reasonable correlation with the real vehicle responses, although the error is large at low speed under the loading condition. Unlike method 1.2, the effect of simulating low torque values was to increase the speed of response at low speed under the loading condition and reduce the speed of response at low speed under the motoring condition. Also, the effect of increasing the velocity transducer lag to 1 s was to create oscillatory low frequency roots under all conditions, becoming unstable at low speed under the motoring condition.

5.5.4 Simulation Method 2.2 (Speed Reference System)

As with method 2.1 it was possible to have high values of proportional plus integral action on the dynamometer controller, although it was necessary to reduce the value of integral action on the prime mover controller (F) in order to maintain adequate damping of the dominant roots:-

Dynamometer Controller (Loading + motoring)	Proportional gain, B = 30 v/v Integral gain, C = 30 s^{-1}
Prime mover Controller (Loading + motoring)	Derivative action, D = 30 s Proportional gain, E = 30 v/v Integral gain, F = 3 s^{-1}

In this case the use of derivative action on the dynamometer controller (A) provided negligible improvement in root positions under all conditions. However, a high value of derivative action on the prime mover controller (D) was necessary to improve the damping of low frequency secondary roots ($\omega_n \triangleq 1$ Hz; $\zeta \triangleq 0.3$) at low and very low speeds under both the loading and motoring conditions. For these controller values the root loci for the system throughout the range of speed are shown in graph G105. The root positions indicate that the system is well damped under all conditions, although the speed of response is much slower than for the fast response dynamometer system.

The dominant response time constants with zero prime mover control were obtained as follows:-

Prime mover speed (rev/min)		<600	600	1500	3000
Time Constant (s)	Loading	594.4	ω_n .75 r/s; ζ .73	12.9	54.8
	Motoring	594.4	-2.05	-16.15	668.6

These values are even closer to those for the real vehicle (section 5.2) than the values obtained for the fast response dynamometer system using method 2.2, although without control on the prime mover oscillatory secondary roots ($\omega_n \doteq 1.5$ Hz; $\zeta \doteq 0.25$) are obtained at low and very low speeds under both the loading and motoring conditions. The effect of simulating low torque levels in the system was small under all conditions, with a slight increase in the speed of response at low speed under the motoring condition, and a slight reduction at low speed under the loading condition. Increasing the velocity transducer time constant (T5) to 1 second once again resulted in low frequency roots becoming unstable under all conditions.

5.6 Discussion

One effect of eliminating the flexible coupling and the input lag for the electric prime mover system is that the order of the system is reduced by 3 in comparison to the internal combustion engine systems. Also, with the electrical dynamometer system, the elimination of the dynamometer input lag (due to thyristor control) further reduces the order and complexity of the system. Hence the choice of controller coefficients is made much easier for the electrical prime mover system (especially with an electric dynamometer) since there are fewer root movements to cause stability problems throughout the range of speed of the system, under both loading and motoring conditions. In fact, with the electrical dynamometer system, using basic simulation method (1) the system becomes fifth order (as shown in graph G103) with all roots residing within a time response band of 0.1 → 1 seconds (assuming velocity transducer lag negligible). Also, since a gearbox is unnecessary for a battery powered vehicle, the range of conditions which may adversely affect the root positions (for given controller values) is much reduced for basic simulation method (2).

Thus from Parts 3, 4 and 5 it may be gathered that from the control point of view the governed diesel engine provides the greatest difficulties, since the root positions vary throughout the range of speed under three different loading conditions (loading mid fuel delivery, loading maximum fuel delivery, motoring) in each gear. Also, for mid fuel delivery, the high governor gain causes the basic system to be highly oscillatory at low speed. In comparison, the petrol engine creates fewer difficulties since the basic engine transfer function remains first order under all conditions, although a single unstable root occurs under the high torque low speed loading condition. The electric prime mover, however, has been shown to have fewer roots than the internal combustion engine systems, which vary with speed under the loading and motoring condition for one fixed gear ratio only.

Although the electric prime mover has fewer roots to cause control problems than the internal combustion engine, the torque/speed characteristics of the electric prime mover have much higher changes in slope throughout the speed range than do the internal combustion engines. Under the motoring condition the slope becomes positive (i.e., the torque required to regenerate a given power level becomes lower as the speed increases). This results in positive feedback, the magnitude of which becomes maximum at low speed (at which point the torque/speed slope is steepest). For the real vehicle the effect of this positive feedback is to create a single unstable root at low and medium speeds, although at high speed the negative feedback effect of the vehicle load is sufficient to overcome the positive feedback of the prime mover. Thus if maximum regeneration conditions are applied at high speed (i.e., maximum braking) the vehicle deceleration will become more rapid as the speed reduces until the very low speed condition is reached, at which point the torque/speed slope of the prime mover becomes zero.

Attempting to simulate these effects can create problems for the control system of a vehicle load simulator. For example, with the hydrostatic dynamometer having a velocity transducer lag of T5 = 1 s (section 5.3) it was found that the use of integral action for speed control of the prime mover under the motoring condition resulted in a secondary root as well as the dominant root occurring on the right-hand side of the complex frequency plane at low speed. At higher speeds the two unstable roots become complex conjugate, so that instead of a smooth transition to low speed occurring, the system will oscillate with increasing order of magnitude. For the fast response dynamometer the system roots are sufficiently far to the left of the imaginary axis to "pull over" the unstable single root of the prime mover so that this problem does not arise. Also, for the electric dynamometer system it is possible to have very high controller gains (since there are no high frequency roots which can go unstable) which once again cause the single unstable root of the prime mover under the motoring condition to be moved to the left-hand side of the complex frequency plane.

It should be noted that under the loading condition the electric prime mover torque/speed slope also becomes positive, thereby resulting in positive feedback. It is for this reason that single unstable roots were obtained under maximum fuel delivery conditions with the diesel engine system in Part 3. However, for the petrol engine and electric prime mover systems it was possible to have sufficiently high gains on the dynamometer controller to stabilise this root without creating stability problems for the remaining roots of the system.

One further effect of large changes in the electric prime mover torque/speed slope throughout the speed range is that of choosing constant controller coefficients which give suitable performance at all speeds. This is especially difficult at low speed, at which point the slope becomes very steep. It is for this reason, coupled with the higher inherent inertia and winding lag of the prime mover, that the correlation between the real vehicle response and that for the simulator using basic method (2) is not as close as obtained with previous systems, especially at low speed under the loading condition.

For the electric prime mover using basic simulation method (1) the use of method 1.2 (prime mover control of torque; dynamometer control of speed) results in slightly better performance than method 1.1 (dynamometer control of torque; prime mover control of speed) especially with the hydrostatic dynamometer system. Also, for basic simulation method (2), the use of the speed reference system (method 2.2) resulted in better performance than the torque reference system (method 2.1) for all dynamometers. Thus method 1.2 provides superior performance to method 1.1, and method 2.2 provides superior performance to method 2.1 for every one of the prime mover/dynamometer systems investigated.

Another difficulty which arises with the electric prime mover system using basic simulation method (2) is in the determination of the system performance by comparison with the real vehicle responses. For the governed diesel engine the maximum fuel delivery condition is frequently encountered in practice. This enables meaningful comparisons to be made with the real vehicle response for zero prime mover control on the load simulation system, since this condition will frequently occur on the simulator. Also, there will be zero prime mover control for both the diesel and petrol engines when operating under the motoring condition.

For the simulation of vehicle loads on the electric prime mover, however, zero prime mover control does not occur under either the loading or motoring conditions. Hence the most suitable approach for the electric prime mover system is to choose dynamometer controller coefficients which give the closest responses to those of the real vehicle under all conditions, and then choose the maximum prime mover coefficients consistent with stability.

Although the hydrostatic and fast response dynamometers have no difficulty in reaching the maximum speed of the electric prime mover, it has been noted that there may be a problem at very low speed due to stick/slip in the positive displacement hydraulic unit (Ref. 20). Also, for all dynamometer systems, it is necessary to have a zero speed sensing device plus control routine in order to prevent possible backward motion of the prime mover, or "hunting" at zero speed, as indicated by the torque response of the low power system in graph G27(b). For the fast response dynamometer system it is necessary to supply a make-up flow of hydraulic fluid to the high pressure side of the hydrostatic unit in order to replenish the leakage flow if high torque/pressure conditions are required at very low speed. Furthermore, since the electric prime mover can provide very high torques at low speed, it is necessary for the hydrostatic unit (pump/motor) to have a power rating much higher than the prime mover, in order that the high torque requirement may be met.

As with previous systems it was noted that high values of integral action on the dynamometer controller eliminated the need for the torque/speed elimination signal (G4). Also, when low values of integral action were necessary for stability purposes the dominant response time constant became much higher. For the electrical dynamometer/prime mover system it was found that the elimination of the mechanical actuators (necessary for the other systems) allowed high values of derivative action to be used which, in turn, enabled the controller gains to be very high. It is for this reason that the electrical dynamometer, with its slow response and large inherent inertia, can provide a high standard of performance in comparison to the hydrostatic and fast response dynamometer systems (for which the electrohydraulic actuators soon create instability if high values of derivative action are used). Finally, it has been shown that signal filtering (necessary for the speed and acceleration signals) can have a large effect upon system performance. It is advisable to use the highest cut off frequency possible for the filter consistent with adequate damping of extraneous signals (e.g., tachogenerator ripple) and taking into account the amplifying effect of the prime mover and dynamometer controllers upon such signals.

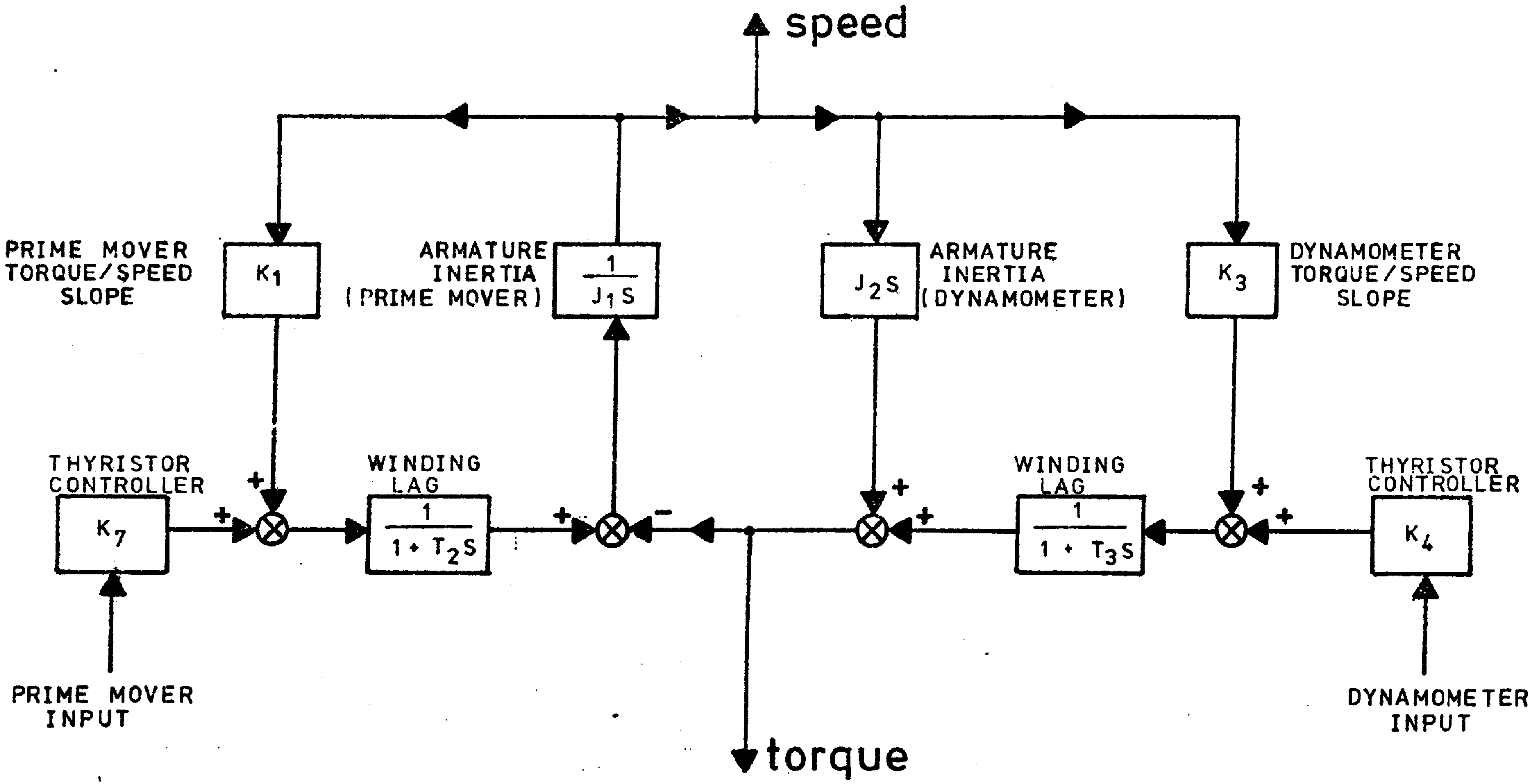

Figure 5.1 Basic block diagram for electric prime mover+dynamometer

PART 6

ANALYSIS AND DESIGN OF THE FAST RESPONSE DYNAMOMETER

6.1 Introduction

It has been shown in previous sections that a fast response dynamometer has an advantage over other dynamometer systems, for the purposes of simulating vehicle loads on a prime mover, in that the secondary root effects (created by the dynamic characteristics of the dynamometer and control system) can be made small. (Although it was also noted in Part 3 that the fast response dynamometer had a limited ability to dampen the oscillatory roots of a governed diesel engine at low speed under the loading condition.) Further need for fast response dynamometer systems arises in the experimental testing of internal combustion engines for identification purposes.

In the past steady state tests using electrical eddy current or water brake type dynamometers (having inherently slow response times) have been used to provide experimental data for the development of mathematical models and simulations of internal combustion engines. However, a large amount of work has recently been undertaken to improve mathematical simulations of the engine dynamics and combustion process, especially for turbocharged diesel engines (Refs. (15), (16), (17), (18)). In order to enable comparisons to be made between the theoretical techniques and experimental observations, it is essential that the engine load is controlled to the required conditions with the inherent dynamic effects of the dynamometer kept to a minimum.

Hence for transient testing, frequency response methods, or pseudo random techniques, where dynamic changes in load are required, the dynamometer should have a fast response with low inherent inertia. It was shown in Part 1 that hydrostatic dynamometer systems can have a much faster speed of response than other types of dynamometer system (e.g., d.c. generator, eddy current, water brake, friction brake or electro-mechanical dynamometers) coupled with a low inherent inertia. In particular, a very fast response may be achieved by means of electrohydraulic servo valve control of the pressure on a hydrostatic pump, as shown in the simplified schematic diagram of Fig. 6.1(a). The pressure may be controlled by the restriction of oil flow with a needle valve arrangement of the type shown in Fig. 6.1(b). The needle position in relation to the valve seating will produce a certain pressure drop at a given flow-rate of hydraulic oil, which, in turn, is dependent upon the prime mover speed.

Depending upon the losses involved in the hydrostatic pump there will be a direct relationship between the controlled pressure drop across the pump and the torque on the connecting shaft to the engine. Hence the torque may be controlled indirectly in this way, or directly by means of a torque transducer placed in the connecting shaft (for which a torque signal takes the place of the pressure transducer signal of Fig. 6.1(a)). Similarly, a speed transducer may be used to control the prime mover speed as long as the overrun (motoring) condition is not required.

Systems of this type have proved very effective for testing of diesel engines at Bath University, Refs. (21), (22). It was found, however, that a highly non-linear relationship was achieved between needle valve settings and the torque produced on the engine shaft. Also, large torque changes were obtained for very small variations in needle valve setting, which results in this type of valve having low discrimination. It was therefore decided to develop a special purpose valve which had greater discrimination in its positioning arrangement.

It is well known that a linear relationship exists between volumetric flowrate and pressure drop in straight ducts for laminar flow after passing through the entrance region, e.g., Refs. (35), (36). Thus by controlling the length of a duct through which hydraulic fluid is flowing it is possible to control the pressure drop across the duct. One method of doing this is to cut the duct out of a solid cylinder in a helical manner, as shown in

Fig. 6.1(c). The helical duct is, in fact, the groove between the shoulders of a square thread machined on the central spool. By moving the spool from its central position the length of duct between the inlet and outlet ports is reduced, so that for a given flowrate there will be a corresponding reduction in pressure drop across the valve.

A small scale valve working on this principle was constructed at Bath University and initial tests performed, Ref. (37). This work has been continued at Kingston Polytechnic with a view to determining design parameters for the construction of a full scale valve for use in the fast response testing of internal combustion engines.

6.2 Analysis of Fluid Conditions

Although no previous work has been reported on a fast response dynamometer valve of this type, a great deal has been written on the effects of fluid flow through curved ducts.

6.2.1 Previous Work

The large amount of work published on fluid flow through curved ducts stems from the widespread industrial use of such ducts for heat exchanger purposes, since it has been found that an enhanced convective heat exchange arises for curved ducts in comparison to straight ducts, Refs. (38), (39). It is, therefore, important to be able to obtain an accurate determination of the pumping power required for such applications (i.e., nuclear reactor coolers, industrial refrigerators).

Other applications arise in reverse osmosis and in certain chemical mixing processes where it is necessary to minimise axial dispersion, Refs. (40), (41). Also it has been suggested that flow through porous media has similar characteristics to flow through strongly curved tubes and that it may be possible to model the porous media as a bundle of such tubes, Refs. (42), (43). Furthermore the analysis of flow in curved ducts has many applications pertaining to the flow of blood in the human arterial system, e.g., for cholesterol deposition on the vascular wall resulting in arterio-sclerosis (Ref. 44), or for the distribution of injected substances and effects of wall shearing stress on arterial lesions (Ref. 45).

One of the earliest investigations into fluid flow through curved pipes was made by Dean in 1927 (Ref. 46) and 1928 (Ref. 47) in which he solved the Navier-Stokes equations analytically using a successive approximation technique for laminar flow in round tubes with large radii of curvature. He found that secondary flow occurred across the plane of the main downstream flow (as shown in Fig. 6.2(a)) and that this flow was characterised by a dimensionless parameter now known as the Dean number, $D_e = R_e(a/r)^{\frac{1}{2}}$

where R_e = Reynolds number

r = radius of curvature

a = radius of tube

Dean's analytical procedure was only valid for small Dean numbers (<17) due to the difficulties in calculating the higher order terms necessary for convergence. Thus Dean's results were limited to very low flowrates, although qualitative agreement was reached with the earlier experimental results obtained by Eustice in 1910 (Ref. 48). The first reliable resistance law to enable pressure loss information to be determined for flow in helical tubes was developed by White in 1929 (Ref. 49). Using experimental data he showed how the resistance coefficient varied with the Dean number for values up to 2000.

This work was extended by Prandtl in 1931 (Ref. 50) who showed that for Dean numbers between 20 and 1000 the resistance ratio between flow in straight and curved pipes in given approximately by:-

$$\lambda_c/\lambda_s = 0.37{D_e}^{0.36}$$

This work was translated into English in 1954 (Ref. 51). In 1934 Adler (Ref.52) obtained experimental results for a range of curved tubes and solved the Navier-Stokes equations using boundary layer approximations to obtain the following resistance ratio:-

$$\lambda_c/\lambda_s = 0.1064 D_e^{0.5}$$

Barua, in 1962 (Ref. 53), extended Adler's boundary layer techniques and obtained a similar resistance ratio:-

$$\lambda_c/\lambda_s = 0.0918 D_e^{0.5} + 0.509$$

In 1967 Topakoglu (Ref. 54) developed the following relationship for the ratio of flow in a curved pipe to the flow in a straight pipe having the same cross section and pressure gradient:-

$$\frac{\text{Flow (curved)}}{\text{Flow (straight)}} = 1 - 0.030575\left(\frac{1}{576}\,\frac{2Re^2}{\sigma}\right)^2$$

where $\sigma = a/r$

This relationship is claimed to give good agreement with Dean's results and is valid only for low Dean numbers. In 1969 Ito (Ref. 55) used boundary layer theory and Pohlhausen's approximate method to solve the Navier-Stokes equations and obtained the following friction factor:-

$$\lambda_c/\lambda_s = 0.1008 D_e^{0.5}(1 + 3.945 D_e^{-.5} + 7.782 D_e^{-1} + 9.097 D_e^{-1.5} + 5.608 D_e^{-2} + \ldots.)$$

He also performed experiments for a range of curved pipes and obtained a similar expression with a modification only to the first term:- $0.1033D_e^{0.5}$. These expressions give close agreement to White's experimental results for Dean numbers ranging from 10 to 4000.

In 1971 Baylis (Ref. 56) presented experimental results for fluid flow in strongly curved ducts of square cross section. For ratios of duct width to radius of curvature ranging from 1.75 to 17.5 and Dean numbers ranging from 500 to 70,000 he found the friction factor closely fitted the following relationship:-

$$\lambda_c/\lambda_s = 0.107D_e^{0.5}$$

which is in close agreement with Adler's results. At Dean numbers lower than 500, however, this relationship gives an under-estimate of the friction factor. Also in 1971 Austin (Ref. 57) produced experimental results to show the effect of flow development in the entrance region of curved tubes. He found that the entrance length fitted the following empirical equation.-

$$D = 49\ (D_e\alpha)^{\frac{1}{3}}$$

(where D is the entrance length in degrees).

In 1972 Lin (Ref. 58) used a Fourier series expansion of the Navier-Stokes equations (based on the method of

McConalogue and Srivastava, Ref. 59) as well as an extension of Ito's method to obtain friction factors for strongly curved tubes over the range of Dean numbers 20 to 1000. In 1973 Austin and Seader (Ref. 60) solved the Navier-Stokes equations using finite difference techniques for flow in curved pipes having curvature ratios from 5 to 100 and Dean numbers from 1 to 1000, achieving close agreement with White's results. The following year Yao and Berger (Ref. 61) extended the boundary layer model of Barua to determine pressure losses for fluid flow in the entrance region of curved pipes. Their analysis indicates that the entrance length for curved pipes is much shorter than for straight pipes, and that pressure losses in the entrance region are lower than for fully developed flow.

Recent work by Joseph et al. 1975 (Ref. 62) and Cheng et al. 1976 (Ref. 63) shows that for helically coiled tubes of square cross section two pairs of vortices occur as the Dean number is increased (rather than the single pair obtained in circular helical tubes), as shown in Fig. 6.2(b). The result of two pairs of vortices occurring in a square duct is shown to increase the resistance ratio compared to a round tube. The friction ratio for a square duct developed numerically by Cheng et al. is given as:-

$$\lambda_c/\lambda_s = 0.1278D_e^{0.5}(1 - 0.257D_e^{-0.5} + 0.669D_e^{-1} + 187.7D_e^{-1.5} - 512.2D_e^{-2})$$

where, in this case, the Dean number is defined as $D_e = R_e(2\alpha)^{\frac{1}{2}}$. Cheng's analysis shows that as the Dean number is increased further the extra vortices disappear, although the analysis is only valid for Dean numbers up to 700. (The analysis of Joseph et al. is for Dean numbers up to 300.)

6.2.2 Initial Investigations

It was initially decided to perform experimental investigations upon an existing valve of the type shown in Fig. 6.1(c), using a range of square thread sizes on the central spool, in order to verify the results of previous workers. A micrometer device was manufactured to enable the spool valve to be positioned to an accuracy of ± 50 microns, as shown in the schematic diagram of Fig. 6.3. The dimensions for each of the spools tested are given in Fig. 6.4.

To enable accurate determination to be made of the Reynolds and Dean numbers it is necessary to be able to accurately measure the oil flowrate and to have a measure of the oil viscosity throughout the temperature range. For the oil used in the experiments (Shell Tellus 27) the manufacturers supply temperature/viscosity charts, although the claimed accuracy is only ± 15%. To determine the viscosity to a greater degree of accuracy, oil samples were taken from the test system and viscosity measurements were made at a range of temperatures using a reverse flow viscometer to B.S.188 . The dynamic viscosities obtained were converted to kinematic viscosity and plotted against temperature on logarithmic graph paper as shown in graph G106.

To determine instantaneous volumetric flowrate with a high degree of accuracy a positive displacement flowmeter provides improved accuracy over turbine type flowmeters, since the former is little affected by viscosity changes in the measured fluid. However, limited funds prevented the purchase of a positive displacement meter and arrangements were made with the manufacturers of a range of turbine meters to supply a flowmeter calibrated over the required temperature and flow range using Shell Tellus 27 oil. The manufacturers claim a repeatability of $\pm$ 0.5% for this type of instrument. To obtain instantaneous volumetric flowrate measurements, a magnetic pick-up was used to provide pulses (from the rotation of the turbine blades) which are converted to a d.c. level and displayed on a meter. The use of a magnetic pick-up did not create magnetic drag effects on the turbine blades over the required flow range of the instrument (1.8 $\rightarrow$ 16 litres/min). Lower flowrates, however, become increasingly affected by magnetic drag and viscosity changes. To avoid the possibility of swirl affecting the turbine meter accuracy, a flow straightener was used at the inlet to the turbine with at least ten pipe diameters of straight pipe before and after the turbine to ensure uniform oil movement.

Pressure measurements were made at the inlet of the special purpose valve using a standard test gauge for which the manufacturers claim an accuracy of $\pm$ 0.25%. The oil system is in a closed loop, as shown in the schematic diagram of Fig. 6.5. The oil temperature is controlled by manual adjustment of the water flow through the heat exchanger so that the tank of oil is at the required temperature prior to the test run. For each setting of the spool position the pressure drop across the valve was measured for a range of flowrates. By this means the oil temperature throughout a test was maintained within $\pm$ 1° C. It was soon discovered that the temperature of the special purpose valve body had a large effect upon the pressures obtained.

For example, if the temperature of the oil in the tank is much higher than that of the valve body, then as the oil flows through the duct formed by the threaded spool, a high proportion of heat is passed from the oil to the surrounding valve body, causing the oil temperature to reduce. This causes the oil viscosity to increase, which consequently increases the pressure drop across the valve. To avoid this effect the oil was passed through the special purpose valve before each test until the valve body temperature (measured by a mercury in glass thermometer mounted in the valve body) reached the level of the oil temperature in the tank. This action enabled a high degree of repeatability to be obtained from test to test.

By this means tests were performed for each of the threaded spools over a wide range of conditions. Typical results of pressure against percentage spool engagement are shown in graph G107 for each of the threaded spools. The slopes obtained in each case are linear with an offset from the origin due to the increased pressure drop in the entry region. Hence these initial tests indicate that the special purpose valve can fulfil the requirements of linearity and high discrimination. Throughout the range of tests the Reynolds numbers lay within the band 600 → 4000 and the Dean numbers 200 → 1500. (Although turbulence occurs in straight tubes for Reynolds numbers greater than 2000, Baylis (Ref. 56) has shown that for strongly curved ducts Reynolds numbers as high as 10^5 can be achieved before turbulence occurs.) To enable a theoretical analysis to be performed for the purposes of comparison, it is necessary to identify two flow regimes within the valve:- (i) entry flow, (ii) fully developed flow.

Comparisons were made between the predicted entrance lengths using the theoretical approach of Yao and Berger (Ref. 61) and the empirical method of Austin (Ref. 57). (The entrance length of a duct is defined as the length at which the centre line velocity reaches 99% of its fully developed value, so that separate analyses must be made for the pressure losses in the entry region compared to those for the downstream region.) For each of the threaded spool valves the entry lengths predicted by the Yao and Berger method were far greater (approximately a factor of 15) than for the values predicted using Austin's method.

Since Austin's method is obtained from experimental data, whereas the method of Yao and Berger is based upon approximate solutions to the Navier-Stokes equations (using approximations which the authors themselves question), it is expected that Austin's method will prove more accurate (especially as the range of Dean numbers in his experimentation lie within the band 200 → 2000). The entrance lengths using Austin's method are marked on the curves obtained for each of the threaded spools in graph G107, and are shown not to conflict with any of the linear fully developed regions. (Whereas Yao and Berger's method indicates that fully developed flow is not reached in any of the tests, which is obviously not the case.)

Pressure measurements were not obtained over the spool engagement range of 0 → 10% since the manually adjusted pressure relief valve could not be controlled to sufficiently low pressures to enable the required flowrate to be reached. For the fully developed flow region it was decided to use the empirical formula for friction factors given by Baylis (Ref. 56), since this covered a wide range of Dean numbers for strongly curved ducts of square cross section. A computer program was written to provide the following information for given spool dimensions and flow conditions:- Curvature ratio, Reynolds number, Dean number, entrance length (Austin), entrance length (Yao and Berger), friction factor (Baylis) and pressure drop for laminar flow in a straight duct having the same dimensions and flowrate as the curved duct.

This pressure drop value was determined using the well known Hagen-Poiseuille formula with a modified friction coefficient for square ducts as given by Purday (Ref. 35):-

$$\frac{dP}{dZ} = \frac{28.6\mu\bar{u}}{(de)^2}$$

where P = pressure loss

Z = duct length

μ = dynamic viscosity

$\bar{u}$ = average fluid velocity in duct

de = effective diameter of duct

$$= \frac{4 \text{ x cross sectional area of duct}}{\text{Wetted perimeter}}$$

The computer program to determine the above information is given in Appendix C(1). The program was used to determine the fully developed pressure losses for each of experimental tests performed on the threaded spools without an allowance being made for the entry region. For the typical experimental results shown in graph G107 the pressure losses were determined using the computer program for the same conditions and the results superimposed upon the actual responses. These graphs show that the theoretically predicted slope of pressure against spool engagement for fully developed flow is in close agreement with the values obtained by experiment. Further analyses were made using the friction factors of other workers (Prandtl, Barua, Ito and Cheng) and the results obtained were also in close agreement with those obtained using the formula due to Baylis (except, as pointed out by Baylis himself, his formula gives an under-estimate of the pressure drop at Dean numbers less than 500).

To further increase the reliability of the experimental data it was decided to undertake further experimental investigations of the four spool valves. These experiments were performed using two different pressure gauges at the inlet to the valve, as well as a replaced turbine flowmeter and a new frequency to d.c. converter (which was further calibrated for an accuracy check). Also, the temperature gauges were checked against a calibrated mercury in glass thermometer and found to be within 1^{o} C (as claimed by the manufacturers). The results of this repeated set of experiments showed no detectable difference compared to the original experiments.

Further theoretical analysis was also undertaken using worst case errors in each of the valve dimensions and fluid coefficients. No reasonable change in these parameters created a significant difference in the correlation between the theoretical and experimental results.

6.2.3 <u>Analysis of Valve Parameters</u>

Having ascertained that the experimental results of the previous section are valid it was decided to determine the effects of various parameters upon the performance of the valve. Parameters having possibly large effects were suggested as follows:-

(i) Oil viscosity changes due to temperature increases in the duct.

(ii) Oil viscosity changes due to pressure effects in the duct.

(iii) Oil viscosity changes due to temperature difference and thermal conductivity of valve body.

(iv) Leakage losses across the threads.

(v) Interruption (or modification) of secondary flow due to leakage across threads.

Each of these effects was investigated in turn.

As the oil flows from the inlet to the exhaust of the valve along the helical duct, the pressure energy of the oil is converted to heat energy which, in turn, creates a temperature gradient along the length of the duct. If all the pressure energy is converted to heat energy in the oil, with negligible heat transfer to the surrounding valve body, it can be shown that there is a direct relationship between pressure and oil temperature:-

A pressure of 1 bar (10^5 N/m^2) is equivalent to an energy of 10^5 Nm per cubic metre = 100 kJ per cubic metre of oil. But the density of Tellus 27 (calculated from data supplied by Shell) is approximately 870 kg/m^3. (The density actually varies from 850 kg/m^3 at 50° C and atmospheric pressure to 887 kg/m^3 at 20° C and 350 bar). Also, the specific heat of Tellus 27 is approximately 0.465 cal/g °C (although it actually varies from 0.45 at 20° C to 0.48 at 50° C).

Hence the specific heat = 0.465 * 4.1868 kJ/kg °C

= 0.465 * 4.1868 * 870 kJ/m^3 °C

$\therefore$ at a pressure of 1 bar an oil temperature increase of

$\frac{100}{0.465 * 4.1868 * 870}$ = 0.05904° C is created in the leakage fluid (provided the heat loss from the oil is negligible). Thus for a given pressure gradient along the length of the square duct there is an equivalent temperature gradient, as shown in Fig. 6.6(a). This temperature gradient will cause changes in the oil viscosity which will result in a viscosity gradient occurring along the length of the duct, as shown in Fig. 6.6(b).

In order to compute the effect of this viscosity gradient upon the pressure drop across the valve it is necessary to obtain a relationship between the oil temperature and viscosity. Such a relationship may be obtained from the logarithmic viscosity chart of graph G106 as follows:-

Above 30° C, viscosity $V = 28726T^{-1.8347}$

Below 30° C, viscosity $V = 2168T^{-1.075}$

(where V is in cs and the temperature T is in $^{\circ}$C)

The viscosity obtained using these equations has an accuracy better than 4% over the temperature range $15 \rightarrow 60^{\circ}$ C. To incorporate the temperature dependent viscosity effects into the analysis an iterative procedure was adopted to determine the changes in pressure at ten points along the length of the duct (neglecting entrance conditions). The first step of the iterative procedure was to determine the pressure gradient for constant viscosity at ten points through the duct. Then, for each point, the change in temperature was determined, followed by the change in viscosity and friction ratio (which is viscosity dependent). Using the new viscosity and friction factor at each point a new pressure gradient was obtained working backwards from the outlet of the duct to determine the new maximum pressure at the inlet. If a large difference existed between the new maximum pressure and the previous maximum pressure ($>$ 0.1 bar) then the iterative procedure was repeated using the new pressure gradient. The computer program is given in Appendix C(2).

In general, the program achieved convergence within five iterations. The reduction in pressure drop was found to be as high as 10% for low inlet temperatures (20° C), reducing to 5% for high inlet temperatures (50° C). In practice, the actual reduction in pressure would be even lower, since heat would be lost from the oil to the valve body. The heat exchange is made greater as a result of the secondary flow (Refs. 38, 39), so that for a sudden increase in flow the initial temperature effect upon the viscosity gradient is quite small.

However, since the greatest temperature difference between the oil and valve body occurs at the downstream end of the duct, then the heat flow to the valve and spool body will be greatest in that region. The temperature of the valve will increase at the downstream end and consequently create a flow of heat through the valve body to the inlet region. This heat flow creates an increase in the temperature of the oil at the inlet, which results in a gradual reduction of the pressure drop across the valve (at a rate which depends upon the thermal conductivity of the oil and valve body). However, under worst case conditions, the maximum reduction in pressure will not be as high as for the case of negligible heat loss from the oil, so that the computer program gives an indication of the greatest possible effects of temperature dependent viscosity changes.

During the course of the experimental investigations this effect was observed in that the initial pressure (obtained as a result of a sudden increase in oil flow-rate) gradually reduced over a time period of approximately 20 seconds. This time dependent response will have negligible effect upon the transient characteristics of the loading valve, since the basic time response will be at least a factor of 1000 times faster than this. However, to avoid the possibility of such lengthy delays creating large temperature changes during the tests with the closed loop system, the experimental results were each obtained within 2 seconds of applying the change in flow conditions. This action eliminates the need for including complex heat exchange equations in the theoretical analysis of the valve, as well as resulting in more accurate transient magnitude characteristics (necessary for the theoretical analysis of the load simulation systems in Parts 3 to 5).

The other parameter which has a large effect upon the oil viscosity (besides temperature) is the oil pressure. Information supplied by Shell shows that the viscosity increases by approximately 30% per 100 bar pressure increase. Hence this effect tends to reduce the pressure loss created by the temperature effect. To determine the relative magnitude of the combined pressure and temperature effects the computer program of Appendix C(2) was modified as follows:-

```
343 V(N)  =  V(N) * (1 + 0.3 * P(N)/100)
```

This modification was found to change the pressure drop from the original program (without the inclusion of the temperature or pressure effects upon viscosity) by only a very small amount (approximately 1%) throughout the temperature and flow range of each threaded spool. This is due to the fact that the viscosity under inlet temperature and atmospheric pressure conditions is a reasonable average of the actual viscosity gradient, as shown in Fig. 6.6(c). Hence it is reasonable to ignore the effects of viscosity changes in the special purpose valve.

The two remaining parameters which may have an important effect upon the valve performance both depend upon the leakage flow across the threads of the central spool.

A simplified theoretical analysis is possible to determine the magnitude of the leakage flow by approximating the leakage path to the form shown in Fig. 6.7(a), where the length of the leakage path is equivalent to the sum of the thread widths along the length of the spool. The height of the leakage path is the clearance between the spool threads and the cylinder walls and the width is the circumference of the spool. The pressure drop across the leakage path is therefore equal to the maximum pressure drop across the spool valve. For fully developed flow through a path of this type the Hagen-Poiseuille formula has a modified friction coefficient (Ref. 35) as shown:-

$$\frac{dP}{dZ} = \frac{12\mu\bar{u}}{(d)^2}$$

where Z becomes L1/2 and d = clearance.

Hence the leakage flow, $Q_L = \bar{u}d\pi D$

$$= \frac{\pi P d^3 D}{6\mu L1} \quad \text{(where D = spool diameter)}$$

Using this equation for a pressure drop of 200 bar and an oil temperature of 50° C with a clearance of 10 microns the leakage rate is approximately 0.017 litres/min. A reduction in the main flowrate of each spool by this value has negligible effect upon the pressure drop across the valve for any of the experimental test conditions (although it should be noted that the leakage flow is proportional to the third power of the clearance, so that for a clearance of 30 microns the leakage flow is approximately .47 litres/min, which is significant).

The last effect which may create important changes in the valve characteristics is that if the spool clearance is large the leakage flow may change the pattern of the secondary flow and thereby reduce the magnitude of its effect. A possible structure for the secondary flow pattern with leakage flow is shown in Fig. 6.7(b), in which the secondary flow effect is much reduced. It is also possible that large values of leakage flow could set up turbulence in the main stream even at Reynolds numbers less than the critical value for straight ducts (2020), so that the secondary flow effect becomes negligible. The friction factor for laminar flow is given in Ref. (66) as $\lambda_1 = 57/R_e$, whereas for turbulent flow $\lambda_t = 0.316/R_e^{\frac{1}{4}}$. Hence the friction ratio between laminar and turbulent flow in straight square section ducts becomes:-

$$\frac{\lambda_t}{\lambda_1} = \frac{0.316}{R_e^{\frac{1}{4}}} * \frac{R_e}{57} = 0.00554 R_e^{\frac{3}{4}}$$

This equation may be used to obtain an indication of the increased pressure drop due to induced turbulence with Reynolds numbers less than the critical value for curved ducts as given in Ref. (56). The equation becomes increasingly inaccurate for Reynolds numbers less than 2020 (critical value for straight ducts) and gives a ratio less than unity for $R_e < 1020$. However, using this equation, the pressure/spool engagement characteristics for turbulent flow with negligible secondary flow effects were found to be approximately 30% lower than the experimentally obtained values.

Since the secondary flow creates the greatest pressures towards the outside of the circular duct (i.e., near the cylinder wall), it was envisaged that any possible leakage effects would be much diminished if the helical duct could be cut into the cylinder wall, rather than on the body of the spool. A further advantage of having the duct in the cylinder wall results from the fact that the great majority of the resistance to the oil flow is provided by the stationary cylinder wall. With the duct on the central spool the tangential component of the resistance force causes the spool to rotate at high speed. Rotational speeds of up to 6000 rev/min were recorded during initial investigations of the valve (Ref. 37), although the assumption was made that the force involved in creating this rotation was due to the change in momentum of the oil as it leaves the threaded spool.

The force involved is, in fact, the tangential component of the pressure acting on the cross sectional area of the duct $(P * L2 * L3)\sin\theta$, where θ is the helix angle. The force available for rotating the spool will be somewhat less than this, since a proportion of the resistance is provided by the stationary cylinder wall. The rotational speed at 200 bar (50° C) for each of the spools was obtained by balancing the torque due to this force with the resistive torque created by the friction between the spool and cylinder wall. This may be approximated by using the formula for the resistive torque of an oiled bearing:-

$$T = \frac{\mu \pi D^3 LN}{4d}$$

where D = spool diameter (.0127 m)

L = length of bearing (.0371 m)

N = speed of rotation

d = clearance (10 microns)

Using these formulae the rotational speeds of each spool (at a pressure of 200 bar) were obtained as follows:-

Spool	A	B	C	D
Speed (rev/min)	1,155	2,070	3,107	4,866

Although a certain level of rotation has the useful feature of overcoming stiction effects in the spool valve, these high speeds are more likely to create problems of wear and overheating of the spool surfaces (with the resultant possibility of seisure).

By having the helical duct cut into the cylinder wall, then only a small proportion of the total friction force is applied to the spool. Hence the rotational speed of the spool should be much lower with an internal thread in the valve body. Such a valve was constructed having a spool diameter of 0.0127 m and internal square thread of 0.00140 x 0.00140 (m) as shown in Fig. 6.7(c). With a clearance of 20 microns between the spool surfaces and the cylinder wall the spool showed no tendency to rotate with applied pressures of up to 200 bar, even though the output shaft could be rotated freely by hand. This indicates that the frictional forces acting on the inside wall of the curved duct are much smaller than on the other walls. The benefits obtained by eliminating stiction effects, however, indicate that a rotating spool could well be useful in a wide variety of fluid metering applications, and further research in this area is recommended.

To verify the previous analysis on leakage dependent pressure losses (without affecting the secondary flow) a range of solid spools was manufactured with varying clearance sizes. Each was tested with the internal thread valve at a flowrate of 1.81 litres/min and an oil temperature of 40.5° C to determine the pressure loss due to leakage:-

Spool	1	2	3	4
Clearance (microns)	10	25	38	51
Pressure (bar)	183	166	131	103
Calculated Leakage (litres/min)	0.010	0.146	0.403	0.766

For a clearance of 51 microns almost half the flow is lost in leakage, causing the pressure drop across the valve to fall by the same proportion. The effect is large with this valve, since the flow range is fairly small. A full scale loading valve used for engine testing may have a flow range in the order of 200 litres/min, which means that a spool clearance of up to 50 microns would have negligible effect upon the valve performance. The valves and equipment used for this range of tests are shown in Plate 6.1.

6.3 Loading Valve Design

It was shown in the previous section that a loading valve based upon the principle of controlling the length of a restricting duct could have certain advantages over standard needle or spool valves with respect to linearity and discrimination. A simple method by which the duct length could be controlled was found to be in the form of a square thread cut on the central spool of a spool valve, for which experimental tests showed high linearity and good discrimination. However, due to the uncertainty of the leakage effect upon the secondary flow in such a valve, as well as the problem of the spool rotating at high speed, a more suitable design was found to be for the square thread to be cut into the valve body. Rather than construct another small scale model based on this principle of operation (for further experimental tests) it was decided to construct the full scale loading valve for use in the engine test cell described in Part 7. The design of the valve is to be based upon the existing theories for fully developed secondary flow, together with Austin's empirical formula for the entrance length.

6.3.1 Basic Considerations

Although the special purpose valve can provide a very high speed of response (for engine testing purposes) in comparison to hydrostatic or electric prime mover systems, there are two possible disadvantages:- (i) the inability to provide the motoring condition to prime movers, as well as the loading condition, (ii) the inability to provide full torque down to zero speed (necessary for testing of electric prime movers, or internal combustion engines + transmission system).

The first of these difficulties may be overcome by the use of two special purpose valves, as shown in the simplified schematic diagram of Fig. 6.8. With the spool of the motoring valve set to minimum engagement the pressure on the inlet to pump (2) is maintained at 10 bar (to avoid the possibility of cavitation) by the use of a spring loaded non-return valve. This valve also prevents recirculation from the outlet of pump (2) to the inlet, which would create overheating in the oil when under load. By controlling the spool position of the loading valve the torque or speed of the engine under test may be controlled (as discussed in section 6.1).

With the loading valve fully open an increase in the spool engagement on the motoring valve causes an increase in pressure on the inlet to pump (2) resulting in the motoring condition. Hence both loading and motoring conditions can be controlled with this system. The disadvantage with the system is that two special purpose valves are required, together with two servo amplifiers and servo valves plus feedback transducers, as well as a control system which changes control from one valve to the other as the motoring/loading boundary is crossed. To overcome these difficulties a valve was designed which combines all the requirements for the loading and motoring conditions. The valve is shown in the simplified schematic diagram of Fig. 6.9.

Under the loading condition the spool is moved to the left of centre to restrict the outflow from the hydrostatic pump/motor unit and unload the pressure on the inlet of the unit to 10 bar. Under the motoring condition the spool is moved to the right of centre to unload the outflow from the pump/motor and increase the pressure at the inlet. Hence, servo control of the spool can be used to create full loading or motoring conditions to the prime mover.

The second possible problem with the special purpose valve arises when full torque capability is required at low speed (including standstill). In order to create torque on the prime mover shaft, a certain level of pressure is required on the outlet of the pump/motor unit. In order to maintain the required pressure it is necessary to have a flow of oil into the pressurised volume in order to make up for the leakage flow. Normally the idling speed of internal combustion engines is sufficiently fast to enable the flowrate from the hydrostatic pump/motor to make up this leakage, although this is not the case for very low prime mover (or transmission output) speeds.

To overcome this problem it is necessary either to have a separate make up supply to the outlet of the pump/motor (which has the disadvantage of being under load at all speeds for the loading condition) or have a modified loading/motoring valve of the type shown in

Fig. 6.10. If the servo supply system has a sufficiently high flowrate and operating pressure, it may be possible to use this as the make up supply by allowing the spool of the system shown in Fig. 6.9(a) to move sufficiently far to the left to let the servo supply feed into the pressurised volume on the outlet of the pump/motor.

Another problem which may be encountered by the spool valve is that of hydraulic lock (Ref. 64). This can occur when a non-uniform clearance exists around the periphery of the spool, allowing a greater flow of leakage oil across one side of the spool compared to the other. The result of this non-uniform leakage flow is to cause a pressure difference across the spool diameter which can force the spool hard into the cylinder wall, creating seizure (hydraulic lock). To avoid this possibility it is necessary to keep the length of contact between the cylinder wall and spool as short as possible and, where necessary, cut grooves in the cylinder wall to equilise the pressure distribution. It should be noted that the threaded section of the valve provides an improvement in this respect.

In order to measure the position of the spool without having some linkage arrangement to the outside of the valve (which may create sealing problems as well as a possible reduction in the speed of response of the spool) it was decided to have the position transducer mounted inside the valve body. A commercially available LVDT (linear variable differential transformer) was purchased with linear characteristics over the required range of displacement (± 0.0254 m). The transducer was stripped from its outer casing to avoid possible problems with pressure distribution, and the LVDT windings were coated in epoxy resin to prevent possible disturbances due to the oil flow. A sectional view of the complete valve is shown in Fig. 6.11. The thread and spool dimensions suitable for control of the 70 kW diesel engine system are determined in the following section.

6.3.2 Analytical Design

Of first importance in the design of the valve it is necessary that the maximum required load torque can be achieved throughout the speed range. In effect the pressure which creates this torque must be achieved by the valve at the oil flowrate delivered by the engine running at its minimum loaded speed (with the oil at its working temperature). This results in low valve discrimination at higher engine speeds (resulting in higher flowrates), as shown in the theoretical linear characteristics of Fig. 6.12(a). To improve the discrimination of the valve at high flowrates it would be necessary to have a variable duct cross sectional area along the length of the spool (e.g., a tapered or variable pitch thread), which would have the theoretical non-linear characteristics shown in Fig. 6.12(b). However, since the entry conditions will become increasingly important at high flowrates (with low valve discrimination) for which there is no reliable method of obtaining the pressure drop in this region, it was decided to design the valve with a constant cross sectional area duct. Although this will result in low discrimination at high speed, it is expected that the experimental results obtained from such a valve will prove of benefit in the design of a variable thread valve having greater discrimination.

From the torque/speed characteristics of the diesel engine an estimated torque of 140 Nm may be achieved at a speed of 600 rev/min. This represents a power level of 8.8 kW which, from the manufacturers' characteristics for the hydrostatic unit acting as a pump, results in a pressure level of approximately 110 bar. At 600 rev/min the pump produces a nominal flow of 40.8 litres/min less the leakage flow at 110 bar. From Part 3 the leakage flow from the system becomes $110 * .087 = 9.57$ litres/min, so that the special purpose valve must have a flowrate of $40.8 - 9.57 = 31.23$ litres/min. In other words, at maximum spool engagement (say 0.0254m as previously) the square thread must have the dimensions such that a pressure of 110 bar is achieved at a flowrate of 28.6 litres/min with the oil at its maximum working temperature.

For convenience of machining the internal thread it was decided to use a spool diameter of 0.01905 m. Using the computer program of Appendix C(2) for a square thread of 0.002616 x 0.002616 m a pressure drop of 125 bar was predicted at 50° C (normal working temperature). Using Austin's empirical formula an entrance length of 20% of the maximum spool engagement was obtained at 50° C, which indicates that the effect of the entry condition may be higher than for the threaded spools tested earlier. At high engine speed (3000 rev/min) to achieve the maximum torque of 200 Nm a pressure of 174 bar is required. This pressure produces a leakage rate of .121 * 174 = 21 litres/min from the hydrostatic system, so that the flow required through the valve becomes 204 - 21 = 183 litres/min. Using the computer program of Appendix C(2) to achieve a pressure drop of 174 bar at a flowrate of 183 litres/min the percentage spool engagement of the valve is required to be 9.8%.

Under these conditions the entrance length predicted by Austin's method becomes 35.3% of the maximum spool engagement, so that the spool operation is well within the entrance region. Since the pressure drop in the entry region is highly dependent upon the form of the flow at the entrance to the duct (Ref. 45) and since the inlet to the duct is of a complex geometrical shape (due to the angle of the helical thread in relation to the spool valve), it is unlikely that any initial analysis of the entry conditions will prove to be very accurate. Furthermore, the Reynolds number at this higher flowrate is 52000, which is approaching the point of transition to turbulent flow (Ref. 56), so that experimental results are necessary to determine the valve performance in this region.

However, it seems likely that since the Reynolds number is high throughout the speed range of the diesel engine (a value of 8100 is obtained even at 600 rev/min) the initial flow may well be turbulent in the entry region before the secondary flow becomes established under all loading conditions. This would result in a much higher pressure drop in the entry region compared to the previous experimental results which had much lower Reynolds numbers.

Under the motoring condition it was decided to use the same thread size as necessary for the loading condition, since the required pressure levels and corresponding flowrates are of the same order. At low speed (600 rev/min) an estimated torque of 16.7 Nm is required to motor the engine (from Part 3). From the manufacturers' characteristics for the hydrostatic unit used as a motor, this torque requires a pressure level of approximately 18.6 bar. From Part 3 the leakage from the motoring side of the system at this pressure becomes 18.6 * 0.34 = 6.3 litres/min. The hydrostatic motor requires a nominal flowrate of 40.8 litres/min at 600 rev/min, whereas a nominal make up supply of 2.8 * 68 = 190.4 litres/min is provided by a similar make up pump powered by a three phase motor running at 2970 rev/min (as shown in Fig. 6.9). Hence under these conditions the valve is required to produce a pressure drop of 22.6 bar at a flowrate of 190.4 - (40.8+6.3) = 143 litres/min.

Using the program of Appendix C(2) a spool engagement of 1.85% is required to provide this pressure level. However, since the program indicates a Reynolds number of 31,000 together with an entrance length of 29.8% of the maximum spool engagement, under these conditions the flow will probably be turbulent and an even smaller spool engagement will be required. In fact, it is possible that the spool will have to be completely withdrawn from the threaded cylinder to achieve the required pressure. At high speed under the motoring condition the picture is somewhat different. The make up supply is only sufficient to run the engine up to 2800 rev/min if no flow is lost due to leakage or through the valve. However, due to the leakage loss created by the pressure necessary to motor the engine, a simple linearised analysis (using the program of Appendix C(2) with no allowance for entry conditions) shows that even with 100% spool engagement the maximum motoring speed will be less than 2200 rev/min.

This is because a pressure of 73.1 bar is required at this speed, resulting in a leakage loss of 27 litres/min. With a flow of 149.6 litres/min required by the hydrostatic motor this leaves a flowrate of 12.5 litres/min for the valve. However, at this flowrate and with 100% spool engagement the valve can only achieve a pressure of 32 bar (which is not sufficient to enable a speed of 2200 rev/min to be reached). In practice a tapered thread could be used to effectively prevent any flow through the valve at high speed under the motoring condition. Also a higher flowrate make up supply could be used, although in this case the same result can be achieved by reducing the swashplate angle on the hydrostatic unit (connected to the diesel engine) if high motoring speeds are required.

Hence the linearised analysis indicates that a uniform duct area based on a square section thread should be capable of providing the required range of loading conditions, although the discrimination will be low at high speed under the loading condition. Also, the discrimination will be low at low speed under the motoring condition, as well as a limit being placed on the maximum speed under the motoring condition.

To improve the accuracy of manufacturing and measuring the dimensions of the internal square thread, the internal components were machined in sections, as shown in Fig. 6.13. The components having mating surfaces with the spool were machined to 100 microns undersize on the internal diameter and 100 microns oversize on the external diameter. These items were then surface hardened (to reduce the abrasive effect of the oil flowing at high velocity) and ground to size (i.e., tight fit into valve body and slide fit for spool). After machining the valve dimensions were measured as follows:-

$L1 = 0.0254$ m; $L2 = .00259$ m; $L3 = .00264$ m;

$L4 = 0.00244$ m; $L5 = 0.01905$ m; clearance = 10 microns.

The theoretical analysis was repeated using these dimensions and the difference with the previous results was found to be negligible. The LVDT housing and the servo supply connections were machined to act as end-stops for the spool at $\pm$ 0.0254 m from the central position. For the initial experimental tests (presented in the following section) the spool was positioned inside the valve by means of a threaded stud connected to the spool through the servo supply side of the valve body (Fig. 6.13).

This method of positioning the spool was necessary since, at the time of the initial tests, a servo supply system was not available in conjunction with the high power main flowrate supply for testing the valve. The LVDT oscillator/demodulator and associated output amplifier system was adjusted to give a 10 volt signal for full scale adjustment of the spool in either direction, for which the manufacturers claim a linearity of 0.5% (at constant temperature). The combined temperature coefficient for the transducer plus oscillator/demodulator and amplifier is 0.05% per °C, so that it is necessary to adjust the output gain at the required operating temperature (i.e., 50 °C for LVDT, room temperature for oscillator/demodulator and amplifier).

6.4 Experimental Results and Discussion

Since the engine test cell was still under construction at the time the special purpose valve was ready for testing, it became necessary to find an existing system which fitted the necessary flow and pressure conditions. By good fortune the main aircraft test frame at Hawker Siddeley Aviation Ltd. (Kingston) was undergoing extensive modifications at that time, for which the hydraulic supply unit met the requirements exactly:- i.e., flow capability of up to 230 litres/min of Shell Tellus 27 oil at a working temperature of 45 - 50° C with a pressure capability of over 200 bar. Permission was kindly granted by the Company to allow the author to test the valve with this system.

The apparatus was set up in an identical manner to the initial experimental system (shown in Fig. 6.5) with the following exceptions:-

(i) The micrometer adjustment of the spool position was replaced by a threaded stud using an LVDT plus oscillator/demodulator and amplifier for position indication on a digital voltmeter.

(ii) A turbine flowmeter was fitted having a flow capability of 30 → 270 litres/min.

(iii) The hydraulic supply system consisted of four separately powered variable capacity hydraulic pumps each having a flow capability of 57 litres/min.

The experimental procedure followed was identical to that of section 6.2.2 in that readings of pressure were recorded within a two second time period of setting up the required flowrate (by adjustment of the pressure relief valve) at a given spool position. For greatest accuracy the experiments were performed at exactly the same flowrates as used by the manufacturers of the turbine flowmeter in their calibration procedure. Identical results were obtained for both the loading and motoring sides of the valve, as shown in graph G108 (pressure plotted against spool displacement at each flowrate).

For the low flowrate characteristics once the fully developed flow has become established the theoretically predicted slope of pressure against spool engagement is shown to be in close agreement with the actual slope.

In the entry region, however, the performance is highly non-linear and the flow conditions are thought to develop as follows;-

In the first 5% of the spool engagement the flow path is probably better described as an orifice (rather than a given length of duct), as shown in Fig. 6.14(a). Hence the pressure drop in this region is relatively small (for flowrates up to 130 litres/min) and the slope is linear. As the spool approaches 10% engagement (equivalent to the duct width, L3) the flow path is much closer to that of a duct, as shown in Fig. 6.14(b). At this point the secondary flow effect is still insignificant and the conditions may be represented by turbulent flow due to the complex path of the duct and the high Reynolds numbers involved. The slope of the pressure/spool engagement characteristic therefore becomes very steep at this point.

As the spool engagement is increased further the centrifugal forces become important and secondary flow begins to develop. Hence a transition takes place from turbulent to laminar flow with a much lower slope for the pressure/spool engagement characteristic. Further spool engagement causes the secondary flow to become more established gradually increasing the pressure drop until the fully developed condition is reached, at which point the slope remains constant. This last region, having a gradually increasing resistance as the secondary flow builds up, is predicted in the theoretical analysis of Yao and Berger (Ref. 44) and is in agreement with the only recorded experimental data for pressure losses in the entry region of gently curved pipes having a curvature ratio $\gg$ 1000 (Ref. 65).

For flowrates greater than 40 litres/min (graph G107) the characteristics all reside well within the entry region of the duct, where the turbulent flow region creates the largest drop in pressure and secondary flow effects are negligible. It would therefore not be expected that the empirical formula for the pressure drop in a curved tube would result in an accurate prediction of the pressure drop in the entrance region. This is particularly noticeable for the characteristics obtained at a flowrate of 65 litres/min for which the theoretical pressure drop at a spool engagement of 13% is approximately a quarter of the actual pressure drop. At the higher flowrates, however, a much closer correlation between the actual and theoretical pressure losses is achieved.

By interpolating the pressure values from the experimental results the approximate torque/spool engagement characteristics were determined at low, medium and high diesel engine speeds, as shown in graph G54. The characteristics were obtained by determining the pressure difference across the hydrostatic pump/motor, which shows that at low speed the zero torque position of the spool is offset from the centre. Referring to Fig. 6.9 this is due to the flowrate on the motoring side of the valve being much higher than on the loading side at low speed, so that the pressure (and therefore torque) is higher on the motoring side with the spool in its central position. At high speed the flowrate on the loading side of the valve is much higher than on the motoring side, so that the pressure builds up on the loading side with the spool in its central position.

Although the characteristics are highly non-linear, graph G54 shows that the required torque levels can be achieved by the fast response dynamometer under all conditions with the exception of the high speed limit under the motoring condition. If the turbulence in the entry region of the valve could be eliminated, then the characteristics would become much more linear, as well as improving the discrimination of the valve for high flowrates (i.e., at high engine speeds).

One method of reducing the magnitude of the initial pressure drop is to increase the cross sectional area of the duct formed by the square thread. However, even for very large duct areas (approaching the cross sectional area of the spool) the Reynolds number is still much higher than 2000, so that the turbulent flow cannot be eliminated, although the pressure drop can be made very small. Also, to achieve the necessary pressure at low flowrates (i.e., maximum torque at low engine speed) a small cross sectional area is necessary. It therefore seems probable that a variable area duct (i.e., tapered thread or variable pitch) could be designed to achieve linear pressure drop characteristics throughout the range of operating conditions with reasonable discrimination at high speed.

A suitable design could be based on obtaining the maximum pressure drop at maximum speed by using the empirical formula of Baylis for a constant duct area at 30% of the maximum spool engagement. The area obtained from this exercise would then be used to give the dimensions of a square thread for which the depth of the duct is reduced to zero over the required length of spool engagement, as shown in Fig. 6.14(c). Although, due to the tapered thread, the required maximum conditions will be obtained at something less than 30% spool engagement, the discrimination should still be greater and the characteristics more linear than for the constant duct valve. Hence, it has been found in this chapter that the following parameters are of importance in the design of the special purpose loading valve:-

The effect of curvature in the square section duct greatly increases the resistance to flow by creating a secondary flow pattern which runs across the axis of the main flow. For fully developed flow, empirical formulae to determine the increase in resistance compared to a straight duct have been well confirmed by theoretical analysis and may be used with confidence in the design calculations. Machining the square thread on the spool is not recommended, since the leakage across the threads of the spool could induce turbulence and the frictional resistance of the spool causes it to rotate at very high speeds.

The most significant non-linear feature of the valve occurs for small spool engagements (at distances approaching the duct width). At this point a very sharp increase in pressure occurs due to turbulence induced by the high Reynolds numbers and complex geometry of the fluid path in this region. In order to linearise the characteristics at this point a large duct area is necessary at the inlet which tapers down towards the outlet to enable high pressure/low flowrate requirements to be met. Further work is necessary in this respect to determine the effect of the taper upon the flow conditions. Finally, the effect of temperature and pressure induced viscosity changes in the valve tend to be self-cancelling, so that these effects can be ignored in the design stage.

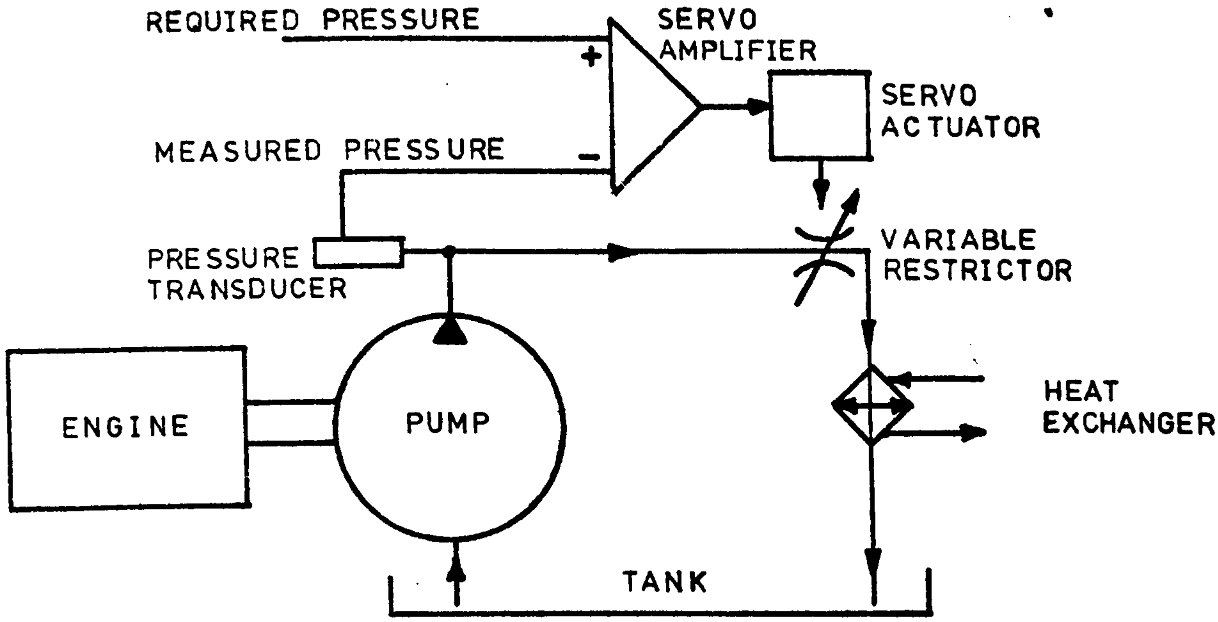

Figure 6.1(a) Fast response system

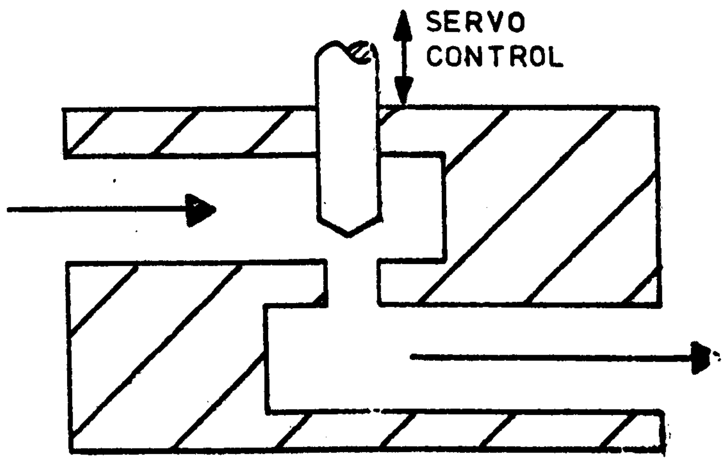

Figure 6.1(b) Needle valve

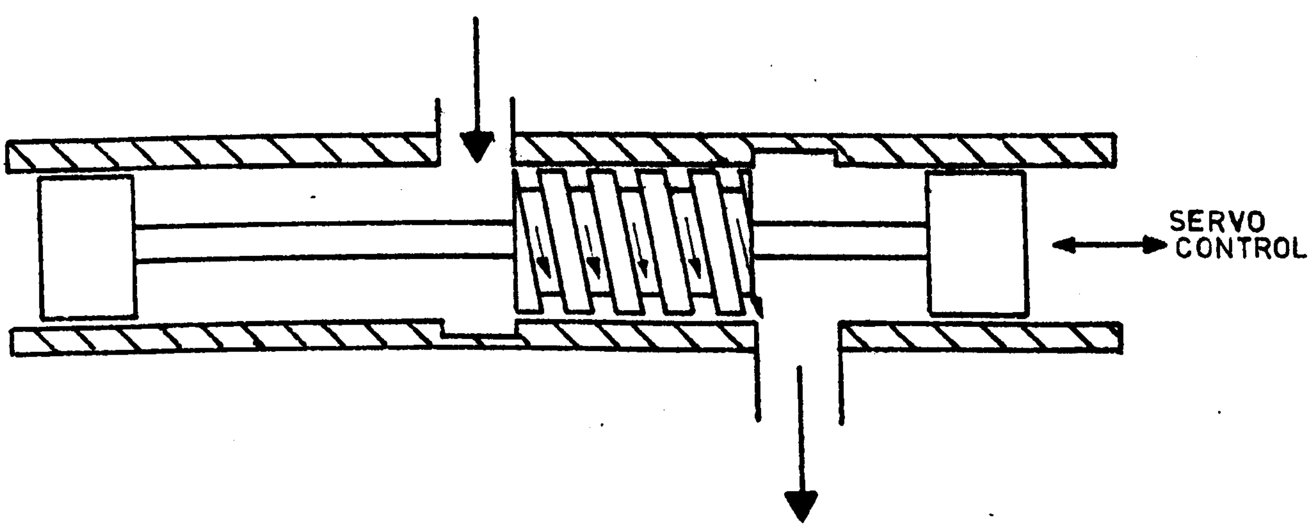

Figure 6.1(c) Special purpose valve

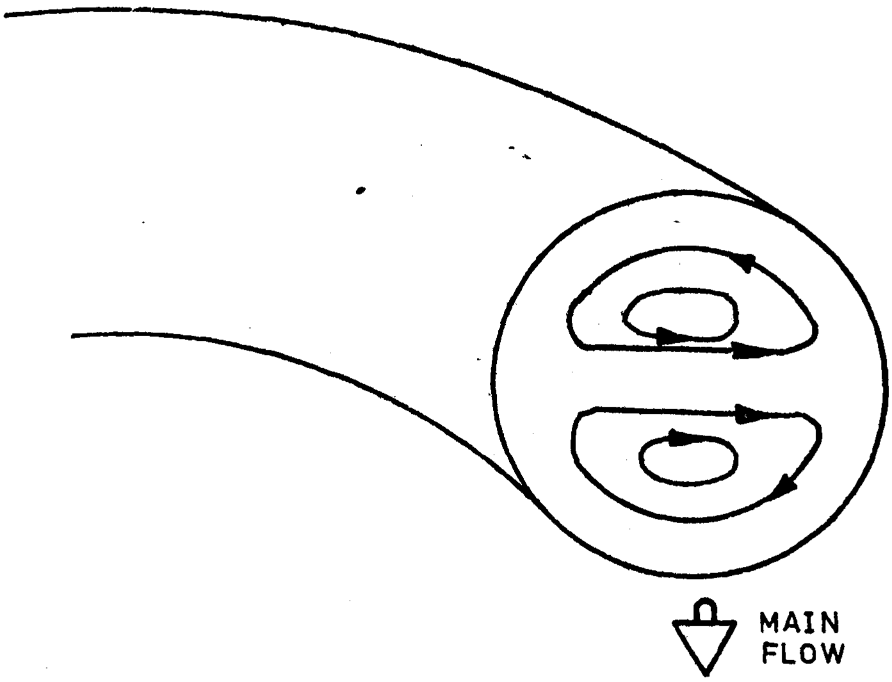

Figure 6.2(a) Secondary flow in curved round tube

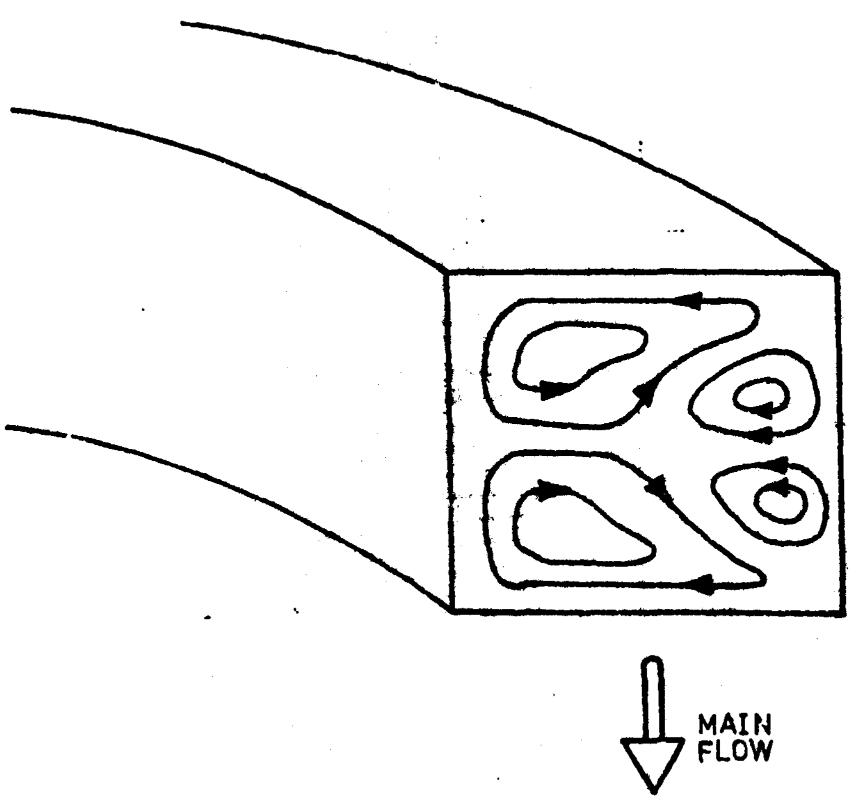

Figure 6.2(b) Secondary flow in curved square duct

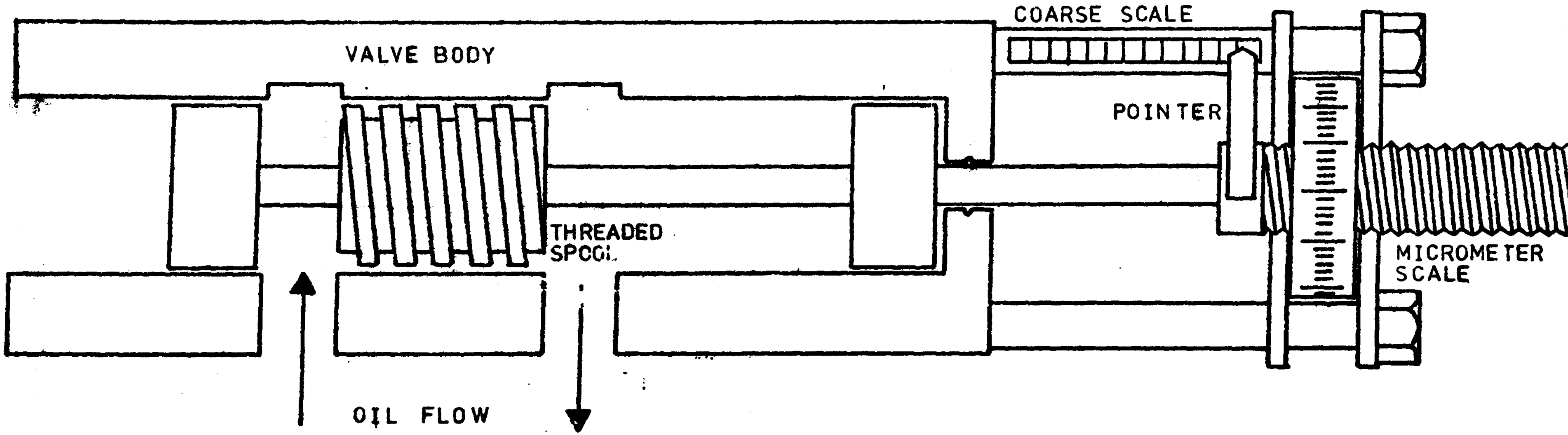

Figure 6.3 Micrometer adjustment of spool position

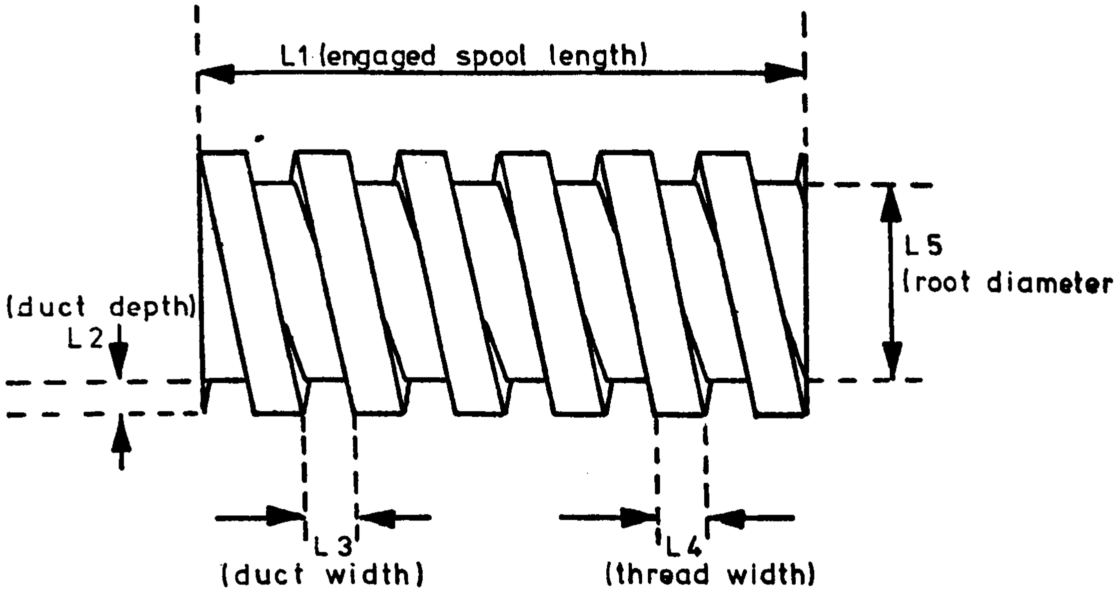

(engaged duct length = L)

DIMENSION (M)	SPOOL DESIGNATION			
	A	B	C	D
L1 (MAX)	0·0254	0·0254	0·0254	0·0254
L2	0·00127	0·00157	0·00178	0·00218
L3	0·00129	0·00152	0·00178	0·00211
L4	0·00127	0·00163	0·00178	0·00173
L5	0·01028	0·00966	0·00925	0·00845

(ALL DIMENSIONS ± 20 MICRONS)

Figure 6.4 Spool dimensions

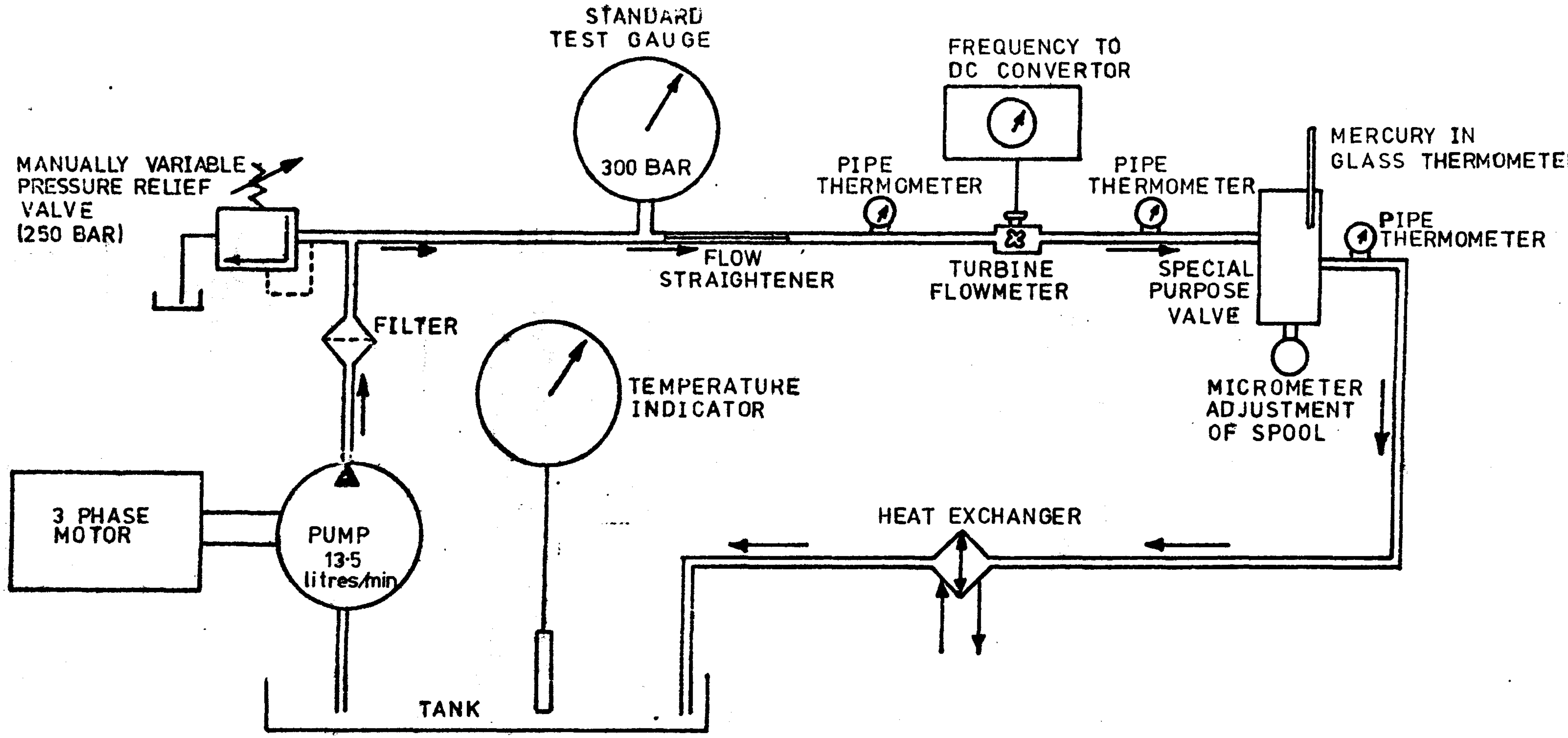

Figure 6.5 Test system for special purpose valve

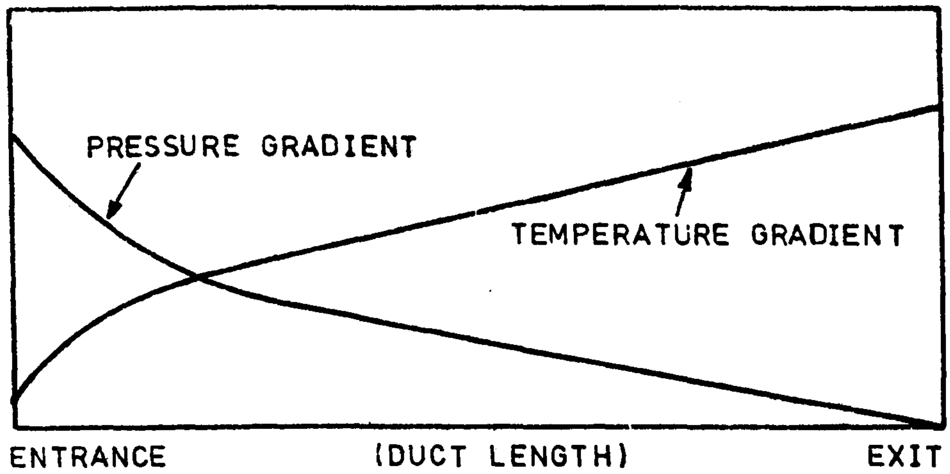

Figure 6.6(a) Temperature gradient for negligible heat loss

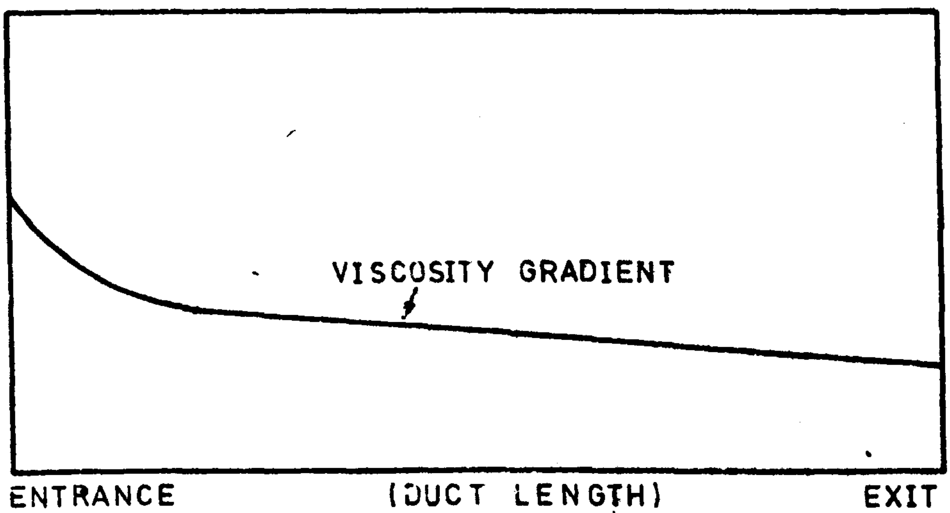

Figure 6.6(b) Viscosity gradient due to temperature change

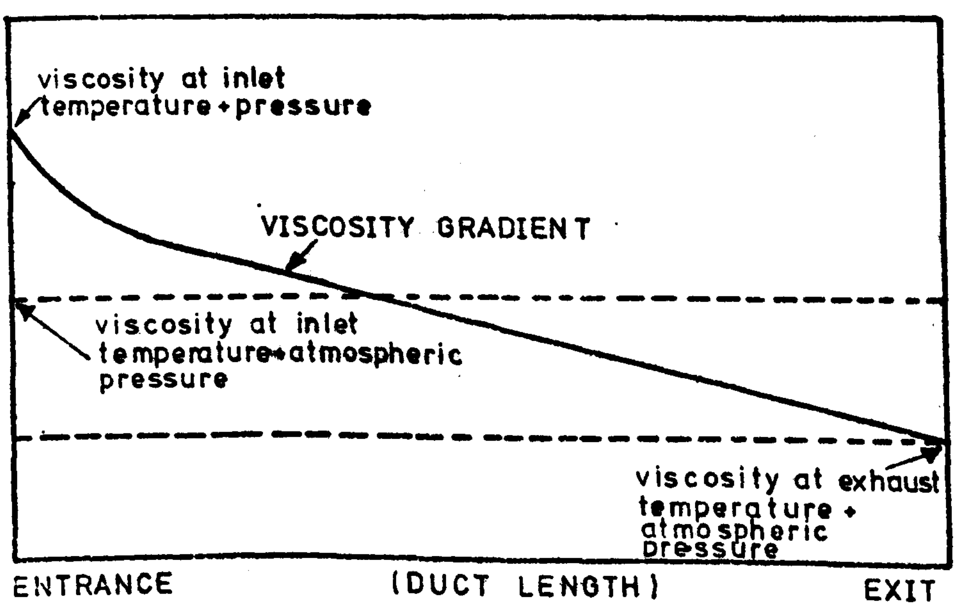

Figure 6.6(c) Viscosity gradient due to temperature + pressure change

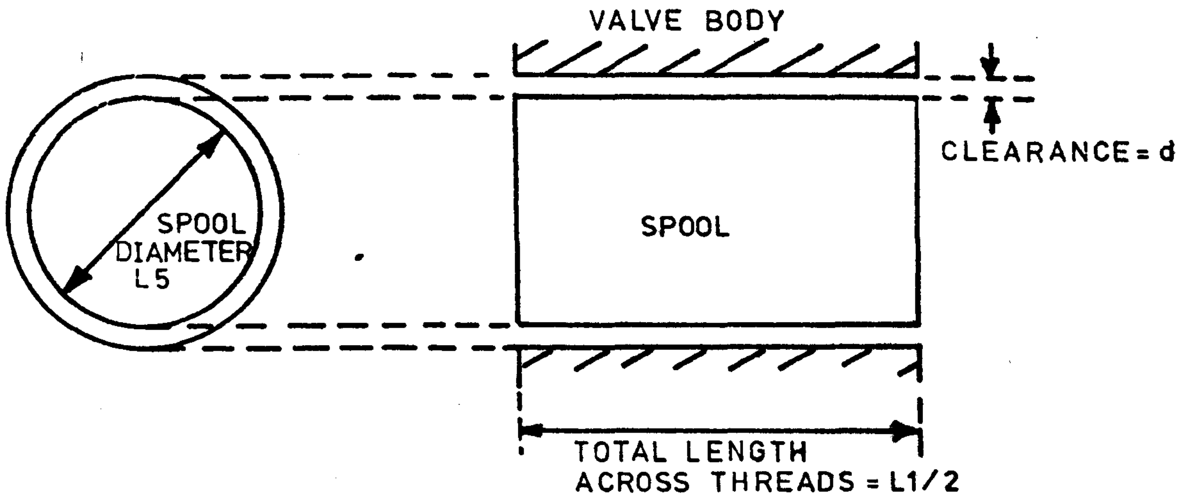

Figure 6.7(a) Leakage path

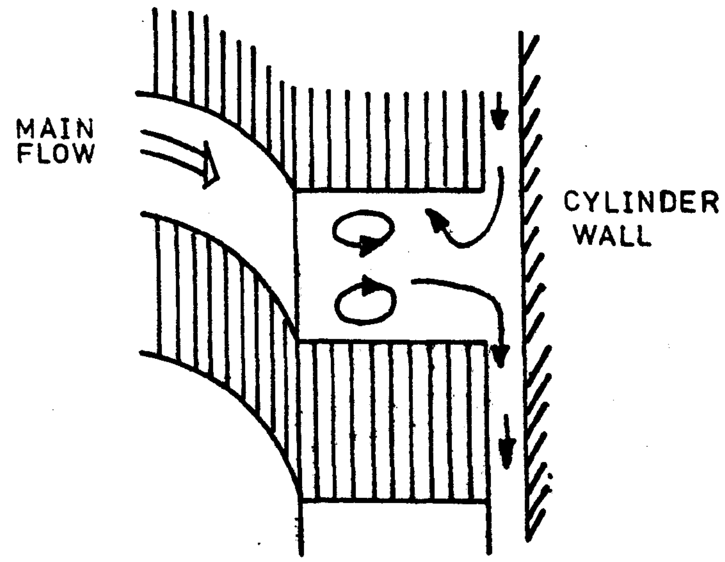

Figure 6.7(b) Possible effect of leakage upon secondary flow

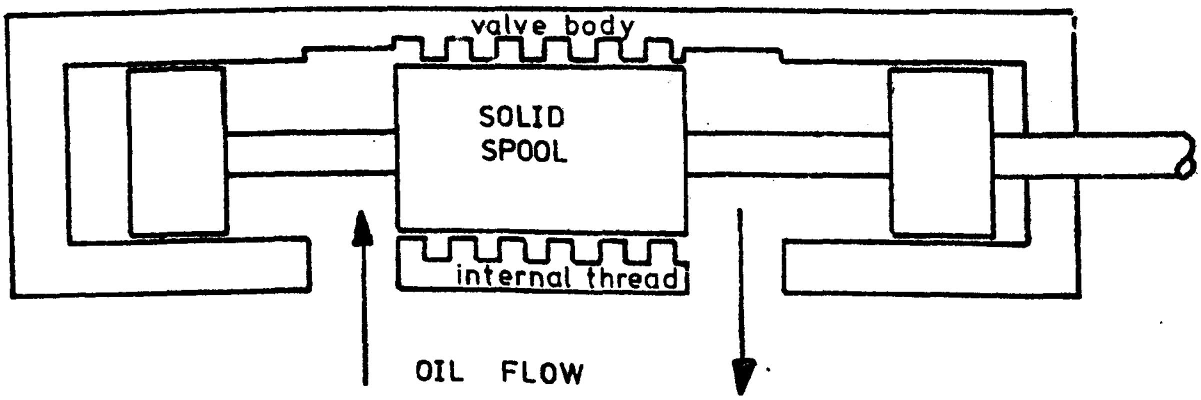

Figure 6.7(c) Internal thread valve

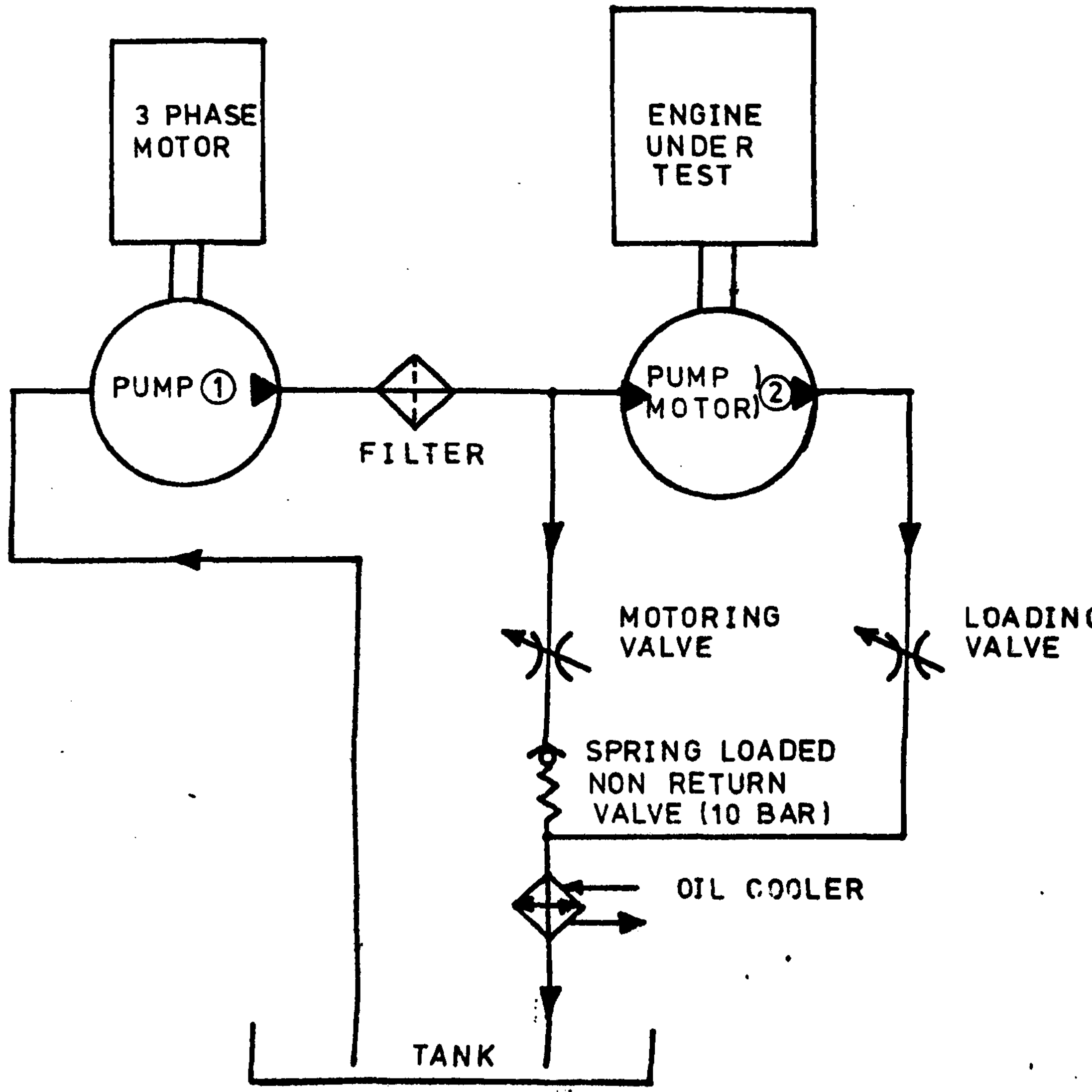

Figure 6.8 Schematic diagram of two valve system for loading and motoring

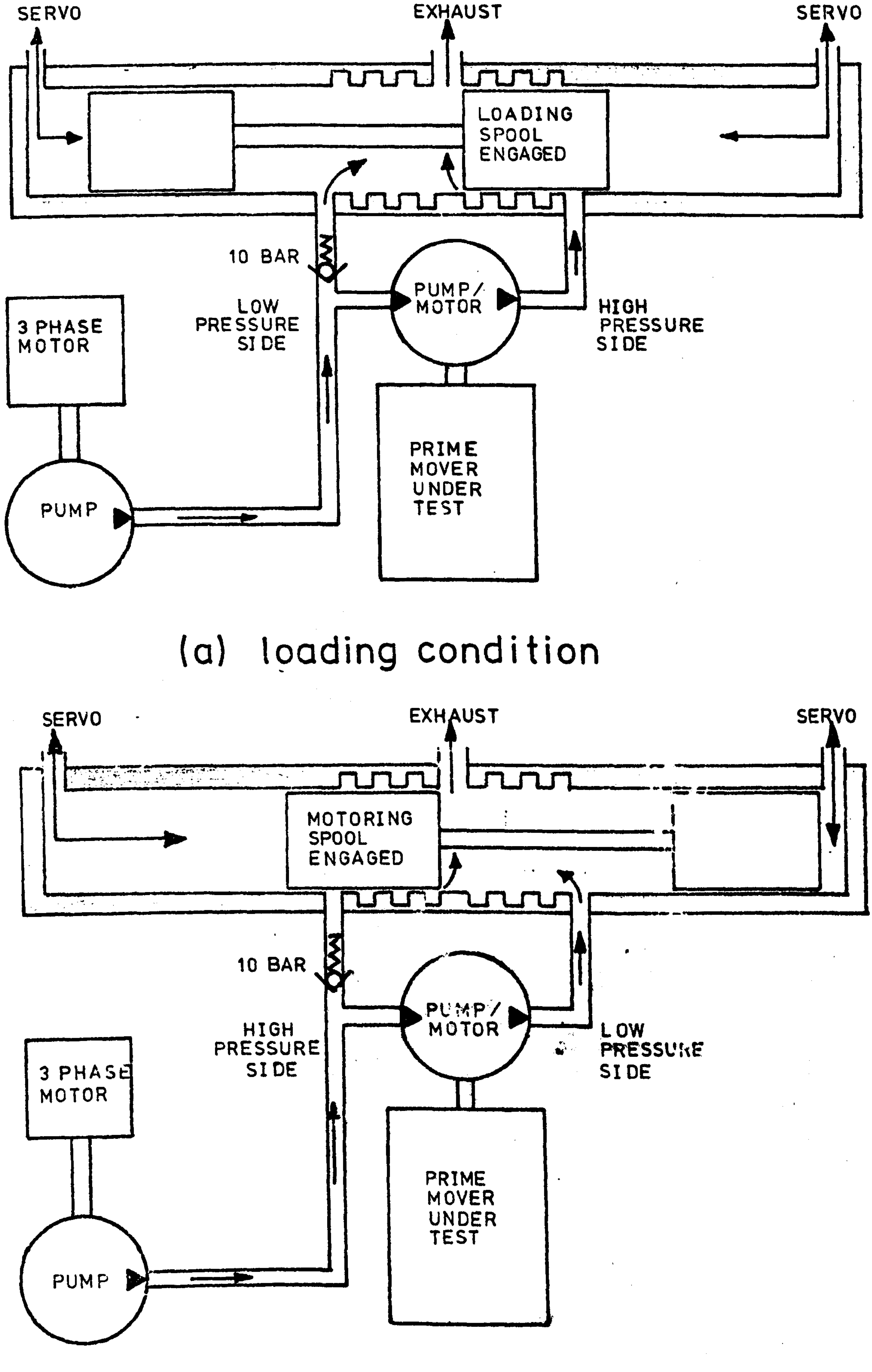

(a) loading condition

(b) motoring condition

Figure 6.9 Loading/motoring valve

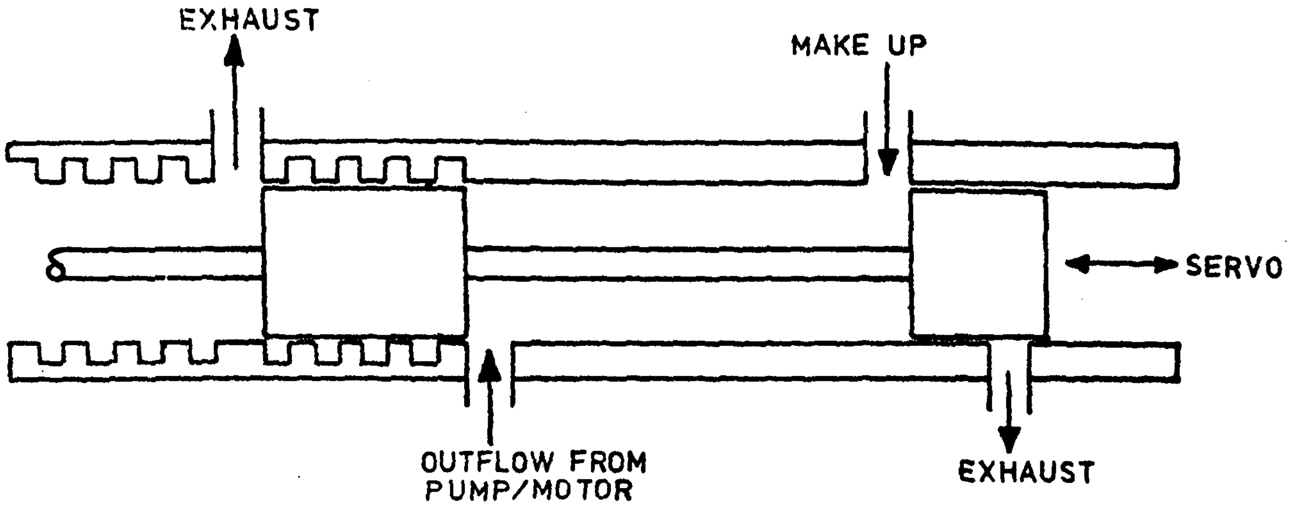

Figure 6.10 Make up supply at low prime mover speed

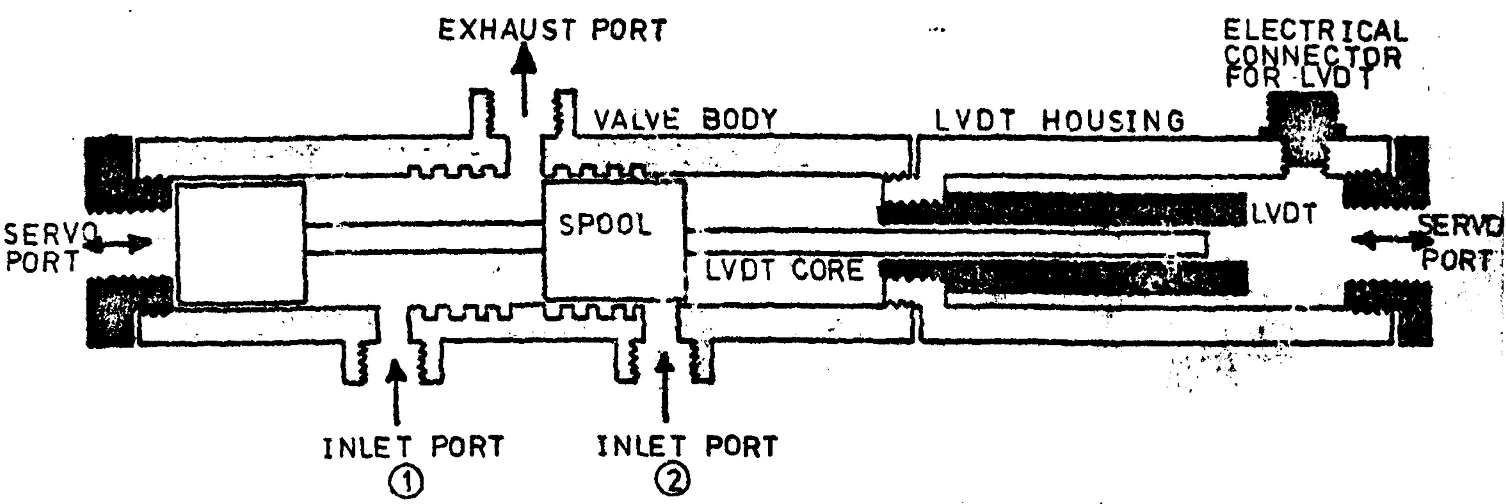

Figure 6.11 Sectional view of complete valve

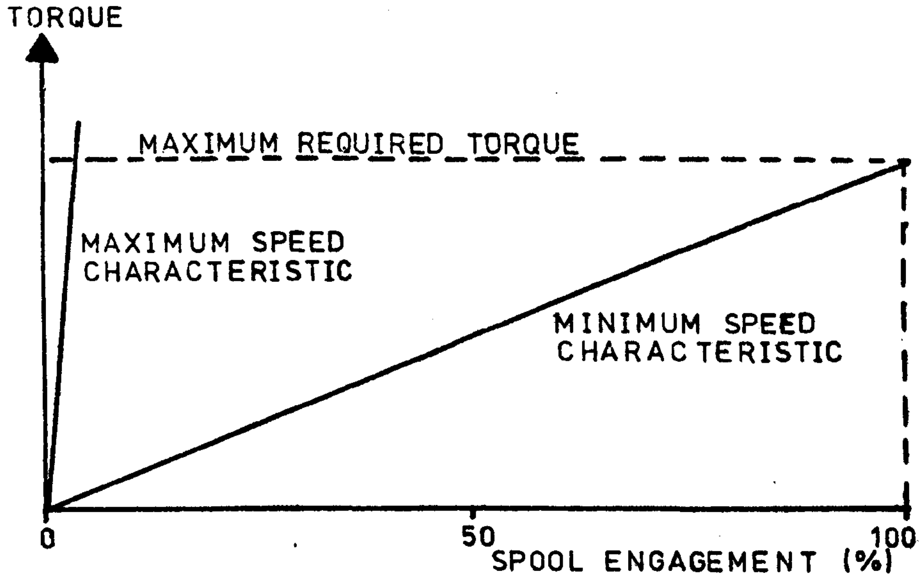

LINEAR CHARACTERISTICS RESULT IN POOR DISCRIMINATION AT HIGH SPEED

Figure 6.12 (a) Theoretical linear characteristics for constant thread valve

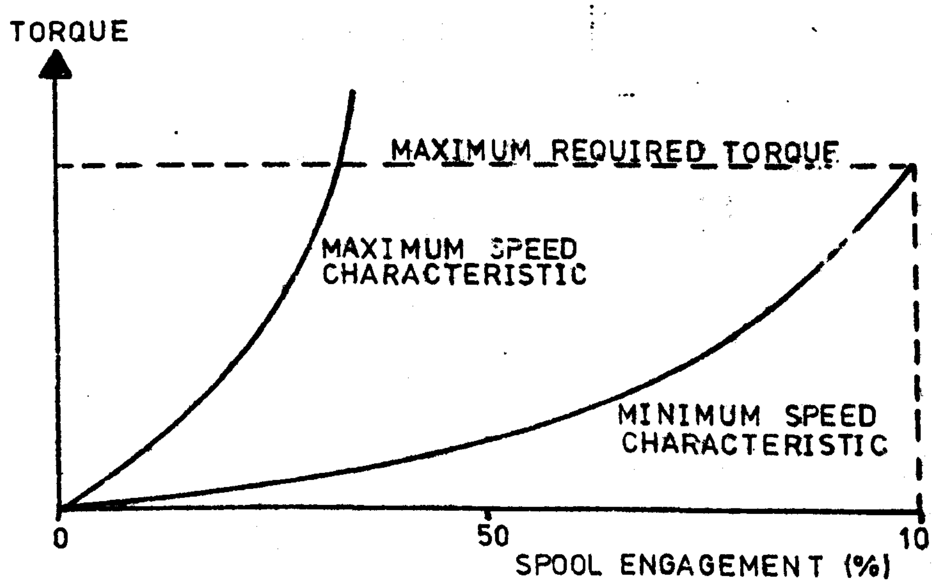

NONLINEAR CHARACTERISTICS REQUIRED FOR GOOD DISCRIMINATION AT HIGH SPEED

Figure 6.12 (b) Theoretical characteristics for varying thread valve

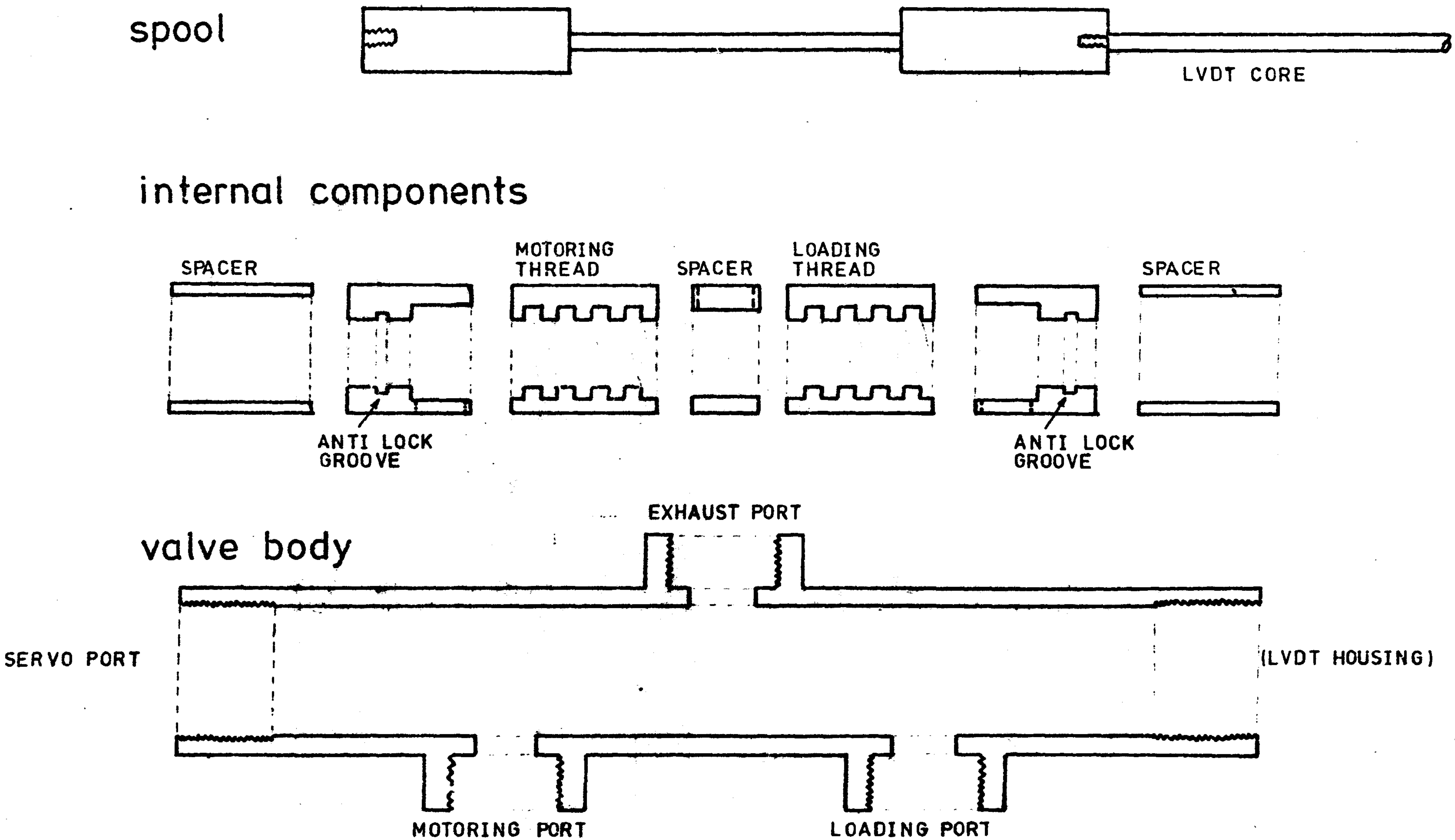

Figure 6.13 Sectional view of components of loading/motoring valve

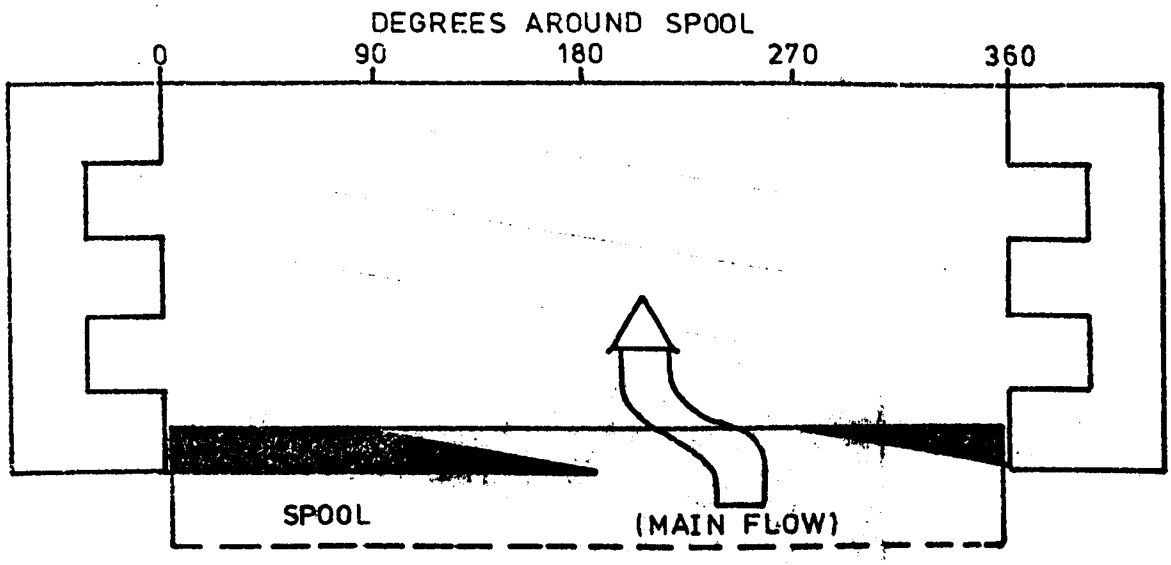

Figure 6.14 (a) Effect of 5% spool engagement on main flow

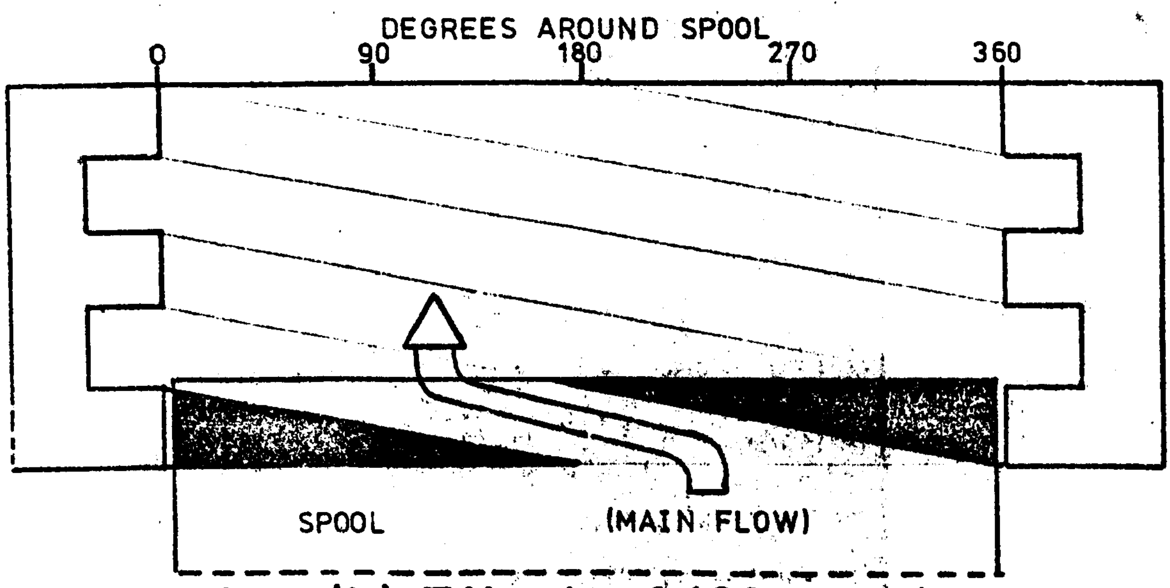

Figure 6.14 (b) Effect of 10% spool engagement on main flow

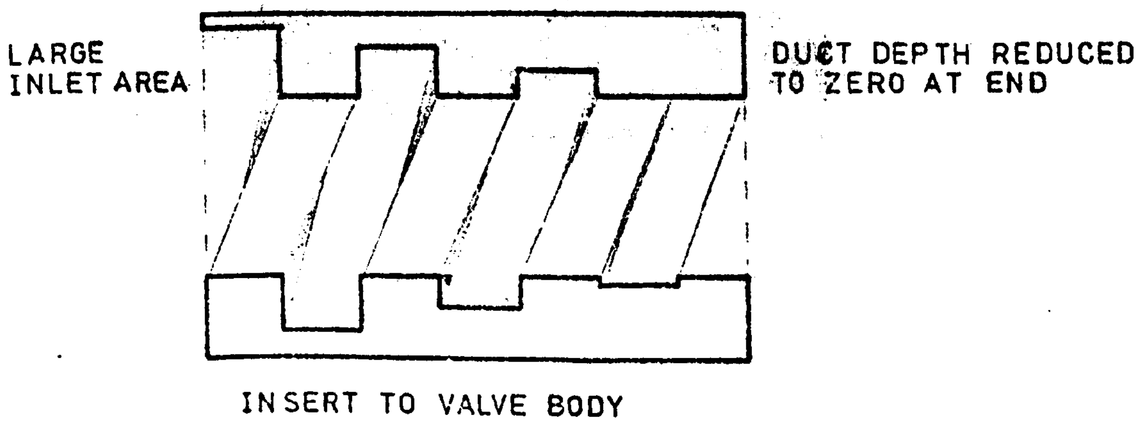

Figure 6.14 (c) Tapered thread valve

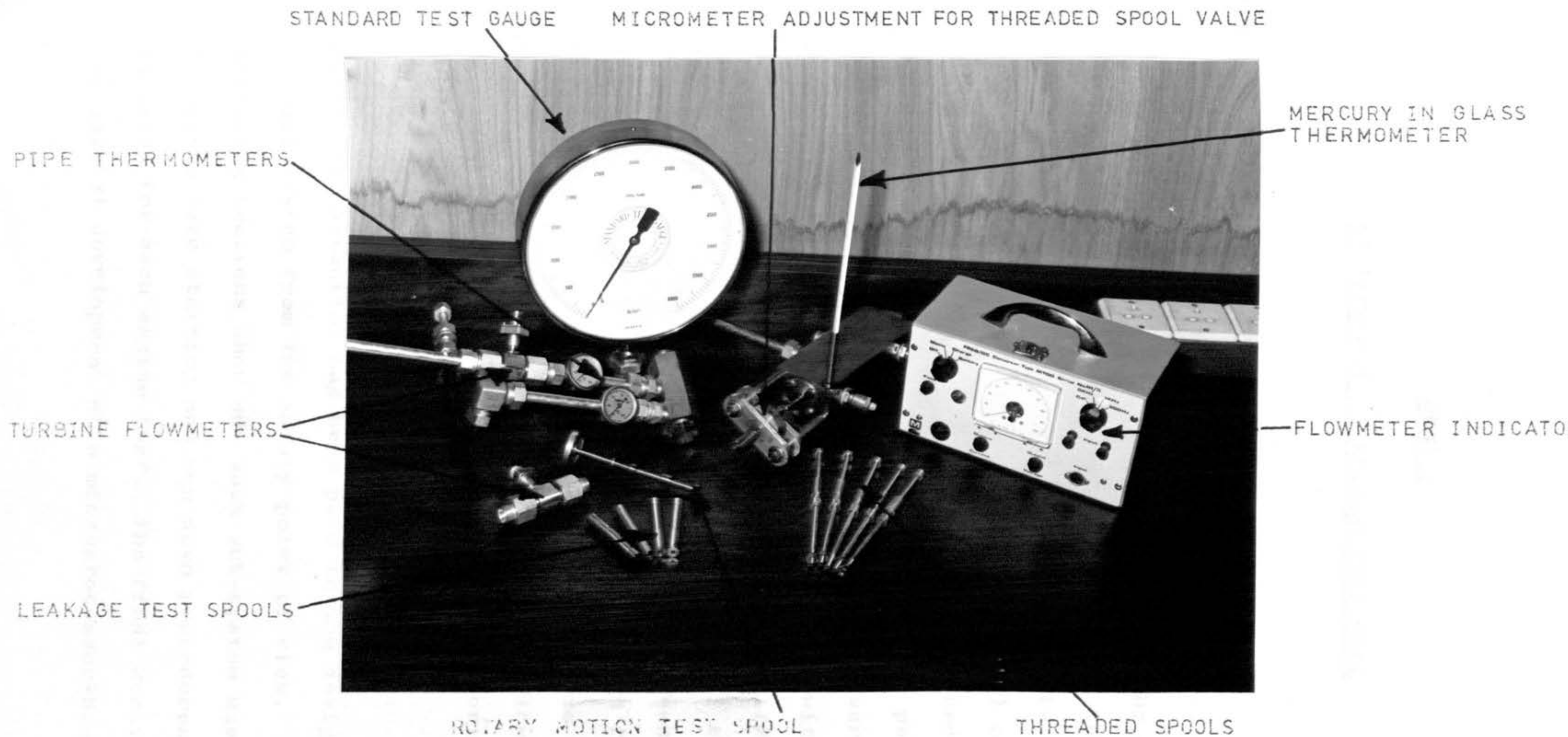

PLATE 6.1 Low power valve test equipment

PART 7

DEVELOPMENT OF ENGINE TEST CELL

7.1 Introduction

First considerations in the development of the dynamometer system for the engine test cell were to enable either a hydrostatic transmission system to be used as the dynamometer (of the type shown in Part 2) or the special purpose loading/motoring valve analysed in Part 6. To enable comparisons to be made between the performance of the two types of dynamometer, it is necessary to be able to change from one system to the other with the minimum of inconvenience. Also, due to the limited electrical power available in the vicinity of the engine test cell, it is necessary to provide some means of reducing the level of power regeneration when full load is applied to the engine using the hydrostatic transmission system. It will be shown in the following section how the special purpose loading/motoring valve can perform this function.

Particular attention has been paid to the design of the overall system from the safety point of view. The following sections show how each sub-system was developed to enable safe starting and run down procedures to be followed for each engine test. The final section shows the initial development of a microprocessor-based monitoring system which will be used for such features as monitoring temperature, pressure, torque and speed levels for safety purposes, as well as data acquisition during transient tests. The system will be extended to provide duty cycles for engine test purposes, and perform on-line control functions for the simulation of vehicle characteristics.

7.2 Hydraulic System

To enable easy interchange between the use of the hydrostatic dynamometer system and the fast response dynamometer system a hydraulic circuit was devised as shown in the simplified schematic diagram of Fig. 7.1. Manual adjustment of the three valves (A, B and C) enables the system to be changed from one dynamometer to the other. For example, with valves A and C closed and B open the dynamometer is of the hydrostatic transmission type. When the spool of the special purpose valve is set to maximum engagement on the motoring side of the valve and the hydrostatic dynamometer is performing the motoring function there is only a small amount of leakage flow through this side of the valve. Also, the loading side of the valve will be fully disengaged under these conditions (refer to Fig. 6.9) so that pump 3 is unloaded.

When the hydrostatic transmission system is to perform the loading function (thereby regenerating power to the

3 ø mains) then as the maximum power level is approached it is necessary to engage the loading side of the special purpose valve. (Although this will cause the motoring side to be disengaged, this is not a problem, since under the loading condition the pressure is reduced on the motoring side of the hydrostatic transmission system. Hence leakage through the motoring side of the valve will only occur if the pressure is greater than the 10 bar rating of the spring loaded non-return valve.) As the loading side of the special purpose valve is engaged the pressure will build up on the outlet of pump 3, causing it to take power from the 3 phase motor and reduce the level of regeneration. Although this action is necessary in this case, due to the limited electrical power supply available in the vicinity of the test cell, such a system may be advantageous where the regeneration of large values of electrical power is not feasible.

With valves A and C open and B closed as well as the swashplate of pump 2 set to its central position, the system becomes a fast response dynamometer, as shown in Fig. 6.9. With pump 2 set to zero flow (swashplate central), this part of the circuit is effectively shut off from the rest of the system, and the oil supply to the special purpose valve is made from pump 3. With the spool engaged on the loading side of the valve, pressure builds up on that side, and the motoring side is unloaded to 10 bar (giving the loading condition).

With the spool engaged on the motoring side of the valve, the pressure builds up on that side and the loading side of the hydrostatic pump is unloaded (giving the motoring condition).

The make up supply is necessary to maintain a minimum pressure in the hydrostatic transmission loop of 10 bar to avoid cavitation at the inlet to pumps 1 and 2, and the boost pump is used for the same reason in conjunction with pump 3. The servo supply pump is used for the servo actuators of the throttle control, special purpose valve control, and the swashplate control for pumps 1 and 2. The make up supply is limited to 10 bar by a relief valve internally mounted in pump 2, and the boost supply to pump 3 is limited to 10 bar by an external high flow spring loaded non-return valve (270 litres/min). Cross port relief valves are mounted internally in pumps 2 and 3 to limit the maximum pressure across these units (initially set to 200 bar). These cross port relief valves are pilot operated and are vented back to tank via a solenoid valve to enable the hydraulic system to be remotely controlled.

The pressure relief valve for the servo supply system is also pilot operated and vented back to tank via a solenoid valve. The control of the solenoid valves is through an electrical interlock system (described in the following section) which ensures that all the servo actuators may be set to their required positions before the main hydraulic power system comes into operation. The full circuit diagram for the complete hydraulic system is shown in Fig. 7.2. The accumulator in the servo supply system is used as a back-up to the servo actuator during transient conditions as well as to maintain servo power for a short period of time if the electrical 3 phase power fails or is "tripped" under emergency shut down conditions.

The pressure is maintained for this short period by using a small bore pipe on the pressure relief outlet (approximately 0.01 m) to reduce the flowrate from the accumulator, which has the additional advantage of reducing the back pressure in the return pipe from the oil cooler. However, to prevent the accumulator from feeding oil back to the servo pump when the 3 phase power goes off (which may cause the 3 phase motor to run backwards at very high speed) a one-way valve is necessary on the outlet of the servo pump. The reason for maintaining the servo pressure as the power goes off is to enable the throttle servo to be moved back through the idling position for the diesel engine, and actuate the fuel shut off lever. This function is performed by using an electromagnetic relay to disconnect the current supply to the torque motor of the throttle servo. By setting a mechanical offset on the servo valve, the hydraulic actuator can be made to automatically move in the direction of the fuel shut off lever when the electrical power is shut down and the relay contacts open. A photograph of the throttle servo system is shown in Plate 7.1.

As with the low power hydrostatic transmission system described in Part 2, a manifold was constructed in order to reduce the volume of oil between the primary and secondary hydrostatic units (thereby reducing the hydrostatic loop time constant under the loading condition). A photograph showing the close positioning achieved between these units is illustrated in Plate 7.2 and the position of the loading/motoring valve in relation to the primary hydrostatic unit is illustrated in Plate 7.6. To improve the damping of the hydrostatic dynamometer when used in conjunction with the governed diesel engine, it was shown in Part 3 that it is necessary to increase the leakage rate from the hydrostatic loop.

From the loading side of the loop an increase in the leakage rate of 0.03 litres/min/bar is required. Using a tube bore of .0014 m at an oil temperature of 50° C the flow becomes turbulent above 3 litres/min. However, at a pressure of 150 bar the required flowrate of 4.5 litres/min is achieved with a tube length of 0.42 m. This result is obtained using the following equation for turbulent flow in circular tubes (Ref. 66):-

$$\frac{dP}{dZ} = \frac{0.316\rho\bar{u}^2}{2R_e^{\frac{1}{4}}d_e}$$, where ρ = fluid density.

Using the same method for the motoring side of the hydrostatic loop, the required increase in leakage rate of 0.07 litres/min/bar is obtained using a tube length of 0.096 m. Although an increase in the tube diameter may be used to obtain laminar flow throughout the pressure range of the system, the necessary tube length to obtain the required leakage rate becomes excessive (<70 m for motoring side).

7.3 Electrical System

The 37 kW three phase motor used to power the hydraulic system may be started either inside the test cell, or remotely from the external control bay, using a star-delta starter with automatic change over. The windings of the solenoids for the servo and cross port relief valve vents are fed from the 3 phase motor side of the overload circuit breaker via the interlocking control circuits in the control bay area. This prevents the motor from being started under load and enables the servo systems to be correctly positioned before engaging the main hydraulic power system. The circuit diagram for the electrical interlock system is shown in Fig. 7.3.

The solenoid supply line is taken between the circuit breaker and overload detectors to enable maximum power interchange for the three phase motor. In the interlock system the "start button" can only provide power to the relay if switch S4 is open and the three phase motor is running. This ensures that the hydraulic control solenoids provide an open path for the vent lines of the servo and cross port relief valves, which causes the system to remain in a low pressure state. Having pressed the start button the relay contacts close, so that the live connection through R3 holds the relay in until the system is shut down or a power failure occurs. A further interlock is provided which prevents switch S3 from operating the solenoid for the cross port relief valve until switch S4 is closed.

Thus under normal start up conditions the three phase motor is initially run up to speed, after which the interlock system start button is pressed, followed by switch S4 being turned on. The servo actuators are then set to their required start positions, and finally switch S3 is turned on. The system can then be used to provide the required running conditions for the diesel engine by means of the servo control signals. Under normal shut down conditions switch S3 is opened and the throttle servo operates the fuel shut off lever on the diesel engine. Once the engine has stopped switch S4 is opened and the delta winding circuit breaker is tripped. Under power fail or emergency shut down conditions a safe shut down will occur as the delta winding circuit breaker opens, under any of the dynamometer running conditions, since the loss of power to the solenoids will cause the relief valves to open and the throttle lever to move to the fuel shut off position.

The control circuit for each of the servo systems is shown in Fig. 7.4. The meters indicate the positions of each of the servo actuators on a console in the control bay. The console also houses the electrical interlock system previously described. Each meter is of the centre zero type giving full scale deflection for a ± 10 volt signal. For the throttle actuator the central position indicates an idling speed setting, with maximum deflection in one direction to indicate maximum fuel delivery, and maximum deflection in the opposite direction to indicate fuel shut off. For the meters indicating the swashplate positions of the hydrostatic units, the central position indicates that the swashplates are set over centre (zero fluid flow).

Since the swashplates are measured by rotary d.c. LVDTs having a voltage output range offset from zero, it is necessary to use operational amplifiers to correct the offset and modify the signal gain to a ± 10 volt level. The use of the operational amplifiers has the additional advantage of buffering the d.c. LVDT signal from impedance changes in the measuring circuit. For the loading valve, the central position indicates no load (only approximately - see graph G54) with deflection to one side giving the motoring condition, and to the opposite side the loading condition.

For each meter there is a separate output for external monitoring of the actuator positions, and an input line for transient testing or computer control purposes. A potentiometer control at each meter enables the servo actuators to be initially set up before the main hydraulic power on sequence, and also to enable steady state tests to be performed on the system. Throughout the construction of the servo control system earth loops have been avoided, and screened leads have been used, making sure that the control signals cannot create interference in the feedback signals (this is of particular importance when high gain controllers are used). Other transducers necessary for preliminary testing of the engine/dynamometer system included:-

(a) Turbine flowmeter plus magnetic pick up and frequency to d.c. convertor to measure the output flow from the loading motoring valve.

(b) Strain gauge type pressure transducers + amplifiers to measure the hydraulic oil pressure on both sides of the hydrostatic loop as well as in the supply line to the loading/motoring valve.

(c) D.c. permanent magnet tachogenerator, connected to the front end of the engine crankshaft, giving 0.4% r.m.s. smoothing for a time constant of 1 ms at an engine speed of 3000 rev/min (reducing to 0.6% smoothing at a speed of 1500 rev/min).

Although it was originally intended to count pulses from a rotating disc connected to the engine flywheel to obtain a measure of the engine speed, this method is still under development. The instrumentation in the control bay of the engine test cell is illustrated in Plate 7.3.

7.4 Cooling System

The cooling system for the test cell has two basic requirements:- to maintain the hydraulic oil temperature at a working level of 50° C (with a maximum of 60° C); and to maintain the engine oil and water temperatures at their normal running level.

For the engine cooling, a header tank (800 litres capacity) provides a maximum flowrate of cooling water to the system of 40 litres/min, as shown in the circuit diagram of Fig. 7.5. The engine water circulator and thermostatic control are used for metering the engine water to heat exchanger (A). For the engine oil a temperature sensor and valve actuator are used to control the flow of cooling water to heat exchanger (B).

To absorb the heat from the hydraulic fluid a high capacity heat exchanger is used, through which coolant is pumped at a maximum rate of 180 litres/min. This coolant forms a closed loop system with the ground level tank having a capacity of 1150 litres. The oil temperature in the hydraulic reservoir is measured by a temperature sensor which actuates a valve in the coolant line to control the rate of flow. A bypass bleed line is used to prevent the high capacity coolant pump from overheating when zero coolant flow is required (valve shut off). A float switch is incorporated in the ground level tank to return the water (at 50 litres/min) when the maximum tank level is reached.

The temperatures of the hydraulic oil as well as the engine oil and cooling water are also measured separately and displayed on large indicator gauges in the test cell (visible from the control bay window). Thermocouple sensing of these variables will also be used for the microprocessor monitoring of the overall system (described at the end of this chapter).

7.5 Fuel System

A schematic diagram of the fuel system for the engine test cell is shown in Fig. 7.6. A standard method of metering a given quantity of fuel to the engine is used, in which a calibrated glass burette tube supplies fuel to the engine pump when solenoid valve (1) is closed. As the fuel level reduces in the burette tube past the light sensitive detector (a), a trigger signal is passed to the monitoring system. The required test conditions are then performed until the fuel level passes detector (b), thereby indicating with high accuracy the volume of fuel used throughout the test (150 ml in this case). At this point solenoid valve (1) is re-opened to take over the fuel supply to the engine and refill the burette tube.

Solenoid valve (2) is placed in close proximity to the engine fuel pump as a safety measure to shut down the engine fuel supply if the electrical power supply to the test cell fails. This acts as a back up to the electrohydraulic actuator control of the fuel shut off lever (described in section 7.2). The solenoid control of the fuel supply at this point is not by itself sufficient to halt the engine immediately, since the small amount of fuel available in the galleries of the fuel pump enable the engine to continue running for a short while. The overflow from the injectors is fed back into the fuel system at the point shown in Fig. 7.6, so that the fuel metering system indicates the volume of oil used by the engine instead of the volume actually fed to the fuel pump.

7.6 Microprocessor-based Monitoring System

To facilitate the data collection and general supervision of the engine test cell a low cost microprocessor-based system has been developed. The system is based upon a Motorola 6800 Evaluation Card which contains the basic microprocessor chip and control logic plus 500 bytes of 8 bit random access memory and peripheral interface logic. The card also contains a mask programmed read only memory which aids the programming and de-bugging of the system by enabling access to and modification of the memory and control registers of the system. Of the two peripheral interface ports provided on the card one was modified to enable full duplex data transfer capabilities with a teletype having an RS232 interface. The other port was used to provide a parallel data interface to a high speed (3.56 m/s) digital cassette recorder for which the interface control programs are presented in Appendix D(1).

The evaluation card was modified to interface to a bus structured data system by allowing external control of the tri-state data input buffers on the card. For this purpose multi-way sockets were soldered to a printed circuit extender card which was then mounted on a case containing the necessary power supplies ($\pm$15 v; $\pm$12 v; +5 v). A schematic diagram for the bus structured system is shown in Fig. 7.7 and the complete microprocessor system is illustrated in Plate 7.4. To enable programs to be written in assembler language (rather than using the hexadecimal base machine language, which becomes tedious to prepare and difficult to de-bug for lengthy programs) an extended memory card of 8 K eight bit words was used to contain the necessary editor and assembler software. This permitted on-line preparation and de-bugging of programs.

However, since the 8 K memory resides in the same memory locations as the 0.5 K memory on the microprocessor evaluation card, it became necessary to change the memory locations on this card. This was done by re-assigning the address lines fed to the chip select inputs of the 0.5 K memory so as to provide consecutive memory locations from 0000 to 227F (hexadecimal). The 8 K memory card is mounted on the external data bus and, during a microprocessor READ MEMORY operation, enables data to be entered to the data lines of the evaluation card by sending an "enable" signal via the control bus to the data input tri-state buffers on the card.

To facilitate further peripheral interfacing a programmable twin port input/output module was also connected to the external bus lines. The "enable" signal for this module (to allow data through the evaluation card tri-state buffer) was taken from the peripheral READ line on the module. One of the ports was interfaced to a low cost 16 channel multiplexed analogue to digital convertor system, for which the software control routines are presented in Appendix D(2). The convertor has a 12 bit accuracy for input signals of up to $\pm$ 10 volts and has a throughput rate of 30 kHz. A faster rate than this is unnecessary for the microprocessor-based system, since the relatively slow instruction times for the MPU limit the speed at which it can process the data.

The second port of the programmable input/output unit is reserved for expansion of the output control facilities of the system, although one output channel may be used as a "trip control" to the test cell electrical power system. This can be used to shut down the system if the analogue data on any of the input channels exceeds certain preset conditions (i.e., speed, power, temperature levels, etc.).

To provide analogue output signals from the micro-processor-based system a twin channel digital to analogue convertor plus interface circuitry (all on a single chip) was connected directly to the external bus. Each channel represents a single memory location to the microprocessor, so that it is unnecessary to write detailed peripheral interface control software in order to output the required analogue signal level on either channel. These channels may be used for providing the required speed and torque levels to the engine/dynamometer system for simulation of vehicle duty cycles, for example, as required by the 1977 Californian emission control legislation (Ref. 1).

For further development of the microprocessor-based system a PROM (Programmable Read Only Memory) programmer system has also been interfaced to the external bus.

This system enables 8 K bit UVE PROMs (Ultra Violet Erasable PROMs) to be programmed under software control of the microprocessor evaluation card. These PROMs may then be used to provide a minimal configuration microprocessor system for monitoring and control of the engine test cell once the necessary software routines have been fully de-bugged on the development system. For example, a one card system containing one 8 K PROM plus a twin channel D/A convertor and one microprocessor chip (with on-chip clock plus control logic and random access memory) may be used to provide the torque/speed signals to the engine/dynamometer system. A similar configuration including a multiplexed A/D convertor plus peripheral interface chip may be used for data acquisition and general supervision of the test cell.

Since the peripheral interface chips of the PROM programmer occupied memory locations used by the mask programmed ROM on the evaluation card, it was necessary to change the address assignments of these chips. Also it was necessary to modify the programming software to enable the programming process to be controlled from the teletype keyboard via the mask programmed monitoring ROM. To enable the data on the PROM to be verified, the READ line of the PROM programmer system was used as the enable line, via the control bus, for controlling the tri-state data buffers of the microprocessor evaluation card.

Further developments in the microprocessor-based system are to replace the teletype with a visual display terminal, and the digital cassette handler with a miniature floppy disc system. Both of these units have much higher performance characteristics than the teletype and cassette handler at a lower cost. This will enable much faster program development on the microprocessor system since the delays in editing, assembling and running programs will be virtually eliminated.

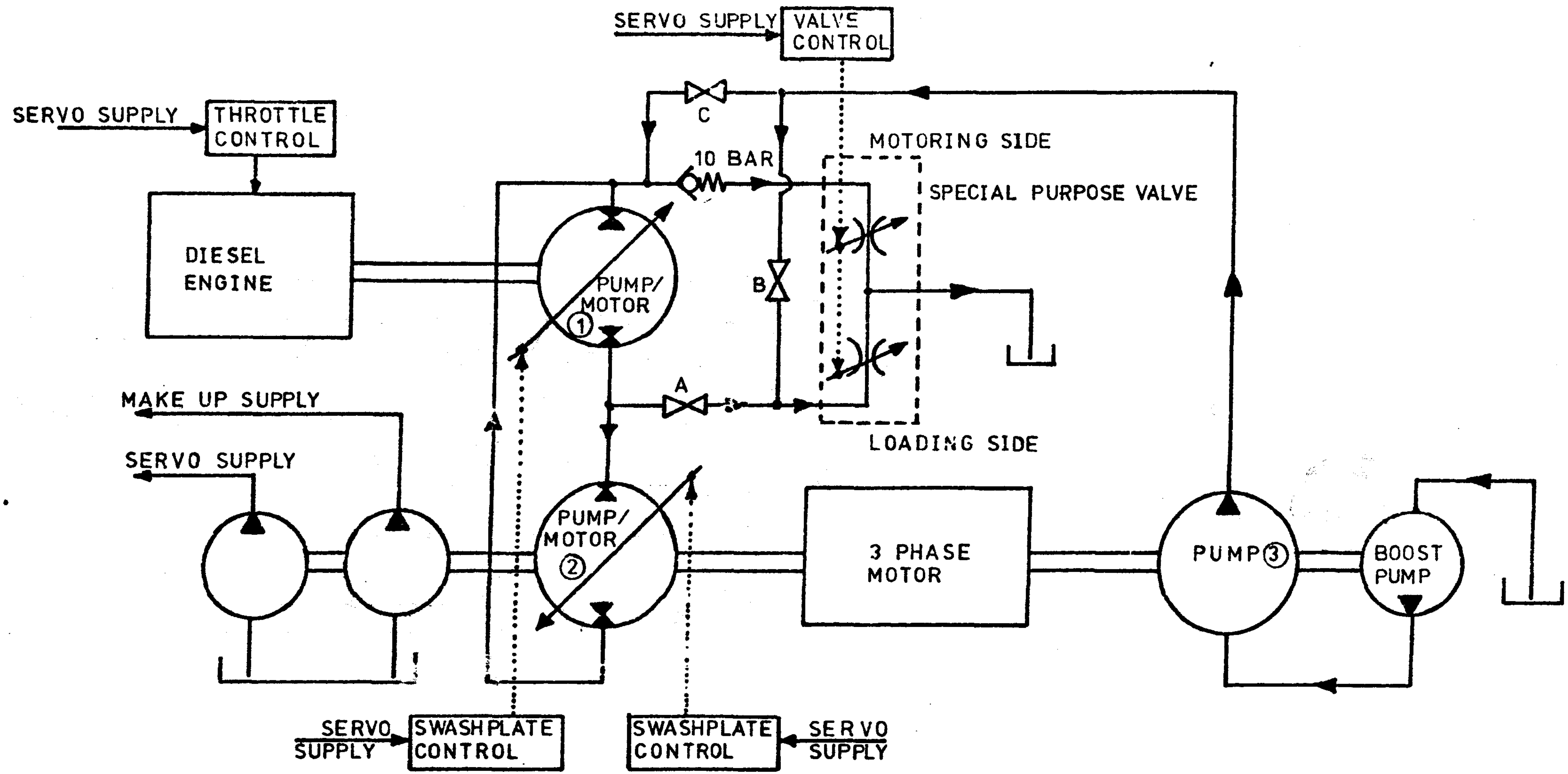

Figure 7.1 Simplified schematic diagram of hydraulic circuit

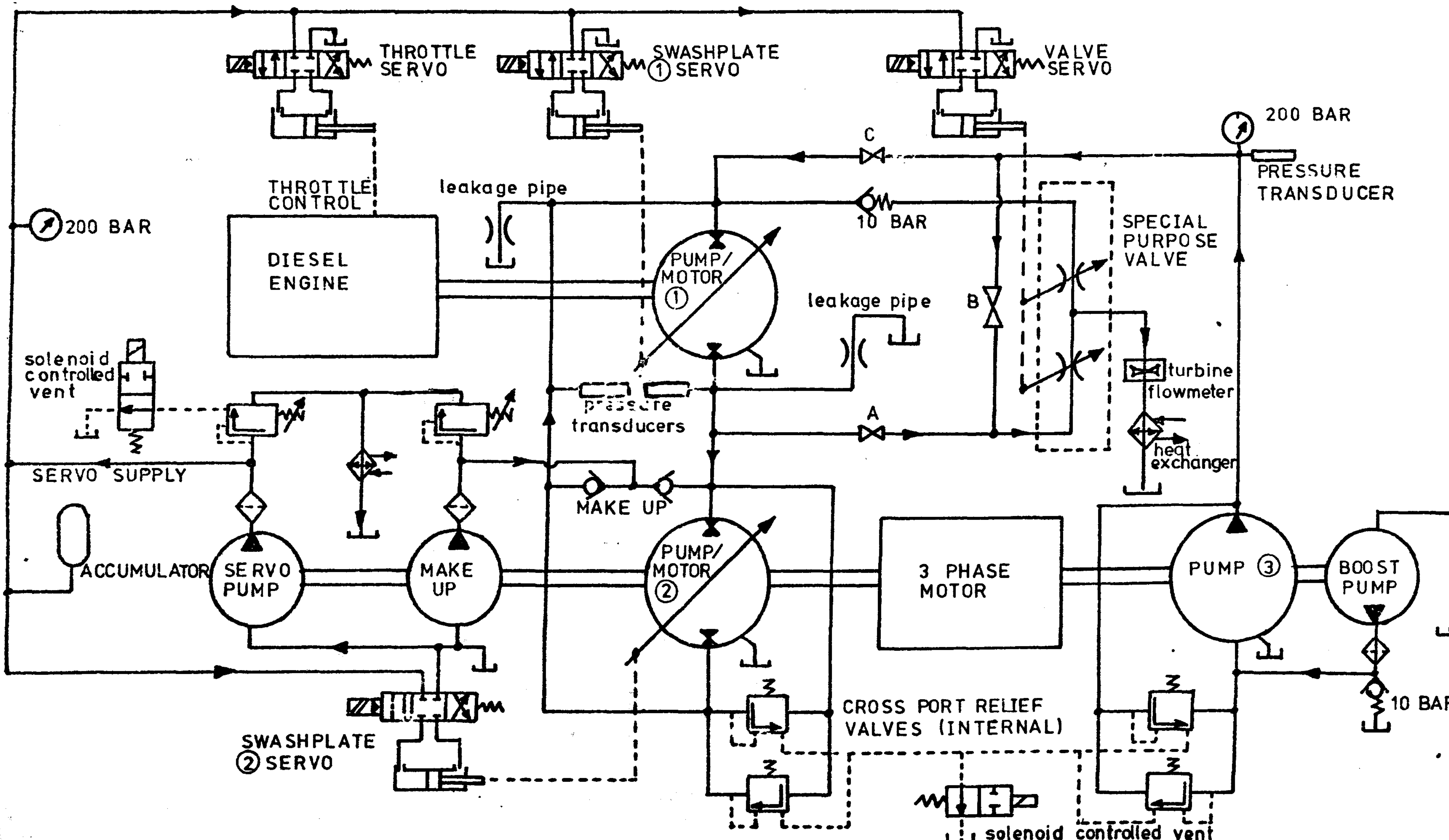

Figure 7.2 Complete hydraulic circuit

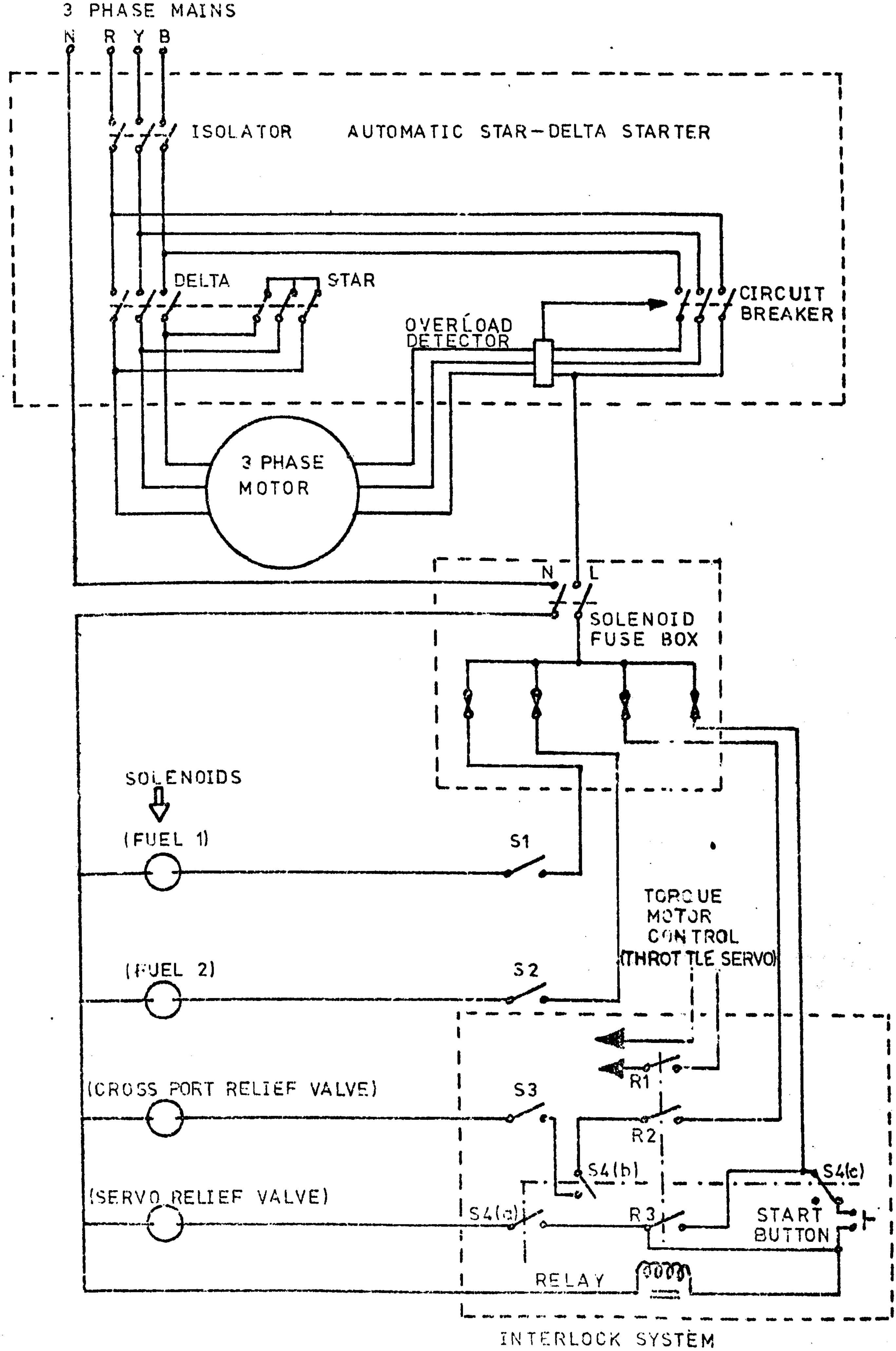

Figure 7.3 Electrical system

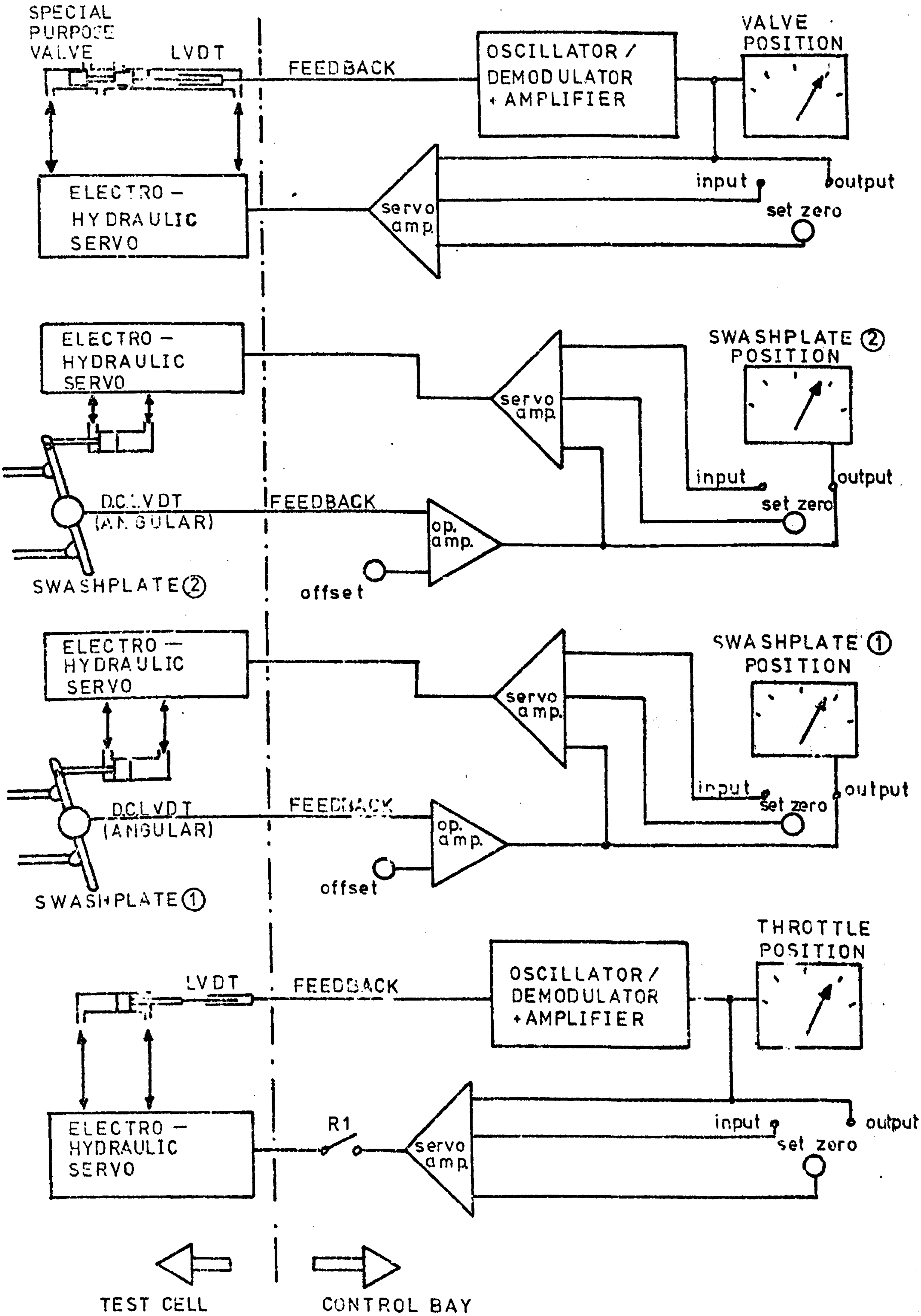

Figure 7.4 Servo control system

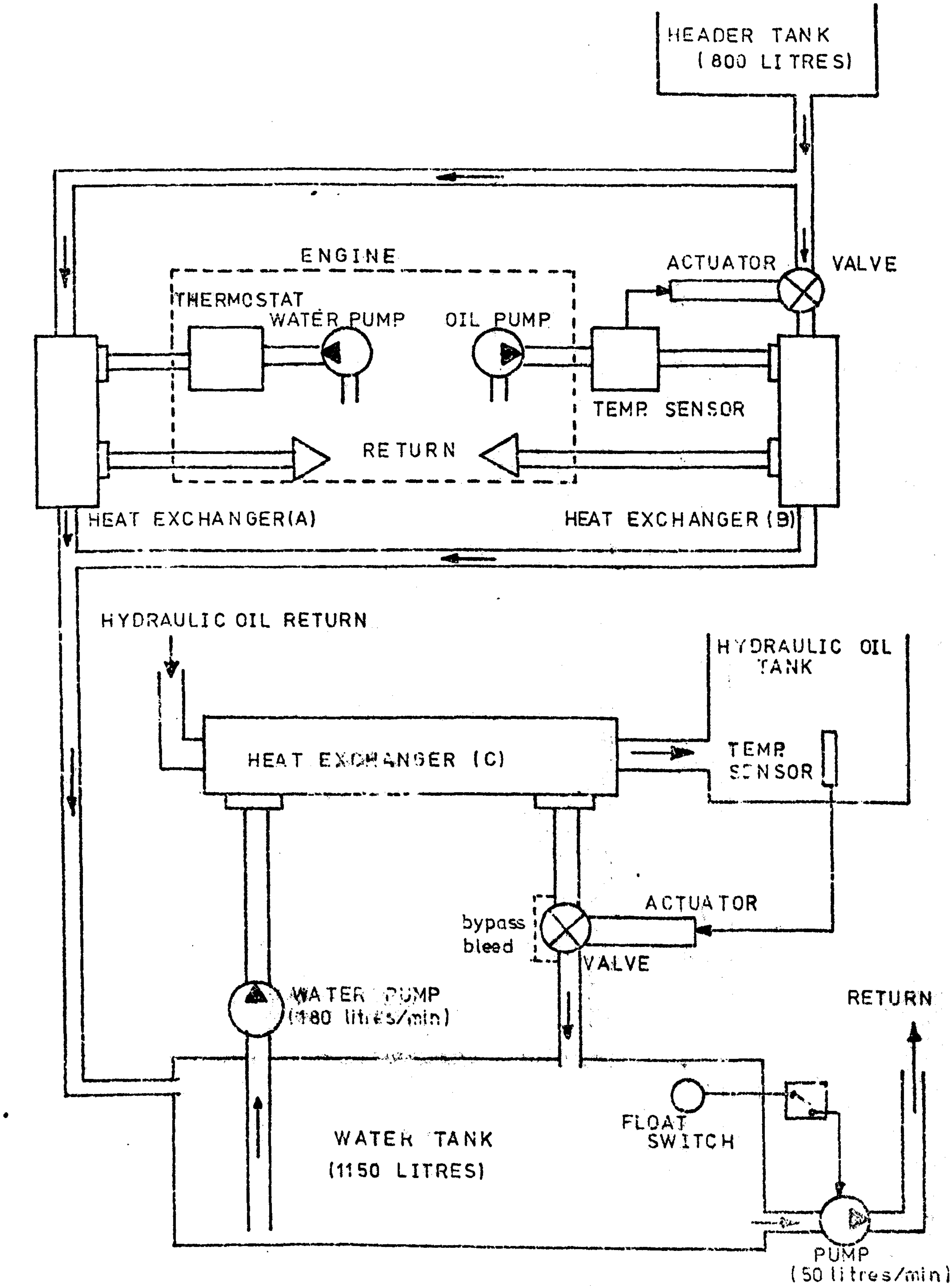

Figure 7.5 Cooling system

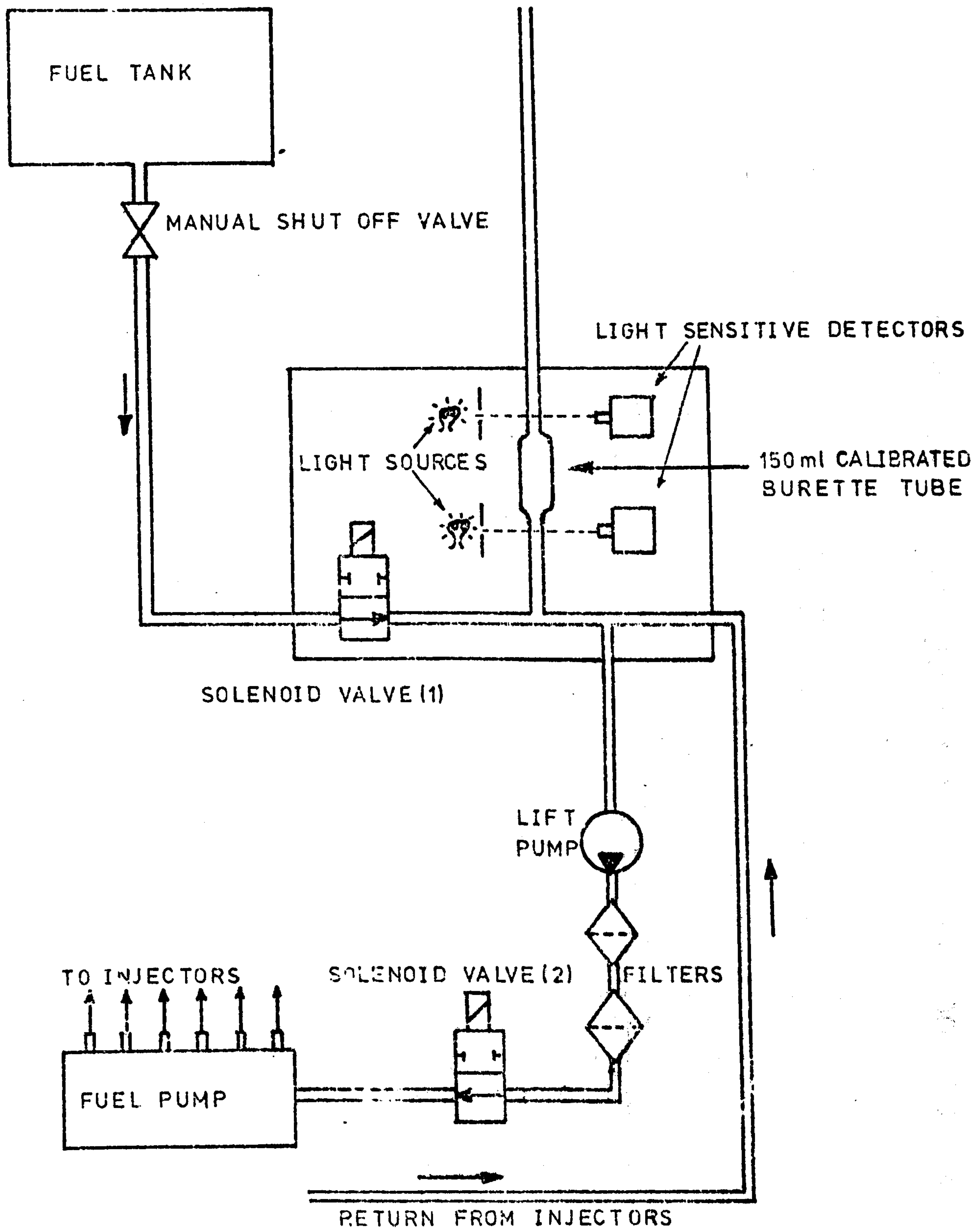

Figure 7.6 Fuel system

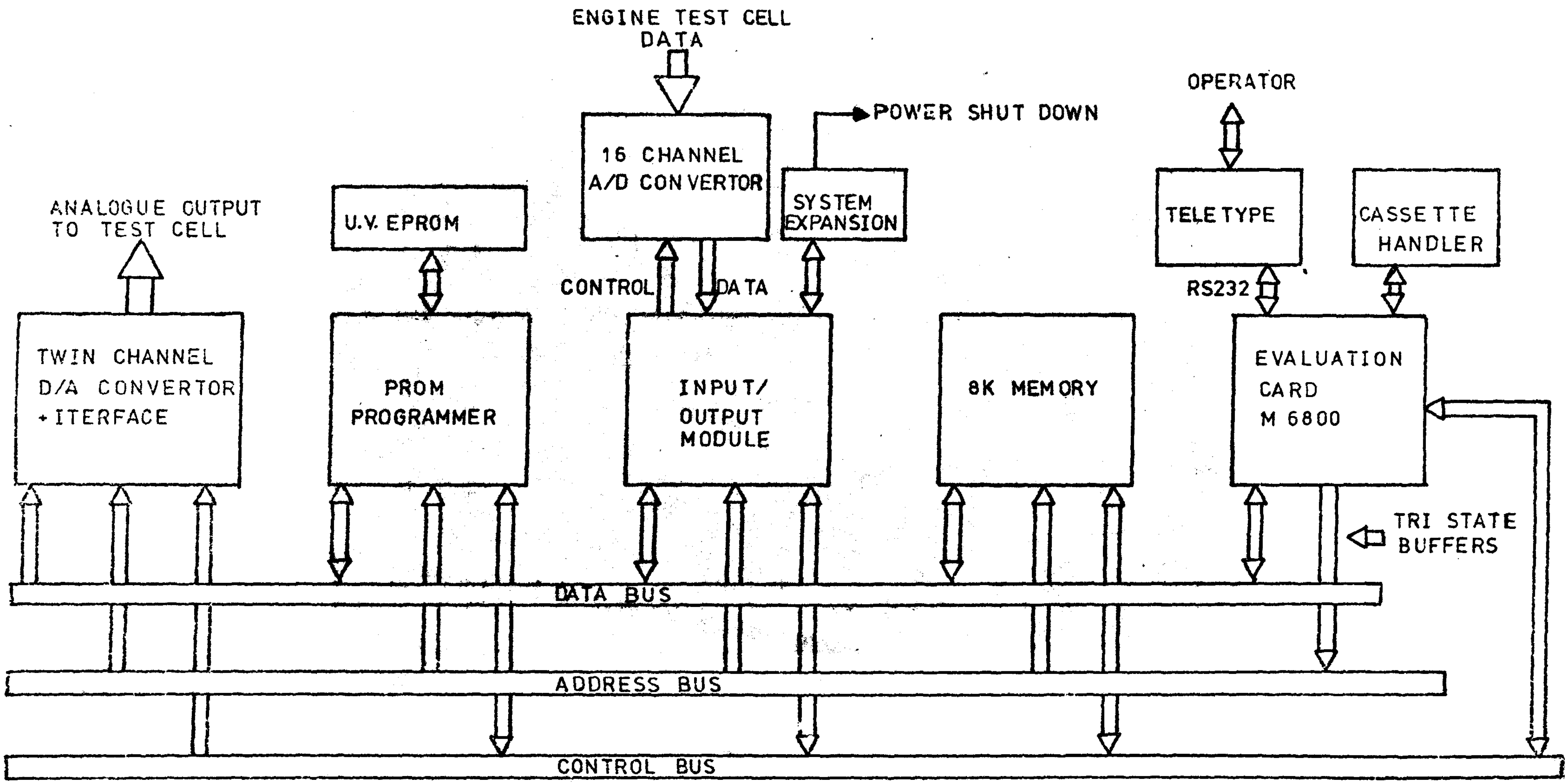

Figure 7.7 Microprocessor based monitoring system

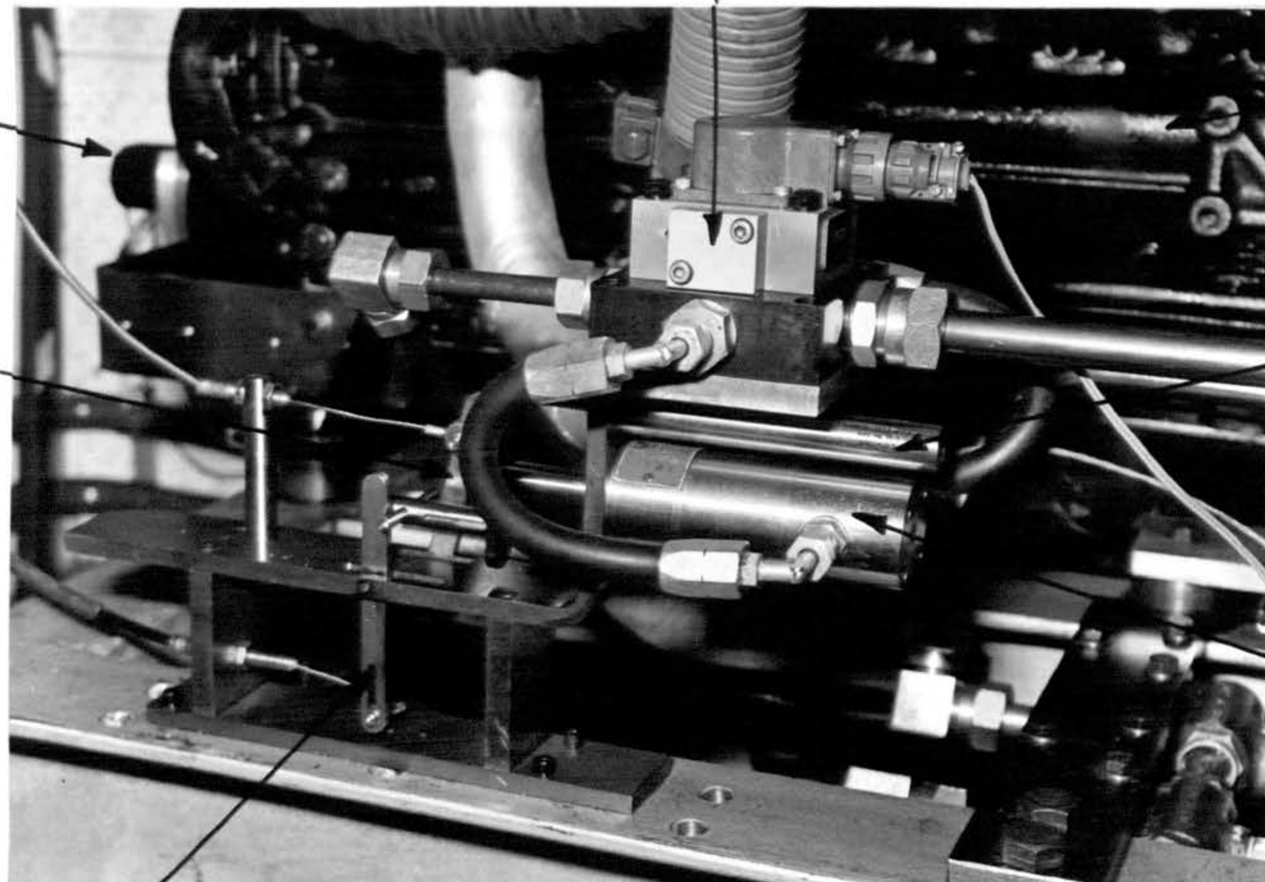

PLATE 7.1 Throttle servo

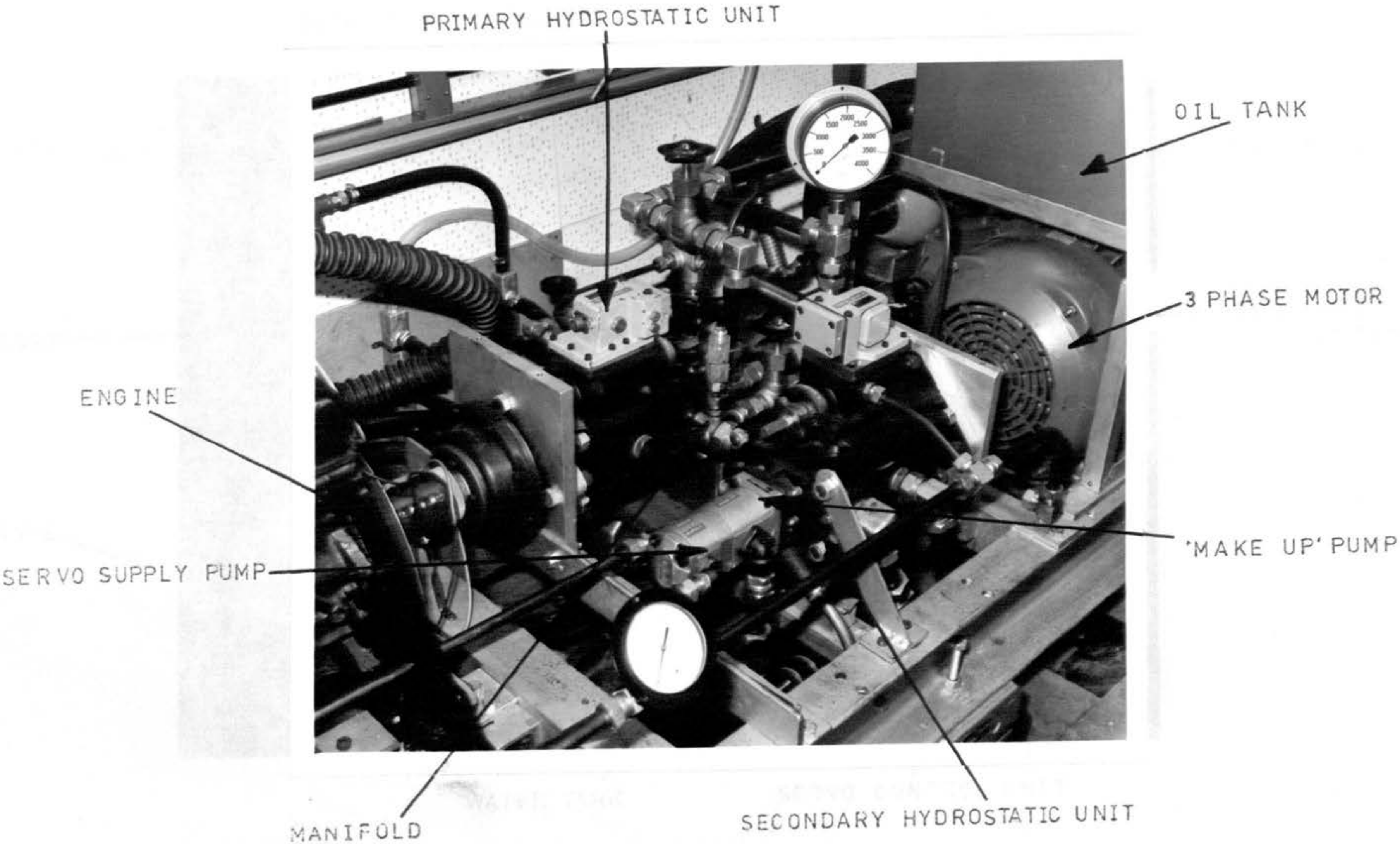

PLATE 7.2 Full power system manifold

PLATE 7.3 Control bay instrumentation

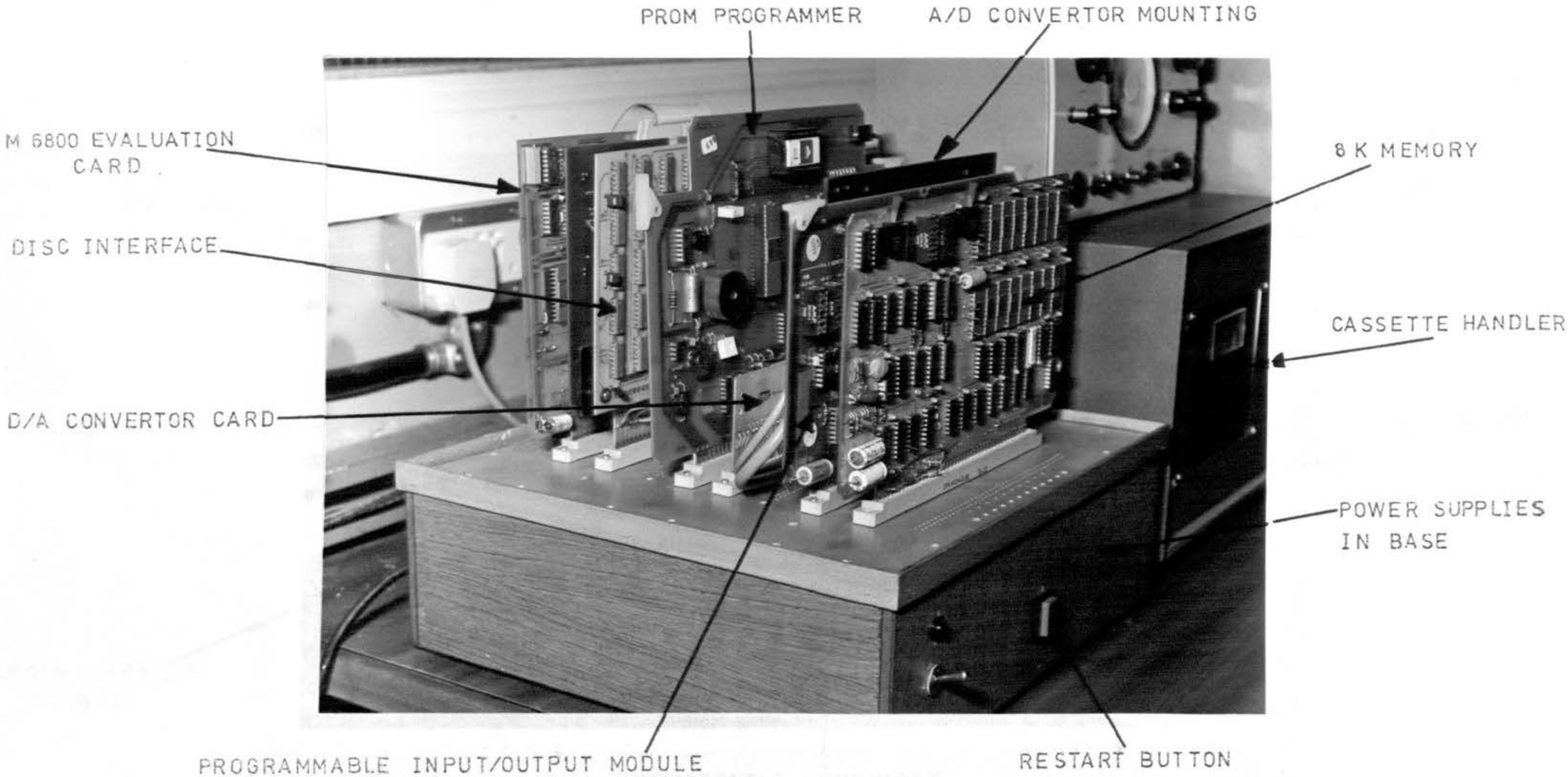

PLATE 7.4 Microprocessor system

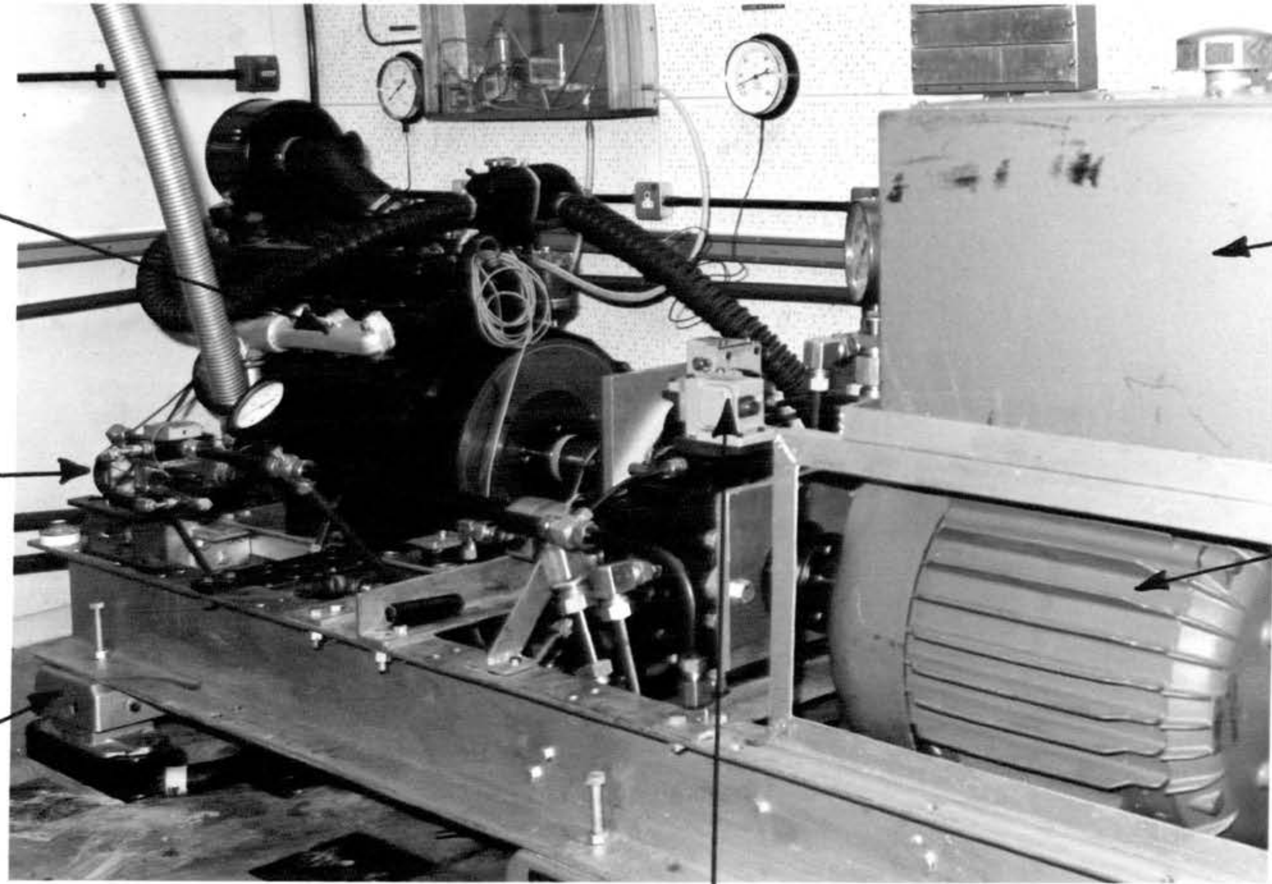

PLATE 7.5 Engine/dynamometer system

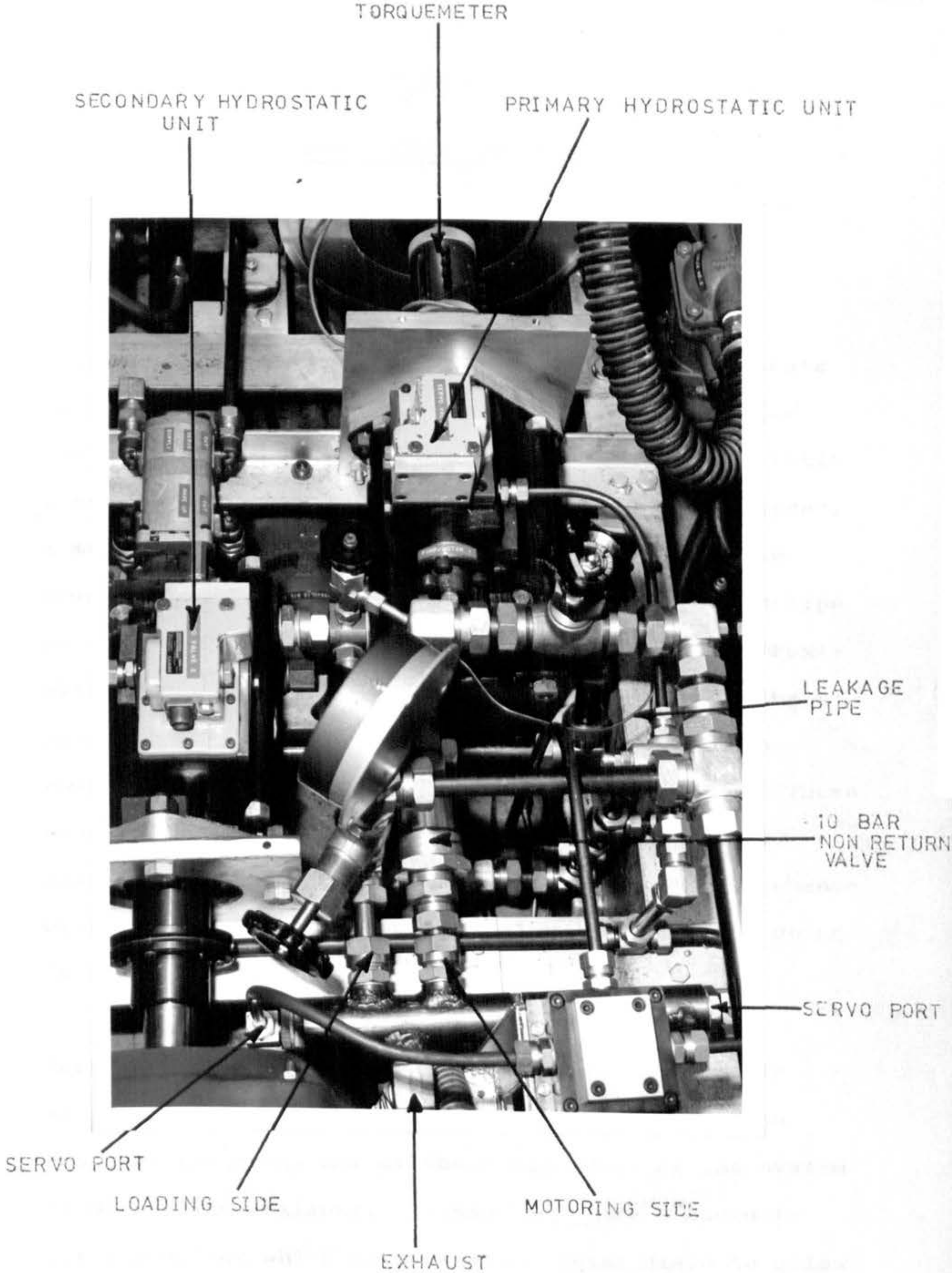

PLATE 7.6 Loading/motoring valve

PART 8

PRELIMINARY RESULTS

8.1 Experimental Determination of System Parameters

It was initially decided to perform steady state tests on the system to verify the predicted parameters for the engine as well as the fast response and hydrostatic dynamometers. On first running up the system, however, a major problem was soon encountered. The flexible coupling recommended by the manufacturers for this type of application was found to reach resonance at approximately 2000 rev/min. This becomes apparent from the analysis of Part 3, which showed that the flexible coupling roots reside at approximately $14 \pm J200$. These root positions result in a natural frequency of 200 radians per second (32 Hz) which indicate that resonance will occur at a shaft speed of 1914 rev/min, this being in close agreement with the actual result.

Further analysis showed that a fourfold increase in stiffness of the coupling was necessary to move the resonant frequency out of the speed range of the system (4000 rev/min maximum). It was therefore decided to fit a coupling which uses flexible metal discs to allow for angular mis-alignment of the engine and dynamometer shafts but which remains torsionally stiff enough to have negligible effect. To prevent over-straining of this coupling under transient conditions the rubber mounting blocks for the engine were replaced by solid connections. Having made these modifications the system could be manually controlled throughout the speed range without further problems.

Initial tests were performed to determine the steady state torque/speed characteristics of the engine under both the loading condition with the fuel control rod at maximum, and the motoring condition with the fuel control rod set to the idling position. The results of these tests are shown in graph G109, which indicates that under the loading condition the slope at low speed is much steeper for the engine than indicated by graph G2. Also, under the motoring condition, the coulomb friction resistance is much larger than that of the viscous friction even at high speed, which results in the value for the engine viscous friction predicted in Part 3 being larger than the actual value. Further tests were performed to verify the predicted coefficients for the governor rating (K8) and the engine input coefficient (K7).

By maintaining the engine speed constant and varying the engine input actuator voltage through the torque range the coefficient K7 was determined at low, medium and high speeds, as shown in graph G110(a). Also, by maintaining the engine actuator voltage constant and varying the shaft speed the governor rating K8 was determined at low, medium and high speeds, as shown in graph G110(b). It should be noted that the large torque/speed slope of the engine at low speed reduces the accuracy of this method of determining K8 (at low speed only), although the value obtained is still a reasonable approximation.

The engine coefficients determined in this way are compared to the values predicted in Part 3 as follows:-

			Experimental	Predicted
K1 (loading)	(Low speed	=	1.53 Nms	0.122 Nms
	(Medium speed	=	0.393 Nms	0
	(High speed	=	-0.297 Nms	-0.154 Nms
K1 (motoring)	(All speeds	=	-0.109 Nms	-0.265 Nms
K7	(Low speed	=	163 Nm/v	498 Nm/v
	(Medium speed	=	267 Nm/v	279 Nm/v
	(High speed	=	235 Nm/v	388 Nm/v
K8	(Low speed	=	5.62 Nms	13.2 Nms
	(Medium speed	=	4.15 Nms	7.4 Nms
	(High speed	=	6.8 Nms	10.3 Nms

The discrepancies are also fairly large for the low speed values of K7 and K8 which result from the predicted maximum engine torque at low speed being much higher than the actual value.

Steady state tests were then performed on the hydrostatic dynamometer in a similar manner. By holding the secondary hydrostatic unit swashplate constant, the dynamometer shaft speed was varied to determine low, medium and high speed values for K3, as shown in graph G111(a). Also, by holding the dynamometer shaft speed constant and varying the secondary unit swashplate control voltage, the dynamometer input coefficient (K4) was determined for each range of speed, as shown in graph G111(b). By the same means the coefficients for the fast response dynamometer were obtained as shown in graph G112. The non-linear transition effect of the special purpose valve (discussed in Part 6) can clearly be seen at medium speed in graph G112(a) and at low speed in graph G112(b). Using suitable linear approximations for these slopes the experimentally determined dynamometer coefficients are compared to the predicted values of Part 3 as follows:-

Hydrostatic Dynamometer			Experimental	Predicted
K3 (loading)	(Low speed	=	8.68 Nms	8.57 Nms
	(Medium speed	=	11.94 Nms	7.77 Nms
	(High speed	=	7.46 Nms	6.17 Nms
K4 (loading)	(Low speed	=	286 Nm/v	252 Nm/v
	(Medium speed	=	286 Nm/v	228 Nm/v
	(High speed	=	157 Nm/v	181 Nm/v

Fast Response Dynamometer			Experimental	Predicted
K3 (loading)	(Low speed	=	2.55 Nms	3.2 Nms
	(Medium speed	=	1.32 Nms	1.27 Nms
	(High speed	=	0.74 Nms	0.637 Nms
K4 (loading)	(Low speed	=	10 Nm/v	20 Nm/v
	(Medium speed	=	333 Nm/v	250 Nm/v
	(High speed	=	500 Nm/v	500 Nm/v

The agreement between these values is quite close except for the low speed value of K4 for the fast response dynamometer, which was once again based upon a much higher engine torque capability at low speed. In performing these tests it was found that the hydraulic oil temperature could be controlled within the range 50 → 55° C for the hydrostatic dynamometer system. For the fast response dynamometer system, however, in which the engine power under the loading condition is dissipated in heating the oil, the oil temperature increased up to a value of 60° C under high speed conditions. This variation in temperature was found to have a much higher effect upon the fast response dynamometer characteristics than on the hydrostatic dynamometer.

Having completed the steady state tests for the system it was decided to verify the transient characteristics where possible. No instrumentation was available to determine the transient characteristics of the injection pump and governor system, or for the oil compressibility characteristics in the hydrostatic system. However, these effects may vary considerably under normal operating conditions (especially in the case of the governor) and further work would be of benefit in this area. Other transient characteristics were investigated using step response tests for the engine and dynamometer input actuators. It was decided to use step response tests since first and second order approximations were being sought for the engine and dynamometer actuator transfer functions respectively, rather than to obtain higher order transfer functions using frequency response or pseudo random techniques.

The step changes were applied for both increasing and reducing signal levels, and the magnitudes of the applied levels were chosen to be characteristic of normal operating conditions. For the engine input actuator, the servo loop gain was adjusted to produce an approximate first order response, with time constant $T6 \simeq 0.01$ s, for step changes of up to 1 volt (which can achieve full torque changes throughout the speed range, as shown in graph G110(a)). For the fast response and hydrostatic dynamometer actuators the servo loop gains were adjusted to give the fastest possible responses consistent with adequate damping. The hydrostatic dynamometer actuator (secondary unit swashplate servo) was provided with step signal changes of up to $\pm$ 1 volt under loaded, no load and motoring conditions, which resulted in an average undamped natural frequency of 50 Hz being obtained with a damping ratio of approximately 0.7. This frequency is considerably higher (factor of 17) than that predicted using information supplied by Lucas (graph G5) due to the following reasons:-

The servo supply pressure used in the Lucas test was approximately one quarter of the pressure used in the dynamometer system.

The flow rating of the electrohydraulic valve used by Lucas is approximately half that of the one used in the dynamometer system.

The stroke used in the Lucas test was ± 80% of the maximum, whereas the stroke used in the dynamometer step response tests (suitable for achieving maximum torque changes) was approximately 6% of this value. Hence the hydrostatic dynamometer has a considerably faster speed of response than that predicted for the fast response dynamometer. In fact, the application of step control voltages up to 10 volts to the fast response dynamometer actuator (special purpose valve servo) which is necessary to achieve full torque at low speed, result in an average undamped natural frequency of 19 Hz being obtained, with a damping ratio of 0.5. The resulting parameters for the transient characteristics of the dynamometer actuators are compared to the values predicted in Part 3 as follows:-

Hydrostatic Dynamometer	Experimental	Predicted
K9	98.7	0.4
K9	0.4398	0.028
Fast Response Dynamometer		
K9	14.25	24.6
K9	0.1194	0.22

One further change in the system parameters predicted in Part 3 arises in the use of a tachogenerator to measure the engine speed. This tachogenerator has a rating of 40 volts per 1000 rev/min, which results in a coefficient of K5 = 0.382 volts per r/s. Using these new values it was possible to make comparisons between the predicted performance of the system using the analytical techniques of Part 1 and the actual performance of the system for a wide variety of conditions. For these preliminary investigations it was decided to use simulation methods 1.2 and 2.2, since the theoretical analysis of Parts 3 → 5 indicates that these methods provide superior performance compared to simulation methods 1.1 and 2.1 respectively for both dynamometer systems.

8.2 Simulation Method 1.2 Torque control on prime mover Speed control on dynamometer

8.2.1 Hydrostatic Dynamometer

The root locus method was employed to determine controller gains for the hydrostatic dynamometer using method 1.2, which resulted in oscillatory roots being created throughout the speed range. This was done in order that these roots could be observed using step response tests on the actual system. Suitable values of controller coefficients were found to be:-

Dynamometer Controller	Proportional gain, B = 0.5 v/v Integral gain, C = 1 s^{-1}
Engine Controller	Proportional gain, E = 0.3 v/v Integral gain, F = 1 s^{-1}

The root locus for the system using these controller coefficients is shown in graph G113 for the range of speed under all conditions. Under maximum fuel delivery conditions the roots are actually well damped throughout the speed range. With the fuel control rod between minimum and maximum, however, second order roots with low damping occur at all speeds. On the actual system the required controller coefficients were set up using an analogue computer and step response tests were performed at 700, 1500 and 2500 rev/min engine speed. The results of these tests for step increases in disturbance torque, applied through the dynamometer input, are shown in graph G114. At 700 rev/min the step disturbance torque causes sufficient oscillation of the engine speed (due to the roots with low damping) for the loading/motoring boundary to be crossed several times. The motoring condition has roots with even lower damping than under the loading condition, as indicated by the root locus of graph G113 for the same controller values, so that several overshoots occur.

The torque response of the actual system at 700 rev/min (graph G114) indicates that the frequency of the oscillatory response under the motoring condition is approximately half that under the loading condition. This result is in agreement with the root positions indicated by graph G113 at low speed for mid fuel delivery ($5.7 \pm j10.3$) and under the motoring condition

(1.6 ± J4.6). At higher speeds for mid fuel delivery the root locus indicates that there is an increase in both the damping and frequency of the oscillatory roots which is also shown by the actual responses of graph G114. The step change in torque at these higher speeds causes the fuel control rod to move to its maximum extent, which results in the initial response being well damped, as indicated by the root locus for maximum fuel delivery. Once the control rod moves back from its maximum position the response becomes oscillatory, as indicated by the root locus for mid fuel delivery.

The low frequency roots indicated by the root locus plots under all conditions can just be seen from the medium and high speed torque responses of graph G114, although the oscillatory nature of the response at low speed tends to hide these roots. Normally the low frequency roots of a system are the most dominant in response to a step input. However, the effect of integral action on both the dynamometer and engine controllers is to create a zero at the origin of the complex frequency plane. This zero cancels the effect of the pole at the origin (resulting from the application of a step disturbance torque) upon the poles of the system. Hence the roots closest to the origin are not necessarily the most dominant. In fact, the closer poles move towards the origin (away from the other roots), the less dominant they become under these circumstances.

The relative magnitude of the response of each pole in this case is determined by its residue (zero vectors to pole/(pole vectors). Applying this criterion to the root locus for mid fuel delivery (graph G113) shows that the oscillatory roots most dominant on the actual responses are also the most dominant on the complex frequency plane. These roots have an order of magnitude approximately twice that of the low frequency roots (shown in the increased scale for mid fuel delivery) and approximately four times that of the real root near the origin.

To further validate the theoretical results under the motoring condition the fuel control rod was held at the idling position and step response tests were performed for a range of dynamometer controller coefficients, as shown in graph G115. The transient characteristics obtained from these tests are in very close agreement with those of the root positions given by the motoring condition of graph G113 for each of the controller values. This would indicate that the mathematical model for this system is highly accurate when the fuel control rod is at either end of its stroke. With the fuel control rod in its mid position, however, the model is not so accurate but still provides a very good indication of the root movements under transient conditions. This result would be expected, since no detailed investigation has been made of the transient characteristics of the governor and injection pump for this system.

Since the hydrostatic dynamometer has been found to have a very fast speed of response (up to 100 times faster than an equivalent electrical system), it was decided to determine the effect of reducing the tacho-generator time constant upon the system performance. For the same controller coefficients the root locus method indicates that reducing the time constant to T5 = 0.1 s causes the system to become virtually unstable at low speed (ζ 0.044; ω_n 35 r/s) with a slight increase in damping at high speed (ζ 0.169; ω_n 42 r/s) under the loading condition. Under the motoring condition the roots remain oscillatory, although with an increased frequency (ζ 0.25; ω_n 14.8 r/s). The actual responses under these conditions are shown in graph G116, which show that the low damping causes the oscillatory response to be sustained with the greatest oscillations occurring at low speed (in agreement with the root locus prediction). To improve the damping of these roots a reduction in the controller gain is necessary, which has a corresponding detrimental effect upon the transient performance (speed of response). Hence the root locus method has been found to be very effective in predicting the performance of the diesel engine and hydrostatic dynamometer for simulation method 1.2. Further comparisons are made for the fast response dynamometer (using method 1.2) in the following section.

8.2.2 Fast Response Dynamometer

In common with the previous section, values of controller gains which gave oscillatory roots throughout the speed range were determined for the fast response dynamometer (using simulation method 1.2) so that comparisons could be made with the actual responses of the system:-

Dynamometer Controller	Proportional gain, B = .05 v/v Integral gain, C = 1 s^{-1}
Engine Controller	Proportional gain, E = 0.1 v/v Integral gain, F = 1 s^{-1}

The root locus for these controller gains is shown in graph G117 throughout the speed range under all conditions. The dominant roots are shown to be most oscillatory at low speed for mid and maximum fuel delivery under the loading condition, and at high speed under the motoring condition. This is in agreement with the actual responses shown in graphs G118 (loading) and G119 (motoring). Under the loading condition the actual response has slightly higher damping at high speed and lower at low speed than indicated by the root locus (for mid fuel delivery), although the agreement shown by the movement of the dominant roots is quite reasonable.

Under the motoring condition the change in damping of the dominant roots throughout the speed range is in close agreement with the actual system damping shown in graph G119. The undamped natural frequencies indicated by the actual responses, however, (obtained from $\omega_n = \omega_d(1 - \zeta^2)^{-0.5}$, where ω_d = actual measured frequency) are much higher than indicated by the root locus plot. This is probably due to errors in the estimation of the dynamometer characteristics under the motoring condition which have not been verified due to the difficulty of changing the load torque (under the motoring condition) at constant speed. In fact, variations in the dynamometer parameters K3 and K4 were found to create large changes in the frequency of the dominant roots using the root locus method for the motoring condition.

Hence the highly non-linear characteristics of the fast response dynamometer which are influenced greatly by temperature changes result in the analysis for this system being less accurate than for the hydrostatic dynamometer system. The root locus method has, however, been successful in showing how the basic system characteristics vary throughout the speed range of the system. Further comparisons for the two dynamometers using simulation method 2.2 are made in the following sections.

8.3 Simulation Method 2.2 Speed Reference System

8.3.1 Hydrostatic Dynamometer

For the hydrostatic dynamometer using method 2.2 it was decided to simulate the low speed loading conditions of a Ford A series truck in fourth gear, in order that comparisons could be made between the theoretical responses indicated by the analytical techniques and the actual responses of the system. Using the root locus technique the following controller values were found to give suitable performance under all conditions:-

Dynamometer Controller	(	Proportional gain, B = 1 v/v
	(	Integral gain, C = 2 s^{-1}
Engine Controller	(	Proportional gain, E = 0.5 v/v
	(	Integral gain, F = 0.2 s^{-1}

At low speed in fourth gear the root positions for all loading conditions are given in the computer printout of Appendix B(i). The step responses of the actual system using these controller coefficients are shown in graphs G120 (loading), G121 (motoring) and G122 (no control over engine input). Under the loading condition for mid fuel delivery the computer printout indicates two pairs of oscillatory roots having a large effect upon the system response (ω_n 1.22 r/s; ζ 0.56 and ω_n 15.4 r/s; ζ 0.57). Both of these roots may be observed in the actual step response of the system under this condition in graph G120.

The somewhat erratic response of the system to a step torque increase resulting from a step change in the dynamometer input signal is probably due to stiction in the fuel control rod and governing system of the engine. The sudden increase in load torque on the engine causes the speed to fall at a steady rate, although the governor does not create an increase in fuel delivery (thereby increasing the engine torque to correct the fall in speed) until over a second later. This effect is also due, in part, to the low value of integral action on the engine controller necessary to maintain stability throughout the speed range.

Under the motoring condition the fuel control rod is at its minimum setting, which eliminates the effect of the integral action upon the engine controller. This causes a pole to appear at the origin which cancels the effect of the zero at the origin (discussed in section 8.2.1). Hence under this condition the roots nearest the origin have the greatest effect upon the system response. The computer printout (Appendix B(i)) indicates that under the motoring condition there is a very slow first order dominant response ($\tau = 92.8$ s) with oscillatory secondary roots (ζ 0.254; ω_n 6.82 r/s). This gives quite a reasonable agreement with the actual response under this condition shown in graph G121.

The performance of the system without feedback control on the engine input is of importance to enable comparisons to be made with the performance of the real vehicle. Since the integral action on the engine controller is eliminated, then the roots closest to the origin also have the greatest effect upon the system response (as under the motoring condition). The computer printout for this condition shows the dominant response to be first order ($\tau = 6.5$ s) with oscillatory secondary roots (ζ 0.55; ω_n 15.7 r/s). Secondary roots closer to the origin than this are also shown, although zeros reside in close proximity and make their effect small. The actual step response under this condition for a step increase and a step reduction of the engine input are shown in graph G122.

Even for such relatively small changes in the engine input (resulting in a speed change of approximately 200 rev/min) the fuel control rod moves to a maximum for a step increase and a minimum for a step reduction in the engine input. The oscillatory secondary roots obtained as the motoring condition is entered show fair agreement with those given by the computer printout for the motoring condition. With the control rod at maximum the speed response is fairly linear, indicating that a ramp change (rather than exponential) is taking place. This is in agreement with the computer printout for maximum fuel delivery, which shows that the dominant root is first order and very close to the origin (even though on the unstable side of the complex frequency plane). Once the control rod moves back from its maximum position (as indicated by the torque response) the speed curve follows an exponential decay. Due to the saturation effect upon the control rod movement the actual time constants measured for these two responses were found to reside just either side of that indicated by the computer printout.

Hence the analytical model developed in Part 1 has (once again) been found to provide a good indication of the performance of the hydrostatic dynamometer system using simulation method 2.2. The effects of using the fast response dynamometer for simulation method 2.2 on the diesel engine are examined in the following section.

8.3.2 Fast Response Dynamometer

As with the hydrostatic dynamometer the loading coefficients of a Ford A series truck in fourth gear were chosen for simulation purposes, although, in this case, the mid speed (1500 rev/min) was used. Suitable controller coefficients for the system under these conditions were determined by the root locus method as follows:-

Dynamometer	(	Proportional gain, B = 0.1 v/v
	(	
Controller	(	Integral gain, C = 0.3 s^{-1}
Engine	(	Proportional gain, E = 0.05 v/v
	(	
Controller	(	Integral gain, F = 0.02 s^{-1}

The root positions for the system using these controller coefficients are given for all loading conditions in the computer printout of Appendix B(ii). The actual step responses of the system under these conditions are shown in graph G123. Under the motoring condition the computer printout indicates a dominant first order response (τ = 52.6 s) with secondary roots (ζ 0.58; ω_n 3.5 r/s). The actual response of the system to a step reduction in the engine input setting (throttle) is to cause the motoring condition to be entered and a gradual fall in speed takes place. When the speed reaches a certain level the governor increases the fuel control rod setting, thereby returning to the loading condition. An estimate of the time constant obtained whilst under the motoring condition from the actual response is in the order of 50 → 60 seconds (in agreement with the computer printout). The secondary roots indicated on the computer printout can also just be seen on the actual response.

Under the loading condition for mid fuel delivery the dominant response indicated by the computer analysis is first order with time constant = 0.606 s (the roots near the origin have negligible dynamic effect, as discussed in section 8.2.1). The actual response under this condition for both a step increase and reduction in the dynamometer input signal causes sufficient change in the fuel control rod for the loading and motoring conditions to be entered initially. However, interpolating the response under these conditions leads to an estimate of the time constant = 0.4 → 0.6 seconds.

With no feedback control on the engine input the computer printout indicates a dominant first order response with time constant = 6.2 s. The actual response under this condition for a step increase in the engine input setting (shown in graph G123) is also first order with a time constant = 6.4 s showing good agreement with the analytical result. The high frequency secondary roots indicated on the computer output (ζ .85; ω_n 30.5 r/s) can also just be observed on the actual response. Hence the analytical techniques developed in Part 1 have been successful in indicating the dynamic characteristics of the diesel engine and the two dynamometer systems under a wide variety of loading conditions for both of the basic load simulation methods.

8.4 Discussion

Preliminary testing of the two dynamometer systems in the engine test cell has shown that the hydrostatic dynamometer has a very fast speed of response (in comparison to the specially developed fast response dynamometer) and also has certain other advantages. In particular the torque/speed characteristics of the hydrostatic dynamometer are linear over the major part of the working range, as shown in graph G111(a). Furthermore, a high degree of discrimination is obtained throughout the speed range, as shown in graph G111(b). For the fast response dynamometer (based upon the operation of the special purpose loading/ motoring valve) it was shown in Part 6 that linearity and discrimination are mutually exclusive throughout the speed range of a prime mover (see Fig. 6.12). However, it was suggested that both the linearity and discrimination of the fast response dynamometer could be improved if a variable pitch thread is used in the special purpose valve (rather than the constant pitch thread of the valve used in this investigation).

Another possible advantage of the hydrostatic dynamometer is that only a small proportion of the engine power goes into heating the hydraulic oil. This means that localised temperature changes are not excessive, so that the performance of the hydrostatic dynamometer remains fairly constant at normal working temperatures. For the fast response dynamometer, however, in which virtually all the engine power is dissipated in heating the oil, large changes in temperature of the valve body can occur under normal working conditions which can create large changes in the dynamometer characteristics.

For testing of engine and transmission systems (i.e., on a chassis dynamometer) or for testing of electric prime mover systems on battery powered vehicles, it is necessary for the dynamometer to be capable of applying high torque values at low speed (including standstill).

Although hydrostatic systems can perform this function, there may possibly be control problems resulting from the stick-slip operation of hydrostatic units at very low speeds (although no difficulties were encountered with the low power system investigated in Part 2). It was shown in Part 6 that for the fast response dynamometer to perform this function some means must be employed for making up the leakage flow from the pressurised side of the system at low speed. In general, for electric prime movers, very high torque levels may be obtained at low speed, which may lead to some incompatibility of the power rating necessary for a hydrostatic system to achieve such levels (since hydrostatic units have an approximately constant maximum torque throughout the speed range).

Although the hydrostatic dynamometer was found to have an undamped natural frequency of approximately 50 Hz, the lag involved in compressing the oil in the hydrostatic loop makes the overall response much slower than this (a factor of five approximately). It was shown in Part 2 that this lag is proportional to the volume of oil in the hydrostatic loop and inversely proportional to the effective bulk modulus and leakage rate from the hydrostatic loop. Due to physical limitations there is a minimum to which the oil volume can be reduced and the effective bulk modulus can be assumed constant. Hence to obtain the fastest time constant the leakage rate from the hydrostatic system must be increased. The maximum allowable leakage rate is governed by the required maximum torque (and hence maximum pressure) at the required maximum speed of the system. The values used for the hydrostatic system incorporated in the engine test cell resulted in a time constant within the range 0.01 → 0.015 s under all conditions, which is approximately a factor of fifteen times faster than an equivalent electrical system (with a time constant of, say, 0.2 s). This speed of response could easily be increased by a factor of three on the present system (by increasing the leakage rate) without affecting the maximum torque requirement.

For the fast response dynamometer it was shown in section 3.3.1 that the lag involved in compressing the oil on either side of the hydrostatic unit has a non-linear time constant which increases in proportion to the oil pressure. Although the time constant can be reduced on the motoring side of the system by reducing the oil volume on this side, it is unlikely that the time constant on the loading side can be reduced by more than a factor of two. The speed of response of the servo system for the spool of the special purpose valve could, however, be significantly increased by suitable valve sizing, although the overall speed of response would be of the same order as for the hydrostatic dynamometer.

Experimental investigations of the hydrostatic dynamometer and diesel engine system showed that a reduction in the lag on the tachogenerator signal required a reduction in the speed control system gain to maintain stability. This reduction in gain also reduces the effect of the tachogenerator ripple upon the swashplate control mechanism, so that the hydrostatic dynamometer can be used in the "fast response" mode if required. However, it was shown in Part 3.3 that a fast response system had difficulty in damping the inherent oscillatory characteristics of the governed diesel engine at low speed. In fact, the high gain governor has an over-riding influence on the transient characteristics of the dynamometer controlled diesel engine system due to its highly non-linear characteristics (i.e., variable spring rate, stiction effects, etc.) as well as to create saturation conditions (i.e., fuel control rod at maximum or minimum) for small changes in speed levels.

To provide a more effective mathematical description of the governing system (for inclusion in the generalised model for prime mover/dynamometer systems developed in Part 1) it is suggested that a second order transfer function may be used which can incorporate gain and phase changes throughout the speed range of the engine, as well as for small changes in signal levels (for which stiction effects become important). Further work in the development of the generalised model will be to use a state space description for each of the basic systems analysed in Parts 3 → 5 to determine whether recently developed modern control theory techniques (Ref. 84) can provide improvements in system performance.

It has been found that the use of the root locus method in conjunction with the generalised model for prime mover/dynamometer systems has given considerable insight into the way in which the system characteristics vary throughout the speed range. Since the majority of the system non-linearities were found to vary with speed, then a root locus varying with speed provides an obvious method of describing the system characteristics under normal working conditions. Also, since other non-linearities vary with changes in torque or signal amplitude then these effects can be superimposed upon the root locus plot, although the analysis applied in Parts 3 → 5 showed that full changes in torque had little effect upon the root positions.

Another advantage of the root locus method is that various parts of the system may be identified with certain root positions (i.e., the roots due to the flexible coupling, or the servo system actuators, etc.). It is therefore possible to determine how these parts of the system are affected by changes in the engine speed, or by any other parameter of the system such as controller gain, torque level, etc. Such techniques are of great benefit in developing improvements in system performance.

It has been shown that the system performance can be judged from an examination of the root positions on the complex frequency plane which have the most significant effect upon the system response to an input stimulus. In particular, it has been shown that the type of stimulus determines which roots are most dominant. With integral control over both the engine and dynamometer servo systems it was found that a zero resides at the origin of the complex frequency plane. This has the effect of eliminating the steady state response to a step disturbance torque and the system roots respond as if to an impulse input (i.e., the magnitude of the response of each root is determined by the proximity of surrounding poles and zeros). Hence, in such cases, the proximity of the roots to the origin does not affect their relative importance in the overall transient response.

If, however, a step change is made in the required torque level of the system, then the effect of the integral control action is to initially convert this signal to a ramp (velocity) disturbance, plus a step disturbance through the proportional controller. The effect of a ramp disturbance is to create an extra pole at the origin, so that, in this case, the dominant roots are determined both from their proximity to surrounding poles and zeros, as well as to the origin (depending upon the relative magnitudes of the proportional and integral action gains). For a ramp change in either the required torque or speed levels the dominant roots are those closest to the origin (this type of input being most often obtained under normal simulated running conditions, i.e., torque/speed curve following). For the governed diesel engine under maximum fuel delivery or motoring conditions the roots nearest the origin give the most dominant response for all changes in the required torque/speed levels under all conditions.

In Part 2 it was found that for basic simulation method (2) (in which the simulated vehicle characteristics are in a feedback path of the system) the torque/speed slope of the dynamometer could create large errors in the simulated characteristics if stability considerations required the integral action of the dynamometer controller to be kept small. To overcome this problem a torque/speed slope elimination signal was introduced which effectively negated the feedback effect of the dynamometer torque/speed characteristics. For the fast response dynamometer (using the special purpose loading/motoring valve) the characteristics have been found to be highly non-linear and vary with temperature. Above low speed, however, the required elimination signal becomes very small (due to the high gain of the loading valve), so that errors in the simulated characteristics are likely to occur only at low speed for this dynamometer.

For the electric dynamometer (separately excited, thyristor controlled, d.c. type) it was found possible to use a high enough integral action gain to make the use of the dynamometer torque/speed elimination signal unnecessary. In general, it was found possible to use higher proportional and integral action gains for the electric dynamometer controller than for the hydrostatic and fast response dynamometer controllers due to the use of derivative action. The winding lag of the electric dynamometer enables high values of derivative action to be used without transmitting high frequency disturbances to the mechanical part of the system (resulting from "noise" amplification of the derivative controller). For the hydrostatic and fast response dynamometers, however, the high speed of response of the electrohydraulic actuators enables the high frequency disturbances to be transmitted directly to the hydro-mechanical system. This is why the analysis for the electrical dynamometer systems in Parts 3 → 5 indicates just as high a standard of performance may be obtained as for the hydraulic dynamometers.

In fact, for simulation method (2) (with the simulated characteristics in a feedback path of the system) the high inertia of the electric dynamometer tends to be more of an advantage than the low inertia of the hydraulic dynamometers, since it lies much closer to the required range of inertia to be simulated. For basic simulation method (1), however, (with the simulated characteristics in a forward path of the system) the high inertia of the electric dynamometer is more of a disadvantage, since the dominant response roots become somewhat slower than those for the hydraulic dynamometers.

In general, the theoretical analysis has shown that simulation method 2.2 (speed reference system) has superior dynamic performance compared to method 2.1 (torque reference system), for which the low pass filter, necessary to eliminate high frequency oscillations, creates errors in the simulated vehicle characteristics. The theoretical analysis has also shown that simulation method 1.2 (speed control by dynamometer, torque control by prime mover) results in superior performance compared to method 1.1 (torque control by dynamometer, speed control by prime mover), for which the dominant response roots are somewhat slower (further from origin) and for which unstable operation may occur when positive torque/speed slopes for the prime mover are encountered. Further experimental analysis is necessary to verify these theoretical findings.

APPENDIX A

GRAPHS G1 $\longrightarrow$ G 123

GRAPH G1

Ford petrol engine model 2614e

(naturally aspirated carburettor)

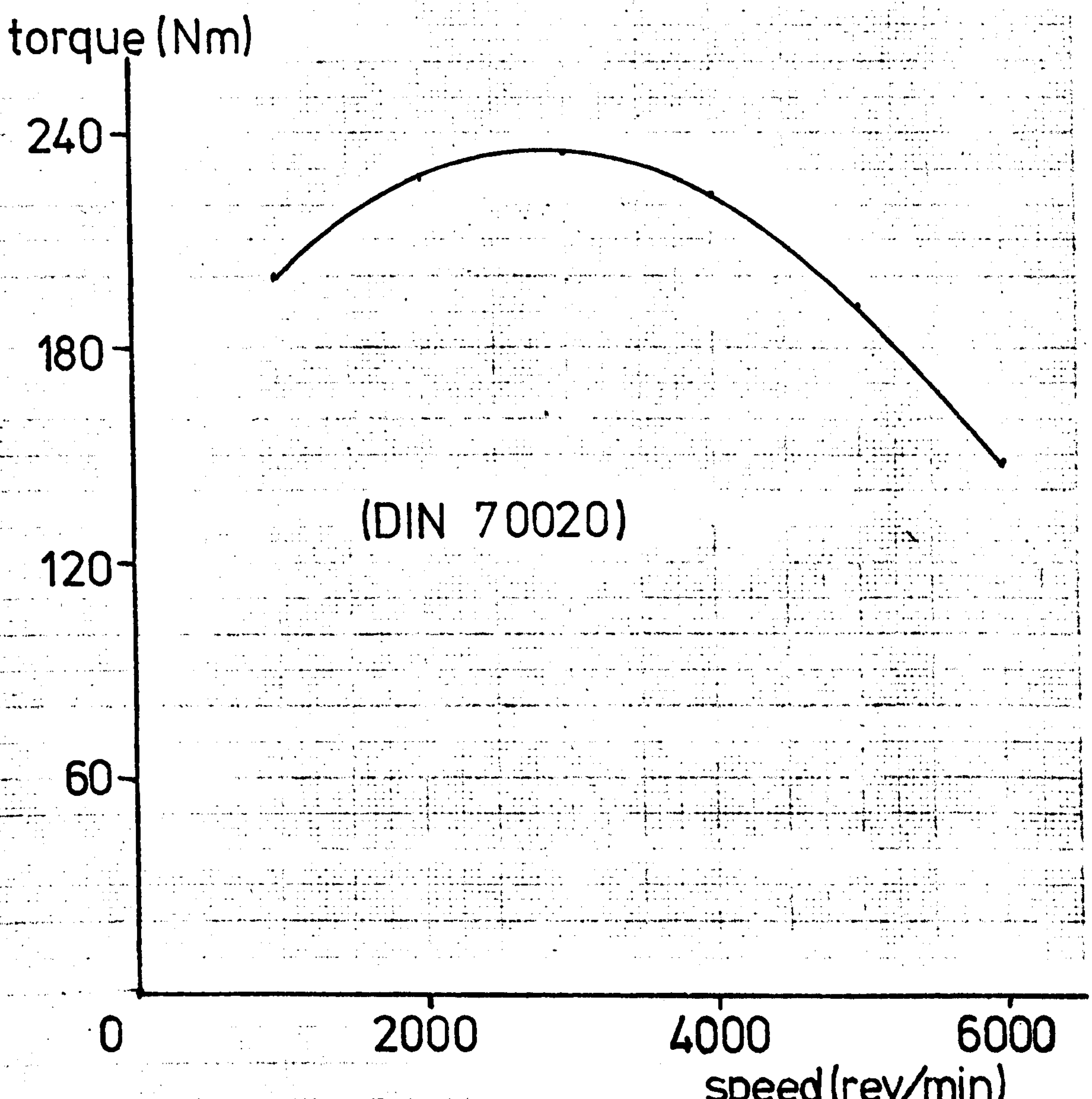

6 cylinder V engine (2994cc)

101·5 kw @ 5000 rev/min

GRAPH G2

Ford diesel engine model 2402e
(high speed minimec governor)

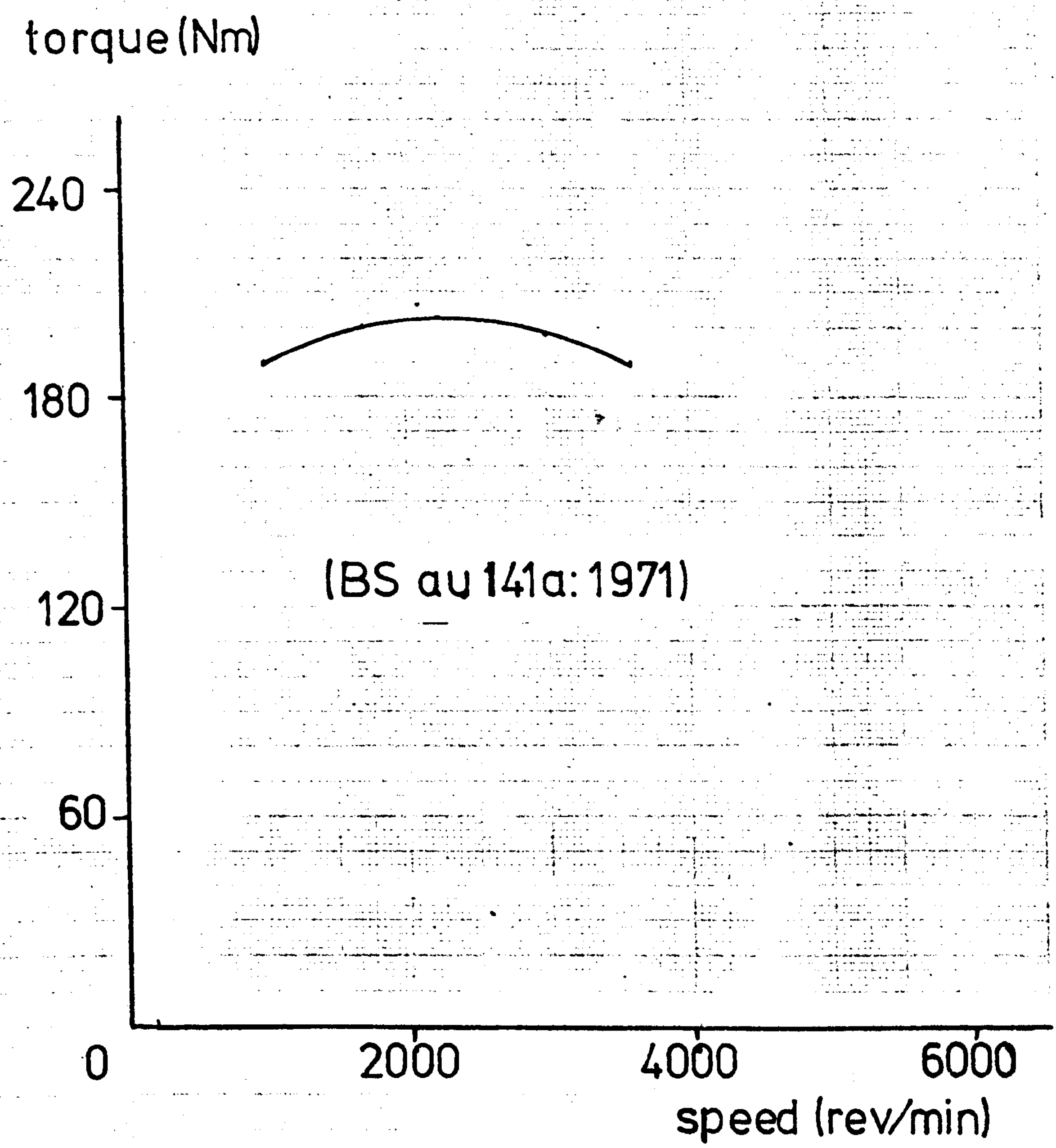

6 cylinder in line (3539 cc)
71·6 kw @ 3600 rev/min

CHLORIDE Ltd. "Silent Karrier"
prime mover characteristics

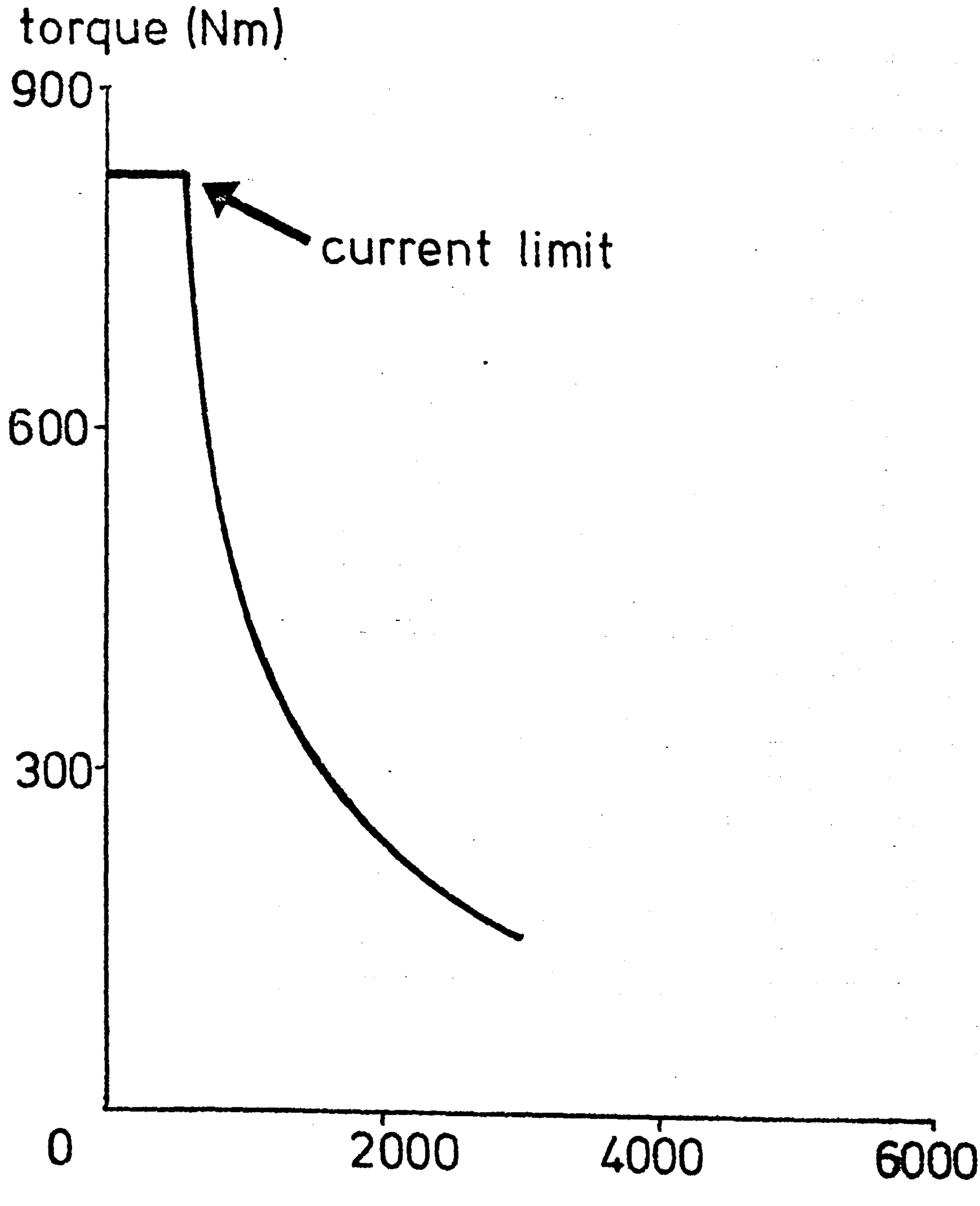

separately excited d.c. traction motor

power limited to 48·5 KW

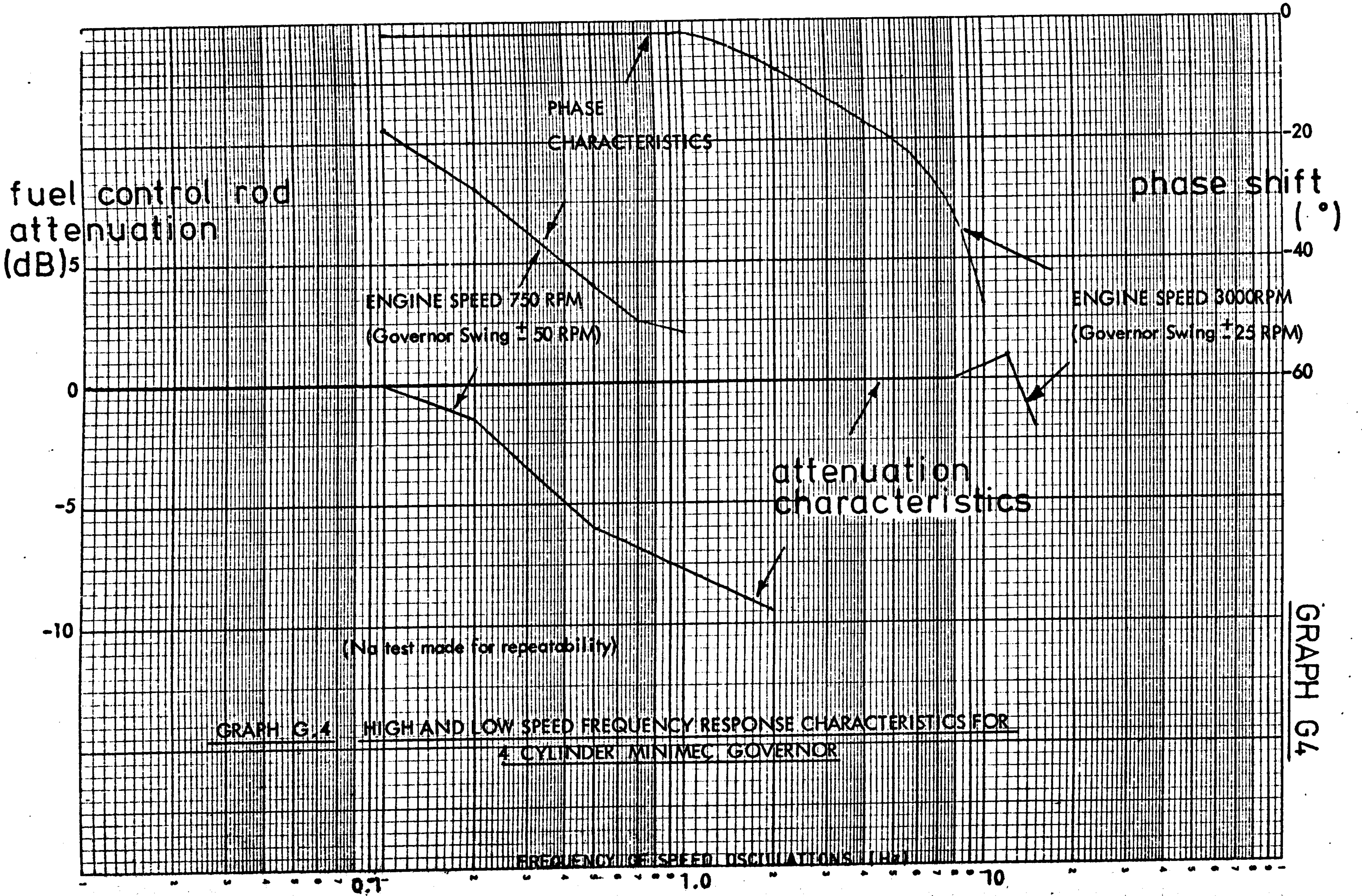

GRAPH G.4 HIGH AND LOW SPEED FREQUENCY RESPONSE CHARACTERISTICS FOR 4 CYLINDER MINIMEC GOVERNOR

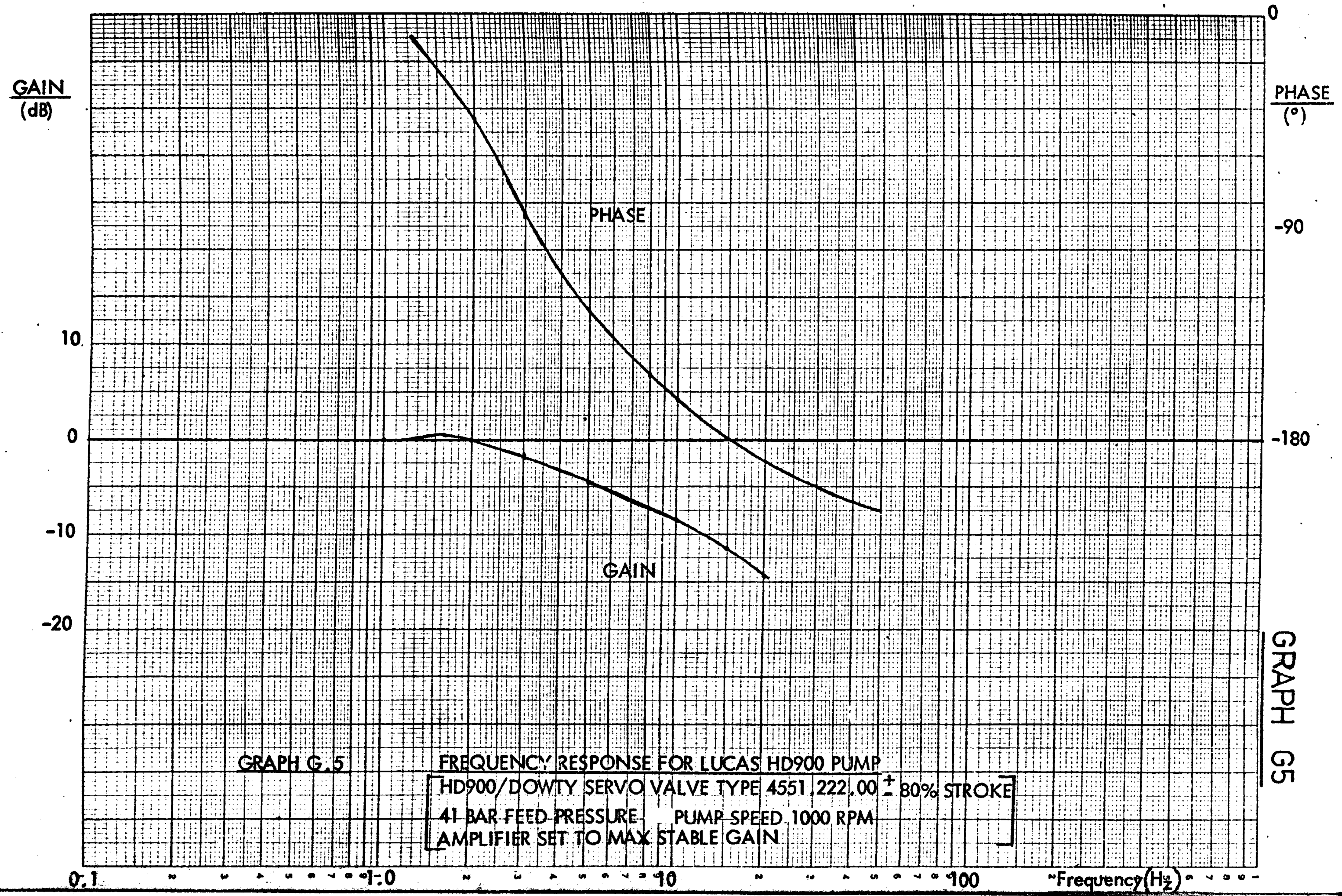

GRAPH G.5 FREQUENCY RESPONSE FOR LUCAS HD900 PUMP
HD900/DOWTY SERVO VALVE TYPE 4551.222.00 ± 80% STROKE
41 BAR FEED PRESSURE PUMP SPEED 1000 RPM
AMPLIFIER SET TO MAX STABLE GAIN

determination of k1

(a) zero prime mover input
(b) medium input
(c) high input

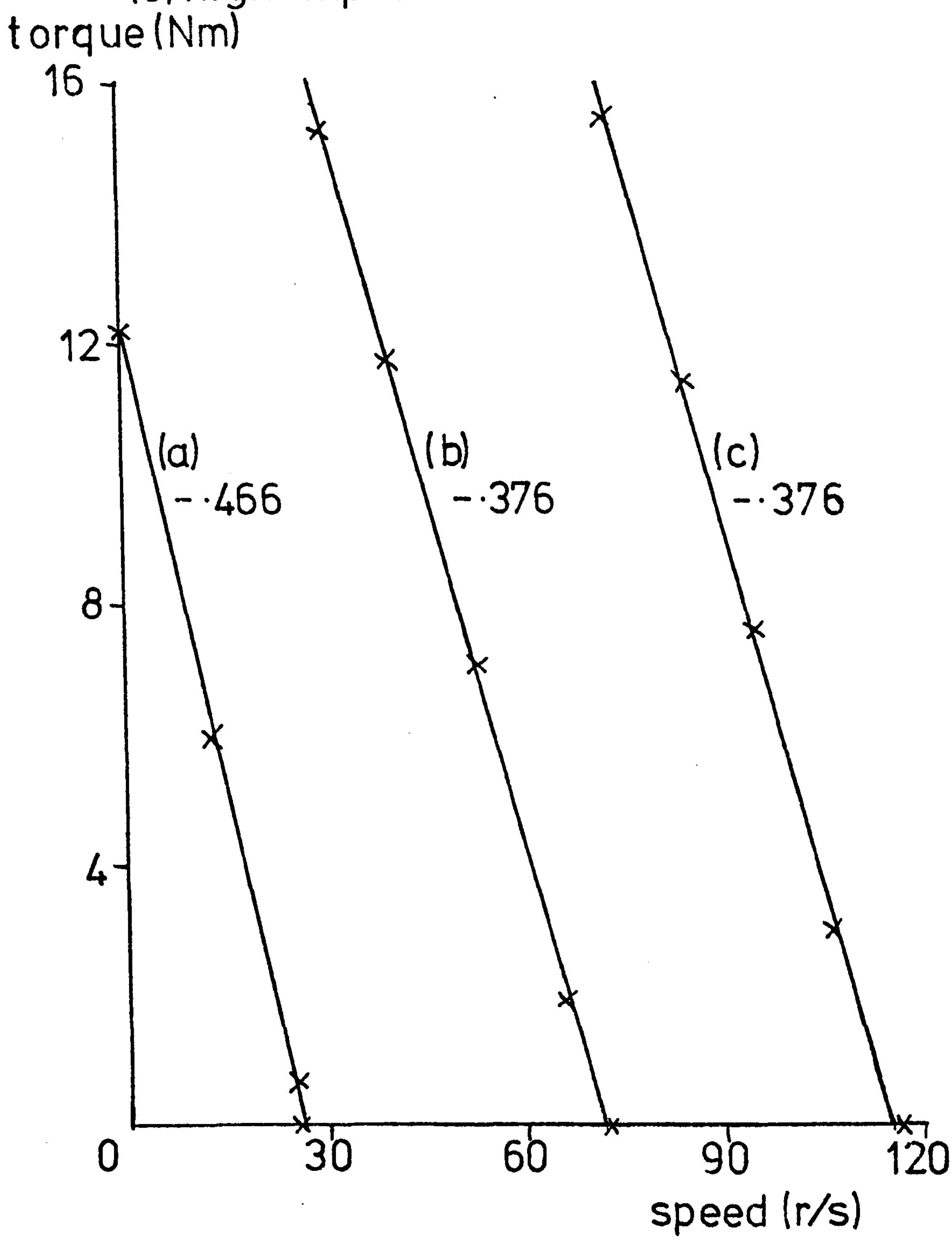

∴ let k1 = -·376 Nms

GRAPH G7

determination of k3

swashplate control held constant:-

range (a) 0 volts (low speed)

range (b) 1 volt (medium speed)

range (c) 2 volts (high speed)

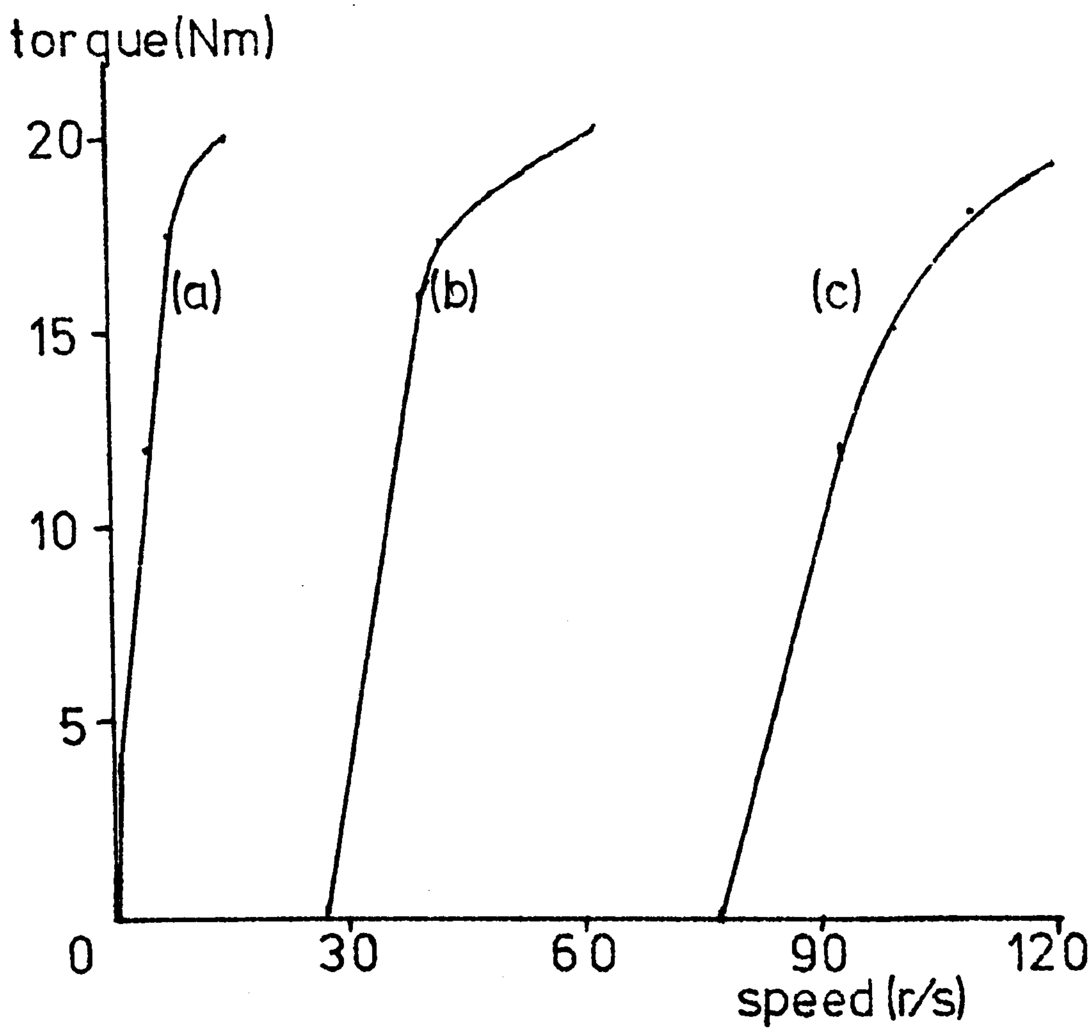

(a) k3 ≏ 2·0 Nms

(b) k3 ≏ 1·267 Nms

(c) k3 ≏ 0·75 Nms

GRAPH G8

determination of k4

prime mover speed:-

(a) 20 r/s

(b) 50 r/s

(c) 100 r/s

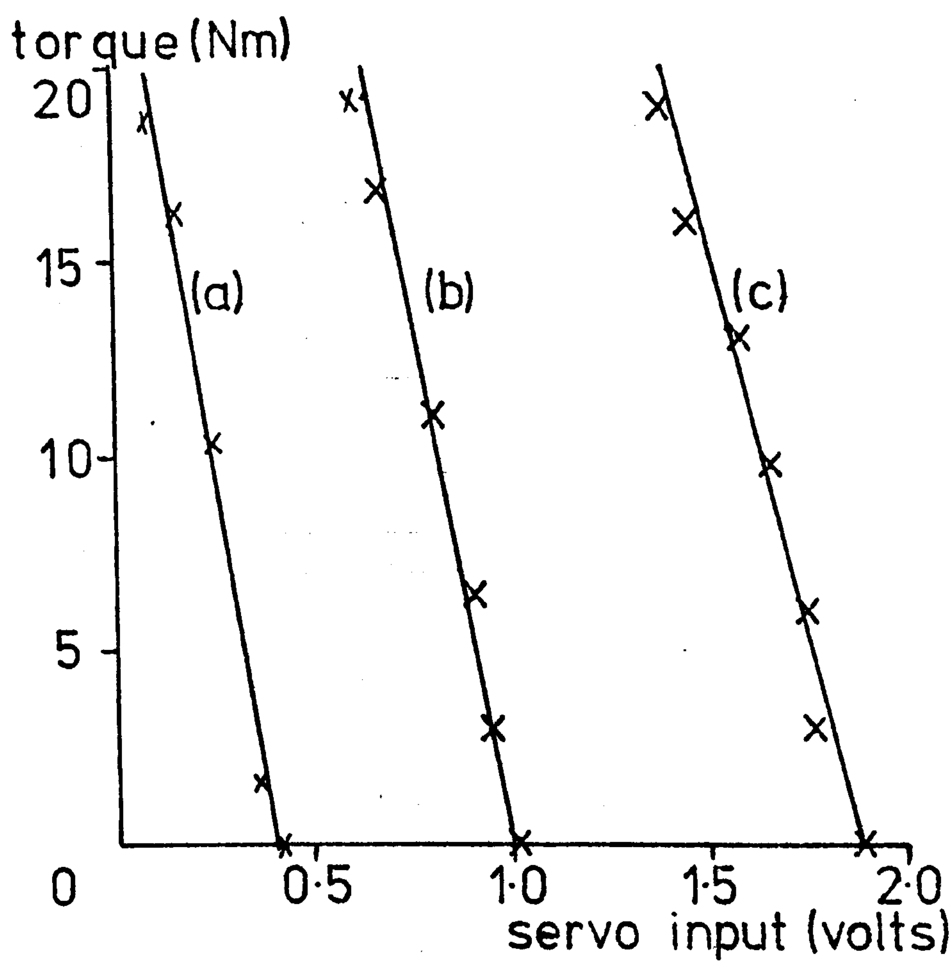

(a) k4 = 64 Nm/v

(b) k4 = 55·7 Nm/v

(c) k4 = 41 Nm/v

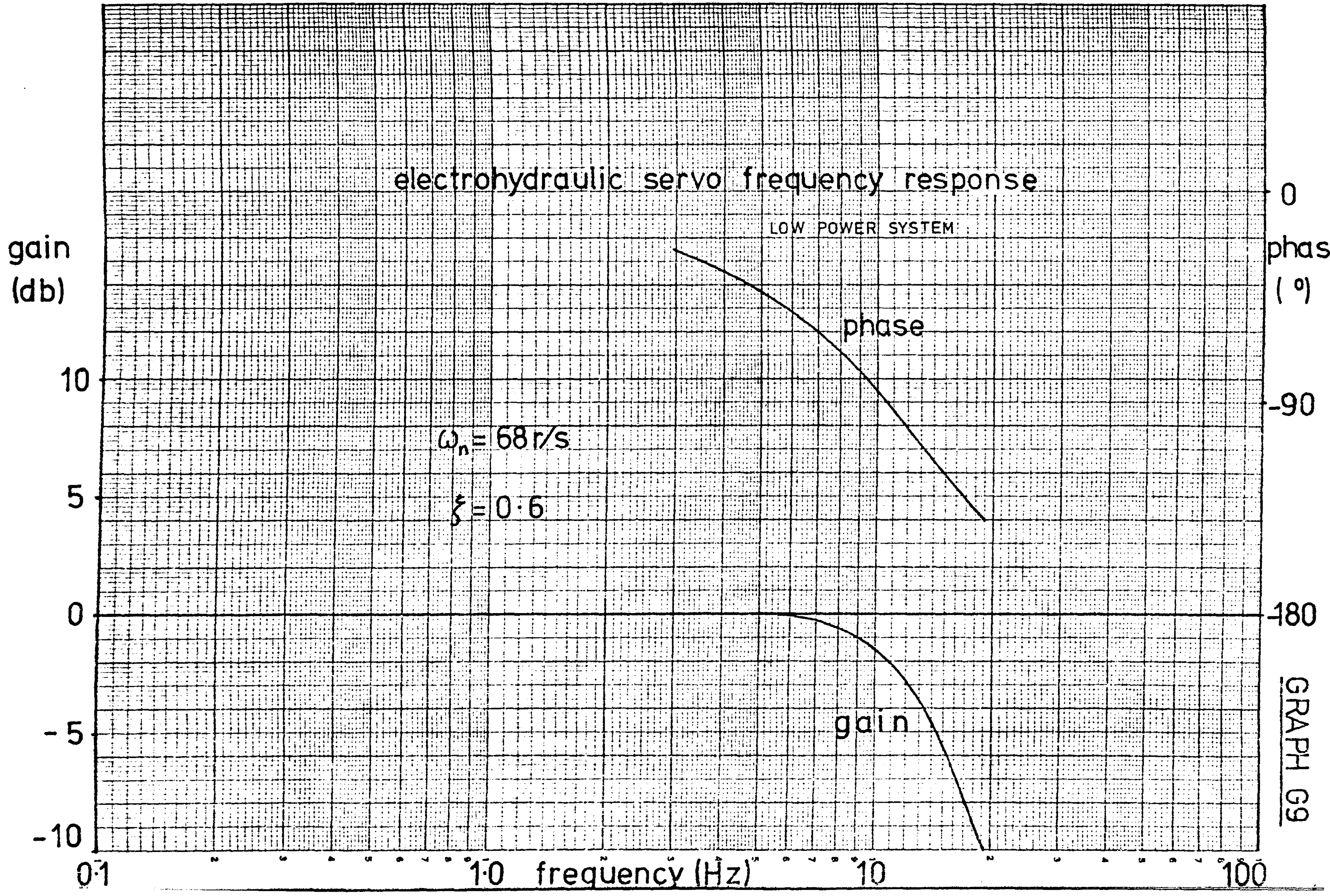
electrohydraulic servo frequency response
LOW POWER SYSTEM
gain
(db)
phas
(°)
phase
gain
$\omega_n = 68$ r/s
$\xi = 0\cdot6$
10
5
0
-5
-10
0
-90
-180
0·1
1·0
10
100
frequency (Hz)
GRAPH G9

GRAPH G10

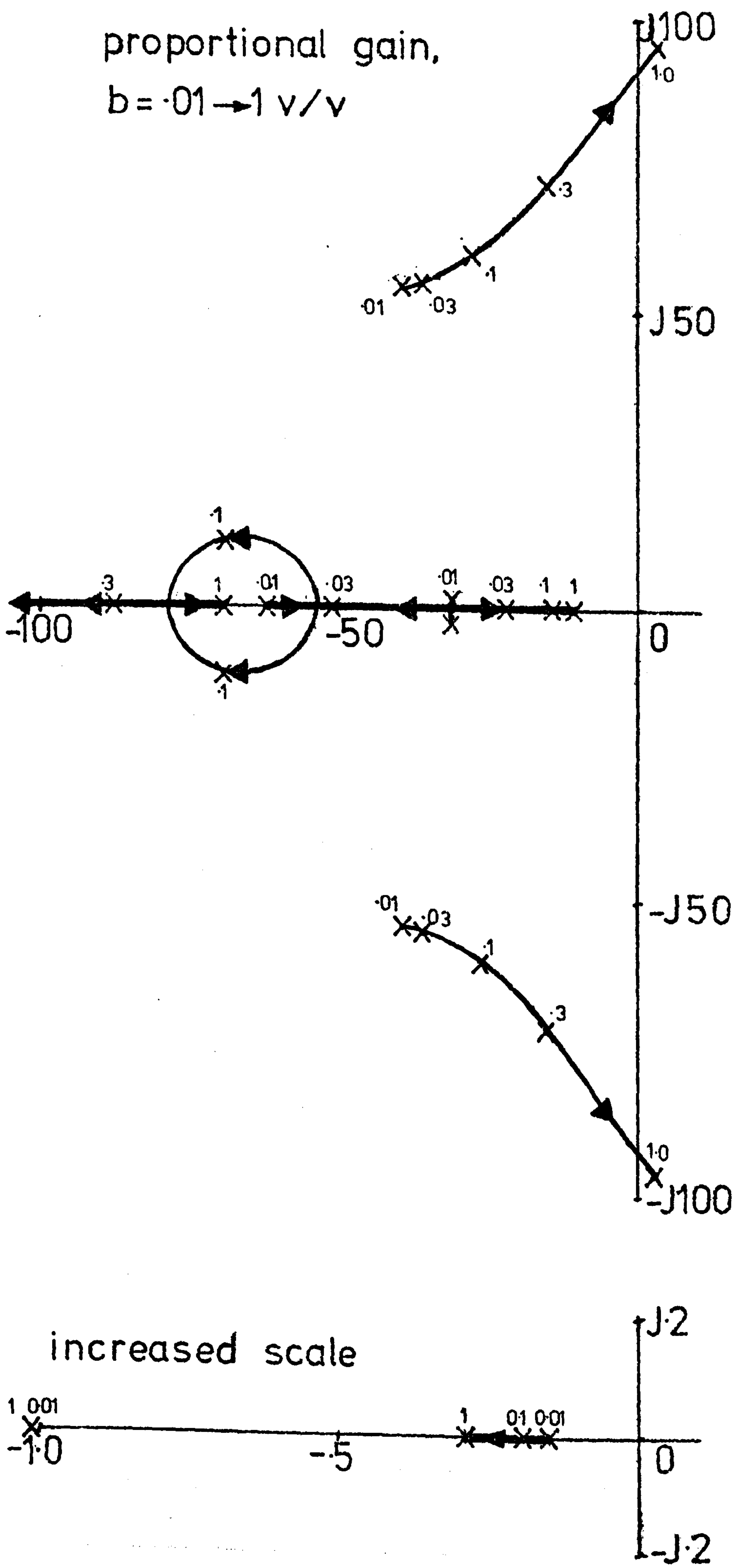
proportional gain,
b = ·01 → 1 v/v
J100
J50
-J50
-J100
-100
-50
0
·01
·03
·1
·3
1·0
1
increased scale
J·2
-J·2
-1·0
-5
1 0·01
01 0·01

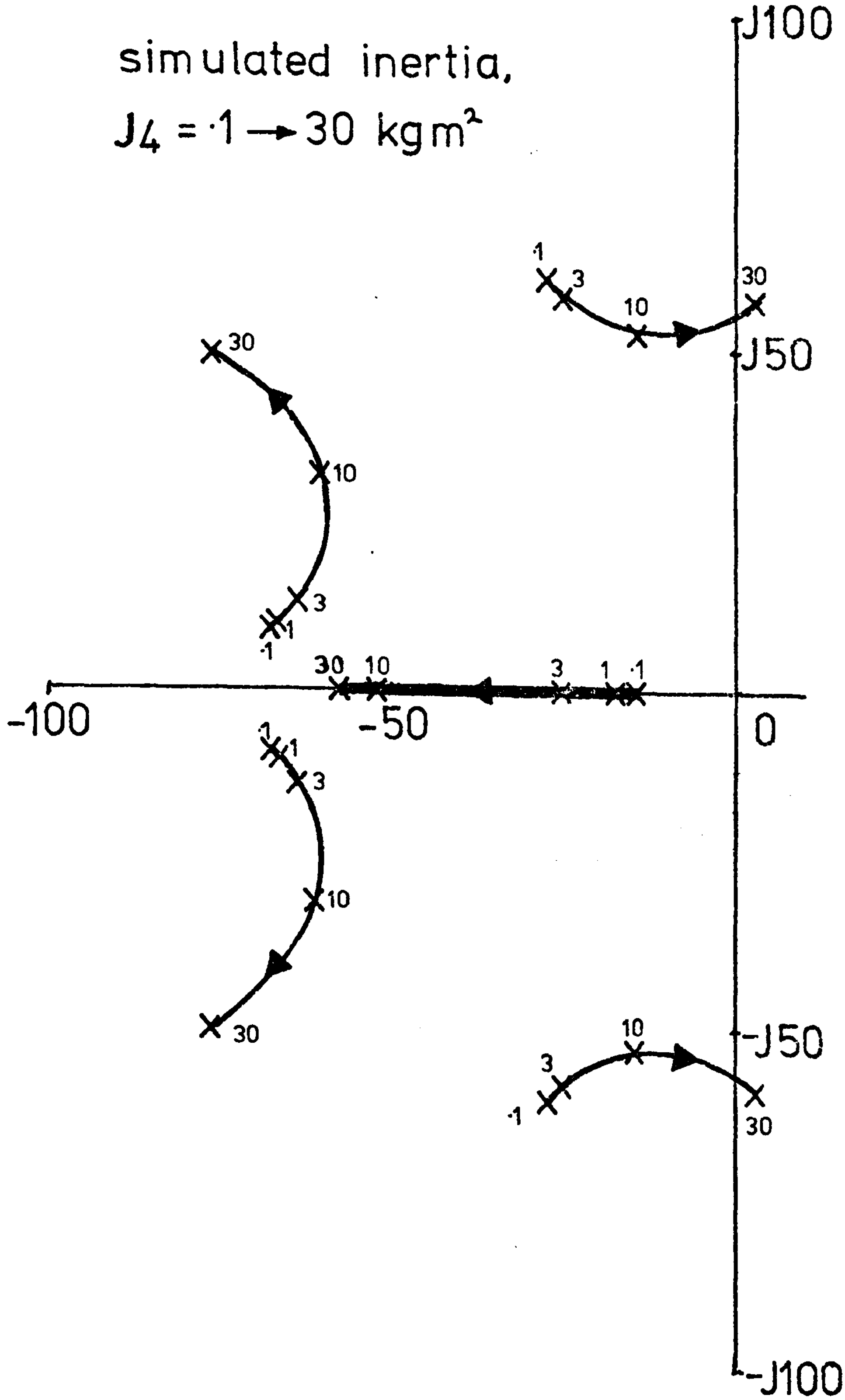
simulated inertia,
$J_4 = \cdot 1 \rightarrow 30$ kgm^2
J100
J50
-J50
-J100
-100
-50
0
30
10
3
1
·1

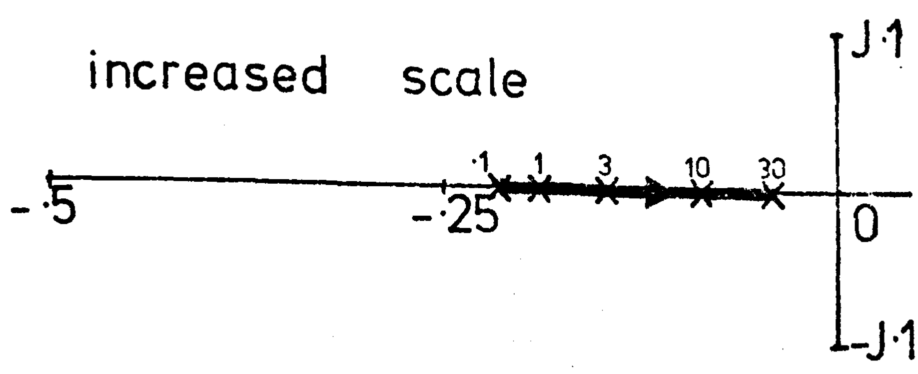
increased scale
J·1
-J·1
-·5
-·25
0
·1
1
3
10
30

GRAPH G12

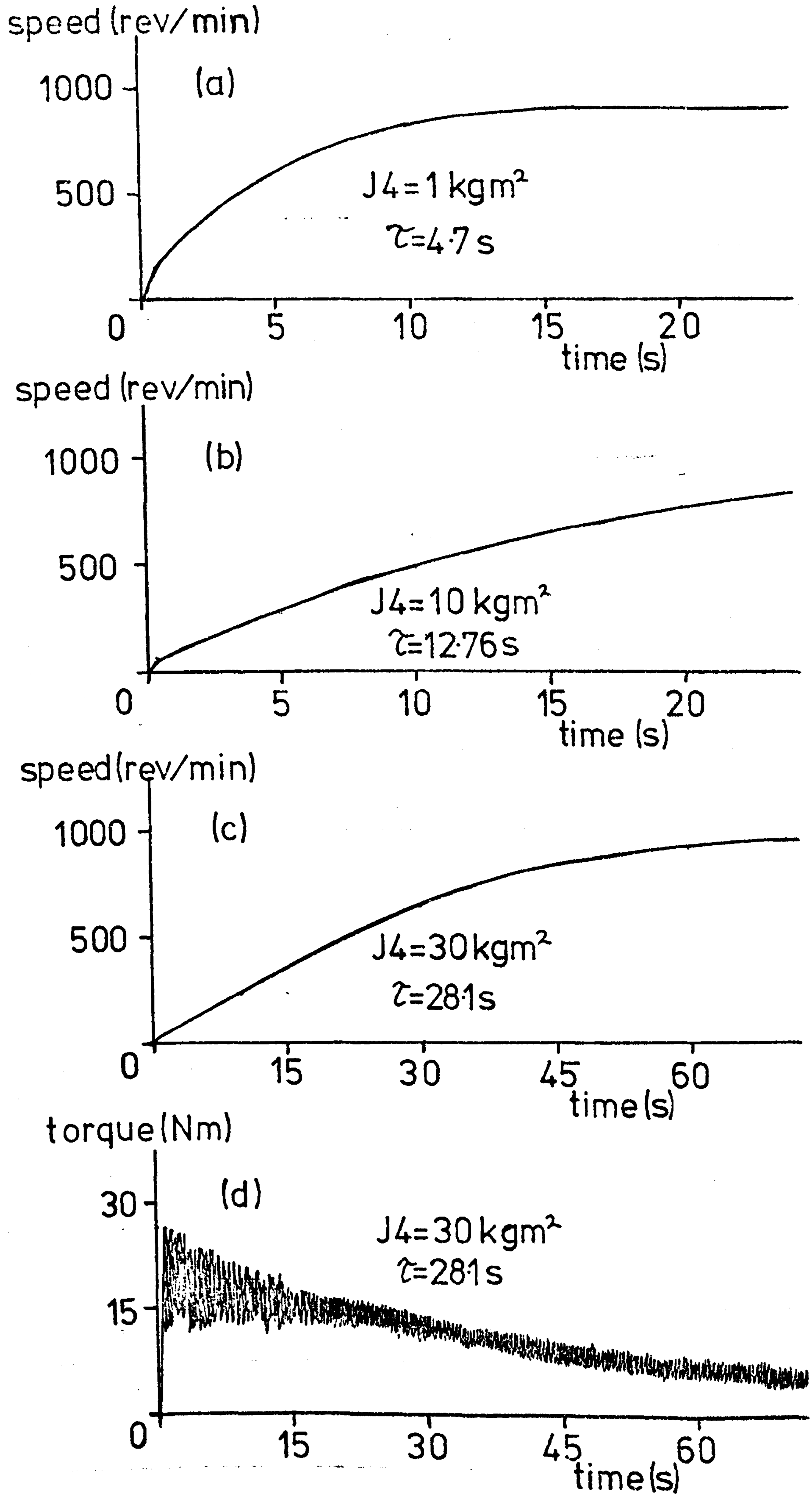
speed (rev/min)
1000
500
(a)
J4=1 kgm²
τ=4·7 s
0
5
10
15
20
time (s)
speed (rev/min)
1000
500
(b)
J4=10 kgm²
τ=12·76 s
0
5
10
15
20
time (s)
speed (rev/min)
1000
500
(c)
J4=30 kgm²
τ=28·1 s
0
15
30
45
60
time (s)
torque (Nm)
30
15
(d)
J4=30 kgm²
τ=28·1 s
0
15
30
45
60
time (s)

(p_g=0·24)

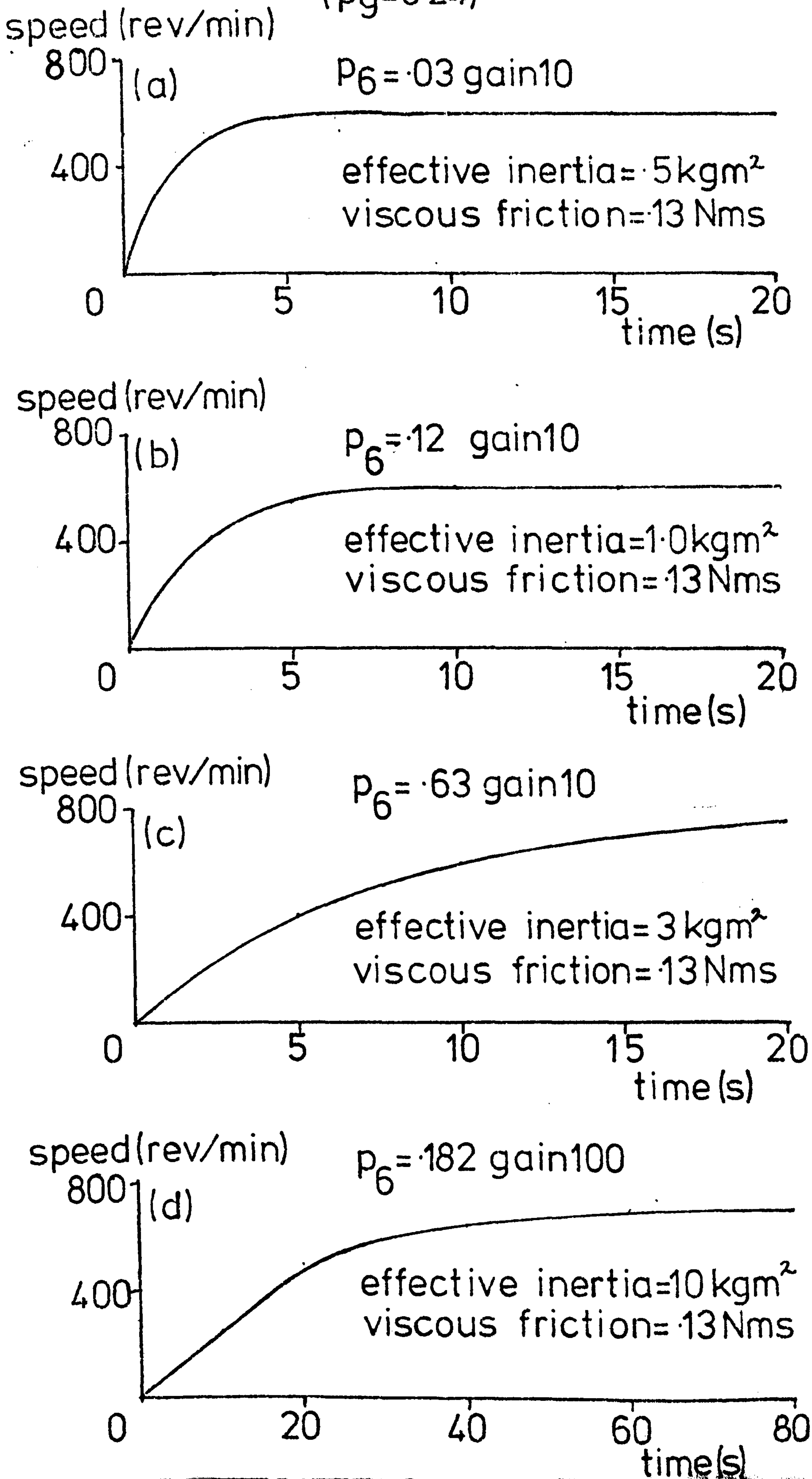
speed (rev/min)
800
400
(a)
P6 = ·03 gain10
effective inertia = ·5 kgm²
viscous friction = ·13 Nms
0
5
10
15
20
time (s)
speed (rev/min)
800
400
(b)
P6 = ·12 gain10
effective inertia = 1·0 kgm²
viscous friction = ·13 Nms
0
5
10
15
20
time (s)
speed (rev/min)
800
400
(c)
P6 = ·63 gain10
effective inertia = 3 kgm²
viscous friction = ·13 Nms
0
5
10
15
20
time (s)
speed (rev/min)
800
400
(d)
P6 = ·182 gain100
effective inertia = 10 kgm²
viscous friction = ·13 Nms
0
20
40
60
80
time (s)

GRAPH G14

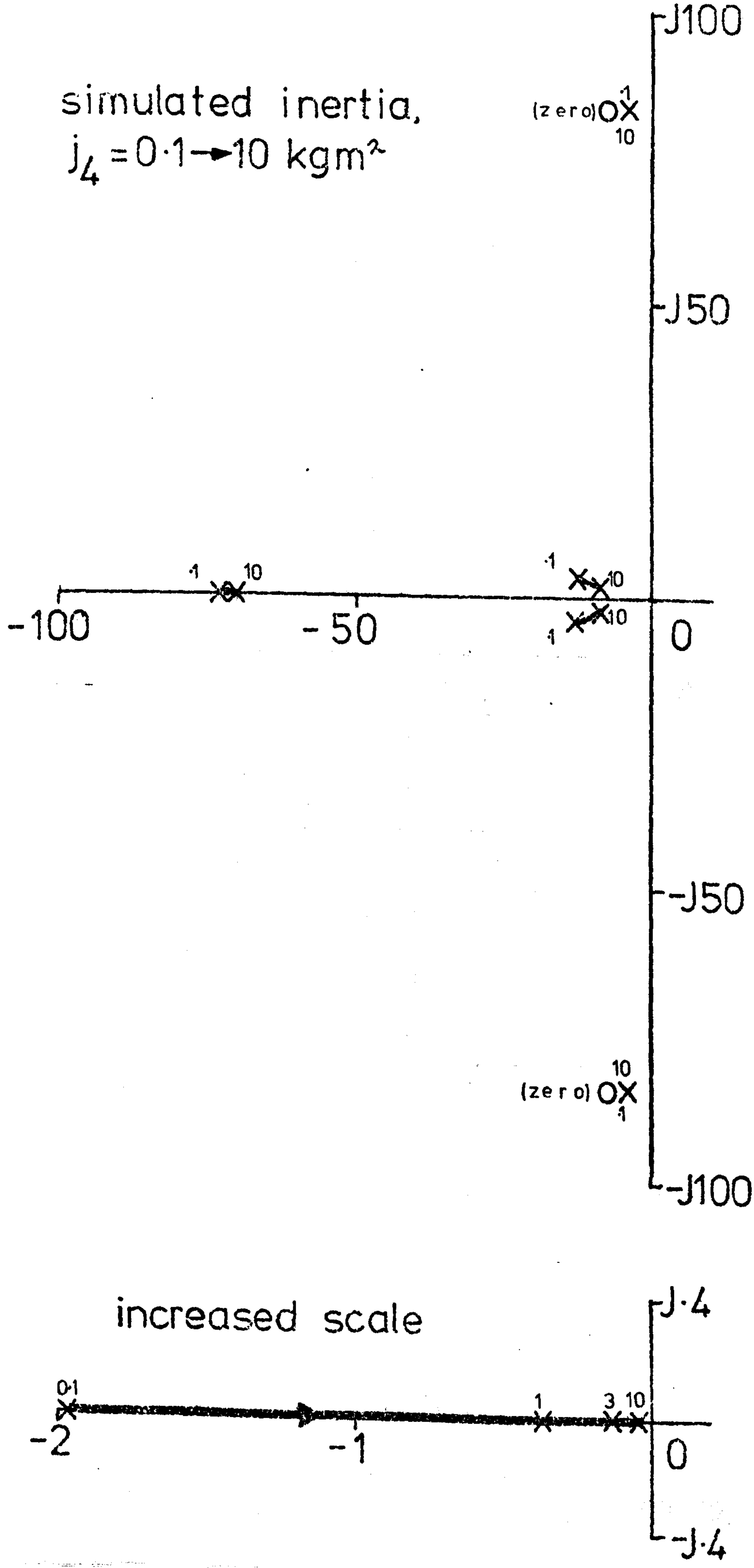

simulated inertia,
$j_4 = 0{\cdot}1 \rightarrow 10\ kgm^2$
J100
J50
-J50
-J100
(zero)
-100
-50
0
increased scale
J·4
-J·4
-2
-1
0·1
1
3
10

LOW POWER SYSTEM

GRAPH G15

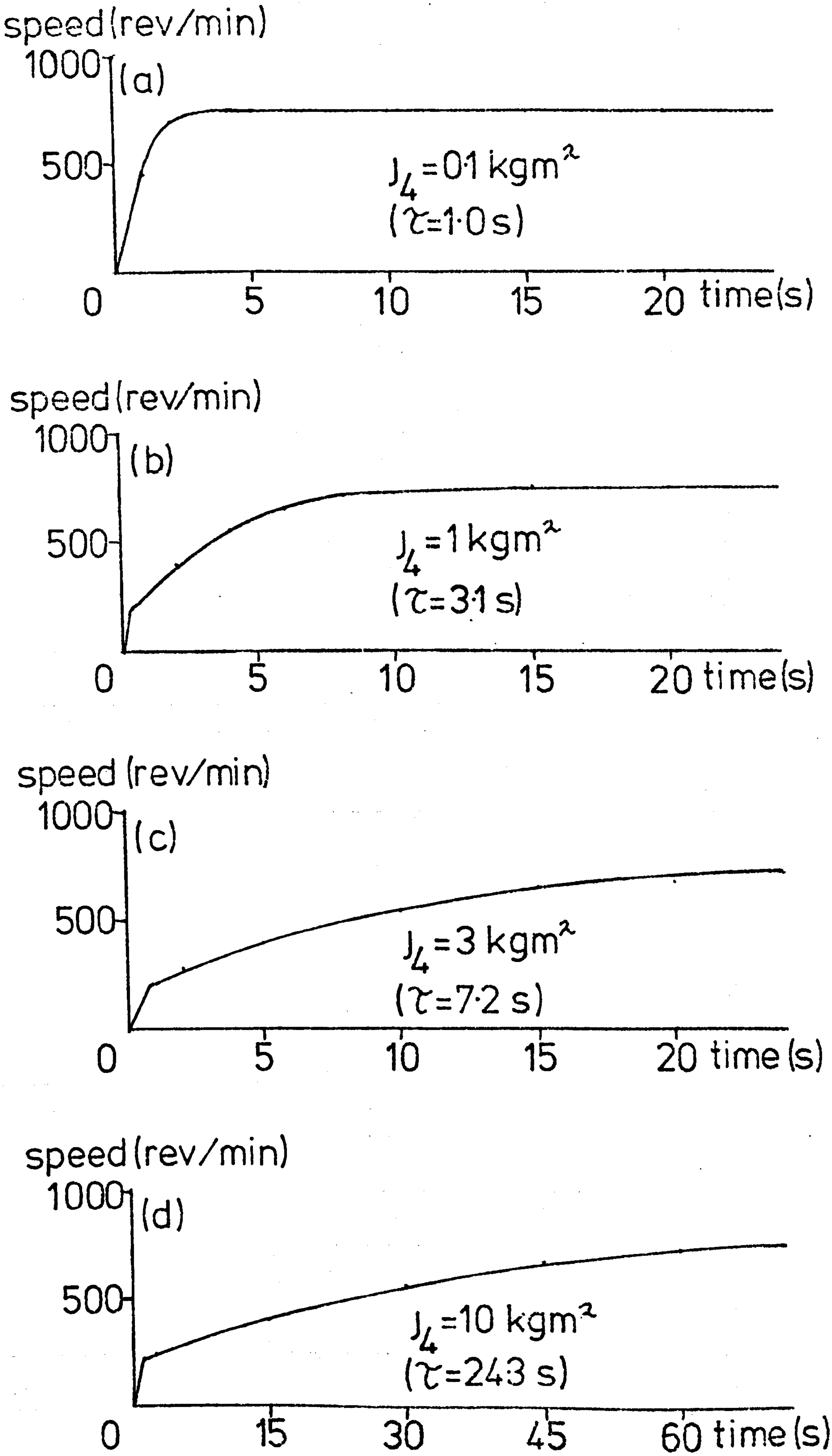

GRAPH G16

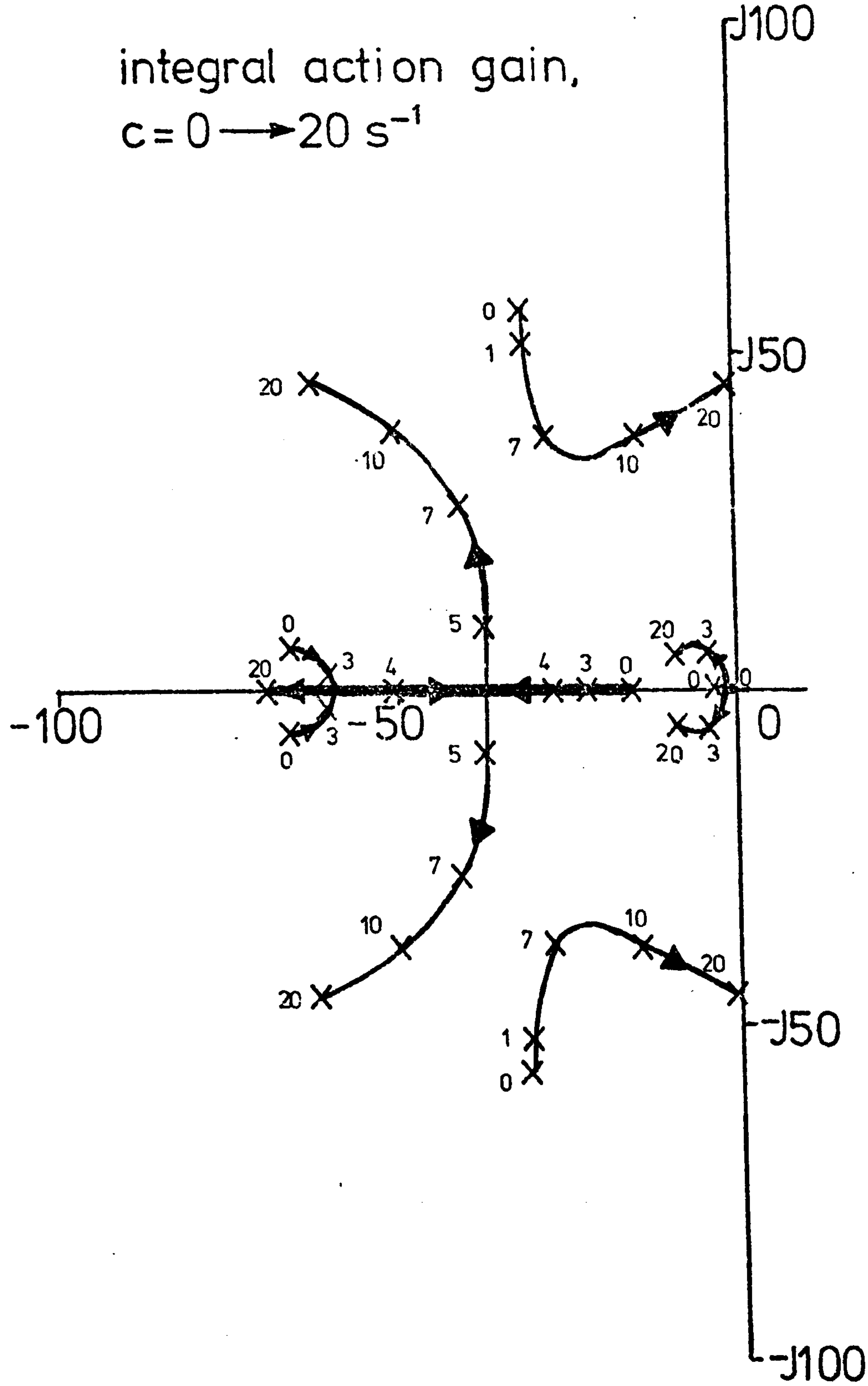

integral action gain,
c = 0 ⟶ 20 s⁻¹
J100
J50
-J50
-J100
-100
-50
0
0
1
7
10
20
5
4
3

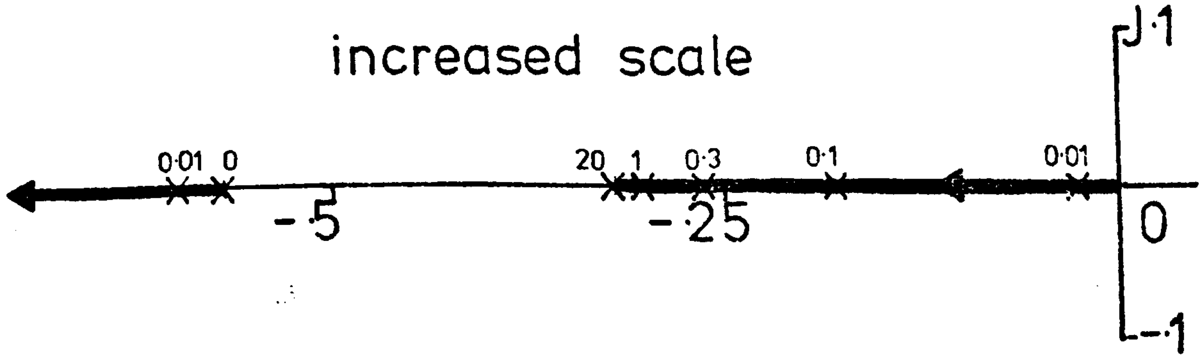

increased scale
J·1
-·1
-·5
-·25
0
0·01
0
20
1
0·3
0·1
0·01

GRAPH G17

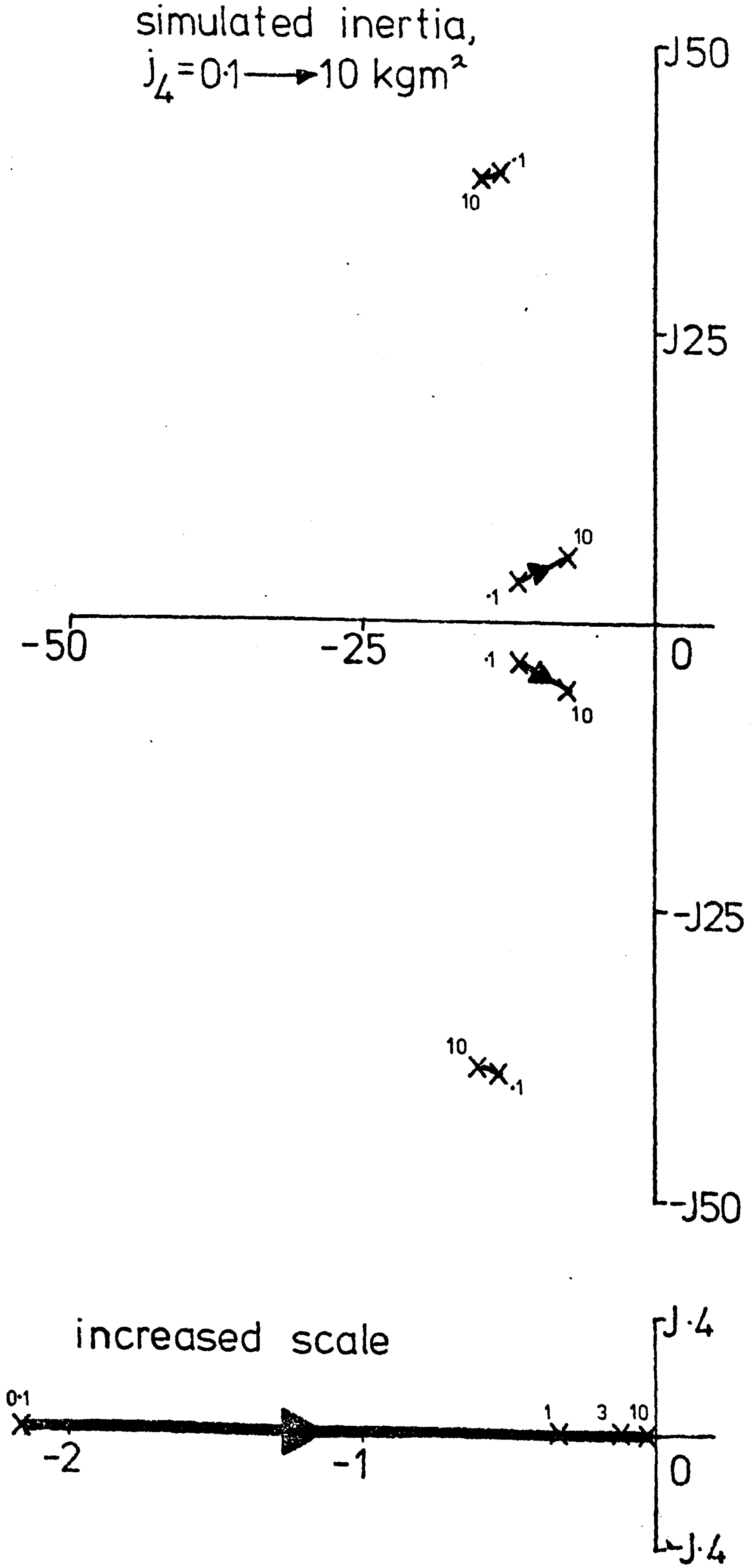
simulated inertia,
$j_4 = 0{\cdot}1 \longrightarrow 10\ kgm^2$
J50
J25
-J25
-J50
-50
-25
0
·1
10
increased scale
J·4
-J·4
0·1
1
3
-2
-1

GRAPH G18

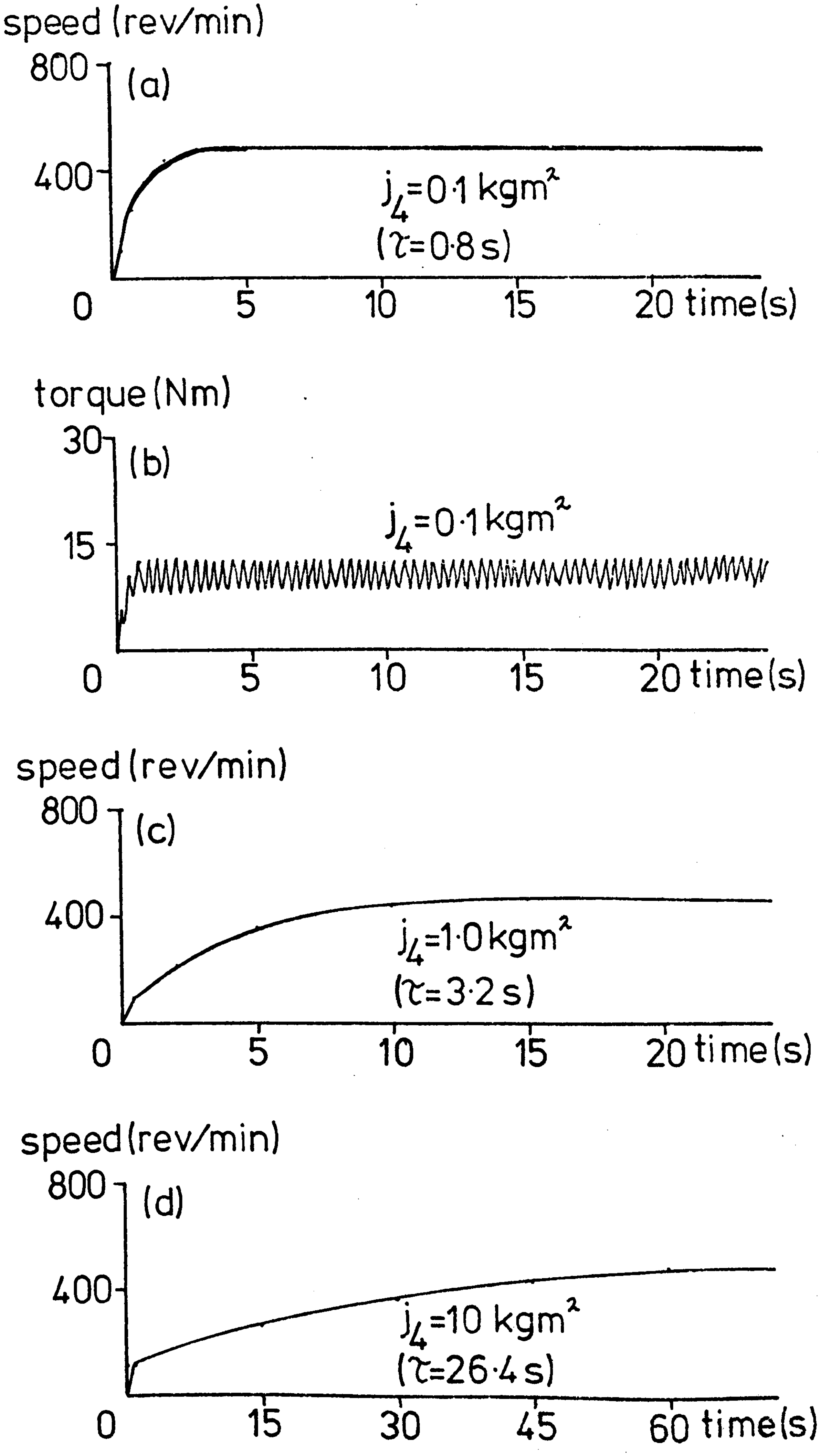
speed (rev/min)
800
400
0
(a)
j_4=0·1 kgm^2
(τ=0·8 s)
5
10
15
20 time(s)
torque (Nm)
30
15
0
(b)
j_4=0·1 kgm^2
5
10
15
20 time(s)
speed (rev/min)
800
400
0
(c)
j_4=1·0 kgm^2
(τ=3·2 s)
5
10
15
20 time(s)
speed (rev/min)
800
400
0
(d)
j_4=10 kgm^2
(τ=26·4 s)
15
30
45
60 time(s)

GRAPH G19

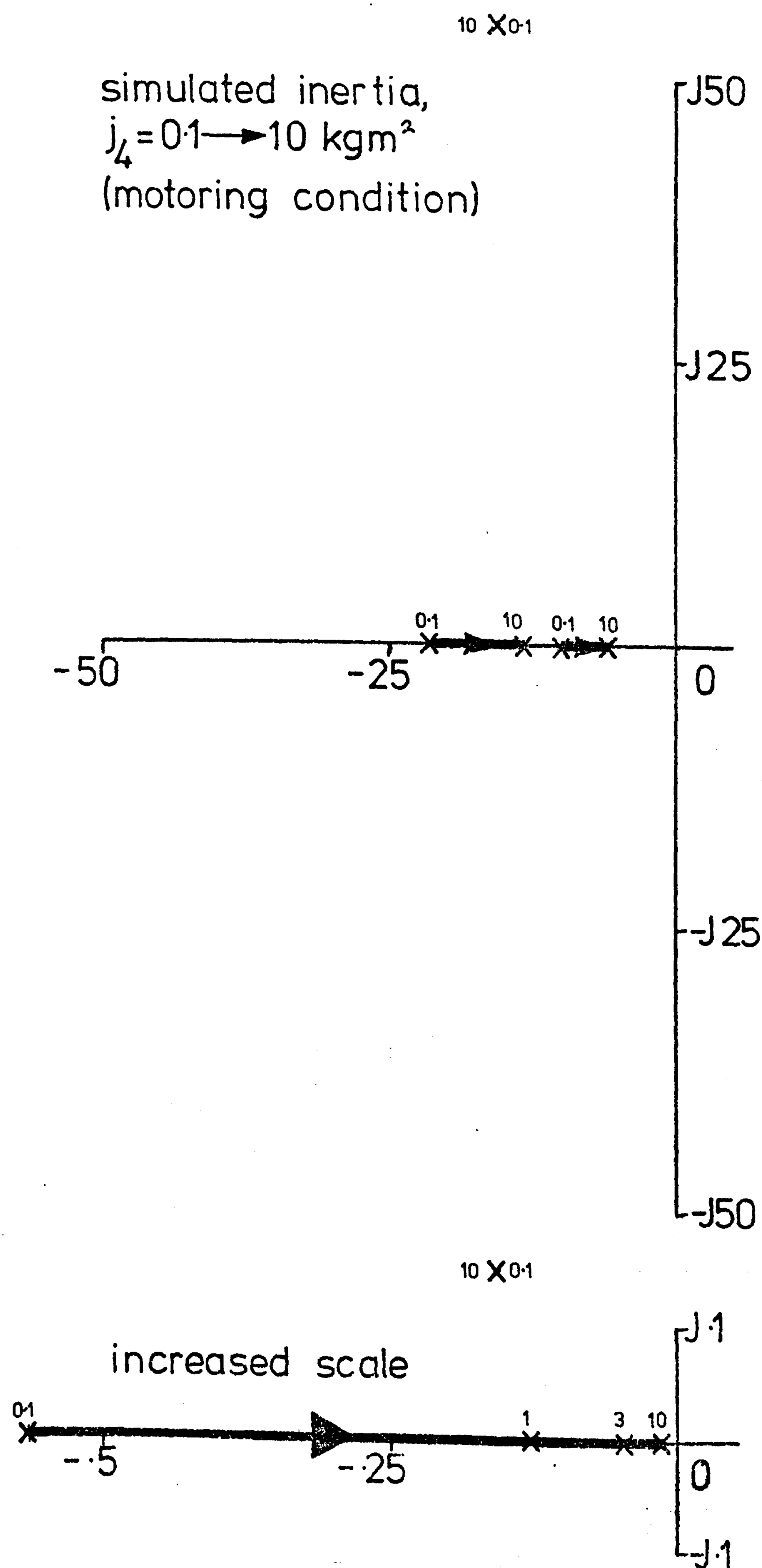
10 X 0·1
simulated inertia,
j_4 = 0·1 → 10 kgm²
(motoring condition)
J50
J25
0·1
10
0·1
10
-50
-25
0
-J25
-J50
10 X 0·1
J·1
increased scale
0·1
1
3
10
-·5
-·25
0
-J·1

LOW POWER SYSTEM

GRAPH G20

(motoring condition)

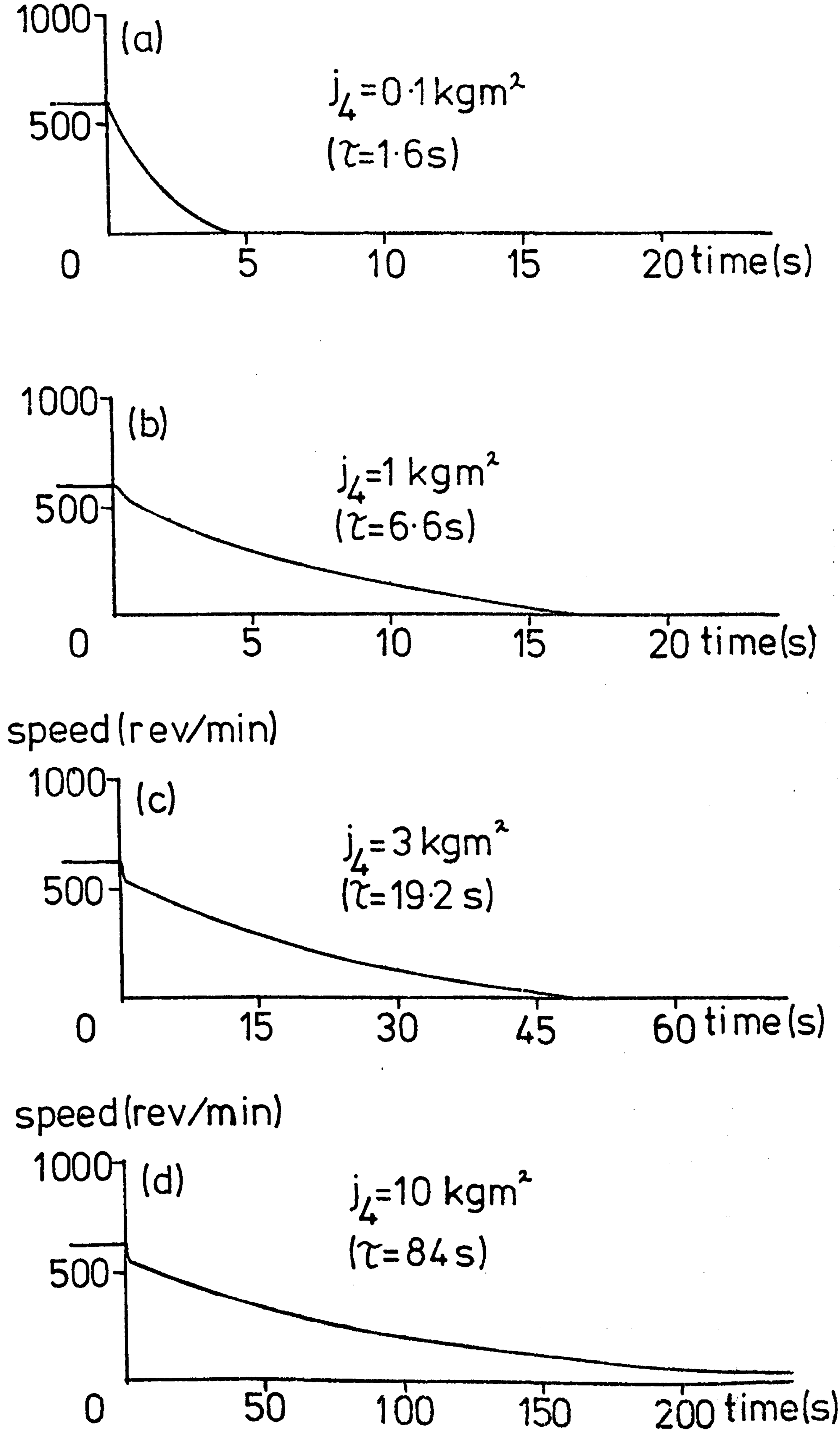

GRAPH G21

oil temperature = 23 → 70 °C

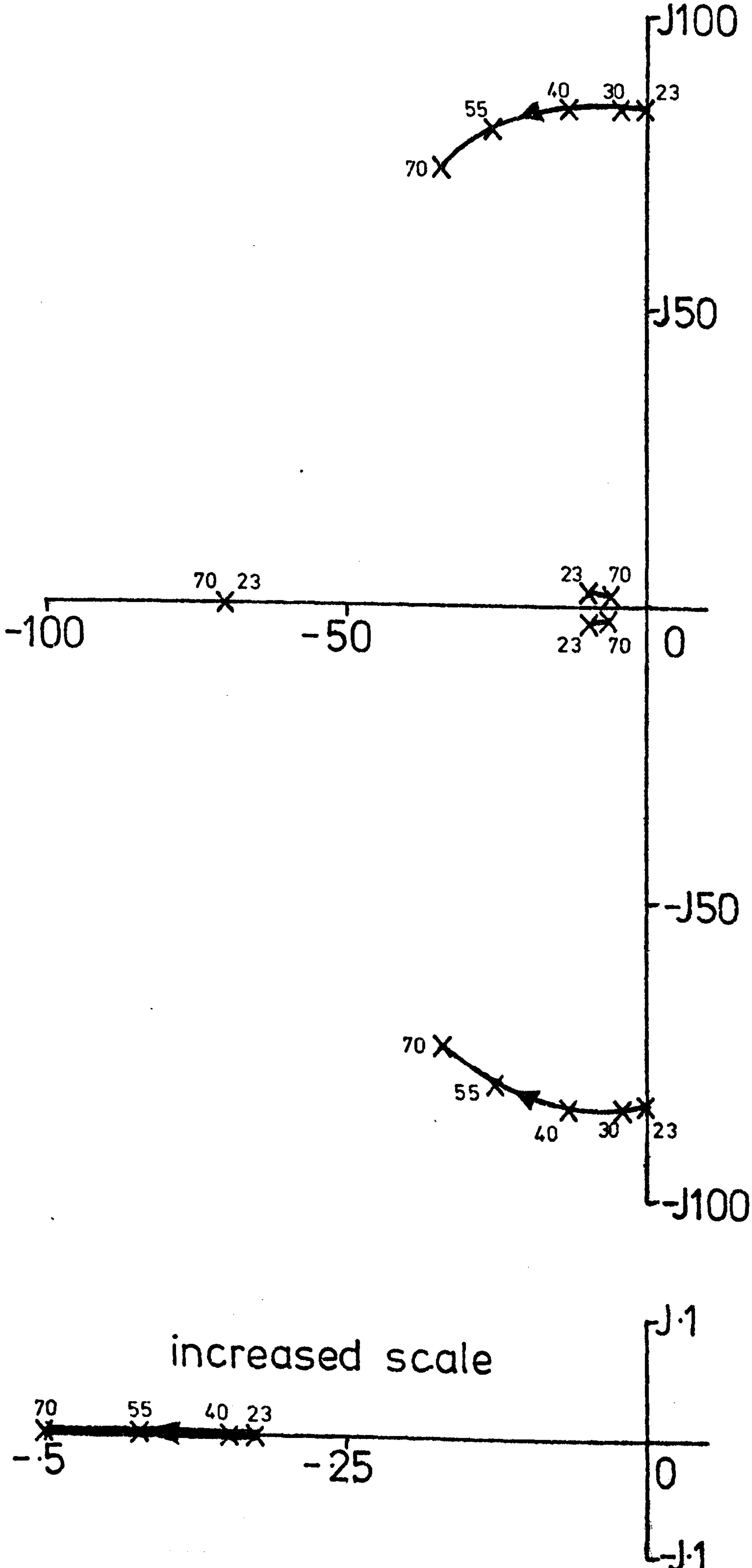

GRAPH G22

proportional gain,
$b = 0{\cdot}01 \longrightarrow 15$ v/v

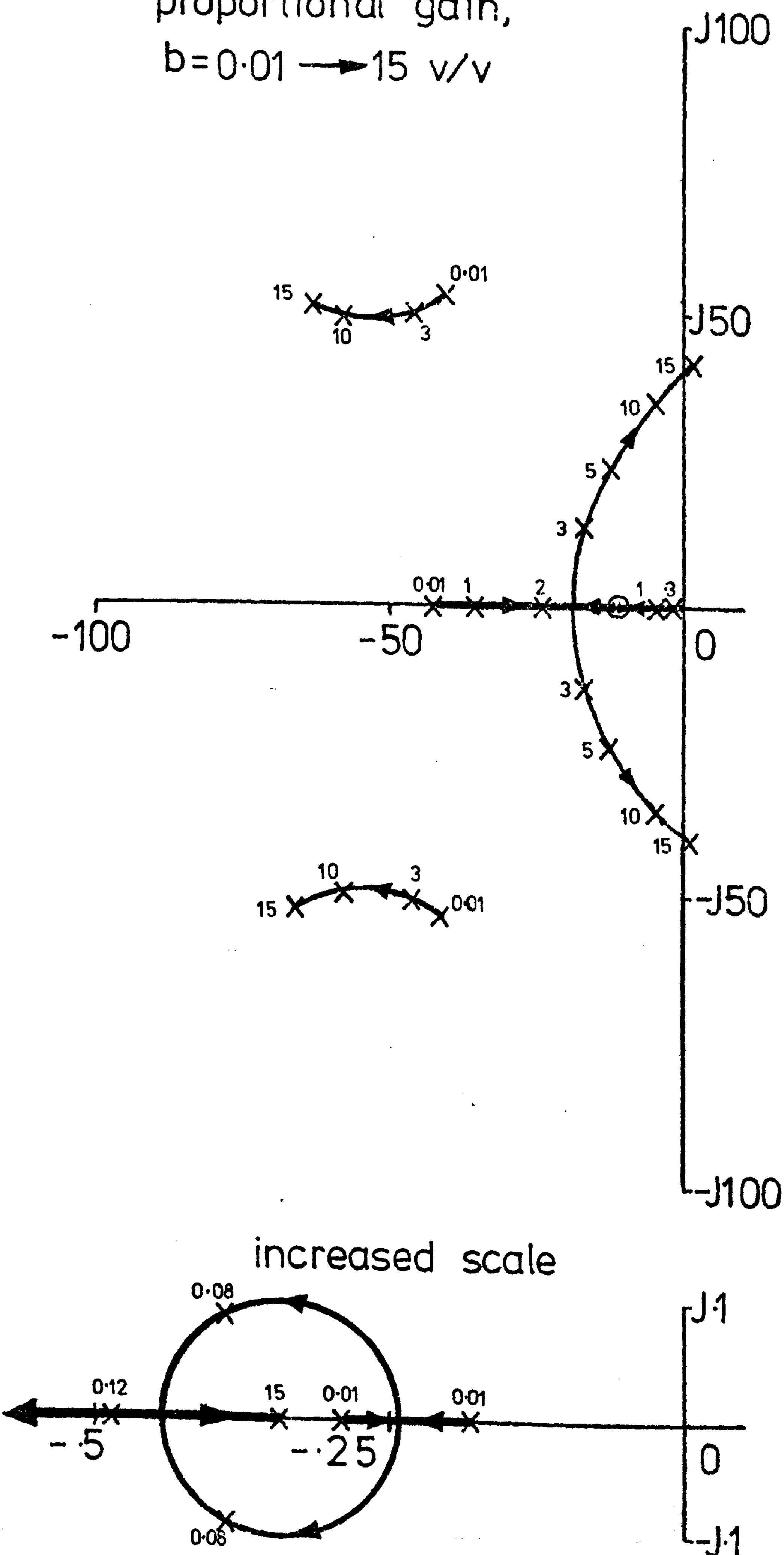

LOW POWER SYSTEM

GRAPH G23

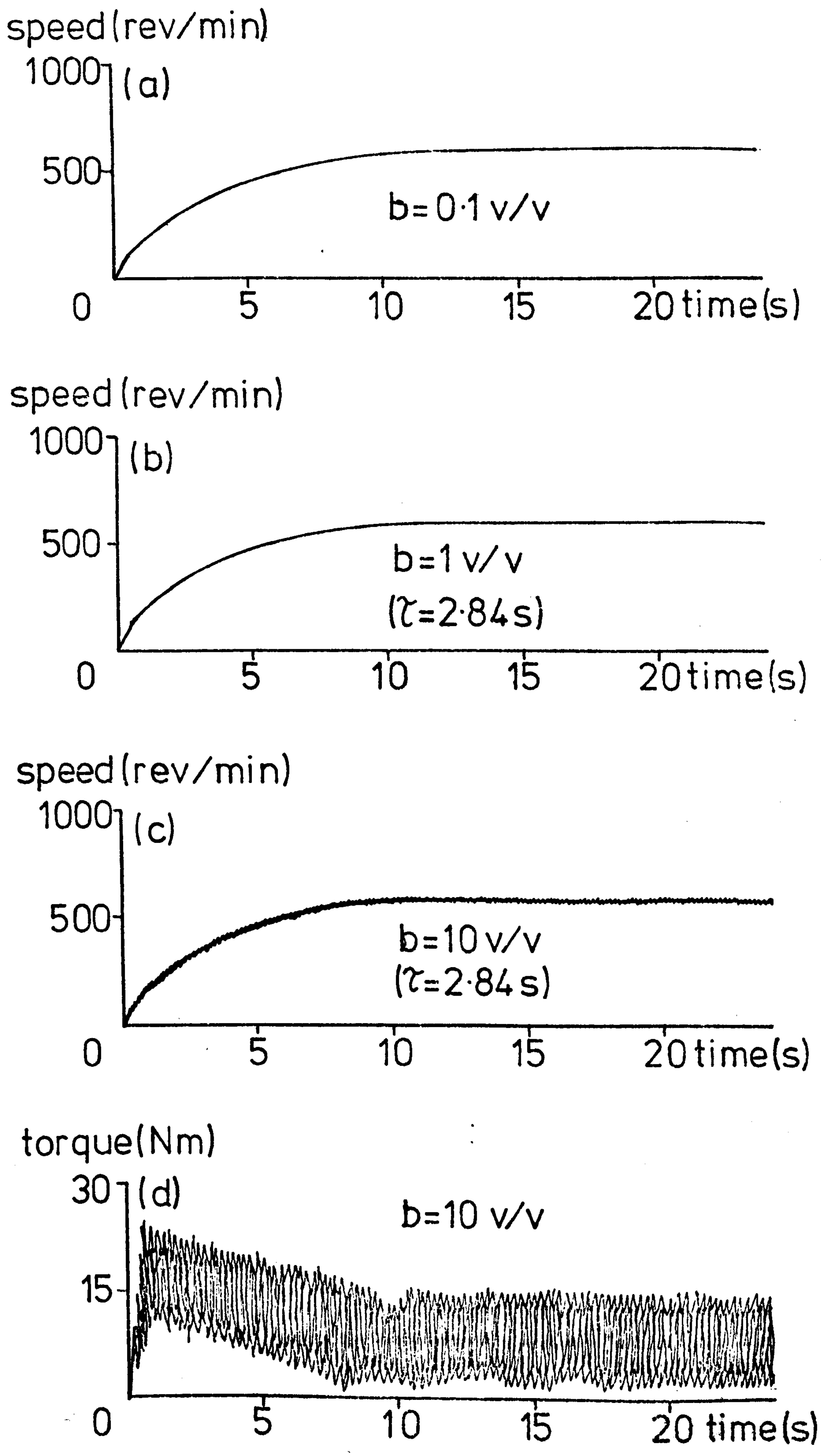

LOW POWER SYSTEM

GRAPH G24

simulated inertia,
$j_3 = 0{\cdot}1$ — $10\ kgm^2$

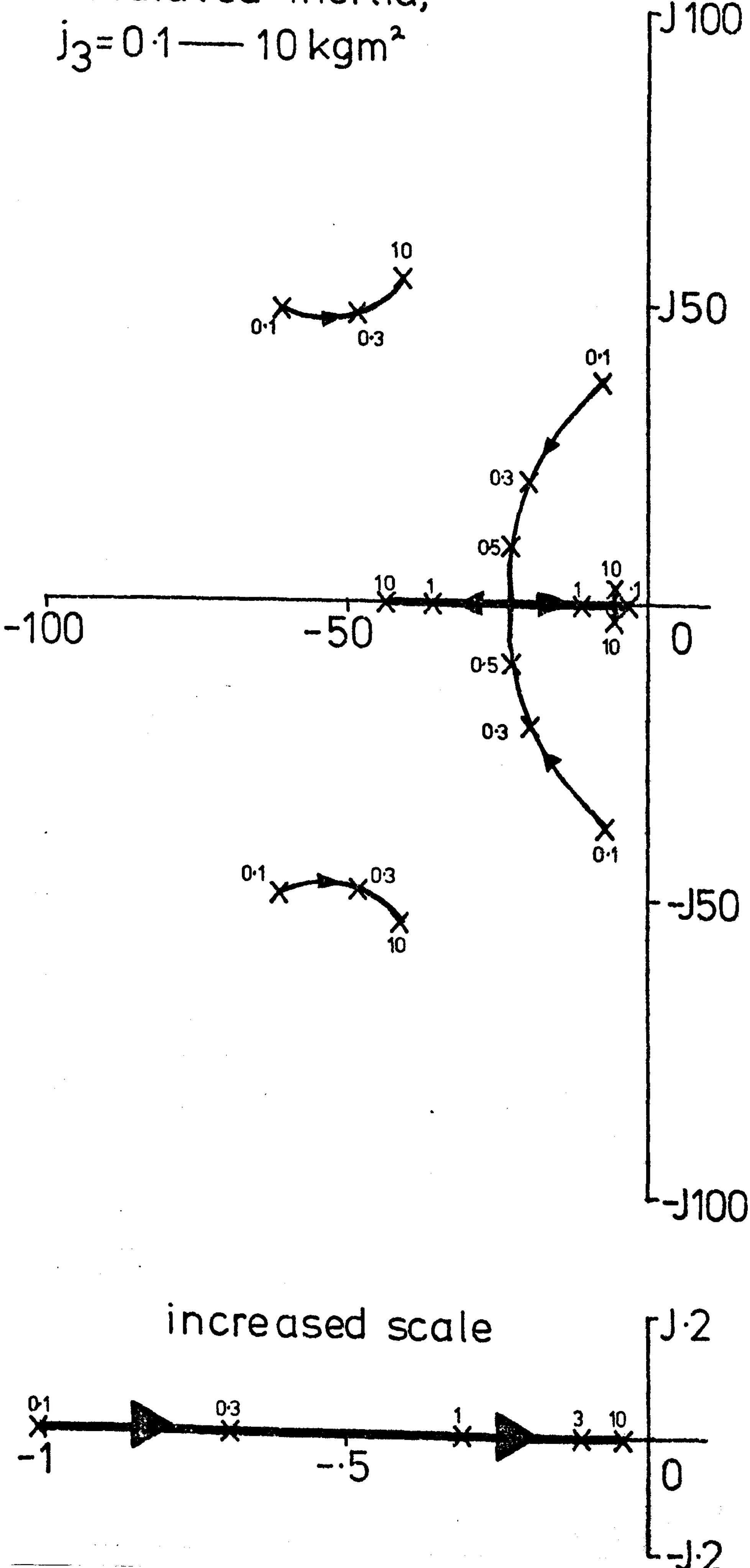

LOW POWER SYSTEM

GRAPH G25

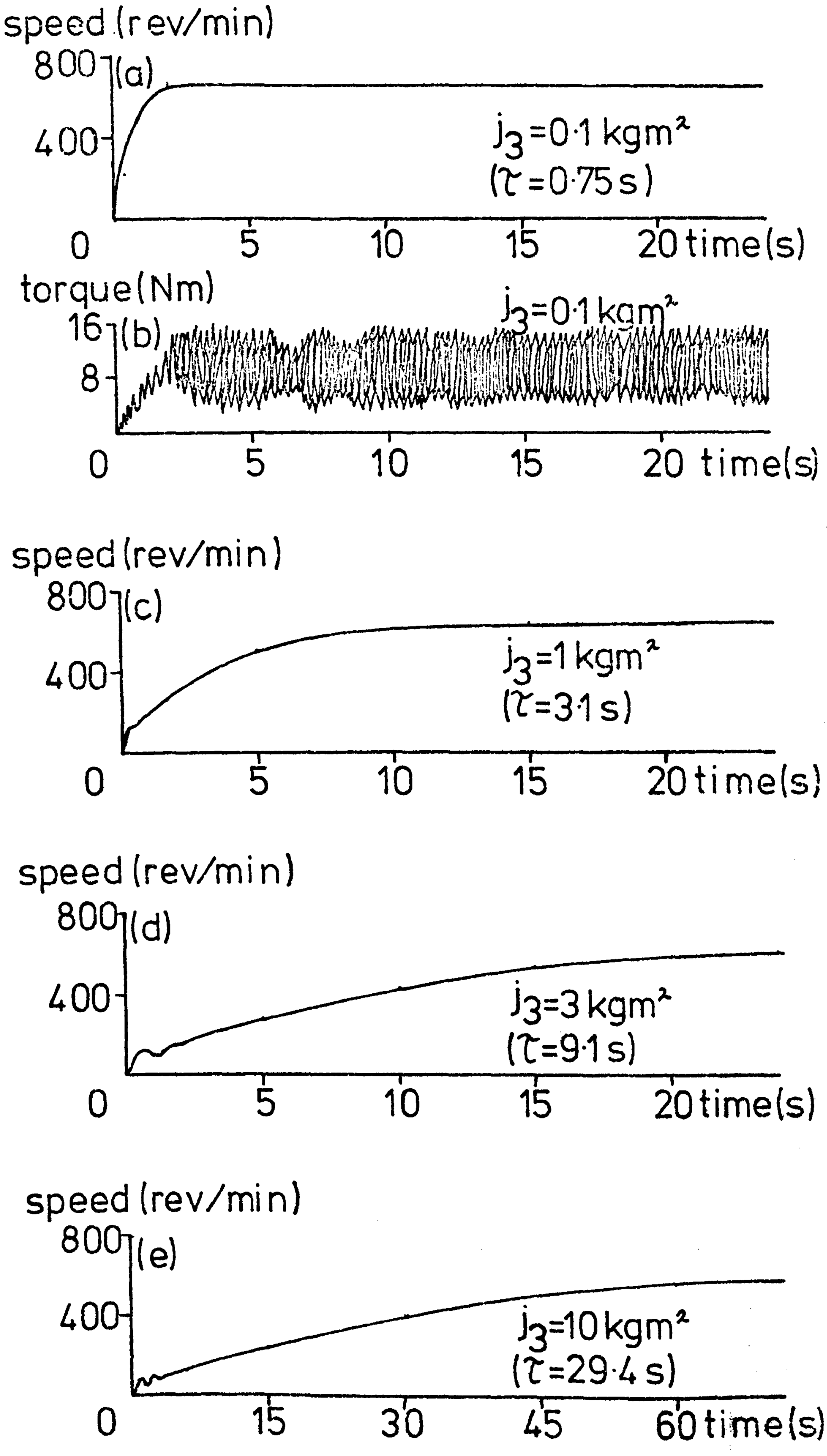

GRAPH G26

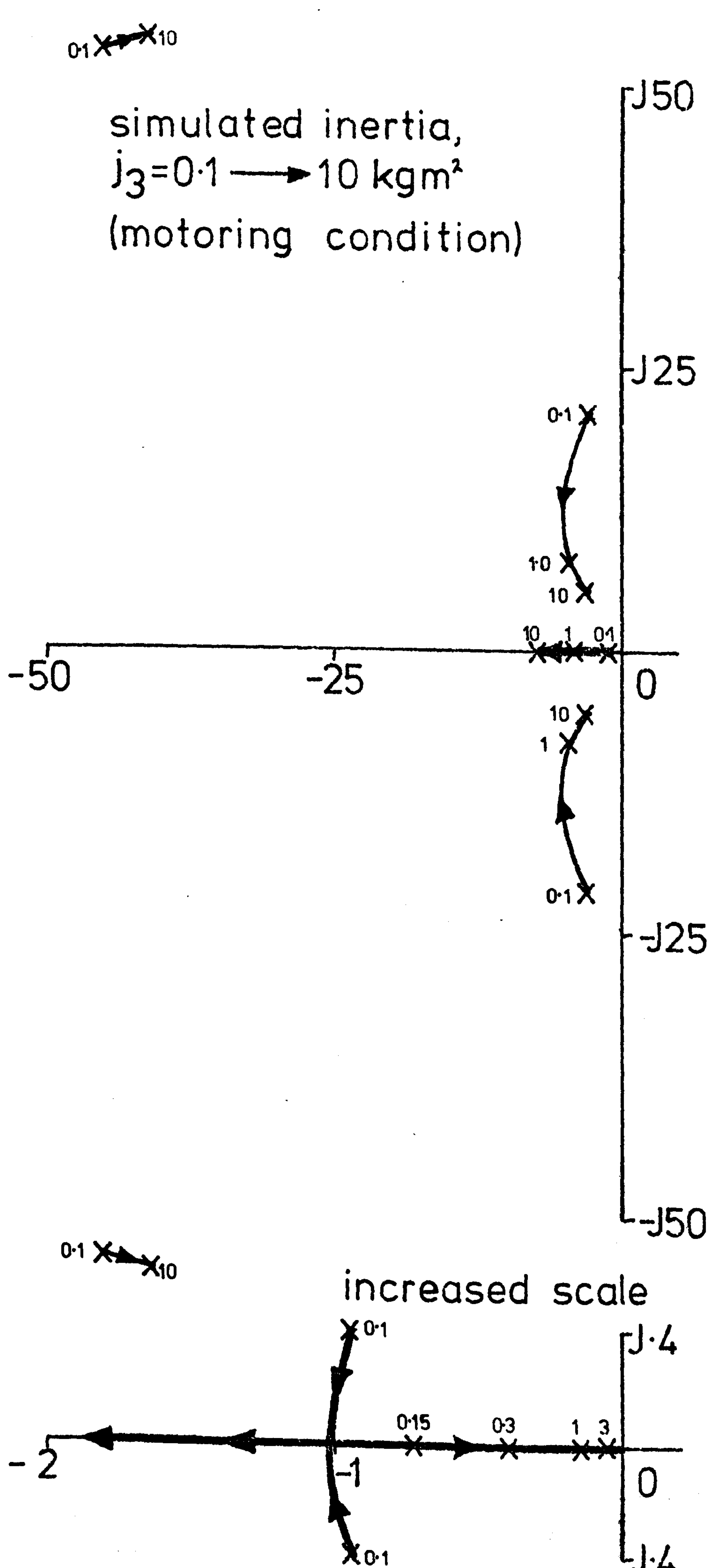

0·1
10
simulated inertia,
j_3=0·1 ⟶ 10 kgm²
(motoring condition)
J50
J25
0·1
1·0
10
10
1
0·1
-50
-25
0
10
1
0·1
-J25
-J50
0·1
10
increased scale
0·1
J·4
0·15
0·3
1
3
-2
-1
0
0·1
J·4

LOW POWER SYSTEM

GRAPH G27

(motoring condition)

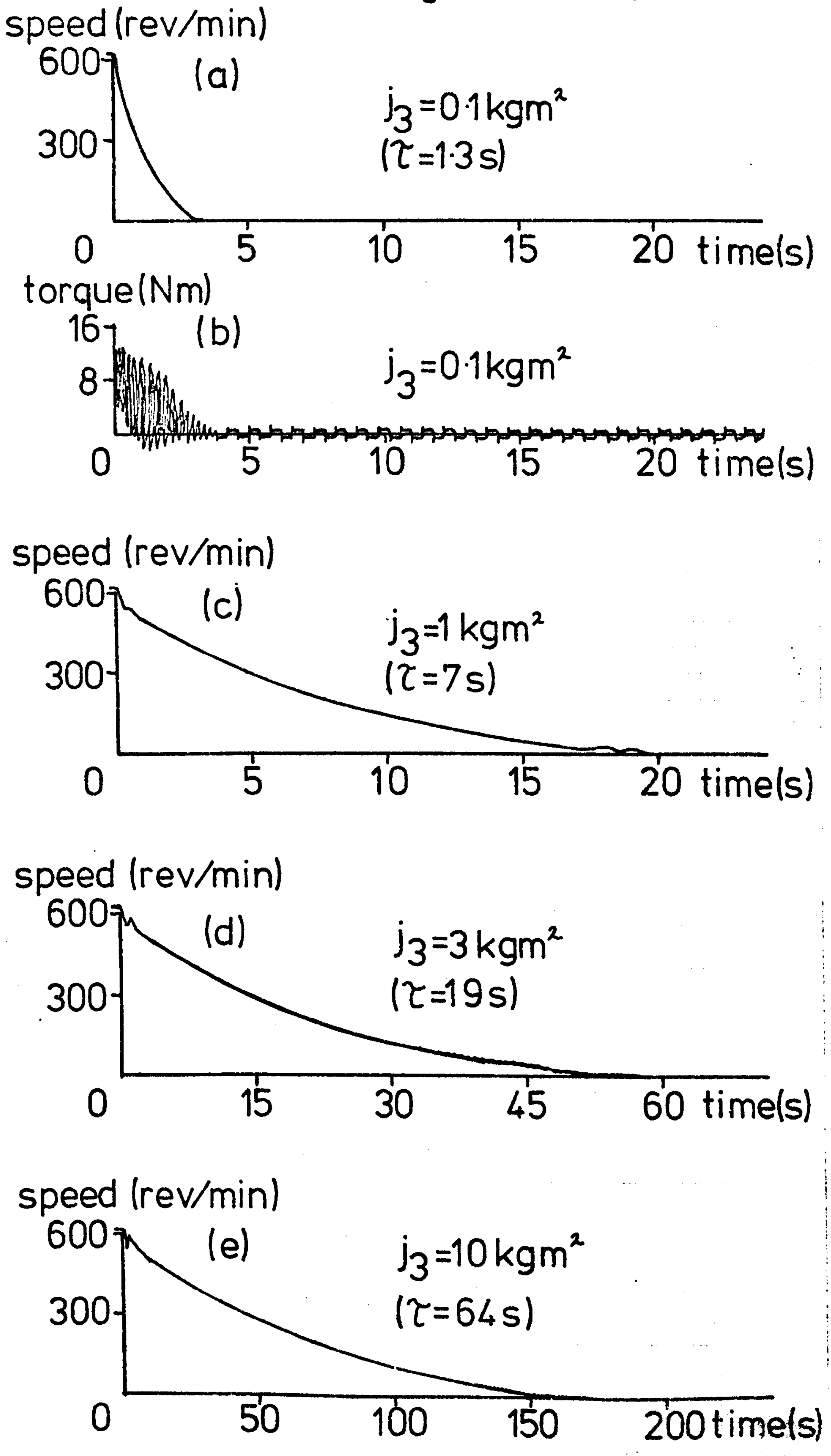

GRAPH G28

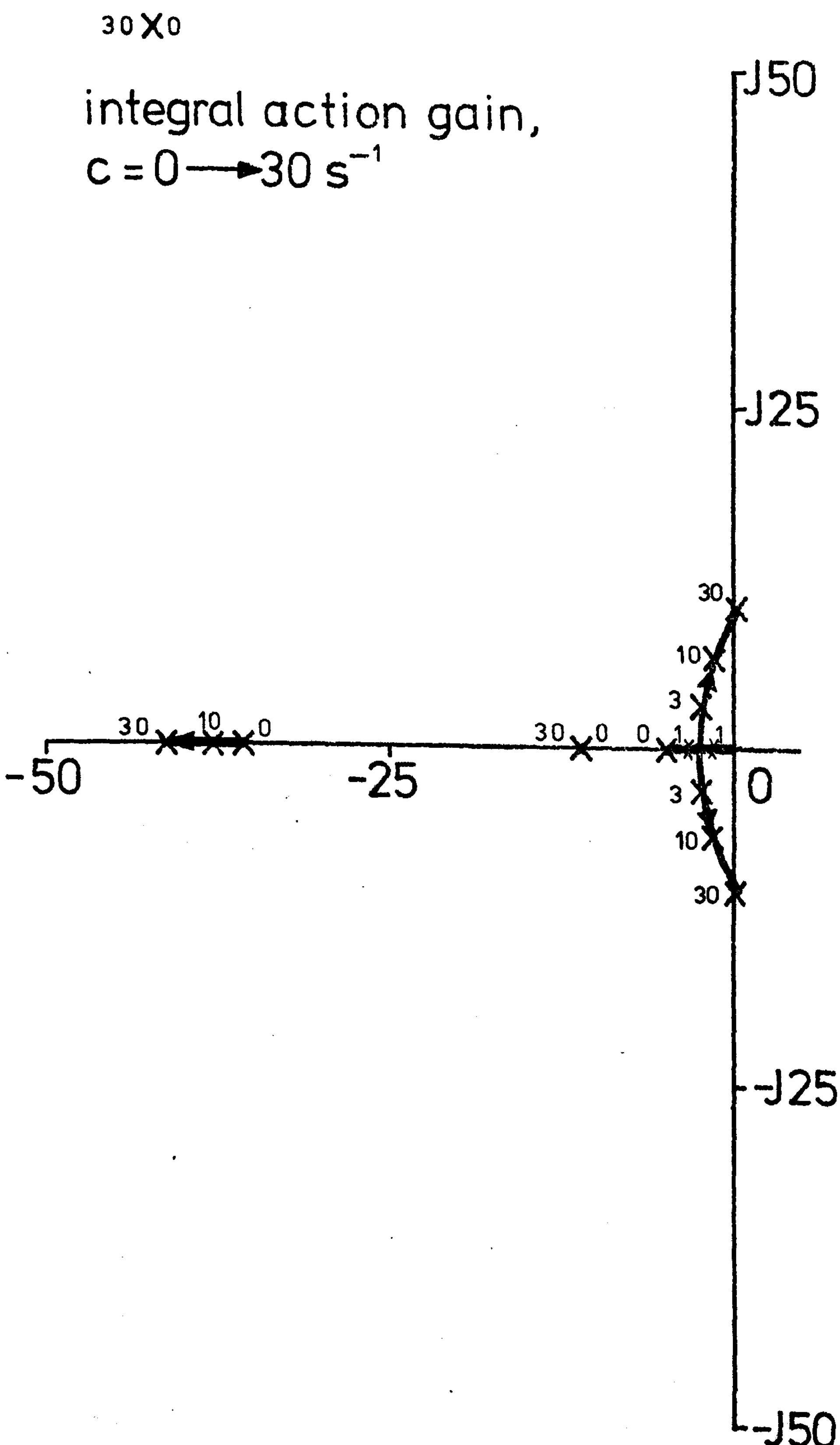

30 X 0
integral action gain,
c = 0 → 30 s^-1
J50
J25
-J25
-J50
30 10 0
30 0
0 1 1
3 10 30
3 10 30
-50
-25
0

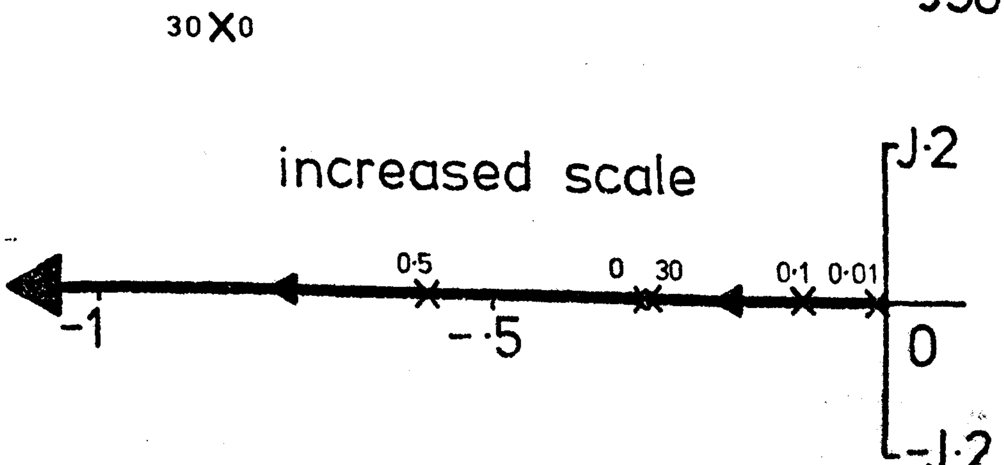

30 X 0
increased scale
J·2
-J·2
0·5
0 30
0·1 0·01
-1
-·5
0

GRAPH G29

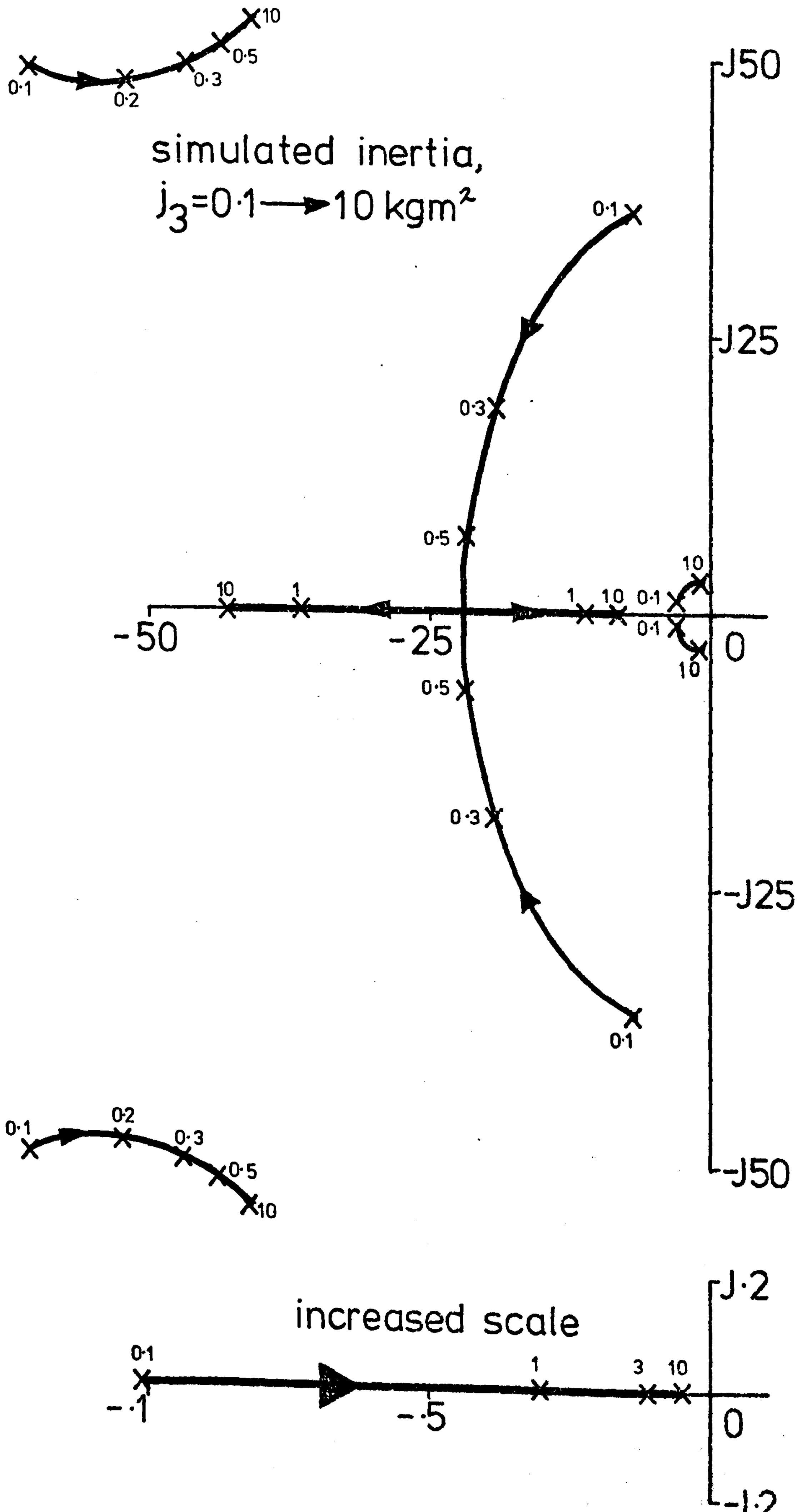
simulated inertia,
j_3=0·1⟶10 kgm²
increased scale
J50
J25
-J25
-J50
-50
-25
0
0·1
0·2
0·3
0·5
1
3
10
J·2
-J·2
-·1
-·5

LOW POWER SYSTEM

GRAPH G30

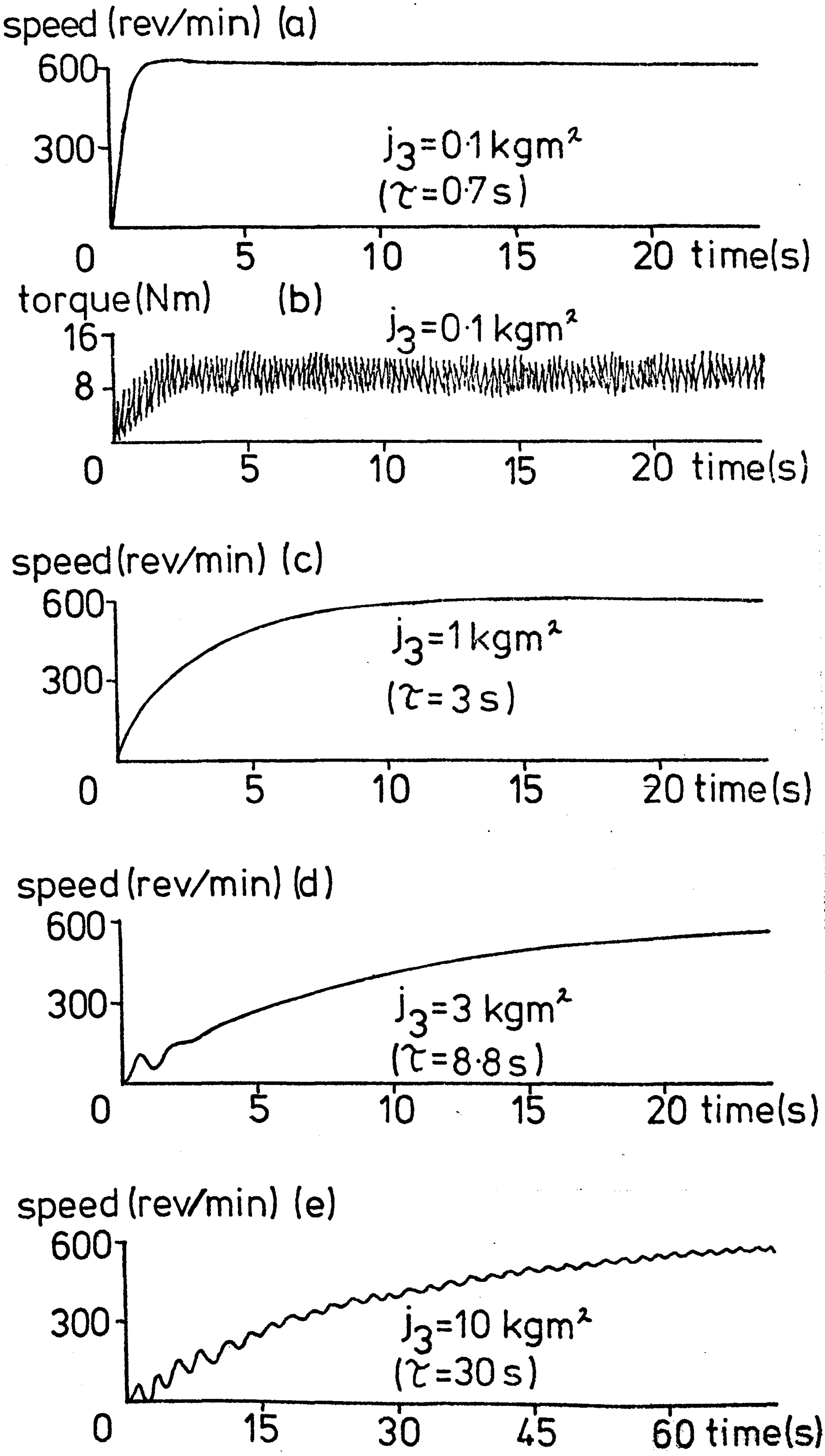

GRAPH G31

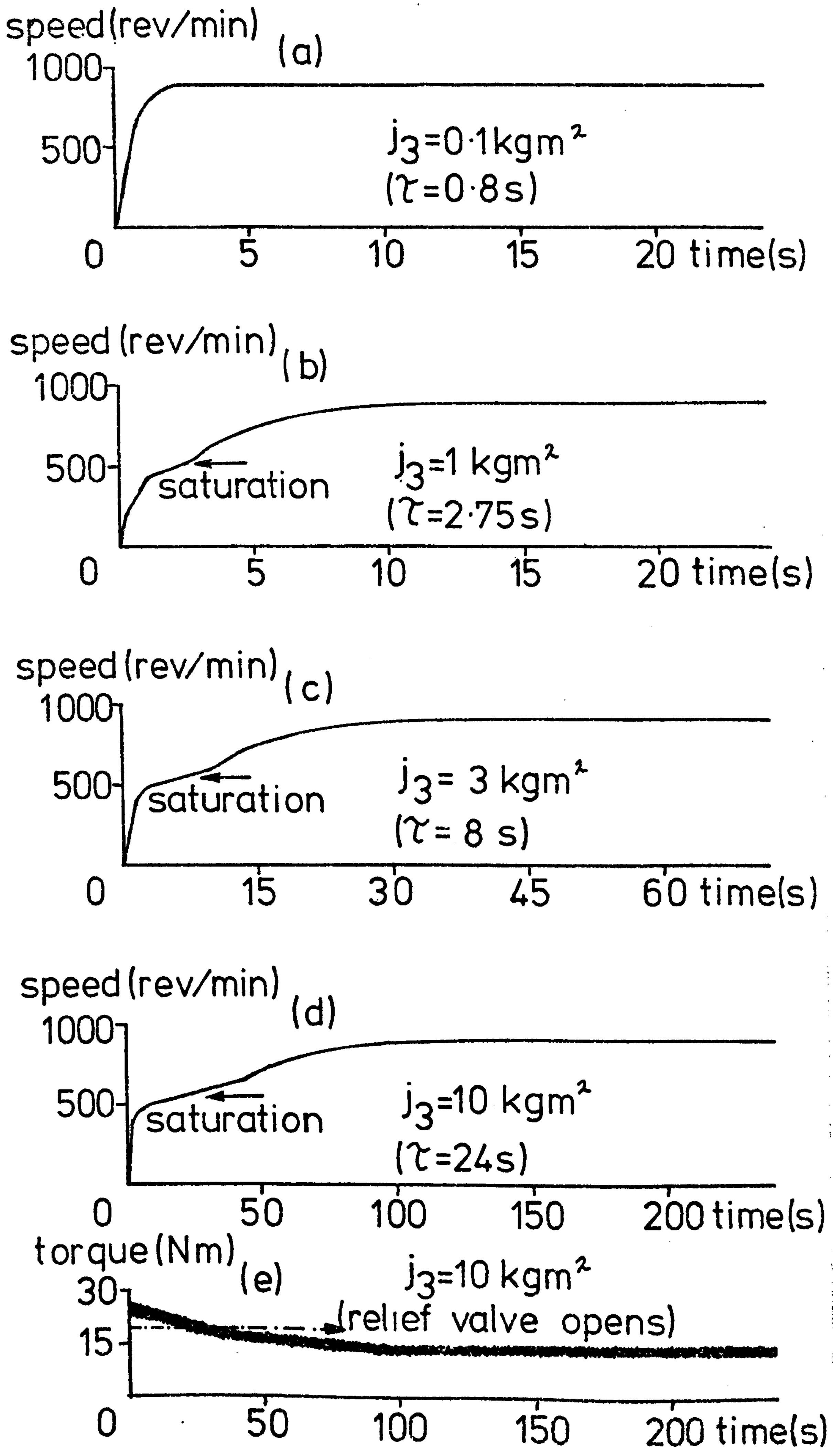
speed(rev/min)
(a)
1000
500
0
$j_3=0{\cdot}1\,kgm^2$
$(\tau=0{\cdot}8\,s)$
5
10
15
20 time(s)
speed (rev/min)
(b)
1000
500
saturation
$j_3=1\,kgm^2$
$(\tau=2{\cdot}75\,s)$
0
5
10
15
20 time(s)
speed (rev/min)
(c)
1000
500
saturation
$j_3=3\,kgm^2$
$(\tau=8\,s)$
0
15
30
45
60 time(s)
speed (rev/min)
(d)
1000
500
saturation
$j_3=10\,kgm^2$
$(\tau=24s)$
0
50
100
150
200 time(s)
torque (Nm)
(e)
$j_3=10\,kgm^2$
30
15
(relief valve opens)
0
50
100
150
200 time(s)

(a) open loop response to sinuscidal swashplate control signal

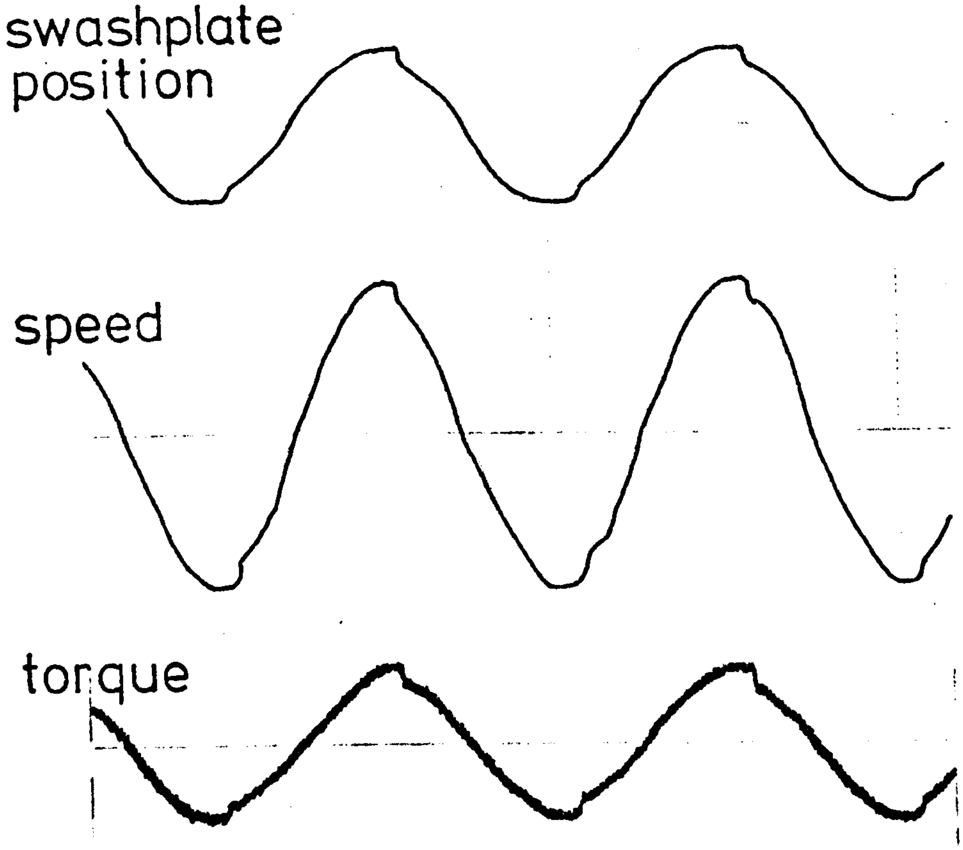

frequency = 0·03 hz
input signal = 1 volt pk–pk

(b) closed loop response to prime mover step input

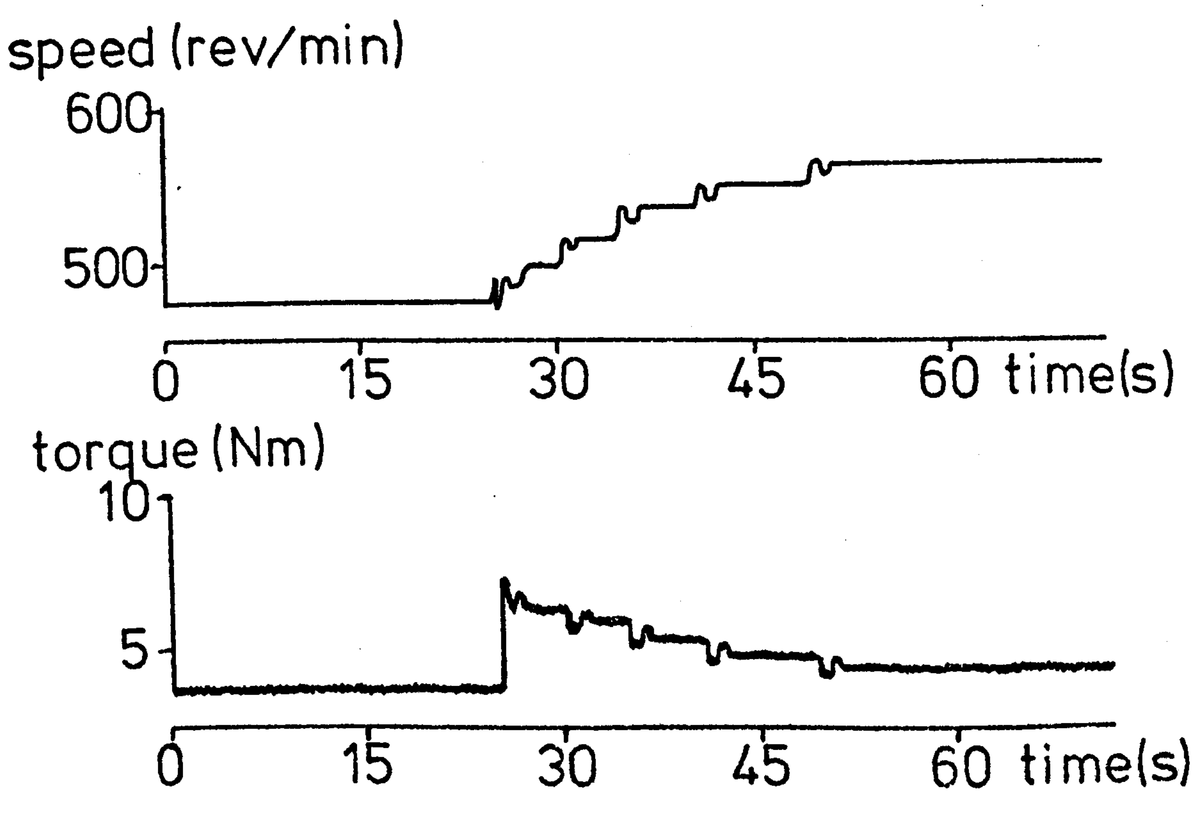

GRAPH G33

diesel engine+hydrostatic dynamometer
(no feedback)
speed range ÷ low → high

(a) loading

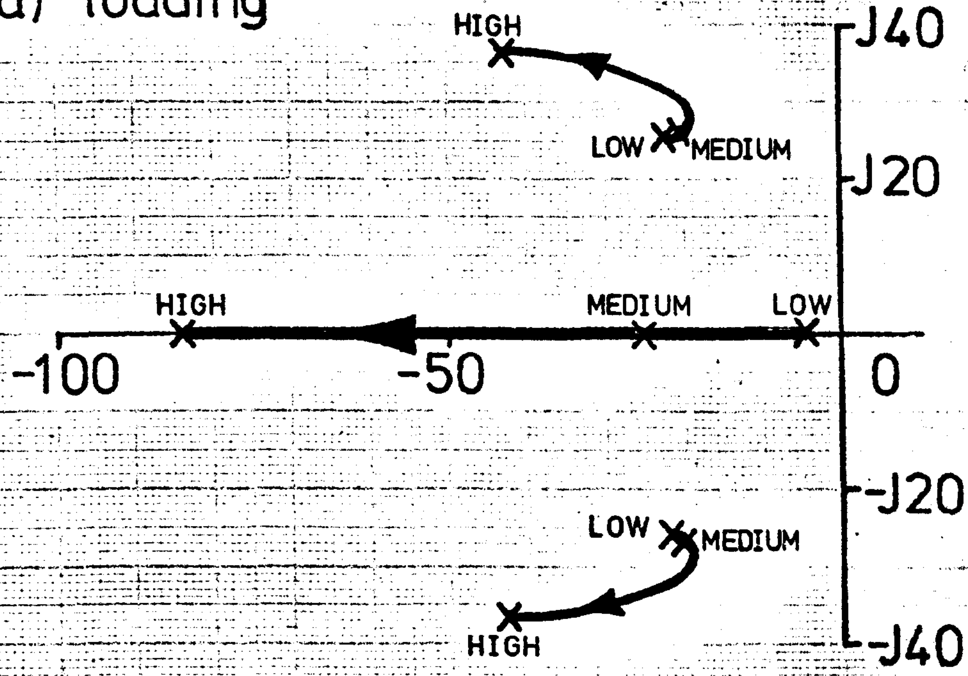

(b) motoring

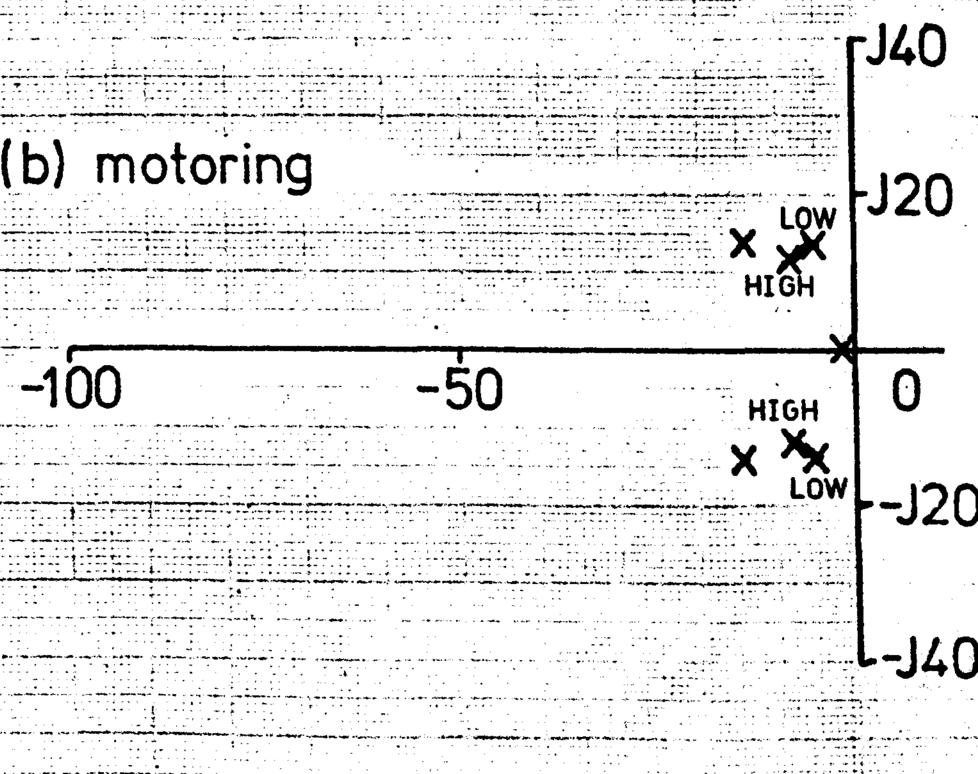

(increased leakage)

speed range ÷ low → high

(a) loading

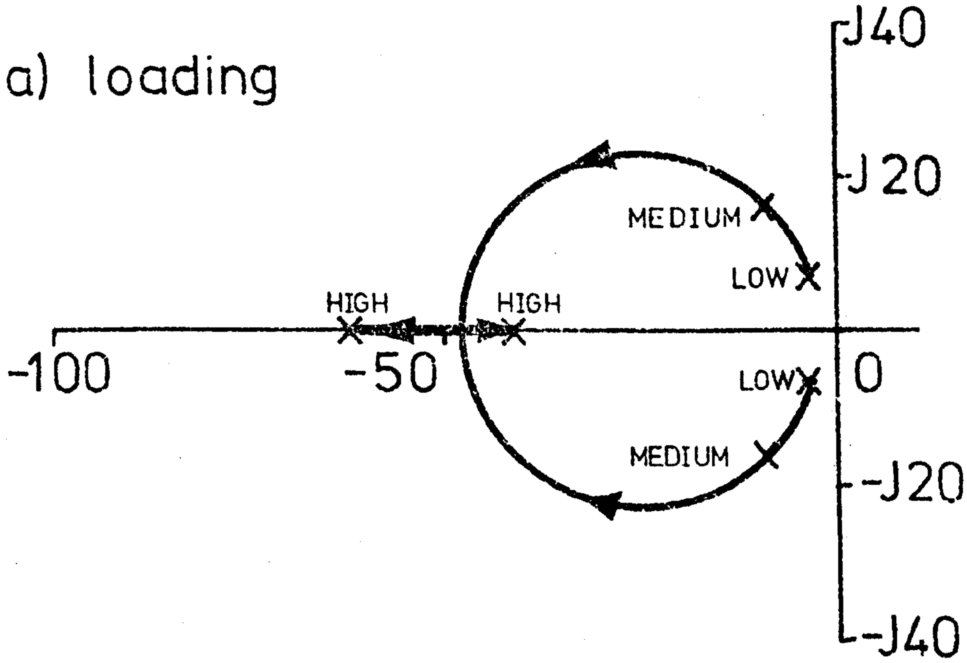

(b) motoring

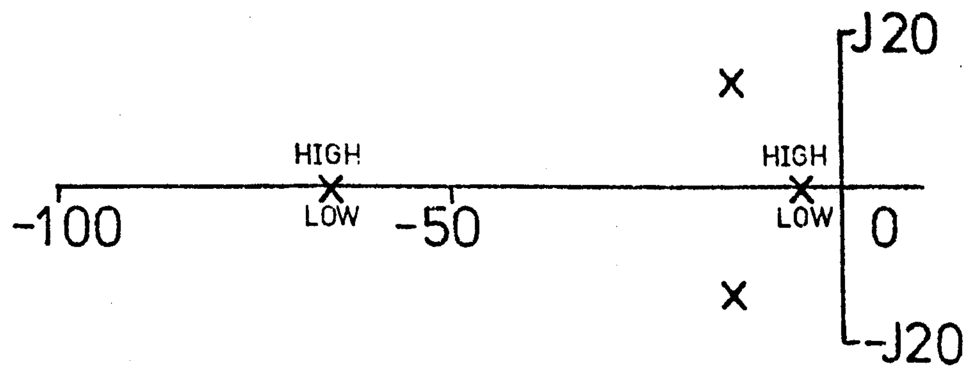

(c) loading (EXTRA LEAKAGE = 0·03 LITRES/MIN/BAR)

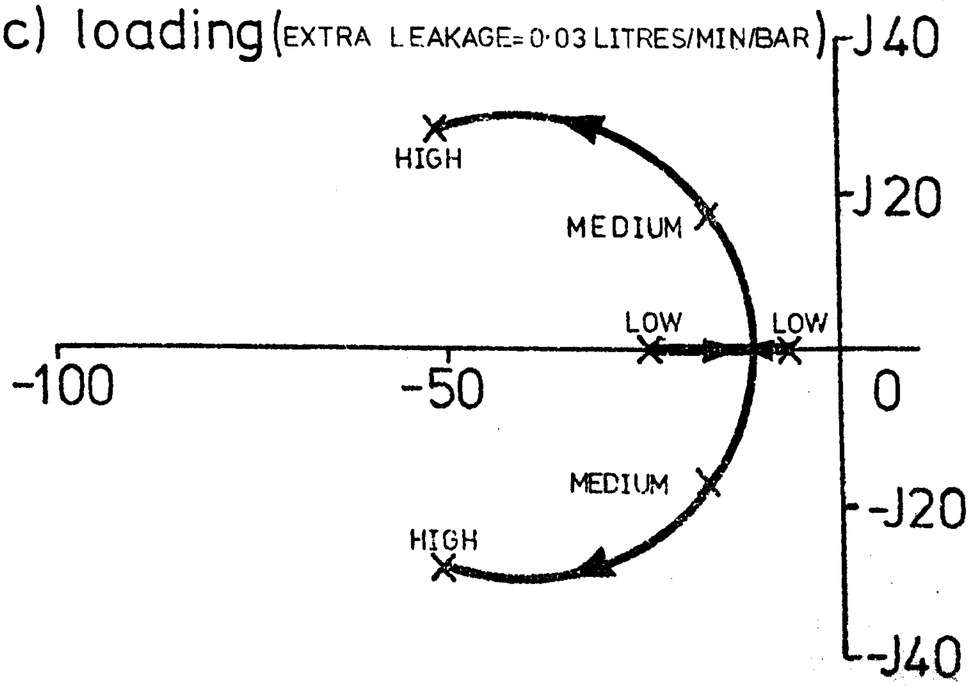

DIESEL ENGINE
HYDROSTATIC DYNAMOMETER

GRAPH G35

method 1.1

torque control signal gain,
b = 0 ⟶ 10 v/v

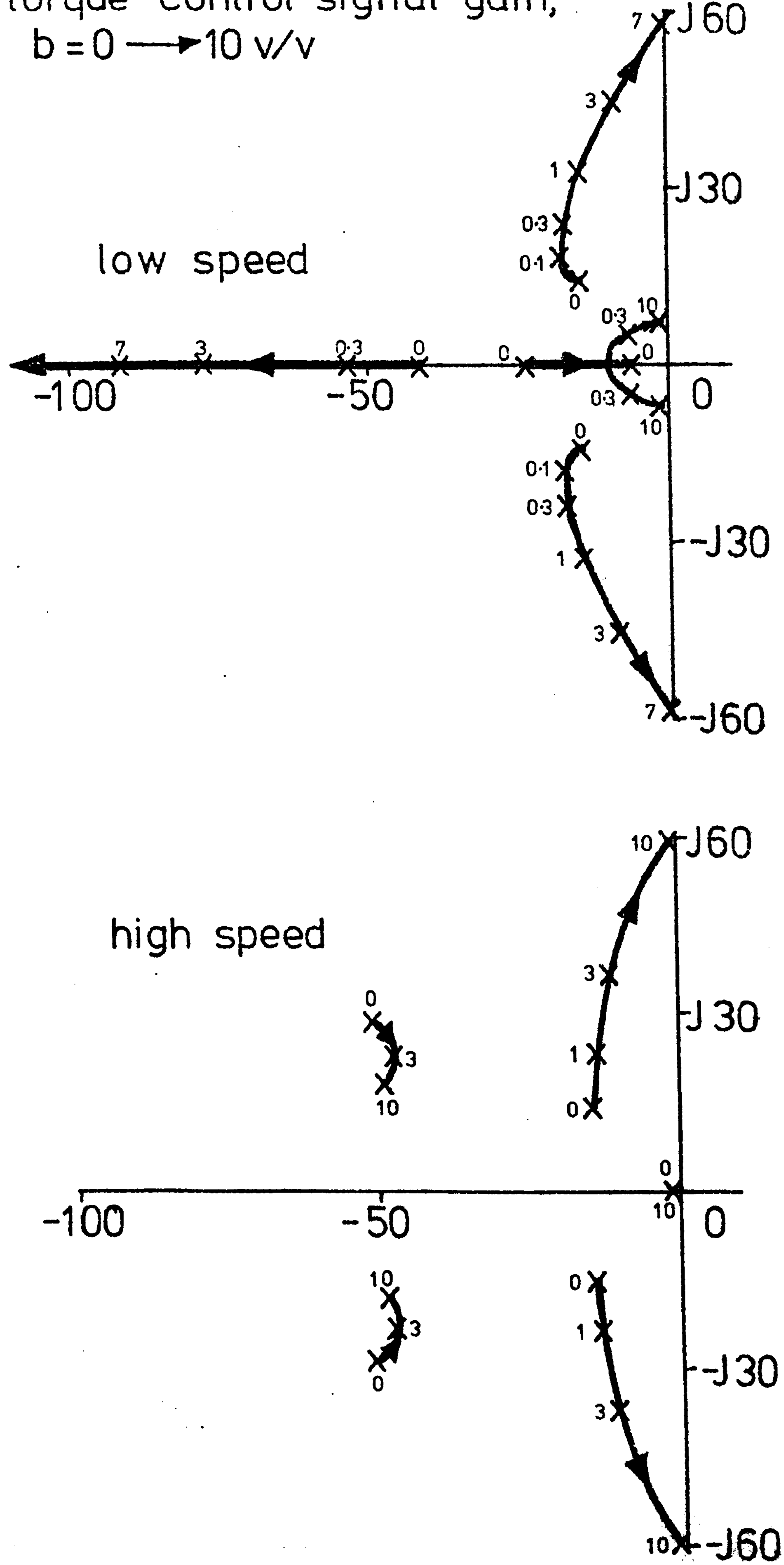

GRAPH G36

method 1.1

varying speed control gain, e
(torque control gain, b=0·3v/v)

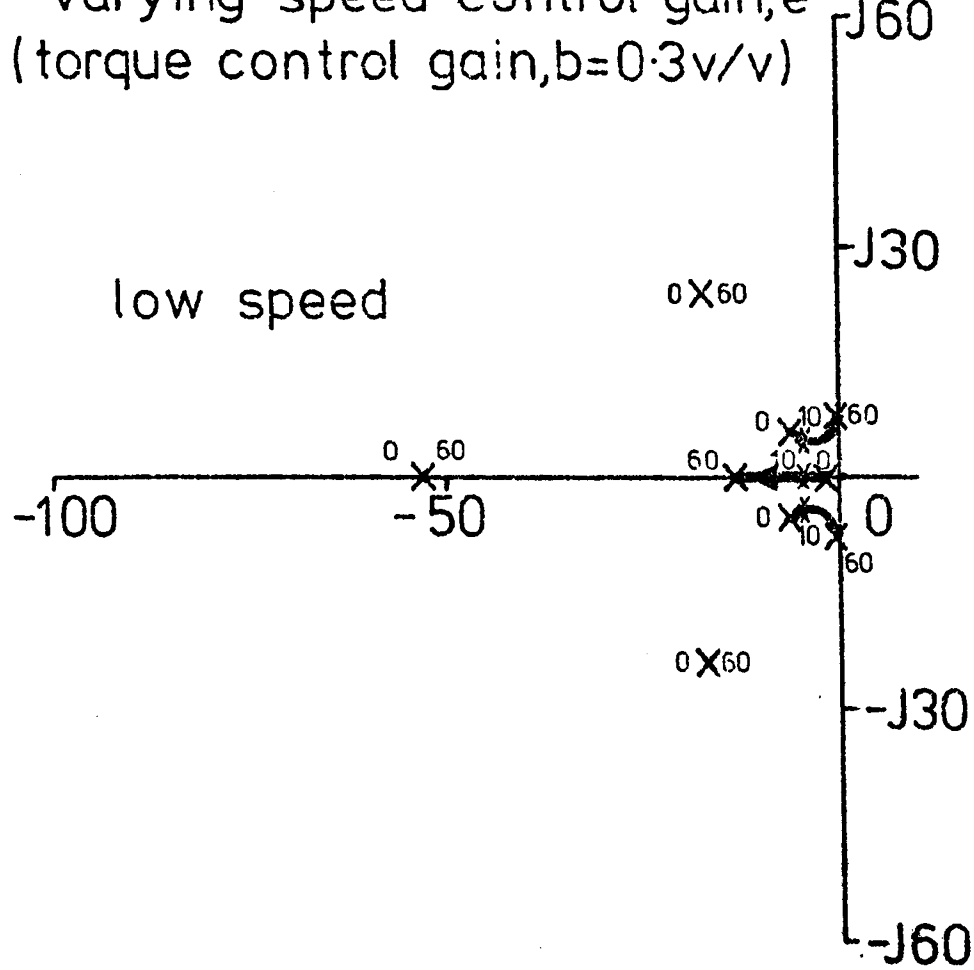

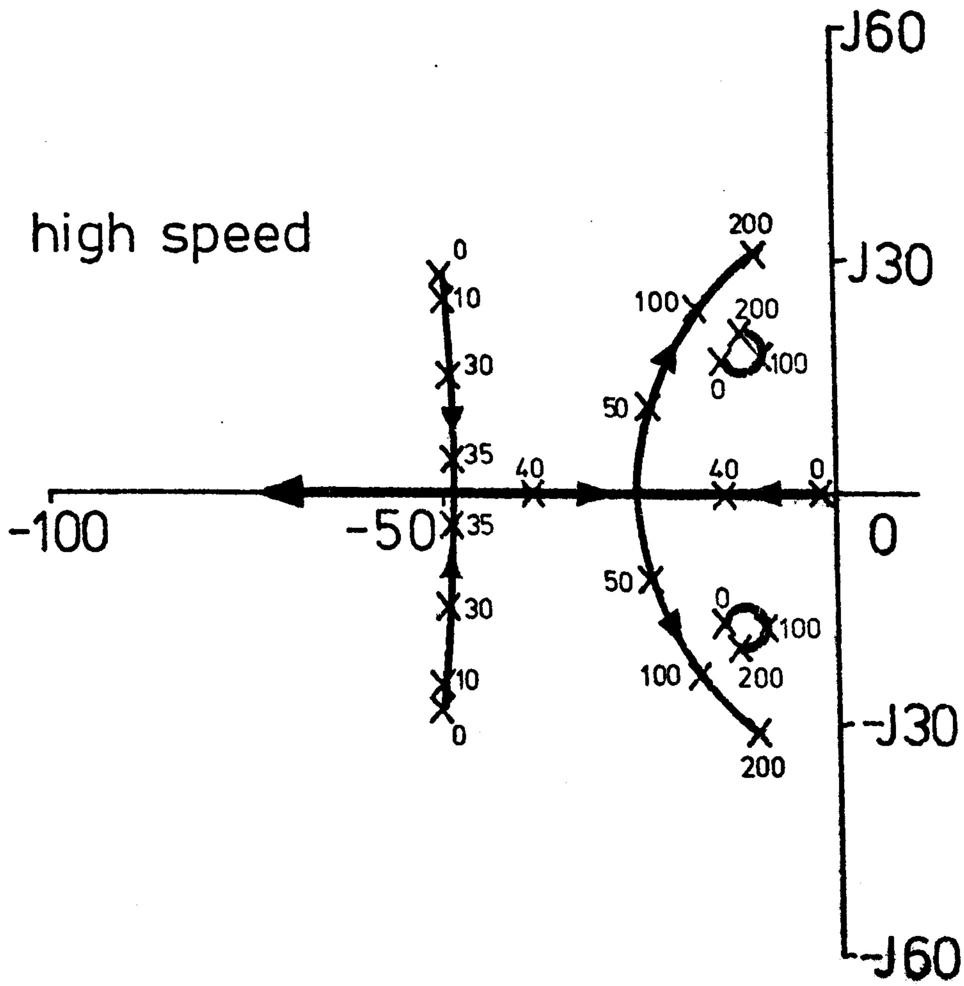

DIESEL ENGINE
HYDROSTATIC DYNAMOMETER

GRAPH G37

method 1.1

effect of integrator gain, c, on torque control signal

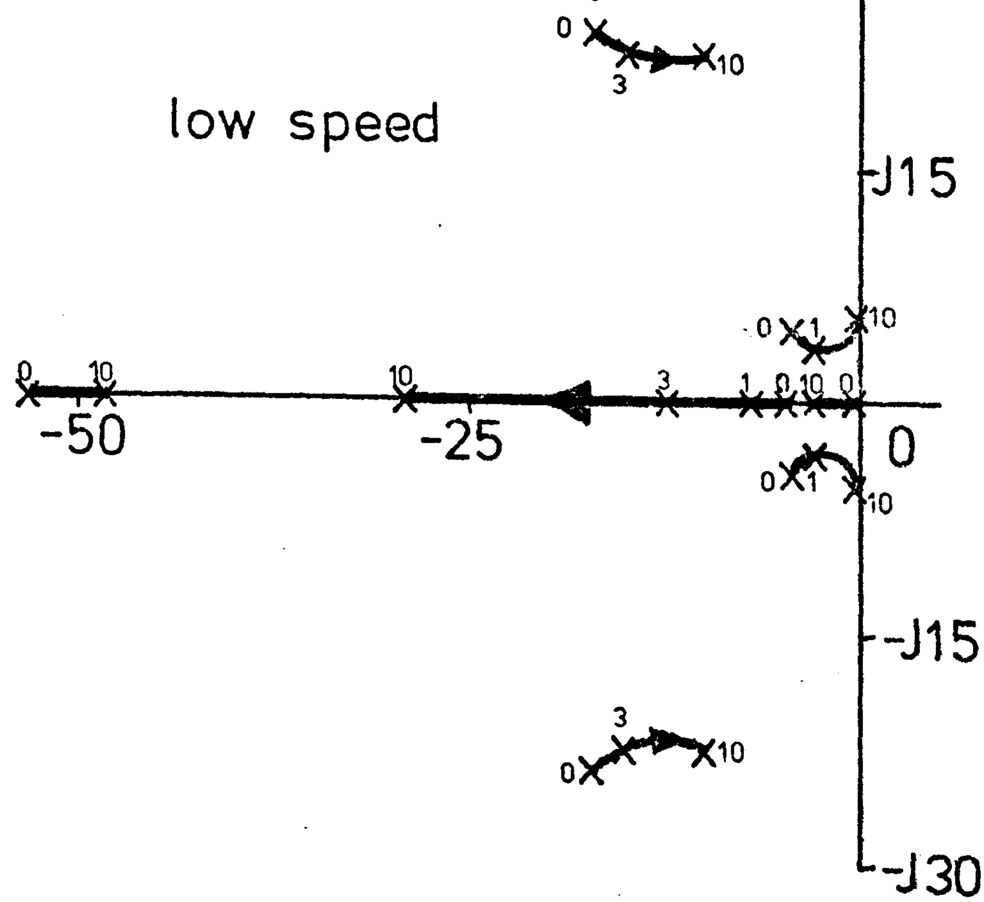

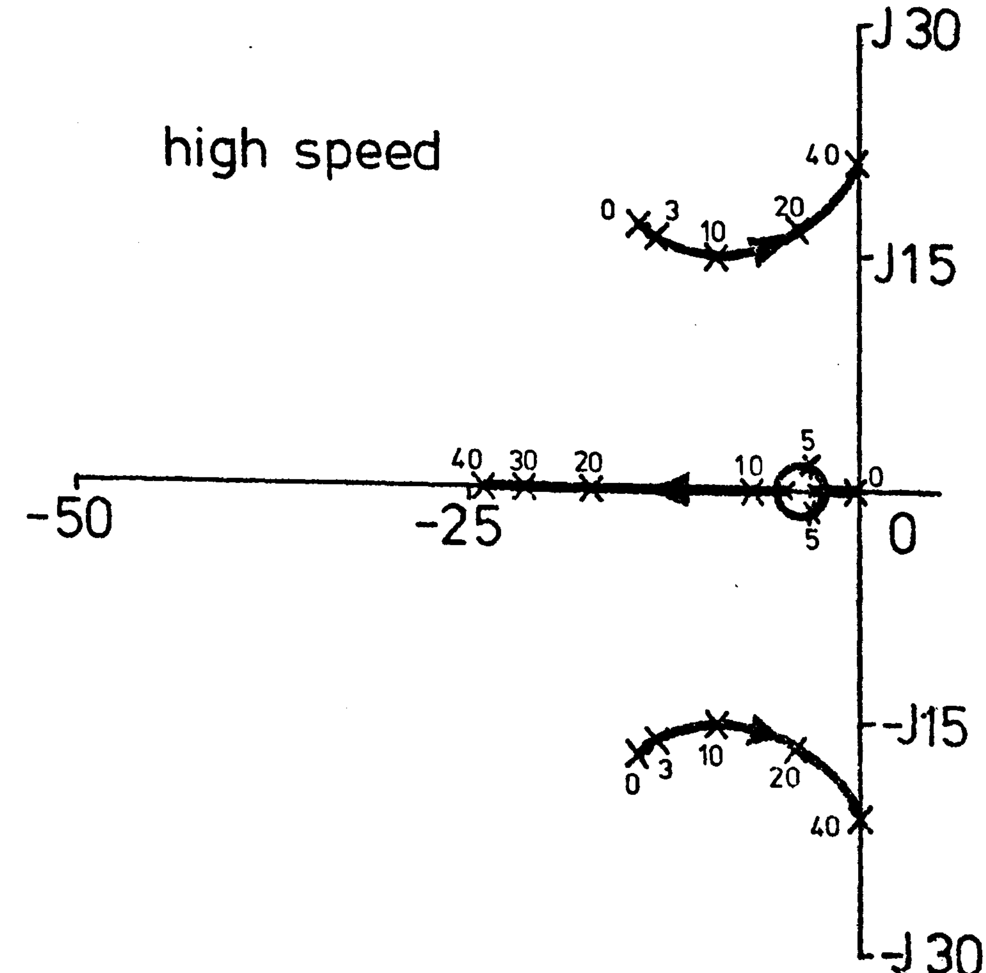

GRAPH G38

method 1.1

effect of integrator gain, f, on speed control signal

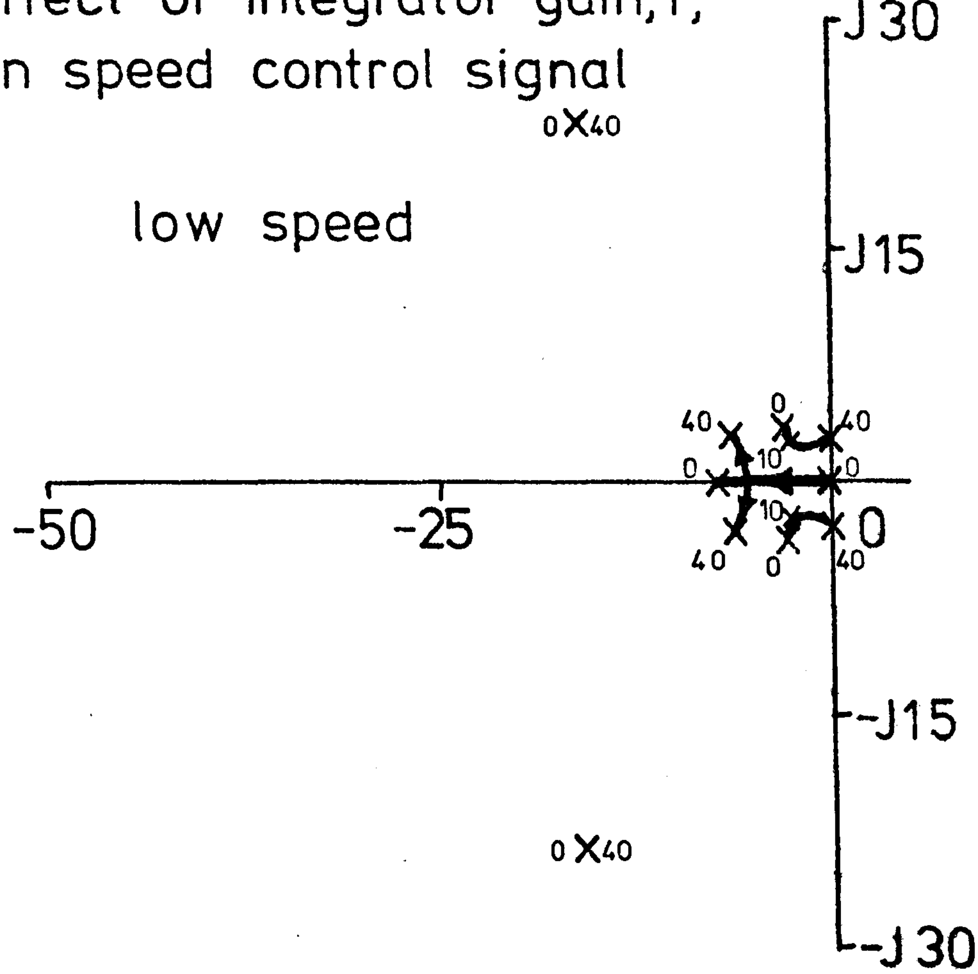

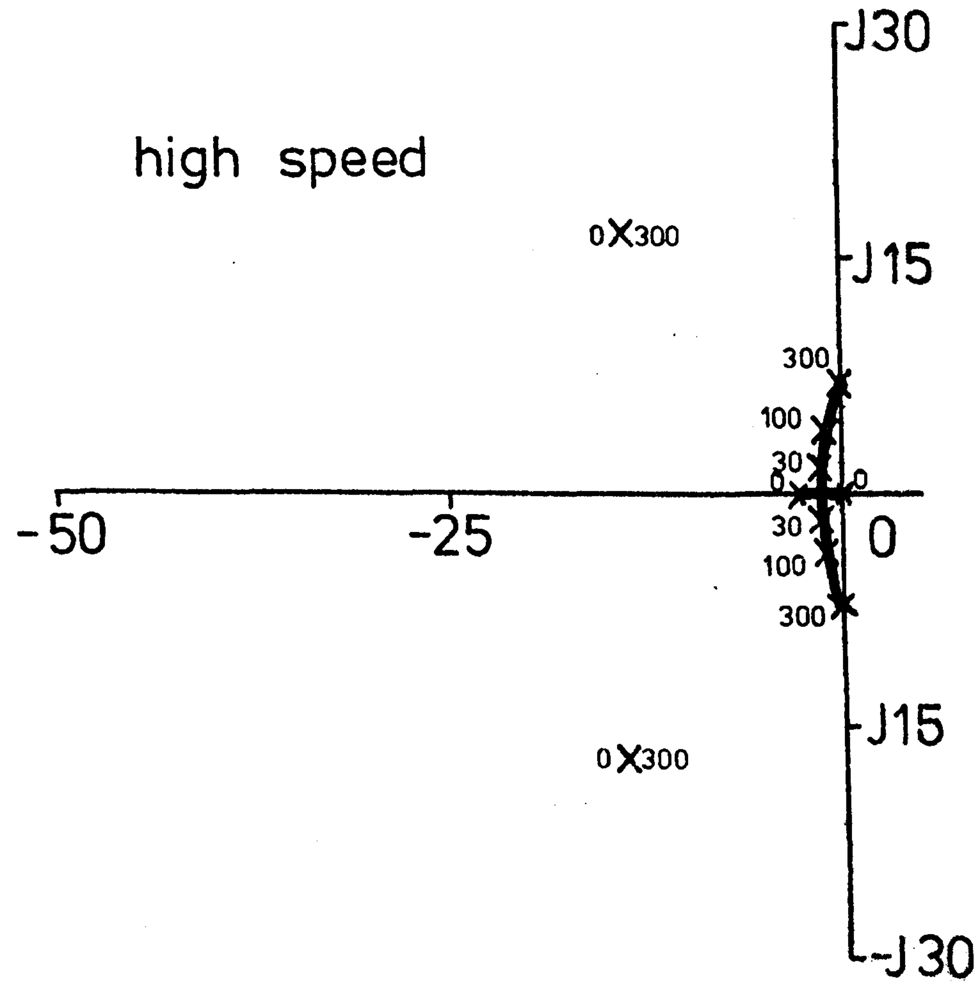

GRAPH G39

method 1.2
(low speed)

dynamometer input gain,
$b = 0 \longrightarrow 70$ v/v

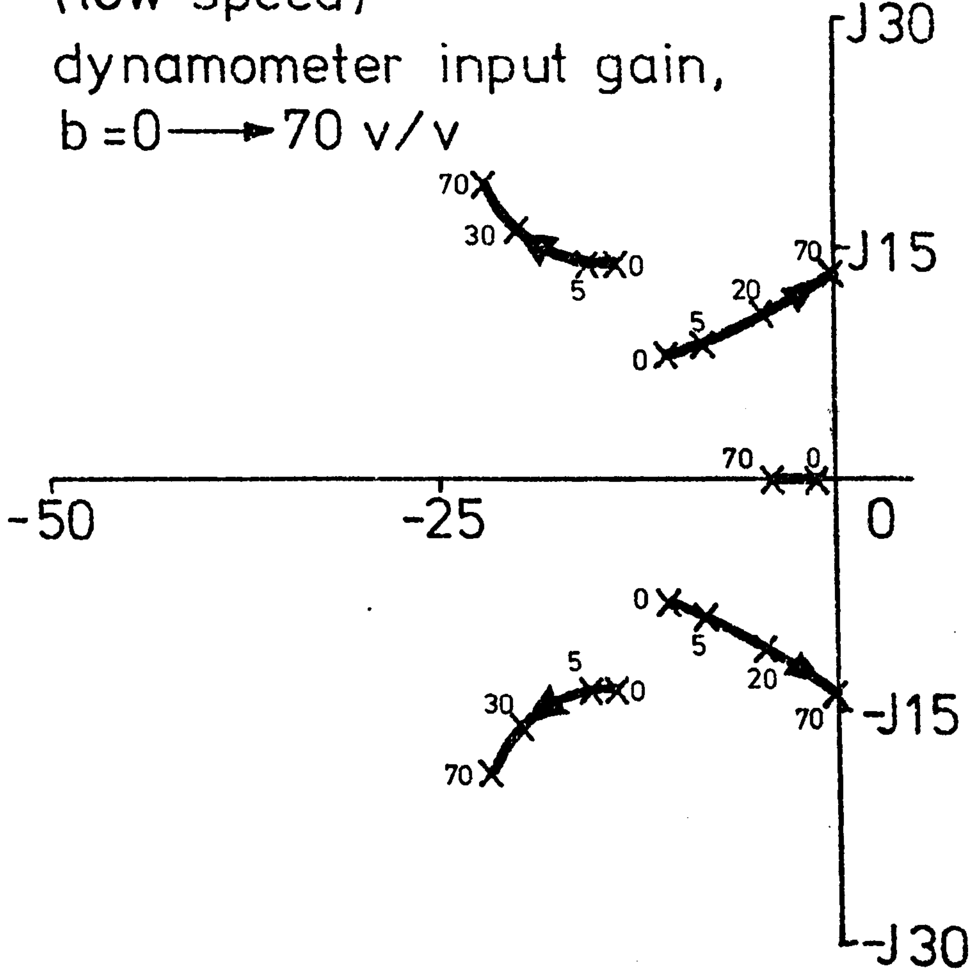

prime mover input gain,
$e = 0 \longrightarrow 3$ v/v

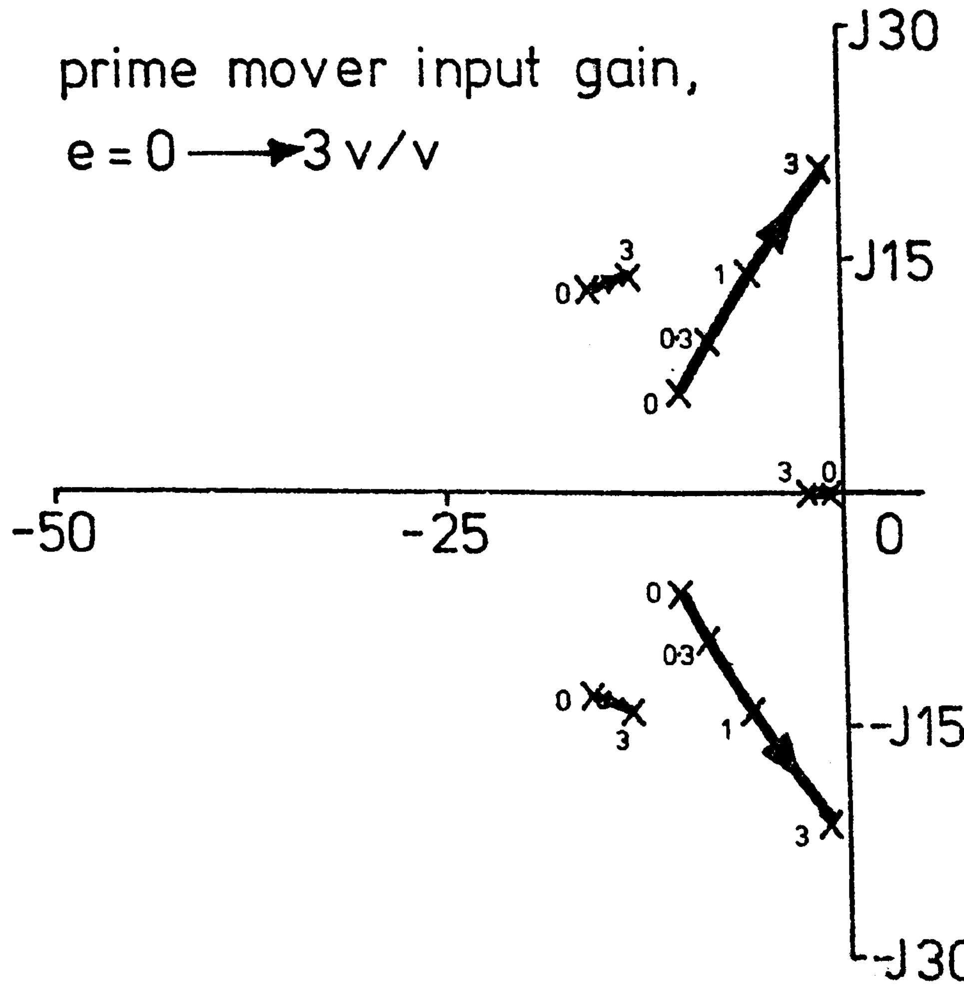

DIESEL ENGINE
HYDROSTATIC DYNAMOMETER

GRAPH G40

method 1.2 .

speed range ÷ low → high

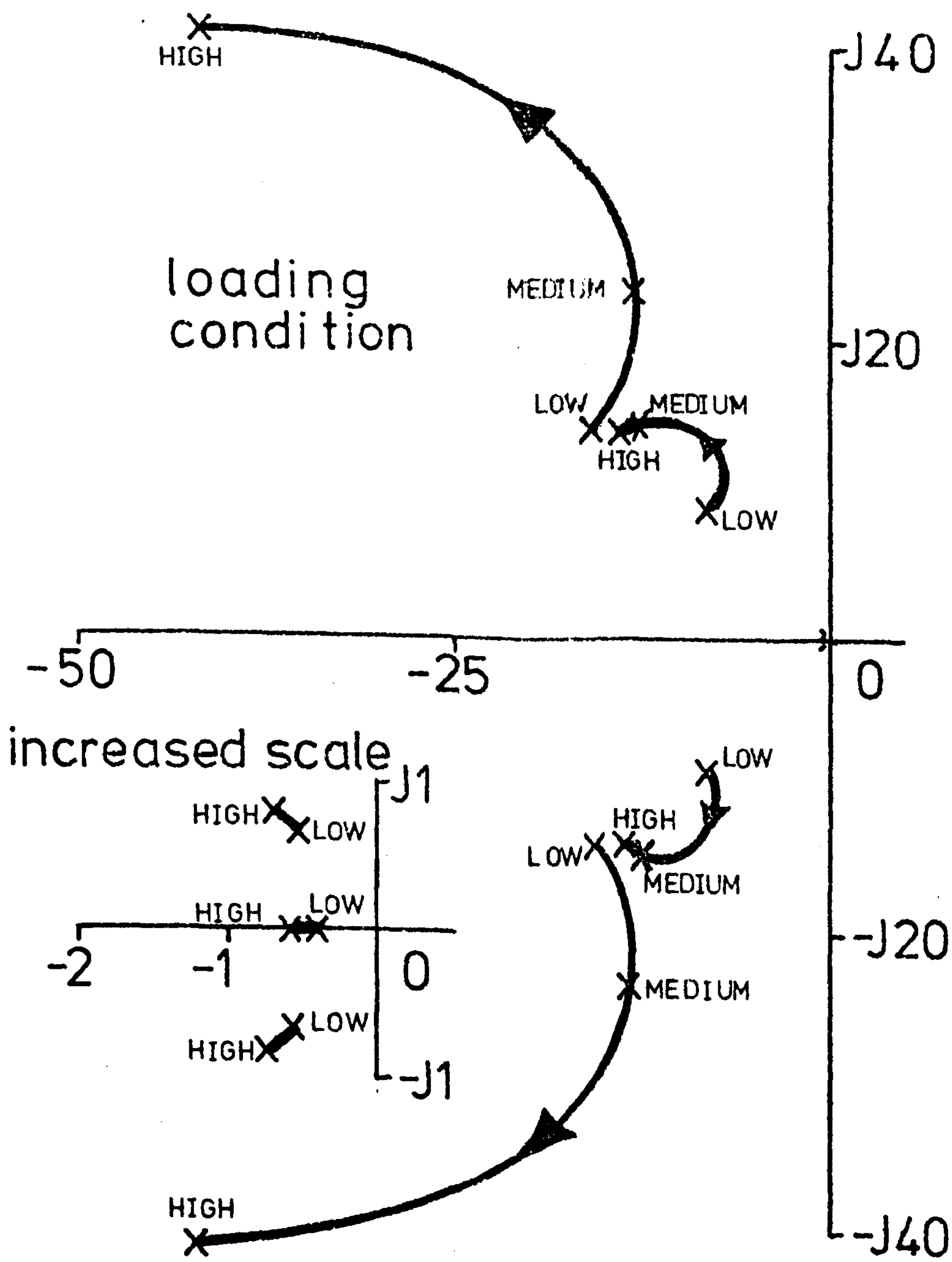

motoring condition

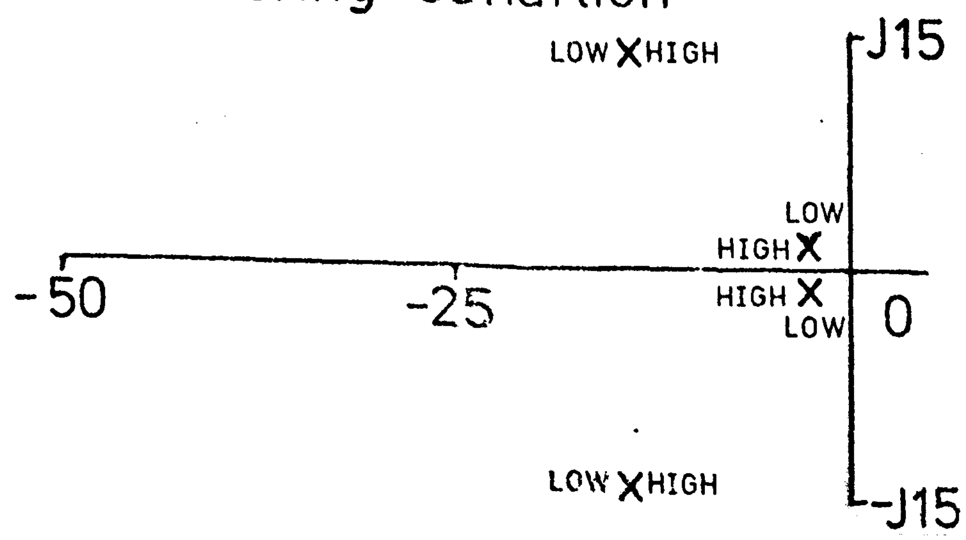

DIESEL ENGINE
HYDROSTATIC DYNAMOMETER

GRAPH G41

control rod at maximum
speed range ÷ low → high

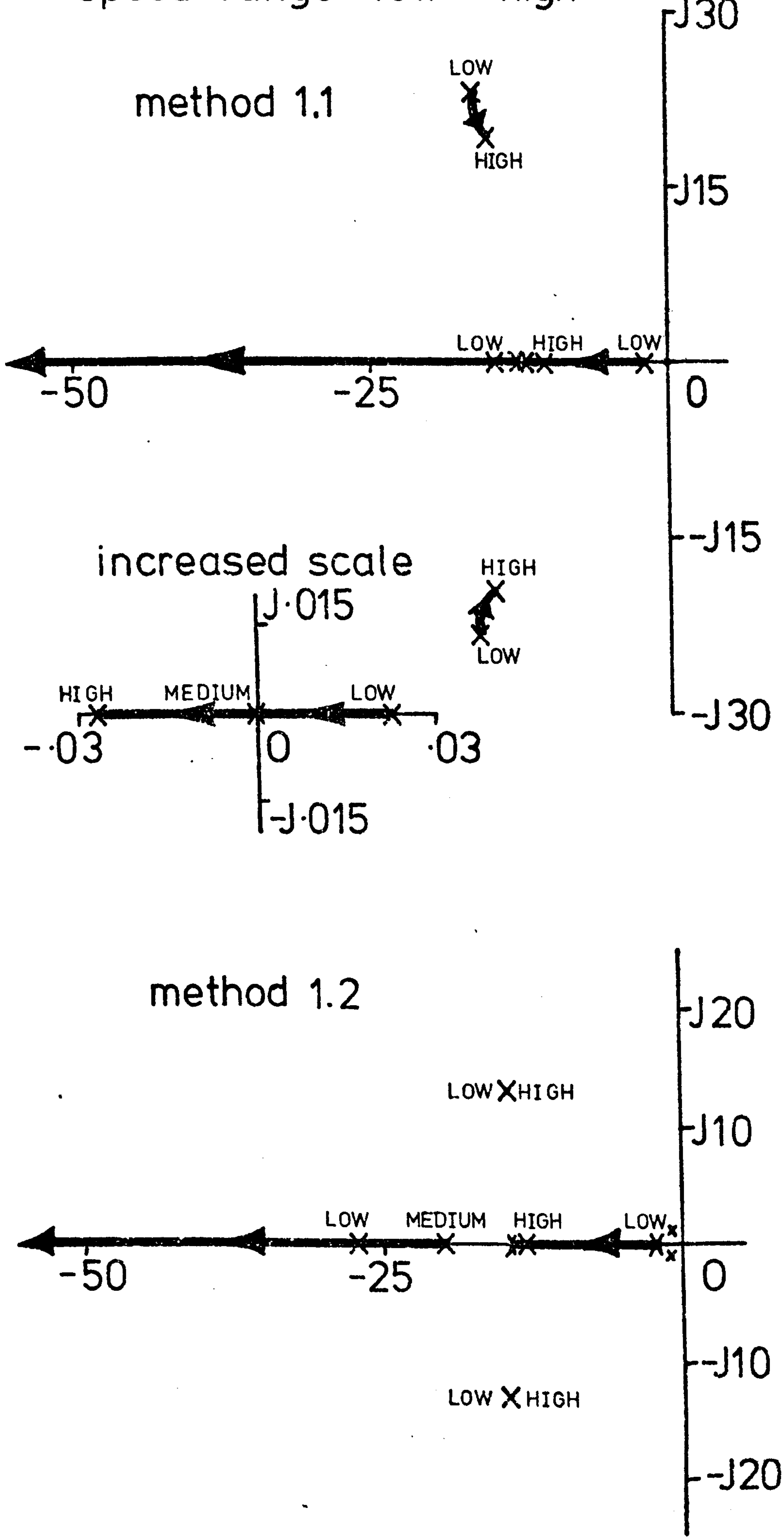

GRAPH G42

friction characteristics
(referred to engine shaft)
Ford A series truck

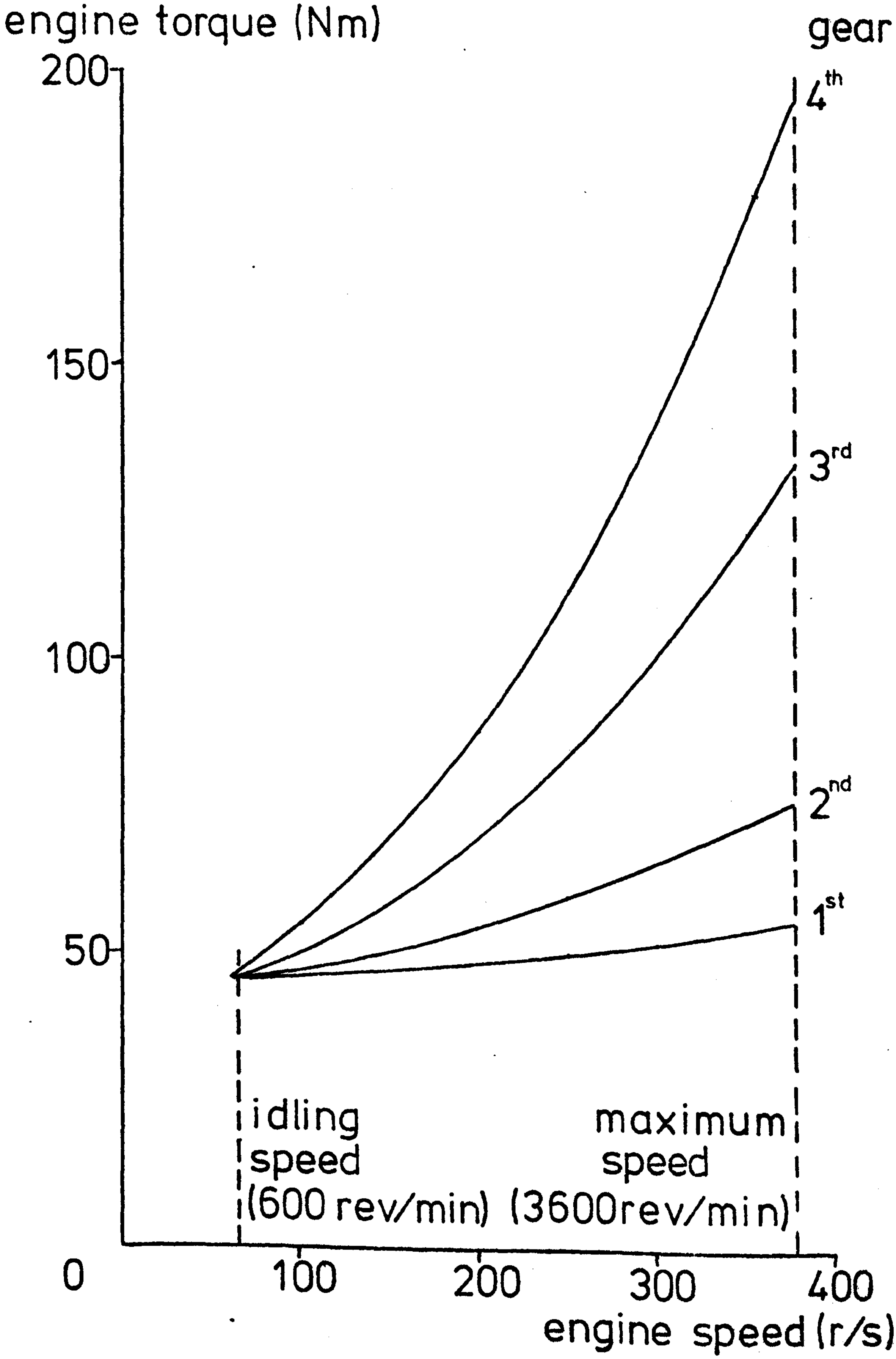

GRAPH G43

method 2.1

high speed 4^{th} gear.

maximum fuel delivery

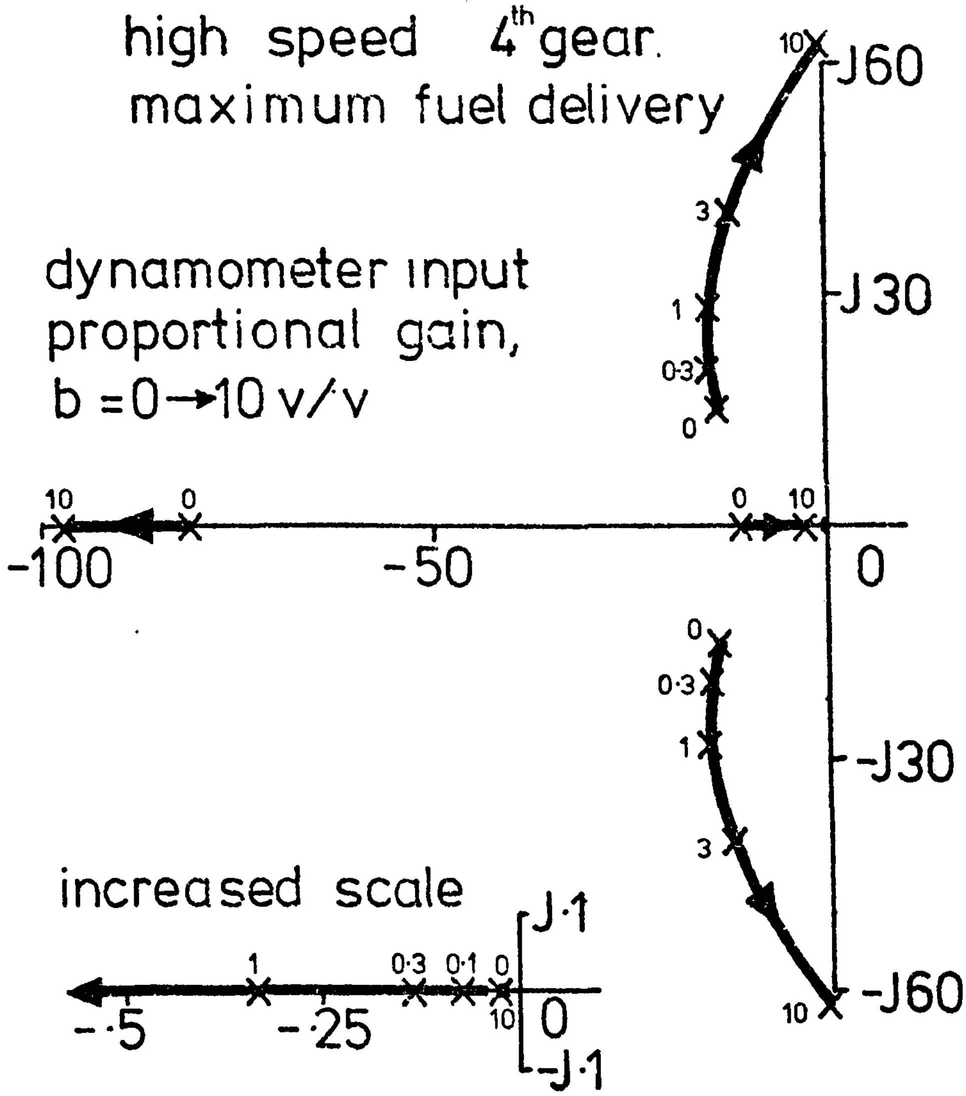

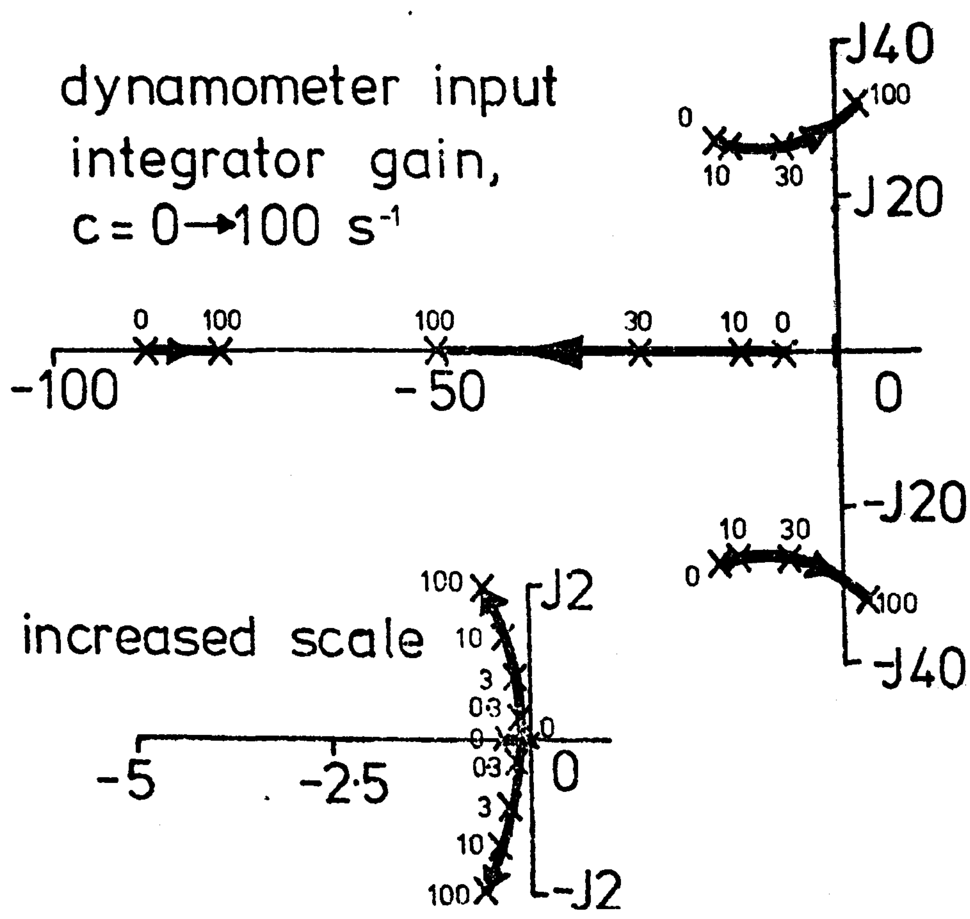

GRAPH G44

method 2.1

speed range ÷ low → high

(4th gear)

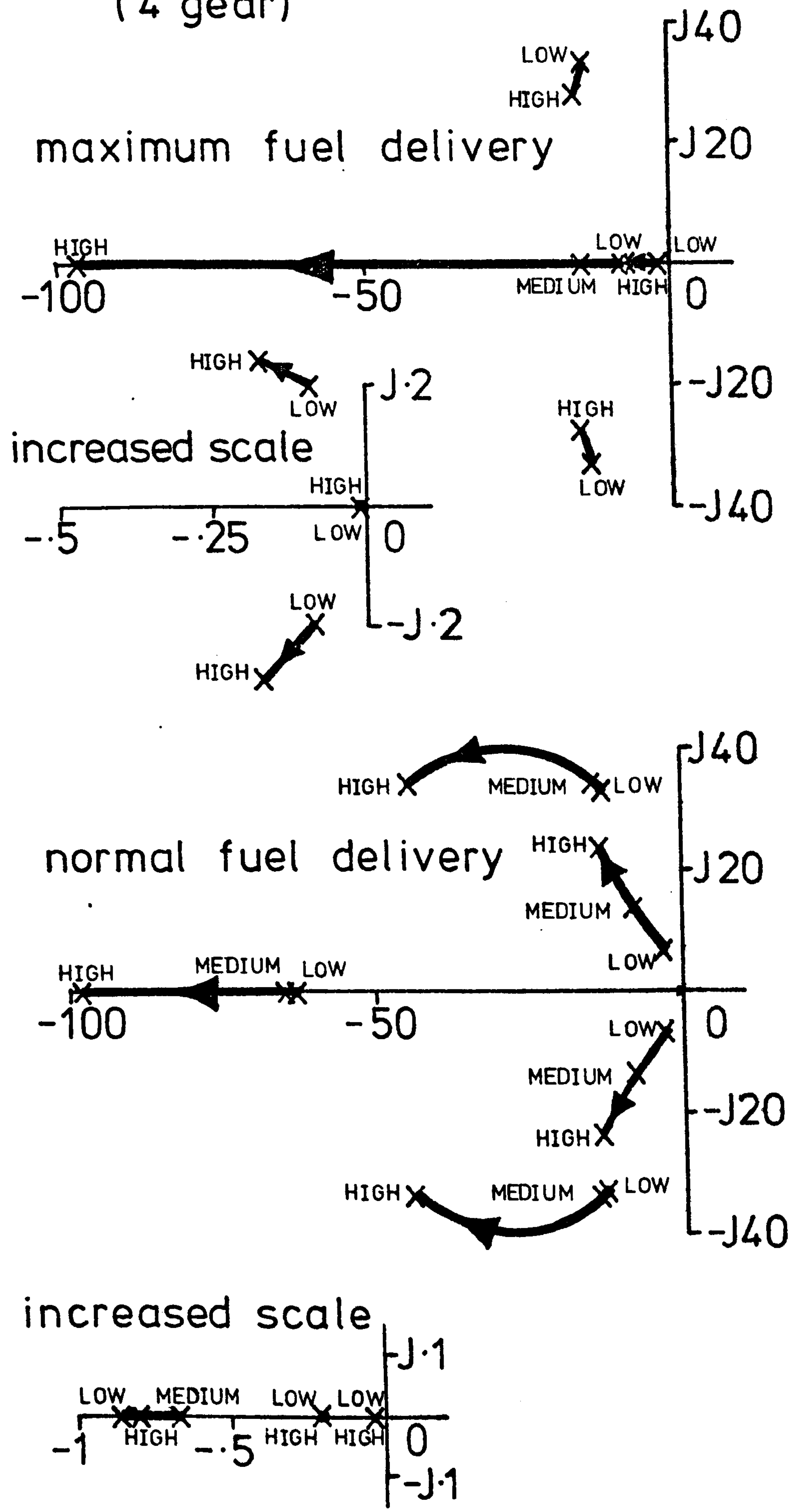

GRAPH G45

method 2.1
speed range ÷ low → high
(1st gear)

normal fuel delivery

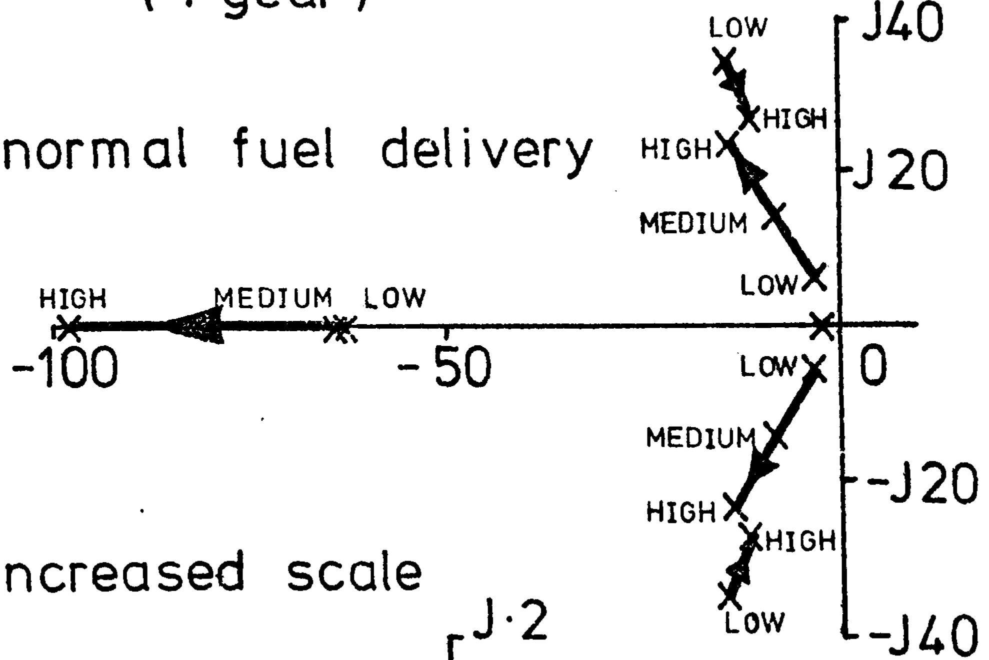

increased scale

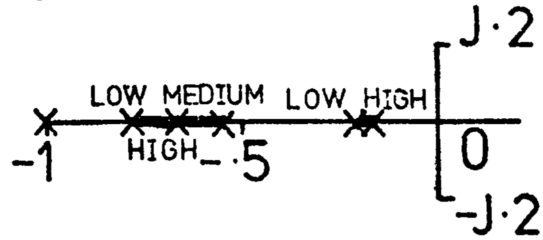

maximum fuel delivery

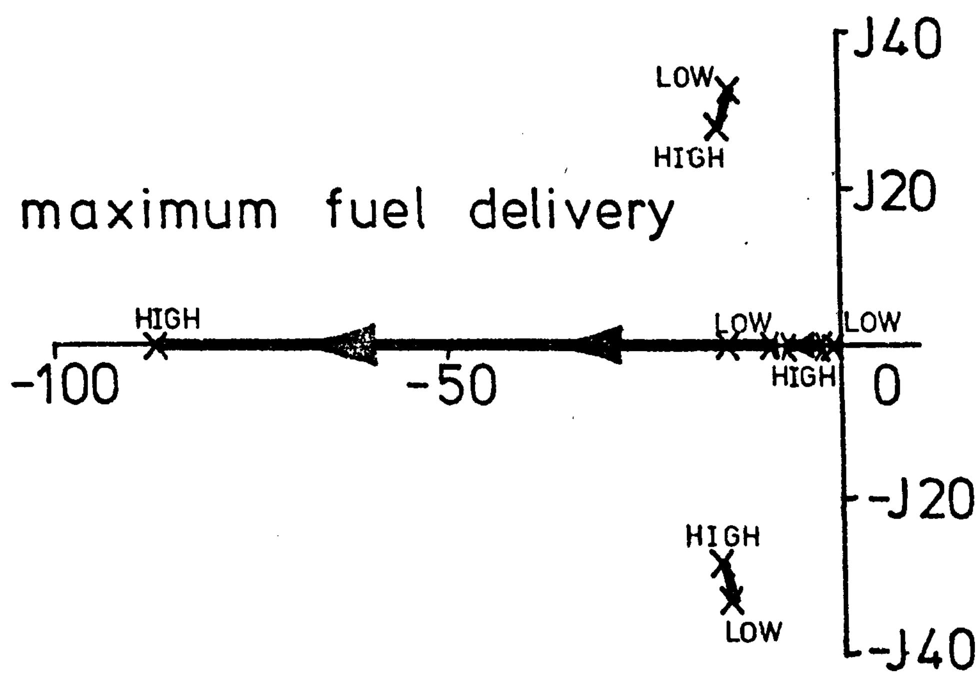

increased scale

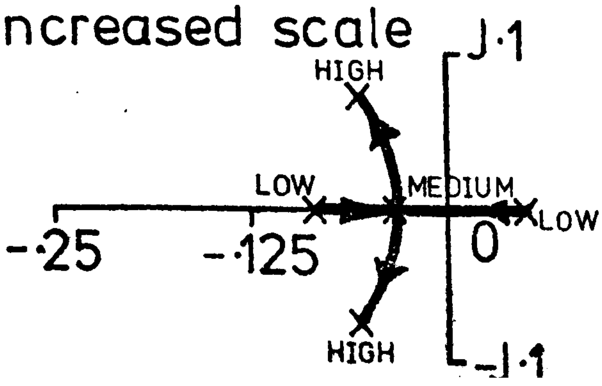

GRAPH G46

method 2.1
speed range ÷ low → high
(motoring)

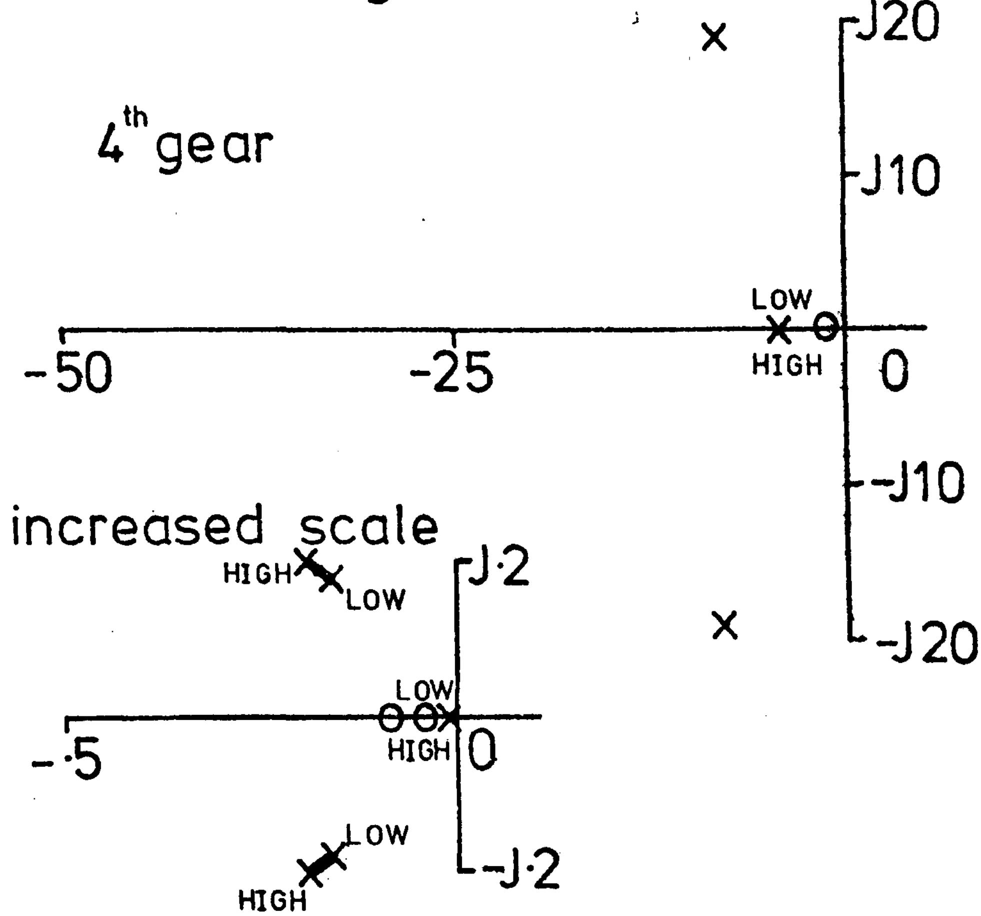

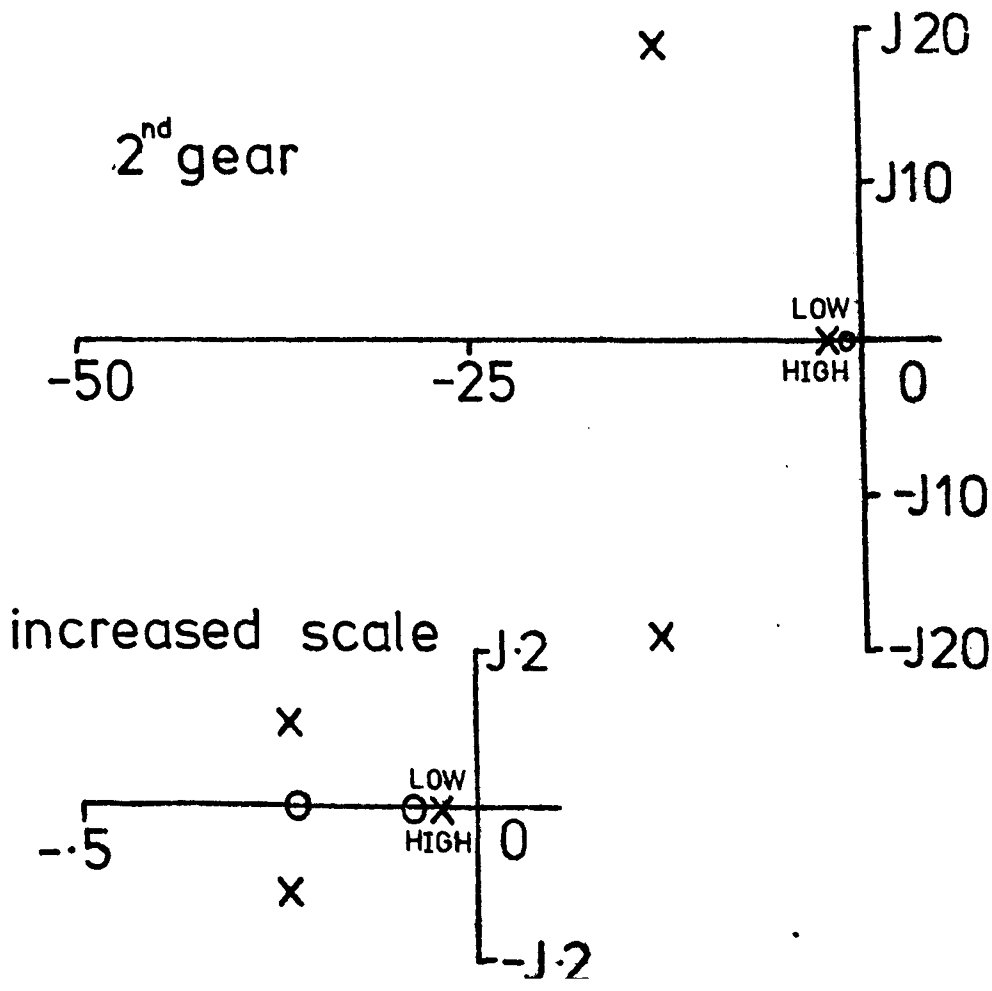

GRAPH G47

method 2.1

varying prime mover controller gains
(low speed; 4th gear; loading)

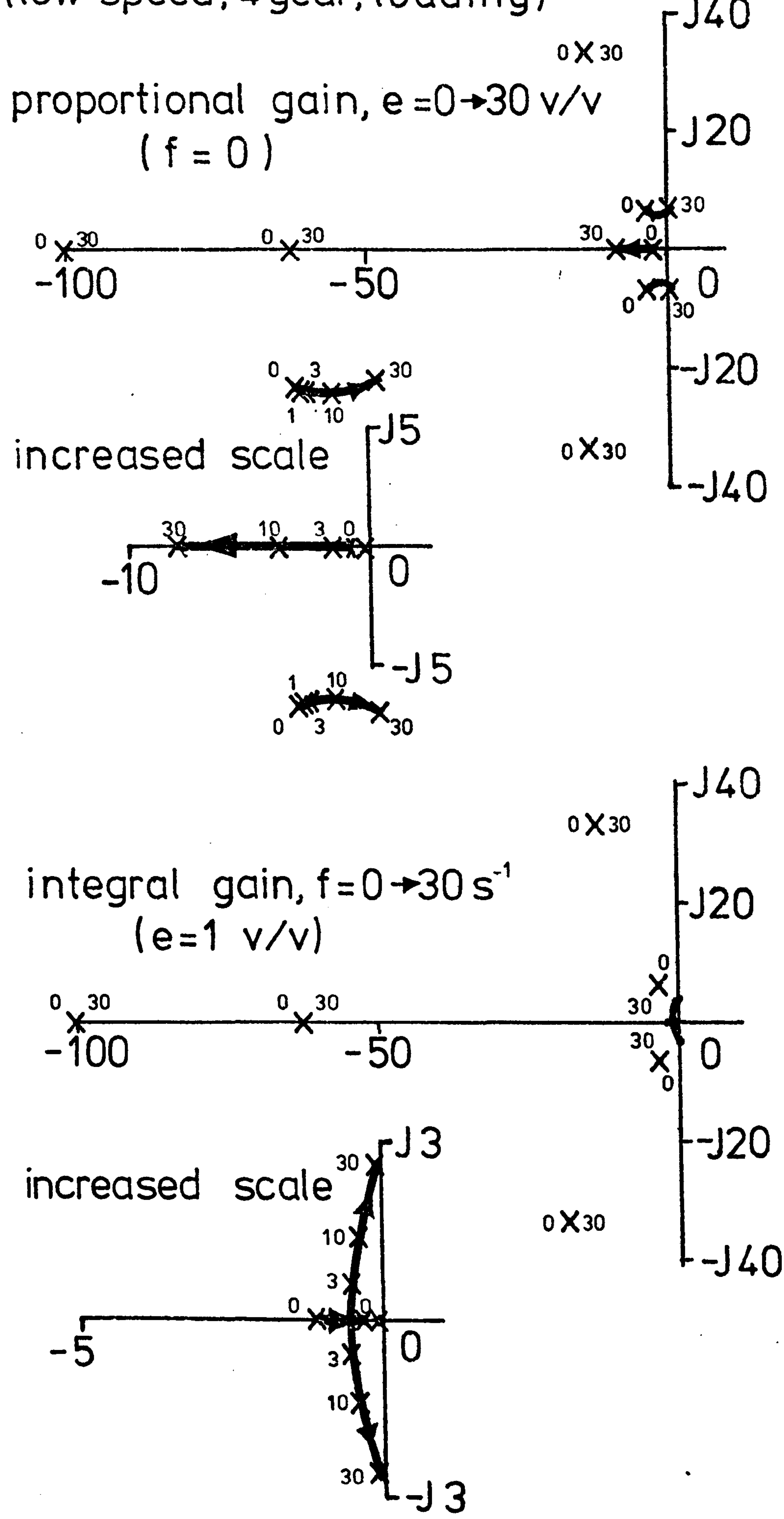

GRAPH G48

method 2.2

varying dynamometer controller gains
(high speed; 4th gear)
(maximum fuel delivery)

proportional gain, b=0→100 v/v
(c = 0)

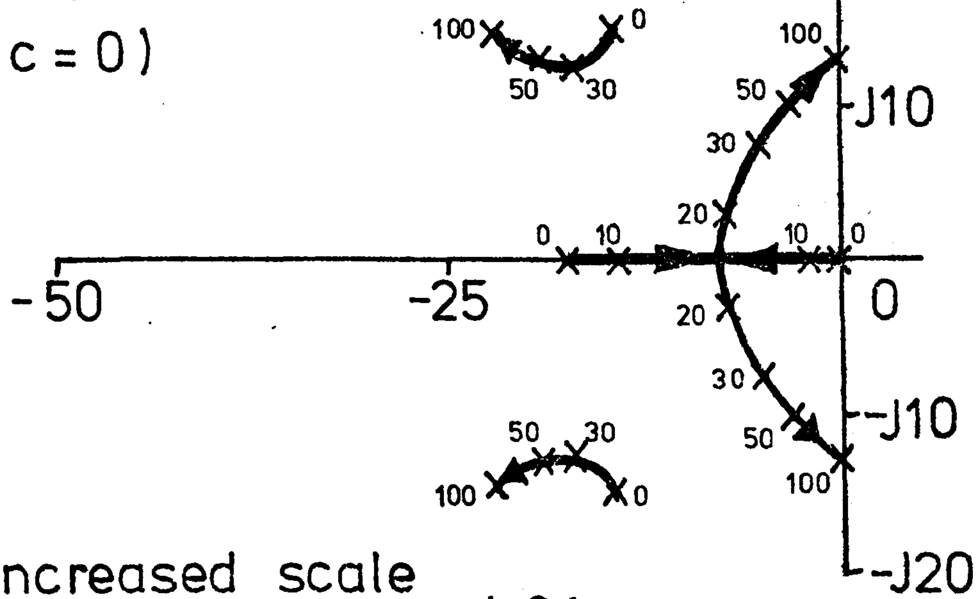

increased scale

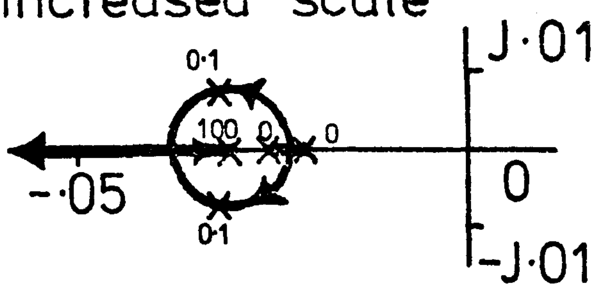

integral gain, c=0→150 s⁻¹
(b=20 v/v)

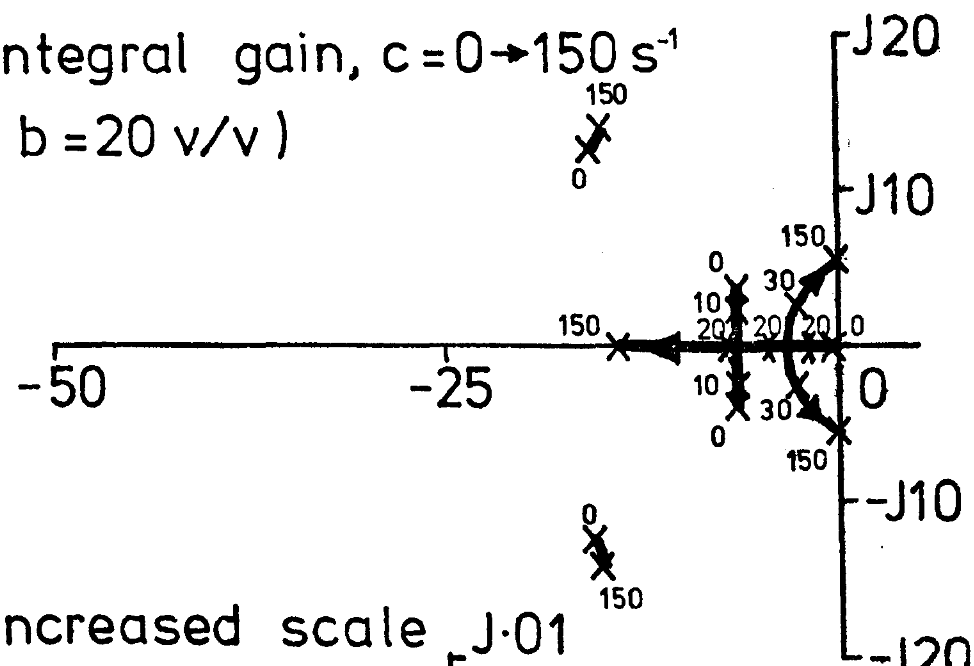

increased scale

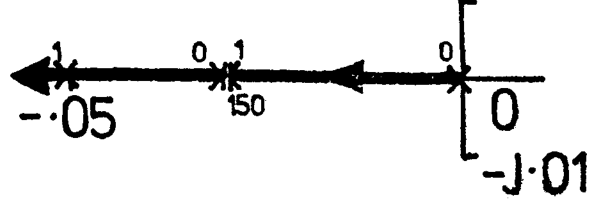

DIESEL ENGINE
HYDROSTATIC DYNAMOMETER

GRAPH G49

method 2.2

varying dynamometer controller gains
(low speed; 1st gear; fuel rod max.)

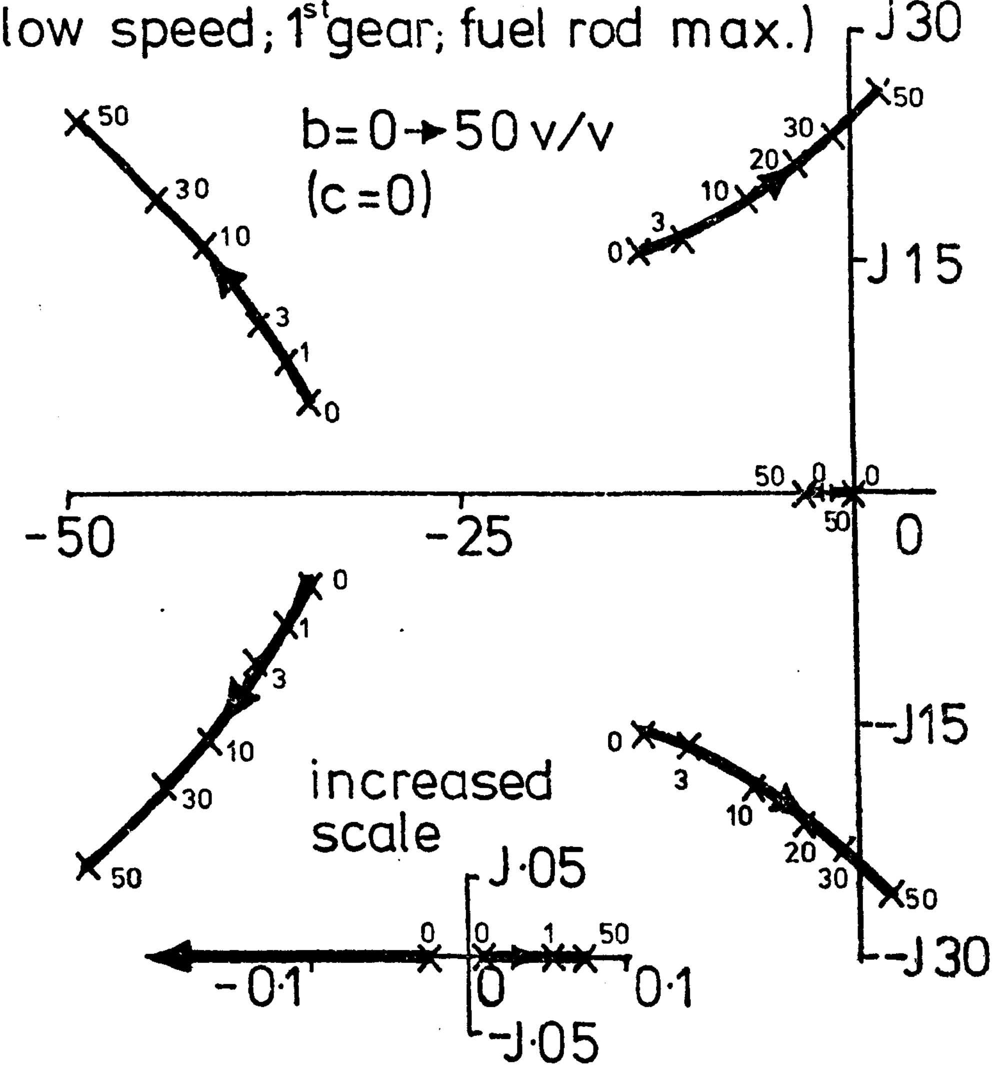

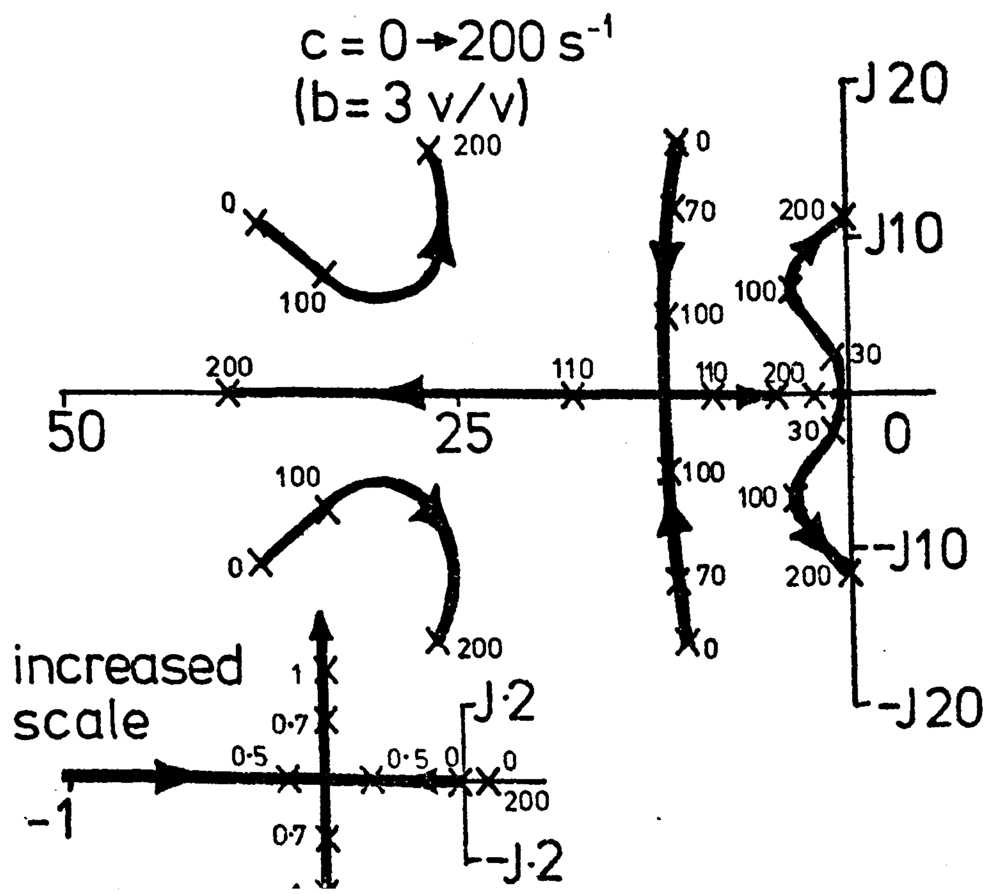

DIESEL ENGINE
HYDROSTATIC DYNAMOMETER

GRAPH G50

method 2.2
speed range ÷ low → high
(1^{st} gear)

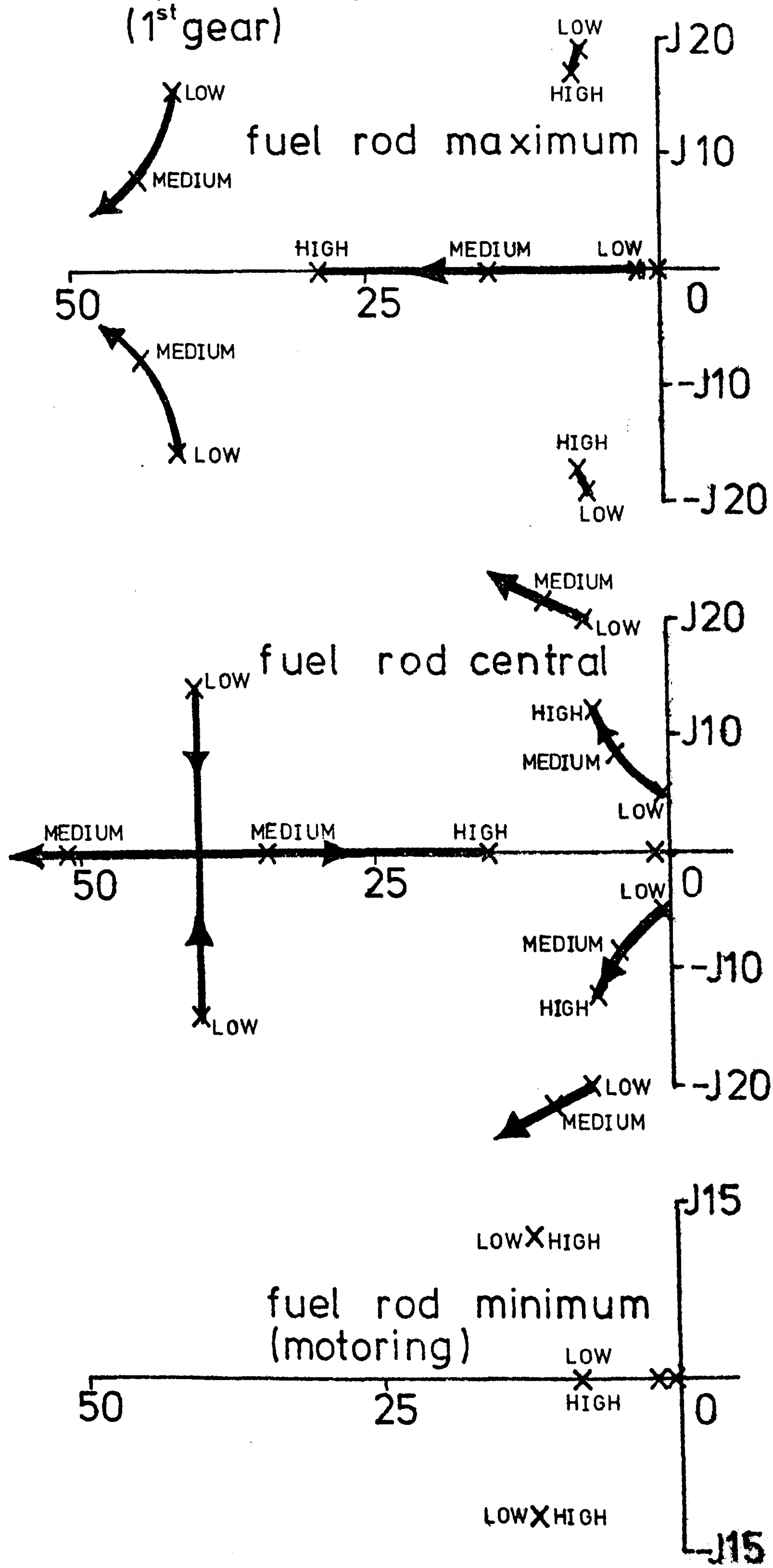

DIESEL ENGINE
HYDROSTATIC DYNAMOMETER

GRAPH G51

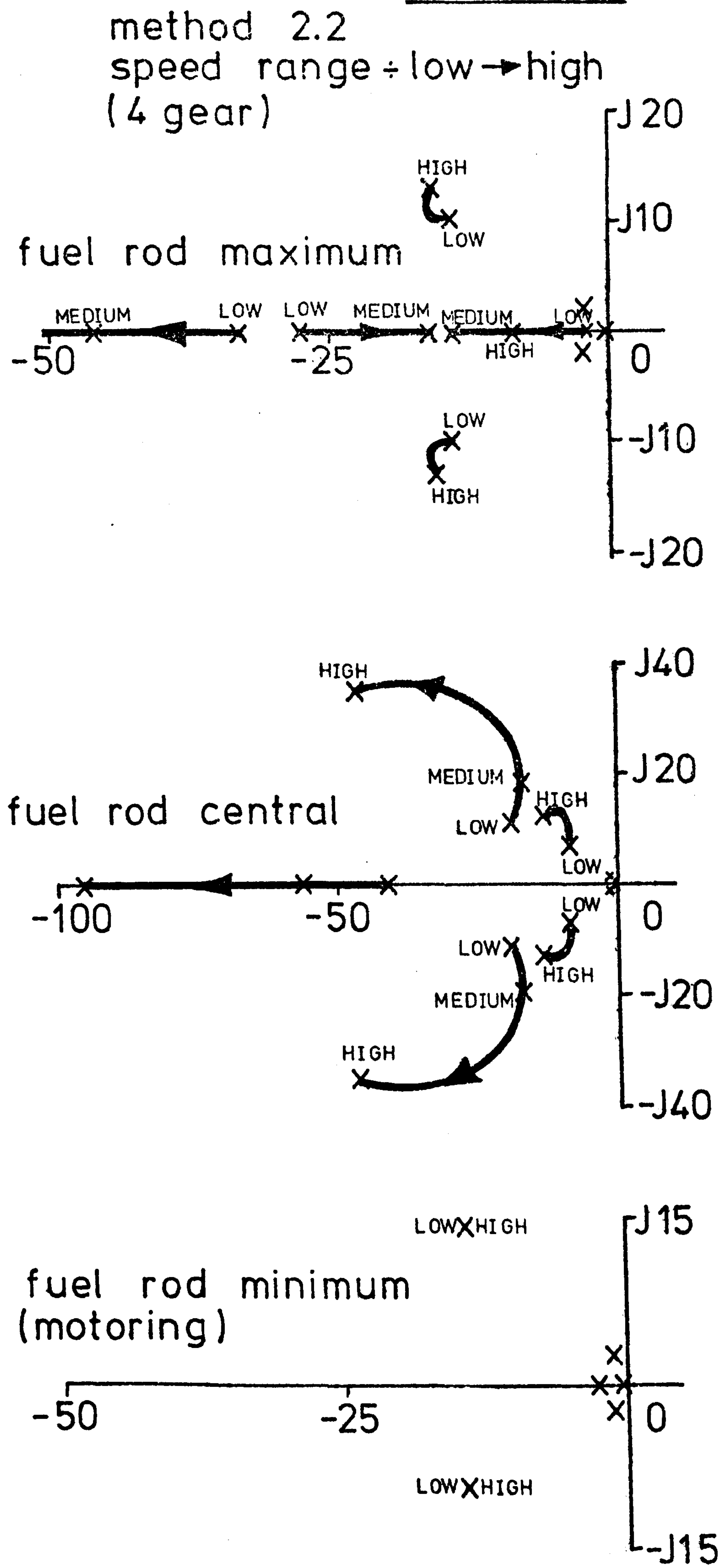

DIESEL ENGINE
HYDROSTATIC DYNAMOMETER

GRAPH G52

method 2.2
varying prime mover controller gains
(high speed; 4^{th} gear)
(normal fuel delivery)

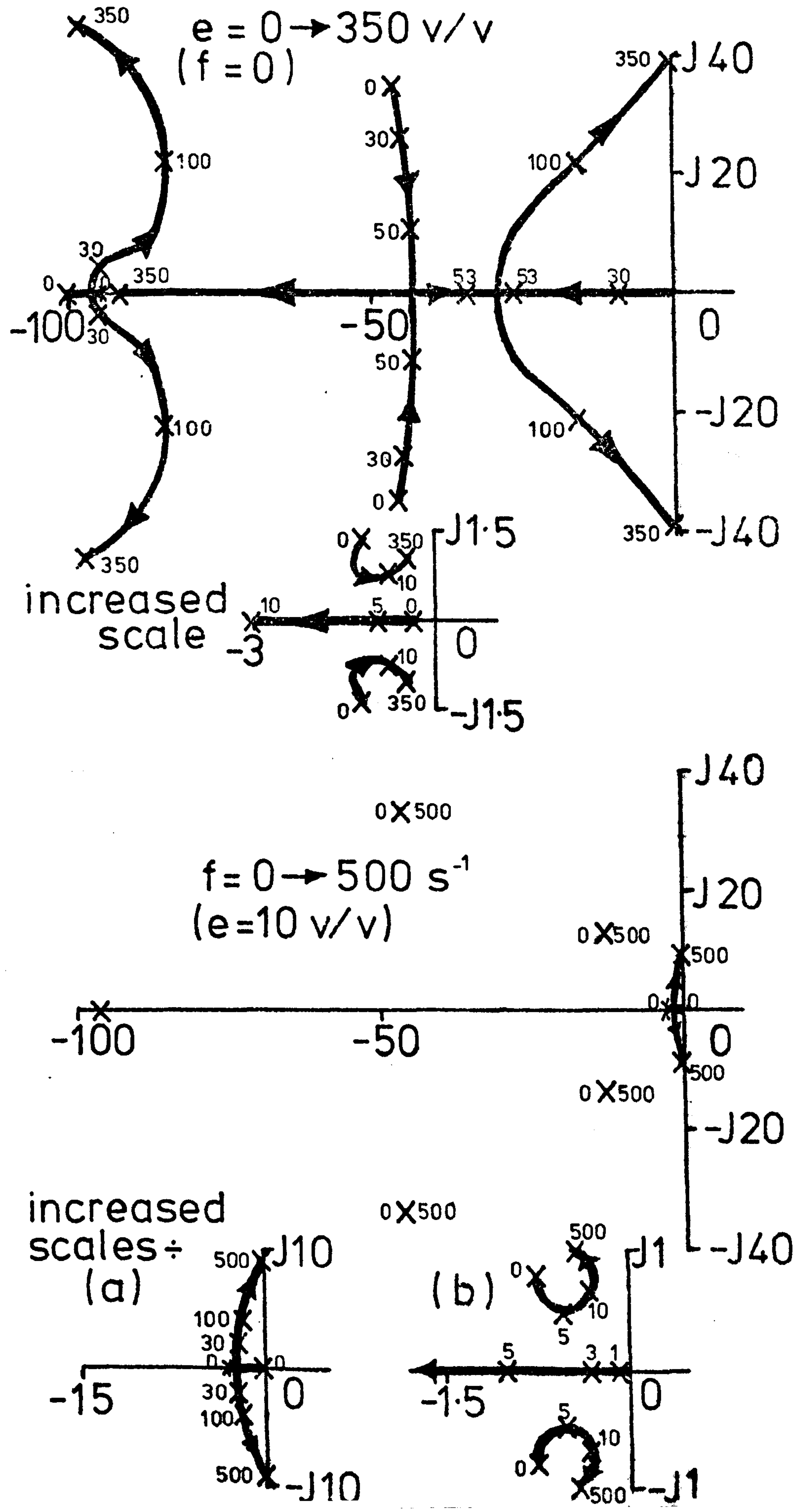

DIESEL ENGINE
HYDROSTATIC DYNAMOMETER

GRAPH G53

method 2.2

speed range ÷ low → high

(1st gear)
(normal fuel delivery)

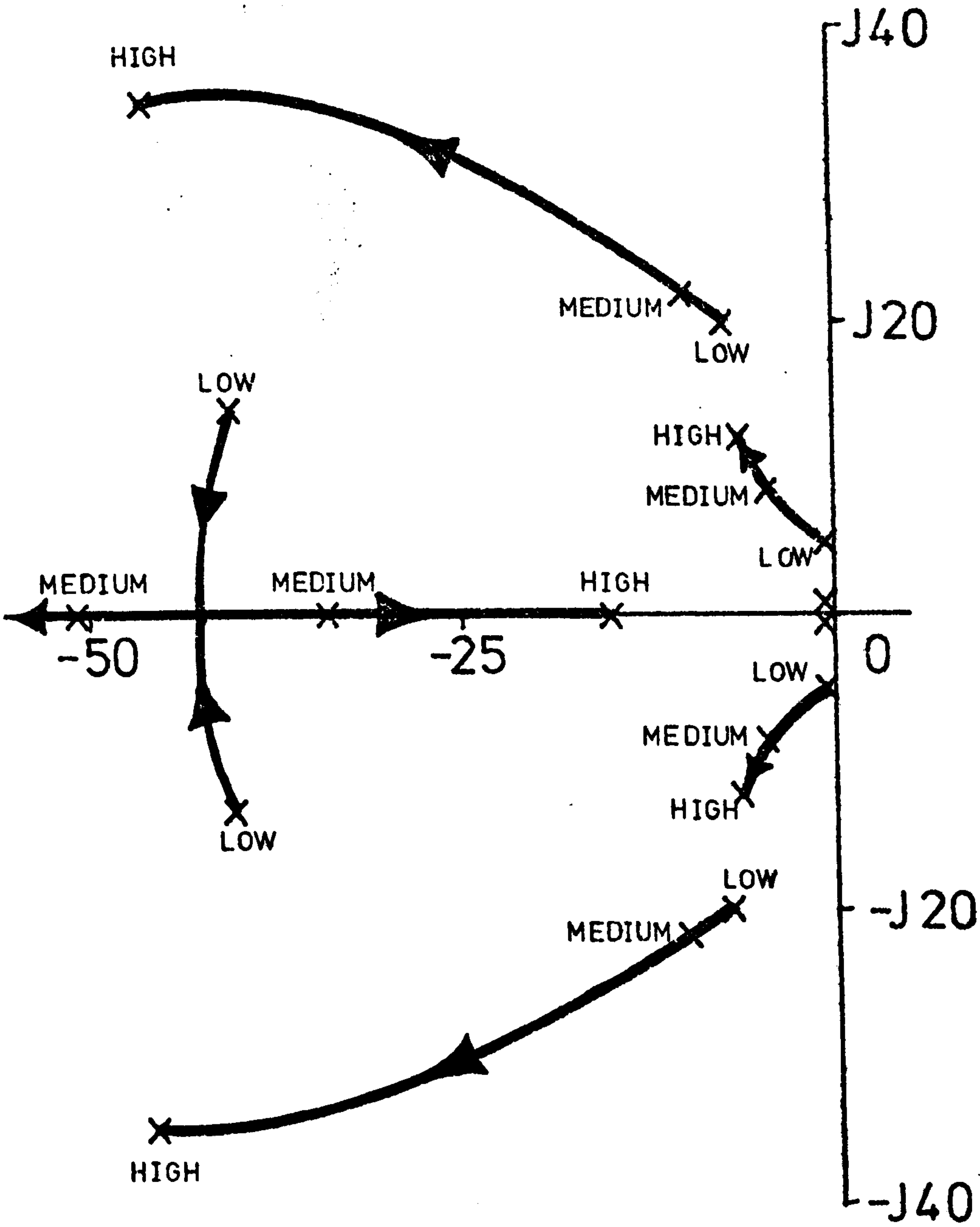

fast response dynamometer predicted characteristics

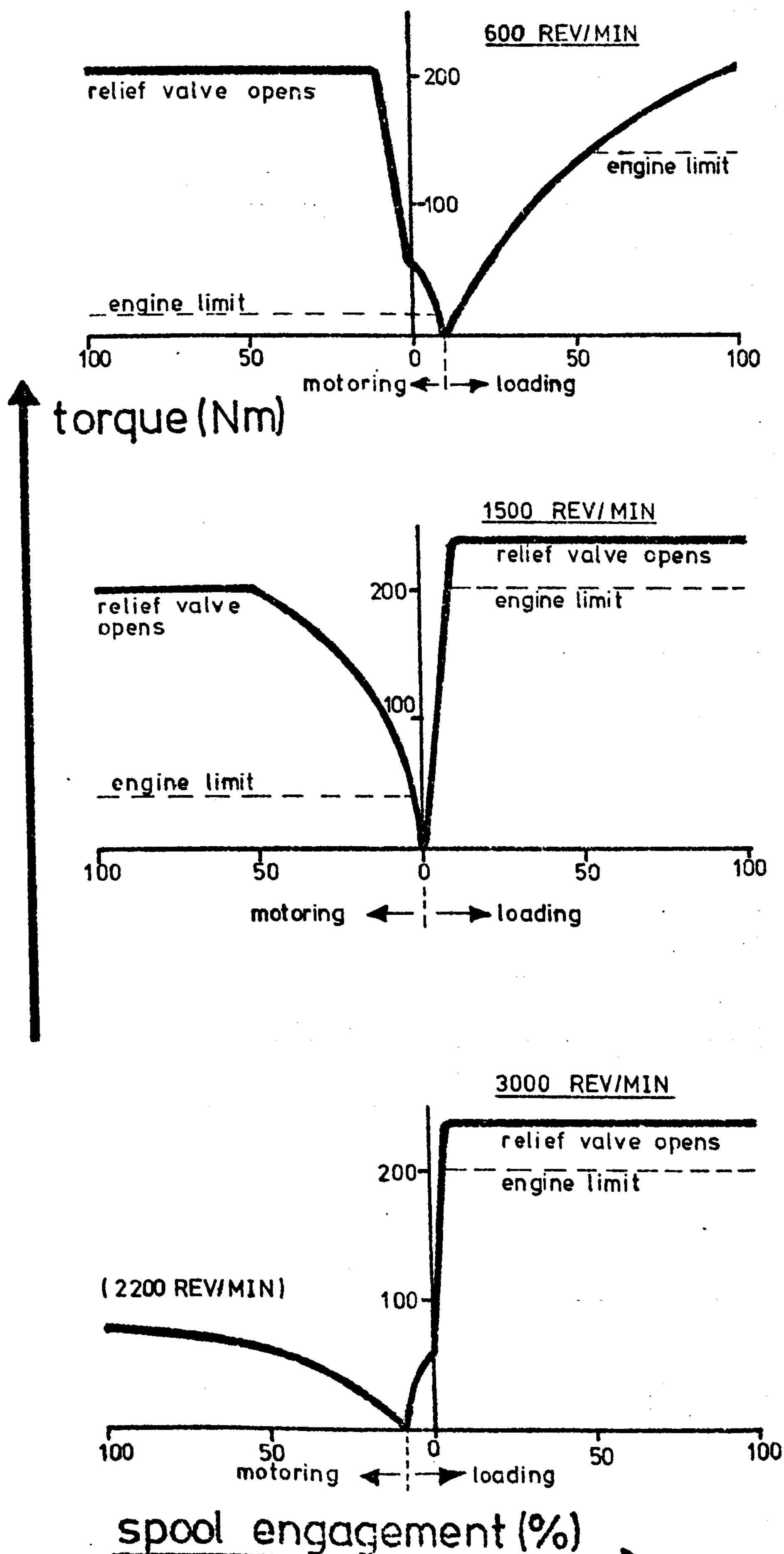

DIESEL ENGINE
FAST RESPONSE DYNAMOMETER

GRAPH G55

no feedback

speed range÷ low → high

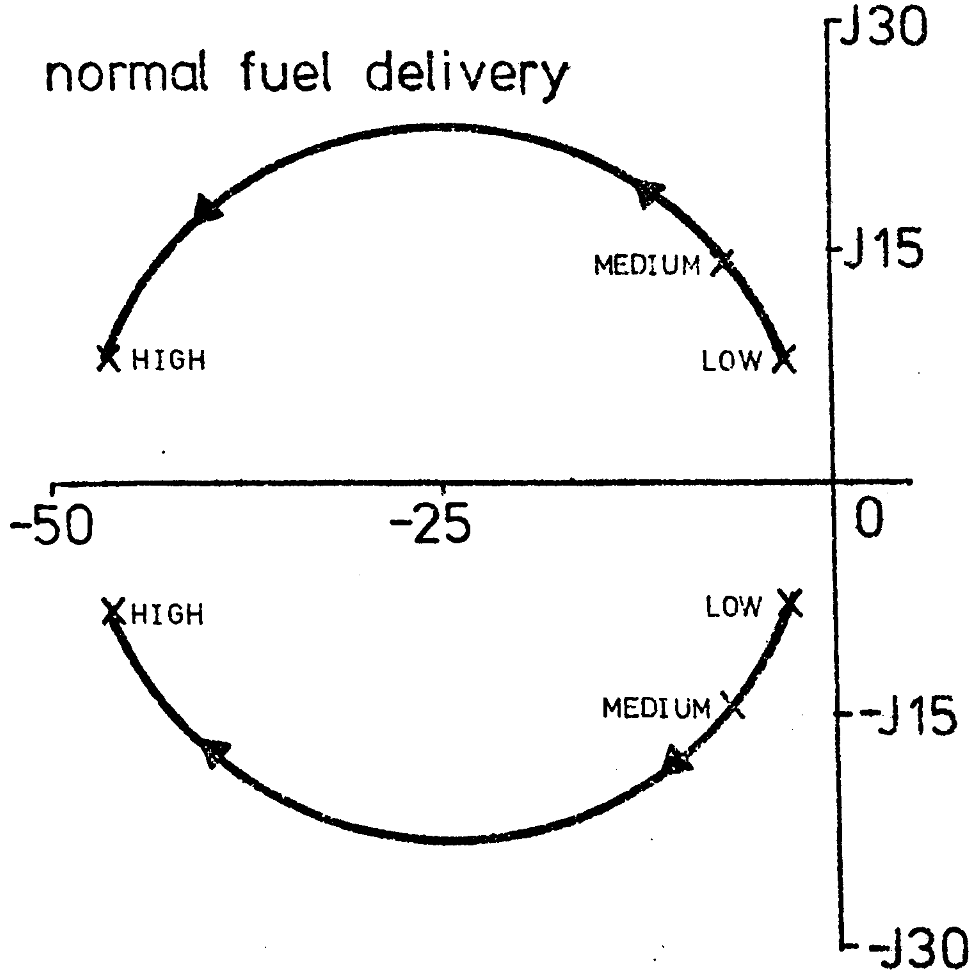

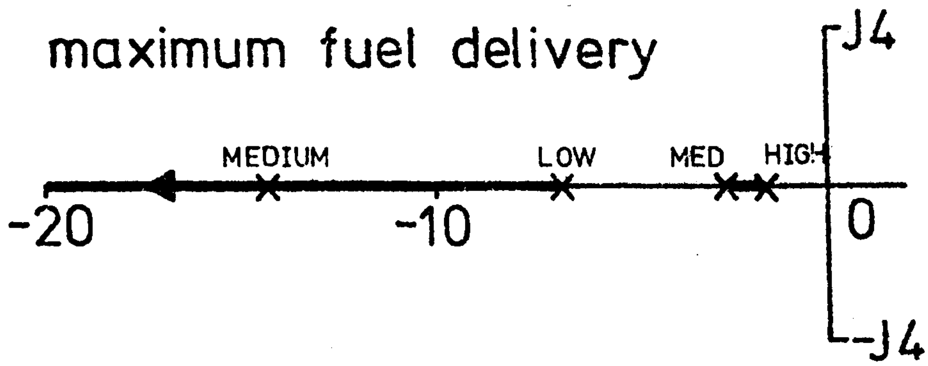

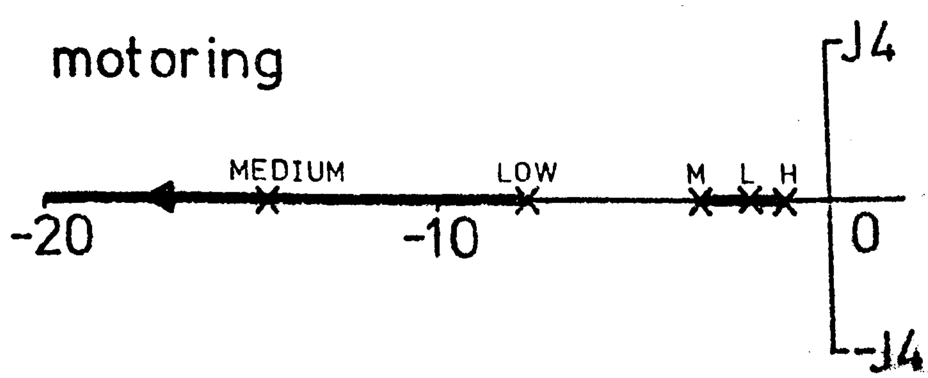

GRAPH G56

method 1.1

speed range ÷ low ⟶ high

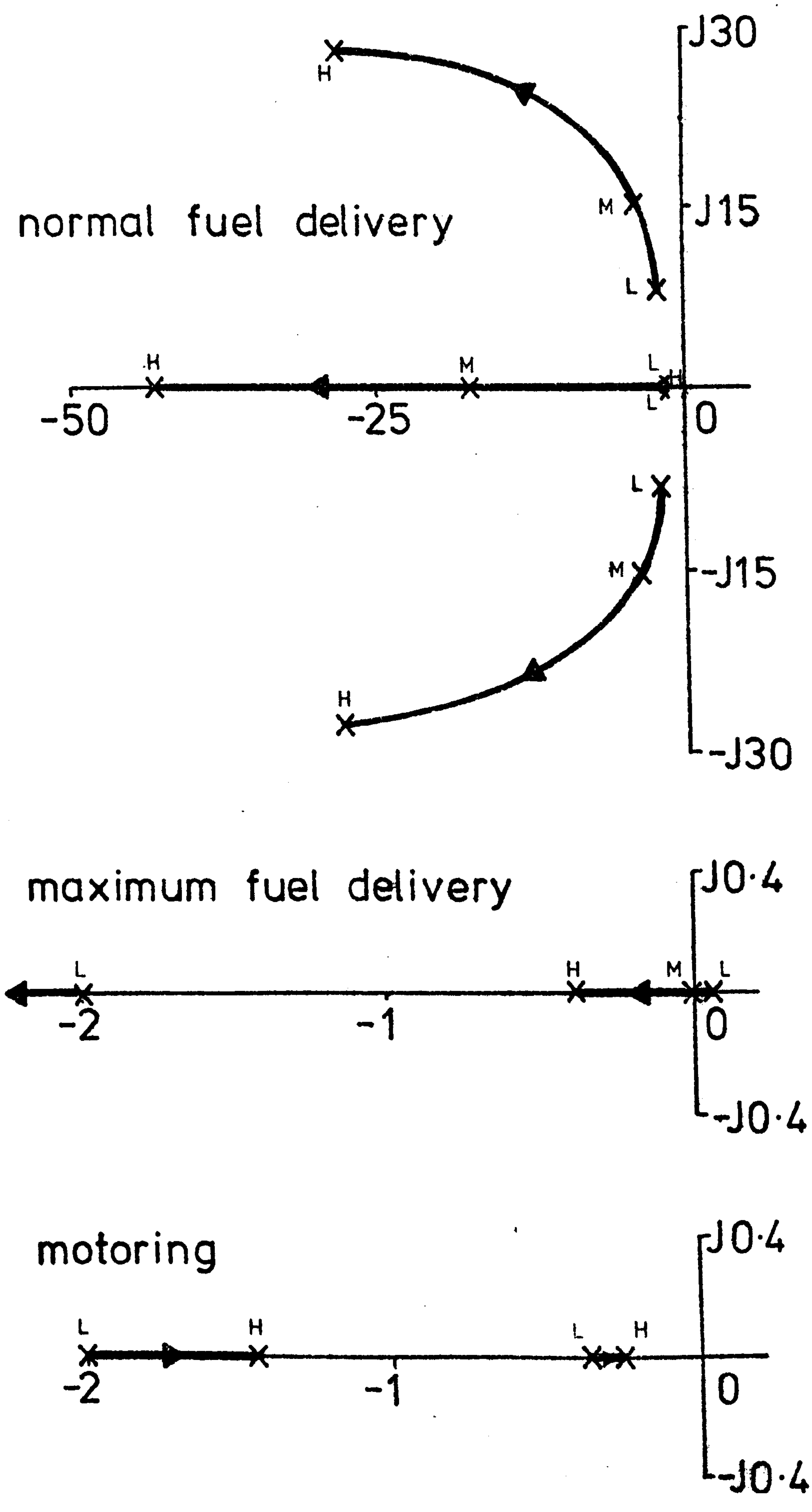

GRAPH G57

method 1.2

speed range ÷ low → high

normal fuel delivery

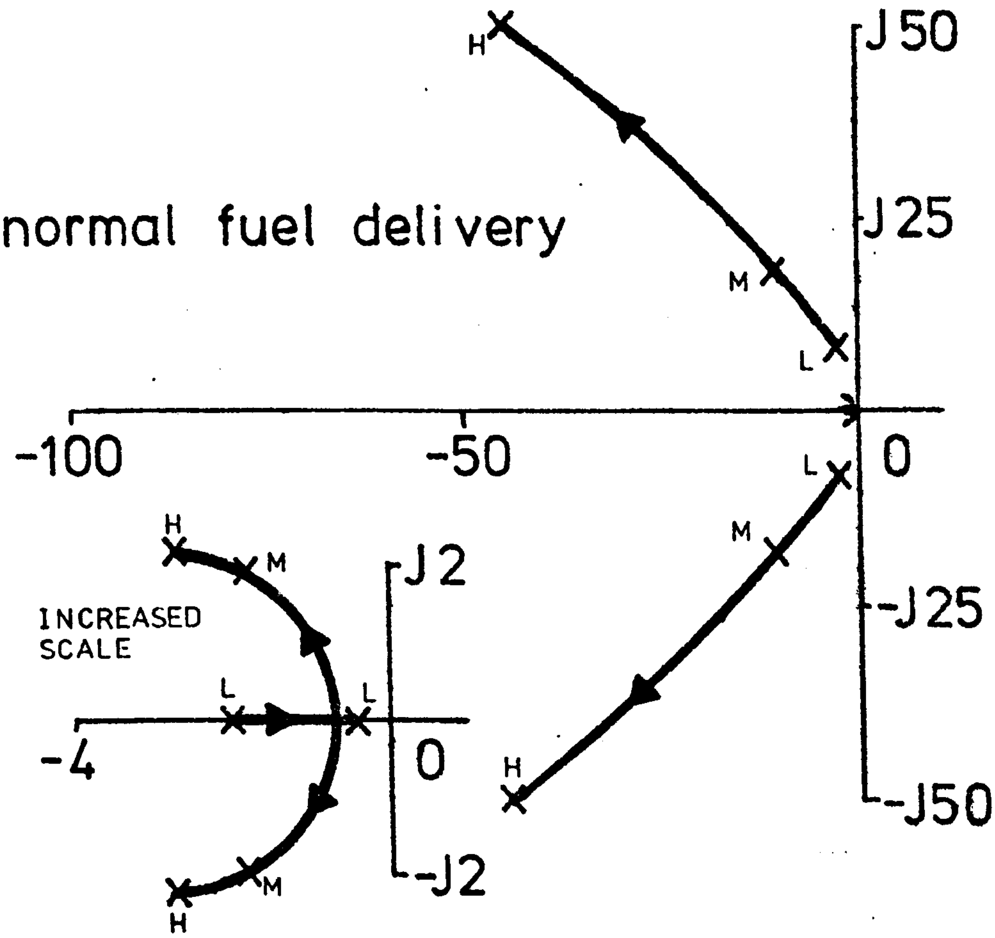

maximum fuel delivery

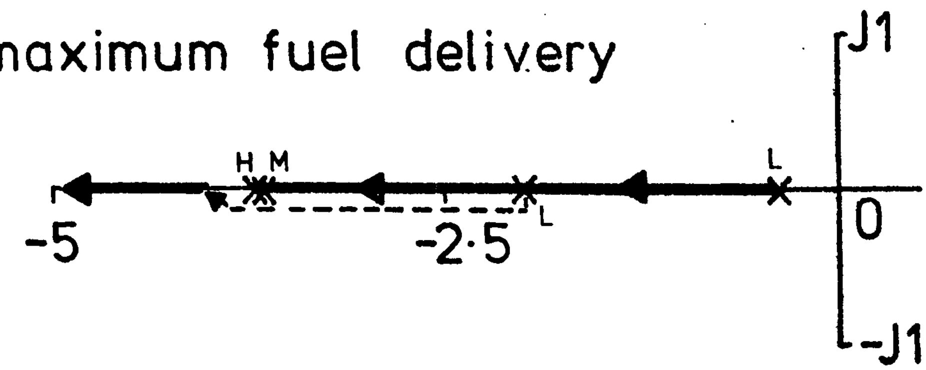

motoring

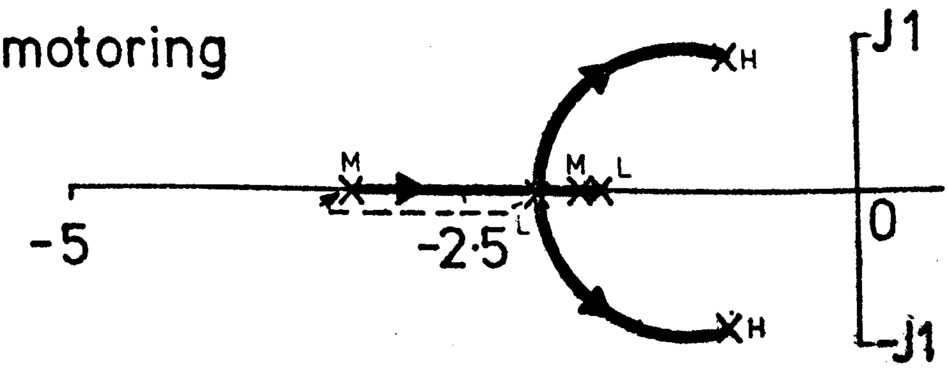

GRAPH G58

basic sytem with dynamometer
torque correction signal

speed range ÷ low ⟶ high

normal fuel delivery

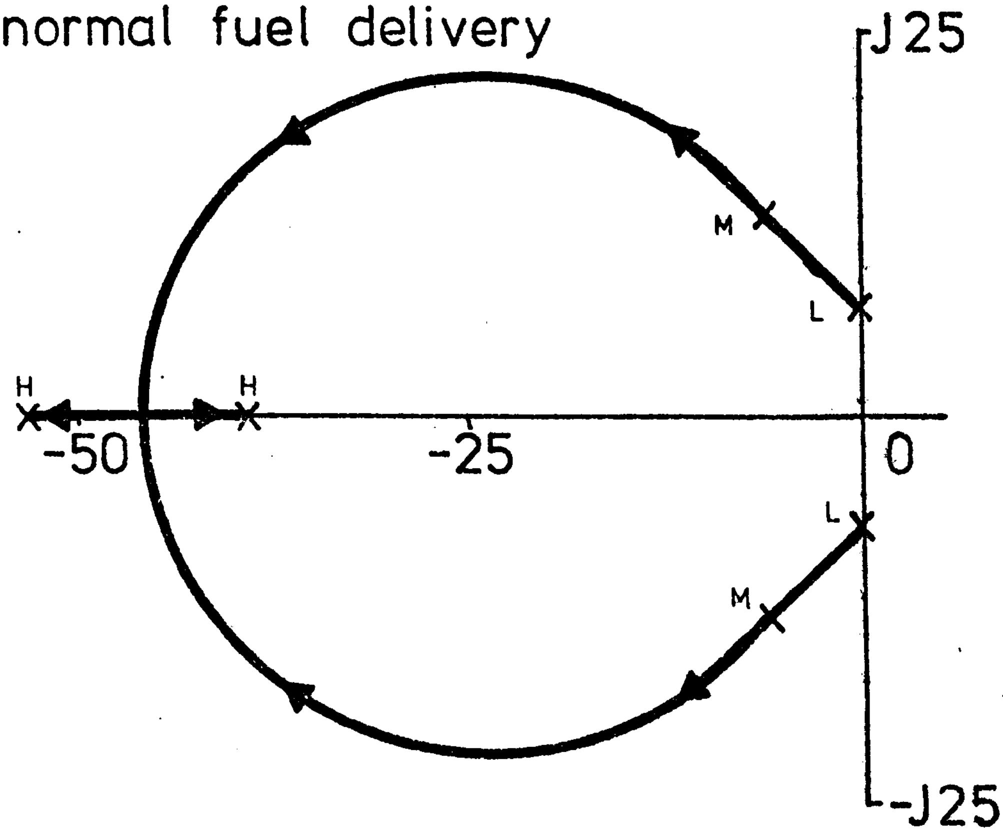

maximum fuel delivery

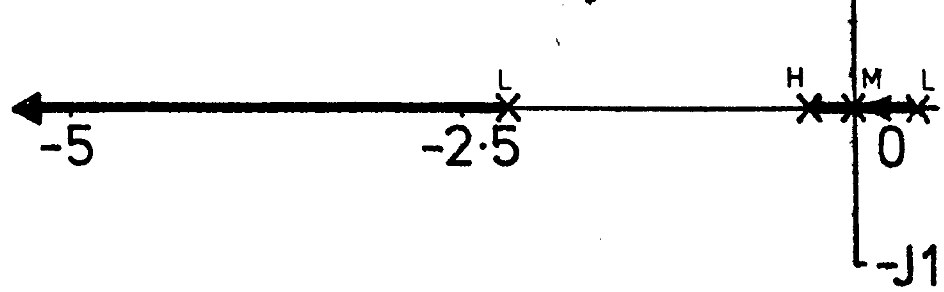

motoring

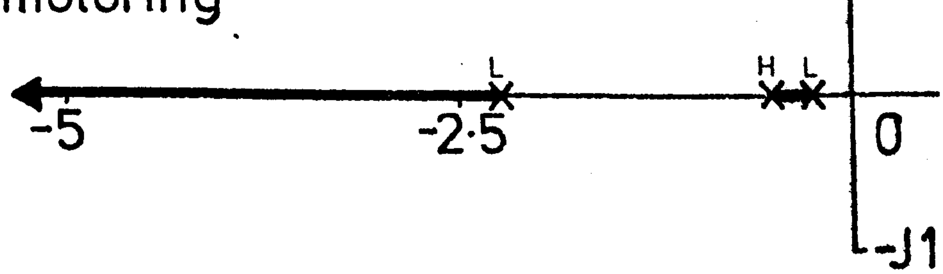

GRAPH G59

method 2.1 4th gear

speed range ÷ low ⟶ high

normal fuel delivery

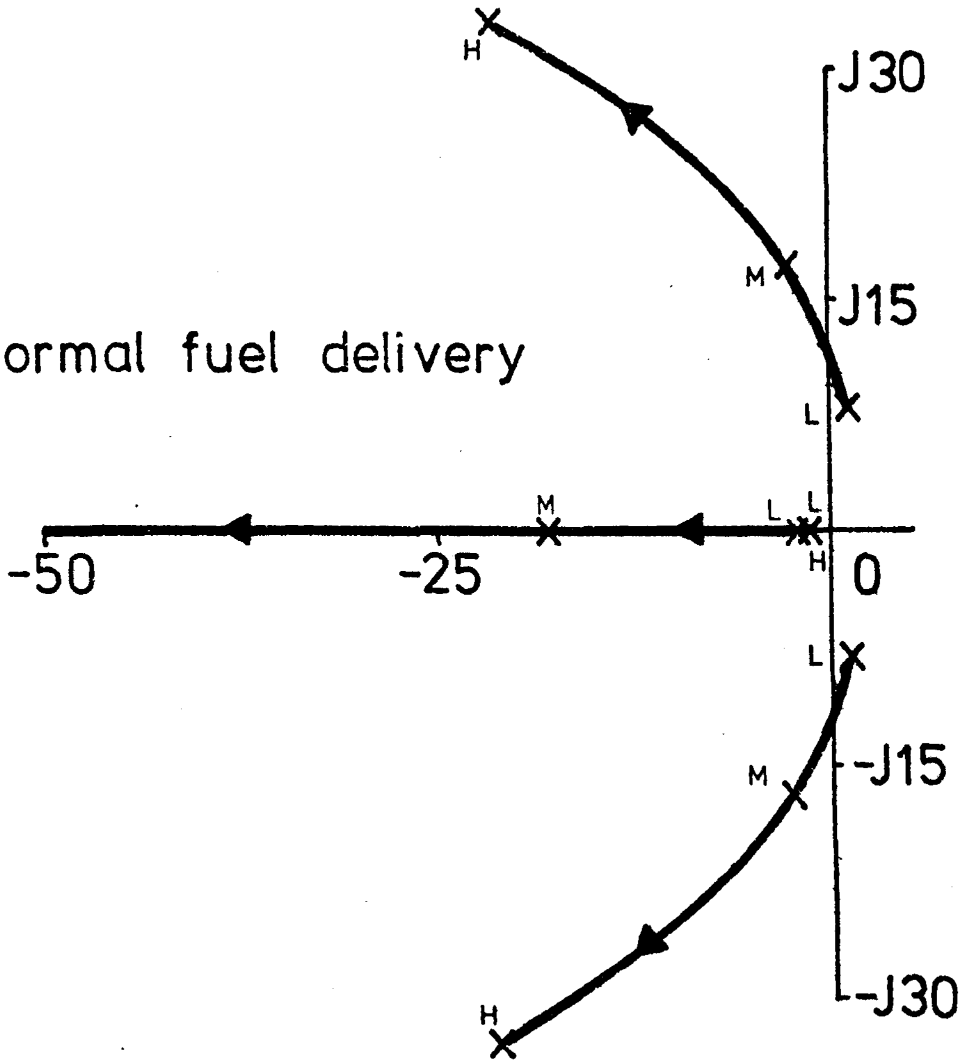

maximum fuel delivery

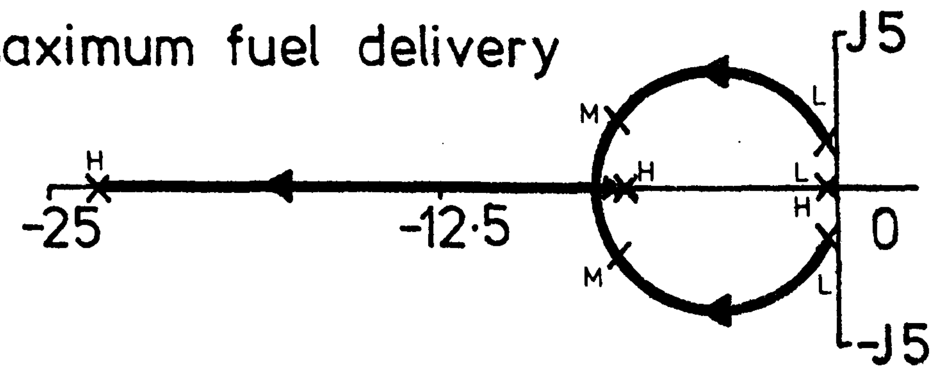

motoring

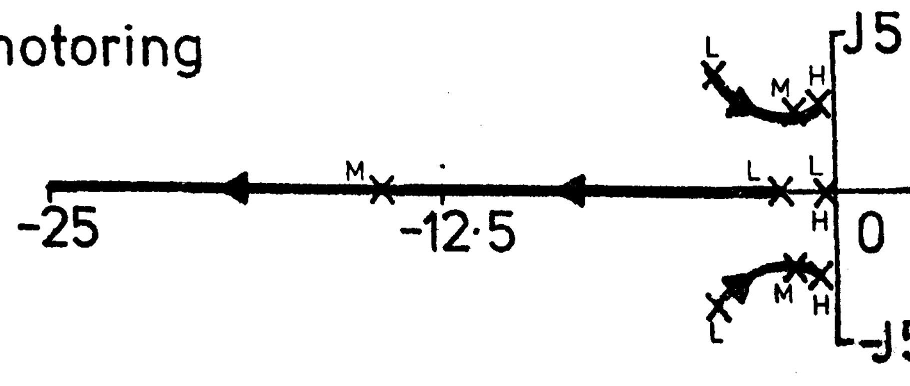

DIESEL ENGINE
FAST RESPONSE DYNAMOMETER

GRAPH G60

method 2.1 1^{st} gear

speed range ÷ low ⟶ high

normal fuel delivery

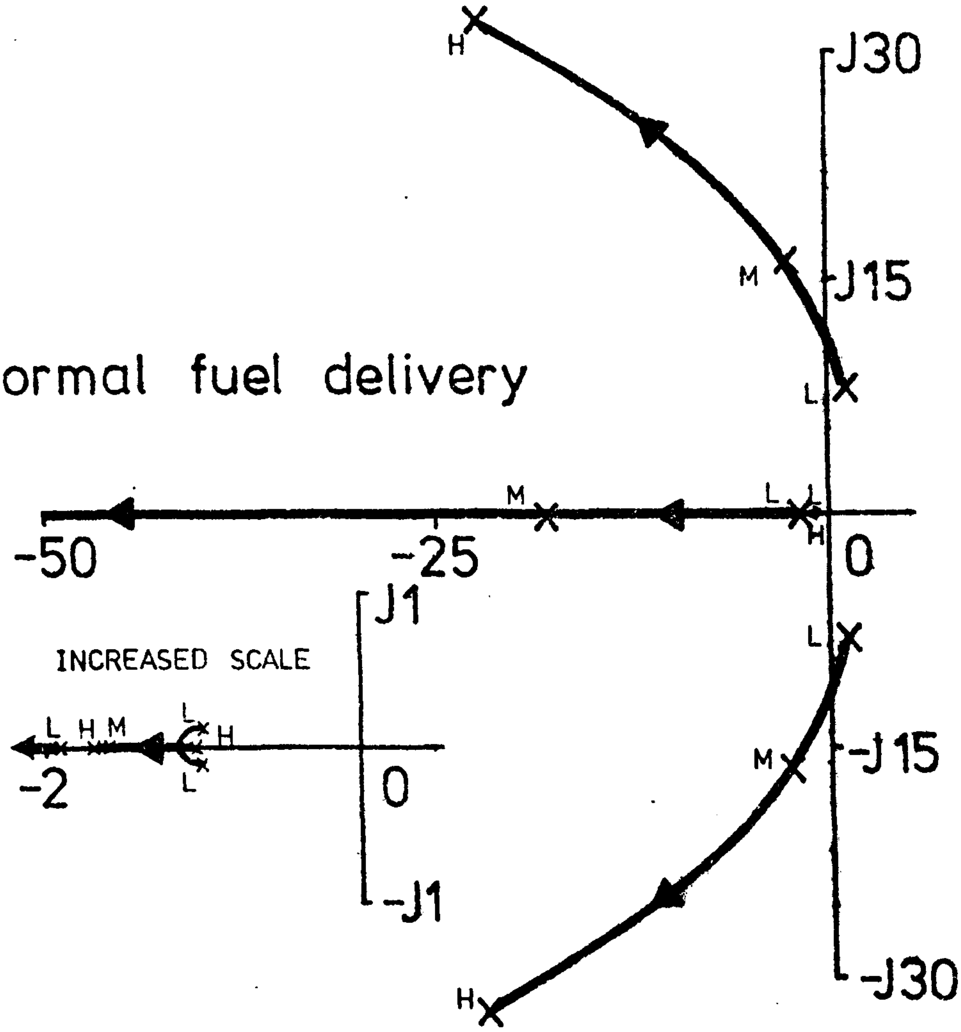

maximum fuel delivery

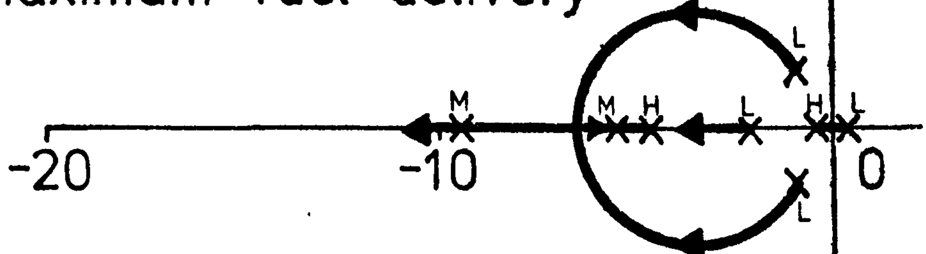

motoring

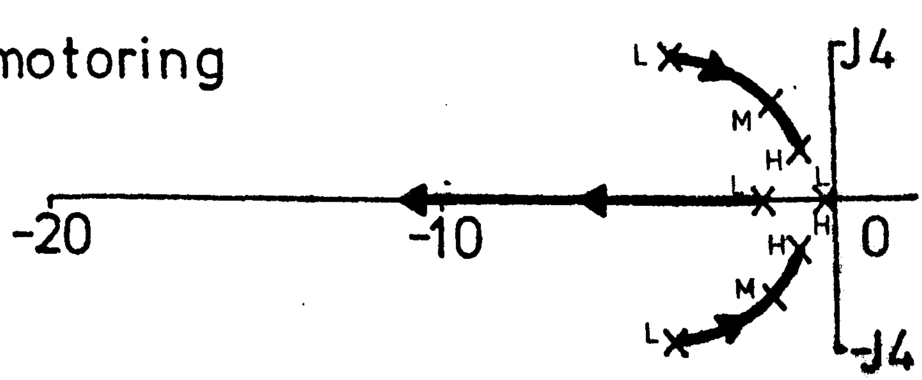

DIESEL ENGINE
FAST RESPONSE DYNAMOMETER

GRAPH G61

method 2.2 1^{st} gear

speed range ÷ low ⟶ high

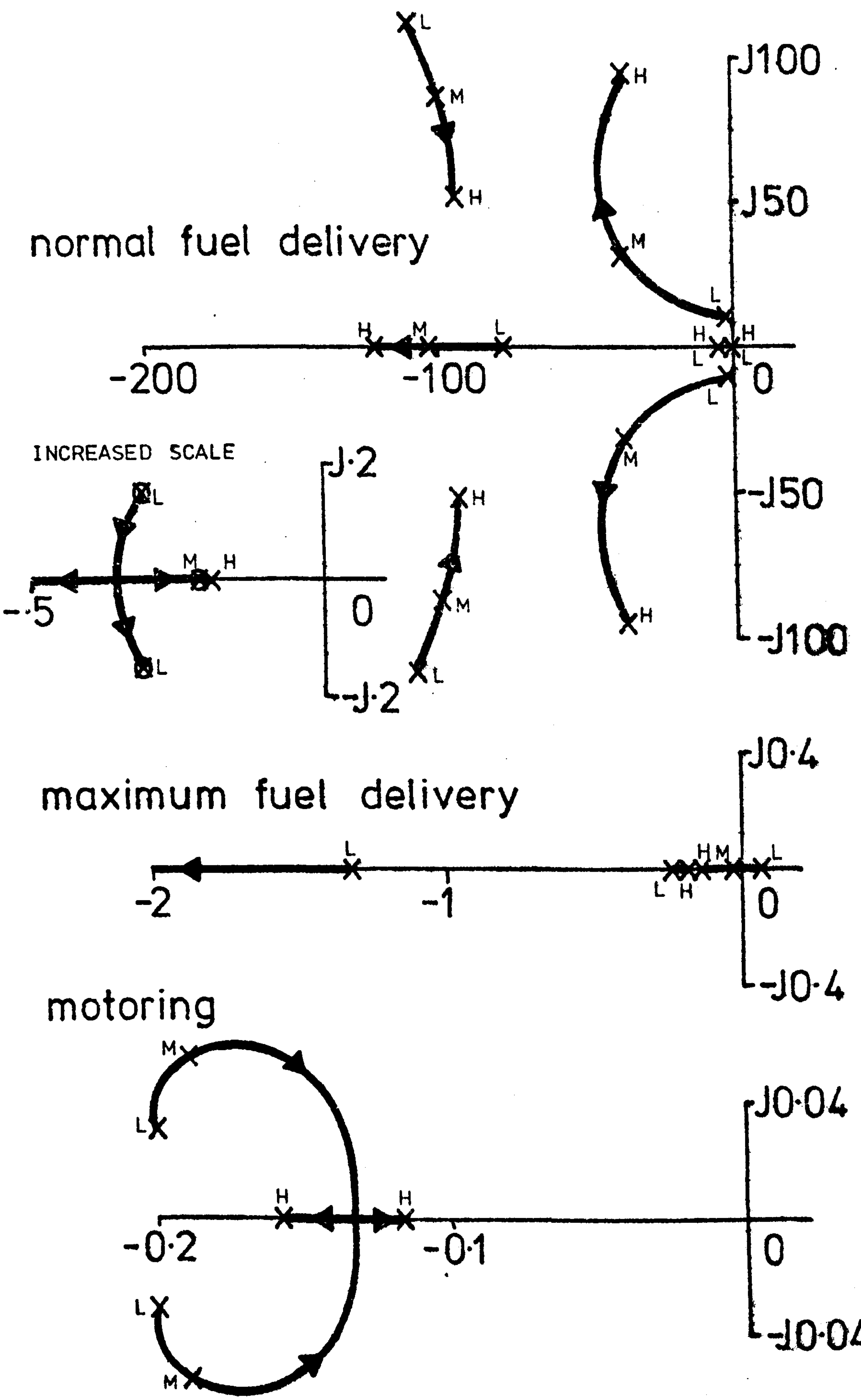

DIESEL ENGINE
FAST RESPONSE DYNAMOMETER

GRAPH G62

method 2.2 4^{th} gear

speed range ÷ low ⟶ high

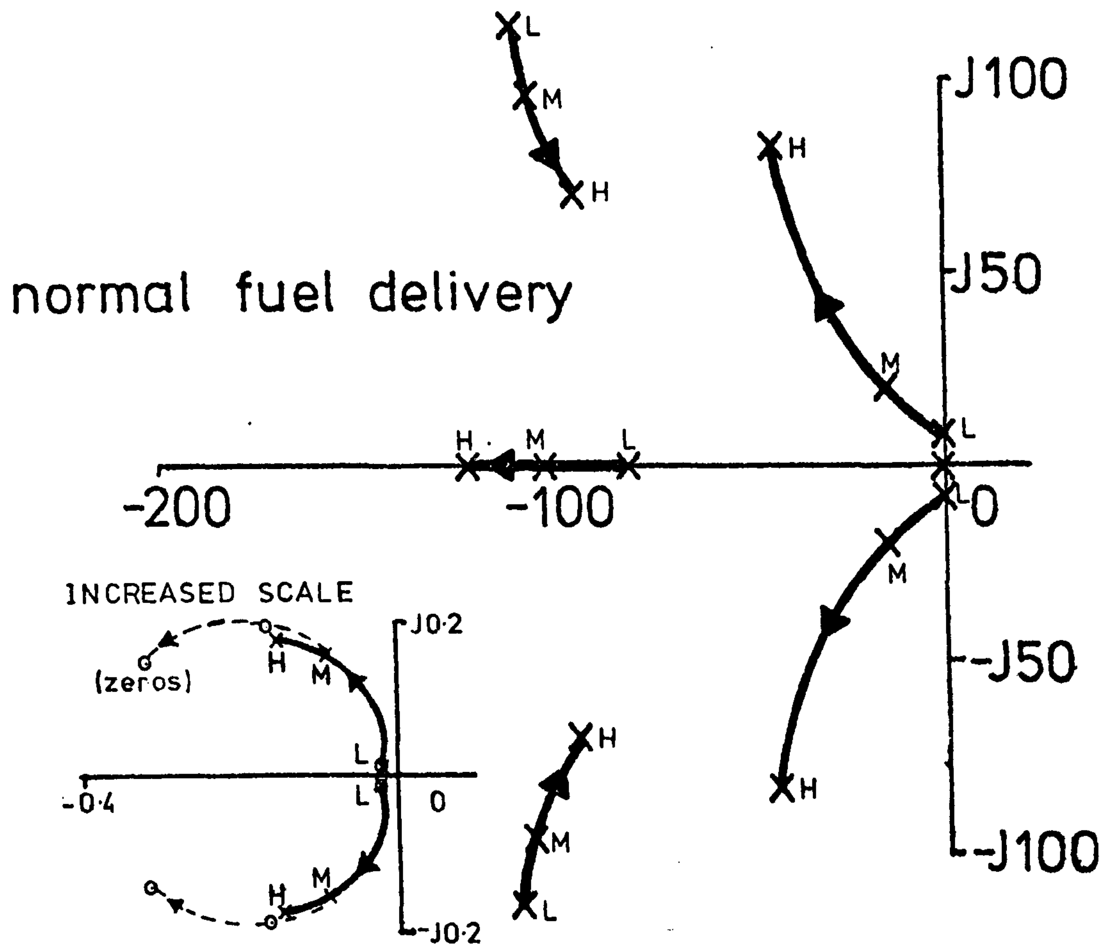

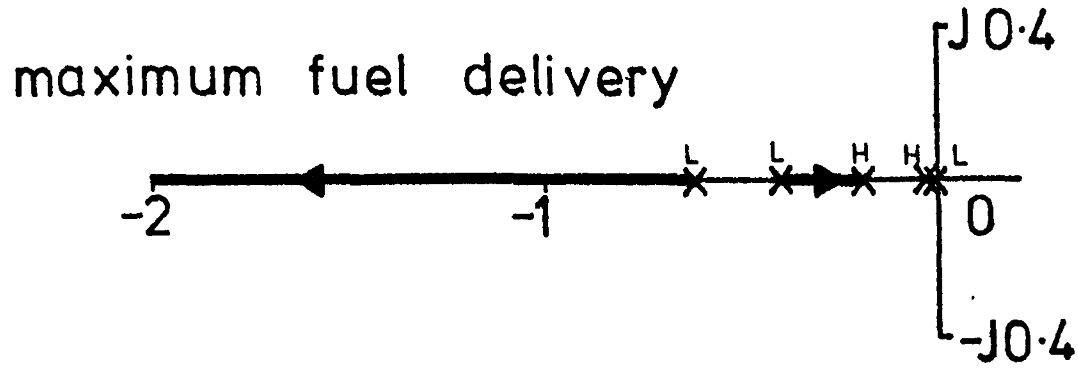

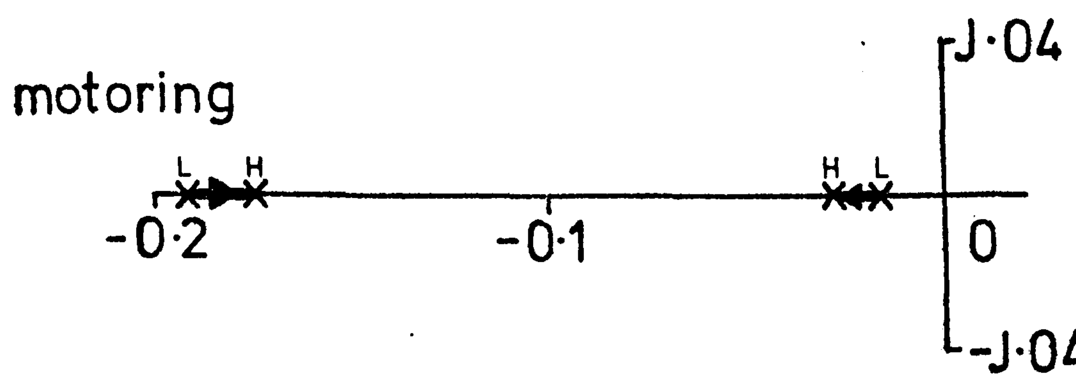

GRAPH G63

electric dynamometer characteristics

100 KW dc motor/generator

(maximum power curve)

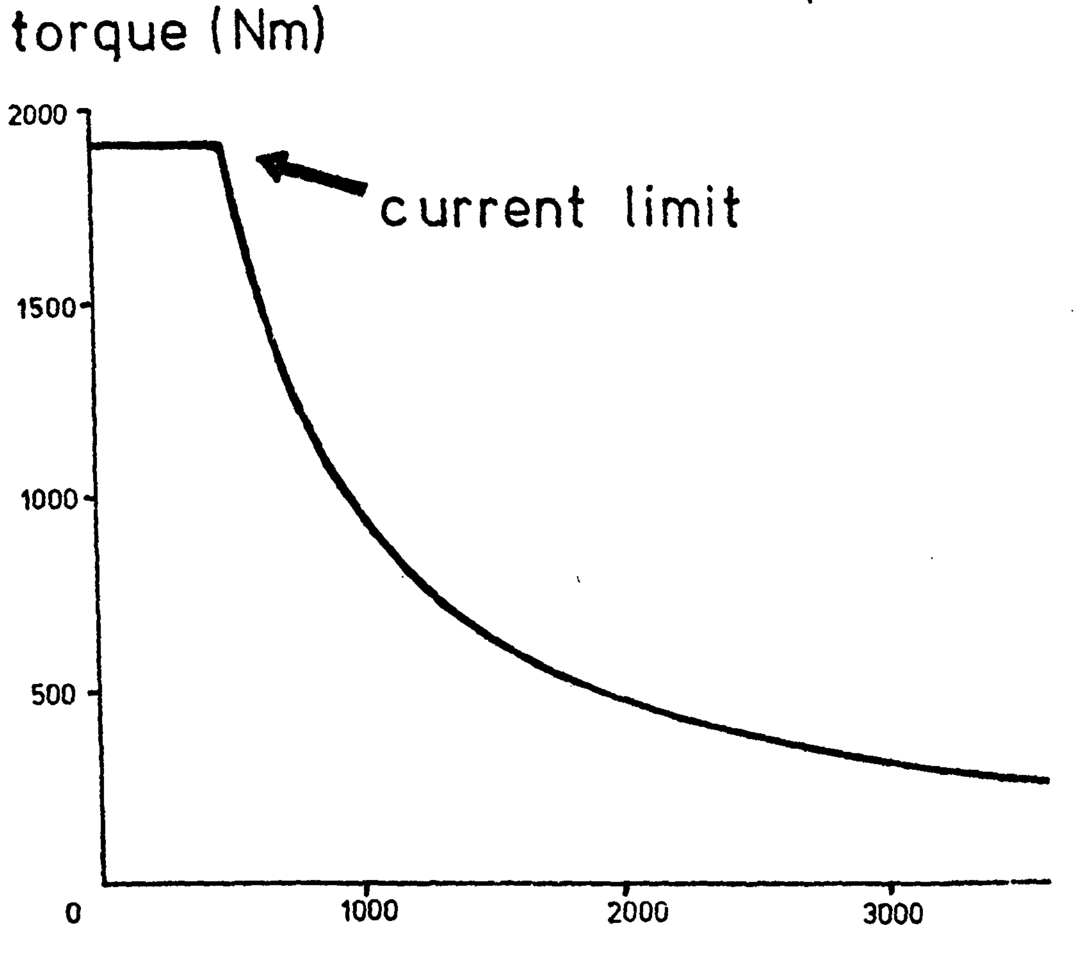

GRAPH G64

basic system (no feedback)

speed range÷ low ⟶ high

mid fuel delivery

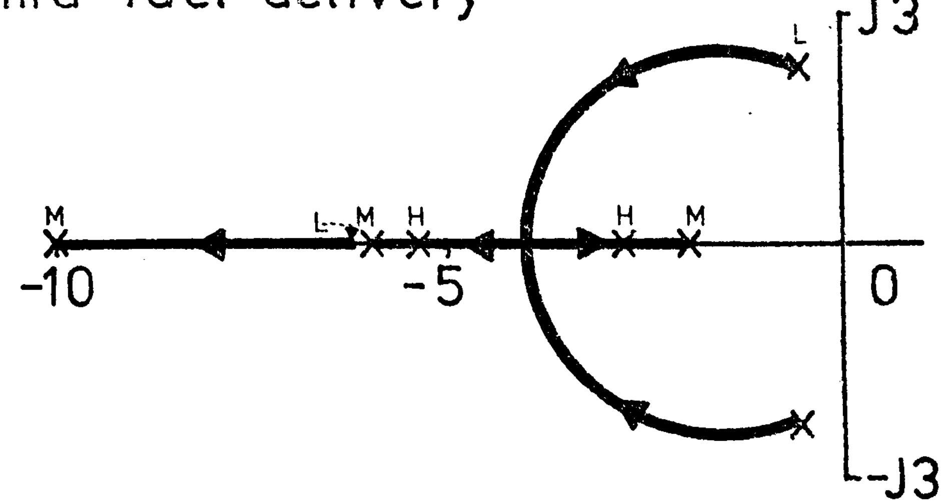

maximum fuel delivery

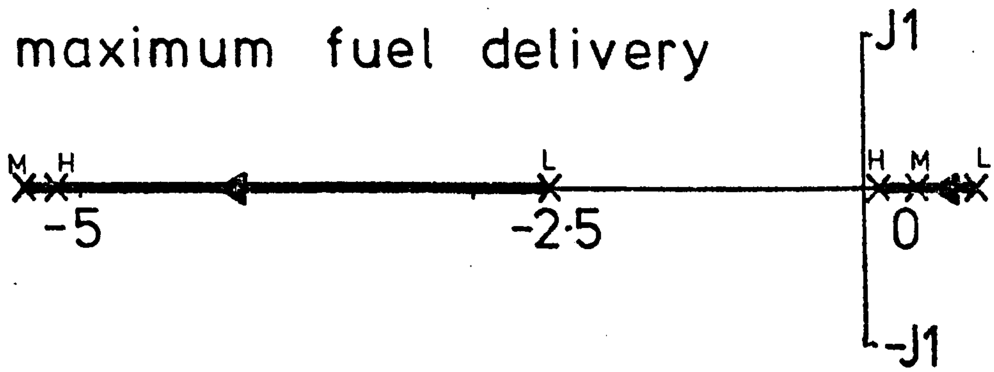

motoring

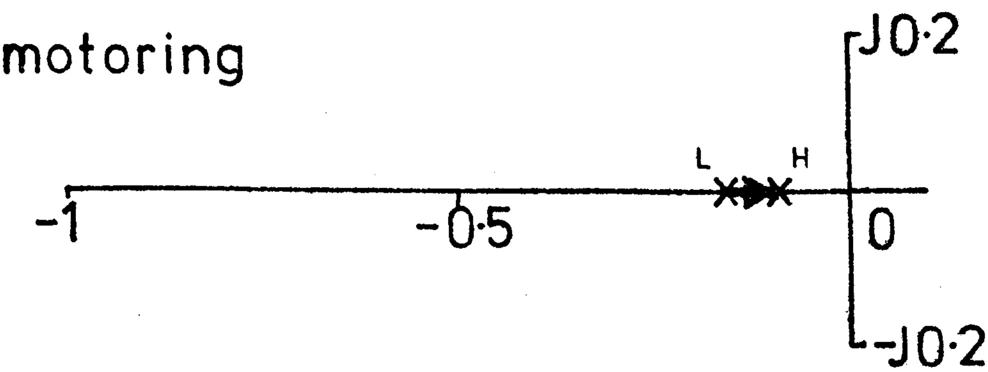

GRAPH G65

method 1.1

speed range ÷ low ⟶ high

mid fuel delivery

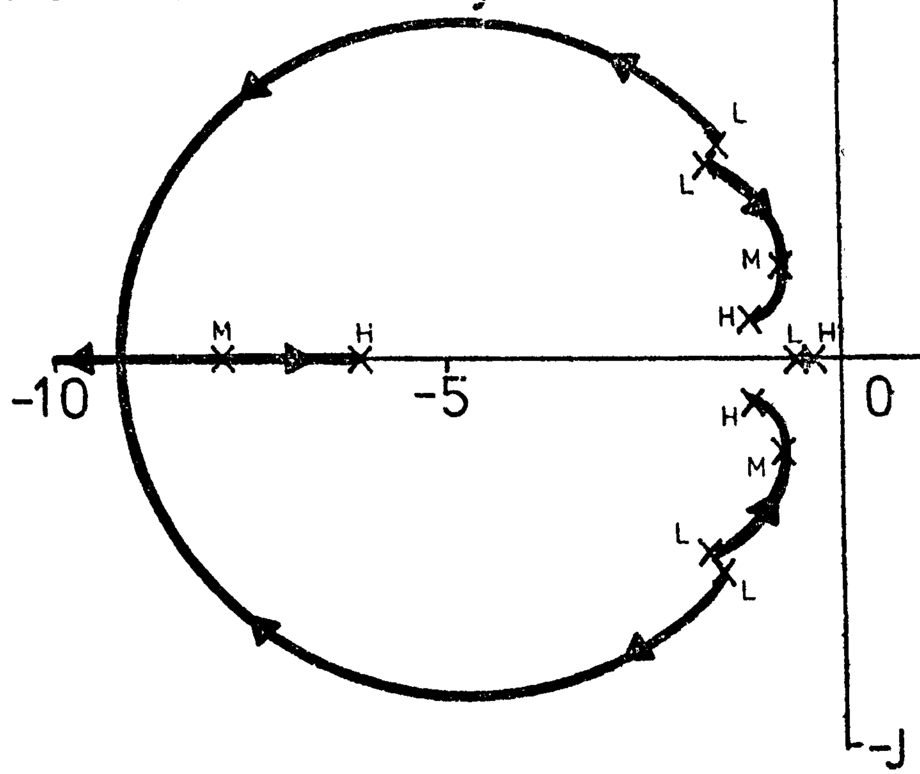

maximum fuel delivery

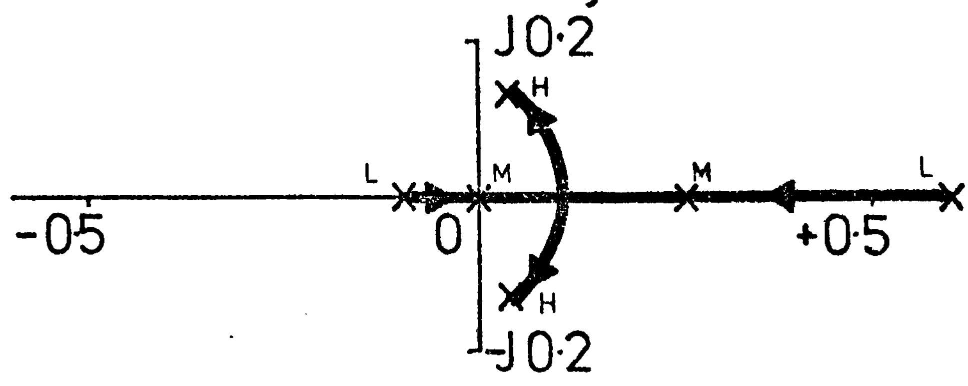

motoring

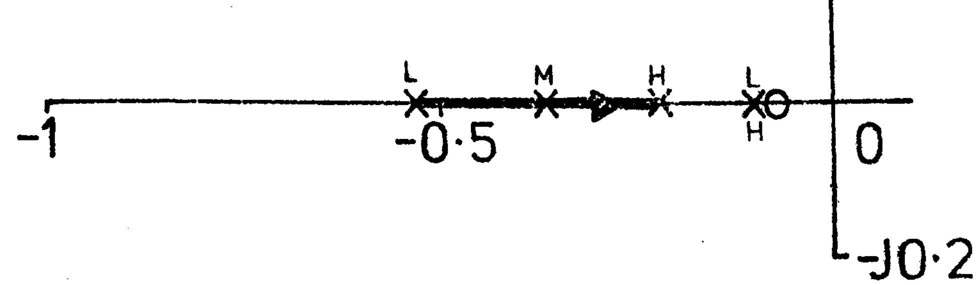

GRAPH G66

method 1.2

speed range ÷ low ⟶ high

mid fuel delivery

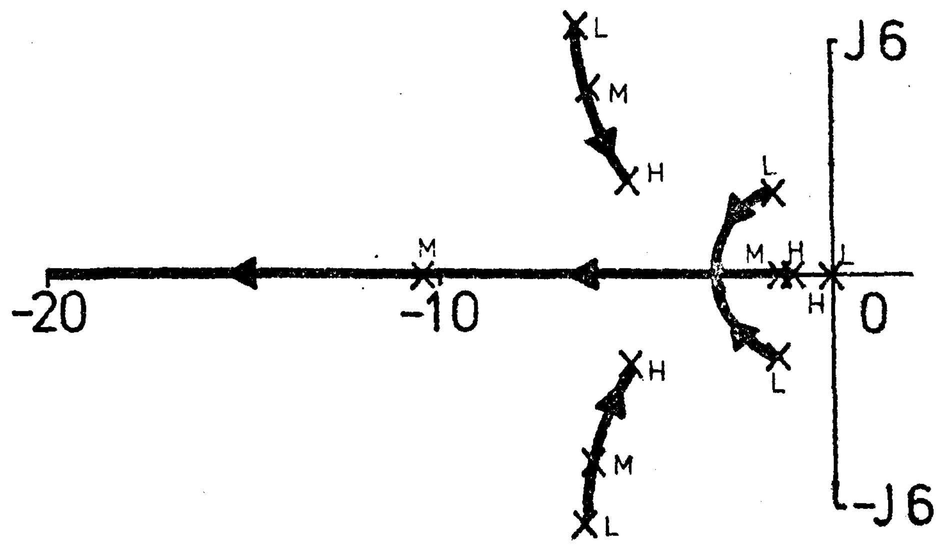

maximum fuel delivery

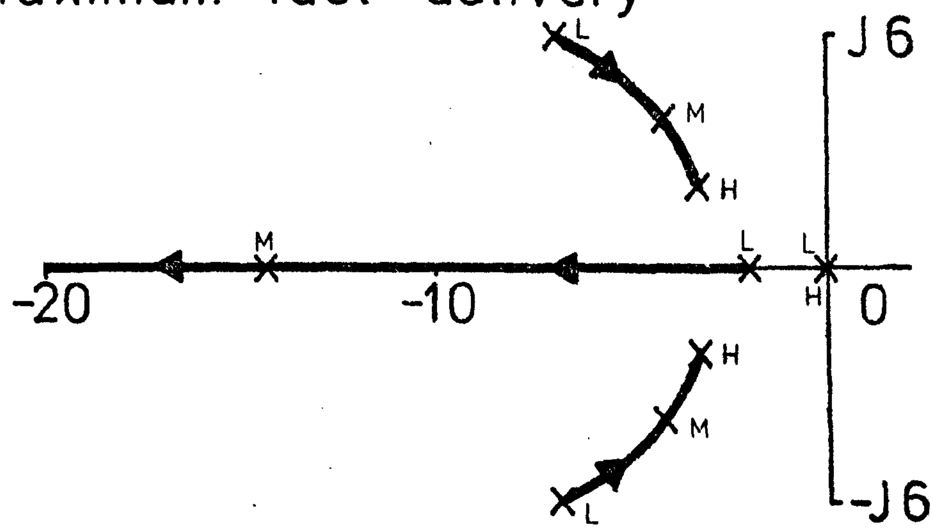

motoring

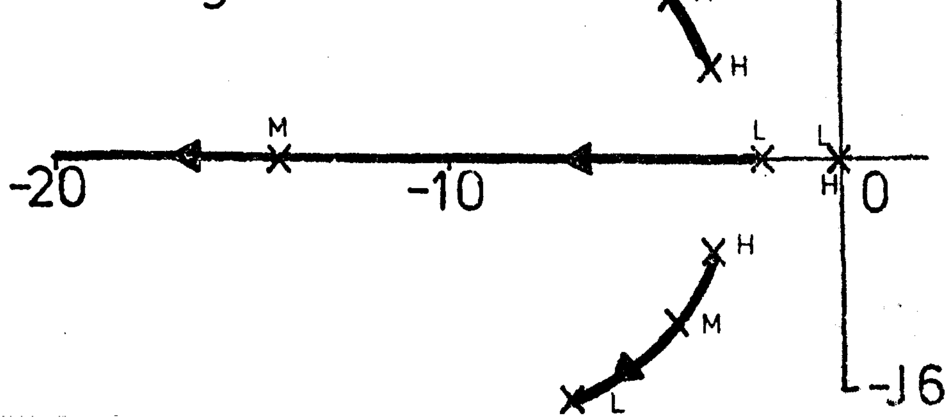

GRAPH G67

basic system with dynamometer torque elimination signal

speed range ÷ low ⟶ high

mid fuel delivery

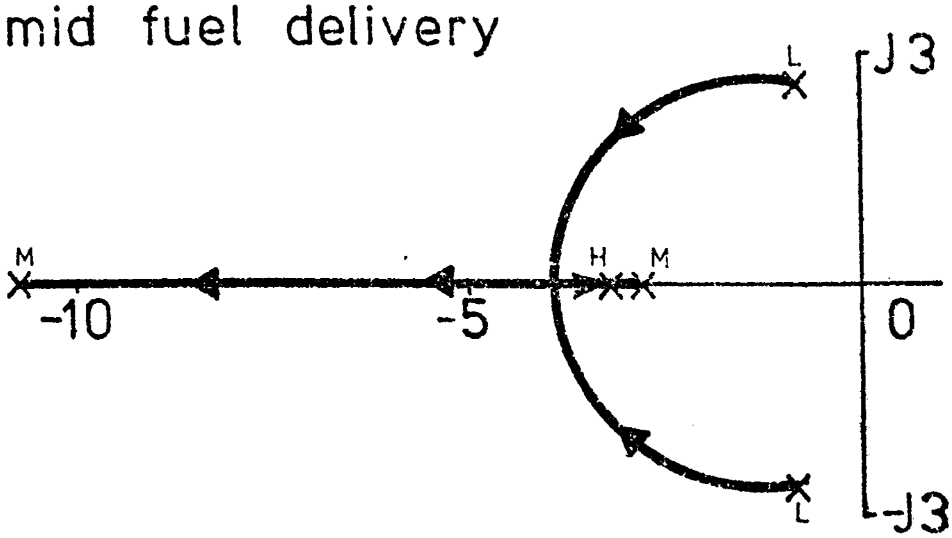

maximum fuel delivery

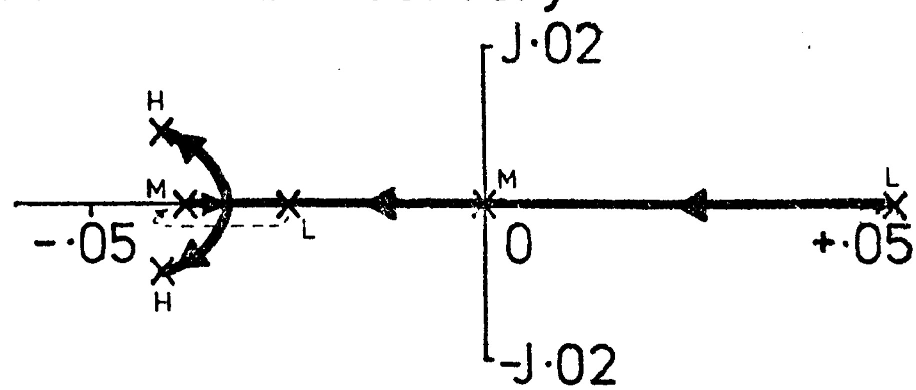

motoring

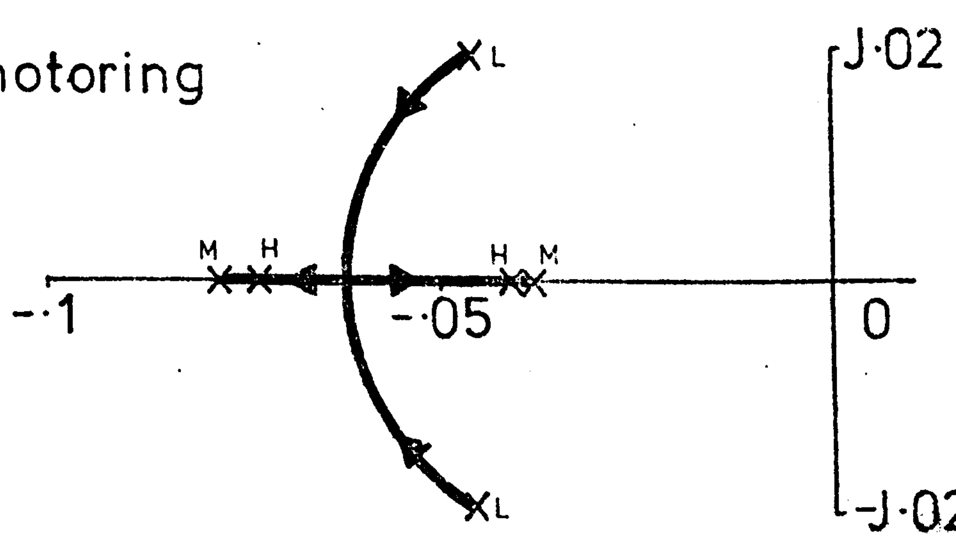

DIESEL ENGINE
ELECTRIC DYNAMOMETER

GRAPH G68

method 2.1 1^{st} gear

speed range ÷ low ⟶ high

mid fuel delivery

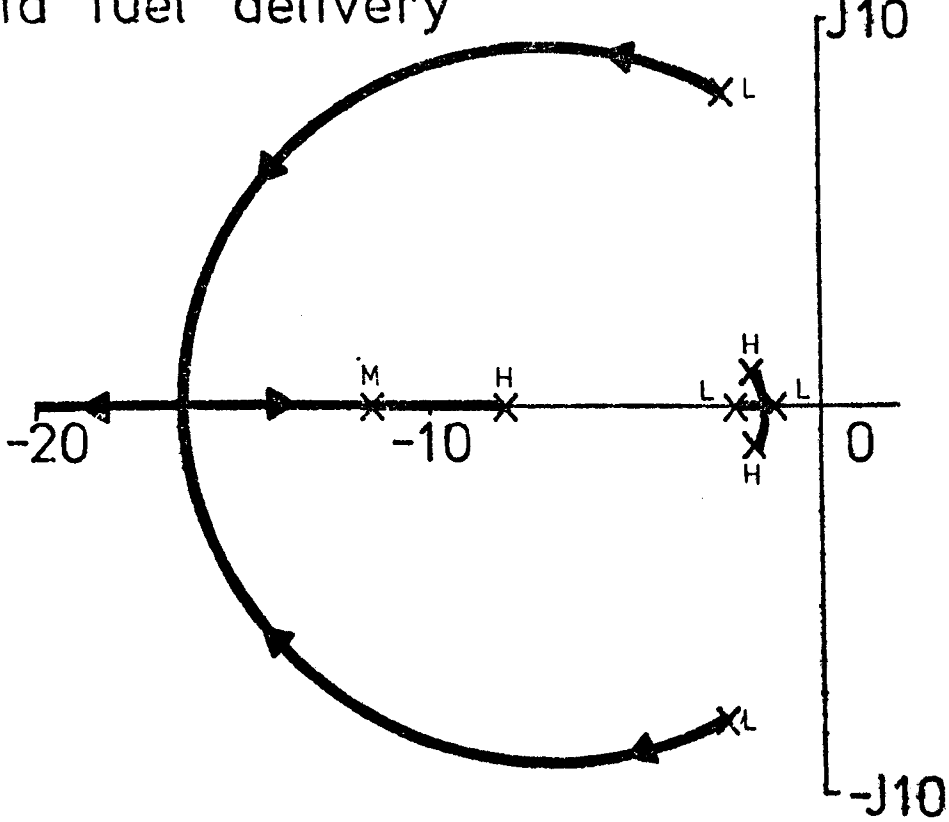

maximum fuel delivery

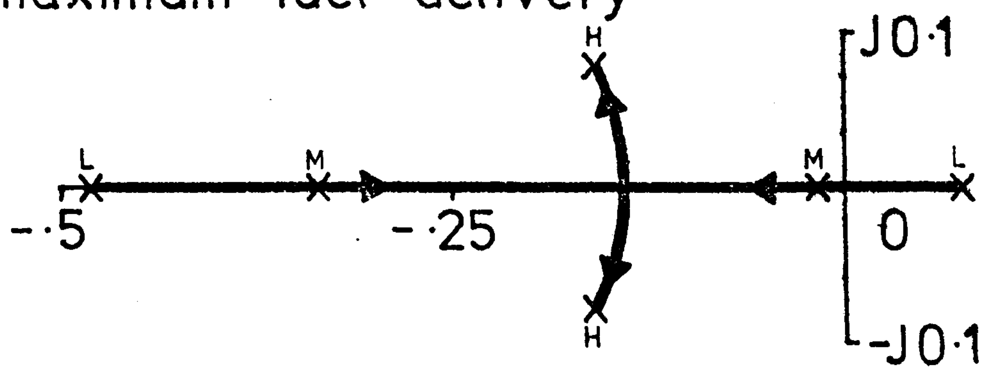

motoring

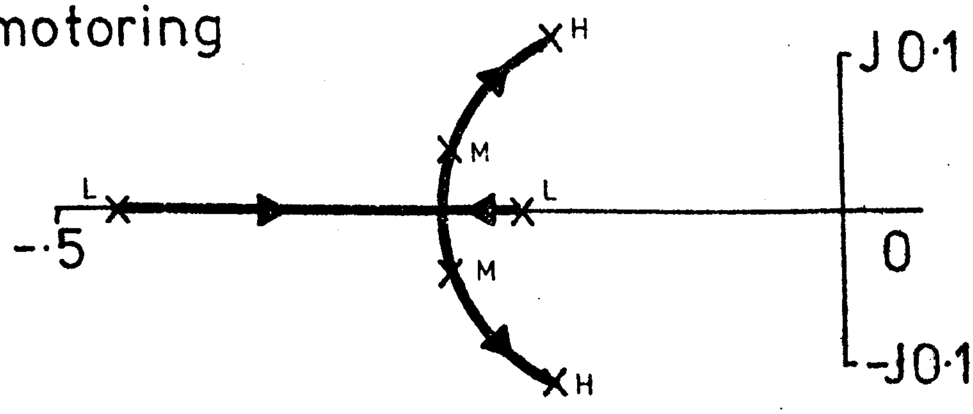

DIESEL ENGINE
ELECTRIC DYNAMOMETER

GRAPH G69

method 2.1 4^{th} gear

speed range ÷ low ⟶ high

mid fuel delivery

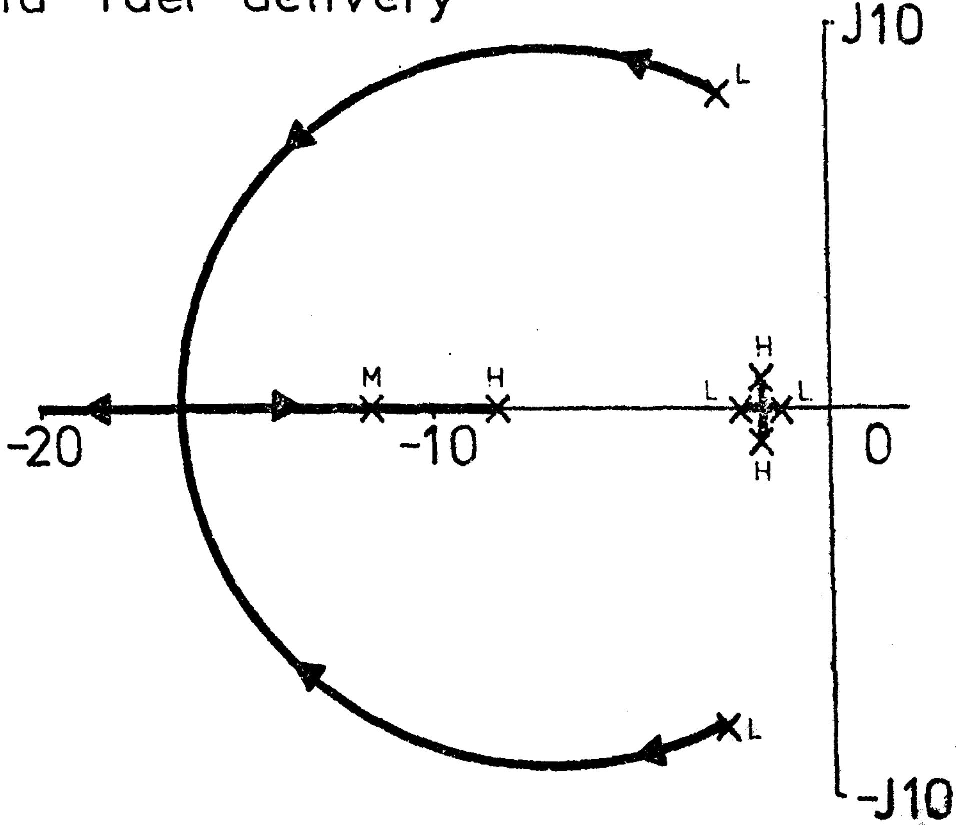

maximum fuel delivery

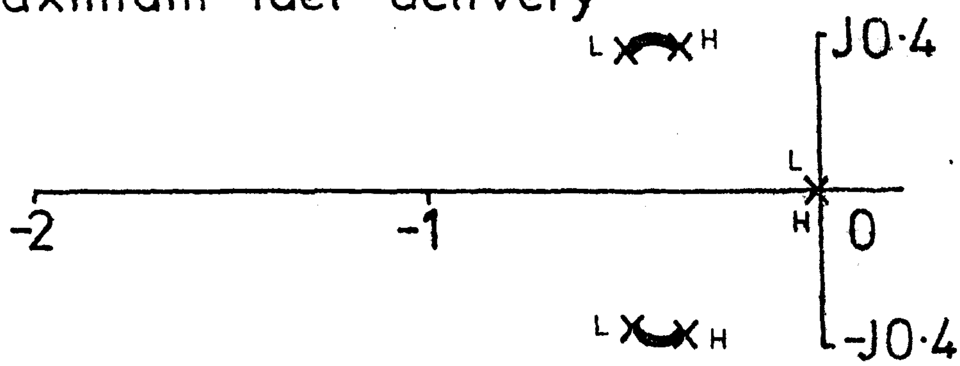

motoring

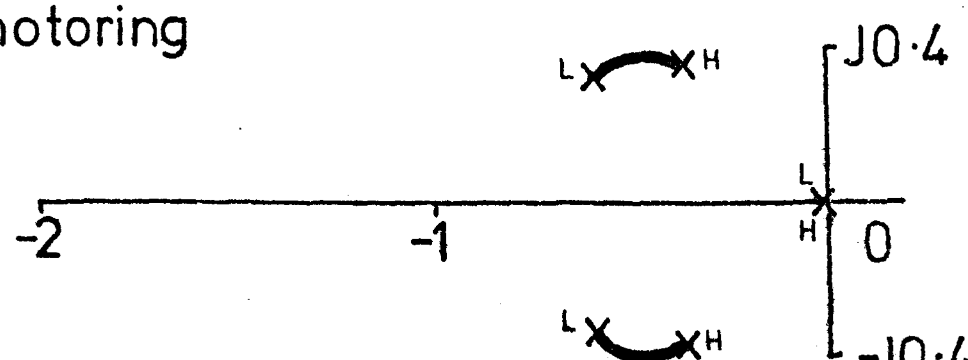

DIESEL ENGINE
ELECTRIC DYNAMOMETER

GRAPH G70

method 2.1 4^{th} gear

speed range ÷ low ⟶ high

no derivative action on dynamometer

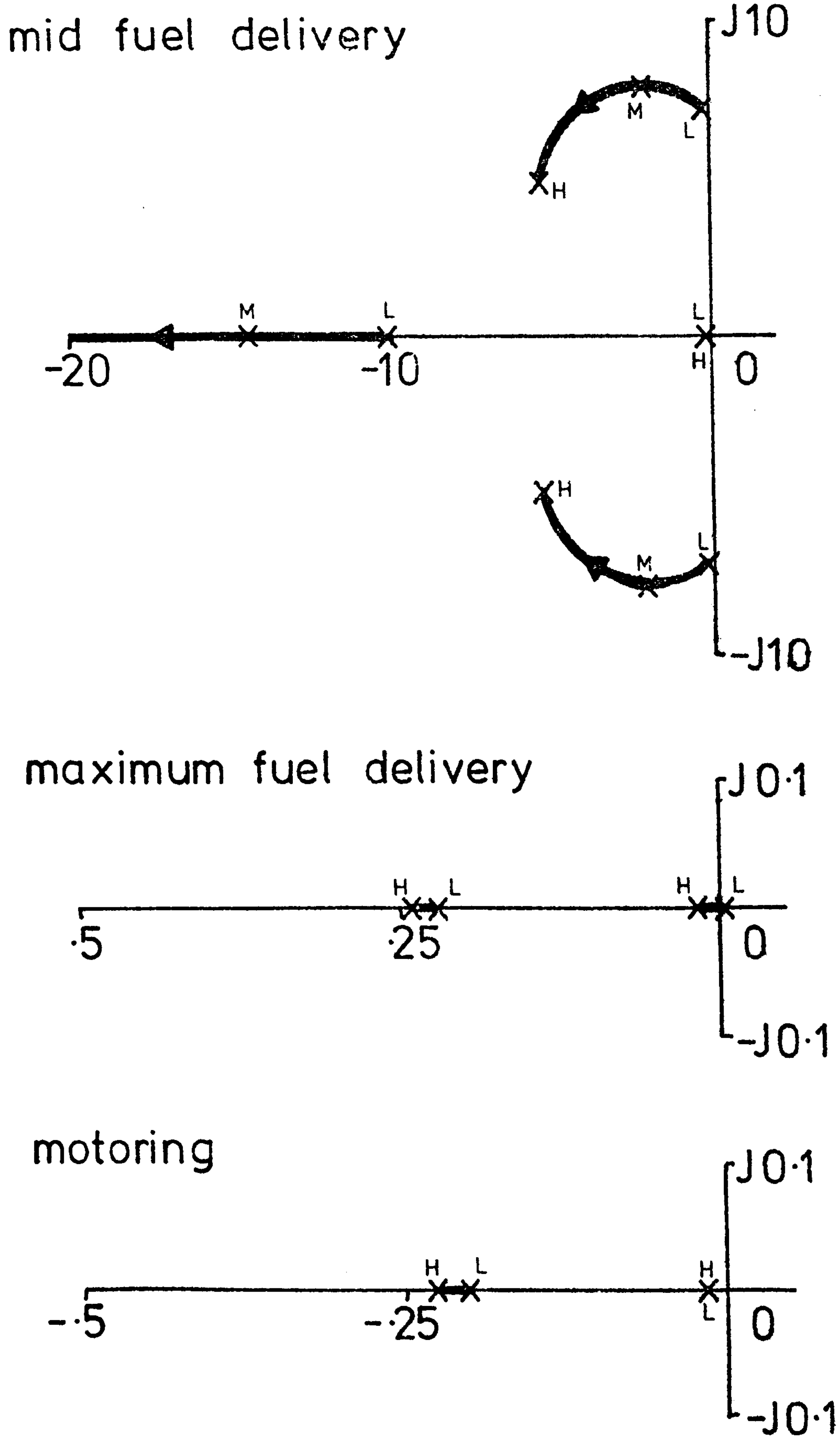

DIESEL ENGINE
ELECTRIC DYNAMOMETER

GRAPH G71

method 2.1 4^{th} gear
speed range ÷ low ⟶ high
acceleration lag = 1 s

mid fuel delivery

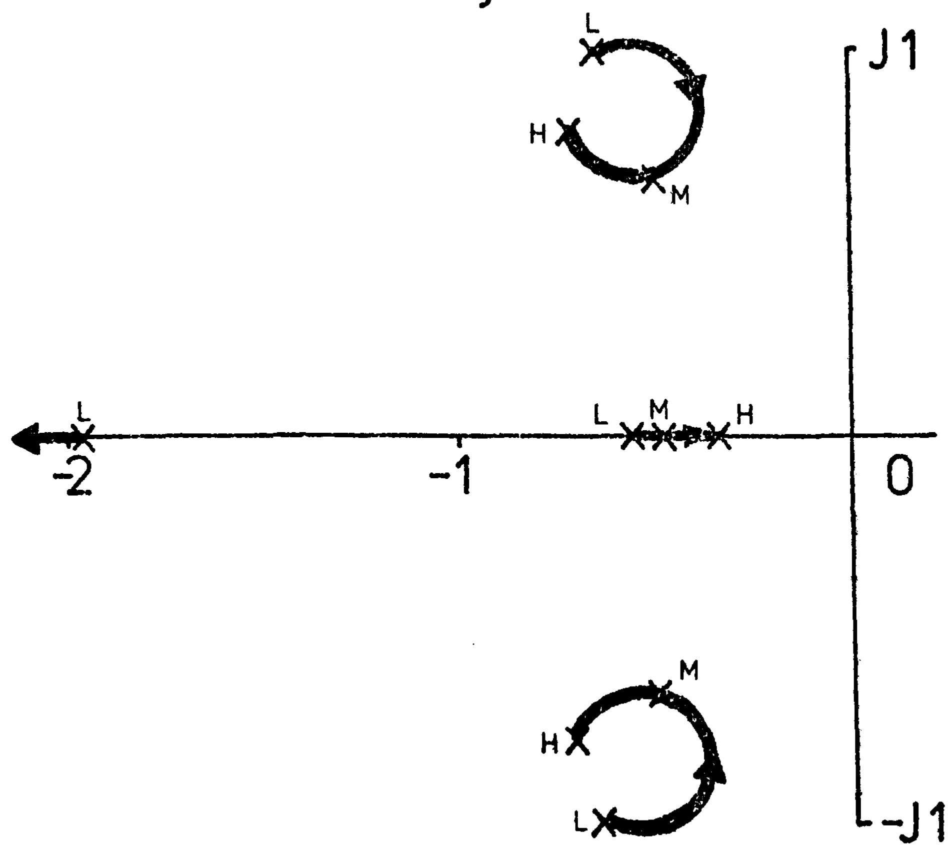

maximum fuel delivery

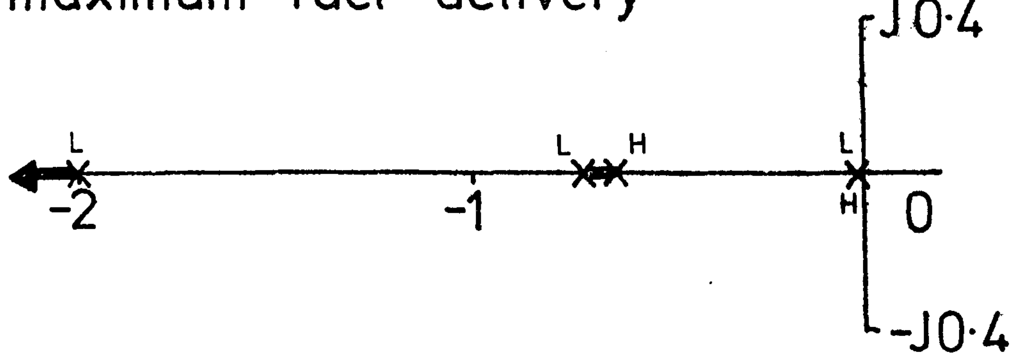

motoring

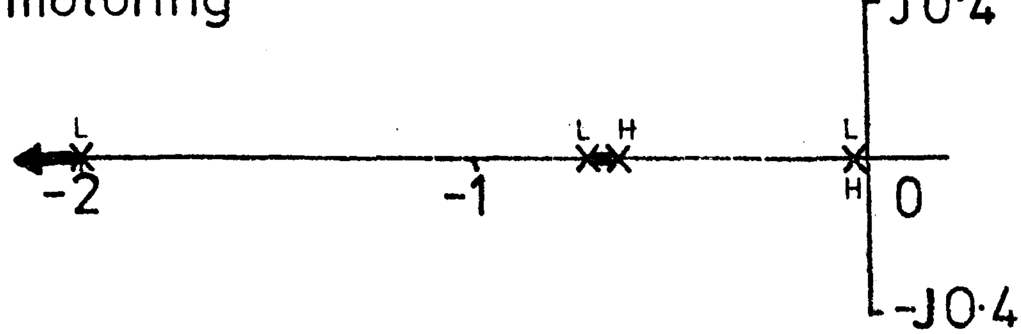

DIESEL ENGINE
ELECTRIC DYNAMOMETER

GRAPH G72

method 2.2 1st gear

speed range ÷ low ⟶ high

mid fuel delivery

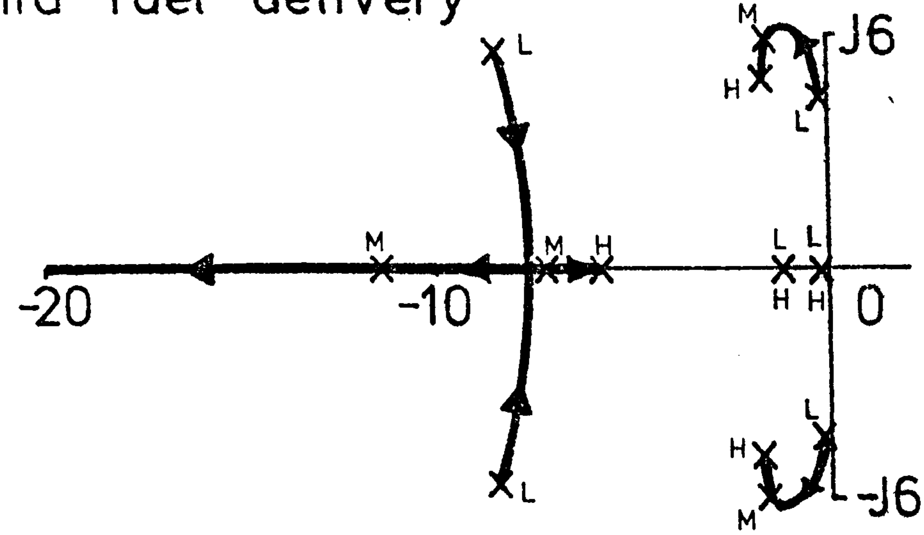

maximum fuel delivery

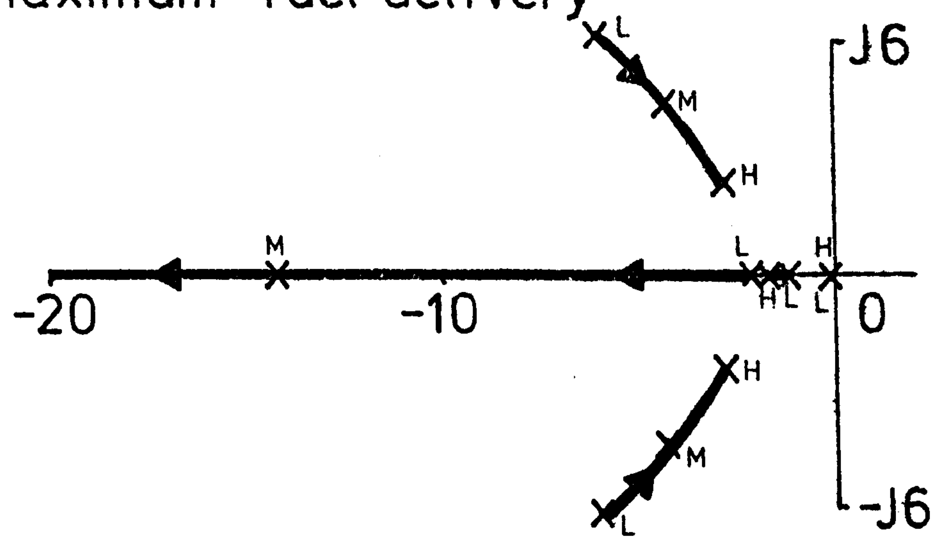

motoring

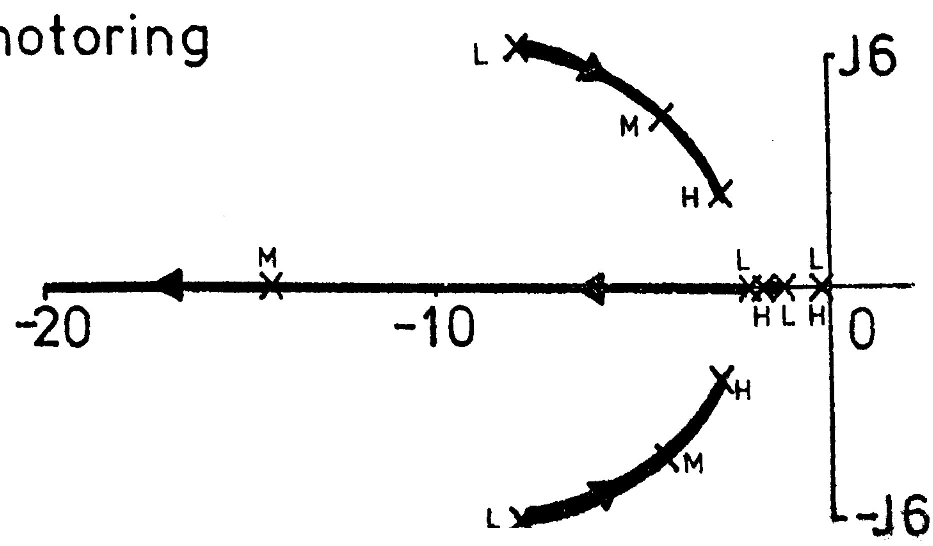

method 2.2 4^{th} gear

speed range ÷ low ⟶ high

mid fuel delivery

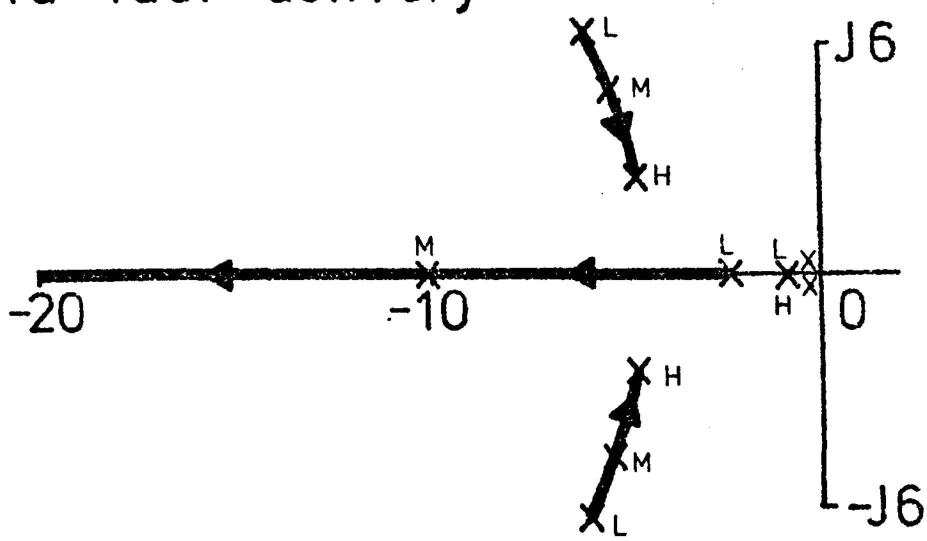

maximum fuel delivery

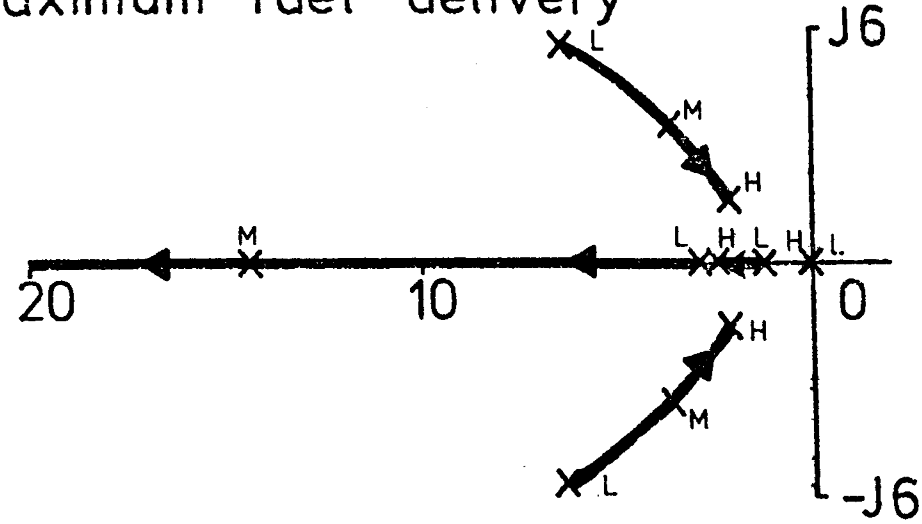

motoring

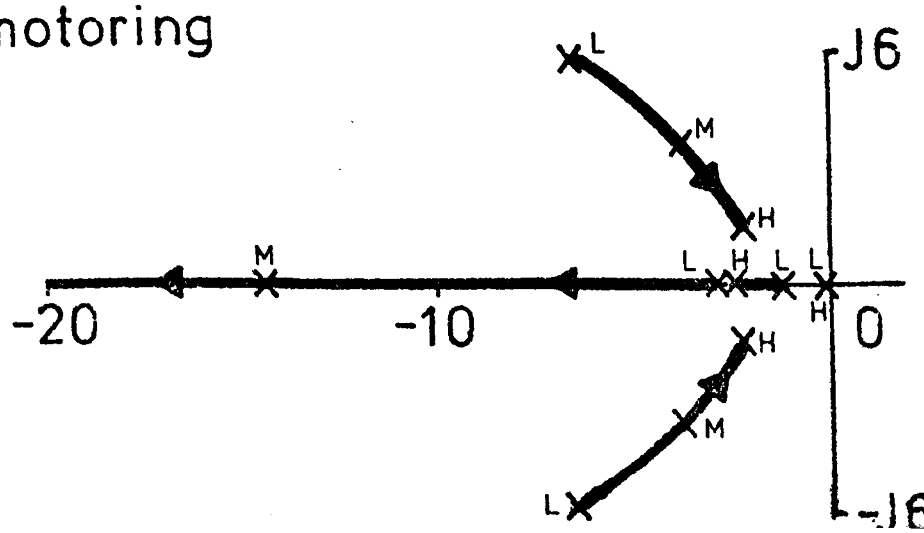

GRAPH G74

basic system (no feedback)

speed range ÷ low ⟶ high
(1000 ⟶ 4000 rev/min)

loading

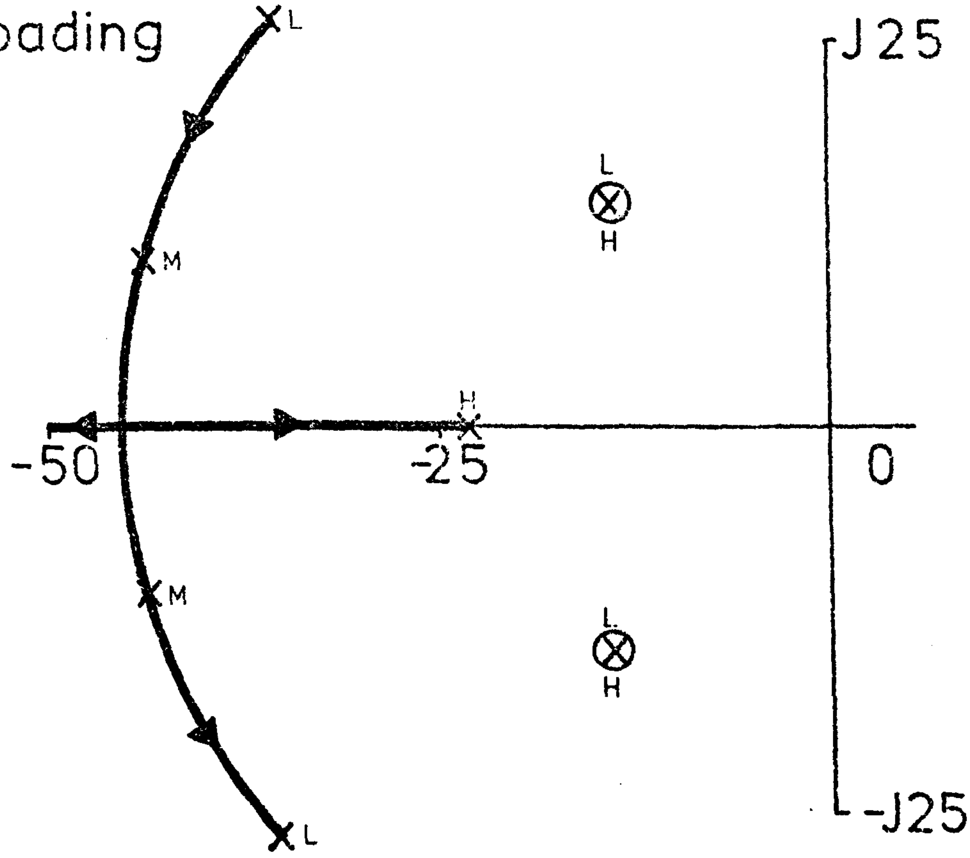

motoring

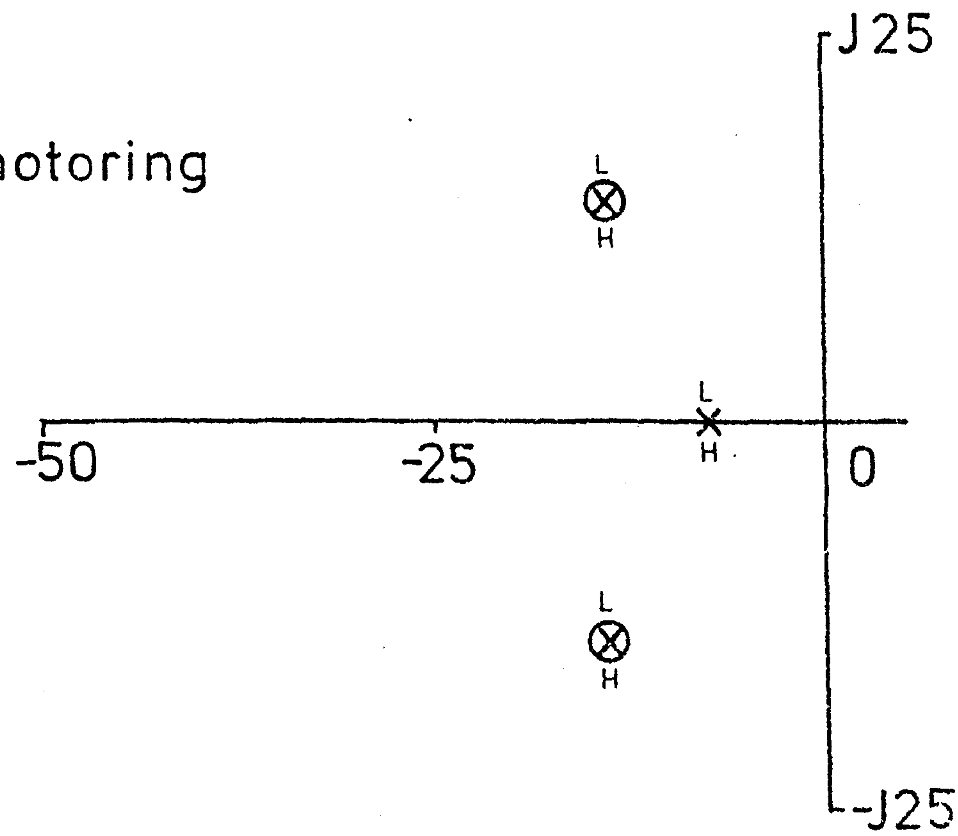

PETROL ENGINE
HYDROSTATIC DYNAMOMETER

GRAPH G75

method 1.1

speed range ÷ low ⟶ high

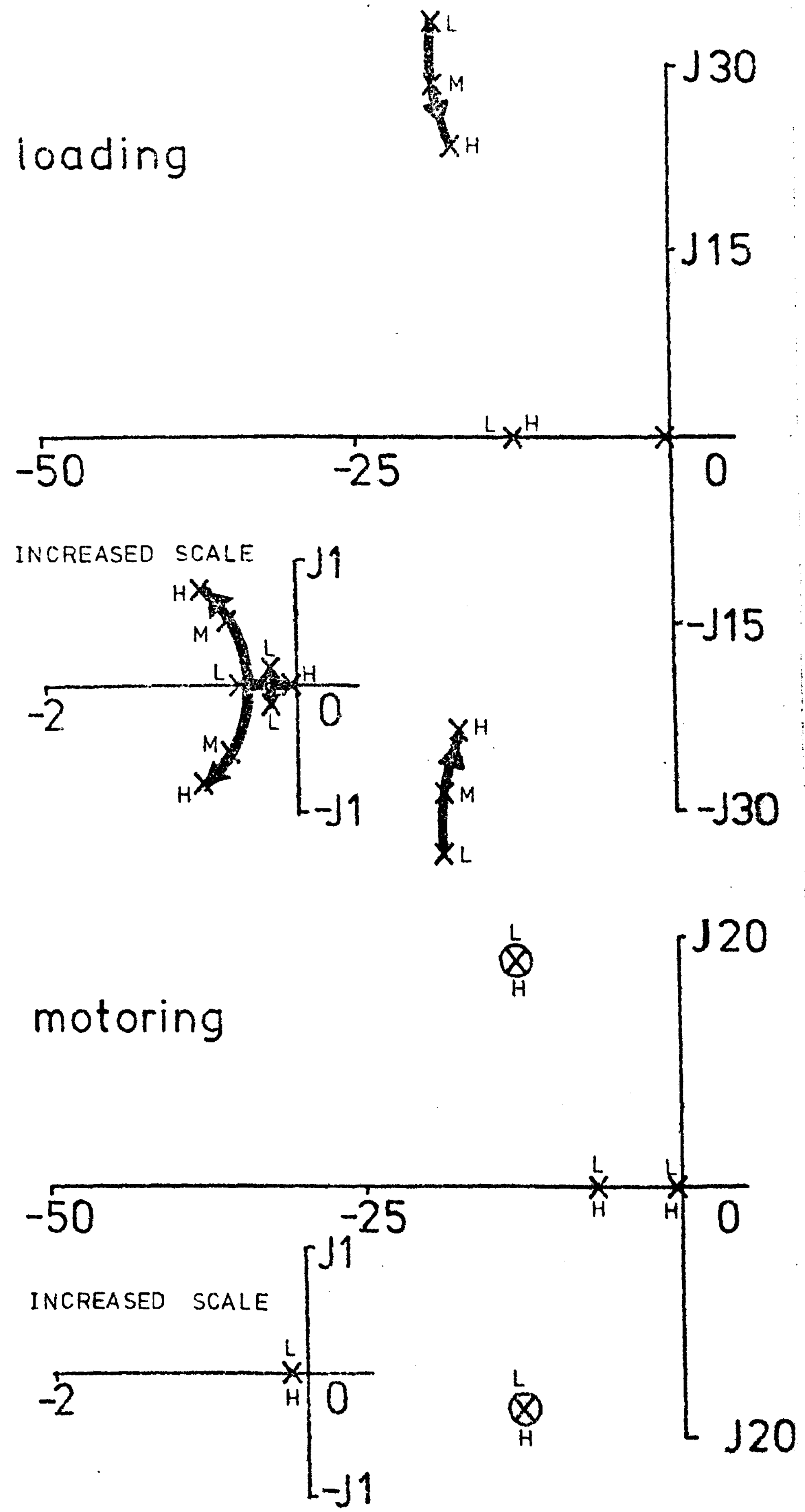

PETROL ENGINE
HYDROSTATIC DYNAMOMETER

GRAPH G76

method 1.2

speed range÷low ⟶ high

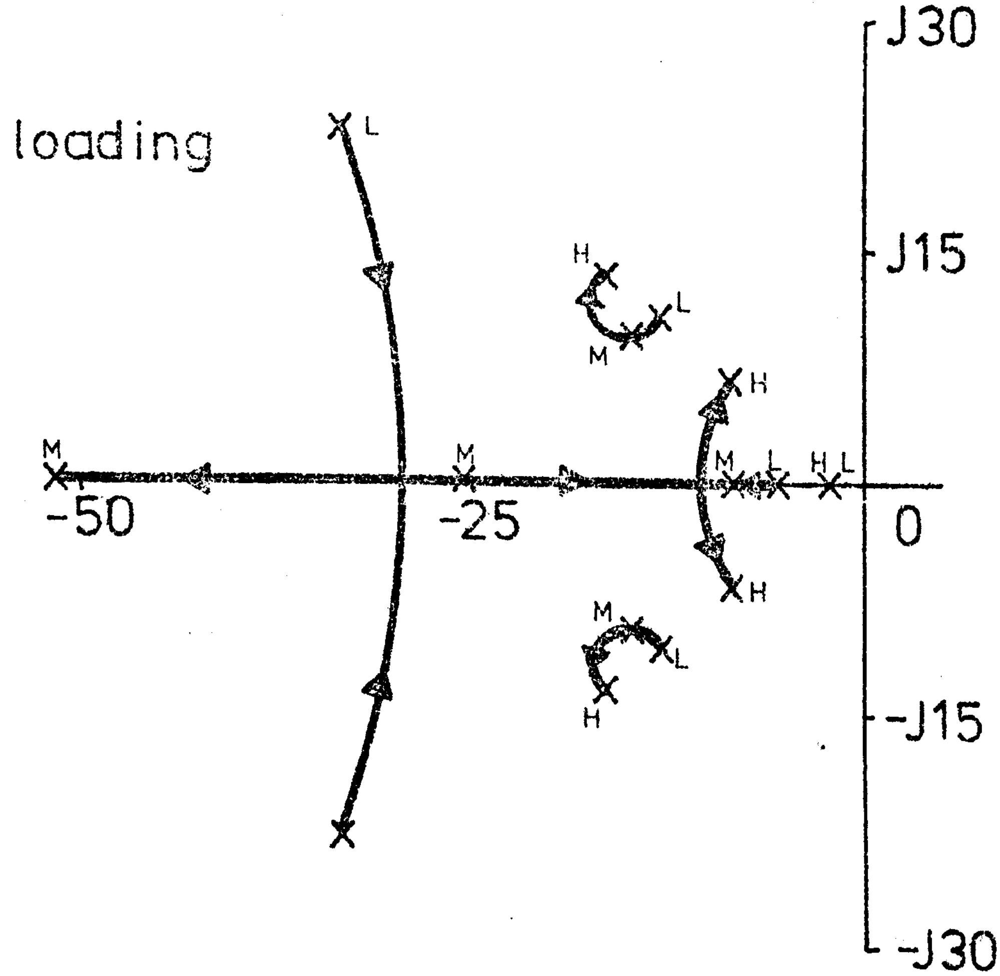

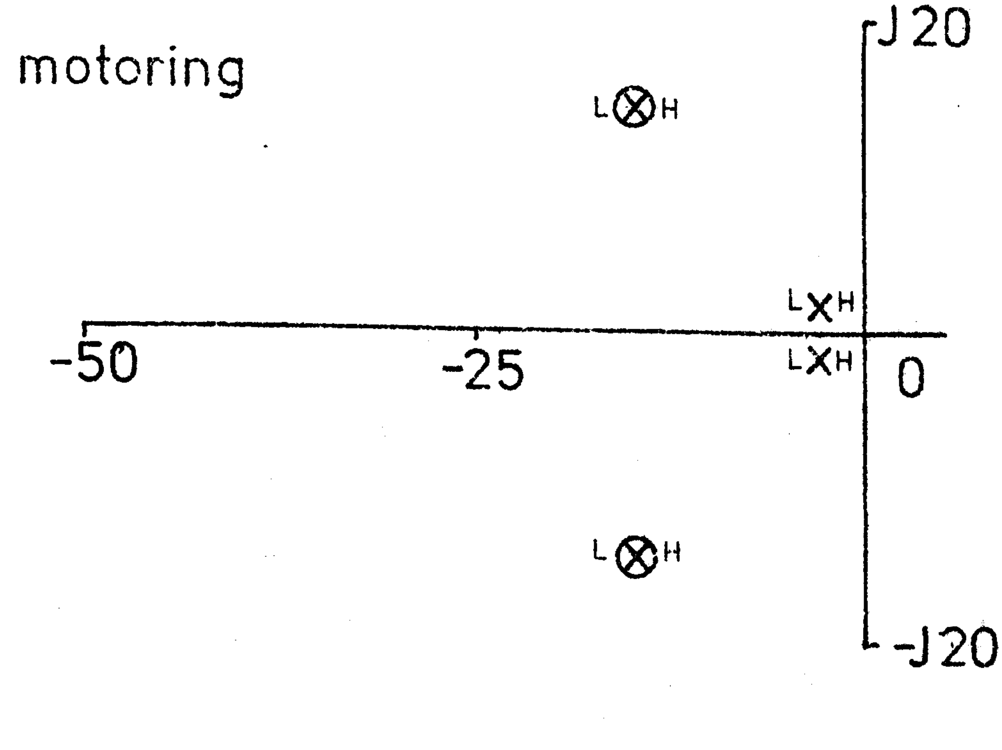

PETROL ENGINE
HYDROSTATIC DYNAMOMETER

GRAPH G77

method 2.1 1^{st} gear

speed range ÷ low ⟶ high

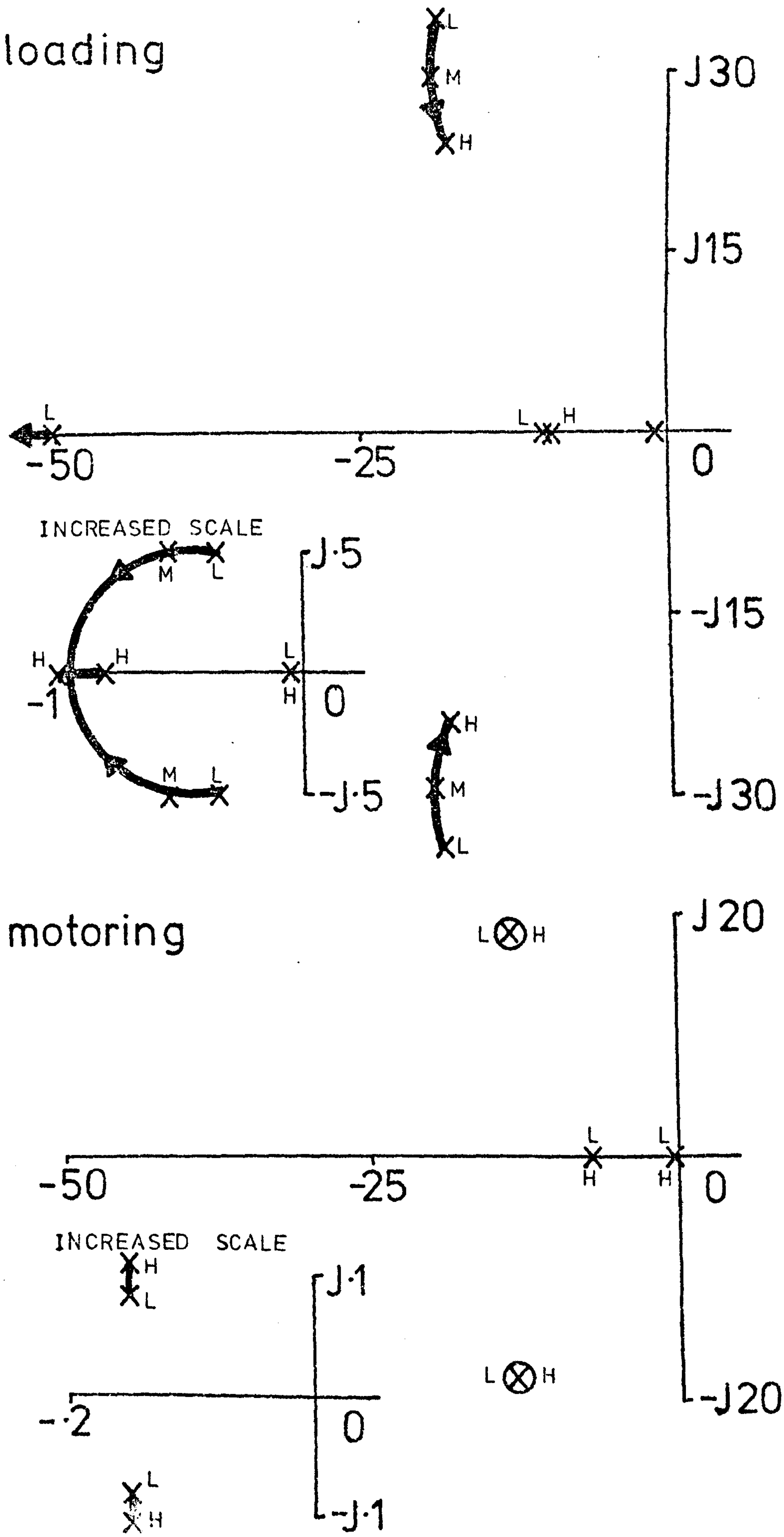

PETROL ENGINE
HYDROSTATIC DYNAMOMETER

GRAPH G78

method 2.1 4th gear

speed range÷ low → high

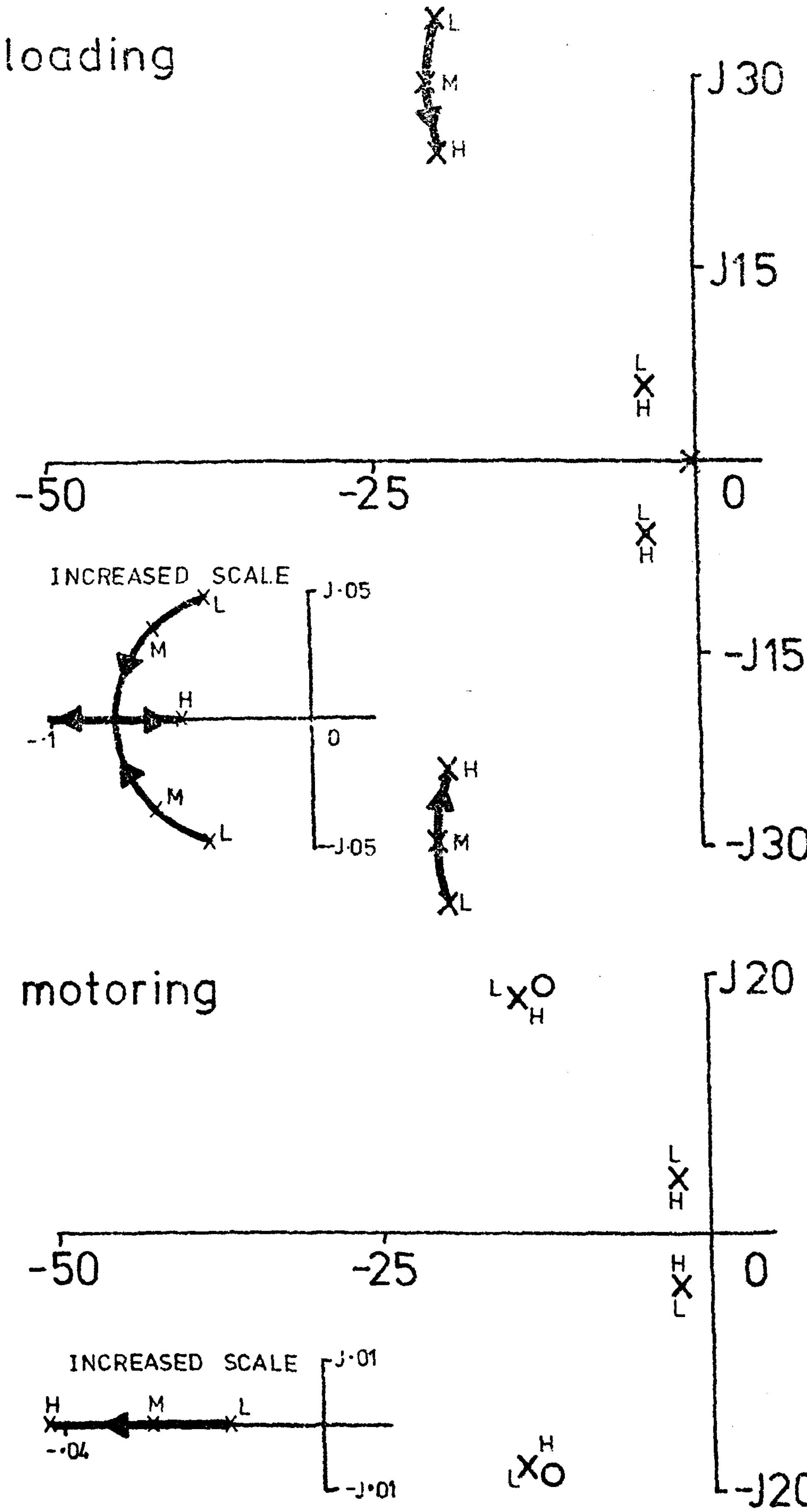

PETROL ENGINE
HYDROSTATIC DYNAMOMETER

GRAPH G79

method 2.2 1st gear

speed range ÷ low ⟶ high

loading

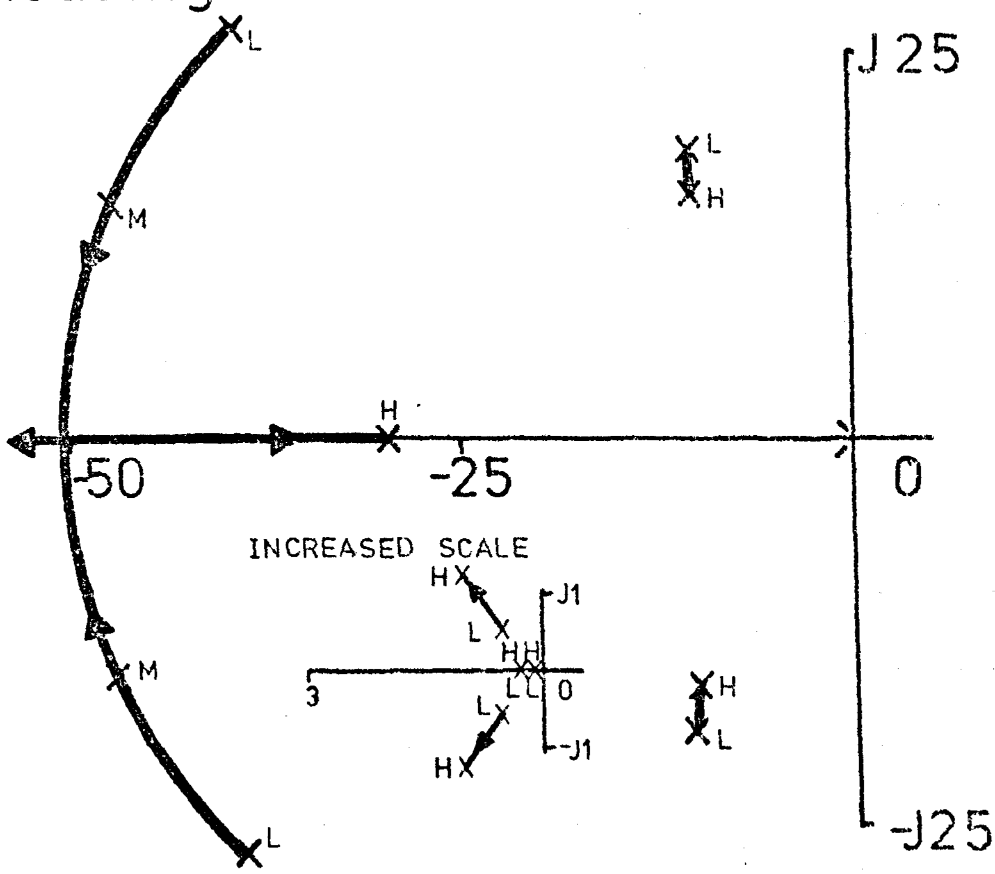

motoring

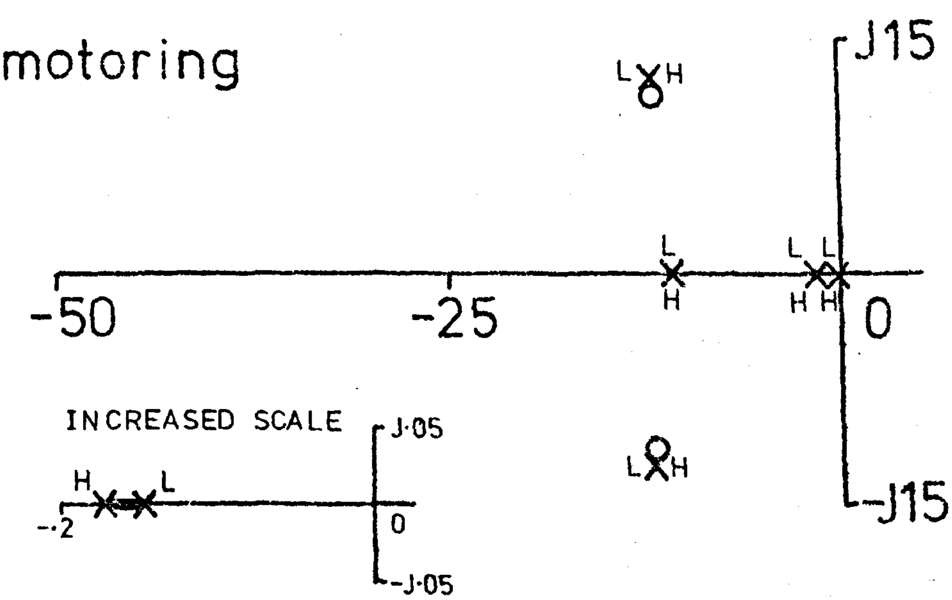

PETROL ENGINE
HYDROSTATIC DYNAMOMETER

GRAPH G80

method 2.2 4^{th} gear

speed range ÷ low ⟶ high

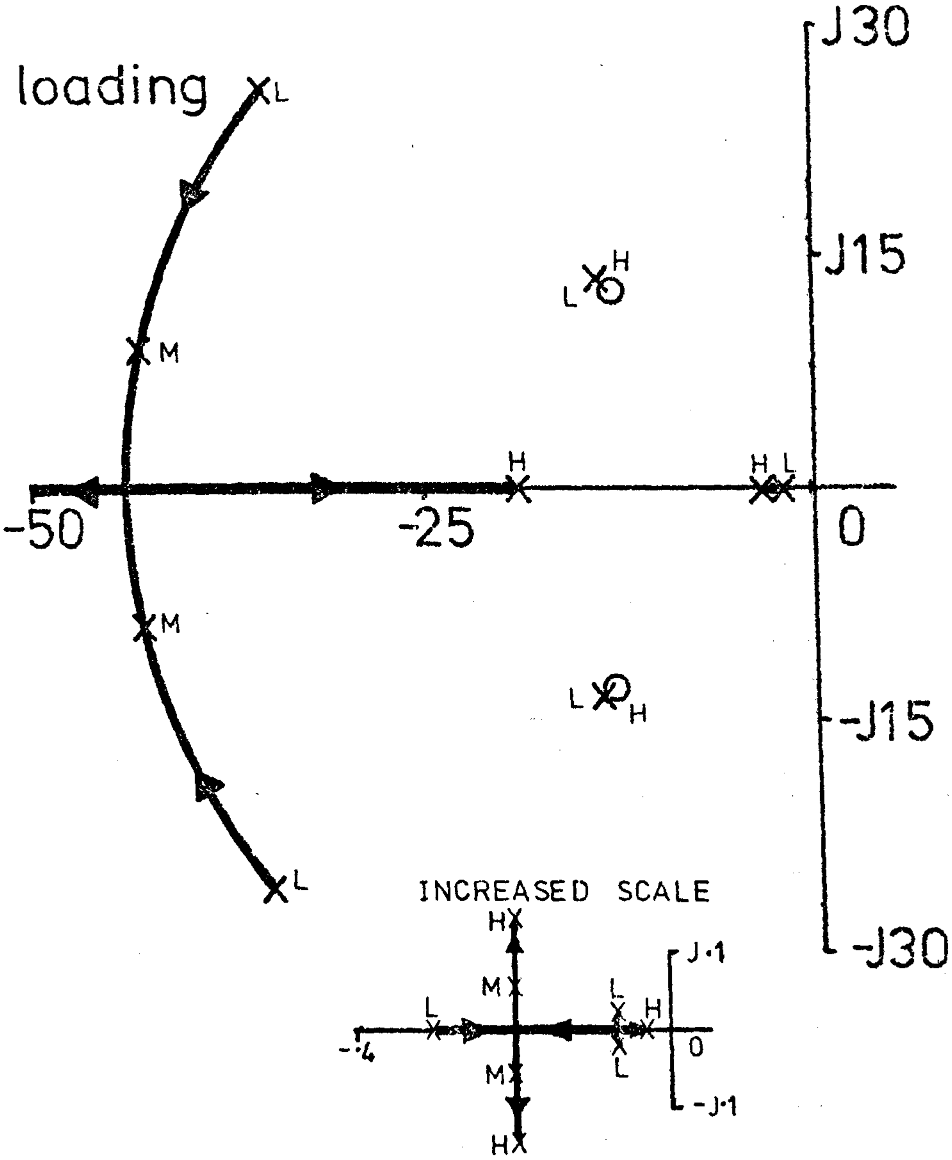

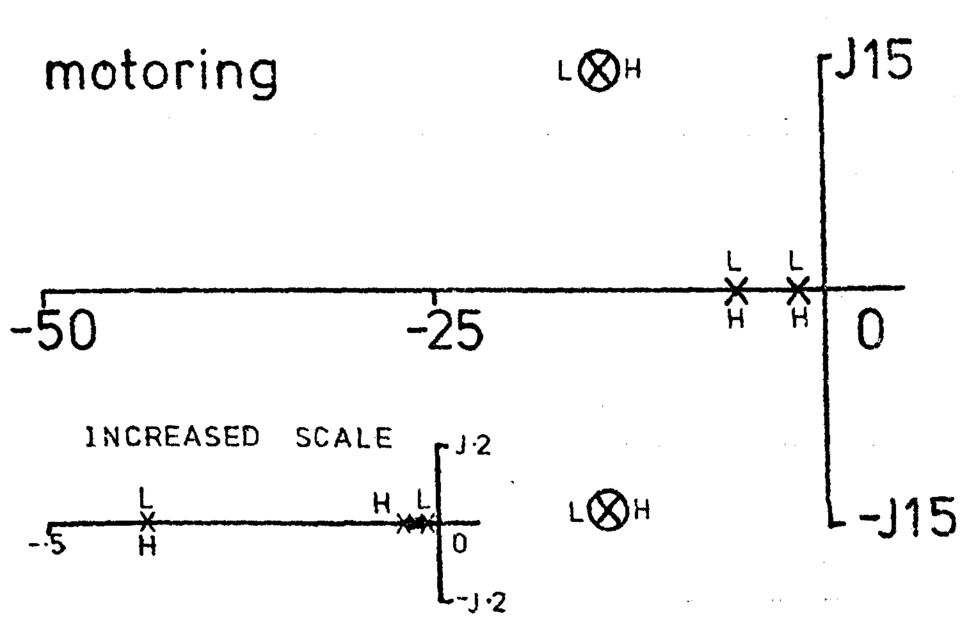

PETROL ENGINE
FAST RESPONSE DYNAMOMETER

GRAPH G81

method 1.1

speed range ÷ low ⟶ high

loading

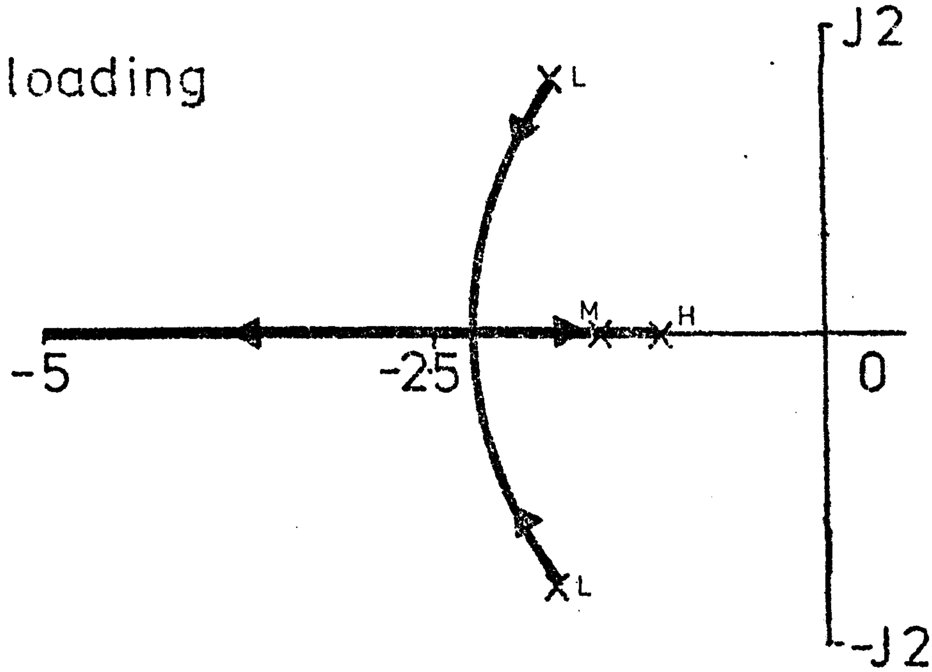

motoring

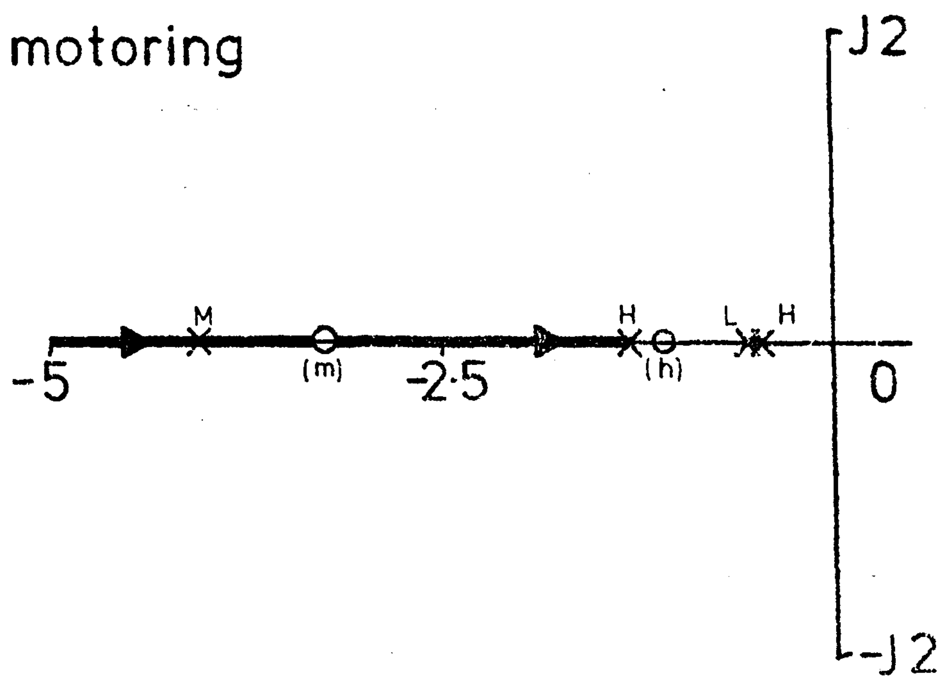

GRAPH G82

method 1.2

speed range÷low ⟶ high

loading

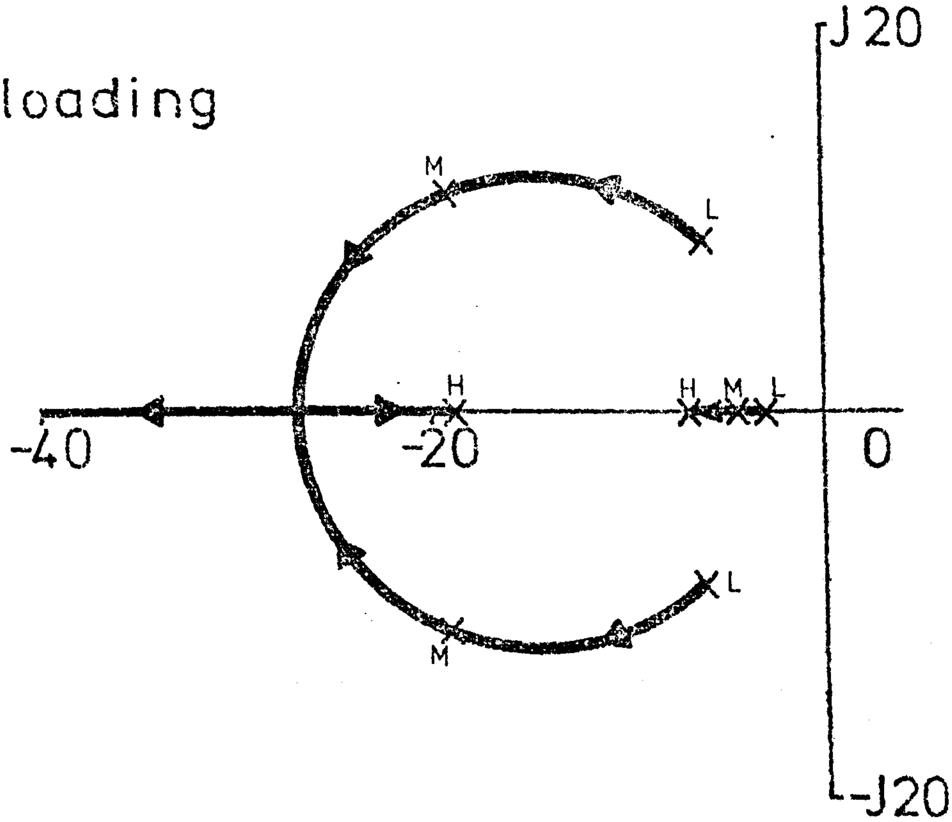

motoring

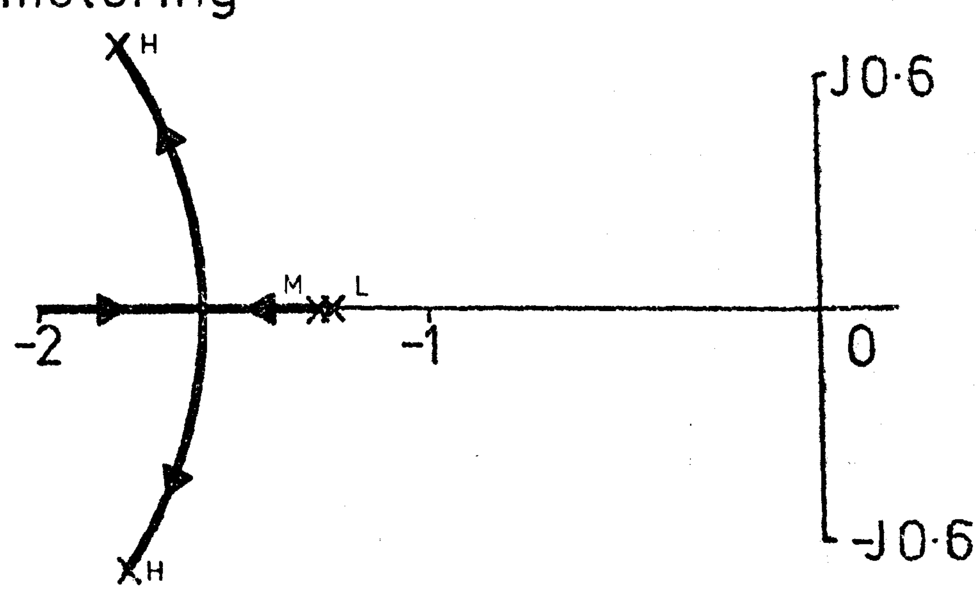

PETROL ENGINE
FAST RESPONSE DYNAMOMETER

GRAPH G83

method 2.1 1st gear

speed range ÷ low ⟶ high

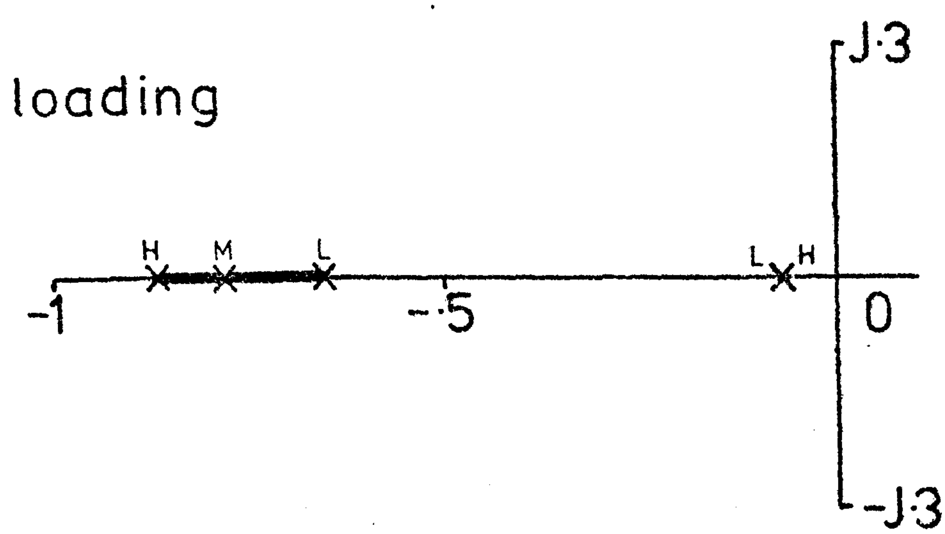

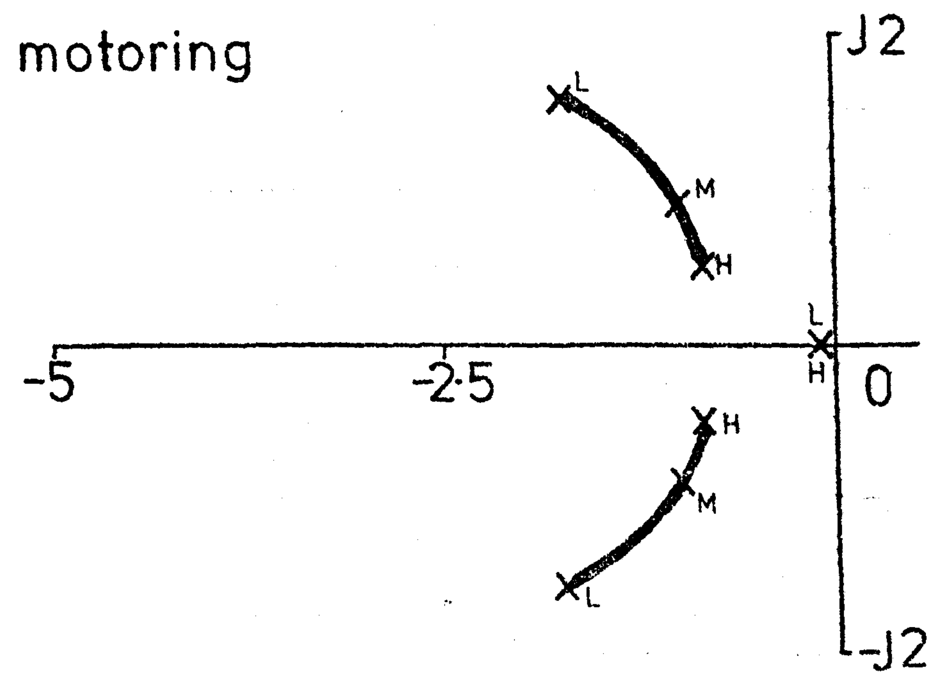

GRAPH G84

method 2.1 4^{th} gear

speed range ÷ low ⟶ high

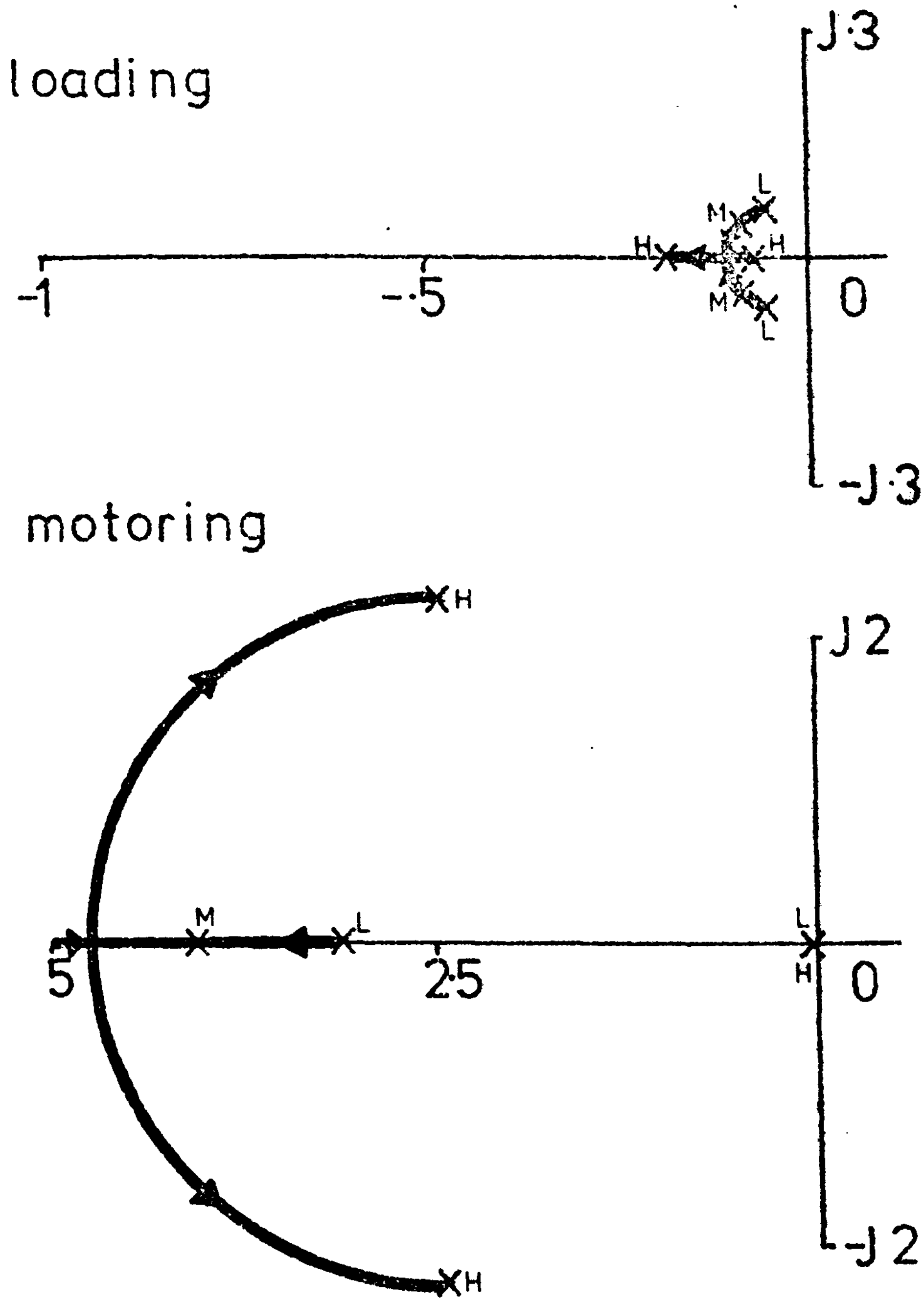

PETROL ENGINE
FAST RESPONSE DYNAMOMETER

GRAPH G85

method 2.2 1st gear

speed range ÷ low ⟶ high

loading

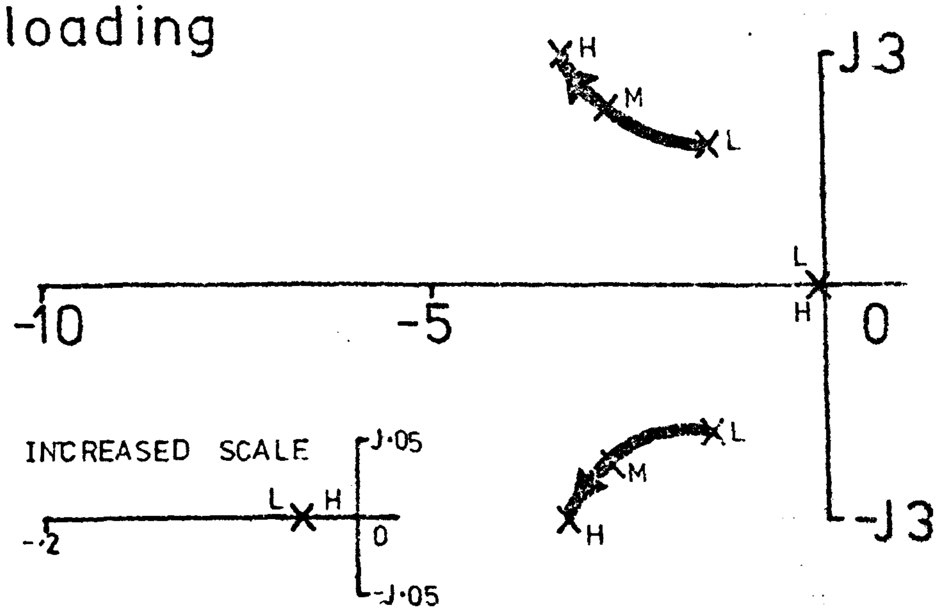

motoring

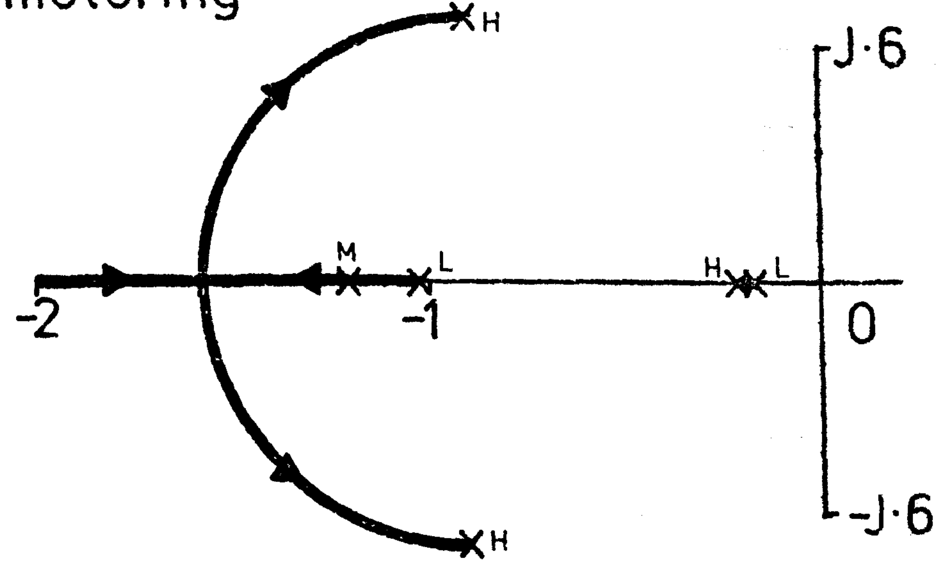

GRAPH G86

method 2.2 4th gear

speed range ÷ low ——▶ high

loading

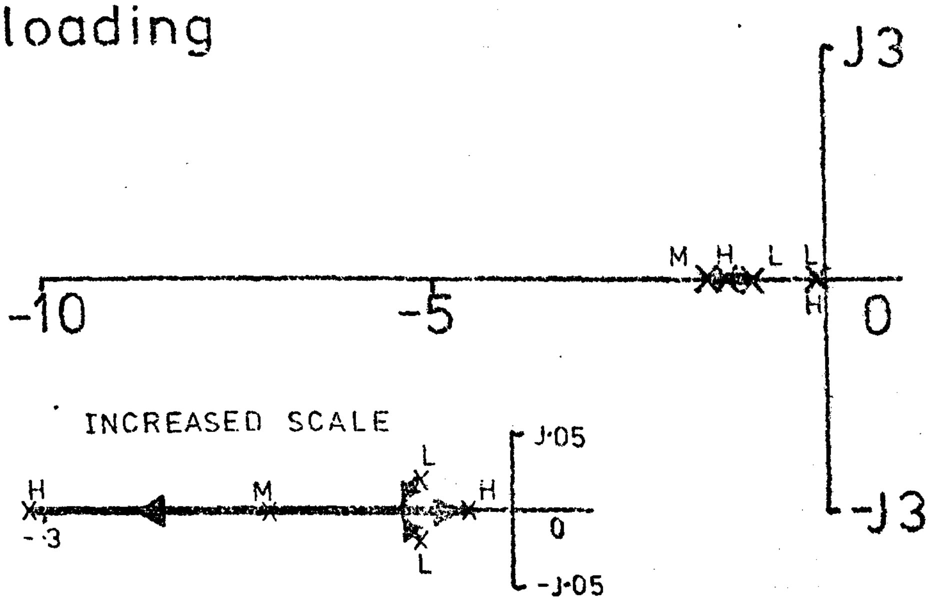

motoring

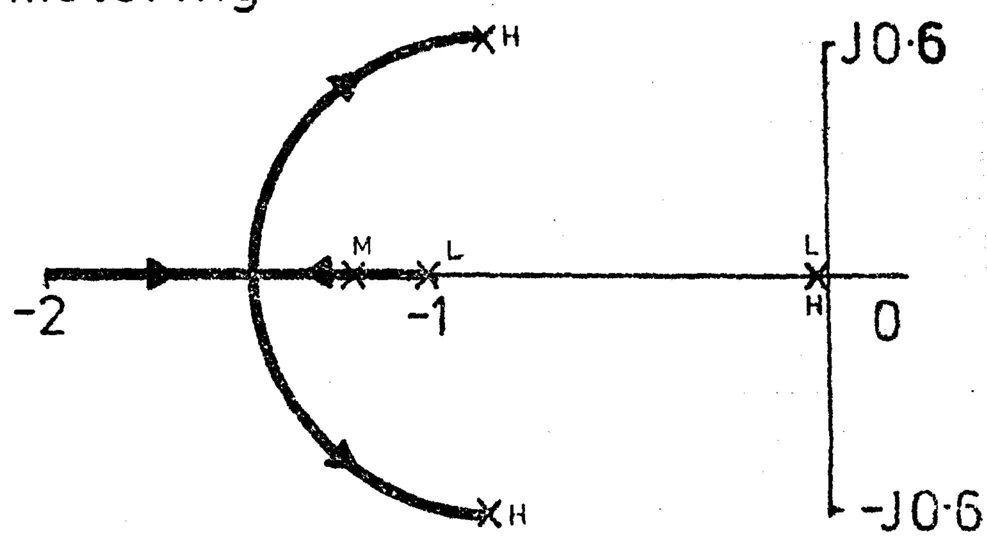

method 1.1

speed range÷low ⟶ high

loading

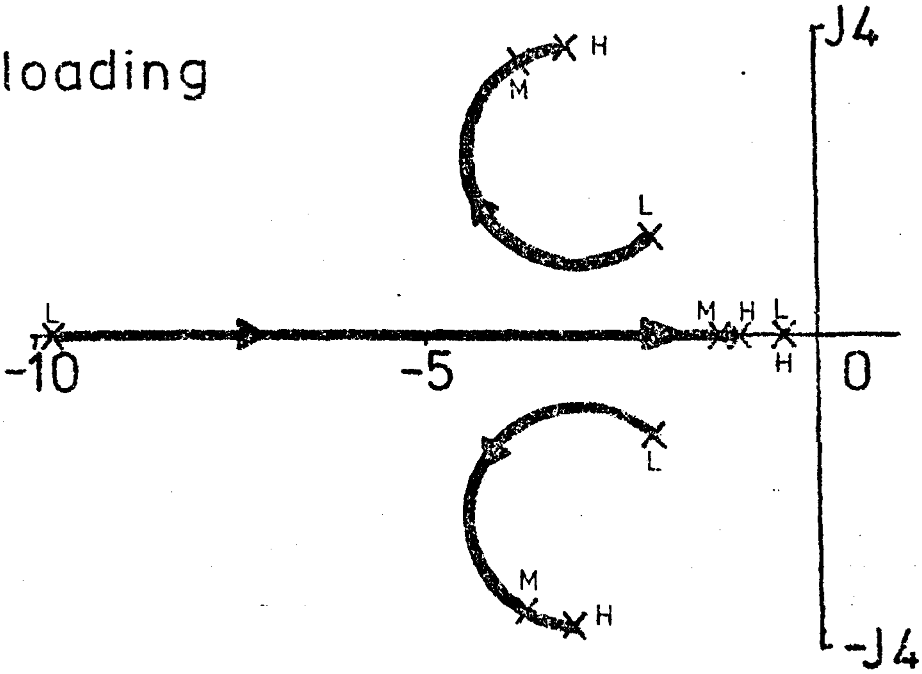

motoring

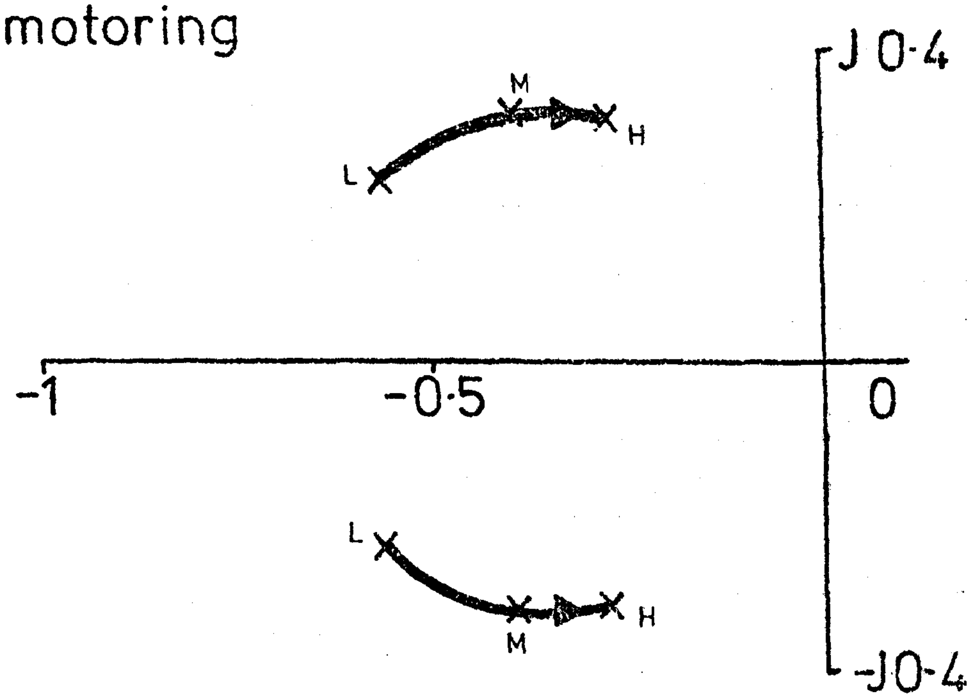

PETROL ENGINE
ELECTRIC DYNAMOMETER

GRAPH G88

method 1.2

speed range÷low ——▶ high

loading

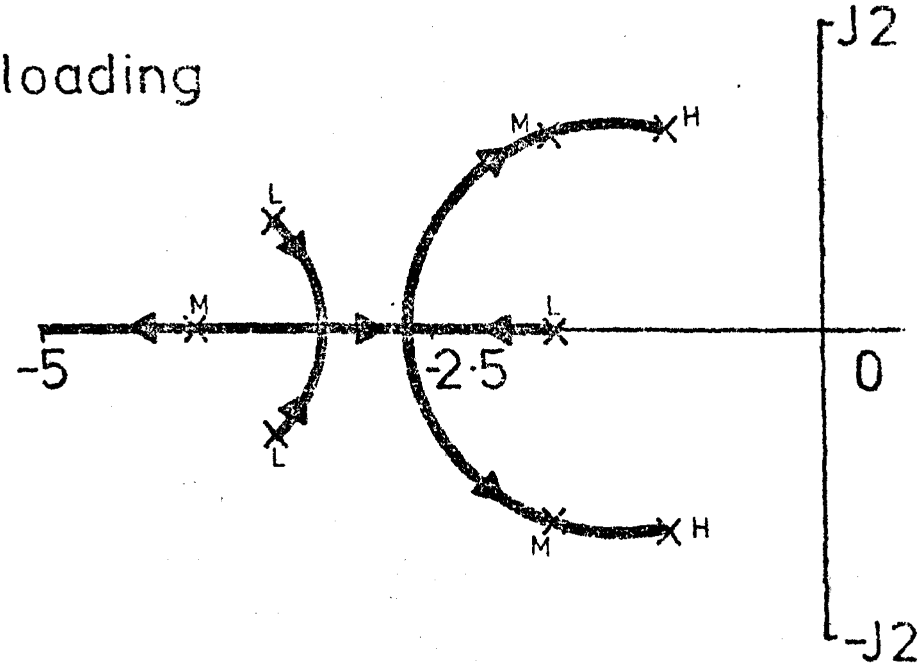

motoring

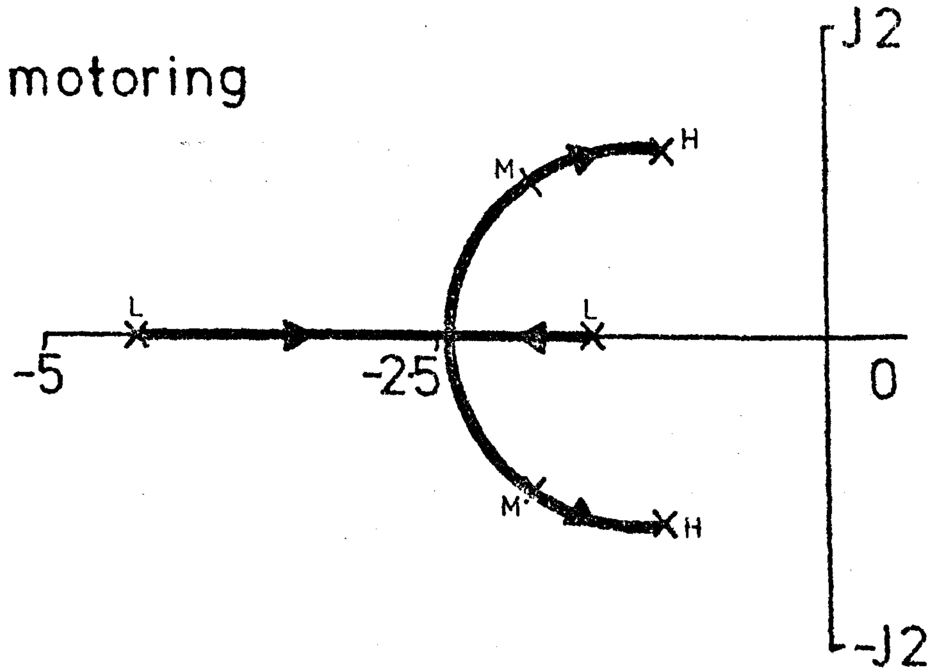

PETROL ENGINE
ELECTRIC DYNAMOMETER

GRAPH G89

method 2.1 1st gear

speed range ÷ low ⟶ high

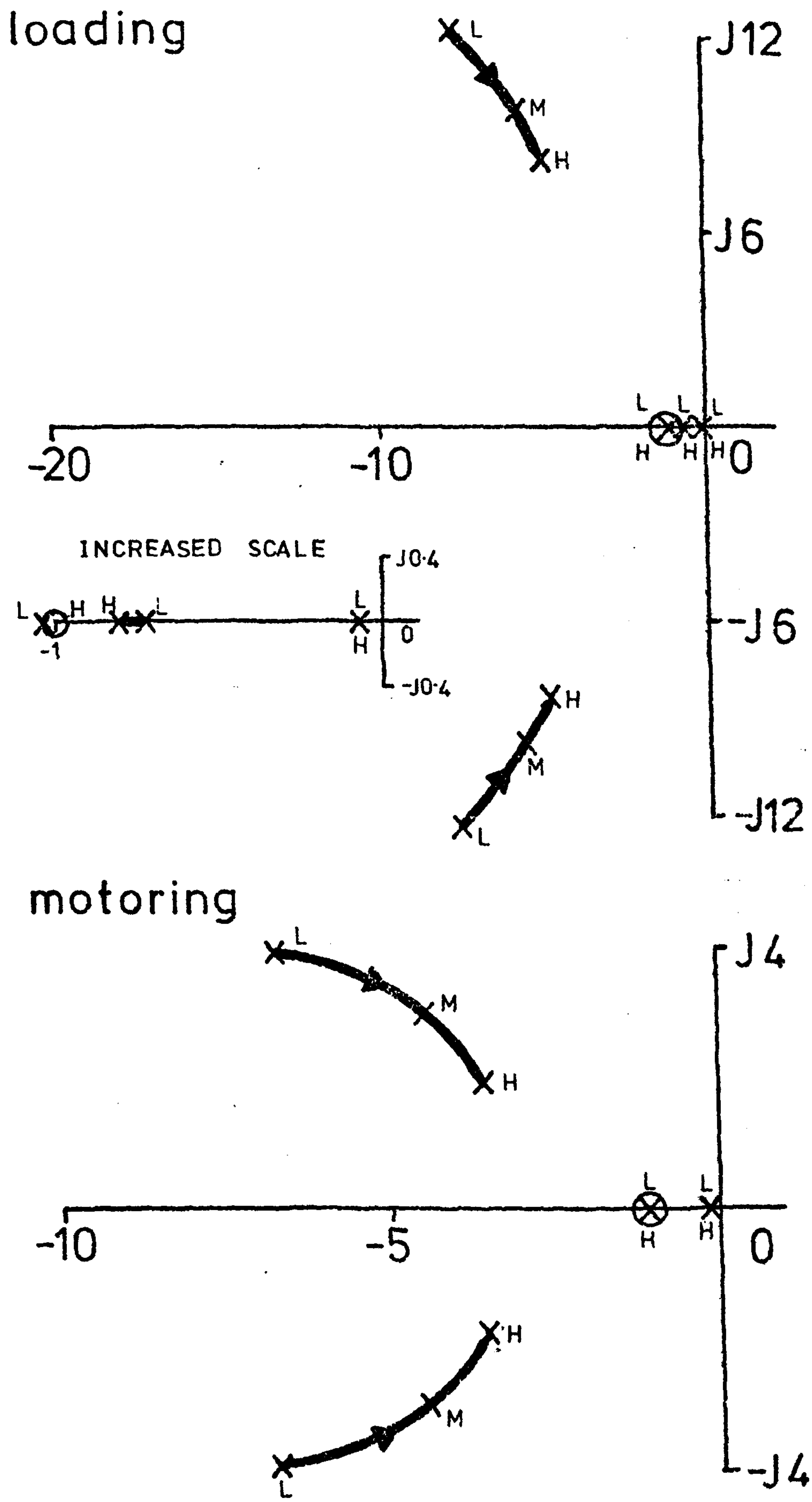

PETROL ENGINE
ELECTRIC DYNAMOMETER

GRAPH G90

method 2.1 4^{th} gear

speed range÷low ⟶ high

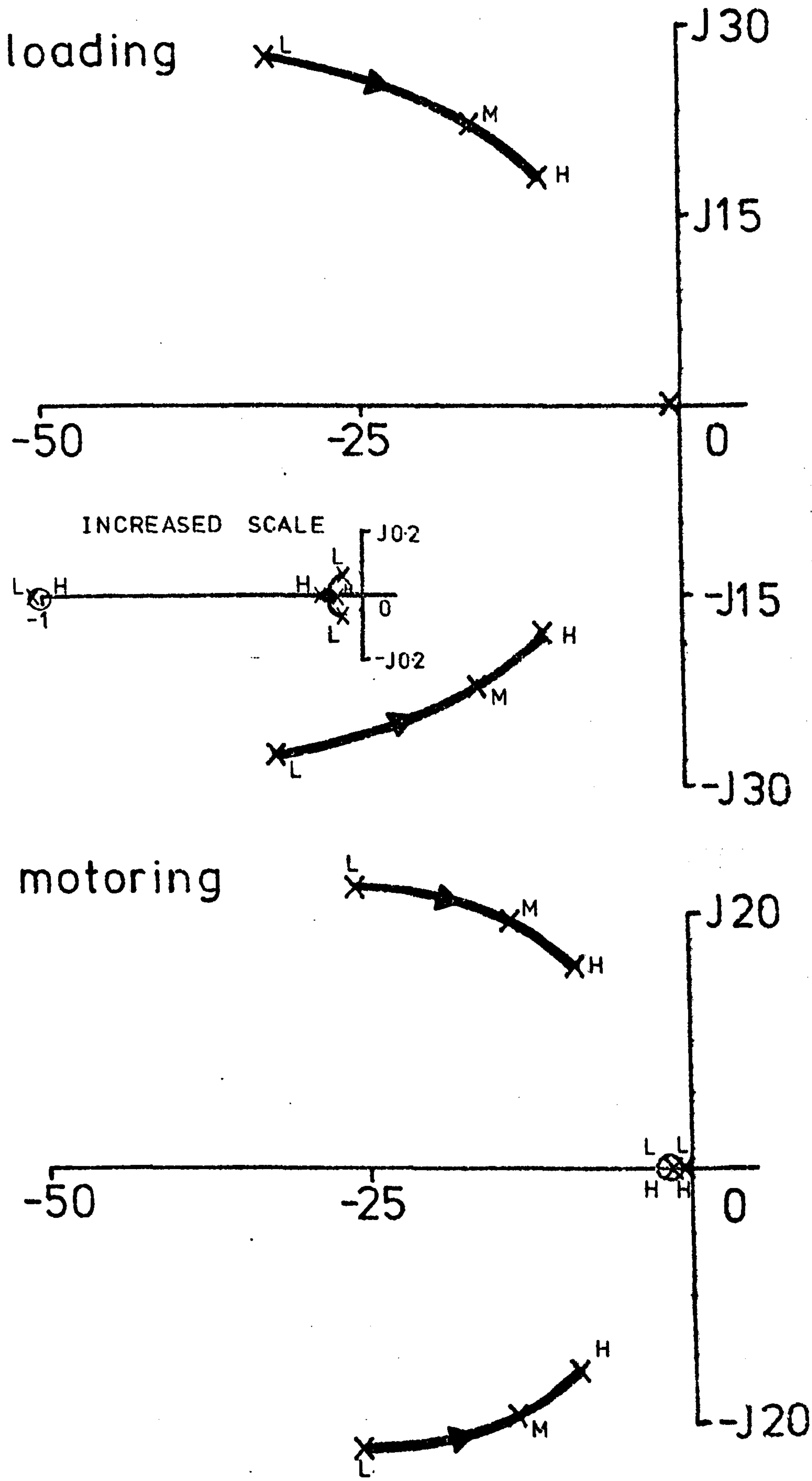

PETROL ENGINE
ELECTRIC DYNAMOMETER

GRAPH G91

method 2.2 1st gear

speed range ÷ low ⟶ high

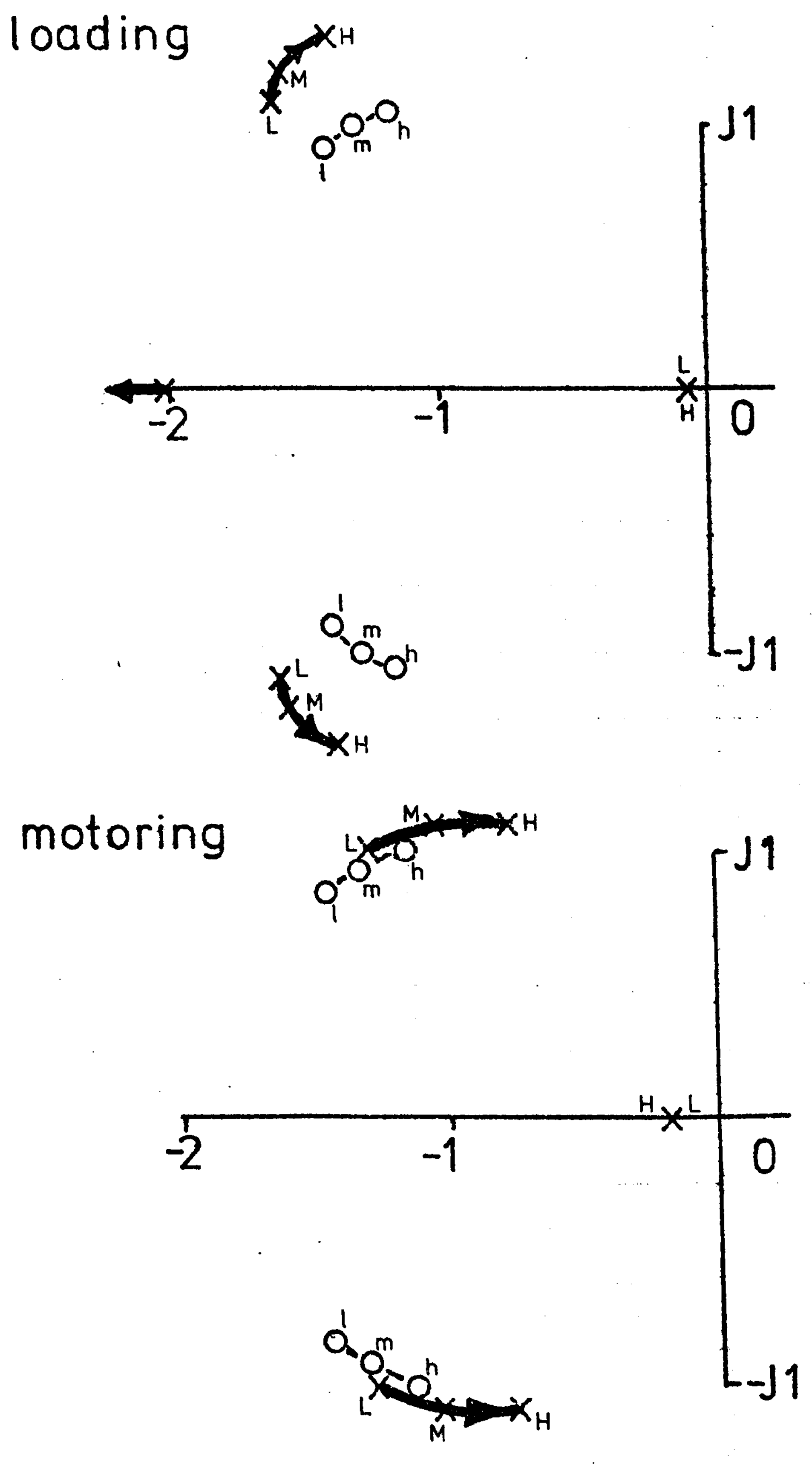

PETROL ENGINE
ELECTRIC DYNAMOMETER

GRAPH G92

method 2.2 4^{th} gear

speed range ÷ low ⟶ high

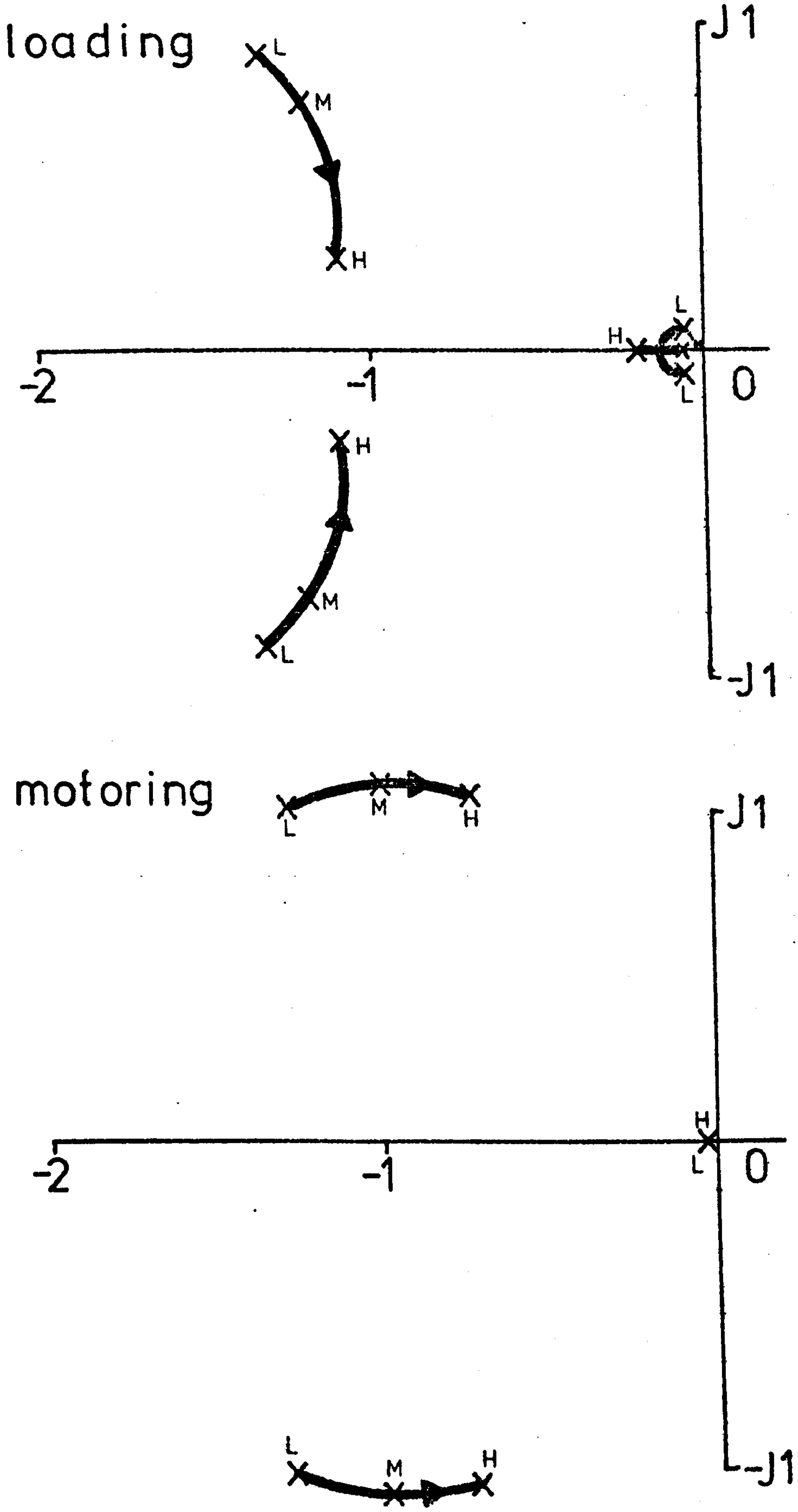

GRAPH G93

resistance characteristics of "Silent Karrier" delivery vehicle (referred to motor shaft)

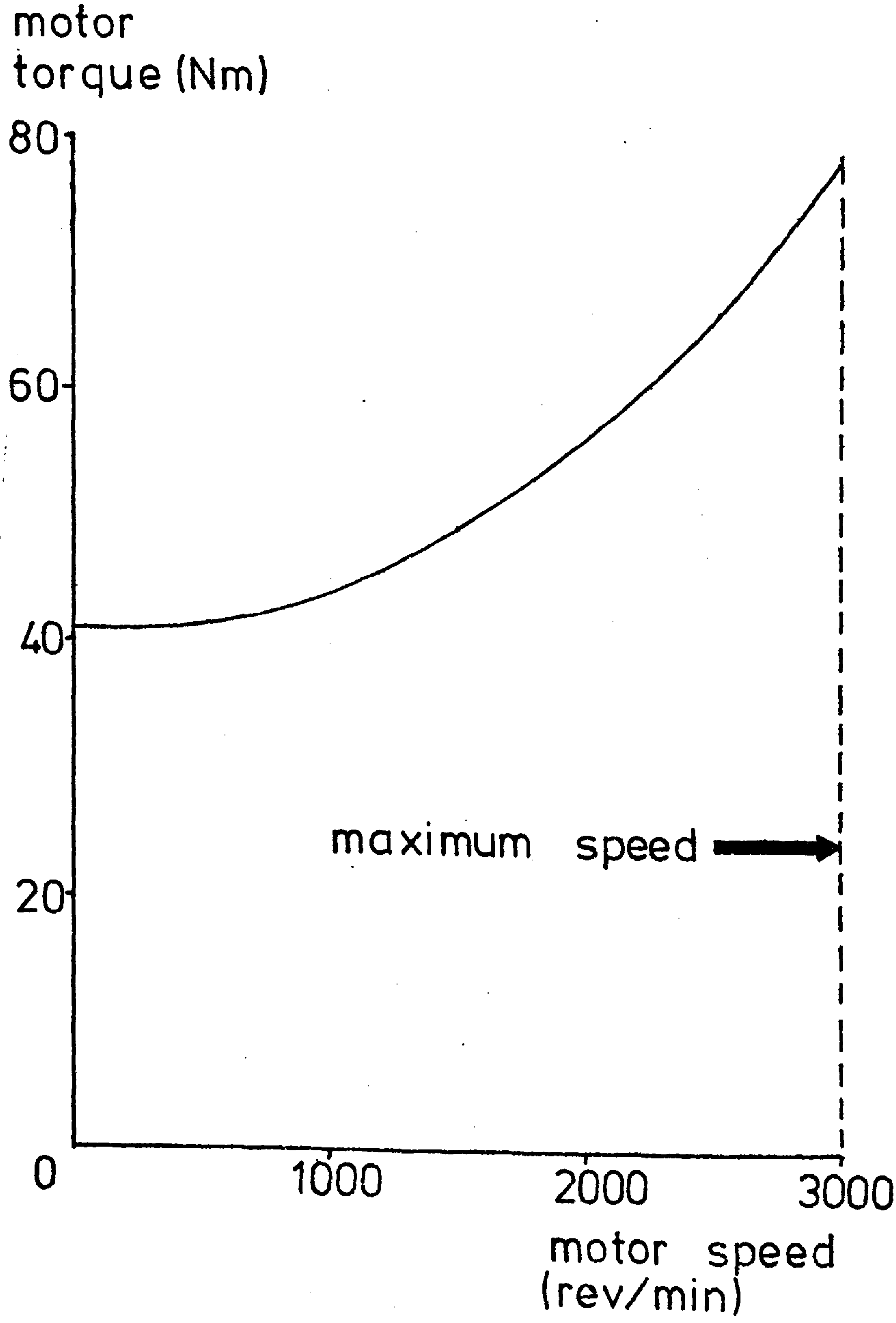

method 1.1

speed range ÷ very low (0 ⟶ 600 r/m)
+low ⟶ high
(600 ⟶ 3000 rev/min)

loading

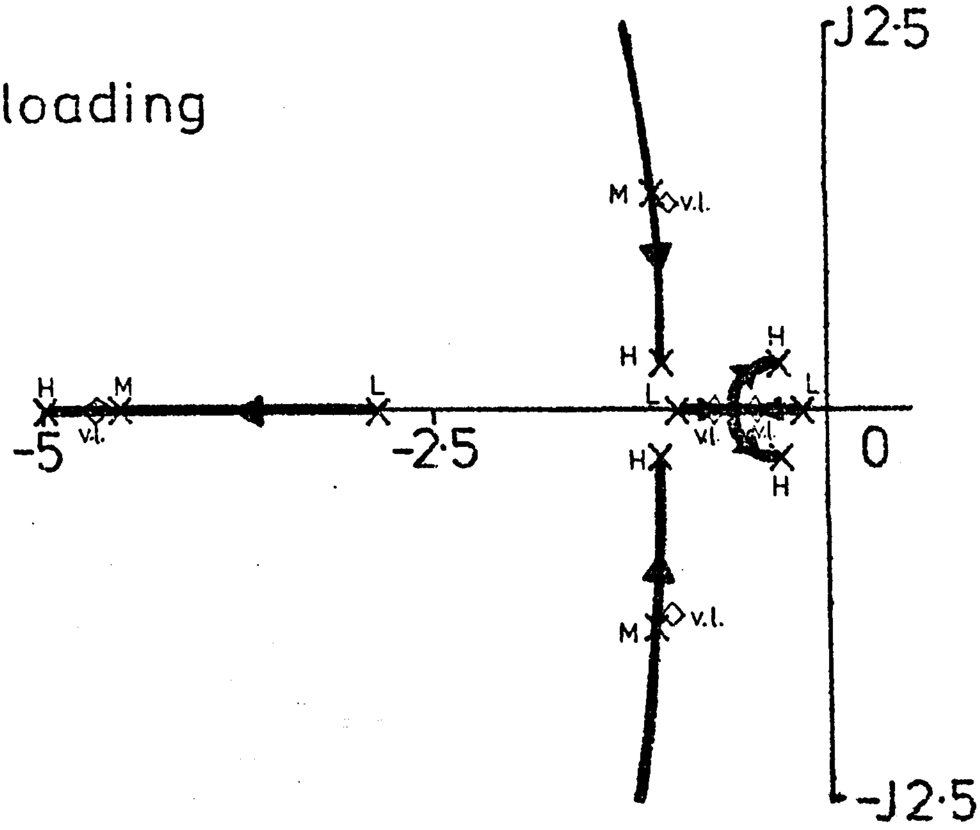

motoring

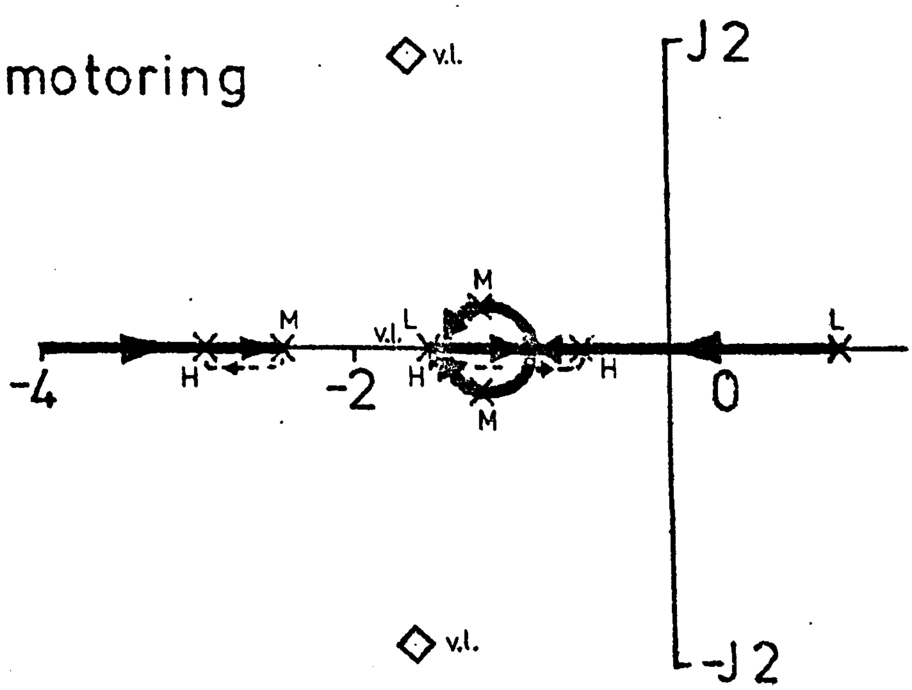

GRAPH G95

method 1.2

speed range ÷ very low
+ low ⟶ high

loading

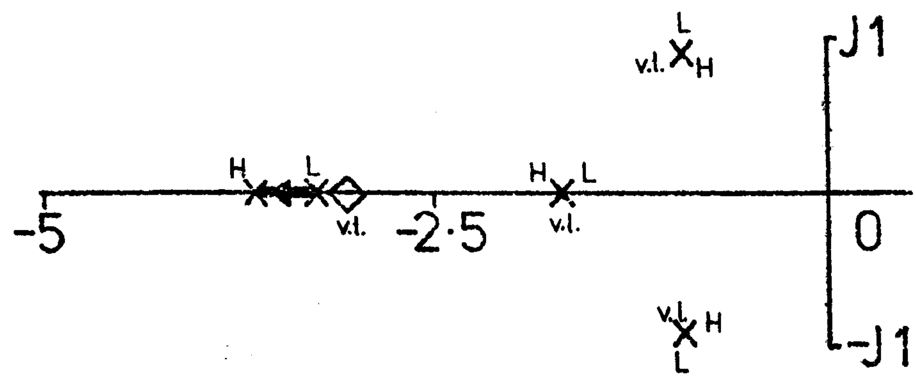

motoring

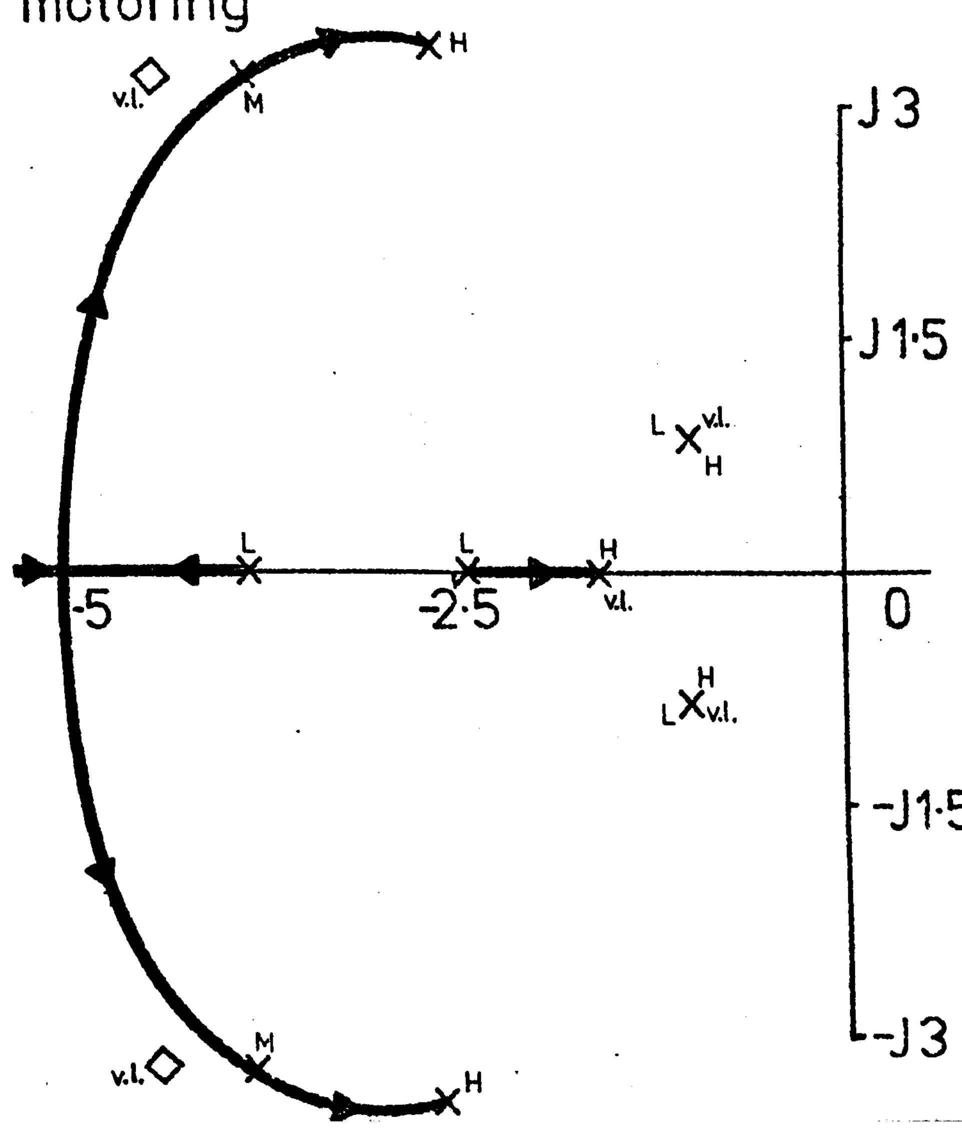

ELECTRIC PRIME MOVER
HYDROSTATIC DYNAMOMETER

GRAPH G96

method 2.1

speed range ÷ very low
+ low → high

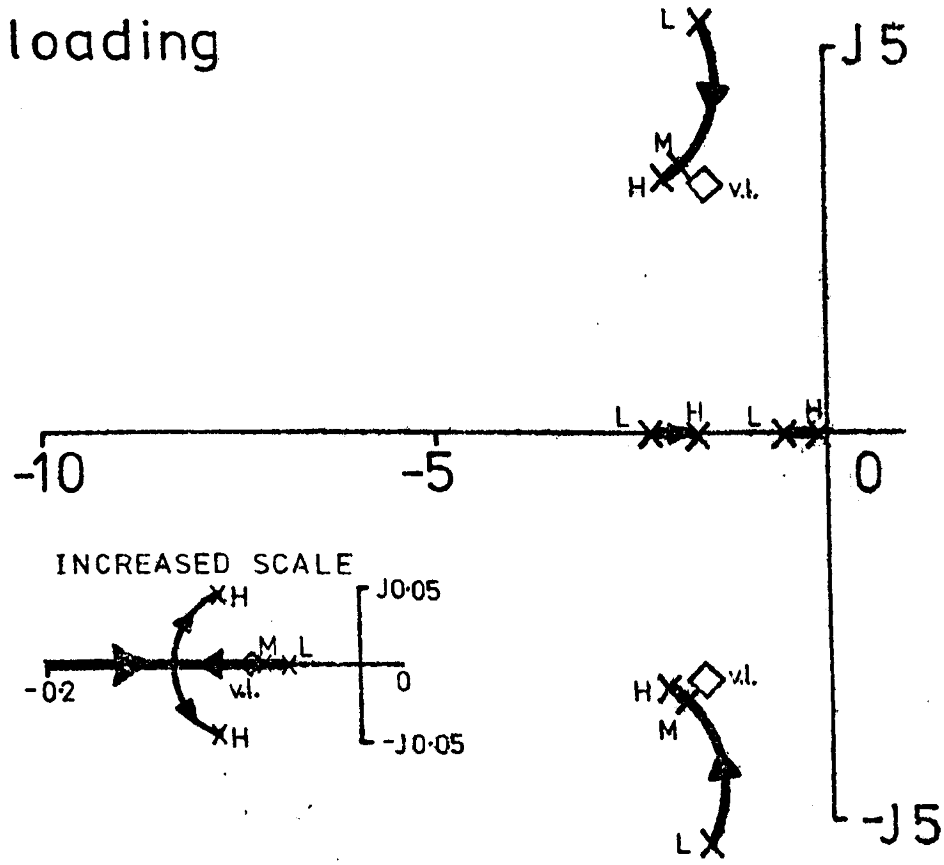

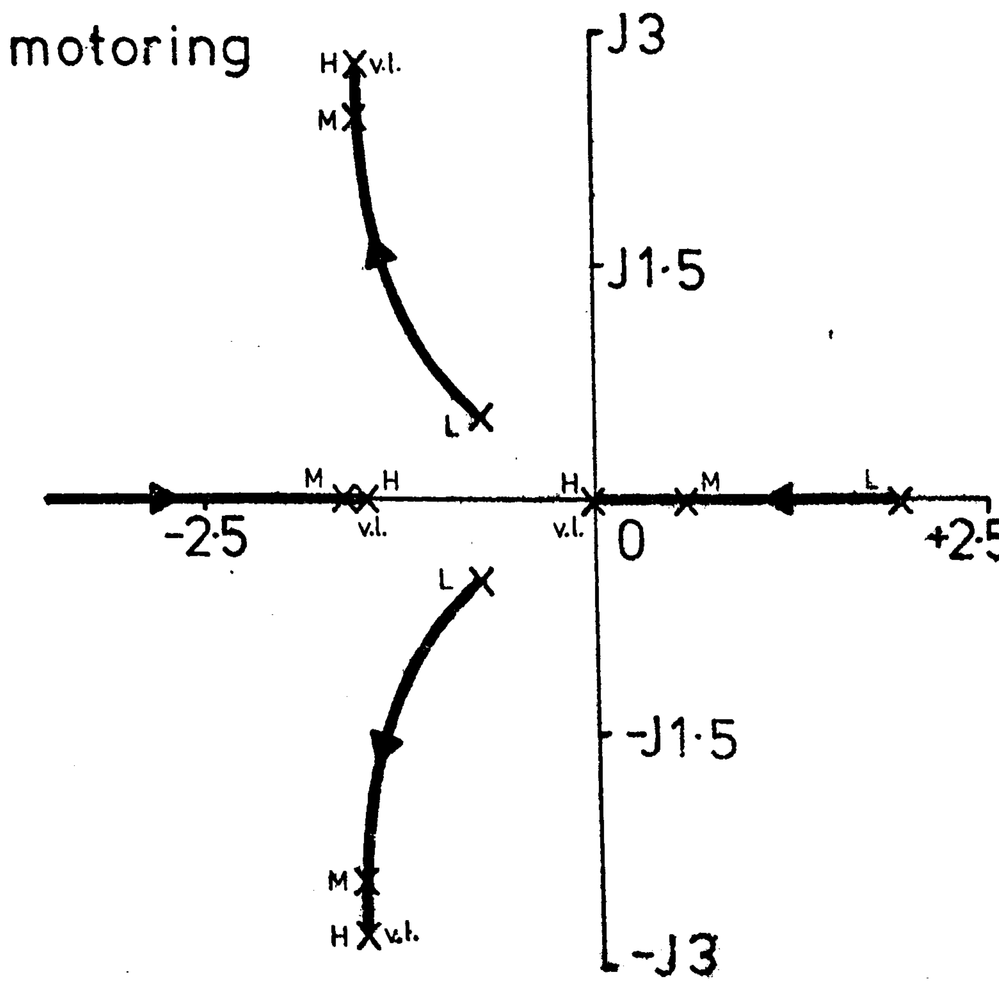

ELECTRIC PRIME MOVER
HYDROSTATIC DYNAMOMETR

GRAPH G97

method 2.2

speed range ÷ very low
+ low ⟶ high

loading

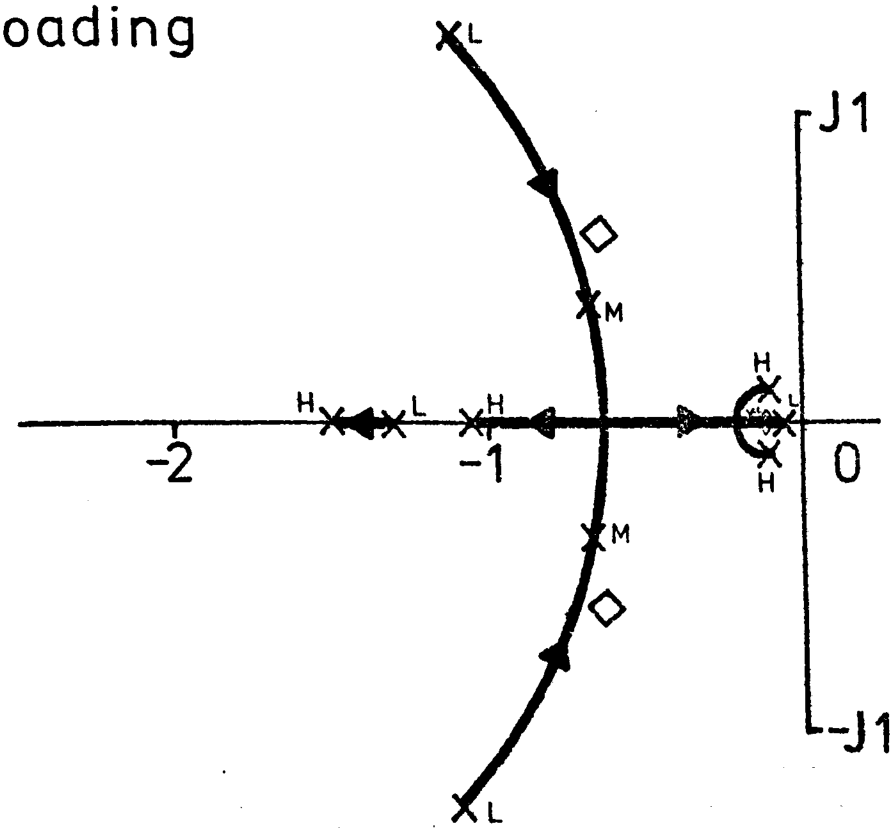

motoring

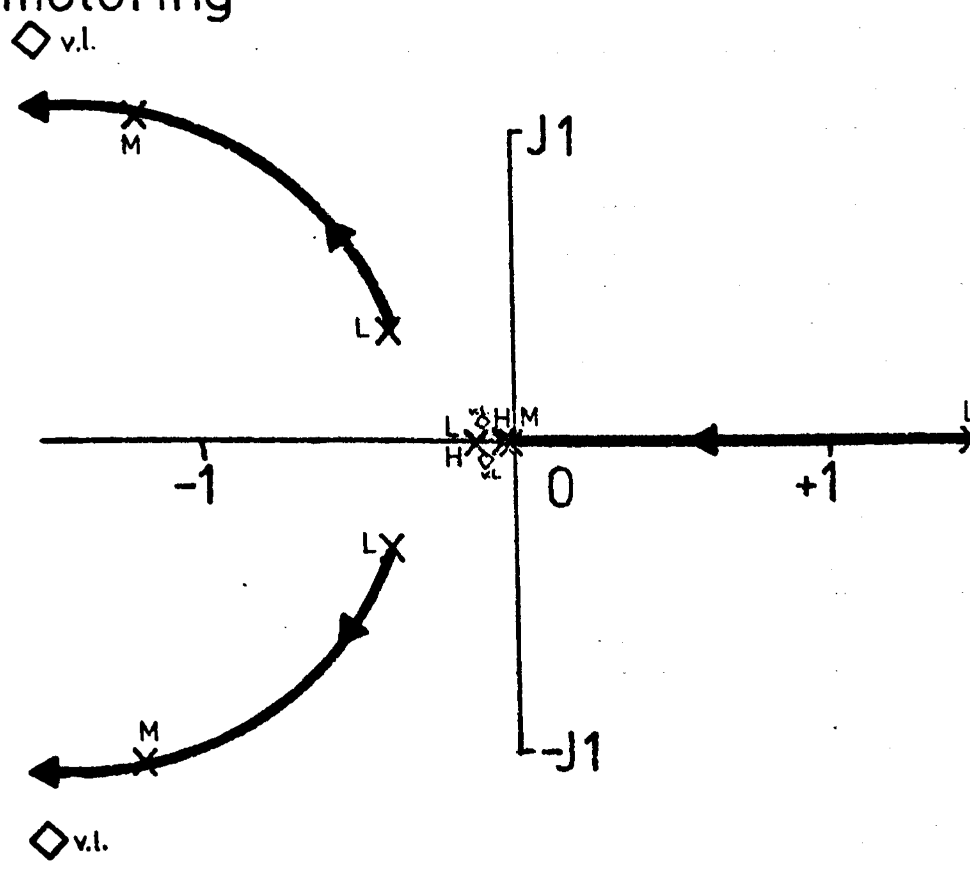

GRAPH G98

method 1.1

speed range ÷ very low
+ low ⟶ high

loading

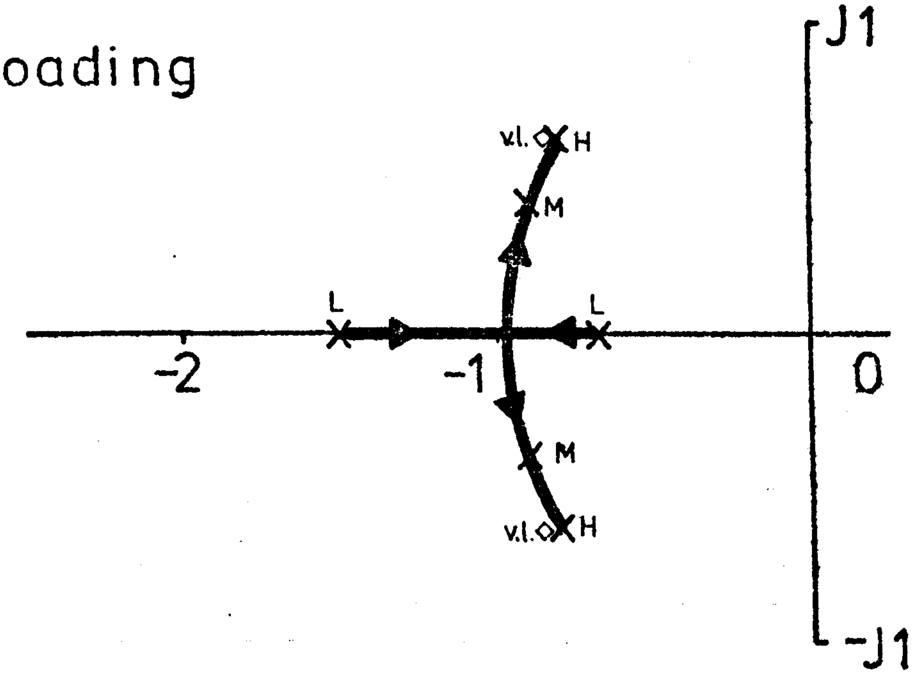

motoring

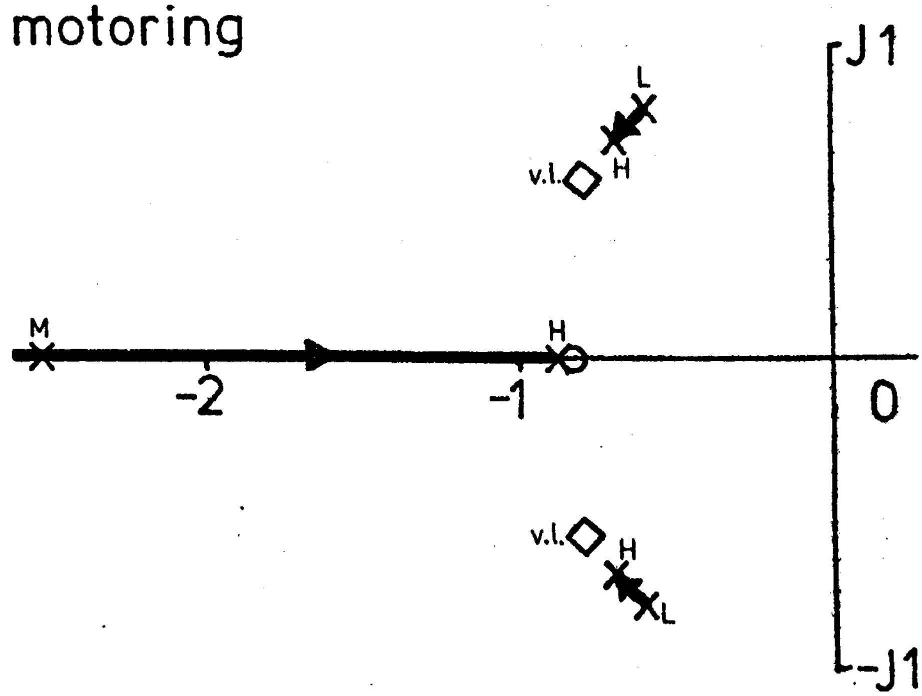

GRAPH G99

method 1.2

speed range÷ very low
+ low ⟶ high

loading

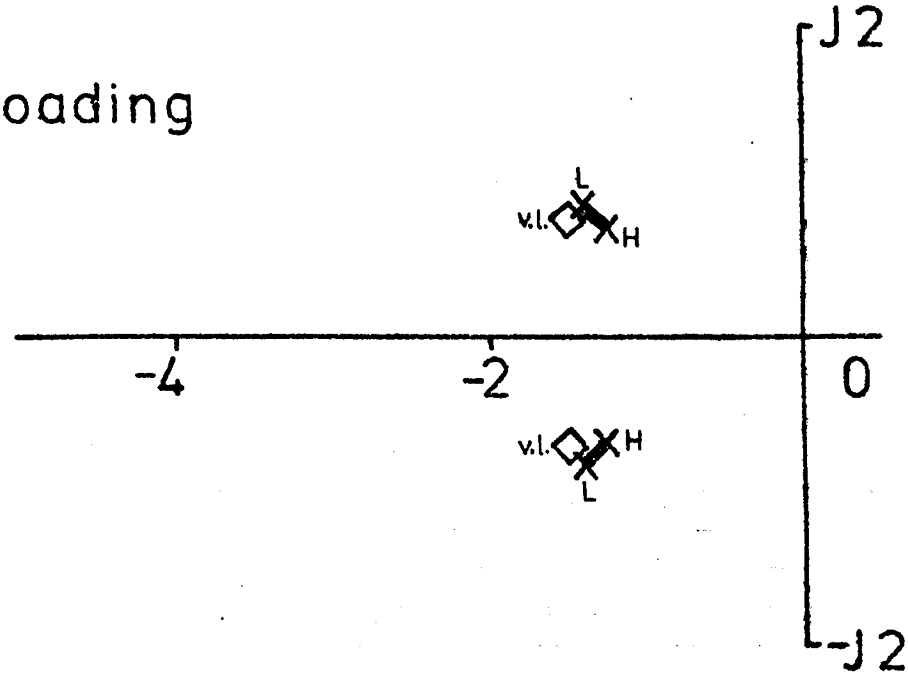

motoring

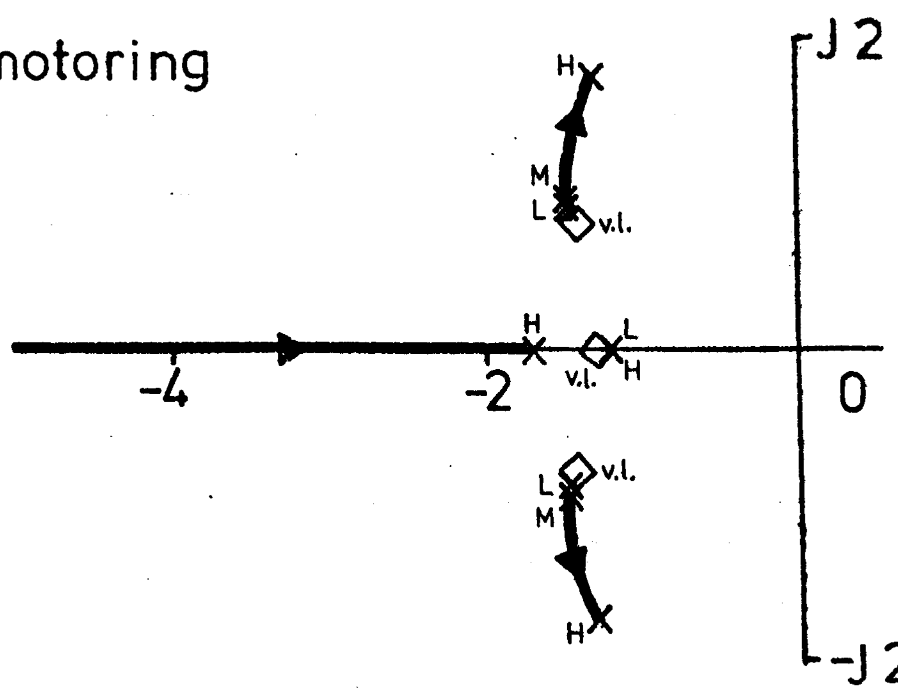

GRAPH G100

method 2.1

speed range÷ very low
+low ⟶ high

loading

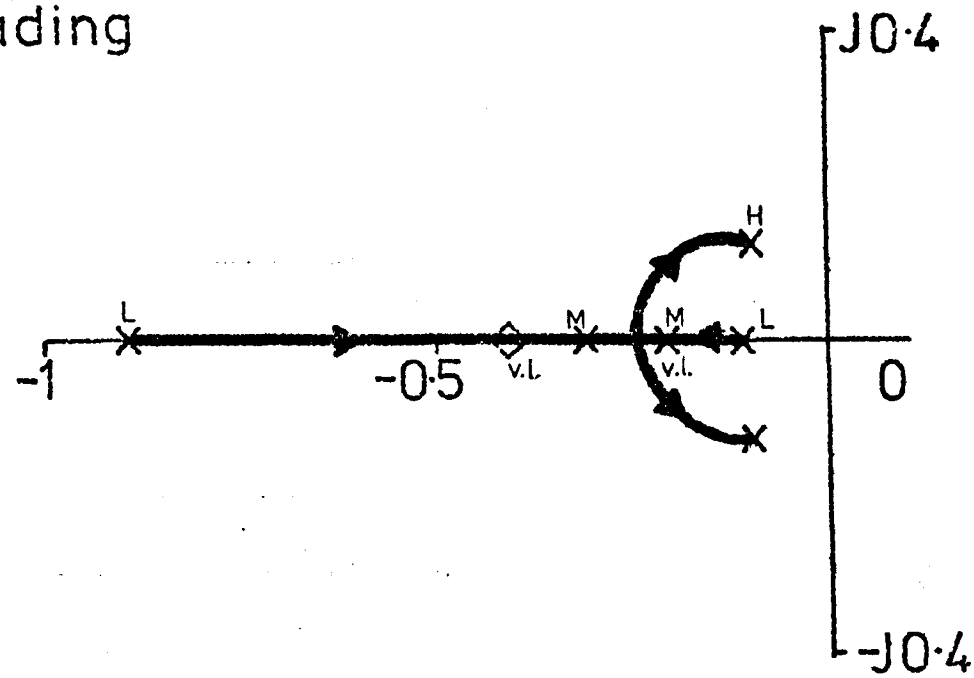

motoring

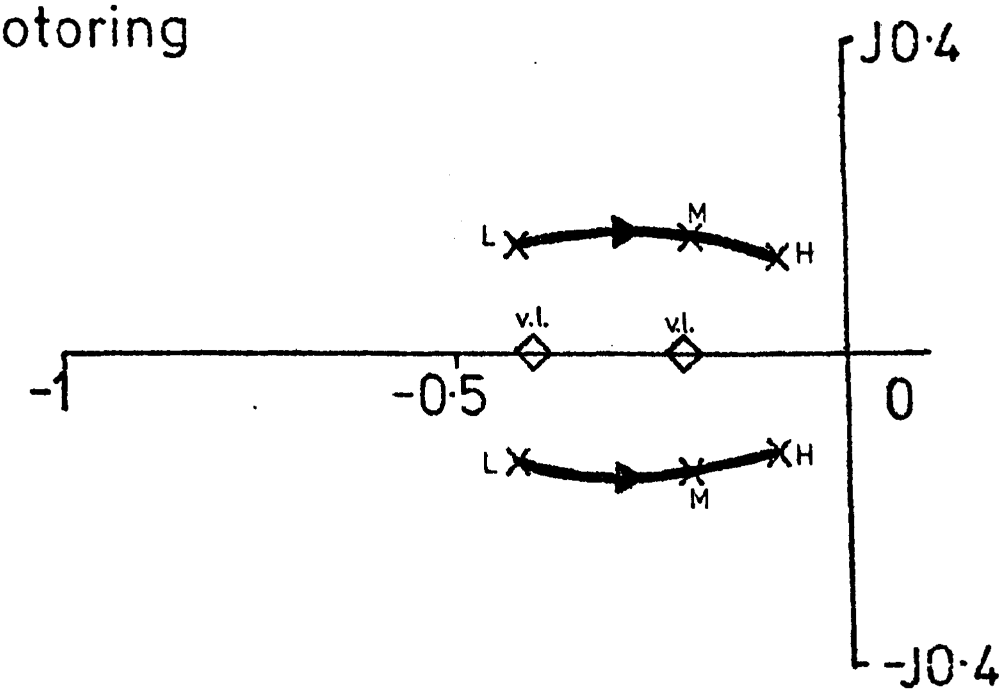

ELECTRIC PRIME MOVER
FAST RESPONSE DYNAMOMETER

GRAPH G101

method 2.2

speed range ÷ very low
+ low ⟶ high

loading

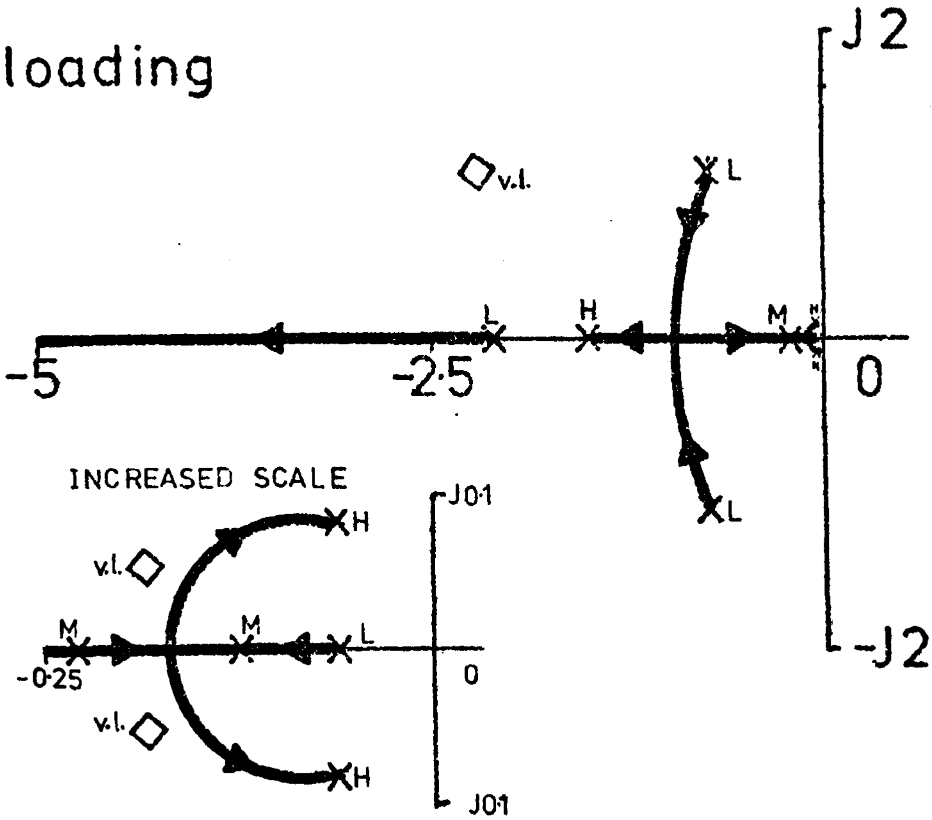

motoring

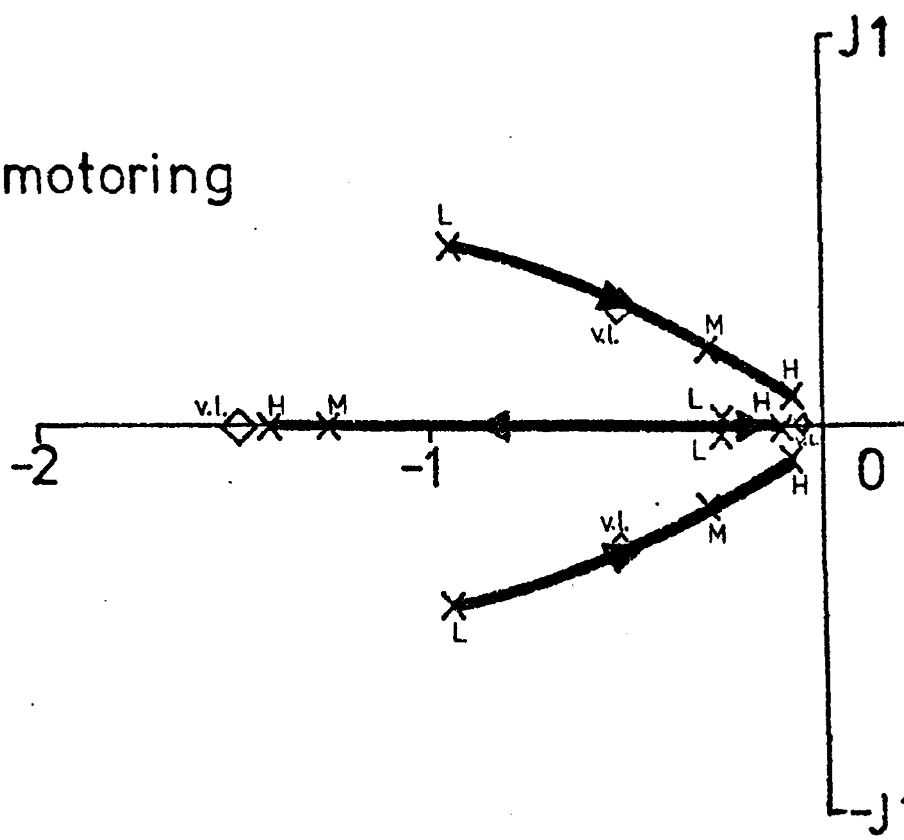

ELECTRIC PRIME MOVER
ELECTRIC DYNAMOMETER

GRAPH G102

method 1.1

speed range ÷ very low
+ low ⟶ high

loading

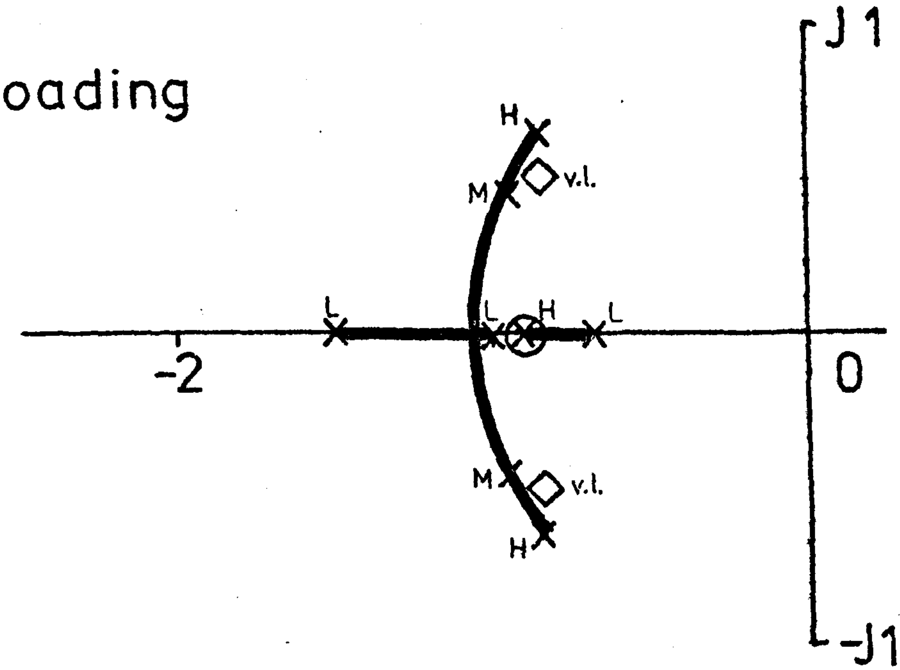

motoring

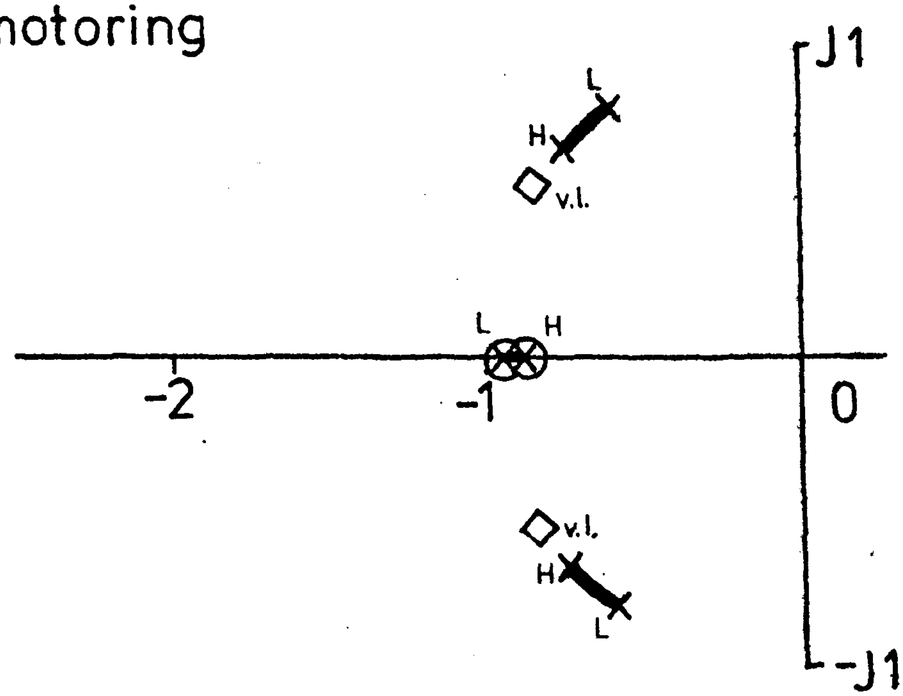

GRAPH G103

method 1.2

speed range ÷ very low
+ low ⟶ high

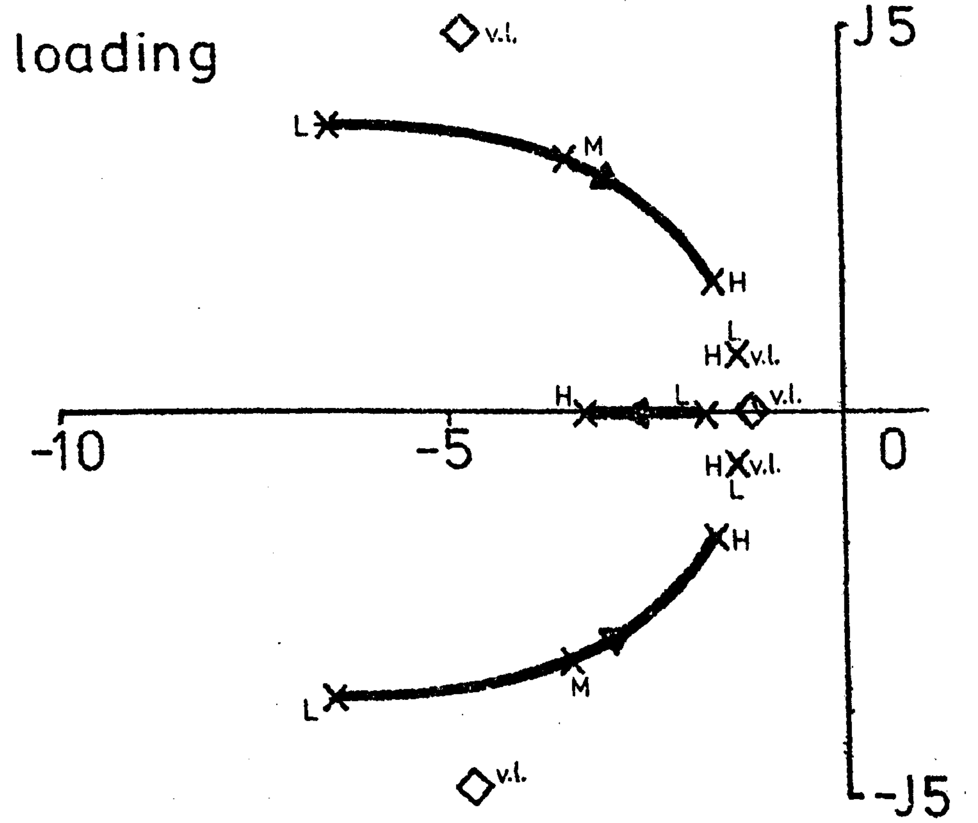

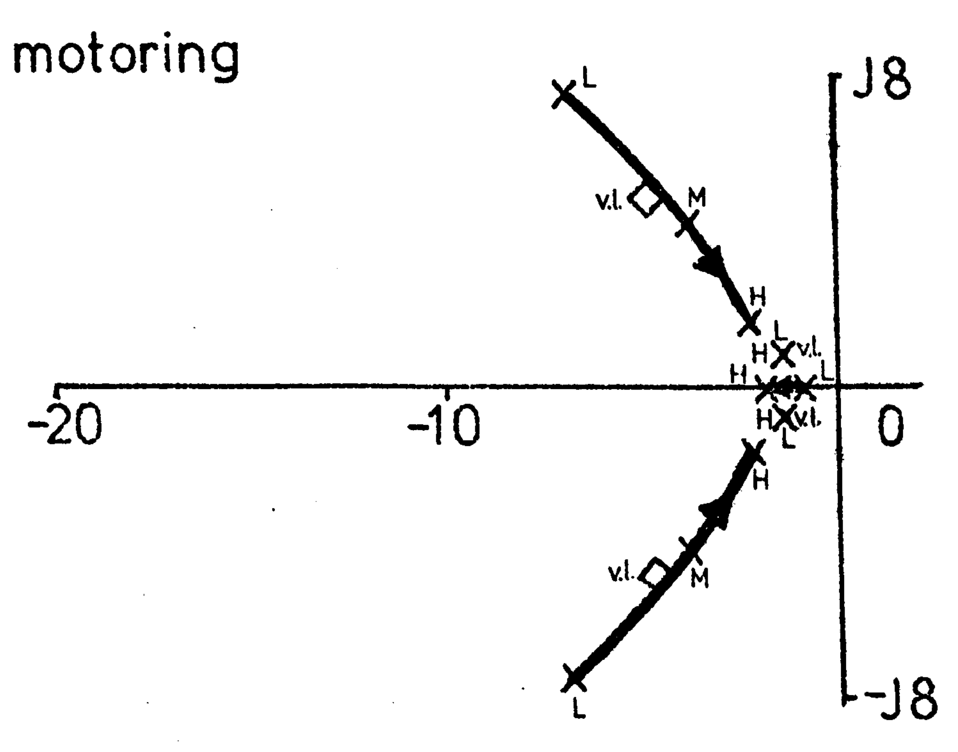

method 2.1

speed range ÷ very low
+ low ⟶ high

loading

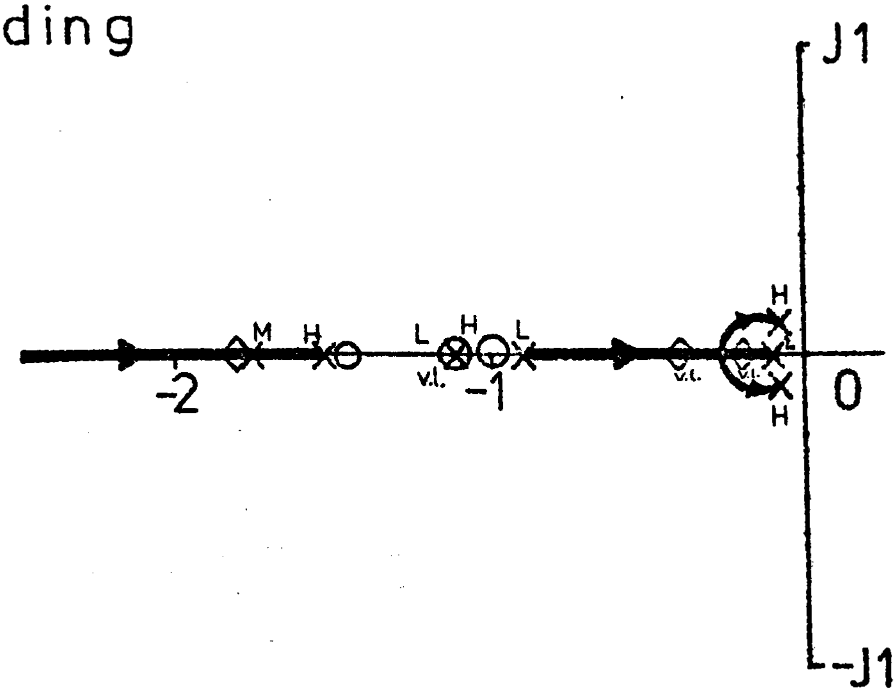

motoring

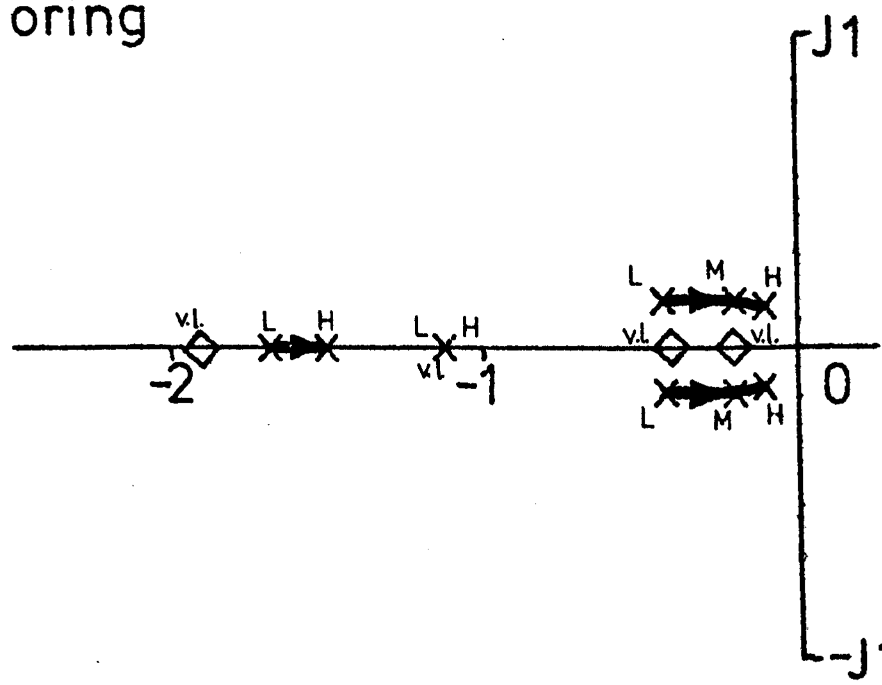

method 2.2

speed range ÷ very low
+ low ⟶ high

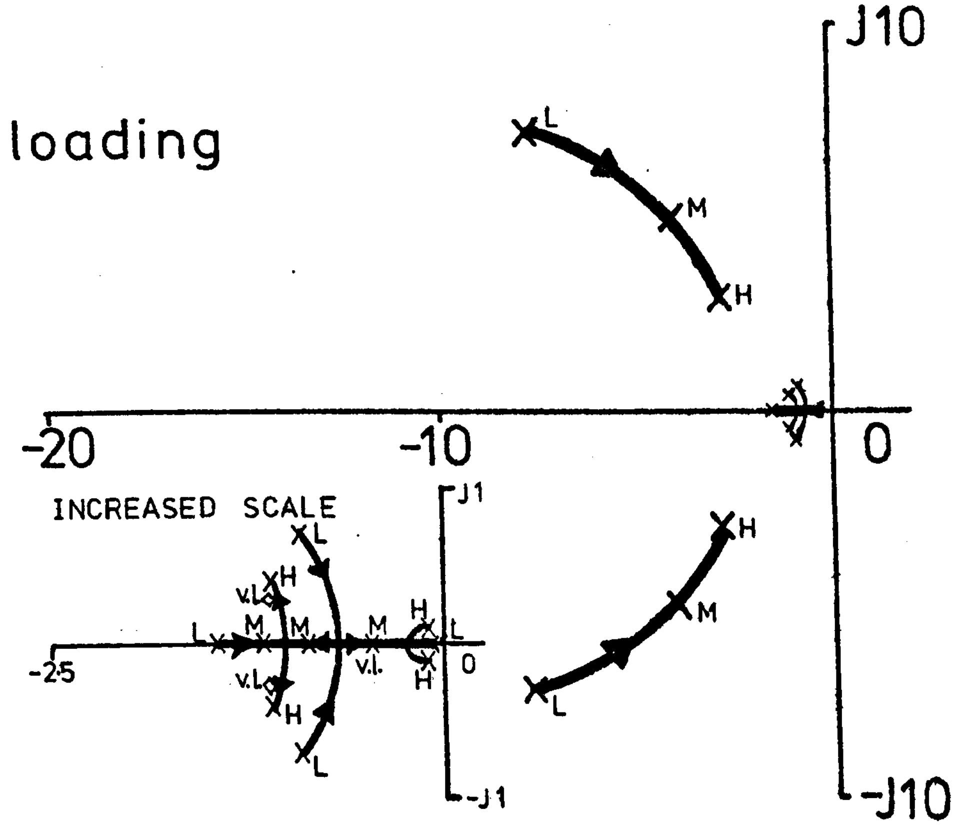

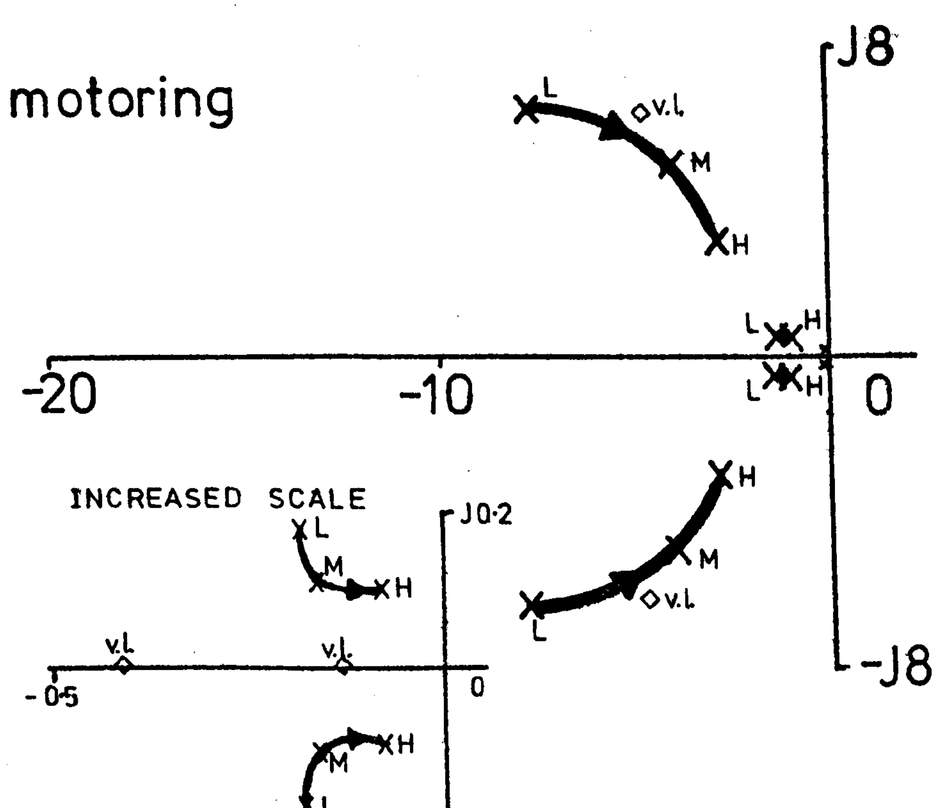

oil calibration chart from reverse flow viscometer test

(Shell Tellus 27)

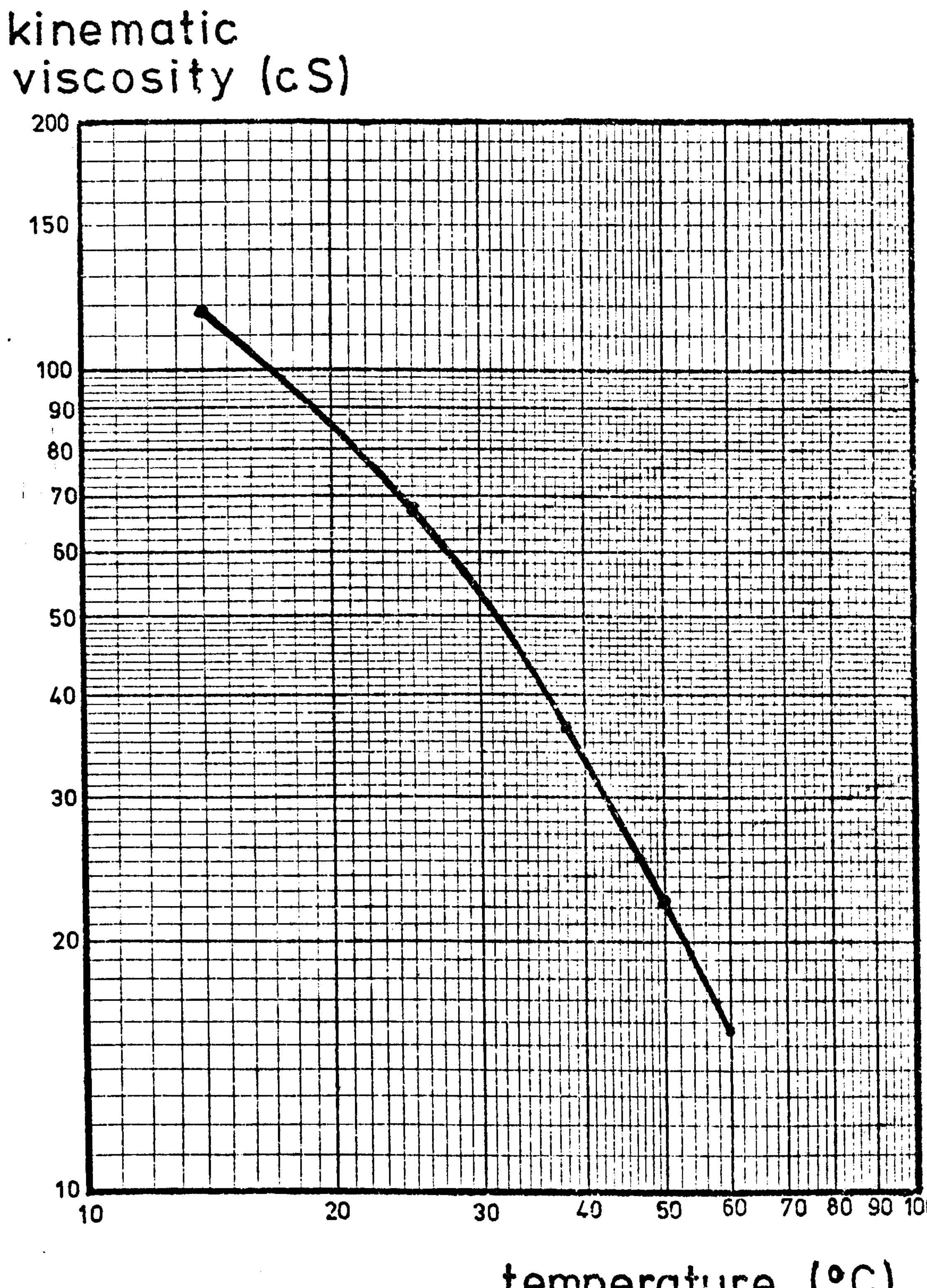

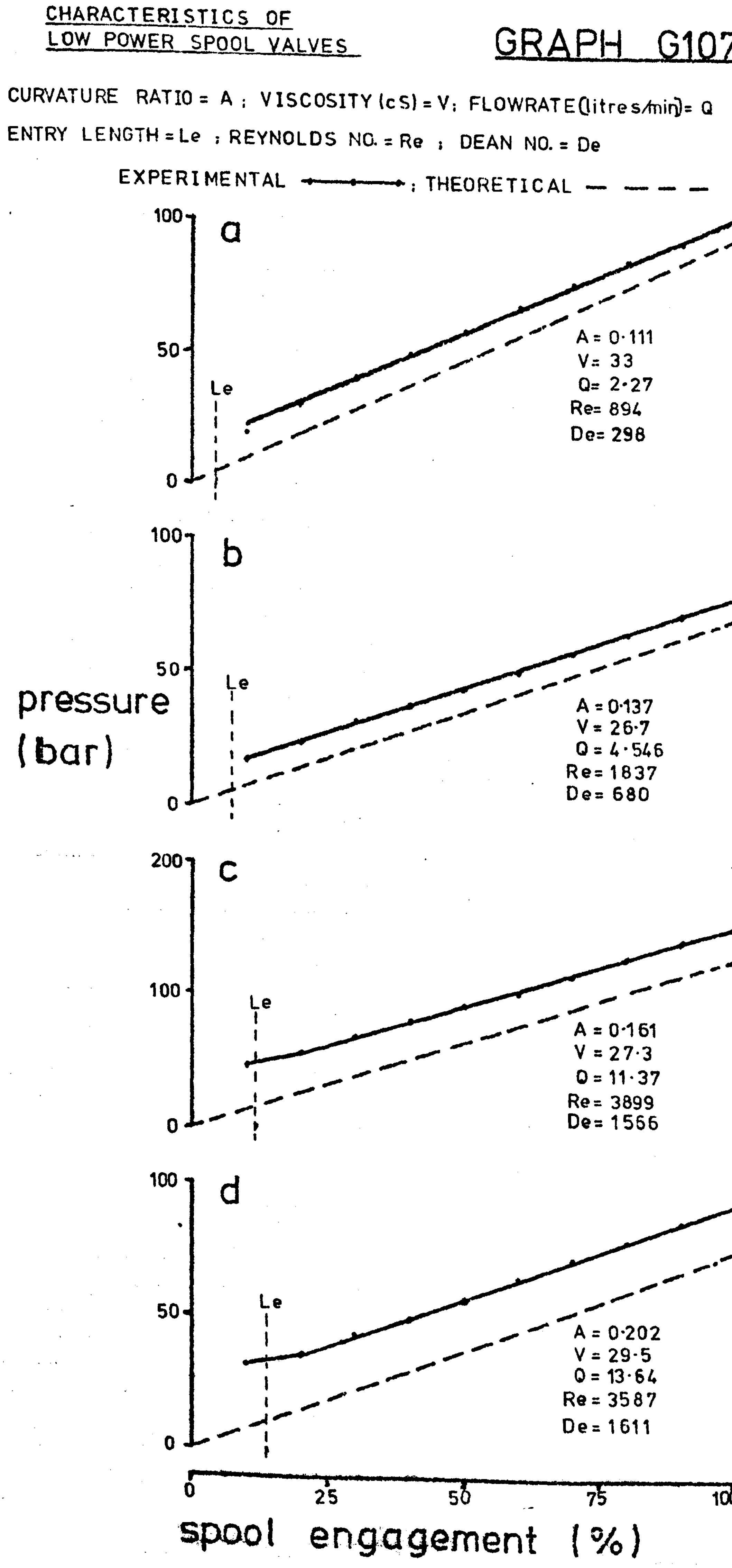
CHARACTERISTICS OF
LOW POWER SPOOL VALVES
GRAPH G107
CURVATURE RATIO = A ; VISCOSITY (cS) = V; FLOWRATE (litres/min) = Q
ENTRY LENGTH = Le ; REYNOLDS NO. = Re ; DEAN NO. = De
EXPERIMENTAL ; THEORETICAL
a
A = 0·111
V = 33
Q = 2·27
Re = 894
De = 298
b
A = 0·137
V = 26·7
Q = 4·546
Re = 1837
De = 680
c
A = 0·161
V = 27·3
Q = 11·37
Re = 3899
De = 1566
d
A = 0·202
V = 29·5
Q = 13·64
Re = 3587
De = 1611
Le
pressure (bar)
0
50
100
200
25
75
spool engagement (%)

CHARACTERISTICS OF HIGH POWER VALVE

GRAPH G108

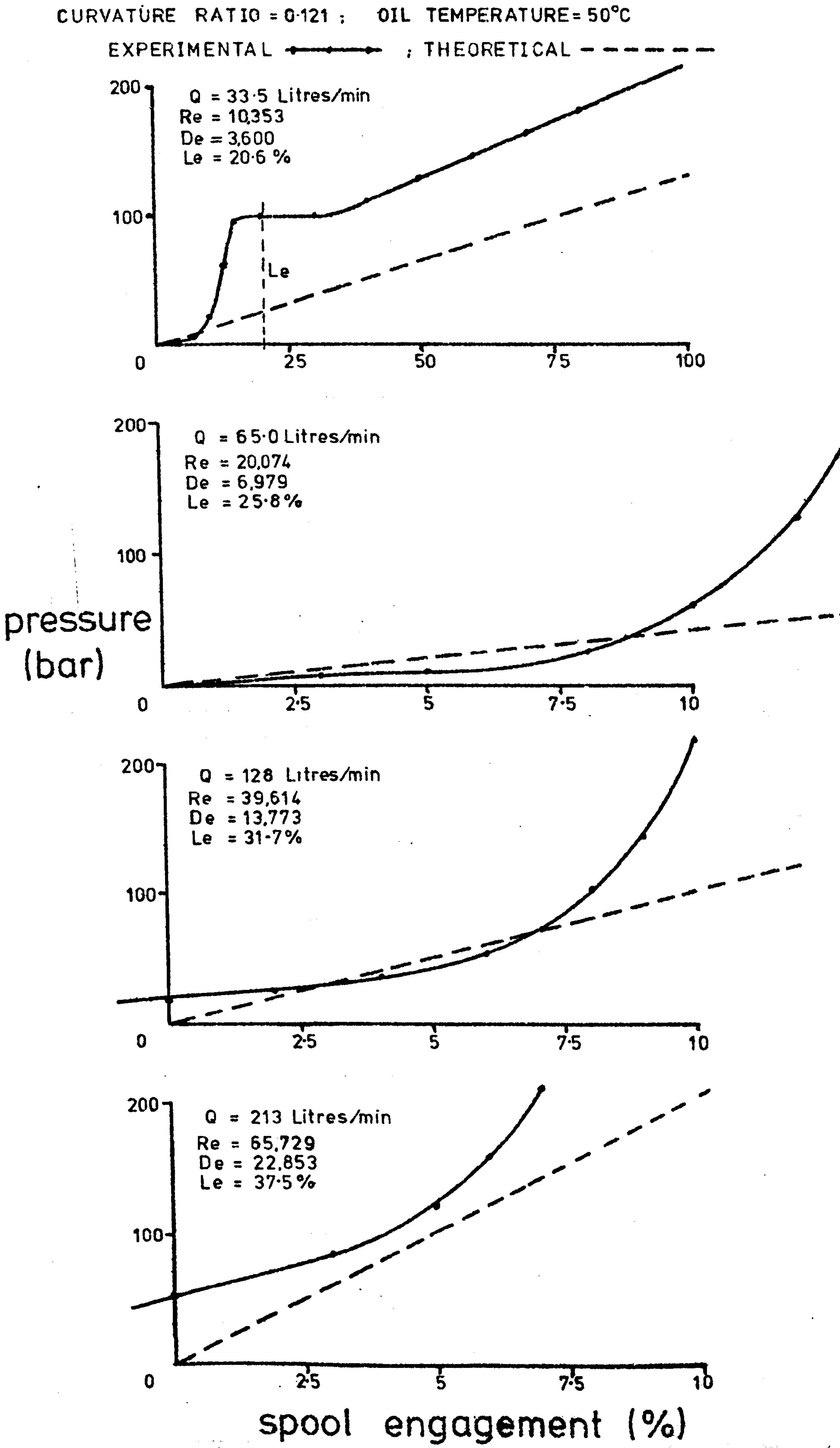

diesel engine characteristics GRAPH G109

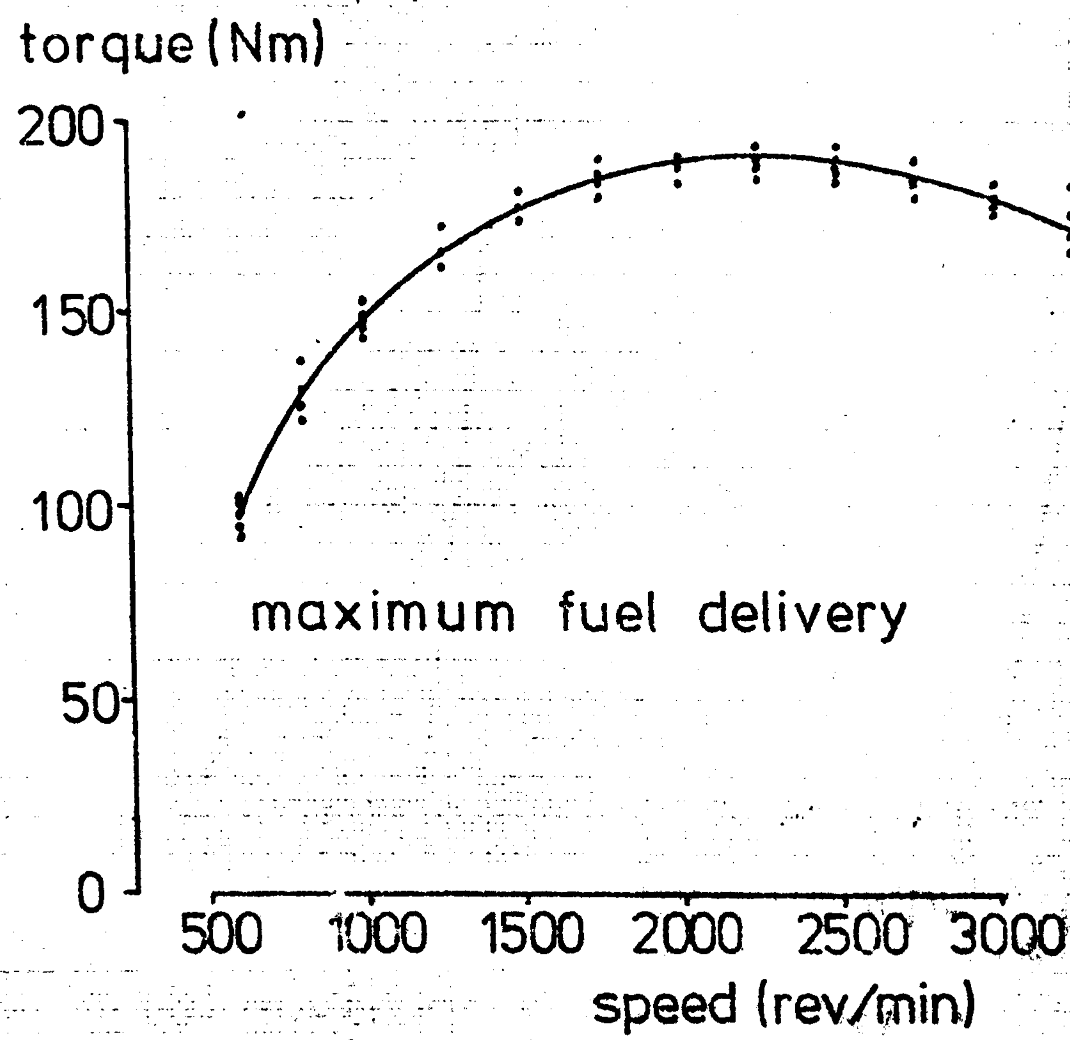

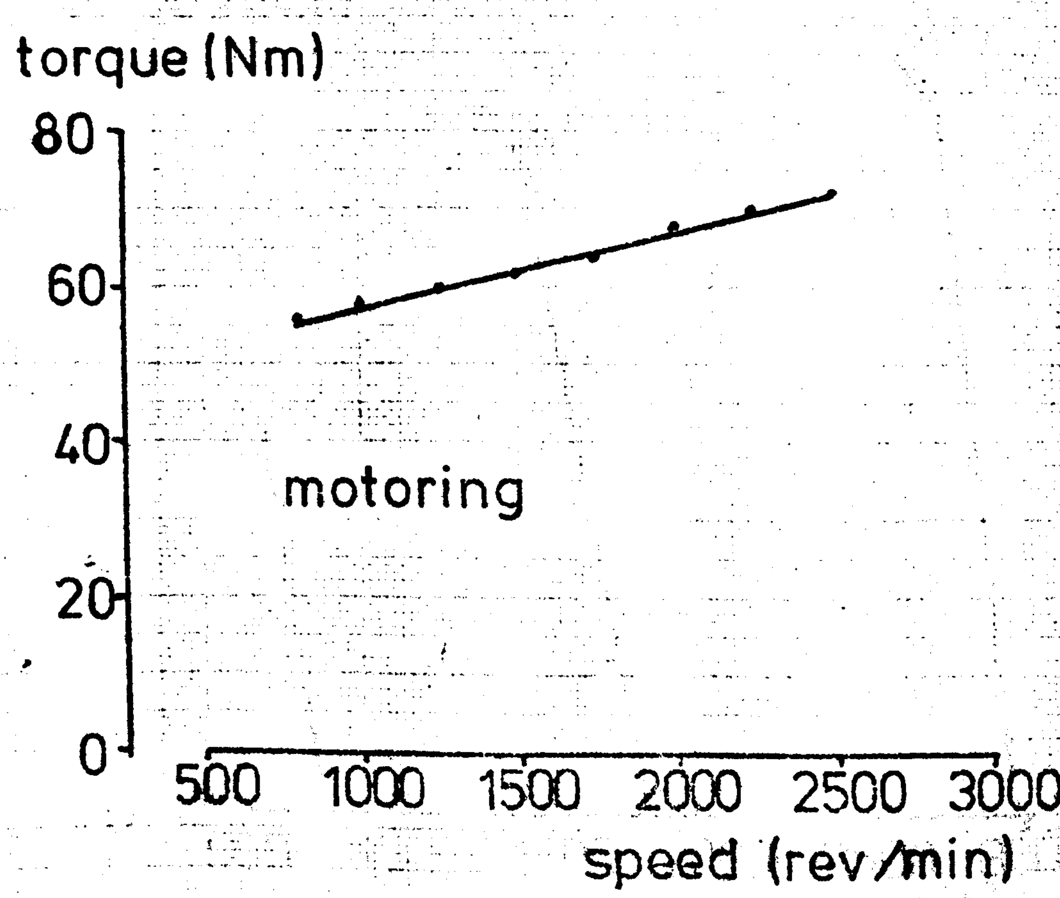

diesel engine characteristics GRAPH G110

(a) torque / throttle — k_7

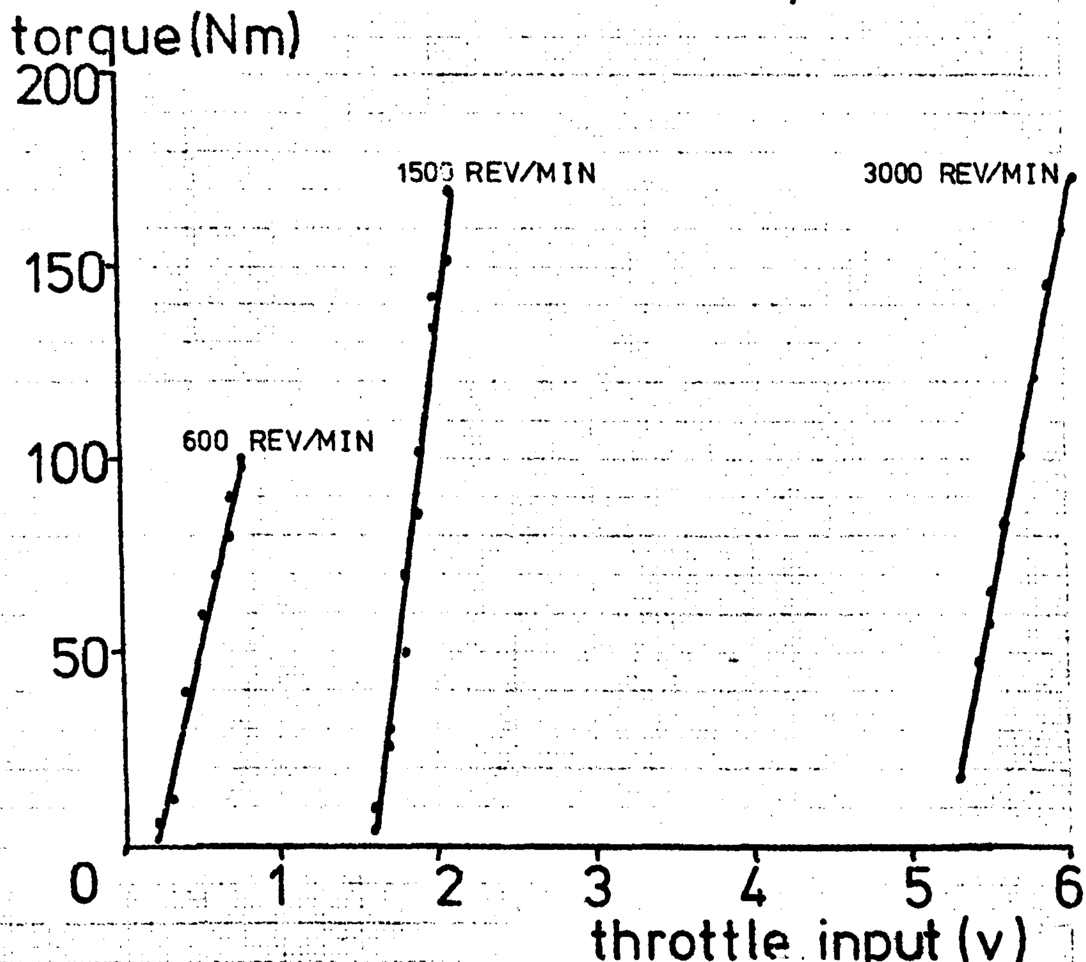

(b) governor rating — k_8

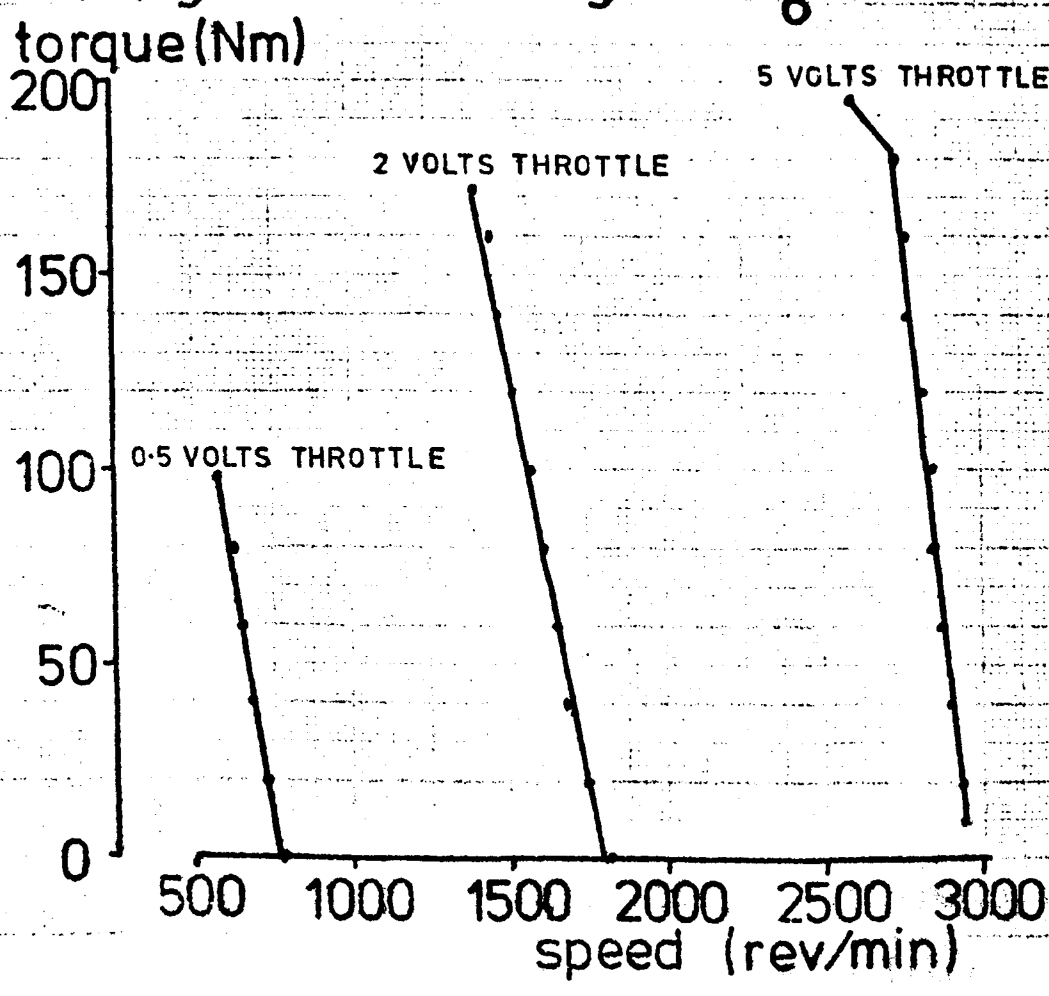

GRAPH G111

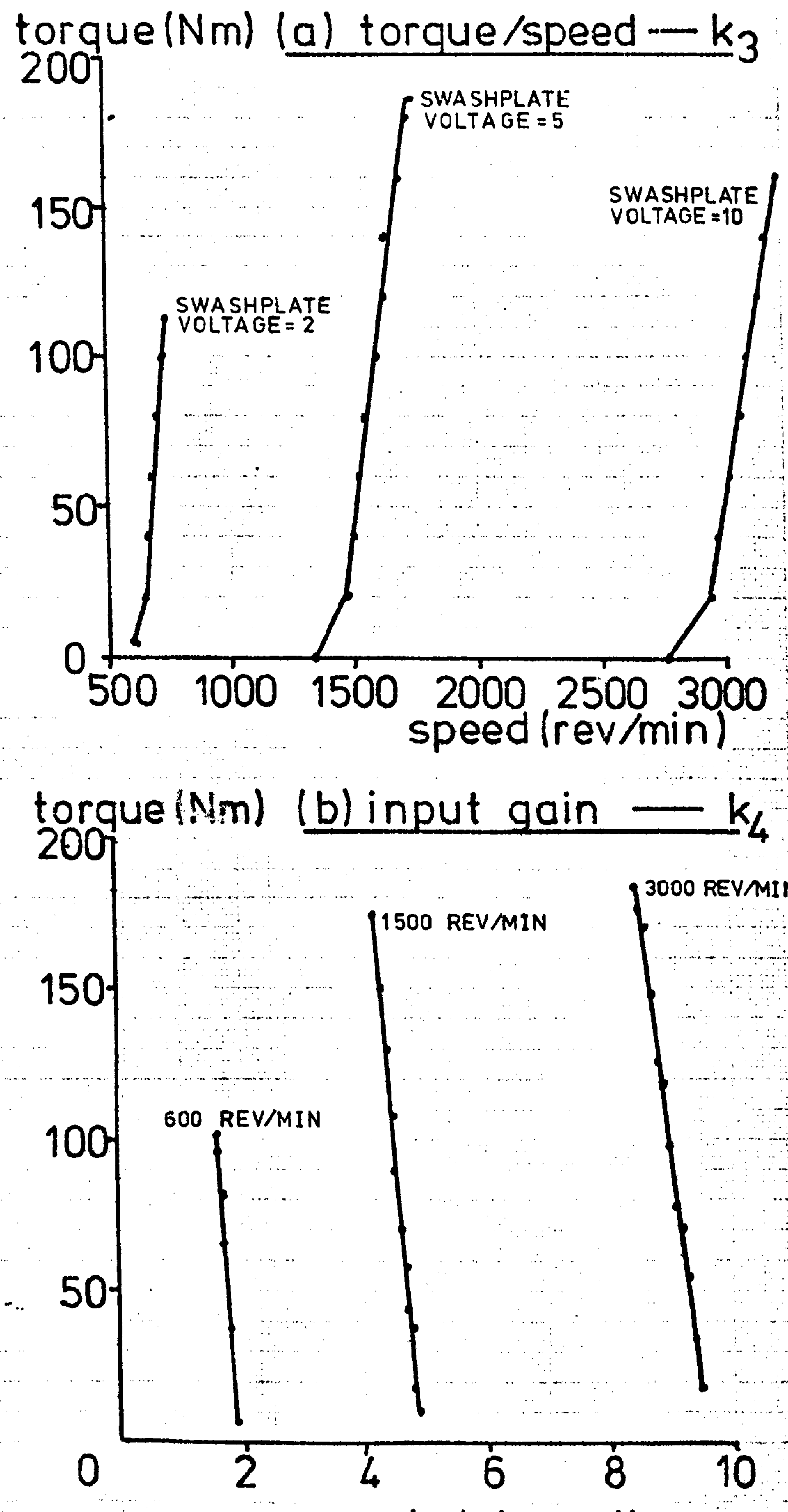
torque (Nm) (a) torque/speed — k_3
200
150
100
50
0
500
1000
1500
2000
2500
3000
speed (rev/min)
SWASHPLATE VOLTAGE = 2
SWASHPLATE VOLTAGE = 5
SWASHPLATE VOLTAGE = 10
torque (Nm) (b) input gain — k_4
200
150
100
50
0
2
4
6
8
10
swashplate voltage
600 REV/MIN
1500 REV/MIN
3000 REV/MIN

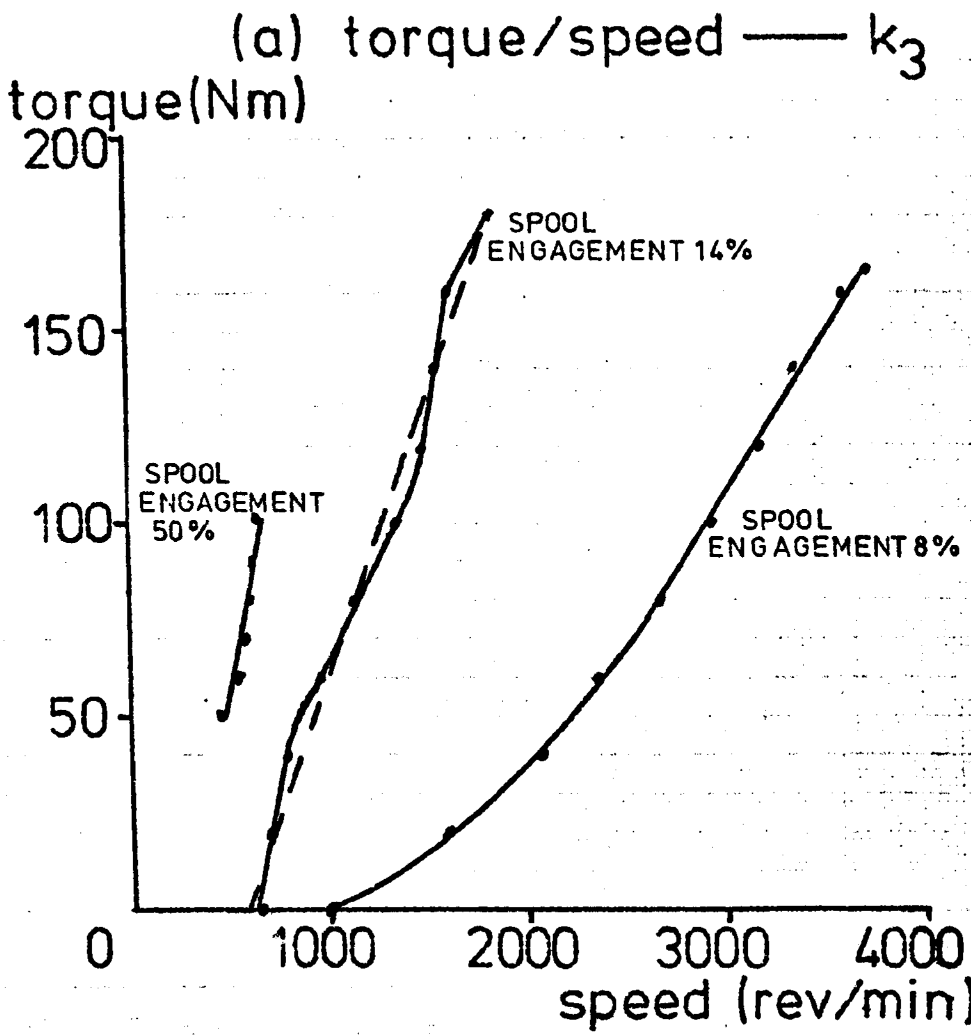
(a) torque/speed —— k_3
torque(Nm)
200
150
100
50
0
1000
2000
3000
4000
speed (rev/min)
SPOOL ENGAGEMENT 14%
SPOOL ENGAGEMENT 50%
SPOOL ENGAGEMENT 8%

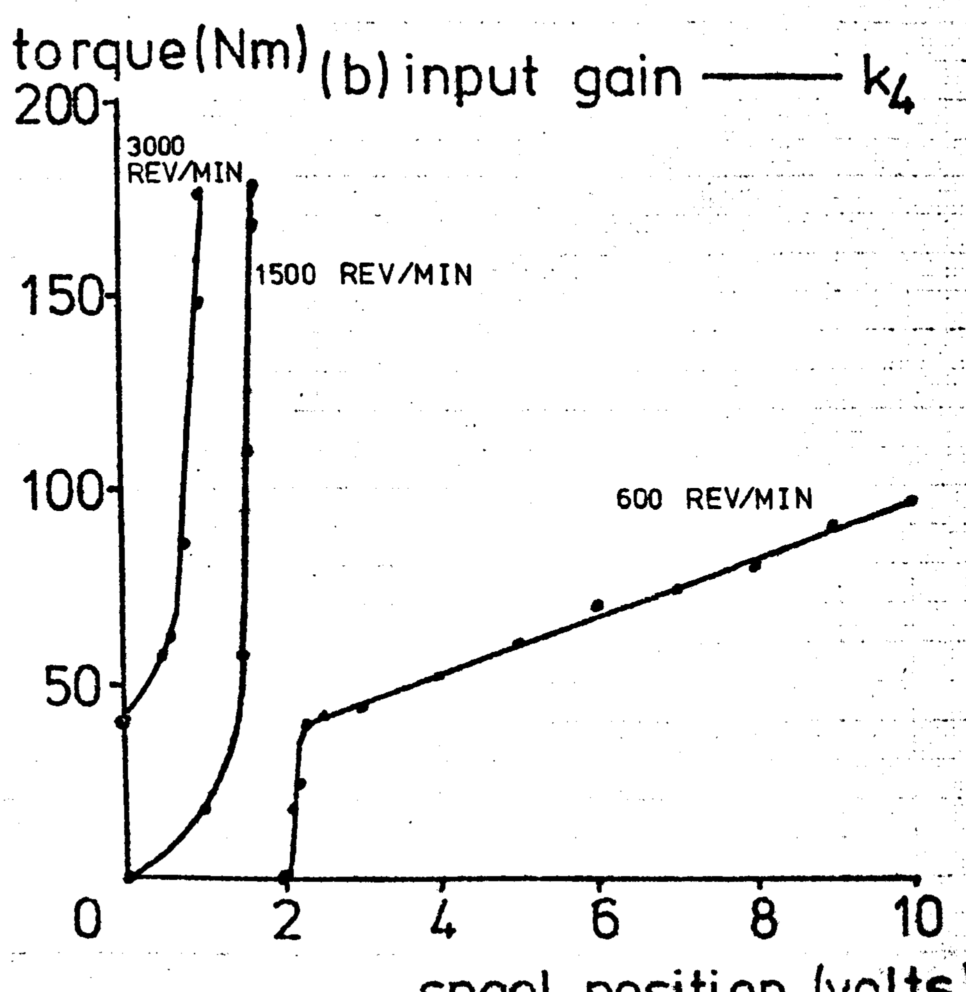
(b) input gain —— k_4
torque(Nm)
200
150
100
50
0
2
4
6
8
10
spool position (volts)
3000 REV/MIN
1500 REV/MIN
600 REV/MIN

method 1.2 speed range÷low→high

(new system coefficients)

mid fuel delivery

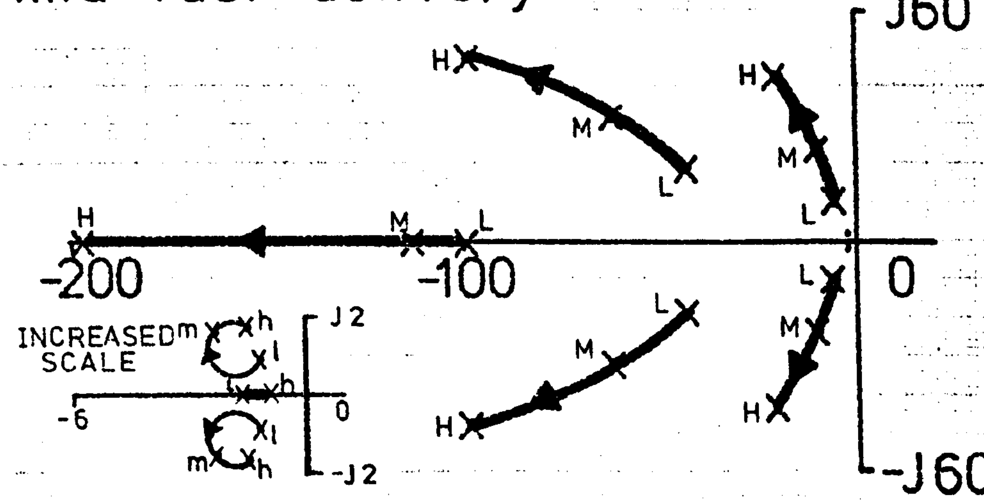

maximum fuel delivery

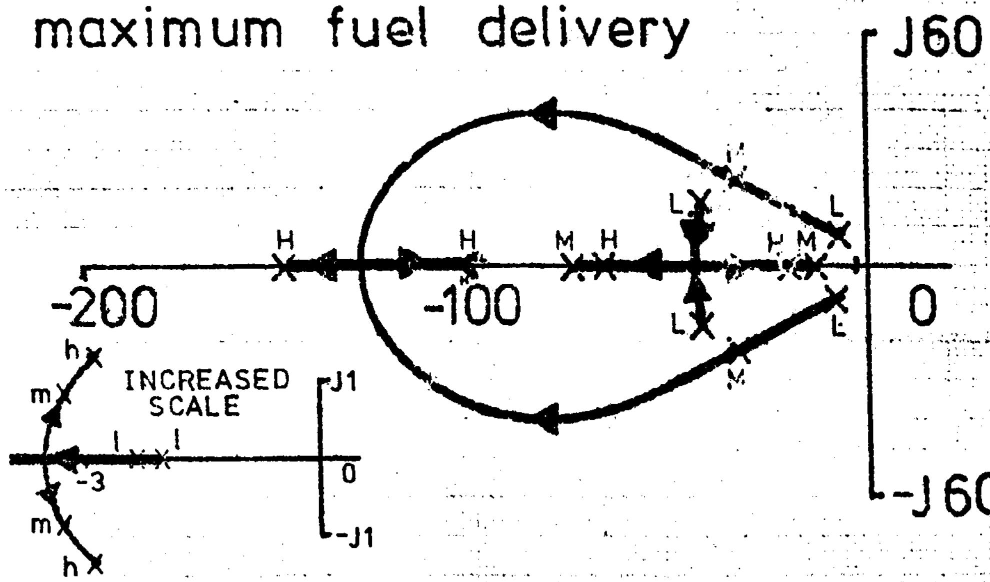

motoring

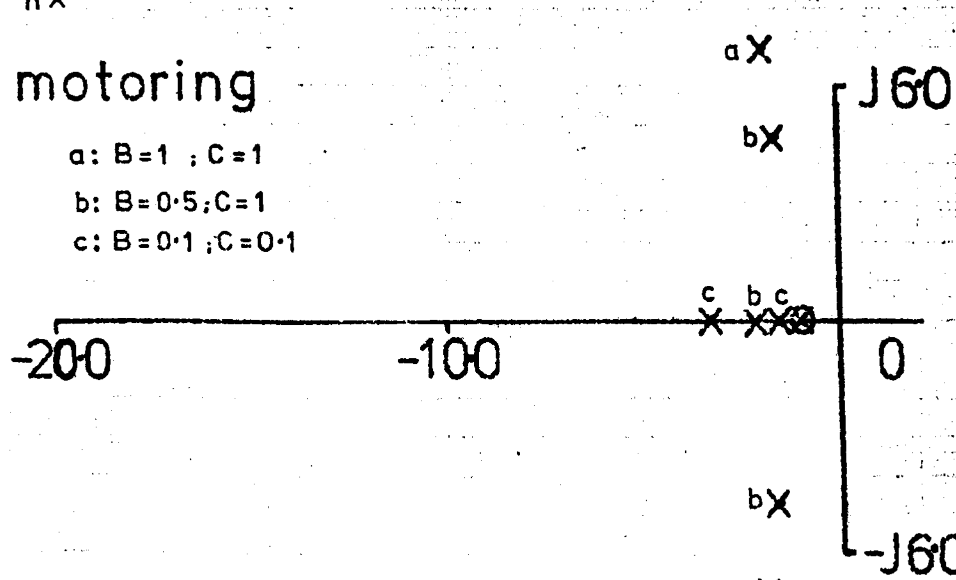

DIESEL ENGINE
HYDROSTATIC DYNAMOMETER

GRAPH G114

TORQUE AND SPEED RESPONSES TO STEP DISTURBANCE OF DYNAMOMETER INPUT SIGNAL

(B = 0·5 ; C = 1 ; E = 0·3 ; F = 1)

METHOD 1.2 LOADING CONDITION

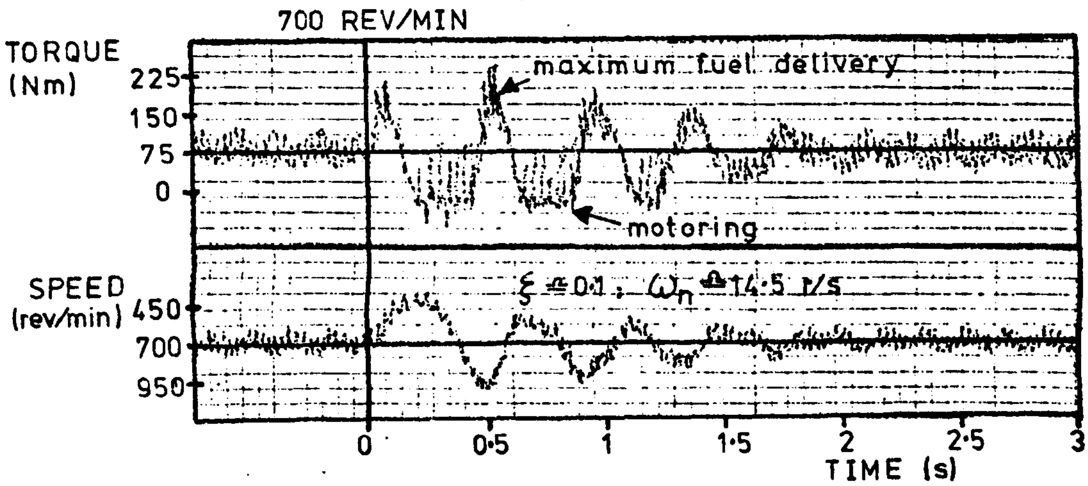

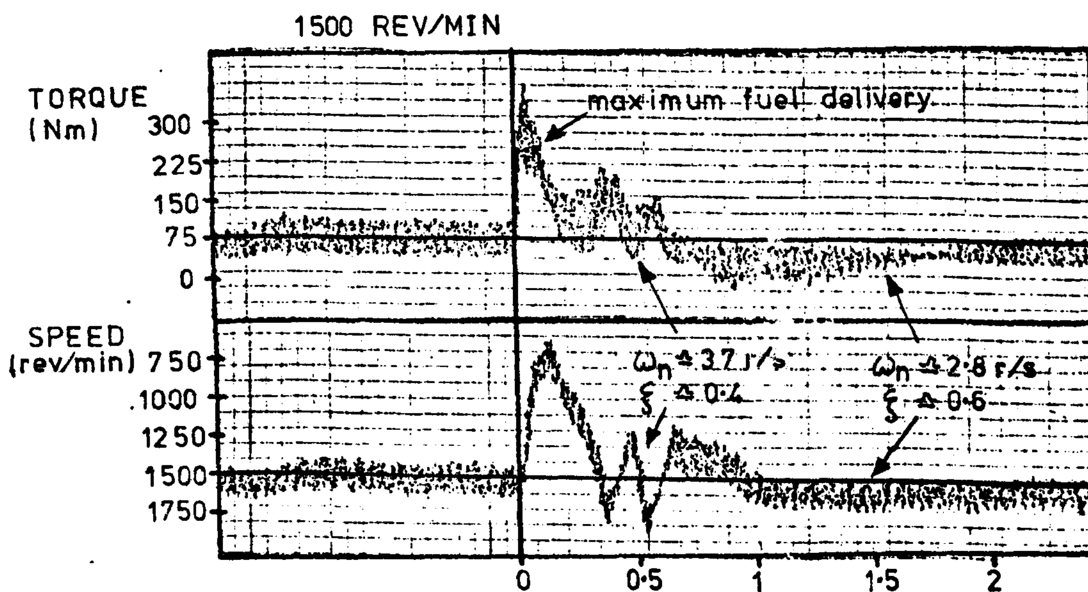

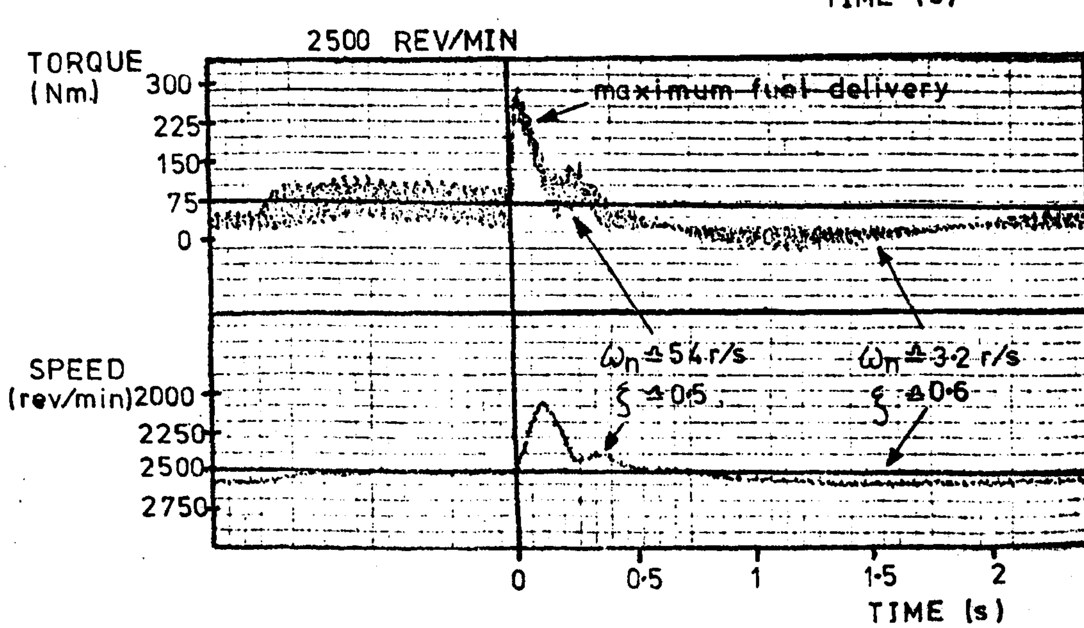

DIESEL ENGINE

HYDROSTATIC DYNAMOMETER

GRAPH G115

TORQUE AND SPEED RESPONSES TO STEP DISTURBANCE OF DYNAMOMETER INPUT SIGNAL

METHOD 1.2 MOTORING CONDITION

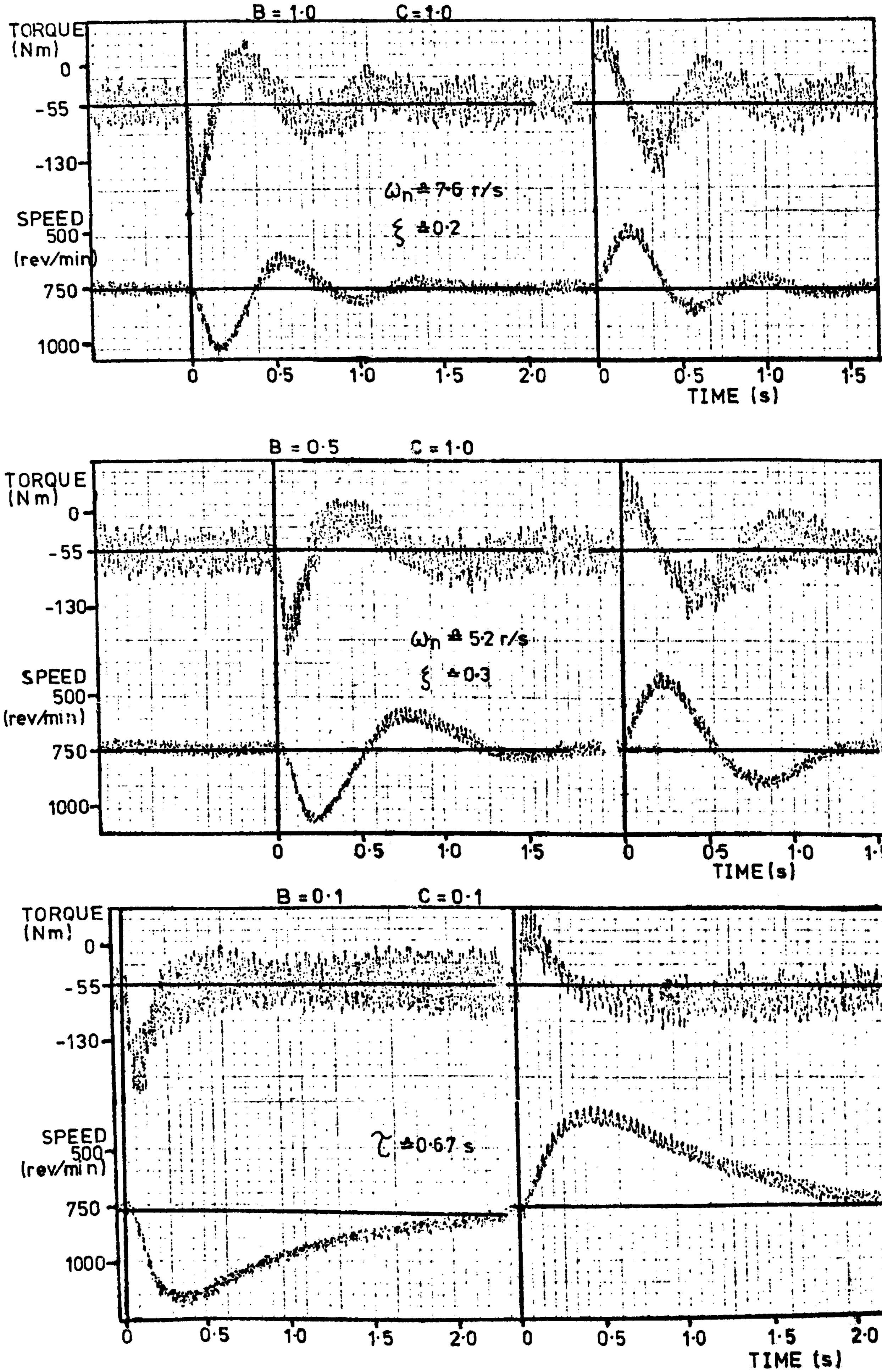

DIESEL ENGINE
HYDROSTATIC DYNAMOMETER

GRAPH G116

METHOD 1.2 UNSTABLE RESPONSES FOR $T_5 = 0{\cdot}1$ (s)

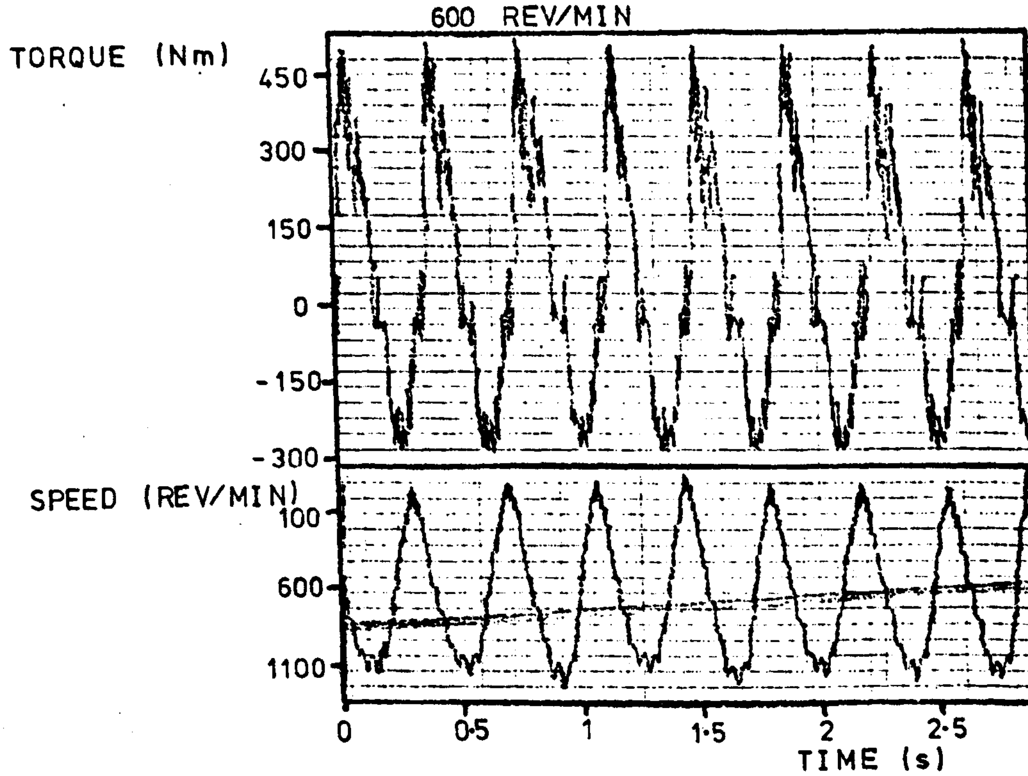

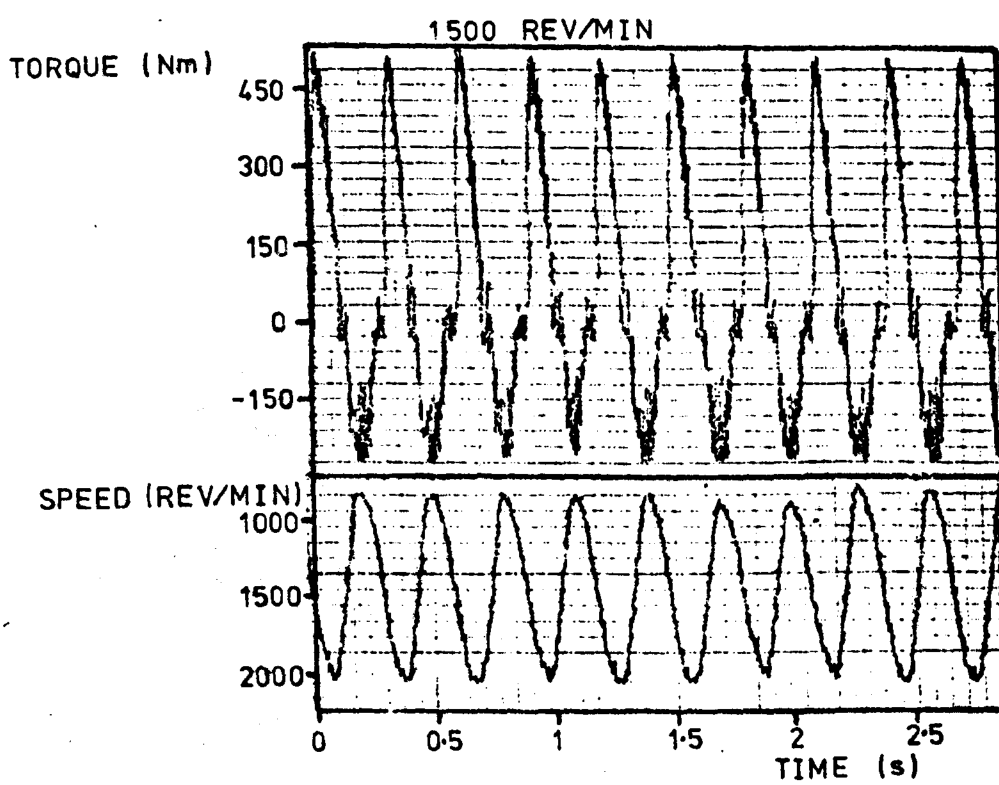

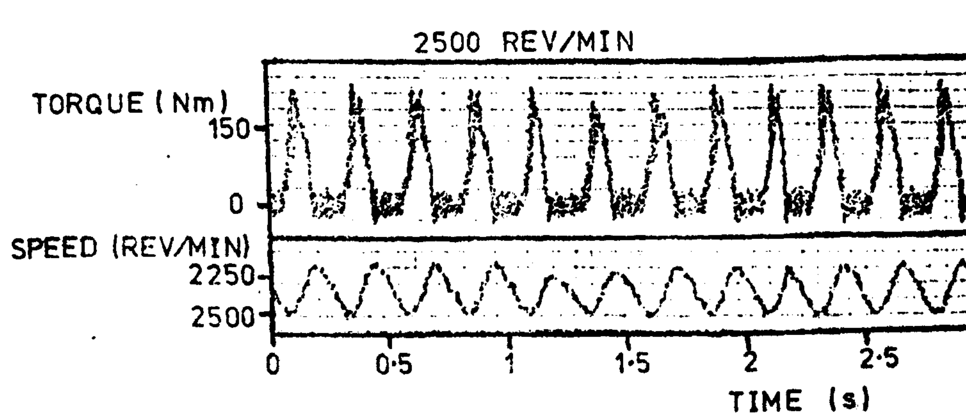

GRAPH G117

method 1.2 ; speed range ÷ low → high

(new system coefficients)

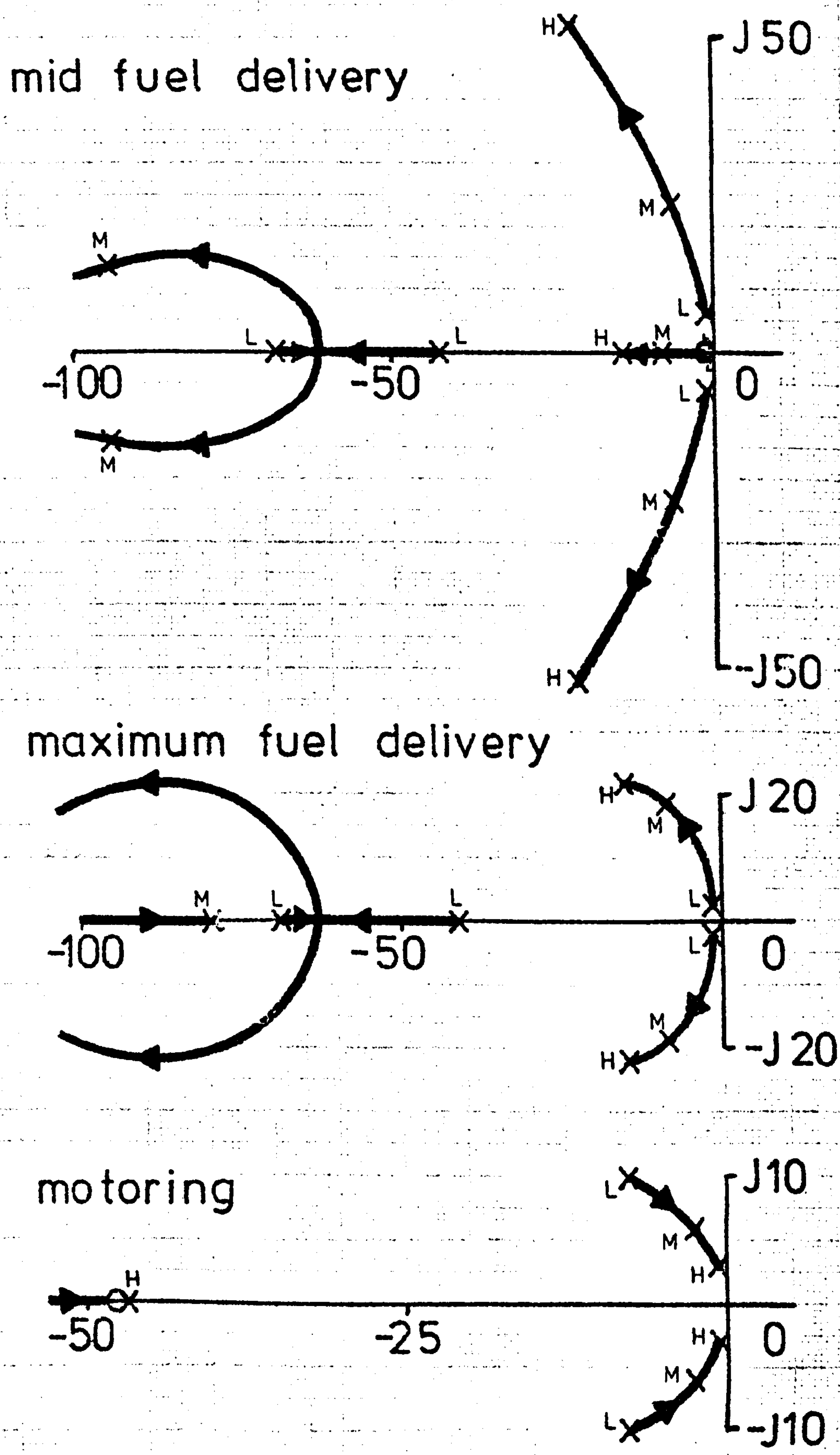

DIESEL ENGINE
FAST RESPONSE DYNAMOMETER

GRAPH G118

TORQUE AND SPEED RESPONSES TO STEP DISTURBANCE OF DYNAMOMETER INPUT SIGNAL

METHOD 1.2 LOADING CONDITION

(B = 0·05 ; C = 1 ; E = 0·1 ; F = 1)

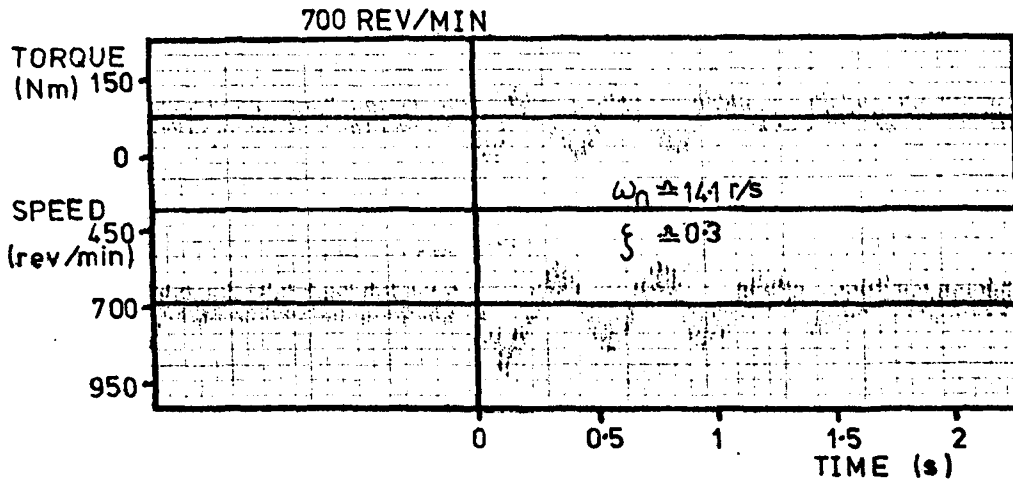

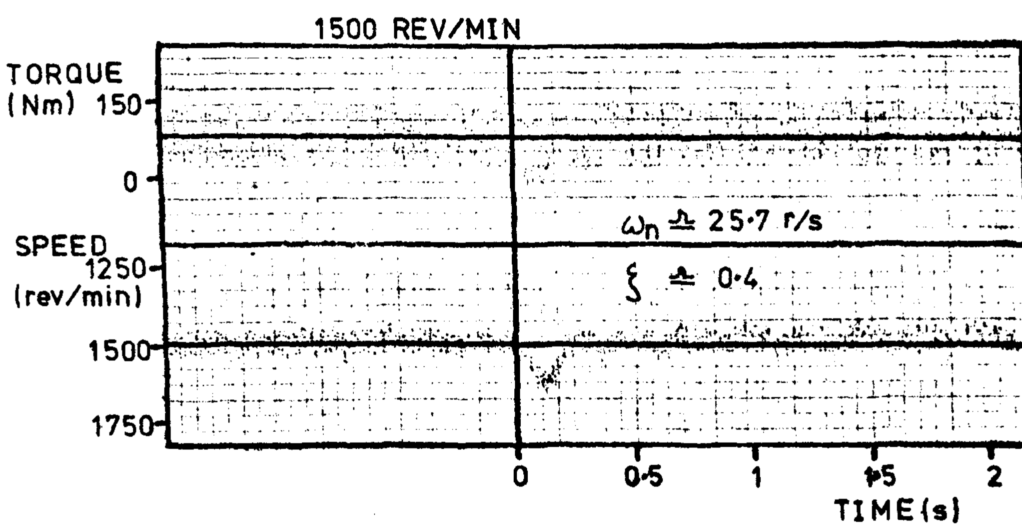

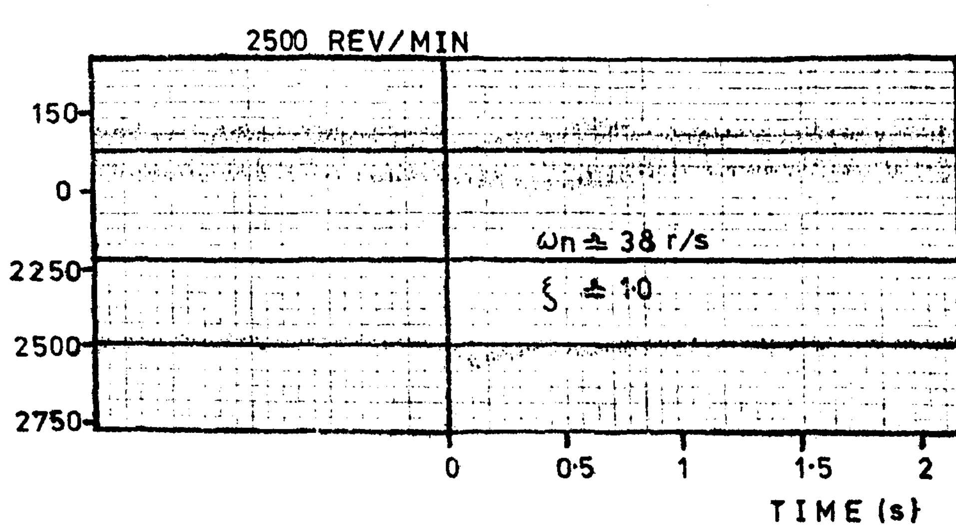

DIESEL ENGINE
FAST RESPONSE DYNAMOMETER

GRAPH G119

TORQUE AND SPEED RESPONSES TO STEP REDUCTION IN THROTTLE LEVER SETTING

METHOD 1.2 MOTORING CONDITION

(B = 0·05 ; C = 1)

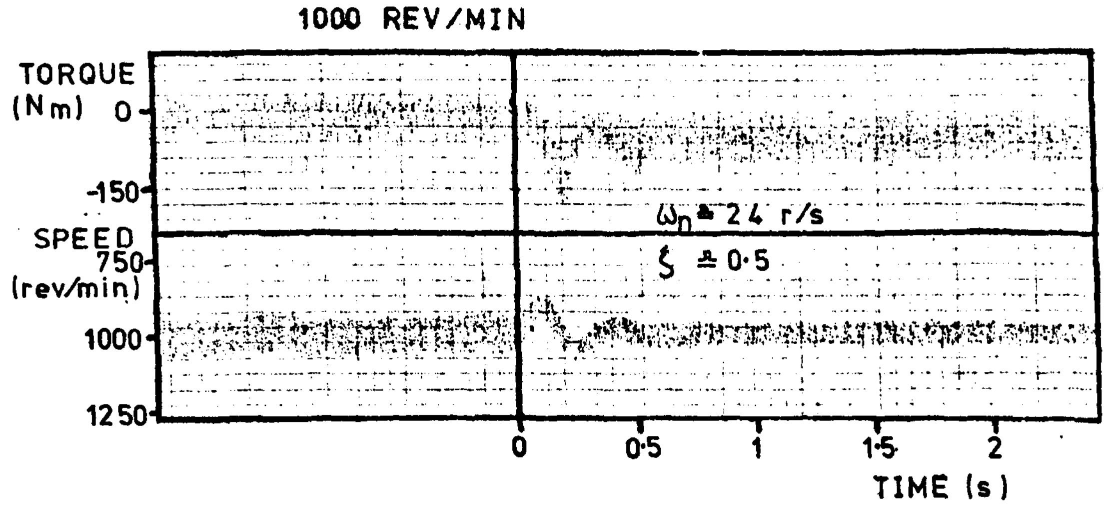

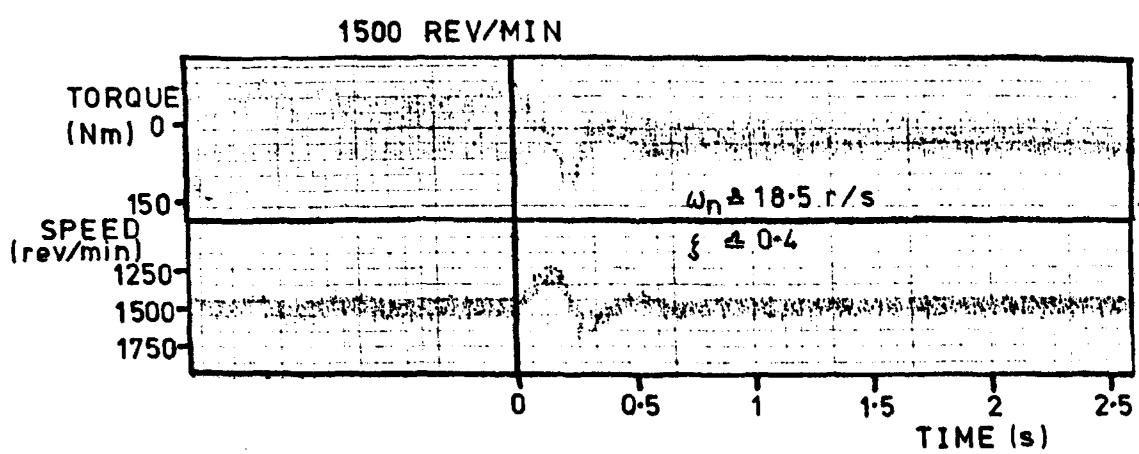

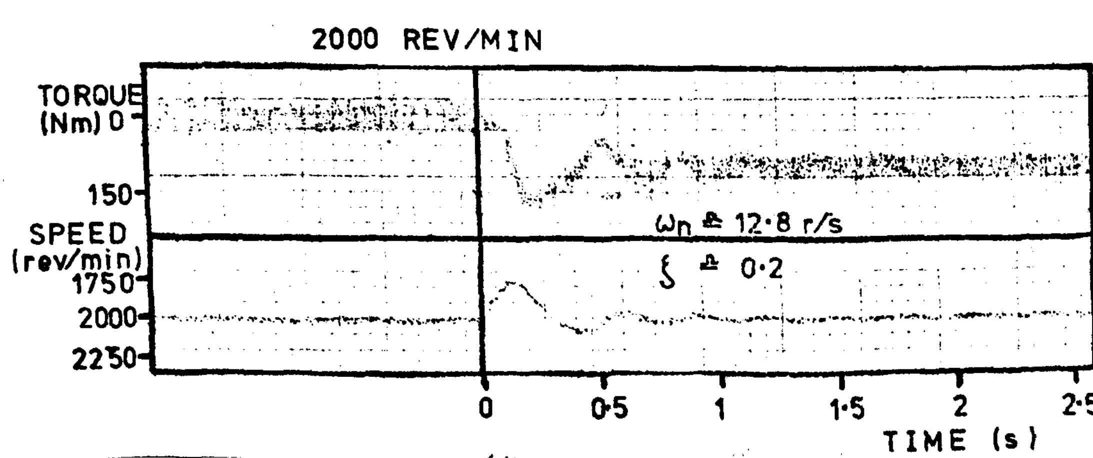

DIESEL ENGINE
HYDROSTATIC DYNAMOMETER

GRAPH G120

TORQUE AND SPEED RESPONSES TO STEP CHANGES IN DYNAMOMETER CONTROL SIGNAL

METHOD 2.2

LOADING CONDITION

SIMULATED CHARACTERISTICS ÷ FORD A SERIES TRUCK
4^{th} GEAR ENGINE SPEED 800 REV/MIN

(B = 1 ; C = 2 ; E = 0·5 ; F = 0·2)

STEP INCREASE TORQUE

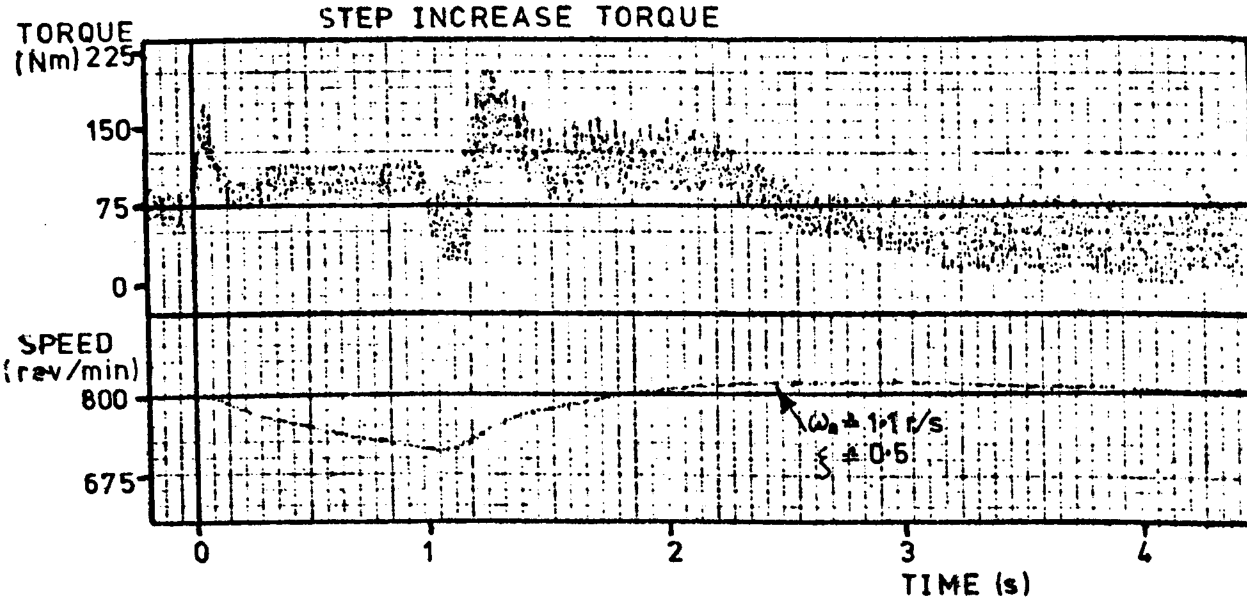

STEP REDUCTION TORQUE

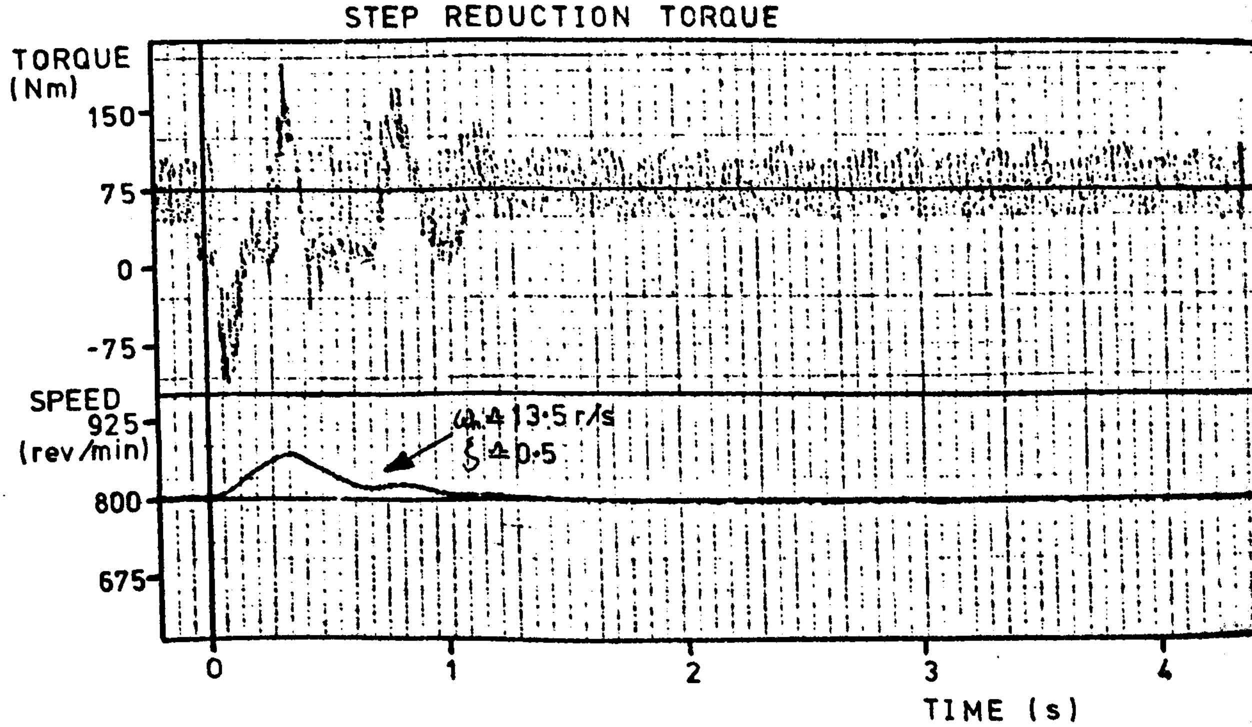

DIESEL ENGINE
HYDROSTATIC DYNAMOMETER

GRAPH G121

TORQUE AND SPEED RESPONSES TO STEP CHANGES IN DYNAMOMETER CONTROL SIGNAL

METHOD 2.2 MOTORING CONDITION

SIMULATED CHARACTERISTICS ÷ FORD A SERIES TRUCK
4th GEAR ENGINE SPEED LOW
(B=1 ; C=2)

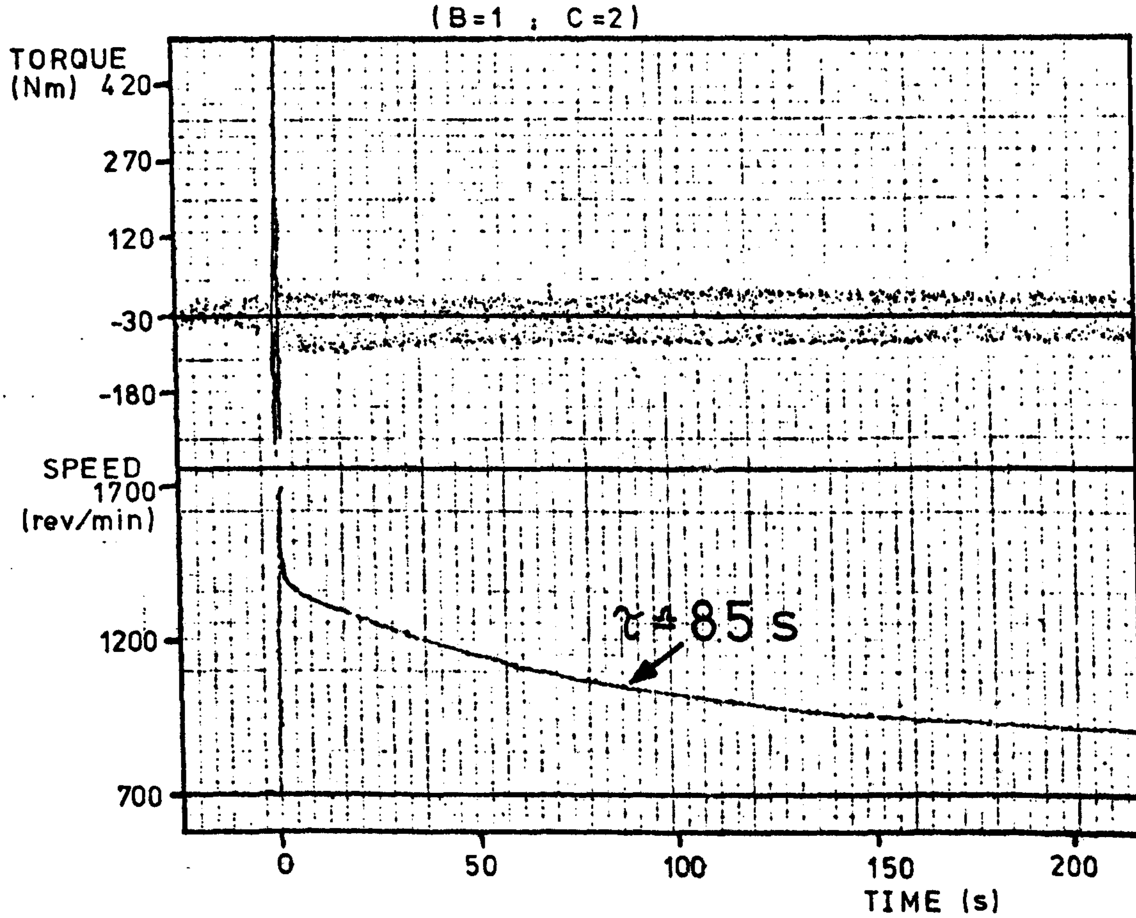

(INCREASED TIME SCALE)

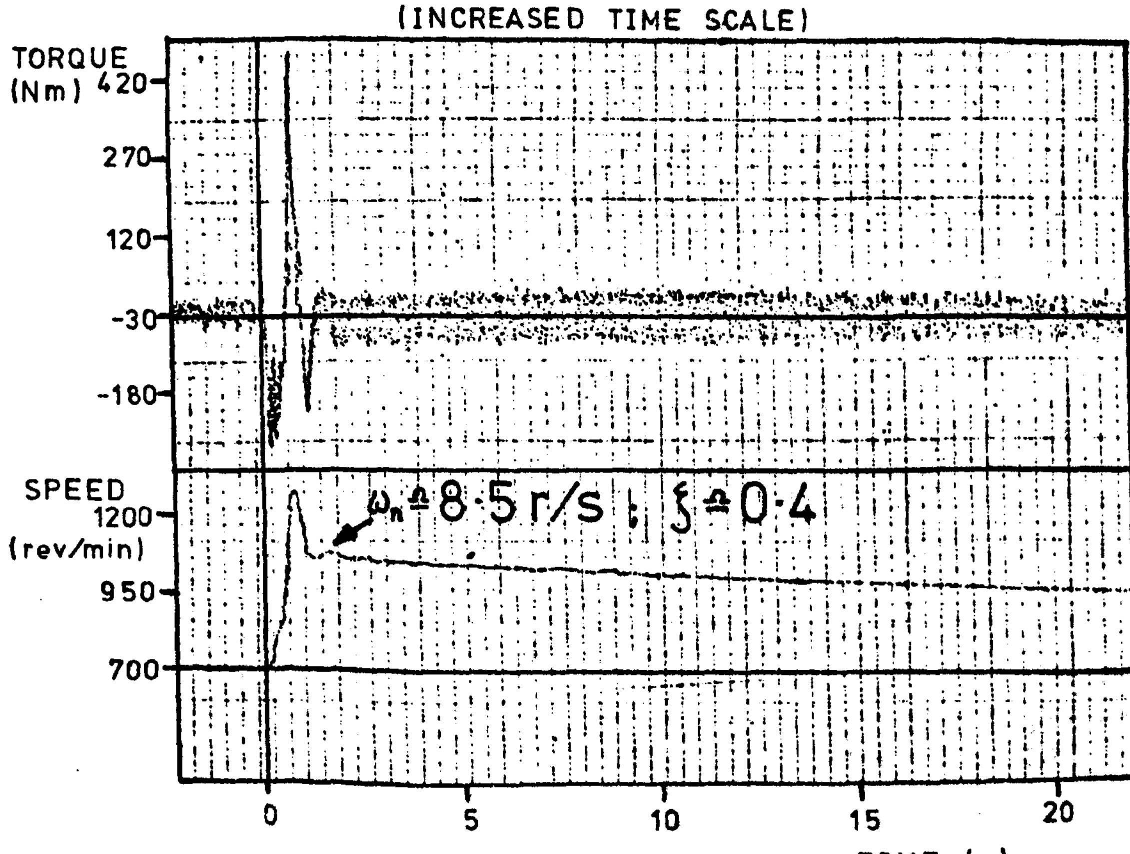

DIESEL ENGINE
HYDROSTATIC DYNAMOMETER

GRAPH G122

TORQUE AND SPEED RESPONSES TO STEP CHANGES IN THROTTLE LEVER SETTING

METHOD 2.2 NO FEEDBACK CONTROL ON THROTTLE

SIMULATED CHARACTERISTICS: FORD A SERIES TRUCK
4th GEAR LOW SPEED

(B = 1 ; C = 2)

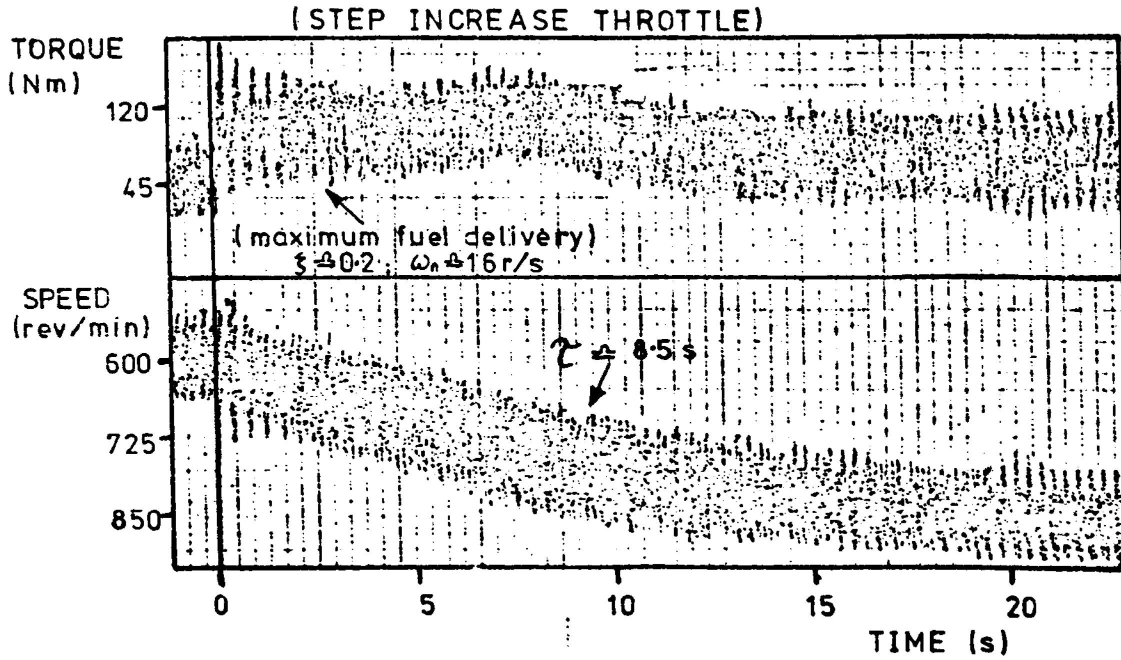

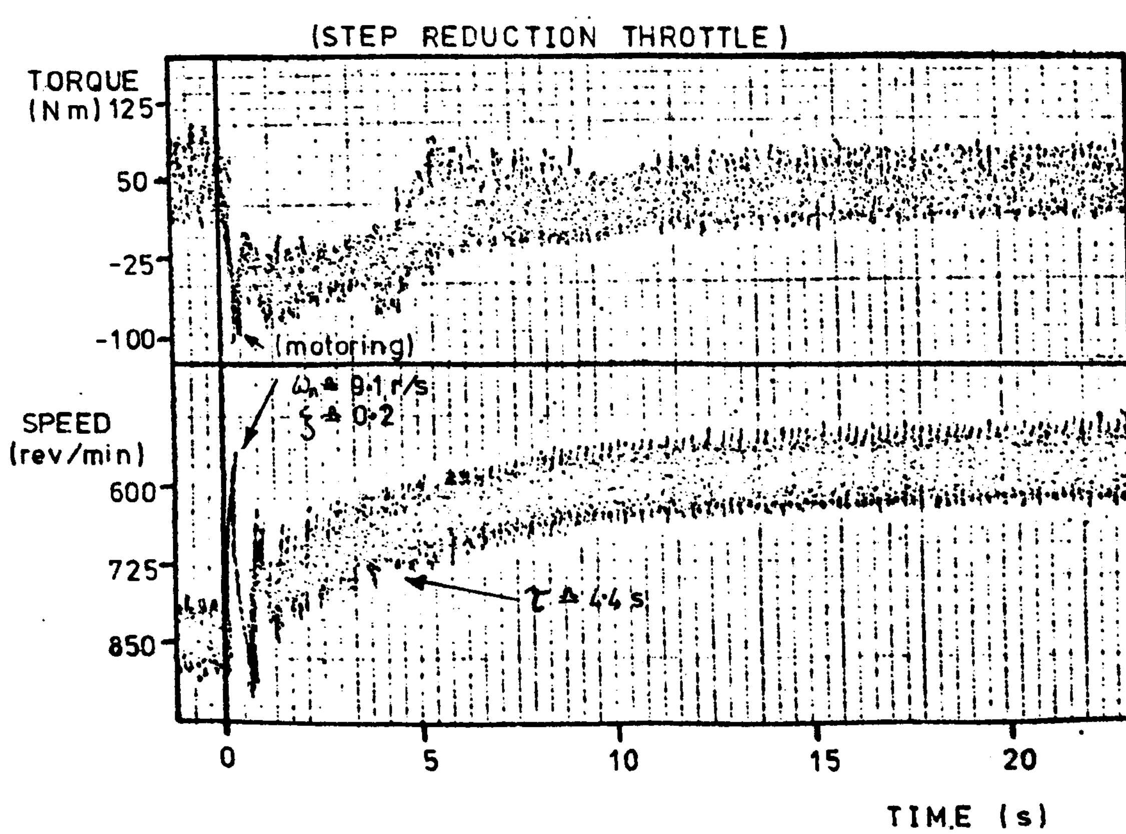

DIESEL ENGINE
FAST RESPONSE DYNAMOMETER

GRAPH G123

TORQUE AND SPEED RESPONSES
TO STEP DISTURBANCE TORQUES

METHOD 2.2

SIMULATED LOAD ÷ FORD A SERIES TRUCK
MEDIUM SPEED 4^{th} GEAR
• (B=0·1 ; C=0·3 , E=0·05 ; F=0·02)

MOTORING (STEP REDUCTION THROTTLE)

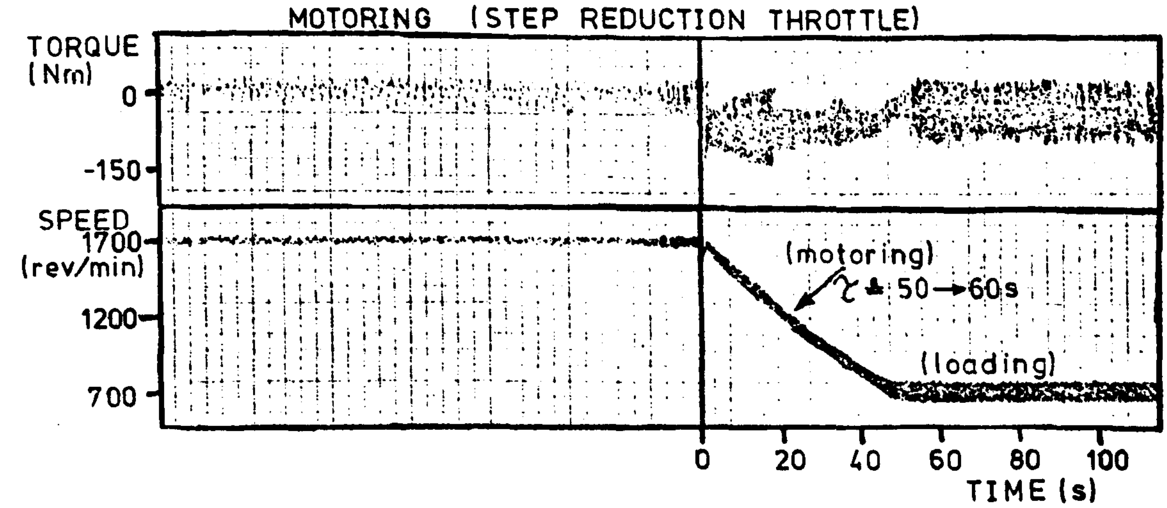

LOADING (STEP DISTURBANCE DYNAMOMETER SIGNAL)

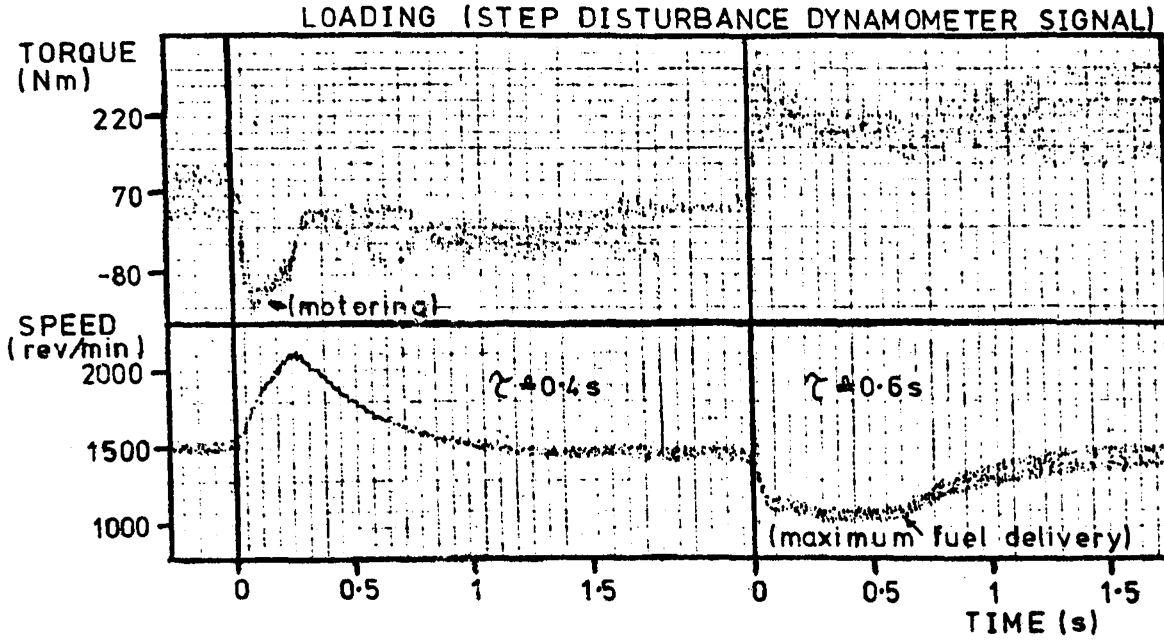

LOADING (STEP INCREASE THROTTLE—NO FEEDBACK)

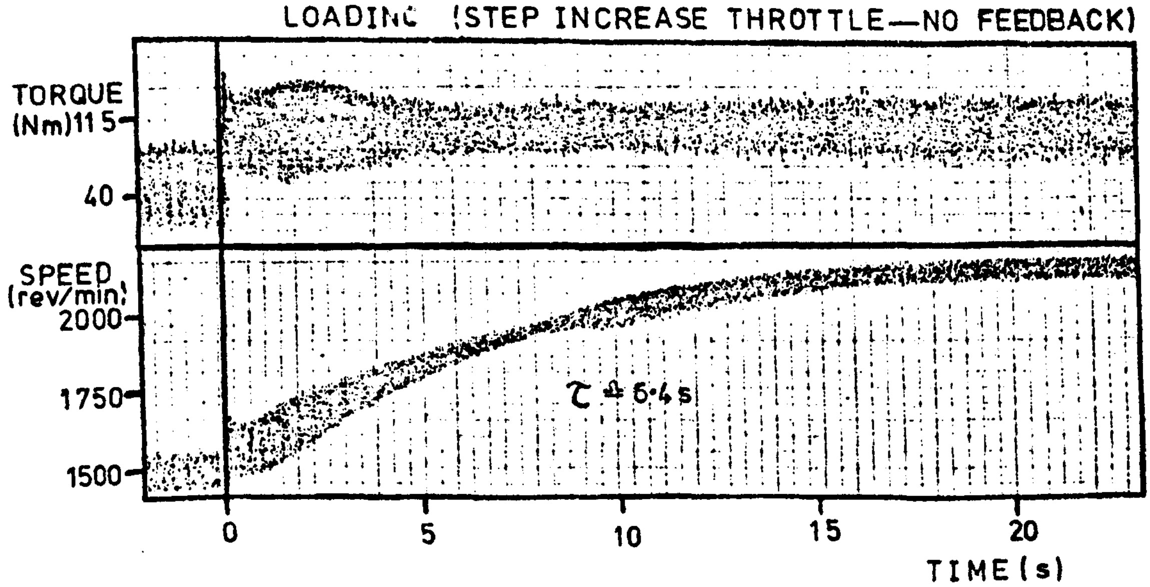

Appendix B

values

```
1 REM    SYSTEM PARAMETERS
2 REM
3 REM
4 REM    GAIN VALUES
5 K1=1.53
10 K2=1
15 K3=8.68
20 K4=286
25 K5=.382
30 K6=.00667
35 K7=163
40 K8=5.62
45 K9=98.7
47 REM    INERTIA VALUES
50 J1=.38
55 J2=.02
60 J3=26.14
62 J3=J3*K6/K5
70 J9=.001
71 REM    VISCOUS FRICTION VALUES
75 F3=.178
77 F3=F3*K6/K5
80 F4=1
85 F9=.4398
87 REM    TIME CONSTANTS
90 T1=.033
92 T2=T1
95 T3=.0152
100 T4=.5
105 T5=1
110 T6=.01
143 REM    CONTROLLER GAINS
150 B=.5
155 C=1
165 E=.3
170 F=.1
175 G1=1
185 G3=1
187 G4=1
189 REM    TELETYPE OUTPUT (IF REQUIRED)
190 A$="DHLO"
192 FILEV #1:"TTY:"\PRINT #1:\PRINT #1:
195 PRINT #1:A$\CLOSE #1
196 G2=-G2
197 DIM A(20),B(20),Q(20)
198 REM    CHECK IF ZEROS REQUESTED
199 IF U9=1 THEN 1500
```

app. B (contd.)

coef

```
200 REM    VARIABLES USED IN BLOCK DIAGRAM REDUCTION
202 W7=T2*T7*J1*T4*T5*T6
210 W6=J1*T7*(T2*T5*T6+T4*T5*T6+T2*T4*T5+T2*T4*T6)
212 W6=W6+J1*T2*T4*T5*T6+K1*T4*T1*T5*T6*T7
220 W5=J1*T7*(T2*T5+T4*T5+T2*T6+T4*T6+T2*T4+T5*T6)
222 W5=W5+J1*(T2*T5*T6+T4*T5*T6+T2*T4*T5+T2*T4*T6)
224 W5=W5-K1*T4*(T5*T6*(T7-T1)-T1*T7*(T5+T6))-(K8-K1)*T1*T5*T6*T7
230 W4=J1*T7*(T2+T4+T5+T6)+J1*(T2*T5+T4*T5+T2*T6+T4*T6+T2*T4+T5*T6)
232 W4=W4-G1*K5*K7*T1*T7*D-K1*T4*((T7-T1)*(T5+T6)-T1*T7+T5*T6)
234 W4=W4+(K8-K1)*(T5*T6*(T7-T1)-T1*T7*(T5+T6))
240 W3=J1*T7+J1*(T2+T4+T5+T6)+G1*K5*K7*(D*(T7-T1)-T1*T7*E)
242 W3=W3-K1*T4*(T7-T1+T5+T6)
244 W3=W3+(K8-K1)*((T7-T1)*(T5+T6)-T1*T7+T5*T6)
250 W2=J1+G1*K5*K7*(E*(T7-T1)-T1*T7+D)
252 W2=W2-K1*T4+(K8-K1)*(T7-T1+T5+T6)
260 W1=(T2+T7)*G1*K5*K7*F+G1*K5*K7*E+K8-K1
270 W0=G1*K5*K7*F
280 X7=J8*J9*T3*J3
290 X6=T3*J3*(J8*F9+F2*J9)+J8*J9*(T3*F3+J3)
300 X5=F3*J8*J9+(T3*F3+J3)*(J8*F9+F2*J9)+J3*T3*(J8*K9+F2*F9+K2*J9)
310 X4=F3*(J8*F9+F2*J9)+T3*J3*(F2*K9+K2*F9)
312 X4=X4+(T3*F3+J3)*(J8*K9+F2*F9+K2*J9)
320 X3=F3*(J8*K9+F2*F9+K2*J9)+(F2*K9+K2*F9)*(T3*F3+J3)
322 X3=X3+K2*K9*T3*J3+K6*G3*K4*K9*F2*A
330 X2=F3*(F2*K9+K2*F9)+K2*K9*(T3*F3+J3)+K6*G3*K4*K9*(F2*B+K2*A)
340 X1=F3*K2*K9+K6*G3*K4*K9*(C*F2+K2*B)
350 X0=K6*G3*K4*K9*C*K2
356 REM    CHECK IF ZEROS REQUESTED
357 IF U9=1 THEN 510
360 Y6=F2*J3*T2*T4*T6
370 Y5=F2*J3*(T4*T6+T2*T4+T2*T6+G2*K6*K7*T1*D)+T2*T4*T6*(F2*F3+K2*J3
380 Y4=F2*J3*(T4+T2+T6+G2*K6*K7*(T1*E-D))+F3*K2*T2*T4*T6
382 Y4=Y4+(F2*F3+K2*J3)*(T4*T6+T2*T4+T2*T6+G2*K6*K7*T1*D)
390 Y3=F2*J3*(1+G2*K6*K7*(T1*F-E))
392 Y3=Y3+(F2*F3+K2*J3)*(T4+T6+T2+G2*K6*K7*(T1*E-D))
394 Y3=Y3+F3*K2*(T4*T6+T2*T4+T2*T6+G2*K6*K7*T1*D)
400 Y2=-F2*J3*G2*K6*K7*F+(F2*F3+K2*J3)*(1+G2*K6*K7*(T1*F-E))
402 Y2=Y2+F3*K2*(T4+T6+T2+G2*K6*K7*(T1*E-D))
410 Y1=-G2*K6*K7*F*(F2*F3+K2*J3)+F3*K2*(1+G2*K6*K7*(T1*F-E))
420 Y0=-F3*K2*G2*K6*K7*F
430 Z7=J2*T3*J9*T5*T7
440 Z6=J2*T3*J9*(T5+T7)+T5*T7*(J2*T3*F9+J2*J9)
450 Z5=J2*T3*J9+(T5+T7)*(J2*T3*F9+J2*J9)
452 Z5=Z5+T5*T7*(J2*T3*K9+J2*F9+K3*J9)
460 Z4=J2*T3*F9+J2*J9+(T5+T7)*(J2*T3*K9+J2*F9+K3*J9)
462 Z4=Z4+T5*T7*(J2*K9+K3*F9)
470 Z3=J2*T3*K9+J2*F9+K3*J9+(T5+T7)*(J2*K9+K3*F9)+K3*K9*T5*T7
472 Z3=Z3+K4*K5*K9*A*(J4+F4*T7)
480 Z2=J2*K9+K3*F9+K3*K9*(T5+T7)
481 Z2=Z2-K9*K3*T7*G4
482 Z2=Z2+K4*K5*K9*(A*F4+B*(J4+F4*T7))
490 Z1=K3*K9+K4*K5*K9*(B*F4+C*(J4+F4*T7))
491 Z1=Z1-K3*K9*G4
500 Z0=K4*K5*K9*C*F4
```

app. B(contd.)

```
507 REM     BLOCK DIAGRAM REDUCTION (CONTD.)
510 A(14)=W7*X7
520 A(13)=W7*X6+Y6*Z7
530 A(12)=W7*X5+W6*X6+W5*X7+Y6*Z6+Y5*Z7
540 A(11)=W7*X4+W6*X5+W5*X6+W4*X7+Y6*Z5+Y5*Z6+Y4*Z7
550 A(10)=W7*X3+W6*X4+W5*X5+W4*X6+W3*X7
552 A(10)=A(10)+Y6*Z4+Y5*Z5+Y4*Z6+Y3*Z7
560 A(9)=W7*X2+W6*X3+W5*X4+W4*X5+W3*X6+W2*X7
562 A(9)=A(9)+Y6*Z3+Y5*Z4+Y4*Z5+Y3*Z6+Y2*Z7
570 A(8)=W7*X1+W6*X2+W5*X3+W4*X4+W3*X5+W2*X6+W1*X7
572 A(8)=A(8)+Y6*Z2+Y5*Z3+Y4*Z4+Y3*Z5+Y2*Z6+Y1*Z7
580 A(7)=W7*X0+W6*X1+W5*X2+W4*X3+W3*X4+W2*X5+W1*X6+W0*X7
582 A(7)=A(7)+Y6*Z1+Y5*Z2+Y4*Z3+Y3*Z4+Y2*Z5+Y1*Z6+Y0*Z7
590 A(6)=W6*X0+W5*X1+W4*X2+W3*X3+W2*X4+W1*X5+W0*X6
592 A(6)=A(6)+Y6*Z0+Y5*Z1+Y4*Z2+Y3*Z3+Y2*Z4+Y1*Z5+Y0*Z6
600 A(5)=W5*X0+W4*X1+W3*X2+W2*X3+W1*X4+W0*X5

602 A(5)=A(5)+Y5*Z0+Y4*Z1+Y3*Z2+Y2*Z3+Y1*Z4+Y0*Z5
610 A(4)=W4*X0+W3*X1+W2*X2+W1*X3+W0*X4
612 A(4)=A(4)+Y4*Z0+Y3*Z1+Y2*Z2+Y1*Z3+Y0*Z4
620 A(3)=W3*X0+W2*X1+W1*X2+W0*X3
622 A(3)=A(3)+Y3*Z0+Y2*Z1+Y1*Z2+Y0*Z3
630 A(2)=W2*X0+W1*X1+W0*X2+Y2*Z0+Y1*Z1+Y0*Z2
640 A(1)=W1*X0+W0*X1+Y1*Z0+Y0*Z1
650 A(0)=W0*X0+Y0*Z0
655 REM     NORMALISE PROCEDURE
660 IF A(0)=0 THEN 680
670 GOTO 700
675 REM     REDUCE LEADING ZERO COEFFICIENTS
680 FOR N=0 TO 14\A(N)=A(N+1)\NEXT N
685 G9=G9+1
690 GOTO 660
700 N=14\C1=0\C2=0
703 REM     PRINT LEADING ZEROS (IF REQUIRED)
705 IF G9=0 THEN 710
707 FOR I=1 TO G9\PRINT 0\NEXT I
710 IF A(N)=0 THEN 730
720 GOTO 740
725 REM     FIND ORDER OF POLYNOMIAL
730 N=N-1\GOTO 710
740 P1=N
750 FOR N=0 TO P1\A(N)=A(N)/A(P1)\NEXT N
```

roots

```
799 REM     FIND COMPLEX ROOTS (LIN'S METHOD)
800 GOTO 1000
805 REM     LIN'S METHOD HASN'T CONVERGED
806 REM     FIND REAL ROOT  (NEWTON-RAPHSON)
810 FOR N=1 TO P1
820 M=N*A(N)*S↑(N-1)+M
830 NEXT N
840 FOR N=0 TO P1
850 S2=A(N)*S↑N+S2
860 NEXT N
870 S1=S-S2/(M+10↑-5)
875 S2=0\M=0
877 REM     CHECK FOR CONVERGENCE
880 IF ABS(S-S1)<ABS(S1)*10↑-6 THEN 925
890 S=S1\GOTO 810
920 REM     PRINT REAL ROOT AND OBTAIN REMAINING COEFS.
925 PRINT S1
927 FILEV #1:"TTY:"\PRINT #1:S1\CLOSE #1
930 B(P1)=0\FOR N=1 TO P1\B(P1-N)=A(P1-N+1)+S1*B(P1-N+1)\NEXT N
935 P1=P1-1\FOR N=0 TO P1\A(N)=B(N)\NEXT N
940 IF P1=0 THEN 1170
```

```
999 REM   LIN'S METHOD FOR COMPLEX ROOTS
1000 N=P1\N1=P1+1
1002 FOR I=1 TO N1\B(I)=A(N1-I)\NEXT I
1005 FOR I=1 TO N1\A(I)=B(I)\NEXT I
1010 L=0\R1=1\R2=A(N1-1)/A(N1-2)\R3=A(N1)/A(N1-2)
1020 L=L+1\T1=A(1)\T2=A(2)\T3=A(3)\K=1\Q(K)=T1
1022 IF L<200 THEN 1030
1024 P1=N\FOR I=0 TO P1\A(I)=B(N1-I)\NEXT I
1026 S=-.1
1027 REM    NO CONVERGENCE. TRY NEWTON-RAPHSON
1028 GOTO 810
1030 S2=T1*R2\S3=T1*R3
1040 FOR I=4 TO N1\T1=T2-S2\T2=T3-S3\T3=A(I)
1050 K=K+1\Q(K)=T1\S2=T1*R2\S3=T1*R3\NEXT I
1060 IF .0001-ABS(1-S2/T2)<=0 THEN 1080
1070 IF .0001-ABS(1-S3/T3)>0 THEN 1090
1080 R2=(R2+T2/T1)/2\R3=(R3+T3/T1)/2\GOTO 1020
1085 REM    CONVERGENCE ACHIEVED. PRINT ROOTS
1090 GOSUB 1300
1095 IF P1-2=0 THEN 1170
1100 N=N-2\N1=N+1\IF N-2<=0 THEN 1130
1110 FOR I=1 TO N1\A(I)=Q(I)\B(I)=Q(I)\NEXT I
1120 GOTO 1010
1130 IF N-2<0 THEN 1160
1140 R1=Q(1)\R2=Q(2)\R3=Q(3)\GOSUB 1300
1150 GOTO 1170
1160 PRINT -Q(2)
1167 FILEV #1:"TTY:"\PRINT #1:-Q(2)\CLOSE #1
1170 STOP
1299 REM   PRINT ROUTINE FOR COMPLEX ROOTS
1300 IF R2*R2-4*R1*R3<0 THEN 1340
1310 PRINT -R2/2+SQR(R2*R2-4*R1*R3)/2
1315 PRINT -R2/2-SQR(R2*R2-4*R1*R3)/2
1323 FILEV #1:"TTY:"
1324 PRINT #1:-R2/2+SQR(R2*R2-4*R1*R3)/2
1326 PRINT #1:-R2/2-SQR(R2*R2-4*R1*R3)/2
1327 CLOSE #1
1330 RETURN
1340 PRINT -R2/2;"+-J";SQR(4*R3*R1-R2*R2)/2
1353 FILEV #1:"TTY:"
1354 PRINT #1:-R2/2;"+J";SQR(4*R3*R1-R2*R2)/2
1356 PRINT #1:-R2/2;"-J";SQR(4*R3*R1-R2*R2)/2
1357 REM    TELETYPE OUTPUT (IF REQUIRED)
1358 CLOSE #1
1360 RETURN
```

zeros

```
1500 PRINT "ZEROS"
1510 FILEV #1:"TTY:"\PRINT #1:\PRINT #1:
1520 PRINT #1:"ZEROS"\CLOSE #1
1530 W6=T5*T7*T4*T2*T6
1540 W5=T2*T4*T5*T7+T6*T4*T2*(T5+T7)+T6*T5*T7*(T4+T2)
1550 W4=T4*T2*(T5+T7)+T5*T7*(T4+T2)
1560 W4=W4+T6*((T5+T7)*(T4+T2)+T5*T7+T4*T2)
1570 W3=(T5+T7)*(T4+T2)+T5*T7+T4*T2
1580 W3=W3+T6*(T2+T4+T5+T7)
1590 W2=T6+T2+T4+T5+T7
1610 W1=1
1620 W0=0
1630 GOTO 280
2000 END
```

Appendix B(i)

diesel engine + hydrostatic dynamometer
low speed 4^{th} gear

MID FUEL DELIVERY

DHLO	ZEROS
-0.4968	
-0.685511 +J 1.01296	
-0.685511 -J 1.01296	-0.999999
-3.15942	-2
-8.7505 +J 12.7137	-2.19184 +J 2.08168
-8.7505 -J 12.7137	-2.19184 -J 2.08168
-39.6146 +J 16.758	-30.3025
-39.6146 -J 16.758	-60.0143
-99.9961	-100.02
-220.485 +J 224.375	-220.589 +J 224.247
-220.485 -J 224.375	-220.589 -J 224.247

MAXIMUMUM FUEL DELIVERY

DHLO	ZEROS
0.0538457	
-2.00015	-0.999999
-2.39693	-2
-10.0801 +J 12.0431	-2.19184 +J 2.08168
-10.0801 -J 12.0431	-2.19184 -J 2.08168
-38.6378 +J 16.4977	-30.3025
-38.6378 -J 16.4977	-60.0143
-99.9751	-100.02
-220.485 +J 224.375	-220.589 +J 224.247
-220.485 -J 224.375	-220.589 -J 224.247

NO THROTTLE CONTROL

DHLO	ZEROS
-0.154231	
-2.11496 +J 0.555832	-0.999999
-2.11496 -J 0.555832	-2
-8.84143 +J 13.3793	-2.19184 +J 2.08168
-8.84143 -J 13.3793	-2.19184 -J 2.08168
-39.8583 +J 16.7762	-30.3025
-39.8583 -J 16.7762	-60.0143
-99.9701	-100.02
-220.485 +J 224.375	-220.589 +J 224.247
-220.485 -J 224.375	-220.589 -J 224.247

MOTORING

DHMO	ZEROS
-0.0107799	
-2.37108	-1
-1.73172 +J 6.59996	-0.378901 +J 1.19148
-1.73172 -J 6.59996	-0.378901 -J 1.19148
-61.8824	-65.6571
-220.009 +J 224.372	-220.029 +J 224.35
-220.009 -J 224.372	-220.029 -J 224.35

Appendix B(ii)

diesel engine + fast response dynamometer
medium speed 4th gear

MID FUEL DELIVERY

DFME	ZEROS
-0.171168 +J 0.227829	
-0.171168 -J 0.227829	
-1.65008	-0.242536 +J 1.18774
-17.3126 +J 25.8963	-0.242536 -J 1.18774
-17.3126 -J 25.8963	-14.2857
-107.153 +J 29.6671	-75.1171
-107.153 -J 29.6671	-100.092
-44.8941 +J 80.2109	-192.054
-44.8941 -J 80.2109	-59.587 +J 103.077
-161.336	-59.587 -J 103.077
-1000.13	-999.988

MAXIMUM FUEL DELIVERY

DFME	ZEROS
-0.00007582	
-3.4749	-0.242536 +J 1.18774
-14.2867	-0.242536 -J 1.18774
-50.646	-14.2857
-88.4023	-75.1171
-99.7828	-100.092
-42.7308 +J 78.7485	-192.054
-42.7308 -J 78.7485	-59.587 +J 103.077
-160.017	-59.587 -J 103.077
-1000.11	-999.988

NO THROTTLE CONTROL

DFME	ZEROS
-0.161356	
-2.27787	-0.242536 +J 1.18774
-25.9186 +J 16.1446	-0.242536 -J 1.18774
-25.9186 -J 16.1446	-14.2857
-100.269 +J 1.39264	-75.1171
-100.269 -J 1.39264	-100.092
-44.1676 +J 78.694	-192.054
-44.1676 -J 78.694	-59.587 +J 103.077
-158.922	-59.587 -J 103.077
-1000.11	-999.988

MOTORING

DFMEMO	ZEROS
-0.0190061	-0.0348742 +J 0.417572
-2.05464 +J 2.85367	-0.0348742 -J 0.417572
-2.05464 -J 2.85367	-71.9071
-67.7891	-99.952
-99.9591	-59.7204 +J 103.342
-59.8824 +J 103.138	-59.7204 -J 103.342
-59.8824 -J 103.138	-999.987
-999.988	

Appendix C(i)

```
5 REM      FLOW CHARACTERISTICS
6 REM      FOR SPECIAL PURPOSE VALVE
7 REM
8 REM
9 REM
10 REM    VALVE DIMENSIONS
20 L2=.102
30 L3=.104
40 L4=.096
50 L5=.75
55 REM     VISCOSITY
60 V=22.43
70 V=V*.00155
75 REM     EFFECTIVE DIAMETER
80 D1=2*L2*L3/(L2+L3)
90 A=D1/(L5+L2)
100 PRINT "CURVATURE RATIO=";A
105 REM    OIL FLOWRATE
110 Q=6.29
115 REM    AVERAGE OIL VELOCITY
120 W=4.62*Q/(L3*L2)
130 R1=D1*W/V
140 PRINT "REYNOLDS NO.=";R1
150 D2=R1*A↑.5
160 PRINT "DEAN NO.=";D2
170 E1=.1361*(L3+L4)*(D2*A)↑(1/3)
180 PRINT "SPOOL ENTRY LENGTH (AUSTIN)=";E1
190 E2=(8*A+1.7)*SQR(D2*A)*D1*(L3+L4)/(3.14159*(L5+L2))
200 PRINT "SPOOL ENTRY LENGTH (Y+B)=";E2
210 F=.107*D2↑.5
220 PRINT "FRICTION FACTOR=";F
225 REM    ENGAGED LENGTH OF SPOOL
230 PRINT "SPOOL LENGTH";\INPUT L1
235 REM    DUCT LENGTH
240 L=SQR((L3+L4)↑2+(3.14159*(L5+L2))↑2)*L1/(L3+L4)
250 P=.361*W*V*L/(D1*D1*10↑5)
260 PRINT "PRESSURE DROP IN STRAIGHT TUBE=";P
270 PRINT "PRESSURE DROP IN CURVED DUCT=";P*F;"PSI"
280 GOTO 230
290 END
```

Appendix C(ii)

```
5 REM    VALVE CHARACTERISTICS INCLUDING
6 REM    TEMPERATURE EFFECT ON VISCOSITY
7 REM
8 REM
9 REM
10 REM   VALVE DIMENSIONS
20 L2=.086
30 L3=.083
40 L4=.068
50 L5=.3326
53 REM    OIL INLET TEMPERATURE
55 T=50
60 IF T>30 THEN 67
63 V=2168*T↑-1.075\GOTO 70
67 V=28726*T↑-1.8347
68 REM    CALCULATED OIL VISCOSITY
70 V=V*.00155
75 REM    EFFECTIVE DIAMETER OF DUCT
80 D1=2*L2*L3/(L2+L3)
90 A=D1/(L5+L2)
100 PRINT "CURVATURE RATIO=";A
105 REM   OIL FLOWRATE
110 Q=3
115 REM   AVERAGE OIL VELOCITY
120 W=4.62*Q/(L3*L2)
130 R1=D1*W/V
140 PRINT "REYNOLDS NO.=";R1
150 D2=R1*A↑.5
160 PRINT "DEAN NO.=";D2
170 E1=.1361*(L3+L4)*(D2*A)↑(1/3)
180 PRINT "SPOOL ENTRY LENGTH (AUSTIN)=";E1
190 E2=(8*A+1.7)*SQR(D2/A)*D1*(L3+L4)/(3.14159*(L5+L2))
200 PRINT "SPOOL ENTRY LENGTH (Y+B)=";E2
210 F=.107*D2↑.5
220 PRINT "FRICTION FACTOR=";F
225 REM   ENGAGED LENGTH OF SPOOL
230 L1=1
235 REM   DUCT LENGTH
240 L=SQR((L3+L4)↑2+(3.14159*(L5+L2))↑2)*L1/(L3+L4)
250 P=232.9*W*V*L/(D1↑2*10↑5)
255 REM    FIRST PRESSURE GRADIENT
260 P(0)=P*F/14.5
265 V(0)=V
270 FOR N=1 TO 10\P(N)=P(0)*(10-N)/10\NEXT N
275 REM    TEMPERATURE GRADIENT
280 T(0)=T
290 FOR N=1 TO 10\T(N)=(P(N-1)-P(N))*.05904+T(N-1)\NEXT N
300 FOR N=1 TO 10
310 IF T(N)>30 THEN 330
315 REM    VISCOSITY GRADIENT
320 V(N)=2168*T(N)↑-1.075\GOTO 340
330 V(N)=28726*T(N)↑-1.8347
340 V(N)=V(N)*.00155
343 V(N)=V(N)*(1+.3*P(N)/100)
345 NEXT N
347 REM    FRICTION FACTOR GRADIENT
350 FOR N=0 TO 9\F(N)=.107*SQR(A↑.5*D1*W/V(N))\NEXT N
360 FOR N=0 TO 9
365 REM    BACK STEP FOR NEXT PRESSURE GRADIENT
370 P(9-N)=P(10-N)+343.35*W*V(9-N)*L*F(9-N)/(145*D1↑2*10↑5)
380 NEXT N
390 IF P(0)-P1<.1 THEN 410
400 P1=P(0)\GOTO 290
405 REM    CONVERGENCE ACHIEVED
410 PRINT P(0)
```

Appendix D(i)

microprocessor program to read data from cassette

```
        NAM     READ        PCD CASSETTE
        OPT O
        OPT S
        ORG     $0000       START ADDRESS
        LDX     #STR1
        JSR     $E07E       READ TAPE REQUEST
        JSR     GET1        RESET CRA7
LOOP    JSR     GET         READ IN ONE BYTE
        CMP A   #'S         IS IT AN S?
        BNE     LOOP        NO. GO BACK
        JSR     GET         YES. GET NEXT BYTE
        CMP A   #'9         IS IT A 9?
        BNE     N1          NO GOTO N1
        LDX     #STR2       YES. STOP TAPE REQUEST
        JSR     $E07E
        JMP     $0103       START EDITOR (CHANGE AS REQUIRED)
N1      CMP A   #'1         IS IT A 1?
        BNE     LOOP        NO. START AGAIN
        CLR     $A00A       YES. CLEAR CHECKSUM
        JSR     GET         NEXT CHARACTER
        DEC A
        DEC A               TAKE AWAY TWO
        STA A   $A00B       STORE BYTE COUNT
        JSR     GET
        STA A   $A00C
        JSR     GET
        STA A   $A00D
        LDX     $A00C        TWO BYTES FOR INDEX REGISTER
N2      JSR     GET          DATA LOOP
        DEC     $A00B
        BEQ     N3
        STA A   0,X          STORE IN MEMORY
        INX
        BRA     N2
N3      INC     $A00A        RECORD IN
        BEQ     LOOP         CHECKSUM OK. GET NEXT RECORD
        LDA A   #'?          CHECKSUM ERROR
        JSR     $E1D1        PRINT ?
        LDX     #STR2        STOP TAPE REQUEST
        JSR     $E07E
        JMP     $E0E3        RETURN TO MIKBUG
STR1    FCB     $D,$A,$A
        FCC     'PRESS READ' MESSAGE
        FCB     04
STR2    FCB     $D,$A,$A
        FCC     'PRESS STOP' MESSAGE
        FCB     04
GET     LDA A   $8009         INPUT ONE BYTE SUBROUTINE
        BPL     GET           BRANCH BACK UNTIL DATA READY
        LDA A   $8008         READ DATA INTO A
GET1    LDA B   #$36
        STA B   $8009         SET CA2 HIGH
        LDA B   #$10
NEXT    DEC B
        BPL     NEXT          WAIT 100 MICROSECONDS
        LDA B   #$3E
        STA B   $8009         SET CA2 LOW
        TAB
        ADD B   $A00A         UPDATE CHECKSUM
        STA B   $A00A
        RTS                   RETURN FROM SUBROUTINE
        END
```

app. D(i) contd.

microprocessor program to write data onto cassette

```
        NAM     WRITE
        OPT O
        ORG     $0100       START ADDRESS
SUBR    LDA A   $800F
        BPL     SUBR        DCH READY?
        LDA A   X           LOAD DATA INTO A
        STA A   $800A
        LDA A   #$3E
        STA A   $800B       INITIALISE WRITE ON CASSETTE
        LDA A   #$10
DELA    DEC A               WAIT 100 MICROSECONDS
        BPL     DELA
        LDA A   $800A
        LDA A   #$36
        STA A   $800B       SET CB2 LOW
        ADD B   X
        INX
        RTS
RED     LDX     $A002
        STX     $A003
RAD     LDA A   $A005       STORE NO. OF BYTES TO BE
        SUB A   $A010       TO BE WRITTEN ON CASSETTE
        LDA B   $A004       IN A AND B
        SBC B   $A00F
        BNE     A1          BRANCH IF B NOT ZERO
        CMP A   #$10
        BCS     A2          BRANCH IF A<10
A1      LDA A   #$0F
A2      ADD A   #4
        STA A   $A011       STORE BYTE COUNT
        SUB A   #3          SUB ADDRESS BYTES+CHECKSUM
        STA A   $A00F       NUMBER OF BYTES FOR TRANSFER
        LDX     #$E13A
        JSR     SUBR        OUTPUT START CHARACTERS 'S1'
        LDX     #$E13B
        JSR     SUBR
        CLR B
        LDX     #$A011      BYTE COUNT
        JSR     SUBR        OUTPUT BYTE COUNT
        LDX     #$A00F
        JSR     SUBR        OUTPUT TWO BYTES CONTAINING
        JSR     SUBR        ADDRESS OF RECORD
        LDX     $A00F       POINTS TO DATA
JAK     JSR     SUBR
        DEC     $A00E
        BNE     JAK         WRITE LOOP
```

```
        STX     $A00F          NEXT ADDRESS
        COM B                  SET UP CHEKSUM
        PSH B                  B TO STACK
        TSX
        JSR     SUBR           WRITE CHECKSUM
        PUL B                  ADJUST STACK POINTER
        LDX     $A00F
        DEX                    COUNTER INX IN SUBR
        CPX     $A004          ALL DATA TRANSFERRED?
        BEQ     JEM            BRANCH IF YES
        JMP     RAD
JEM     LDX     #$E13A         TRANSFER 'S9'
        JSR     SUBR
        LDX     #S9
        JSR     SUBR           END OF RECORD
        LDX     #STR3
        JSR     $E07E          STOP TAPE REQUEST
        JMP     $E0E3          RETURN TO MIKBUG
S9      FCB     $39            '9
STR3    FCB     $D,$A,$A
        FCC     'PRESS STOP'   STOP MESSAGE
        FCB     04
        END
```

Appendix D(ii)

microprocessor subroutine to control 16 channel multiplexed A/D convertor

```
        NAM     ATOD
        OPT     O,S
        ORG     CONT1
*CHANNEL ADDRESS STORED IN A
*RETURN ADDRESS FOR DATA GIVEN BY INDEX REGISTER
PIAD    EQU     $8010           PIA ADDRESS
SAVX    RMB     2               SAVE RETURN ADDRESS
DATIN   STX     SAVX
        LDX     #PIAD
        LDA B   #$38            PROGRAM PIA
        STA B   1,X
        LDA B   #$0F
        STA B   X
        LDA B   #$3C
        STA B   1,X             ENABLE PIA REG A
        LDA B   #$4
        STA B   3,X             ENABLE PIA REG B
        STA A   PIAD
        LDA A   #$34
        STA A   PIAD+1          TRIGGER A/D
WAIT    LDA A   1,X
        BPL     WAIT            CONVERSION COMPLETE?
        LDA B   X
        LDA A   2,X             LOAD DATA
        LDX     SAVX            GET RETURN POINTER
        STA A   X               HAND BACK MS BITS
        STA B   1,X             HAND BACK LS BITS
        RTS
CONT2   EQU     *
        END
```

REFERENCES

1. "Emission Standards for Model Year 1977", Federal Register, Vol. 40, No. 126, June 30, 1975.

2. E.E.C. Council directives:- March 20, 1970 (petrol engines); August 2, 1972 (diesel engines). Reported in official journal Nos. L76/1 and L190/1 respectively.

3. "Dynamic modelling of a turbocharged diesel engine", Ledger, J.D., Benson, R.S., Whitehouse, N.D., Engine Performance Modelling Conference, I.Mech.E., 1973.

4. "The prediction of diesel engine performance and combustion chamber component temperatures using digital computers",
Janota, M.S., Hallam, A.J., Brock, E.K., Dexter, S.G., Proc.I.Mech.E., Vol. 182, Part 3L, pp. 58-70, 1967-68.

5. "A summary of current research in the field of combustion - University of Nottingham",
Hay, N., Proc. UNICEG Meeting, University of Bath, September 1975.

6. "Mathematical model for displacement pumps and motors", Schlösser, W.M.J., Hydraulic Power Transmission, April 1961.

7. "How to estimate the bulk modulus of hydraulic fluids", Hayward, A.T.J., Hydraulic Pneumatic Power, January 1970.

8. "The compressibility of hydraulic fluids", Hayward, A.T.J., Journal of the Institute of Petroleum, Vol. 51, No. 494, February 1965.

9. "The dynamic characteristics of a hydrostatic transmission system", Bowns, D.E., Worton-Griffiths, J., Proc. I.Mech.E., Vol. 186, 55/72, 1972.

10. "Mathematical model of an internal combustion engine and dynamometer test rig", Monk, J., Comfort, J., Measurement and Control, Vol. 3, June 1970.

11. "Automation in an engine laboratory", Laborn, A., Proc. I.Mech.E., Vol. 179, Part 2A, No. 8, 1964-65.

12. British Standard, engine test corrections, AU141a, 1971.

13. "Electrohydraulic Vehicle Load Simulation", Karwatzki, J.M., M.Phil. Thesis, CNAA, 1973.

14. "Federal Driving Schedule", Federal Register, revised Vol. 36, No. 55, March 1971.

15. "Transient response of turbocharged diesel engines", Winterbone, D.E. et al., SAE Paper No. 770122, 1977.

16. "A wholly dynamic model of a turbocharged diesel engine for transfer function evaluation", Winterbone, D.E., Thiruarooran, C., Wellstead, P.E., SAE Paper No. 770124, 1977.

17. "Mathematical simulation of a large turbocharged two-stroke diesel engine", Streit, E.E., Borman, G.L., SAE Paper No. 710176, 1971.

18. "A comprehensive digital computer program to simulate a compression ignition engine including intake and exhaust systems", Benson, R.S., SAE Paper No. 710173, 1971.

19. "Some problems in diesel engine research with special reference to computer control and data acquisition", Marzouk, M., Watson, N., Proc.I.Mech.E., Vol. 190, 23/76, 1976.

20. "Speed varying loads affect the stability of hydrostatic transmissions", Olson, J.R., 26th National Conference on Fluid Power, 1970.

21. "The dynamic transfer characteristics of reciprocating engines", Bowns, D.E., Proc.I.Mech.E., Vol. 185, 16/71, 1970-71.

22. "Transient characteristics of turbocharged diesel engines",
Bowns, D.E. et al., Engine Performance Modelling Conference, I.Mech.E., 1973.

23. "Transient engine testing by computer control", Cassidy, J.F. Jr., Rillings, J.H., SAE Paper No. 720454, 1972.

24. "Using analog function modules for measurement and control",
Huffman, J.G., Gibson, T.V., Rose, S.T., Instruments and Control Systems, December 1972.

25. "Developments in dynamometer control methods", Clements, R.W., Richard, M.A., SAE Paper No. 720453, 1972.

26. "Hybrid simulation in the automotive industries", Soliman, J.I., Journal of Automotive Engineering, August 1973.

27. "A hybrid model of an automated engine test bed", Soliman, J.I., Journal of Automotive Engineering, October 1973.

28. "An automatic diesel engine test plant", Oatley, J.W., Industrial Electronics, April 1966.

29. "An engine test bed model for dynamic control studies", Al-Bermani, S.A., Gravestock, R.E., Journal of Automotive Engineering, I.Mech.E., February 1975.

30. "Automatic testing of electric vehicle drives", Pacey, K., Edwards, J.B., Int. Electric Vehicle Expo. and Conf., Chicago, April 1977.

31. "Introduction to the ERDA electric and hybrid demonstration program", U.S. Energy Research and Development Administration, Electric Vehicle News, May 1977.

32. "An engine test language for computer control of engine tests", Warman, E.A., Third International Symposium on Automation of Engine Testing, September 1974.

33. "Processing engine test data using SPEED", Warman, E.A., Scott, S.W., Ibid.

34. "Internal combustion engine instrumentation for on-line computer applications", Connor, W.A., Int. Journal of Mech. Eng. Education, Vol. 2, No. 4, 1974.

35. "Streamline Flow", Purday, H.F.P., Constable, 1949.

36. "Developing laminar flow in a circular tube", Collins, M.W., Symposium on Internal Flows, Salford University, 1971.

37. Bath University of Technology, Engineering Department Report No. 113, 1968.

38. "Study on forced convective heat transfer in curved pipes", Mori, Y., Nakayama, W., Int. Journal of Heat and Mass Transfer, Vol. 8, 1965.

39. "Boundary vorticity method for laminar forced convection heat transfer in curved pipes", Akiyama, M., Cheng, K.C., Ibid., Vol. 14, 1971.

40. "Reverse osmosis in laminar flow through curved tubes", Nunge, R.J., Adams, L.R., Desalination, Vol. 13, 1973.

41. "Minimisation of axial dispersion by use of secondary flow in helical tubes", Koutsky, J.A., Adler, R.J., Canadian Journal of Chemical Engineering, December 1964.

42. "Viscous drag and secondary flow in granular beds", Jones, W.M., Brit. J. Appl. Phys. (J. Phys. D), Vol. 1, 1968.

43. "Non-linear flow through granular media",
Wright, D.E., Proc. ASCE, J. Hyd. Div., HY4, 1968.

44. "Entry flow in a curved pipe",
Yao, L.S., Berger, S.A., J. Fluid Mech., Vol. 67, Part 1, 1975.

45. "Entry flow in a curved pipe",
Singh, M.P., J. Fluid Mech., Vol. 65, Part 3, 1974.

46. "The streamline motion of fluid in a curved pipe",
Dean, W.R., Phil. Mag. iv, p. 208, 1927.

47. "The streamline motion of fluid in a curved pipe (second paper)",
Dean, W.R., Ibid., Vol. 5, No. 30, 1928.

48. "Experiments in streamline motion in curved pipes",
Eustice, J., Proc. Royal Soc., Series A, Vol. 85, 1911.

49. "Streamline flow through curved pipes",
White, C.M., Proc. Royal Soc., Series A, Vol. 123, 1929.

50. "Abriss der Stromungslehre",
Prandtl, L., Braunschweig, 1931.

51. "Essentials of Fluid Dynamics",
Prandtl, L., Blackie, 1954.

52. "Strömung in gekrümmten Rohren",
Adler, M., ZAMM, October 1934.

53. "On secondary flow in stationary curved pipes",
Barua, S.N., Quart. J. Mech. and App. Math.,
Vol. XVI, Part 1, 1963.

54. "Steady laminar flows of an incompressible viscous fluid in curved pipes",
Topakoglu, H.C., Journal of Mathematics and Mechanics,
Vol. 16, No. 12, 1967.

55. "Laminar flow in curved pipes",
Ito, H., ZAMM, Vol. 49, 1969.

56. "Experiments on laminar flow in curved channels of square section",
Baylis, J.A., J. Fluid Mech., Vol. 48, Part 3, 1971.

57. "The development of viscous flow within helical coils",
Austin, L.R., Ph.D. Thesis, University of Utah, 1971.

58. "Laminar convective transport processes in strongly curved tubes",
Lin, T.S., Ph.D. Thesis, Clarkson College of Technology, 1972.

59. "Motion of fluid in a curved tube",
McConalogue, D.J., Srivastava, R.S., Proc. Royal Soc.,
Series A, Vol. 307, 1968.

60. "Fully developed viscous flow in coiled circular pipes", Austin, L.R., Seader, J.D., AIChE Journal, Vol. 19, No. 1, January 1973.

61. "Numerical treatment of fully developed laminar flow in helically coiled tubes", Truesdell, L.C. Jr., Adler, R.J., AIChE Journal, November 1970.

62. "Numerical treatment of laminar flow in helically coiled tubes of square cross section", Joseph, B., Smith, E.P., Adler, R.J., AIChE Journal, Vol. 21, No. 5, September 1975.

63. "Fully developed laminar flow in curved rectangular channels", Cheng, K.C., Lin, R.C., Ou, J.W., Journal of Fluids Engineering, March 1976.

64. "A general approach to hydraulic lock", Dransfield, P., Bruce, D.M., Wadsworth, M., Proc. I.Mech.E., Vol. 182, Part 1, No. 27, 1967-68.

65. "Pressure losses for fluid flow in curved pipes", Keulegan, G.H., Beij, K.H., Journal of Research of the National Bureau of Standards, research paper RP965, Vol. 18, January 1937.

66. "Boundary Layer Theory",
Schlichting, H., McGraw-Hill, 1968.

67. "A computer controlled engine test cell for engineering experiments",
Rillings, J.H., Wendell, D.C., Lakshmi, S.V., Proc. IEEE, Vol. 61, No. 11, November 1973.

68. "Simulation of massive inertia loads using feedback techniques",
Bates, J.J., Grimshaw, K.P., Proc. IEE, Vol. 113, No. 3, March 1966.

69. "A comparison of dynamic exhaust emissions tests: chassis dynamometer vs. engine dynamometer",
Cassidy, J.F., SAE Paper No. 720455, 1972.

70. "A dynamometer on which the dynamic behaviour of a passenger car can be simulated",
Odier, J., Proc. I.Mech.E., Vol. 186, 7/72, 1972.

71. "Advancing electric vehicles",
Harding, G.G., The Transport Engineer, May 1976.

72. "Batteries and controls for c.v. traction",
Pearson, M.G., Ibid.

73. "The development of cost effective electric road vehicles",
Mangan, M.F., Internal report, Chloride Technical Ltd.

74. "Computer simulation of a turbocharged diesel engine operating under transient load conditions",
Ledger, J.D., Walmsley, S., SAE Paper No. 710177, 1971.

75. "Hybrid computer simulation of the sampled-data model for compression-ignition engines",
Burrows, C.R., Van Eetvelt, P.W., Windetl, G.P., Int. J. Control, Vol. 14, No. 4, 1971.

76. "Discrete modelling of spark-ignition engines for control purposes",
Hazell, P.A., Flower, J.O., Ibid., Vol. 13, No. 4, 1971.

77. "Sampled-data theory applied to the modelling and control analysis of compression-ignition engines",
Flower, J.O., Hazell, P.A., Ibid.

78. "Survey of research by universities internal combustion engine group",
University of Manchester, Inst. of Science and Tech., 1971.

79. "Scientific design of a diesel governor",
Massey, A.G., Oldenburger, R., Trans. ASME, Paper No. 58-OGR11, 1958.

80. "Governing of compression-ignition oil engines",
Welbourn, D.B., Roberts, D.K., Fuller, R.A., Proc. I.Mech.E., Vol. 173, No. 22, 1959.

81. "Instability due to static and coulomb friction in autonomous control systems", Parnaby, J., 2nd Fluid Power Symposium, Guildford, January 1971.

82. "Dynamic characteristics of a naturally aspirated compression-ignition engine", Bowns, D.E., Engine Performance Modelling Conference, I.Mech.E., 1973.

83. "Modelling and control of a spark-ignition engine", Marshall, S.A., Oversby, K., Ibid.

84. "Multi-variable control of an engine/dynamometer test rig", Munro, N., Hirbod, S., UMIST Control Systems Centre, Report No. 373, 1977.

85. "Hydrostatic dynamometers - a step forward", Anon., Fluid Power International, December 1967.

86. "Fast response dynamometer", Woolvet, G.A., Karwatzki, J.M., CME, December 1973.

87. "A fast response dynamometer", Caputo, C., Carnevale, E., 3rd Int. Symp. on Automation of Engine Testing, September 1974.

88. "Mathematical models and effective performance of hydrostatic machines and transmissions",
Thoma, J., Hydraulic Pneumatic Power, November 1969.

89. "Analysis of a dynamically loaded hydrostatic transmission system",
McCallion, H., Dudley, B.R., Knight, G.C., 1st Fluid Power Symposium, Cranfield, January 1969.

90. "An analysis of the control mechanism used in variable delivery hydraulic pumps",
Green, W.L., Crossley, T.R., Proc. I.Mech.E., Vol. 185, 6/71, 1970-71.

91. "The application of optimising control to an hydraulic drive",
Steel, G.K., Measurement and Control, Vol. [illegible],
February 1973.